THE FINITE ELEMENT SOLUTION OF SOME TWO- AND THREE-DIMENSIONAL VISCOUS FLOW PROBLEMS USING PRIMITIVE VARIABLES

by

CLAUDIO RIGON

BE (Hons), University of Adelaide, 1976

A Thesis presented to the Faculty of Engineering
of the University of Adelaide for the
Degree of Doctor of Philosophy.

Civil Engineering Dept
University of Adelaide

March 1981

CONTENTS

		Page
ABSTRACT		iv
DECLARATION		vi
ACKNOWLEDGEMENTS		vii
NOTATION		viii
LIST OF FIGURES		x
LIST OF TABLES		xiii
CHAPTER 1	INTRODUCTION	1
1.1	Background	1
1.2	Aims and Scope of Thesis	4
1.3	Layout of Thesis	7
CHAPTER 2	LITERATURE SURVEY	11
CHAPTER 3	THEORY	20
3.1	Governing Equations and Boundary Conditions	20
3.2	Equation Formulation in Terms of Finite Elements	33
3.3	Assembly of Global Simultaneous Finite Element Equation System	44
3.4	Solution of Global Simultaneous Equation System	54
CHAPTER 4	FINITE ELEMENT AND COMPUTER PROGRAM DETAILS	69
4.1	Isoparametric Finite Elements	69
4.2	Numerical Integration Details	94
4.3	Some Important Computer Programming Aspects	99
CHAPTER 5	RESULTS OF ANALYSES AND COMPARISONS IN TWO DIMENSIONS	106
5.1	Computational Test Program Details	106
5.2	Entrance Flow Problem Details	112
5.3	Cavity Flow Problem Details	131
5.4	Results of Formulation Comparison	142
5.5	Results of Element Comparison	178
5.6	Presentation of Entrance and Cavity Flow Problem Results and Comparison with Other Published Solutions	214
CHAPTER 6	ANALYSES IN THREE DIMENSIONS	265
6.1	Extension of Two-dimensional Comparisons Results to Three Dimensions	265
6.2	Details of Three-dimensional Flow Problems	270
6.3	Results of Three-dimensional Analyses	278
CHAPTER 7	SUMMARY, CONCLUSIONS AND RECOMMENDATIONS	301
APPENDIX A	DERIVATION OF MOMENTUM AND MASS CONSERVATION EQUATIONS AND STRESS-STRAIN RATE RELATIONSHIP	305

Page

APPENDIX B	THREE-DIMENSIONAL COMPUTER PROGRAM DETAILS	317
APPENDIX C	ELEMENT STIFFNESS, NUMERICAL VALUES FOR 1x1 ELEMENT	347
APPENDIX D	SOLUTION OF POISEUILLE FLOW USING EIGHT AND NINE NODED ELEMENTS	350
BIBLIOGRAPHY		359

ABSTRACT

The fundamental aim of the investigation described in this dissertation was to clarify two aspects associated with the use of primitive variables in the finite element solution of the two-dimensional steady and incompressible Navier-Stokes equations and then to use this knowledge in an attempt to solve the more general three-dimensional equations.

By deriving the Navier-Stokes equations from first principles it is shown that terms containing the quantity $\frac{\partial v_i}{\partial x_i}$ appear at several stages in the derivation. Traditionally some of these have always been eliminated by making use of the incompressible Continuity equation $\frac{\partial v_i}{\partial x_i} = 0$. Others however, have sometimes been eliminated and sometimes retained, it being argued that because the solution method adopted is approximate, the quantity $\frac{\partial v_i}{\partial x_i}$ will not be identically equal to zero everywhere, and hence the Continuity equation should not be used to eliminate the $\frac{\partial v_i}{\partial x_i}$ terms. In order to determine the effects of the inclusion of these terms several versions of the Navier-Stokes equations are set up and the solutions of two two-dimensional viscous flow problems are used to show that although the different formulations give rise to essentially the same results, they do not all have the same ability to converge, nor do they all produce the same quality solutions as Reynolds number is increased.

When primitive variables are used it has been shown that the order of polynomial approximation for the pressure should be one less than that for the velocity. Two finite elements that have commonly been used with this type of mixed interpolation are the Serendipity and the Lagrangian isoparametric elements. In order to determine which is the optimal, a computer program for each of these elements in two dimensions was set up and developed. The solutions of the same two viscous flow

problems mentioned earlier were then used to show that although both elements give rise to almost identical results, the Lagrangian requires considerably more computation time and space to produce the same solution and is therefore the lesser efficient.

By extending the results of the above investigations to three dimensions, a third computer program was developed and used to solve several three-dimensional viscous flow problems. Although a comprehensive study of these problems was not carried out, and although some questions still remain unanswered, it has been shown that the primitive variables finite element method can be used successfully to solve the steady and incompressible three-dimensional Navier-Stokes equations.

DECLARATION

This thesis contains no material which has been accepted for the award of any degree or diploma in any University and, to the best of the candidate's knowledge and belief, contains no material previously published or written by another person, except where due reference is made in the text.

ACKNOWLEDGEMENTS

The author wishes to express his sincere gratitude to his advisers Dr M.F. Yeo and Dr S.G. Hutton for their invaluable advice and guidance during the course of this work. Thanks are also due to Dr G. Sved and Professor R.F. Warner for their unfailing enthusiasm and assistance during the preparation of this thesis.

In addition, the author thanks Mr G. Joss and Mr C.R. Jones and the staff of the Adelaide University Computing Centre for their continuous assistance and willingness to help in all matters of computing.

The patience and gentle encouragement of my wife Margot, made this work possible.

The efforts of Christine Gradolf in typing this thesis are gratefully appreciated and the financial support of the Commonwealth of Australia Department of Education in the form of a Postgraduate Research Award is gratefully acknowledged.

NOTATION

A_i	area of element i
a_j	position of jth Gauss point
$[C(\underset{\sim}{x})]$	non-linear convective stiffness matrix
C_1, C_2, C_3	constants, equal to one or zero depending on formulation
F_i	body force per unit mass in i direction
F_{ij}	equivalent nodal force at node j in element i
$[J]$	Jocobian transformation matrix
det J	determinant of Jacobian matrix
$[K]$	linear diffusive stiffness matrix
K'	number of velocity nodes per element
K"	number of pressure nodes per element
L_D	development length for entrance flows
$\bar{L}$	characteristic length used for non-dimensionalization
N'_{ij}	velocity shape function for node j of element i
N''_{ij}	pressure shape function for node j of element i
N_e	number of elements in finite element meshes
n	number of Gauss points per coordinate direction
n_i	ith component of vector normal to element boundary
p, p^*, p^*_{ij}	pressure, exact, approximate, nodal
q	excess pressure drop
$[R_i]$	matrix of finite element equation system
R_{ij}	residual functions
Re	Reynolds number
$[S_i]$	matrix of Jacobian finite element equation system
S_i	surface of element i
s, s_1, s_2	tangential surface or edge shear stress
T^o_i	specified boundary stress component in ith direction
u, u^*, u^*_{ij}	x component of velocity, exact, approximate, nodal

$\bar{V}$	characteristic velocity used for non-dimensionalization
V_i	volume of element i
v, v^*, v^*_{ij}	y component of velocity, exact, approximate, nodal
v^o_i	specified velocity component in ith direction
w_j	weight for jth Gauss point
w, w^*, w^*_{ij}	z component of velocity, exact, approximate and nodal
x, y, z	global coordinates
(x_{ij}, y_{ij}, z_{ij})	global coordinates of node j in element i
ρ	fluid density
μ	coefficient of fluid viscosity
ω	vorticity
ψ	stream function
δ_{ij}	Kroneker delta
λ	coefficient of bulk viscosity
ξ, η, ζ	local coordinates
$(\xi_{ij}, \eta_{ij}, \zeta_{ij})$	local coordinates of node j in element i
$\sigma_{ij}, \sigma^*_{ij}$	stress tensor, exact, approximate

LIST OF FIGURES

Figure		Page
3.1	Typical Nodal Positionings	45
4.1	Typical Triangular and Quadrilateral Two-dimensional Finite Elements	72
4.2	Typical Eight Noded Serendipity and Nine Noded Lagrangian Elements	74
4.3	Parent Eight Noded Serendipity and Nine Noded Lagrangian Elements	76
4.4	Typical Boundary Element with Applied Normal and Tangential Shear Stress Components	80
4.5	Typical Twenty Noded Serendipity and Twenty-seven Noded Lagrangian Elements	84
4.6	Parent Twenty Noded Serendipity and Twenty-seven Noded Lagrangian Elements	85
4.7	Typical Boundary Element with Applied Normal and Tangential Shear Stress Components	89
4.8	Positive Directions of Normal and Shear Stresses in Three Dimensions	90
4.9	Positions of Gauss Points in a Two-dimensional Element for n=3	97
4.10	Example of Loss of Information Resulting from Computer Round-off	102
5.1	Entrance Flow Problem Details	113
5.2	Non-dimensionalized Entrance Flow Problem Details	115
5.3	Mesh ENFLM1 (not to scale)	118
5.4	Mesh ENFLM2 (not to scale)	120
5.5	Entrance Flow Boundary Conditions	123
5.6	(a) Specified Entrance Velocity Profile, and (b) Typical Downstream Velocity Profile	126
5.7	Entrance Edge Wall Corner Velocity Specification	127
5.8	Cascade of Plates	130
5.9	Cavity Flow Problem Details	132
5.10	Non-dimensionalized Cavity Flow Problem Details	134

Figure		Page
5.11	Mesh CAVFLM1 (not to scale)	136
5.12	Mesh CAVFLM2 (not to scale)	137
5.13	Cavity Flow Boundary Conditions	139
5.14	(a) Specified Moving Wall Velocity Profile, and (b) Typical Moving Wall Velocity Profile Specified by Previous Workers	141
5.15	Formulation Comparison, Entrance Flow, Variation of u on y=0.5 at Various Reynolds Numbers	151
5.16	Variation of u on y=0.1	156
5.17	Variation of p on y=0.5	161
5.18	Formulation Comparison, Cavity Flow, Variation of u on x=0.5 at Various Reynolds Numbers	166
5.19	Variation of p on x=0.5	171
5.20	Element Comparison, Entrance Flow, Variation of u on y=0.5 at Various Reynolds Numbers	186
5.21	Variation of u on y=0.1	191
5.22	Variation of p on y=0.5	196
5.23	Element Comparison, Cavity Flow, Variation of u on x=0.5 at Various Reynolds Numbers	201
5.24	Variation of p on x=0.5	206
5.25	Variation of u Along y=0.5 for the Entrance Flow Problem at Various Reynolds Numbers	217
5.26	Variation of u Along y=0.1 for the Entrance Flow Problem at Various Reynolds Numbers	225
5.27	Transverse Velocity Profiles at Various Reynolds Numbers	231
5.28	Variation of p Along y=0.1 and y=0.5 for the Entrance Flow Problem at Various Reynolds Numbers	241
5.29	Variation of u Along x=0.5 for the Cavity Flow Problem at Various Reynolds Numbers	246
5.30	Velocity Vector Fields for Various Reynolds Numbers	252
5.31	Pressure Contour Plots for Various Reynolds Numbers	259
6.1	Typical Three-dimensional Finite Element Mesh	269
6.2	Details of Meshes M1, M2, M3, M4 and M5	273

Figure		Page
6.3	Boundary Conditions for the (a) Poiseuille Flow, (b) Square Duct Flow, and (c) Developing Square Duct Flow	275
6.4	(a) Typical Layout of Matrix of Coefficients of Finite Element Equations, and (b) Its Reduced Form	280
6.5	Exact Numerical Values of w(x,y,z) Over Quarter Duct Cross-Section	288
6.6	Exact and Calculated Values of Axial Component of Velocity for Fully Developed Duct Flow	291
6.7	Variation of w Along Centreline for the Developing Flow in a Square Duct	297
6.8	Variation of p Along Centreline	299
A1	Position of a Mass of Viscous Fluid at Times t and $t+\delta t$	306
A2	Typical Element of Fluid, $\delta x\,\delta y\,\delta z$	306
A3	Positive Directions of Nine Three-dimensional Stress Components	310
A4	Flow Between Two Parallel Plates Moving Relative to Each Other	315
D1	(a) Actual Three-dimensional Poiseuille Flow, and (b) Two-dimensional Representation	351
D2	Details of Meshes 1, 2 and 3 for Poiseuille Flow	352
D3	Details of Meshes 2A, 2B and 2C	354
D4	Typical Elements, (a) General Quadrilateral, (b) Trapezoidal, and (c) Rectangular	356

LIST OF TABLES

Table		Page
4.1	Positions of Gauss Points and Associated Weights for n=3	98
5.1	Computer Runs Carried Out in Test Series 1	110
5.2	Computer Runs Carried Out in Test Series 2	112
5.3	Details of Meshes and Elements Used to Solve the Entrance Flow Problem	122
5.4	Details of Meshes and Elements Used to Solve the Cavity Flow Problem	138
5.5	Number of Iterations and Execution Times for Runs in Test Series 1	146
5.6	Number of Iterations and Execution Times for Runs in Test Series 2	181
5.7	Average Execution Times and Computer Storage Required by Runs in Test Series 2	182
5.8	Average Execution Time per Iteration per Node	185
5.9	Development Lengths at Re = 1 to 2000 and at the Large Reynolds Number Limit	223
5.10	Location and Magnitude of Local Maxima for Various Reynolds Numbers	237
5.11	Excess Pressure Drop for Various Reynolds Numbers	244
5.12	Coordinates of Vortex Centre at Various Reynolds Numbers	258
6.1	Details of Poiseuille Flow Test Runs in Three Dimensions	285
D1	Solution to Poiseuille Flow Obtained Using Mesh 2C and Eight and Nine Noded Elements	355

CHAPTER 1

INTRODUCTION

1.1 Background

1.2 Aims and Scope of Thesis

1.3 Layout of Thesis

1. INTRODUCTION

In this introductory chapter the use of approximate numerical solution procedures for solving problems in fluid mechanics is discussed briefly. More specifically, the class of flow problem that will be treated in this study, and the approach adopted to analyse it are defined. Finally, the aims and scope of this thesis are set out and its overall layout briefly summarized.

1.1 Background

The equations that are encountered in fluid mechanics are, in general, of such a nature that no closed-form solution is available. In order to obtain answers to such problems it is therefore necessary to resort to approximate solution techniques. Of the variety of approximate methods introduced in the last several decades to solve flow problems in general, the finite difference technique has, until recently, been the most commonly used. Since 1965 however, the finite element method, originally developed for application in the analysis of complex structural systems, has gradually replaced the finite difference method and has been successfully applied to most areas of fluid mechanics. Its success has been, in part, due to its ability to accommodate complex boundary geometries, and to the fact that it is not restricted to establishing the solution only at points on a regularly spaced grid. It also allows greater flexibility in the choice of local approximation. The development of the method is well documented and Zienkiewicz (37) provides a comprehensive list of references in his review of the method.

The finite element method as it applies to the solution of potential flow fields was first described by Zienkiewicz and Cheung (38) in 1965. This marked the beginning of the use of finite elements in the field of fluid mechanics. Since then the method has been vigorously

exploited, with research and application expanding at an exponential rate. As a result, three major conferences on the use of finite element methods in fluid mechanics have been held in the six years since 1974. Several surveys with the same theme, such as that published by Norrie and de Vries (22) in 1976, have also been made during this time.

The main reason for this sudden increase in interest in computational fluid dynamics is twofold. Firstly improvements in the numerical models, such as the introduction of the finite element method, have now made it possible to solve complex flow problems for which no closed-form solution exists and which are either costly or difficult to determine experimentally. Secondly, the introduction of improved computer hardware, more efficient both in terms of calculating and access speeds and storage capabilities, has made the use of numerical simulation possible and more attractive to both the engineer, who is concerned with cost-effective derivation of design data, and the scientist or researcher who requires a deeper understanding of fluid processes through detailed analysis.

The range of fluid mechanics problems to which the finite element method has been applied include potential flow, viscous flow, subsonic, supersonic and transonic compressible flow, free surface and open channel flow and porous media flow. The equations governing each of these types of flows can be derived in terms of various sets of dependent variables of which the following are the most frequently encountered: the primitive variables such as velocity, pressure, temperature and density, the velocity potential alone or with other variables, and the stream function alone or with other variables such as vorticity. Depending on the type of problem to be solved, one approach may have advantages over another, but in general the choice of approach is usually based on the equation system that the researcher prefers to handle and his familiarity with the techniques available for solving it.

The primitive variables approach has often been preferred because not only are the boundary conditions more easily determined and applied, but also because the solution obtained is in an immediately usable form. When the velocity potential, the stream function or the stream function and vorticity approaches are adopted, additional manipulation of the finite element results is required to obtain the fluid velocity and pressure fields, the quantities most useful to the analyst. The use of primitive variables also leads to the lowest order governing differential equations and this approach is the only one that is directly applicable to both two- and three-dimensional flows.

Although recently some consideration has been given to the solution of some three-dimensional problems, in the main the finite element method has been restricted to solving two-dimensional or plane flows. Probably there are two reasons for this. Firstly, most of the research effort to date has been directed towards investigating and understanding the numerous aspects involved in the application of the finite element method to solving a basic viscous flow problem, and this is done most easily in two dimensions. Secondly and perhaps more likely, the amount of computing time and computer size required to perform even a moderately sized finite element analysis of a three-dimensional flow have, in the past, prevented many researchers from proceeding with such an analysis simply because these facilities were not available. However, with the development of computer technology progressing at such a high rate, coupled with the knowledge we now have from comprehensive two-dimensional studies, this situation is rapidly changing and research on a large scale using the finite element method to solve general three-dimensional flow problems will soon be possible.

The common types of finite element methods that have been used in the past include the classical variational, restricted variational, Galerkin, least squares and the global balance forms, with the first

three being the most widely used. However, since it is often difficult or even impossible to construct the necessary functionals, the two variational methods are limited in their applicability, and although they are still widely accepted the Galerkin method is becoming increasingly used, particularly for non-linear problems.

In this study the Galerkin finite element method is used exclusively to analyse both two- and three-dimensional steady, viscous flows with the equations describing them expressed in terms of the primitive variables, velocity and pressure.

1.2 Aims and Scope of Thesis

The purpose of this thesis is threefold; firstly to determine the optimal finite element formulation of four versions of the two-dimensional Navier-Stokes equations, secondly to determine the more efficient of two two-dimensional quadrilateral finite elements, and thirdly to determine whether the results of the above two investigations can be extended to three dimensions and be used successfully to obtain the finite element solution of a typical three-dimensional viscous flow. As mentioned earlier, the actual technique that was adopted for this study is the Galerkin finite element method, and although this procedure has already been successfully applied to the analysis of two-dimensional viscous flows, to the author's knowledge, it has never been used to solve the more general three-dimensional problem. In this study therefore, the Galerkin finite element method is used in conjunction with the primitive variables approach to solve the steady two- and three-dimensional Navier-Stokes equations describing the fully contained flow of a viscous and incompressible Newtonian fluid.

In their derivation from first principles, it is shown that the Navier-Stokes equations contain three terms, each of which contains

the quantity $\frac{\partial v_i}{\partial x_i}$. Some of these terms have been traditionally always eliminated by using the incompressible Continuity equation $\frac{\partial v_i}{\partial x_i} = 0$, while others have sometimes been retained and sometimes eliminated. In order to determine the effects of the inclusion of each of these terms, four versions of the Navier-Stokes equations are set up. These range from the first in which all such terms are eliminated to the fourth in which all terms are retained and include the two which have traditionally been most favoured by previous researchers. As far as the author can ascertain, no comparison has previously been made to determine which of these versions leads to the best numerical solution, or which is the most efficient in terms of computational effort. Therefore, in order to ensure that the optimal version is used in the subsequent two- and three-dimensional analyses, a formulation comparison is made using the solutions of two independent two-dimensional viscous flow problems. The results of this formulation comparison are presented and the optimal version of the Navier-Stokes equations used in all subsequent work.

As a result of investigations carried out by previous researchers, which show that when primitive variables are used, the order of interpolation for the pressure should be one less than that for the velocity, a quadratic velocity and linear pressure mixed interpolation is used. Two quadrilateral finite elements capable of allowing the velocity and pressure to be approximated in this manner are the Serendipity and the Lagrangian isoparametric elements. In two dimensions these elements have eight and nine nodes respectively, while in three dimensions they have twenty and twenty-seven. Suggestions have been made by some previous researchers that of these two elements, the Lagrangian is the superior. In this thesis these suggestions are investigated by comparing the solutions of two independent two-dimensional viscous flow problems obtained using the eight and the nine noded elements. Particular attention is paid to their respective abilities to represent accurately the

pressure fields. The results of this comparison, together with the velocity and pressure fields obtained for both the two-dimensional flows considered, are presented, and the three-dimensional element corresponding to the more efficient of the two two-dimensional elements is used in the final three-dimensional analyses.

The solutions required by the above two investigations were obtained by using two computer programs, one incorporating the eight noded and the other the nine noded element, and both developed during the course of this study. Also, in order to keep the total computing time to within a reasonable limit and because solutions evaluated by other researchers for these problems are most readily available, the same two flow problems are considered in both comparisons.

The finite element equations that are presented are formulated in dimensionless form for a general three-dimensional viscous flow and a general finite element. The two-dimensional finite element equations can be easily obtained by disregarding the third momentum equation and eliminating all terms in the remaining three equations that are associated with the third coordinate direction.

Having determined, in two dimensions, the optimal formulation and the more efficient finite element, these results are used in three dimensions in an attempt to solve a typical three-dimensional viscous flow. In order to do this, a third computer program incorporating the Frontal solution procedure was written and developed. The results of several three-dimensional analyses together with a discussion of each of the two major problems that were encountered in carrying them out are presented. The second problem was eventually overcome but the first which involved the necessity to specify additional pressure boundary conditions before a solution can be obtained, requires further investigation. Nevertheless, it is shown that the primitive variables finite element method can be used successfully to solve the steady and incompressible three-dimensional Navier-Stokes equations. All three-

dimensional solutions that are presented in this thesis were obtained by supplying, where required, the additional pressure values. Full details of all three-dimensional flows analysed have therefore been included with special care being taken over the prescribed boundary conditions.

1.3 Layout of Thesis

Essentially, this thesis consists of three basic sections comprising viscous flow and finite element theory, numerical solution details and the two- and three-dimensional results. At the start of each chapter, a short introductory discussion defines its purpose and contents. The specific usage and meaning of all symbols and variables encountered in all chapters are defined in the section entitled Notation which is found at the start of this thesis.

Chapter 2 is devoted entirely to giving a detailed account of work carried out previously and which directly affects many of the decisions made during this study. It is not intended, however, that this chapter be a complete survey of all work done in the field of computational fluid dynamics, since the amount of published material is already very large. Only selected works have therefore been included. Where applicable, after the relevant work of other researchers has been presented, the approach or technique adopted for this study is set out.

The Navier-Stokes equations describing a general three-dimensional viscous flow are discussed in the first section of Chapter 3 and are derived from first principles in Appendix A. Tensor notation, in which the summation convention holds for subscripted variables with repeated lower case indices, is used only in these two sections. Also in the first section of Chapter 3, the boundary conditions that are most likely to be encountered in the problems to be solved are reviewed and these,

together with the governing equations are non-dimensionalized and expressed in terms of a single dimensionless parameter, the Reynolds number. Finally, the four versions of the Navier-Stokes equations that arise because of the inclusion of terms containing the quantity $\frac{\partial v_i}{\partial x_i}$ are set out and the reasons for these inclusions explained.

The finite element formulation of the governing equations is set out and discussed in the second section of Chapter 3. The finite element equations that are constructed are based on a general finite element which is capable of allowing the pressure to be interpolated differently if necessary, from the velocity. The meaning of the surface integrals that result as a consequence of the use of the Gauss theorem to reduce the order of differentiation, is also explained. The remaining two parts of Chapter 3 deal firstly with the theory of the assembling process, the technique used to combine the equations of individual finite elements into one overall global equation system and secondly, with the multi-dimensional Newton-Raphson iterative solution technique, the method adopted for solving this system. The general j-kth component of the non-linear element "stiffness" matrix corresponding to the four versions of the Navier-Stokes equations is set out in full in the last section of Chapter 3.

In Chapter 4, the choice of interpolation for the velocity and pressure variables is explained and both the two- and three-dimensional elements that have the ability to represent the required variations are presented in detail. Since the elements chosen are isoparametric and therefore considerably more complicated than the simpler ordinary quadrilateral and hexahedral elements, a detailed description of the required adjustments to the area and line integrals for two dimensions and the volume and surface integrals for three dimensions is included. The evaluation of these integrals is done numerically and is described in the second section of Chapter 4. The remainder of Chapter 4 is

devoted to discussing the problems encountered in setting up and developing the three computer programs written to analyse the selected two- and three-dimensional viscous flows. A listing of the three-dimensional computer program is given in Appendix B.

The results of the two comparisons, namely the comparison to determine which version of the Navier-Stokes equations leads to the most efficient finite element formulation and the best solutions, and the comparison made to determine which of the two elements, the Serendipity or the Lagrangian, has the better characteristics, are presented in Chapter 5. The two two-dimensional viscous flow problems that are used in both comparisons are the flow in the entrance region between two semi-infinite parallel plates and the recirculating flow in a square cavity. Care is taken to ensure that complete details of all boundary conditions, mesh configurations and other relevant aspects for each problem are clearly presented so that all problems are fully defined and readily reproducable. The optimal element type and the most efficient version of the Navier-Stokes equations that are selected for use in the three-dimensional analyses, and the reasons for choosing them are presented in the discussion at the conclusion of each of the relevant sections of Chapter 5.

Finally, in Chapter 6, the finite element method and the results of the two-dimensional comparisons are used in an attempt to find the solution to some typical three-dimensional viscous flows. In all, three flow problems are considered. The first is the fully developed flow between two infinite parallel plates, which was previously solved in two dimensions. A second, more complex problem, namely the fully developed flow in a duct of arbitrary cross-section, is then attempted. Since it is not possible to set up one general finite element mesh for a duct with an arbitrary cross-section, a typical square duct is analysed. In both cases it is shown that additional pressure data is required

on the outer boundary of the flow before a correct solution is obtained. A detailed account of the investigation carried out in order to obtain a fuller understanding of the nature of this difficulty is given in the final section of Chapter 6. The analysis of a third three-dimensional viscous flow problem, namely the developing flow in the entrance region of a square duct, confirmed the findings of this investigation. The results of this third analysis are also presented in the final section of Chapter 6. The other two sections of this chapter are used to describe in detail, firstly the reasons for the choice of formulation and element type adopted for the three-dimensional analyses, and secondly the meshes and boundary conditions used to analyse the particular flows.

A summary of all conclusions arrived at during the course of this study, together with some concluding remarks concerning this thesis and the direction of probable future research in this field, are made in the final chapter.

In order to remove excessive detail from the main text, use is made of four Appendices. The details of Appendix A are well known and are included for completeness. A listing of the three-dimensional computer program is given in Appendix B, together with data input details, user instructions and a basic flow chart. Appendix C contains the numerical values of the linear portion of the "stiffness" matrix for a two-dimensional element of unit width and depth for formulation B and for each of the eight and nine noded element types. It has been included to enable future workers in this field to compare their formulations with those in this study on a numerical level. Finally, a comparison of the results of two analyses of the Poiseuille flow using the eight and the nine noded elements is made in Appendix D.

CHAPTER 2

LITERATURE SURVEY

2. LITERATURE SURVEY

In this section the research into the application of the various finite element methods to the solution of steady, incompressible and viscous flow problems is reviewed with particular emphasis placed on the more recent developments. To facilitate classification of the approaches used by the researchers mentioned in this survey, the three commonly used forms of the two-dimensional Navier-Stokes equations are discussed first. The solution techniques adopted for solving the resulting equations are then briefly described. A more detailed discussion of all relevant material follows in the body of the thesis later.

As was mentioned previously, the two-dimensional equations governing the flow of an incompressible viscous fluid can be expressed in terms of three basic sets of dependent variables. In terms of the primitive variables, the two velocity components u and v and the pressure p, these equations, more commonly known as the Navier-Stokes equations, can be written as

$$u\frac{\partial u}{\partial x} + v\frac{\partial u}{\partial y} = \frac{1}{Re}\left(\frac{\partial^2 u}{\partial x^2} + \frac{\partial^2 u}{\partial y^2}\right) - \frac{\partial p}{\partial x} \qquad 2.1.1$$

$$u\frac{\partial v}{\partial x} + v\frac{\partial v}{\partial y} = \frac{1}{Re}\left(\frac{\partial^2 v}{\partial x^2} + \frac{\partial^2 v}{\partial y^2}\right) - \frac{\partial p}{\partial y} \qquad 2.1.2$$

and

$$\frac{\partial u}{\partial x} + \frac{\partial v}{\partial y} = 0 \qquad 2.1.3$$

where non-dimensionalization has been carried out with respect to a reference length $\bar{L}$ and a reference velocity $\bar{v}$ and where Re is the dimensionless parameter, the Reynolds number, which is defined as

$$Re = \frac{\rho \bar{v} \bar{L}}{\mu} \qquad 2.2$$

ρ and μ are the fluid density and viscosity respectively. Introducing the stream function ψ and the vorticity ω which are defined as

$$\frac{\partial \psi}{\partial y} = u, \qquad \frac{\partial \psi}{\partial x} = -v \tag{2.3.1}$$

and

$$\omega = \frac{\partial v}{\partial x} - \frac{\partial u}{\partial y} \tag{2.3.2}$$

enables the equations to be rewritten as

$$\frac{\partial \psi}{\partial y}\frac{\partial \omega}{\partial x} - \frac{\partial \psi}{\partial x}\frac{\partial \omega}{\partial y} = \frac{1}{Re}\left(\frac{\partial^2 \omega}{\partial x^2} + \frac{\partial^2 \omega}{\partial y^2}\right) \tag{2.4.1}$$

and

$$\frac{\partial^2 \psi}{\partial x^2} + \frac{\partial^2 \psi}{\partial y^2} = \omega \tag{2.4.2}$$

where equation 2.4.2 takes the place of the Continuity equation which is satisfied identically. If only the stream function is introduced the governing equations for a viscous flow can be reduced to the single fourth order differential equation

$$\frac{\partial \psi}{\partial y} \cdot \nabla^2\left(\frac{\partial \psi}{\partial x}\right) - \frac{\partial \psi}{\partial x} \cdot \nabla^2\left(\frac{\partial \psi}{\partial y}\right) = \frac{1}{Re}\nabla^2(\nabla^2 \psi) \tag{2.5}$$

where

$$\nabla^2 = \frac{\partial^2}{\partial x^2} + \frac{\partial^2}{\partial y^2}$$

To date all theoretical and numerical modelling of incompressible viscous flows have used one or other of these three forms of the Navier-Stokes equations.

It will be noted that because of the inclusion of the inertia terms the equations in each case are non-linear. It will also be noted that as the Reynolds number is increased the dominance of these non-linear terms also increases. It is not surprising therefore that because the difficulty of solving a problem increases with the degree of non-linearity of its governing equations, most of the finite element solutions presented to date are for low to moderate Reynolds numbers. This applies equally to all three approaches described above. Also,

although some consideration has been given to the finite element solution of three-dimensional problems, in the main the finite element formulations have been for two-dimensional flows.

Finite element formulations based on each of the three forms of the Navier-Stokes equations have been devised during the past ten years. Within the general context of the primitive variables approach, several schemes have been developed. As noted by Olson (24) and confirmed by this review, finite element methods using this approach fall into three basic groups

(a) Integrated formulation type

(b) Segregated formulation type

and (c) Solenoidal velocity formulation type.

The integrated formulation type finite element methods in which the velocity component and pressure fields are solved for simultaneously, use either a variational or a weighted residual approach. The former has the advantage of yielding a better understanding of the significance of the equations but its use in some cases is limited by the non-existence of the required equivalent variational functional. To date most of the finite element work in viscous fluid dynamics has been carried out using the primitive variables and integrated formulations, with the Galerkin weighted residual approach being the most favoured.

In his book, Zienkiewicz (36) presents the Galerkin finite element formulation of the Stokes and Continuity equations which are applicable only to creeping flows. The resulting matrix of equation coefficients otherwise referred to as the element "stiffness" matrix, was shown to be unsymmetrical. This was in contrast with element stiffness matrices resulting from similar formulations of structural problems, which are always symmetrical. However, by a slight change in the theory presented by Zienkiewicz, Yamada et al. (35) were able to show that element stiffness symmetry could be retained. They also noted that, at least for

Stokes flows the Galerkin approach produced the same formulation of the primitive equations as did the classical variational method. Because the equations governing creeping flows are linear, the finite element solutions for these problems are easily obtained and a large number are readily available in the literature. However, because creeping flows represent only a very restricted class of viscous flow problems, in order to solve a more general viscous flow, the more general Navier-Stokes equations must be considered.

The next stage in the development of the finite element method as it applies to viscous fluid dynamics was therefore to solve the full non-linear Navier-Stokes equations. In 1973, Taylor and Hood (30), following the same procedure as Zienkiewicz, set up a Galerkin finite element formulation for the complete two-dimensional Navier-Stokes equations in terms of the primitive variables. They showed that solutions could be obtained for the flow in a square cavity and around a cylinder with Reynolds numbers as high as 600 and 100 respectively. In a subsequent paper, Hood and Taylor (16) modified their previous theory to include mixed interpolation and showed that when a primitive variables formulation is used the pressure field approximation must be a polynomial of one degree lower than the approximation of the velocity component fields. This they argued, ensures that consistently accurate results are obtained simultaneously for both velocity and pressure, and that rigid body modes are suppressed. They noted that poor accuracy had been obtained by previous researchers who had disregarded or had not accounted for this fact in their formulations. This was confirmed by the subsequent studies of Kawahara et al. (19) and Tuann and Olson (32), both of whom used a Galerkin integrated formulation and the same mixed interpolation as Hood and Taylor, namely a quadratic velocity and a linear pressure approximation.

Many other studies have been carried out since these. Some of the typical two-dimensional viscous flow problems that have been solved using the Galerkin integrated formulation in terms of the primitive variables are the Poiseuille and Couette flows, the flow in a slider bearing, the flow in a square cavity, the flow past a circular cylinder, the flow over a backward facing step, the developing flow in the entrance region between two parallel plates and the flow between two converging plates. In almost all cases the Newton-Raphson iterative method was used to obtain a solution to the resulting non-linear discretized equation system which can be expressed generally as

$$\{C(\underset{\sim}{x}) + K\}\,\underset{\sim}{x} = \underset{\sim}{f} \qquad 2.6$$

where C and K, are respectively the non-linear convective and the linear diffusive stiffness matrices, $\underset{\sim}{f}$ the load vector resulting from surface stresses and specified boundary quantities, and $\underset{\sim}{x}$ the vector of unknown nodal velocities and pressures. In addition to making the problem non-linear, matrix C is also unsymmetric. Three other methods that have been used in the past to solve equation system 2.6 include two which make symmetric the coefficient matrix by placing either all or the unsymmetric part of $C(\underset{\sim}{x}).\underset{\sim}{x}$ evaluated for the previous iteration step on the right hand side as part of the load vector for the next iteration and a third which, like the Newton-Raphson method, retains the unsymmetric coefficient matrix and uses successive substitution to linearize it.

Gartling et al. (13) recently completed a detailed comparison of these four methods and found the following. Firstly the methods that solved the full unsymmetric equation system were far superior and more generally applicable than their symmetric counterparts, and secondly, of the unsymmetric algorithms, the Newton-Raphson procedure was clearly the most rapidly convergent and therefore the most efficient. From these studies therefore, it appears essential that, at least for the

primitive variables approach the non-linear unsymmetric effects be retained in the coefficient matrix, and if maximum efficiency is desired the Newton-Raphson procedure be adopted.

The second type of primitive variables finite element method involves a segregated formulation in which the velocity and pressure are sufficiently uncoupled to allow their alternate solution in an iterative sequence. This approach was pioneered by Olson and Tuann (24, 25, 32), and although it has been used extensively in finite differences, it has received relatively little attention from finite element workers. The procedure involves the derivation of two restricted functionals, the first of which allows the pressure to be calculated if the velocity is known and the second of which allows the reverse. The Newton-Raphson method or any of its equivalents are not needed in this procedure.

The main advantage of this method for finite elements is that the pressure interpolation can be of any order and independent of the velocity interpolation. This is important because the pressure accuracy is often the limiting factor in the overall solution accuracy.

Although some work has been done using this method, many questions still remain unanswered. For example, how well is continuity satisfied (since it is not built in as it is in the integrated formulation), and what are the convergence characteristics for this approach at higher Reynolds numbers?

The third alternative for the primitive variables finite element method involves the use of solenoidal velocity interpolations; that is, assumed velocity fields which satisfy the Continuity equation exactly. By using such interpolations, the assumed velocity field has zero divergence and hence the incompressibility constraint is satisfied explicitly. Therefore the Continuity equation is not required and by eliminating the pressure from the remainder of the equation system only

the velocity components are retained as the dependent variables. Although the procedure appears simple, the construction of the solenoidal field or null divergence finite element is very difficult. Further, it appears almost impossible to have both incompressibility and compatibility of velocity satisfied simultaneously.

Fortin (12) was the first to make a significant contribution to this area and was able to produce an equivalent variational formulation of the primitive system with incompressibility satisfied explicitly. Hutton (17) used the same theory as Fortin to analyse regions of flow in the vicinity of singular points on wall boundaries. However no numerical results were presented in either case and, as with the segregated formulation, it appears that much more research needs to be done, particularly into the characteristics and the effects of the use of the null-divergence but non-conforming elements.

Finite element formulations based on the derived variables, stream function ψ and vorticity ω have arisen as a result of the desire to avoid the difficulties inherent with the pressure variable. The main disadvantage of this approach is that the vorticity boundary condition is not known a priori, and therefore the stream function and the vorticity cannot both be solved simultaneously. Nevertheless the finite element work in this area is still quite extensive, with the analysis of unsteady flows taking precedence over steady. Because ψ and ω cannot be solved for simultaneously, the Newton-Raphson method is not practical. The solution procedure that is usually adopted is a calculation scheme that alternates between ψ and ω. That is, ψ is assumed known when equation 2.4.1 is to be solved and vice versa for 2.4.2.

Both the Galerkin and restricted variational approaches have commonly been used with the stream function and vorticity equations. Baker (2) used the former to predict the development in time of imbedded regions of recirculating flow, while Cheng (8) and Tong (31) used the

latter in an attempt to solve the flow in a channel with a contraction and the flow around a cylinder (two-dimensional) and a sphere (axi-symmetric). In all cases good results were claimed even with the use of the simplest triangular elements. However, as was reported by Olson (24), although considerable progress has been made in this area, there still remain many questions unanswered, particularly regarding the stability and the accuracy of the adopted solution schemes at higher Reynolds numbers.

The only other approach that has been used in the finite element modelling of the two-dimensional Navier-Stokes equations is based on the fourth order, biharmonic type differential equation 2.5, expressed in terms of the stream function alone. The main work in this area has been done by Olson (23) who has used this approach to analyse the flow around a cylinder and in a constricted cylindrical tube with Reynolds numbers up to 100. Few other researchers have adopted this approach, perhaps because of their lack of familiarity with the higher order elements it requires. Olson used a restricted variational principle together with an 18 degree of freedom triangular element which has the stream function and all of its first and second derivatives as nodal variables. He found that this produced good stability in the two-dimensional analyses but behaved relatively poorly in the axisymmetric case.

Olson and Tuann (32, 25) have compared the primitive variables and stream function approaches using variational methods and concluded by saying that the stream function method is the least difficult and perhaps the more accurate as applied to their particular test flows. Taylor and Hood (30) compared the primitive variables and the stream function-vorticity approaches using Galerkin and concluded that the primitive variables method was the more efficient and the one most easily extended to three dimensions. From this review therefore it becomes

evident that for the analysis of two-dimensional viscous flows, no one approach or formulation is considerably more advantageous than another. Each has its advantages and its disadvantages, with the overall picture remaining very complicated. As a result different people have chosen different formulations and their preferences have undoubtedly been influenced by their experiences and the availability of certain algorithms and computer packages.

In this study the author has elected to use primitive variables because this approach appears to be the most easily extended to three dimensions, the Galerkin weighted residual method because this appears to be the most general, and the Newton-Raphson iterative method because this has proven to be the most efficient solution technique available.

CHAPTER 3

THEORY

3.1 Governing Equations and Boundary Conditions

3.2 Equation Formulation in Terms of Finite Elements

3.3 Assembly of Global Simultaneous Finite Element Equation System

3.4 Solution of Global Simultaneous Equation System

3. THEORY

All the theory that is used during the course of this study is presented in this chapter. It covers the derivation of the Navier-Stokes equations and the asssociated boundary conditions, a discussion of certain terms not normally included in these equations, the non-dimensionalization of the equations and the boundary conditions, the construction of the primitive variables finite element formulation, a discussion of the assembly of individual element equation systems into one global system and a discussion of the application of the Newton-Raphson method to the solution of this system. Although much of this theory is commonly accepted and well documented it has been repeated here for the sake of completeness and to maintain a consistent form of presentation. Also certain aspects such as the process of assembling the global equation system and the application of the Newton-Raphson method to its solution are not as well covered in the literature as one would have expected. In these cases additional care has been taken to ensure that their explanations and discussions are as clear and as concise as possible.

3.1 Governing Equations and Boundary Conditions

In the study of viscous fluid motion we are concerned with three basic laws:

(a) Conservation of mass

(b) Newton's second law of motion

and (c) Conservation of energy (the first law of thermodynamics).

The respective equations that result from the application of these laws are the Continuity equation, the three components of the Momentum equation and the Energy equation. These equations are generally expressed in terms of the five basic or primitive variables, the three components of velocity and the two thermodynamic quantities, pressure and temperature. In incompressible flows, since the density is constant the energy

equation becomes uncoupled and if the temperature is assumed to remain constant, it becomes redundant.

The general differential equations governing the steady and incompressible flow of a viscous fluid at constant temperature and expressed in tensor notation and in terms of the velocity and stress components are therefore as follows.

$$\frac{\partial \sigma_{ji}}{\partial x_j} = \rho \left(v_j \frac{\partial v_i}{\partial x_j} + C_2 \, v_i \frac{\partial v_j}{\partial x_j} - F_i \right) \qquad 3.1$$

and

$$\frac{\partial v_j}{\partial x_j} = 0 \qquad 3.2$$

where v_i is the velocity of the fluid in the x_i direction, ρ is the fluid density, F_i is the body force per unit mass in the x_i direction and σ_{ij} is the stress tensor. Equations 3.1 and 3.2 are the equations for the conservation of momentum and mass respectively, and when expressed only in terms of velocity and pressure, are often referred to as the Navier-Stokes and the Continuity equations. It will be noted that an additional term prefixed by the constant C_2 and not generally found in the momentum equation has been included in Equation 3.1. The significance of the inclusion of this term and others similar to it subsequently will be explained at a later stage. It will suffice to say that this term is a normal part of the momentum equation which has been traditionally always eliminited by the use of the Continuity equation. Its origin is explained in Appendix A where both Equations 3.1 and 3.2 have been derived from first principles.

In order to obtain the commonly used form of the Navier-Stokes equation it is necessary to write the momentum equation entirely in terms of the primitive variables, velocity v_i and pressure p. The stress-strain rate relationship that was chosen to express the stress tensor σ_{ij} found on the left hand side of equation 3.1 in terms of velocity and pressure is

$$\sigma_{ij} = \mu\left(\frac{\partial v_i}{\partial x_j} + \frac{\partial v_j}{\partial x_i} - \frac{2}{3} C_3 \delta_{ij} \frac{\partial v_k}{\partial x_k}\right) - p\,\delta_{ij} \qquad 3.3$$

where μ is the first coefficient of viscosity, or simply the fluid viscosity and δ_{ij} is the Kronecker delta defined as

$$\delta_{ij} = 1 \quad \text{if} \quad i = j$$

and $$\delta_{ij} = 0 \quad \text{if} \quad i \neq j$$

In general the fluid viscosity is temperature and to a lesser extent, pressure dependent. In this study however, because it has been assumed the fluid temperature is constant, and because the secondary pressure effects will be ignored, the viscosity will be constant. The stress-strain rate relationship that results is therefore linear and characteristic of Newtonian fluids.

The pressure, as it appears in equation 3.3 and in subsequent references is, by definition, the negative mean of the three normal stresses acting at any particular point. That is

$$p = -\frac{1}{3}\sigma_{kk} \qquad 3.4$$

It can easily be verified that by using equation 3.3, the value of the sum $-\frac{1}{3}(\sigma_{xx} + \sigma_{yy} + \sigma_{zz})$ is in fact equal to p provided C_3 equals one or $\frac{\partial v_j}{\partial x_j} = 0$. The term containing the constant C_3 is similar to the one found in the momentum equation and containing the constant C_2. It is normally eliminated by the use of the Continuity equation and does not generally appear in the stress-strain rate relationship. The derivation of this relationship has also been included in Appendix A in order to explain the origin of the term.

The necessity to define the pressure at any point in a moving fluid in the above manner arises from the fact that in establishing equation 3.3 one requires a scalar quantity, donated p for convenience, that at any point is equal in all directions, and is analogous to the static-fluid pressure in the sense that it is a measure of the local

intensity of the "squeezing" of the fluid. It can easily be shown that at any point $\frac{1}{3}\sigma_{kk}$ is the average value of the normal components of stress over the surface of a small sphere centred on that point. Thus the quantity p defined by equation 3.4 is a real parameter of the fluid system and is accessible to direct observation.

Equation 3.3 can now be substituted into equation 3.1 to give,

$$\mu\left(\frac{\partial^2 v_i}{\partial x^2_j} + \frac{\partial^2 v_j}{\partial x_j \partial x_i} - \frac{2}{3} C_3 \delta_{ij} \frac{\partial^2 v_k}{\partial x_j \partial x_k}\right) - \frac{\partial p}{\partial x_j} \delta_{ij}$$

$$= \rho\left(v_j \frac{\partial v_i}{\partial x_j} + C_2 v_i \frac{\partial v_j}{\partial x_j} - F_i\right) \qquad 3.5$$

The third and fourth terms of this equation can be simplified as follows.

$$-\frac{2}{3} C_3 \delta_{ij} \frac{\partial^2 v_k}{\partial x_j \partial x_k} = -\frac{2}{3} C_3 \frac{\partial^2 v_k}{\partial x_i \partial x_k}$$

since this term is non zero only when j = i,

$$= -\frac{2}{3} C_3 \frac{\partial^2 v_j}{\partial x_i \partial x_j}$$

because the extra subscript k is not necessary when j is the summation subscript within each equation, and

$$-\frac{\partial p}{\partial x_j} \delta_{ij} = -\frac{\partial p}{\partial x_i}$$

since this term also is non zero only when j = i. By rewriting the second term of equation 3.5 as $\frac{\partial}{\partial x_i}\left(\frac{\partial v_j}{\partial x_j}\right)$ it can be seen that the Continuity equation could be used to eliminate it. However, because the significance of the inclusion of this term and the previous two similar to it are being investigated in this study, this term will be prefixed by the constant C_1 and retained in the governing equations.

Thus the form of the Navier-Stokes equation that will be used throughout this study is

$$\mu \left(\frac{\partial^2 v_i}{\partial x^2_j} + C_1 \frac{\partial^2 v_j}{\partial x_j \partial x_i} - \frac{2}{3} C_3 \frac{\partial^2 v_j}{\partial x_i \partial x_j}\right) - \frac{\partial p}{\partial x_i}$$

$$= \rho\left(v_j \frac{\partial v_i}{\partial x_j} + C_2 v_i \frac{\partial v_j}{\partial x_j} - F_i\right)$$

or rearranged is

$$\frac{\mu}{\rho}\left(\frac{\partial^2 v_i}{\partial x^2_j} + \left(C_1 - \frac{2}{3} C_3\right) \frac{\partial^2 v_j}{\partial x_i \partial x_j}\right) - \frac{1}{\rho}\frac{\partial p}{\partial x_i}$$

$$= v_j \frac{\partial v_i}{\partial x_j} + C_2 v_i \frac{\partial v_j}{\partial x_j} - F_i \qquad 3.6$$

and

$$\frac{\partial v_j}{\partial x_j} = 0$$

The above equations of motion require boundary conditions that are mathematically tenable and also physically realistic. The two types of boundary that will be encountered in this study are

(1) solid-fluid interface

and (2) inlet or outlet regions.

The fluid-fluid interface, which includes the free surface case if one of the fluids has a relativity negligible density, will not be considered here since it is not directly amenable to the solution technique chosen.

At the solid-fluid interface it will be assumed that the fluid takes on exactly the velocity of the solid; that is

$$v_{i_{fl}} = v_{i_{sol}}.$$

If, as will be the case in most of the problems to be solved in this study, the solid at the interface is a stationary and impermeable wall, then on these sections of the flow boundary the fluid velocity will be zero in all coordinate directions. In addition, it will be convenient in many of the problems to limit the analysis to a finite region through

which the flow passes. This is permissible provided the properties of the flow at both the inlet and outlet are specified. That is, at the inlet and outlet boundaries, the fluid pressure and either the fluid velocity or the velocity gradients must be known. Where the velocity is known the boundary condition can be applied directly. However, if only the velocity gradients are known, then these must be used in conjunction with the pressure and equation 3.3 to establish the fluid state of stress in these regions. The fluid stress boundary condition can then be specified. If either the fluid pressure or the fluid velocity (or the velocity gradients) is unknown at the inlet or outlet boundary then a unique solution to the problem cannot be found because the flow is not totally contained.

The above conditions may be expressed formally as

$$v_i = v_i^o \qquad \text{on boundary } S_{v_i}$$

$$\text{and} \qquad \sigma_{ji}.n_j = T_i^o \qquad \text{on boundary } S_{T_i} \qquad 3.7$$

where S_{v_i} is the portion of the total boundary on which the velocity v_i^o in the x_i direction is prescribed, and S_{T_i} is the remainder of the boundary on which the stress T_i^o in the x_i direction is specified and on which n_j is the j^{th} component of the outward pointing normal. $S_{v_i} + S_{T_i} = S$ where S is the total boundary enclosing the flow being analysed. It is important to note that at every point on S either a velocity or stress component must be specified in each coordinate direction. This fact will become more evident when the assembly process is discussed in more detail later in Section 3.3. It is not necessary, however, that the portion of boundary on which a velocity is specified be the same for each coordinate direction. For example, if u (the velocity component in the x direction) is specified on boundary S_u and v (the velocity component in the y direction) is specified on boundary S_v, then S_u and S_v need not be coincident. Similarly for stresses; if T_y

(a stress in the y direction) is specified on boundary S_{T_z} and T_z is specified on boundary S_{T_z}, then S_{T_y} and S_{T_z} need not be the same portion of S.

Thus the system of differential equations and boundary conditions that describe the steady flow of an incompressible fluid through a region V, on whose boundary S, forces as well as flow restrictions have been imposed, and for which the body force per unit mass F_i is zero in all directions is

$$\frac{\mu}{\rho}\left(\frac{\partial^2 v_i}{\partial x^2_j} + \left(C_1 - \frac{2}{3}C_3\right)\frac{\partial^2 v_j}{\partial x_i \partial x_j}\right) - \frac{1}{\rho}\frac{\partial p}{\partial x_i}$$

$$= v_j \frac{\partial v_i}{\partial x_j} + C_2 v_i \frac{\partial v_j}{\partial x_j} \qquad 3.8.1$$

and

$$\frac{\partial v_j}{\partial x_j} = 0 \qquad 3.8.2$$

over region V, with boundary conditions

$$v_i = v_i^o \quad \text{on boundary } S_{v_i} \qquad 3.8.3$$

and

$$\sigma_{ji} \cdot n_j = T_i^o \quad \text{on boundary } S_{T_i} \qquad 3.8.4$$

Before proceeding any further, it is necessary to non-dimensionalise the above relationships so that dimensional problems in subsequent derived formulations and flow solutions are not encountered. By selecting a velocity $\bar{v}$ and length $\bar{L}$ characteristic of the flow to be analysed, all variables in the governing equations and boundary conditions can be non-dimensionalised or written in dimensionless or normalised form by using the following transformations.

Length: $$x_i' = \frac{x_i}{\bar{L}} \qquad 3.9.1$$

Velocity: $$v_i' = \frac{v_i}{\bar{v}} \qquad 3.9.2$$

Pressure or Stress: $p' = \dfrac{p}{\rho \bar{V}^2}$ or $\sigma'_{ij} = \dfrac{\sigma_{ij}}{\rho \bar{V}^2}$ 3.9.3

Equations 3.8.1-4 become

$$\frac{\mu}{\rho \bar{V} \bar{L}} \left(\frac{\partial^2 v'_i}{\partial x'^2_j} + \left(C_1 - \frac{2}{3} C_3\right) \frac{\partial^2 v'_j}{\partial x'_i \, \partial x'_j} \right) - \frac{\partial p'}{\partial x'_i}$$

$$= v'_j \frac{\partial v'_i}{\partial x'_j} + C_2 v'_i \frac{\partial v'_j}{\partial x'_j}$$

and $$\frac{\partial v'_j}{\partial x'_j} = 0$$

with $v'_i = v'^{o}_i$ on boundary S_{v_i}

and $\sigma'_{ji} . n_j = T'^{o}_i$ on boundary S_{T_i}

The dash notation for dimensionless variables can now be dropped with the understanding that all variables used from now on, unless otherwise stated, have been non-dimensionalised using relationships 3.9.1-3. The final form of the governing equations that are to be used in this study is therefore

$$\frac{1}{Re} \left(\frac{\partial^2 v_i}{\partial x^2_j} + \left(C_1 - \frac{2}{3} C_3\right) \frac{\partial^2 v_j}{\partial x_i \, \partial x_j} \right) - \frac{\partial p}{\partial x_i}$$

$$= v_j \frac{\partial v_i}{\partial x_j} + C_2 v_i \frac{\partial v_j}{\partial x_j} \qquad 3.10.1$$

and $$\frac{\partial v_j}{\partial x_j} = 0 \qquad 3.10.2$$

with $v_i = v_i^{o}$ on boundary S_{v_i} 3.10.3

and $\sigma_{ji} . n_j = T_i^{o}$ on boundary S_{T_i} 3.10.4

and where $Re = \dfrac{\rho \bar{V} \bar{L}}{\mu}$ 3.10.5

is the resulting dimensionless parameter known as the Reynolds number and is the only quantity of importance affecting all laminar viscous flows at constant temperature.

It should be pointed out that the characteristic quantities $\bar{v}$ and $\bar{L}$ that are chosen to non-dimensionalise the above equations for a given problem, must both be unity when the equivalent dimensionless problem is solved. For convenience, $\bar{v}$ and $\bar{L}$ are usually selected as quantities that are independent of the solution that is to be obtained and that can be used regardless of the Reynolds number. For example, in pipe flow, $\bar{L}$ is chosen to be the pipe diameter rather than the pipe length because the length of pipe that must be considered may depend on the Reynolds number. The diameter of the pipe for a given problem is usually known beforehand and in the equivalent dimensionless problem is set to unity, thus fixing one of the dimensions of the flow geometry for all Reynolds numbers. Similarly, $\bar{v}$ is usually chosen as one of the velocities in the velocity boundary conditions which are also known prior to solving a problem. For example, in pipe flow, $\bar{v}$ is usually the entry velocity while for the flow around an object, $\bar{v}$ is the free stream velocity. In all cases $\bar{v}$ and $\bar{L}$ are chosen in such a manner that enables a flow of any Reynolds number to be solved without too many changes to the boundary conditions or the flow geometry. The Reynolds number therefore should be the only parameter that affects a given class of flow problems.

The governing equations and boundary conditions have now been set up and are in a form suitable for solving. They have been written out in full below in order to show their full extent and complexity. The assumptions that have been made in obtaining them are summarised as follows. It is assumed that

(1) the temperature of the fluid is uniform,

(2) the fluid density and viscosity are constant,

(3) the fluid is isotropic and Newtonian,

(4) the flow is steady,

(5) the flow is laminar and continuous,

(6) the flow is fully contained (no free surfaces),

(7) the fluid is not subject to body forces.

$$\frac{1}{Re}\left(\left(\frac{\partial^2 u}{\partial x^2}+\frac{\partial^2 u}{\partial y^2}+\frac{\partial^2 u}{\partial z^2}\right)+\left(C_1-\frac{2}{3}C_3\right)\left(\frac{\partial^2 u}{\partial x^2}+\frac{\partial^2 v}{\partial x\,\partial y}+\frac{\partial^2 w}{\partial x\,\partial z}\right)\right)-\frac{\partial p}{\partial x}$$

$$=\left(u\frac{\partial u}{\partial x}+v\frac{\partial u}{\partial y}+w\frac{\partial u}{\partial z}\right)+C_2\left(u\frac{\partial u}{\partial x}+u\frac{\partial v}{\partial y}+u\frac{\partial w}{\partial z}\right) \qquad 3.11.1$$

$$\frac{1}{Re}\left(\left(\frac{\partial^2 v}{\partial x^2}+\frac{\partial^2 v}{\partial y^2}+\frac{\partial^2 v}{\partial z^2}\right)+\left(C_1-\frac{2}{3}C_3\right)\left(\frac{\partial^2 u}{\partial y\,\partial x}+\frac{\partial^2 v}{\partial y^2}+\frac{\partial^2 w}{\partial y\,\partial z}\right)\right)-\frac{\partial p}{\partial y}$$

$$=\left(u\frac{\partial v}{\partial x}+v\frac{\partial v}{\partial y}+w\frac{\partial v}{\partial z}\right)+C_2\left(v\frac{\partial u}{\partial x}+v\frac{\partial v}{\partial y}+v\frac{\partial w}{\partial z}\right) \qquad 3.11.2$$

$$\frac{1}{Re}\left(\left(\frac{\partial^2 w}{\partial x^2}+\frac{\partial^2 w}{\partial y^2}+\frac{\partial^2 w}{\partial z^2}\right)+\left(C_1-\frac{2}{3}C_3\right)\left(\frac{\partial^2 u}{\partial z\,\partial x}+\frac{\partial^2 v}{\partial z\,\partial y}+\frac{\partial^2 w}{\partial z^2}\right)\right)-\frac{\partial p}{\partial z}$$

$$=\left(u\frac{\partial w}{\partial x}+v\frac{\partial w}{\partial y}+w\frac{\partial w}{\partial z}\right)+C_2\left(w\frac{\partial u}{\partial x}+w\frac{\partial v}{\partial y}+w\frac{\partial w}{\partial z}\right) \qquad 3.11.3$$

and
$$\frac{\partial u}{\partial x}+\frac{\partial v}{\partial y}+\frac{\partial w}{\partial z}=0 \qquad 3.11.4$$

with boundary conditions:
$$u = u^o \quad \text{on boundary } S_u$$
$$v = v^o \quad \text{on boundary } S_v \qquad 3.11.5$$
$$w = w^o \quad \text{on boundary } S_w$$

and
$$\sigma_{xx}n_x+\sigma_{yx}n_y+\sigma_{zx}n_z = T_x^o \quad \text{on boundary } S_{T_x}$$
$$\sigma_{xy}n_x+\sigma_{yy}n_y+\sigma_{zy}n_z = T_y^o \quad \text{on boundary } S_{T_y} \qquad 3.11.6$$
$$\sigma_{xz}n_x+\sigma_{yz}n_y+\sigma_{zz}n_z = T_y^o \quad \text{on boundary } S_{T_z}$$

Before these equations are formulated in terms of the finite element method it is necessary to explain the reasons for retaining

the terms containing the constants C_1, C_2 and C_3 and the quantity $\frac{\partial v_j}{\partial x_j}$. Until recently, it has been customary to use the Continuity equation wherever possible in the momentum equation to eliminate all terms containing the quantity $\frac{\partial v_j}{\partial x_j}$. Some researchers however argued that because their method of solving the governing equations is approximate, the quantity $\frac{\partial v_j}{\partial x_j}$ is not exactly zero everywhere and therefore cannot be used to eliminate certain of the viscous terms in the momentum equation. These additional viscous terms were therefore retained in the governing equations. Recently the author and others carried this argument further and applied it to certain acceleration terms (18). These were then also retained. Finally in this study, all terms that contain the quantity $\frac{\partial v_j}{\partial x_j}$, including an additional viscous one, have been included and prefixed by a constant whose value is either one or zero depending on whether the term is to be retained or eliminated. The various approaches that have traditionally been used can thus be compared and their relative merits confirmed.

By setting $C_1 = C_2 = C_3 = 0$, no terms containing $\frac{\partial v_j}{\partial x_j}$ are retained and the governing equations reduce to

$$\frac{1}{Re} \frac{\partial^2 v_i}{\partial x_j^2} - \frac{\partial p}{\partial x_i} = v_j \frac{\partial v_i}{\partial x_j} \qquad \text{Formulation A}$$

$$\frac{\partial v_j}{\partial x_j} = 0$$

The finite element formulation based upon these equations will be subsequently referred to as "formulation A".

The governing equations for "formulation B", obtained by setting $C_1 = 1$ and $C_2 = C_3 = 0$ are

$$\frac{1}{Re}\left(\frac{\partial^2 v_i}{\partial x^2_j} + \frac{\partial^2 v_j}{\partial x_i \partial x_j}\right) - \frac{\partial p}{\partial x_i} = v_j \frac{\partial v_i}{\partial x_j}$$

$$\frac{\partial v_j}{\partial x_j} = 0$$

Formulation B

This is perhaps the most commonly used form of the Navier-Stokes equation since the physical interpretation of all terms that result in the finite element formulation based on these equations is well known. The additional term is referred to as a "viscous term" because, like the term prefixed by $\frac{1}{Re}$ in the equations governing formulation A, it is the result of the inclusion in the equations of motion of stresses that occur because of the viscous nature of the fluids considered.

The equations governing "formulation C", $C_1 = C_2 = 1$ and $C_3 = 0$ are

$$\frac{1}{Re}\left(\frac{\partial^2 v_i}{\partial x^2_j} + \frac{\partial^2 v_j}{\partial x_i \partial x_j}\right) - \frac{\partial p}{\partial x_i} = v_j \frac{\partial v_i}{\partial x_j} + v_i \frac{\partial v_j}{\partial x_j}$$

$$\frac{\partial v_j}{\partial x_j} = 0$$

Formulation C

and "formulation D", $C_1 = C_2 = C_3 = 1$ are

$$\frac{1}{Re}\left(\frac{\partial^2 v_i}{\partial x^2_j} + \frac{\partial^2 v_j}{\partial x_i \partial x_j} - \frac{2}{3}\frac{\partial^2 v_j}{\partial x_i \partial x_j}\right) - \frac{\partial p}{\partial x_i} = v_j \frac{\partial v_i}{\partial x_j} + v_i \frac{\partial v_j}{\partial x_j}$$

$$\frac{\partial v_j}{\partial x_j} = 0$$

Formulation D

The additional term in the equations governing formulation C, often referred to as an acceleration or inertia term because it results from the right hand side of the equation of motion F = m.a, and the extra viscous term in the equations governing formulation D have, to the author's knowledge, traditionally always been omitted. The first arises from changes in momentum associated with the lack of satisfaction of the Continuity equation, inherent in an approximate method of solution

such as the finite element method. The second results from the fact that the approximated pressure is not the same as the negative mean direct stress as calculated from the approximated velocity field if this term is omitted. By definition, the pressure at any point in the flow is the negative mean of the three normal stresses at that point regardless of whether the fields are exact or approximate, or whether the Continuity equation is satisfied exactly or not. Using the non-dimensionalised form of equation 3.3, it can be shown that if the term containing C_3 is omitted then

$$p_{defn} = -\frac{1}{3}\sigma_{k,k} = \frac{2}{3}\frac{1}{Re}v_{k,k} + p$$

Therefore if Continuity is not satisfied exactly, as is assumed in formulation D, the pressure in the flow is not the same as the p appearing in the equations governing that flow. To ensure that it does, the term containing C_3 must be included. Formulation D therefore has retained all terms that have at one stage or another been eliminated by making use of the Continuity equation. It should be pointed out at this stage that if the finite element approximation happens to coincide with the exact solution, all the terms containing the constants C_1, C_2 and C_3 will vanish leaving the Navier-Stokes and the Continuity equations unchanged. It is also important to note that the boundary conditions for all four formulations are the same and given by 3.11.5 and 6.

3.2 Equation Formulation in Terms of Finite Elements

The exact solution to any viscous flow problem is attained when the solution {u(x,y,z),v(x,y,z),w(x,y,z),p(x,y,z)} satisfies the governing equations at every point within the flow domain V, and the boundary conditions at every point on the flow boundary S. This situation however occurs only in a handful of elementary problems and the exact solution to a general viscous flow problem is as yet impossible to find, simply because of the complex nature of the governing partial differential equations and their boundary conditions, and the limitations of known methods for solving such equations exactly. It has therefore been necessary to resort to approximation or numerical techniques in order to find some form of approximate solution. Of these techniques, the finite element method has proved to be the most versatile, both in the field of fluid dynamics and in the field of structural and stress analysis where it was first applied. Its widespread use however, has only come about with the recent introduction of the faster and relatively large new generation digital computers. The finite element method is used exclusively throughout this study and is described in detail below.

Let the flow domain over which the governing equations must be satisfied, be divided into N_e similar non-overlapping subdivisions otherwise known as finite elements or simply elements. The elements should be similar only to the extent that they have the same number of edges or faces. It should be noted that the elements need not necessarily have this restriction, but it does simplify the formulation and the computer programming without too much loss of generality. Assume that each element has the same number of nodes internally and per edge or face, so that the total number per element is K. Assume that any two adjacent elements both contain the whole of the common face or edge and that all nodes on this face or edge are common to both elements.

With the geometry of each element and the positions of its K nodes thus fixed, it is then possible to set up for each element, K polynomial functions in terms of x, y and z, subsequently referred to as shape functions and denoted $N_{ij}(x,y,z)$, with the characteristic that for any element i,

$$\begin{aligned} N_{ij}(x,y,z) &= 1 \qquad \text{at the } j^{th} \text{ node} \\ &= 0 \qquad \text{at the other K-1 nodes} \end{aligned} \tag{3.12}$$

Any function $\Phi(x,y,z)$ operative in the region defined as element i, can now be expressed approximately in terms of its values at the K nodal points of element i by using the shape functions. If Φ_{ij} is the value of $\Phi(x,y,z)$ at the j^{th} node of element i, then within element i,

$$\Phi(x,y,z) \simeq \Phi_i^*(x,y,z)$$

$$\text{where} \qquad \Phi_i^*(x,y,z) = \sum_{j=1}^{K} \Phi_{ij}\, N_{ij}(x,y,z) \tag{3.13}$$

The function Φ_i^* has the exact value of Φ at the K nodes but elsewhere within element i it is only an approximation, the degree of which depends on the shape functions and therefore on the number and position of the nodes. It is evident that as K increases the order of the polynomial shape functions also increases and with them the number of points at which Φ_i^* equals Φ exactly.

This method of approximating a function can now be applied to the required solution $\{u(x,y,z), v(x,y,z), w(x,y,z), p(x,y,z)\}$ of the governing Navier-Stokes and Continuity equations. By expressing the unkown solution functions in terms of their unknown values at K points within a series of elements comprising the flow domain V, the task of finding the overall solution is reduced to one of finding its numerical value at a finite number of discrete points. Within each element the individual approximations, which are obtained by interpolation using the element's shape functions, are then combined in a piecewise fashion to give the overall approximate solution at all points in V. Some elements on S, the boundary of V, will have nodes at which the velocity

and pressure has been specified. For these elements, the approximation for velocity and pressure is summed only over those nodes at which the solution is unknown.

The three components of velocity and the pressure can be expressed approximately within any element i as follows.

$$u(x,y,z) \simeq u_i^*(x,y,z) = \sum_{j=1}^{K'} u_{ij} N'_{ij}(x,y,z) \qquad 3.14.1$$

$$v(x,y,z) \simeq v_i^*(x,y,z) = \sum_{j=1}^{K'} v_{ij} N'_{ij}(x,y,z) \qquad 3.14.2$$

$$w(x,y,z) \simeq w_i^*(x,y,z) = \sum_{j=1}^{K'} w_{ij} N'_{ij}(x,y,z) \qquad 3.14.3$$

and

$$p(x,y,z) \simeq p_i^*(x,y,z) = \sum_{j=1}^{K''} p_{ij} N''_{ij}(x,y,z) \qquad 3.14.4$$

where u_{ij}, v_{ij} and w_{ij} are the unknown values of the three velocity components at the j^{th} velocity node (j=1, .. K'), and p_{ij} is the unknown value of the pressure of the j^{th} pressure node (j=1, .. K"), in element i. The K' velocity and K" pressure shape functions are defined as follows.

$$N'_{ij}(x,y,z) = 1 \quad \text{at the } j^{th} \text{ node}$$
$$= 0 \quad \text{at the other K'-1 velocity nodes,} \qquad 3.15.1$$

and

$$N''_{ij}(x,y,z) = 1 \quad \text{at the } j^{th} \text{ node}$$
$$= 0 \quad \text{at the other K"-1 pressure nodes.} \qquad 3.15.2$$

In these approximations the summations for the velocity components and for the pressure are taken over different numbers of nodes to enable the pressure, if necessary, to have a different order of approximation from that of the velocity components. In fact, since in the governing equations the highest order of differentiation of the pressure is one less than the highest order of differentiation of velocity, the pressure is given a lower order of approximation than the velocity components. Therefore K" is less than K', and as a result, within each element all nodes are used in the approximation of the velocity components but only

a given subset of the same nodes is used in the pressure approximation. The maximum number of nodes per element is K = K'. An alternative arrangement would be to set up two finite element subdivisions or meshes, over the same flow domain, one for the velocity approximation and the second containing elements with less nodes for the pressure approximation. However this approach would require considerable additional effort both in setting up the extra finite element mesh and in the solution procedure, and is therefore not often used.

Having constructed an approximate function for each component of velocity and the pressure within each element of the flow domain, four residual functions can be set up by substituting the approximations 3.14.1-4 into the governing equations 3.11.1-4.

$$R_{i1} = \frac{1}{Re}\left(\left(\frac{\partial^2 u_i^*}{\partial x^2} + \frac{\partial^2 u_i^*}{\partial y^2} + \frac{\partial^2 u_i^*}{\partial z^2}\right) + \left(C_1 - \frac{2}{3}C_3\right)\left(\frac{\partial^2 u_i^*}{\partial x^2} + \frac{\partial^2 v_i^*}{\partial x\,\partial y} + \frac{\partial^2 w_i^*}{\partial x\,\partial z}\right)\right) - \frac{\partial p_i^*}{\partial x}$$

$$-\left(u_i^* \frac{\partial u_i^*}{\partial x} + v_i^* \frac{\partial u_i^*}{\partial y} + w_i^* \frac{\partial u_i^*}{\partial z}\right) - C_2\left(u_i^* \frac{\partial u_i^*}{\partial x} + u_i^* \frac{\partial v_i^*}{\partial y} + u_i^* \frac{\partial w_i^*}{\partial z}\right) \qquad 3.16.1$$

$$R_{i2} = \frac{1}{Re}\left(\left(\frac{\partial^2 v_i^*}{\partial x^2} + \frac{\partial^2 v_i^*}{\partial y^2} + \frac{\partial^2 v_i^*}{\partial z^2}\right) + \left(C_1 - \frac{2}{3}C_3\right)\left(\frac{\partial^2 u_i^*}{\partial y\,\partial x} + \frac{\partial^2 v_i^*}{\partial y^2} + \frac{\partial^2 w_i^*}{\partial y\,\partial z}\right)\right) - \frac{\partial p_i^*}{\partial y}$$

$$-\left(u_i^* \frac{\partial v_i^*}{\partial x} + v_i^* \frac{\partial v_i^*}{\partial y} + w_i^* \frac{\partial v_i^*}{\partial z}\right) - C_2\left(v_i^* \frac{\partial u_i^*}{\partial x} + v_i^* \frac{\partial v_i^*}{\partial y} + v_i^* \frac{\partial w_i^*}{\partial z}\right) \qquad 3.16.2$$

$$R_{i3} = \frac{1}{Re}\left(\left(\frac{\partial^2 w_i^*}{\partial x^2} + \frac{\partial^2 w_i^*}{\partial y^2} + \frac{\partial^2 w_i^*}{\partial z^2}\right) + \left(C_1 - \frac{2}{3}C_3\right)\left(\frac{\partial^2 u_i^*}{\partial z\,\partial x} + \frac{\partial^2 v_i^*}{\partial z\,\partial y} + \frac{\partial^2 w_i^*}{\partial z^2}\right)\right) - \frac{\partial p_i^*}{\partial z}$$

$$-\left(u_i^* \frac{\partial w_i^*}{\partial x} + v_i^* \frac{\partial w^*}{\partial y} + w_i^* \frac{\partial w_i^*}{\partial z}\right) - C_2\left(w_i^* \frac{\partial u_i^*}{\partial x} + w_i^* \frac{\partial v_i^*}{\partial y} + w_i^* \frac{\partial w_i^*}{\partial z}\right) \qquad 3.16.3$$

and $$R_{i4} = \frac{\partial u_i^*}{\partial x} + \frac{\partial v_i^*}{\partial y} + \frac{\partial w_i^*}{\partial z} \qquad 3.16.4$$

An indication of the accuracy of the approximate solution can now be obtained by examining these four residual functions. If all four residuals are zero at all points within each element, then the exact solution has been obtained. In general however, a trial approximate

solution as is described by equations 3.14.1-4, will not result in residuals that are identically zero everywhere. Therefore the best approximate solution that can be set up is the one whose nodal values of velocity and pressure in some average sense, reduces the residual functions to a least value within each element. An obvious way of achieving this is to make use of the fact that if the function R(x,y,z) is identically equal to zero everywhere in a volume V_i, then

$$\int_{V_i} W(x,y,z)\, R(x,y,z)\, dV = 0 \qquad 3.17$$

for all functions W. Conversely, by using a finite number of linearly independent functions W, equation 3.17 can be used to ensure that the four residual functions are zero at least in an average sense over each element. Therefore by using 3K' + K" linearly independent functions, equation 3.17 can be used to generate sufficient simultaneous equations to solve for the 3K' unknown velocity and K" unknown pressure values at the nodes of each element. This process is known as the weighted residual method and W are the weighting functions. The Galerkin method of weighted residuals leads in general to the best approximate solution and is therefore the one chosen for this study. In this particular process the weighting functions are coincident with the linearly independent shape functions used in the approximations for velocity and pressure. Two types of shape functions are used in these approximations and both are therefore used as weighting functions. The required 3K' + K" simultaneous equations for element i are:

$$\int_{V_i} N'_{ij}(x,y,z)\, R_{i1}\, dV = 0 \qquad 3.18.1$$

$$\int_{V_i} N'_{ij}(x,y,z)\, R_{i2}\, dV = 0 \qquad \text{for } j=1, \ldots K' \qquad 3.18.2$$

$$\int_{V_i} N'_{ij}(x,y,z)\, R_{i3}\, dV = 0 \qquad 3.18.3$$

$$\int_{V_i} N''_{ij}(x,y,z)\, R_{i4}\, dV = 0 \qquad \text{for } j=1, \ldots K'' \qquad 3.18.4$$

where V_i is the volume of element i.

This now completes the basic theory behind the finite element formulation of the Navier-Stokes and Coninuity equations. All that remains to be done is to substitute equations 3.14.1-4 into 3.16.1-4 and these into 3.18.1-4, rearrange and solve the resulting set of non-linear simultaneous equations to obtain the required nodal values of velocity and pressure. The finite element equations as they presently stand have been written out in full below.

$$\int_{V_i} N'_{ij} \{ \frac{1}{Re} ((\frac{\partial^2 u_i^*}{\partial x^2} + \frac{\partial^2 u_i^*}{\partial y^2} + \frac{\partial^2 u_i^*}{\partial z^2}) + (C_1 - \frac{2}{3} C_3) (\frac{\partial^2 u_i^*}{\partial x^2} + \frac{\partial^2 v_i^*}{\partial x \partial y} + \frac{\partial^2 w_i^*}{\partial x \partial z})) - \frac{\partial p_i^*}{\partial x} - (u_i^* \frac{\partial u_i^*}{\partial x} + v_i^* \frac{\partial u_i^*}{\partial y} + w_i^* \frac{\partial u_i^*}{\partial z}) - C_2 (u_i^* \frac{\partial u_i^*}{\partial x} + u_i^* \frac{\partial v_i^*}{\partial y} + u_i^* \frac{\partial w_i^*}{\partial z}) \} dV = 0$$

for j=1,..K' 3.19.1

$$\int_{V_i} N'_{ij} \{ \frac{1}{Re} ((\frac{\partial^2 v_i^*}{\partial x^2} + \frac{\partial^2 v_i^*}{\partial y^2} + \frac{\partial^2 v_i^*}{\partial z^2}) + (C_1 - \frac{2}{3} C_3) (\frac{\partial^2 u_i^*}{\partial y \partial x} + \frac{\partial^2 v_i^*}{\partial y^2} + \frac{\partial^2 w_i^*}{\partial y \partial z})) - \frac{\partial p_i^*}{\partial y} - (u_i^* \frac{\partial v_i^*}{\partial x} + v_i^* \frac{\partial v_i^*}{\partial y} + w_i^* \frac{\partial v_i^*}{\partial z}) - C_2 (v_i^* \frac{\partial u_i^*}{\partial x} + v_i^* \frac{\partial v_i^*}{\partial y} + v_i^* \frac{\partial w_i^*}{\partial z}) \} dV = 0$$

for j=1,..K' 3.19.2

$$\int_{V_i} N'_{ij} \{ \frac{1}{Re} ((\frac{\partial^2 w_i^*}{\partial x^2} + \frac{\partial^2 w_i^*}{\partial y^2} + \frac{\partial^2 w_i^*}{\partial z^2}) + (C_1 - \frac{2}{3} C_3) (\frac{\partial^2 u_i^*}{\partial z \partial x} + \frac{\partial^2 v_i^*}{\partial z \partial y} + \frac{\partial^2 w_i^*}{\partial z^2})) - \frac{\partial p_i^*}{\partial z} - (u_i^* \frac{\partial w_i^*}{\partial x} + v_i^* \frac{\partial w_i^*}{\partial y} + w_i^* \frac{\partial w_i^*}{\partial z}) - C_2 (w_i^* \frac{\partial u_i^*}{\partial x} + w_i^* \frac{\partial v_i^*}{\partial y} + w_i^* \frac{\partial w_i^*}{\partial z}) \} dV = 0$$

for j=1,..K' 3.19.3

and $$- \int_{V_i} N''_{ij} \{ \frac{\partial u_i^*}{\partial x} + \frac{\partial v_i^*}{\partial y} + \frac{\partial w_i^*}{\partial z} \} dV = 0 \qquad \text{for } j=1,..K'' \qquad 3.19.4$$

where the approximate functions u_i^*, v_i^*, w_i^* and p_i^* are given by equations 3.14.1-4.

In order to enable the stress boundary conditions to be incorporated in the finite element equations and to facilitate subsequent integral transformations (explained in Section 4.1), it is necessary to reduce by one order all second order velocity and first order pressure derivatives in equations 3.19.1-3. This can be done by first applying the product rule of differentiation to each of the first three terms of these equations and then rearranging so that

$$\int_{V_i} \frac{\partial}{\partial x}\{N'_{ij}(\frac{1}{Re}((\frac{\partial u_i^*}{\partial x}+\frac{\partial u_i^*}{\partial x})-\frac{2}{3}C_3(\frac{\partial u_i^*}{\partial x}+\frac{\partial v_i^*}{\partial y}+\frac{\partial w_i^*}{\partial z}))-p_i^*)\}$$
$$+\frac{\partial}{\partial y}\{N'_{ij}(\frac{1}{Re}(\frac{\partial v_i^*}{\partial x}+\frac{\partial u_i^*}{\partial y}))\}+\frac{\partial}{\partial z}\{N'_{ij}(\frac{1}{Re}(\frac{\partial w_i^*}{\partial x}+\frac{\partial u_i^*}{\partial z}))\}\,dV$$
$$+\int_{V_i}\frac{\partial}{\partial x}\{(C_1-1)\frac{1}{Re}N'_{ij}\frac{\partial u_i^*}{\partial x}\}+\frac{\partial}{\partial y}\{(C_1-1)\frac{1}{Re}N'_{ij}\frac{\partial v_i^*}{\partial x}\}$$
$$+\frac{\partial}{\partial z}\{(C_1-1)\frac{1}{Re}N'_{ij}\frac{\partial w_i^*}{\partial x}\}\,dV-\int_{V_i}\frac{1}{Re}\{\frac{\partial N'_{ij}}{\partial x}\frac{\partial u_i^*}{\partial x}+\frac{\partial N'_{ij}}{\partial y}\frac{\partial u_i^*}{\partial y}+\frac{\partial N'_{ij}}{\partial z}\frac{\partial u_i^*}{\partial z}\}$$
$$+C_1\frac{1}{Re}\{\frac{\partial N'_{ij}}{\partial x}\frac{\partial u_i^*}{\partial x}+\frac{\partial N'_{ij}}{\partial y}\frac{\partial v_i^*}{\partial x}+\frac{\partial N'_{ij}}{\partial z}\frac{\partial w_i^*}{\partial x}\}-\frac{2}{3}C_1\frac{1}{Re}\{\frac{\partial N'_{ij}}{\partial x}\frac{\partial u_i^*}{\partial x}$$
$$+\frac{\partial N'_{ij}}{\partial x}\frac{\partial v_i^*}{\partial y}+\frac{\partial N'_{ij}}{\partial x}\frac{\partial w_i^*}{\partial z}\}-\frac{\partial N'_{ij}}{\partial x}p_i^*+N'_{ij}\{(u_i^*\frac{\partial u_i^*}{\partial x}+v_i^*\frac{\partial u_i^*}{\partial y}+w_i^*\frac{\partial u_i^*}{\partial z})$$
$$+C_2(u_i^*\frac{\partial u_i^*}{\partial x}+u_i^*\frac{\partial v_i^*}{\partial y}+u_i^*\frac{\partial w_i^*}{\partial z})\}\,dV=0$$

for $j=1,..K'$ 3.20.1

and $$-\int_{V_i}N''_{ij}\{\frac{\partial u_i^*}{\partial x}+\frac{\partial v_i^*}{\partial y}+\frac{\partial w_i^*}{\partial z}\}\,dV=0 \qquad \text{for } j=1,..K'' \qquad 3.20.4$$

For obvious reasons equations 3.20.2 and 3 corresponding to the y and z directions, have not been written out in full here. However they can be obtained in a similar manner.

By using the non-dimensionalised form of the stress tensor given by equation 3.3, that is

$$\sigma^*_{ij} = \frac{1}{Re}\left(\frac{\partial v^*_i}{\partial x_j} + \frac{\partial v^*_j}{\partial x_i} - \frac{2}{3} C_3\, \delta_{ij} \frac{\partial v^*_k}{\partial x_k}\right) - p^* \delta_{ij} \qquad 3.21$$

the three terms in the first integral in each of equations 3.20.1 to 3 can be rewritten in terms of stress components. The Gauss Divergence Theorum can then be applied to the first two volume integrals in each of these equations to reduce them to surface integrals. The resulting equations are:

$$\int_{V_i} \frac{1}{Re}\left\{\frac{\partial N'_{ij}}{\partial x}\frac{\partial u^*_i}{\partial x} + \frac{\partial N'_{ij}}{\partial y}\frac{\partial u^*_i}{\partial y} + \frac{\partial N'_{ij}}{\partial z}\frac{\partial u^*_i}{\partial z}\right\} + \frac{C_1}{Re}\left\{\frac{\partial N'_{ij}}{\partial x}\frac{\partial u^*_i}{\partial x} + \frac{\partial N'_{ij}}{\partial y}\frac{\partial v^*_i}{\partial x} + \frac{\partial N'_{ij}}{\partial z}\frac{\partial w^*_i}{\partial x}\right\}$$
$$- \frac{2}{3} C_3 \frac{1}{Re}\left\{\frac{\partial N'_{ij}}{\partial x}\frac{\partial u^*_i}{\partial x} + \frac{\partial N'_{ij}}{\partial x}\frac{\partial v^*_i}{\partial y} + \frac{\partial N'_{ij}}{\partial x}\frac{\partial w^*_i}{\partial z}\right\} - \frac{\partial N'_{ij}}{\partial x} p^*_i + N'_{ij}\left\{\left(u^*_i \frac{\partial u^*_i}{\partial x}\right.\right.$$
$$\left.\left. + v^*_i \frac{\partial u^*_i}{\partial y} + w^*_i \frac{\partial u^*_i}{\partial z}\right) + C_2\left(u^*_i \frac{\partial u^*_i}{\partial x} + u^*_i \frac{\partial v^*_i}{\partial y} + u^*_i \frac{\partial w^*_i}{\partial z}\right)\right\} dV$$

$$= \int_{S_i} N'_{ij}\left\{\sigma^*_{xx} n_x + \sigma^*_{yx} n_y + \sigma^*_{zx} n_z\right\} dS$$
$$+ \int_{S_i} (C_1 - 1)\frac{1}{Re} N'_{ij}\left\{\frac{\partial u^*_i}{\partial x} n_x + \frac{\partial v^*_i}{\partial x} n_y + \frac{\partial w^*_i}{\partial x} n_z\right\} dS \quad \text{for } j=1,..K' \qquad 3.22.1$$

$$\int_{V_i} \frac{1}{Re}\left\{\frac{\partial N'_{ij}}{\partial x}\frac{\partial v^*_i}{\partial x} + \frac{\partial N'_{ij}}{\partial y}\frac{\partial v^*_i}{\partial y} + \frac{\partial N'_{ij}}{\partial z}\frac{\partial v^*_i}{\partial z}\right\} + \frac{C_1}{Re}\left\{\frac{\partial N'_{ij}}{\partial x}\frac{\partial u^*_i}{\partial y} + \frac{\partial N'_{ij}}{\partial y}\frac{\partial v^*_i}{\partial y} + \frac{\partial N'_{ij}}{\partial z}\frac{\partial w^*_i}{\partial y}\right\}$$
$$- \frac{2}{3} C_3 \frac{1}{Re}\left\{\frac{\partial N'_{ij}}{\partial y}\frac{\partial u^*_i}{\partial x} + \frac{\partial N'_{ij}}{\partial y}\frac{\partial v^*_i}{\partial y} + \frac{\partial N'_{ij}}{\partial y}\frac{\partial w^*_i}{\partial z}\right\} - \frac{\partial N'_{ij}}{\partial y} p^*_i + N'_{ij}\left\{\left(u^*_i \frac{\partial v^*_i}{\partial x}\right.\right.$$
$$\left.\left. + v^*_i \frac{\partial v^*_i}{\partial y} + w^*_i \frac{\partial v^*_i}{\partial z}\right) + C_2\left(v^*_i \frac{\partial u^*_i}{\partial x} + v^*_i \frac{\partial v^*_i}{\partial y} + v^*_i \frac{\partial w^*_i}{\partial z}\right)\right\} dV$$

$$= \int_{S_i} N'_{ij}\left\{\sigma^*_{xy} n_x + \sigma^*_{yy} n_y + \sigma^*_{zy} n_z\right\} dS$$
$$+ \int_{S_i} (C_1 - 1)\frac{1}{Re} N'_{ij}\left\{\frac{\partial u^*_i}{\partial y} n_x + \frac{\partial v^*_i}{\partial y} n_y + \frac{\partial w^*_i}{\partial y} n_z\right\} dS \quad \text{for } j=1,..K' \qquad 3.22.2$$

$$\int_{V_i} \frac{1}{Re}\left\{\frac{\partial N'_{ij}}{\partial x}\frac{\partial w^*_i}{\partial x} + \frac{\partial N'_{ij}}{\partial y}\frac{\partial w^*_i}{\partial y} + \frac{\partial N'_{ij}}{\partial z}\frac{\partial w^*_i}{\partial z}\right\} + \frac{C_1}{Re}\left\{\frac{\partial N'_{ij}}{\partial x}\frac{\partial u^*_i}{\partial z} + \frac{\partial N'_{ij}}{\partial y}\frac{\partial v^*_i}{\partial z} + \frac{\partial N'_{ij}}{\partial z}\frac{\partial w^*_i}{\partial z}\right\}$$

$$- \frac{2}{3}C_3\frac{1}{Re}\left\{\frac{\partial N'_{ij}}{\partial z}\frac{\partial u^*_i}{\partial x} + \frac{\partial N'_{ij}}{\partial z}\frac{\partial v^*_i}{\partial y} + \frac{\partial N'_{ij}}{\partial z}\frac{\partial w^*_i}{\partial z}\right\} - \frac{\partial N'_{ij}}{\partial z}p^*_i + N'_{ij}\left\{\left(u^*_i\frac{\partial w^*_i}{\partial x}\right.\right.$$

$$\left.\left. + v^*_i\frac{\partial w^*_i}{\partial y} + w^*_i\frac{\partial w^*_i}{\partial z}\right) + C_2\left(w^*_i\frac{\partial u^*_i}{\partial x} + w^*_i\frac{\partial v^*_i}{\partial y} + w^*_i\frac{\partial w^*_i}{\partial z}\right)\right\}\, dV$$

$$= \int_{S_i} N'_{ij}\left\{\sigma^*_{xz}n_x + \sigma^*_{yz}n_y + \sigma^*_{zz}n_z\right\} dS$$

$$+ \int_{S_i}(C_1-1)\frac{1}{Re}N'_{ij}\left\{\frac{\partial u^*_i}{\partial z}n_x + \frac{\partial v^*_i}{\partial z}n_y + \frac{\partial w^*_i}{\partial z}n_z\right\} dS \quad \text{for } j=1,..K' \qquad 3.22.3$$

and $$-\int_{V_i} N''_{ij}\left\{\frac{\partial u^*_i}{\partial x} + \frac{\partial v^*_i}{\partial y} + \frac{\partial w^*_i}{\partial z}\right\} dV = 0 \qquad \text{for } j=1,..K'' \qquad 3.22.4$$

where S_i is the surface area of element i, and (n_x, n_y, n_z) is its unit outward pointing normal vector,

and where $u^*_i = \sum_{k=1}^{K'} u_{ik} N'_{ik}$, $v^*_i = \sum_{k=1}^{K'} v_{ik} N'_{ik}$, $w^*_i = \sum_{k=1}^{K'} w_{ik} N'_{ik}$

and $$p^*_i = \sum_{k=1}^{K'} p_{ik} N''_{ik} \qquad \text{for } i=1, ..N_e$$

The 3K' + K" equations that are thus produced can now be set up for each of the N_e elements in the flow domain. The equations are non-linear because certain of their terms contain products of summations which when expanded produce the full range of cross products of all the nodal velocity components in each element. It is this non-linearity, characteristic of viscous flows with moderate to high Reynolds numbers that causes convergence problems and makes the obtaining of a good approximate solution difficult. For flows with low Reynolds numbers the relative importance on the non-linear terms, often referred to also as the acceleration terms, is considerably less. If these terms are omitted the solution of the resulting simultaneous equations is easily obtainable, but the class of problems that can be solved is very

restricted. In this project all linear and non-linear terms in the Navier-Stokes equations will be retained.

The significance of the right hand side surface integrals that have resulted as a consequence of the application of the Divergence Theorem can be explained as follows. If any element i of the flow domain is isolated from the remainder of the flow, the fluid within this element will continue to move as it did when it was part of the whole, provided the stresses required to maintain its equilibrium are applied to the surface of the element. These surface stresses can then be replaced by a set of equivalent point forces acting in each of the three co-ordinate directions and at each of the nodes on the boundary of the element. The value of these equivalent nodal forces is found by ensuring that the rate of work done by the surface stresses is equal to that done by the point forces when an arbitrary increment is applied to each of the nodal velocity components of the element. For example, if the velocity in the x direction at node j is incremented by δu_j to $u_{ij} + \delta u_j$, the increment in velocity in the x direction at any other point in the element is $N'_{ij}\, \delta u_j$. The rate of work done by the surface stresses when δu_j is applied is therefore

$$\int_{S_i} N'_{ij}\, \delta u_j\, T_{ix}\, dS \qquad 3.23.1$$

where T_{ix} is the stress in the x direction on the surface of element i and is given by

$$T_{ix} = (\sigma_{xx}\, n_x + \sigma_{yx}\, n_y + \sigma_{zx}\, n_z)_{\text{on boundary of element i}}$$

The rate of work done by the equivalent nodal force, F_{ijx} in the x direction at node j is

$$F_{ijx}\, \delta u_j \qquad 3.23.2$$

Therefore $F_{ijx}\, \delta u_j = \int_{S_i} N'_{ij}\, \delta u_j\, (\sigma_{xx}\, n_x + \sigma_{yx}\, n_y + \sigma_{zx}\, n_z)\, dS$

$$\text{or} \quad F_{ijx} = \int_{S_i} N'_{ij} \, (\sigma_{xx} \, n_x + \sigma_{yx} \, n_y + \sigma_{zx} \, n_z) \, dS \qquad 3.24$$

A similar argument can be applied to each of the other two coordinate directions. The right hand side surface integrals containing the stress components are therefore simply the equivalent point forces whose effect is the same as that of the distributed surface stresses. The remaining surface integral occurring only in formulation A and containing the velocity gradients, has no physical significance of importance and in most cases can be made to vanish by suitable choice of boundary conditions.

It will be noticed that if node j is an internal node then the surface integrals of the j^{th} equation in each of equations 3.22.1-3 will be zero since on the boundary of element i, N'_{ij} is everywhere zero. Furthermore, it appears that the value of the stress components at each point on the surface of each element must be known beforehand so that the surface integrals may be evaluated to enable the system of equations to be solved. This will not be the case however, and it will be shown in the following section that by making a realistic assumption about the continuity of the pressure and the velocity gradients across element interfaces, only the surface integrals in equations that correspond to nodes on the outer surface of the whole flow domain need be retained. In most cases the boundary conditions of the problem will then supply sufficient information to enable the surface integrals to be evaluated or eliminated.

It should be mentioned at this point that when the phrase "equations corresponding to node k" is used, all that is implied is that the equations in question have been weighted by the shape functions N'_{ik} or N''_{ik}, and that the surface stress integrals containing the stress tensor components are the equivalent point forces acting at that node. It does not imply that the equations were derived at that node or that they are valid only at that node.

3.3 Assembly of Global Simultaneous Finite Element Equation System

Equations 3.22.1-4 could now be solved for each element individually without further manipulation, provided the value of the right hand side surface integrals can be evaluated for each of the 3K' momentum equations. To do this the velocity gradients as well as the pressure variations on the surface S_i of each element must be known. Since this implies that the solution should be known before the equations can be solved, this approach is not very useful. A better technique, and one which is universally used in the finite element method, is the one in which the equations corresponding to nodes common to neighbouring elements are added in such a way as to enable the surface integrals of the momentun equations to cancel each other. This eliminates the necessity of evaluating these integrals for all momentum equations except those corresponding to nodes on the boundary of the flow domain. At these nodes, either the fluid velocity or its stress state must be specified. This is why it was emphasized in Section 3.1 that at every point on the flow boundary either the velocity or the stress components must be known for each coordinate direction. If the velocity is given, then the equations corresponding to the velocity at these nodes become redundant and there is no need to evaluate the surface integrals. If the stress is specified, then the surface integrals can be evaluated without further ado.

In order to explain the process of assembling the equations for each element into one global equation system, it will be necessary to refer to the diagrams in Figure 3.1 which, for the sake of convenience, show only a two-dimensional element arrangement rather than the more general three-dimensional one. Each of the four diagrams shows a typical node positioning in a general element mesh and each case will be considered individually as follows.

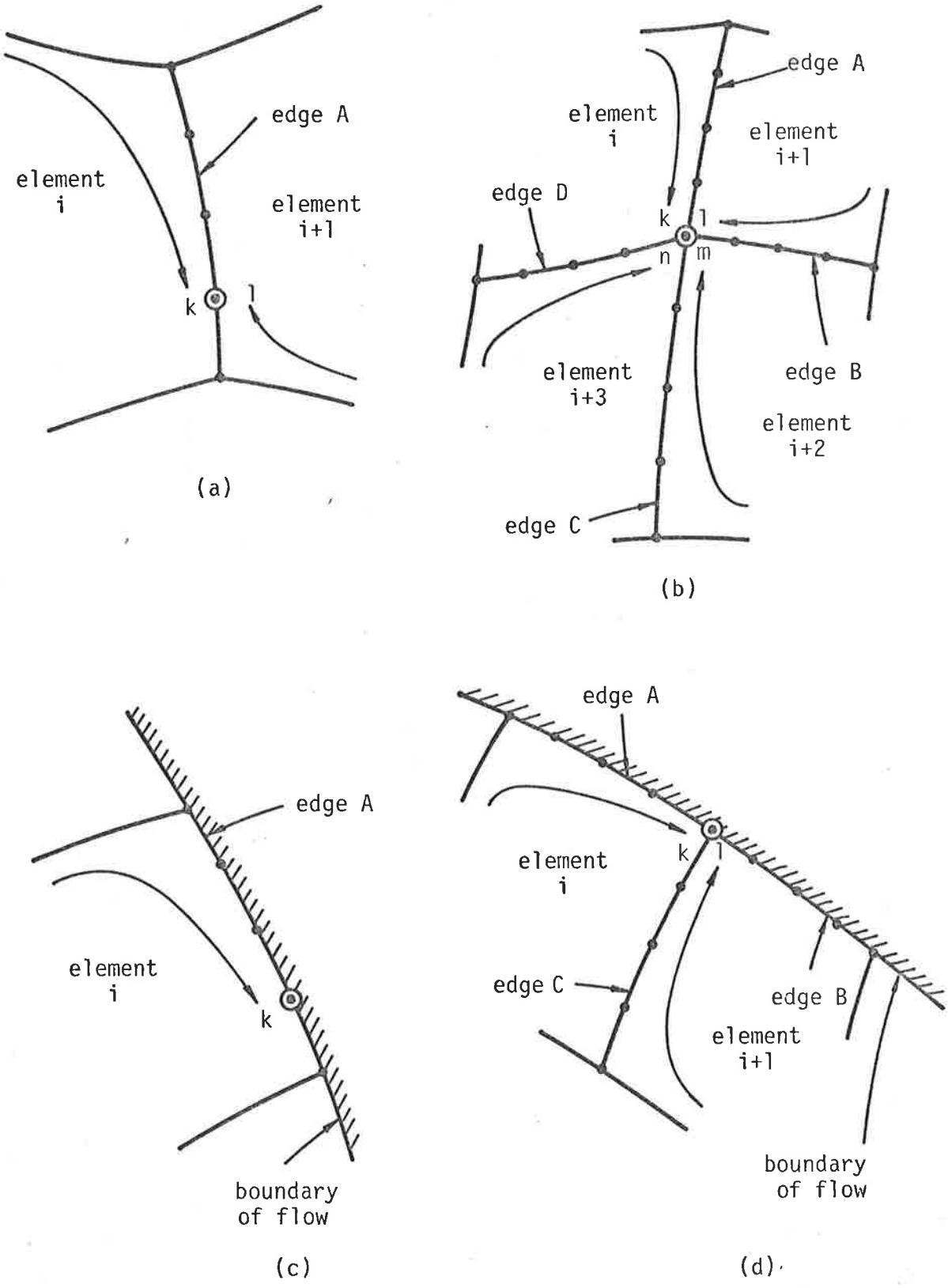

Figue 3.1 Typical Nodal Positionings. (a) internal edge, (b) internal corner, (c) boundary edge, (d) boundary corner.

Consider diagram a in Figure 3.1 showing a typical internal edge. Let this edge, common to elements i and (i+1) be called edge A. All nodes on edge A, except the two corner nodes will have associated velocity shape functions in both elements i and (i+1) that are zero everywhere except along the common edge A. This means that if (a) the values of the shape functions N'_{ik} and $N'_{(i+1)1}$ are the same at all points on edge A, and (b) the value of the velocity gradients and pressure along edge A in element i is the same as their value along edge A in element (i+1), then for the x direction,

$$\int_{S_i} N'_{ik}(\sigma_{xx}n_x + \sigma_{yx}n_y)_{eli}\, dS + \int_{S_{i+1}} N'_{(i+1)1}\,(\sigma_{xx}n_x + \sigma_{yx}n_y)_{el(i+1)}dS$$

$$= \int_{\text{edge A}} N'_{ik}(\sigma_{xx}n_x + \sigma_{yx}n_y)_{eli}dS + \int_{\text{edge A}} N'_{(i+1)1}(\sigma_{xx}n_x + \sigma_{yx}n_y)_{el(i+1)}dS$$

$$= \int_{\text{edge A}} N'_{ik}(\sigma_{xx}n_x + \sigma_{yx}n_y)_{eli}dS - \int_{\text{edge A}} N'_{ik}(\sigma_{xx}n_x + \sigma_{yx}n_y)_{eli}dS$$

$$= 0 \qquad 3.25.1$$

and for the y direction,

$$\int_{S_i} N'_{ik}(\sigma_{xy}n_x + \sigma_{yy}n_y)_{eli}dS + \int_{S_{i+1}} N'_{(i+1)1}(\sigma_{xy}n_x + \sigma_{yy}n_y)_{el(i+1)}dS$$

$$= 0 \qquad 3.25.2$$

where the k^{th} node of element i coincides with the 1^{th} node of element (i+1) and lies on edge A. By the same argument

$$\int_{S_i} N'_{ik}\left(\frac{\partial u_i^*}{\partial x}n_x + \frac{\partial v_i^*}{\partial x}n_y\right)_{eli}dS + \int_{S_{i+1}} N'_{(i+1)1}\left(\frac{\partial u_i^*}{\partial x}n_x + \frac{\partial v_i^*}{\partial x}n_y\right)_{el(i+1)}dS$$

$$= 0 \qquad 3.26.1$$

and

$$\int_{S_i} N'_{ik}\left(\frac{\partial u_i^*}{\partial y}n_x + \frac{\partial v_i^*}{\partial y}n_y\right)_{eli}dS + \int_{S_{i+1}} N'_{(i+1)1}\left(\frac{\partial u_i^*}{\partial y}n_x + \frac{\partial v_i^*}{\partial y}n_y\right)_{el(i+1)}dS$$

$$= 0 \qquad 3.26.2$$

The change in sign results from the fact that the outward facing normal vector for element (i+1) along edge A is of the same magnitude as, but in the opposite direction to the outward facing normal vector for element

i. By adding the momentum equations corresponding to node k of element i in the x and y directions, to the equations corresponding to node l of element (i+1), the above combinations of surface integrals are obtained. By using the argument presented above the right hand sides of the combined equations can then be reduced to zero. This process can be applied to the momentum as well as the continuity equations corresponding to all "non-corner" nodes on all internal edges.

A similar but slightly more involved argument can be applied to the momentum equations corresponding to any internal corner node that belongs to three or more elements. Consider diagram b in Figure 3.1 showing a typical internal corner node shared by four elements, i, i+1, i+2, and i+3. Let the four edges common to the four pairs of adjacent elements be called edges A to D. The velocity shape functions in these four elements for the corner node are zero everywhere except along the common edges A to D. If at all points along these edges (a) the shape functions for neighbouring elements have the same value, and (b) the value of the velocity gradients and pressure for adjacent elements is the same, then for the x direction,

$$\int_{S_i} N'_{ik}(\sigma_{xx}n_x + \sigma_{yx}n_y)_{eli}\,dS + \int_{S_i} N'_{(i+1)l}(\sigma_{xx}n_x + \sigma_{yx}n_y)_{el(i+1)}\,dS$$

$$+ \int_{S_i} N'_{(i+2)m}(\sigma_{xx}n_x + \sigma_{yx}n_y)_{el(i+2)}\,dS + \int_{S_{i+3}} N'_{(i+3)n}(\sigma_{xx}n_x + \sigma_{yx}n_y)_{el(i+3)}\,dS$$

$$= \int_{\text{edge D}} N'_{ik}(\sigma_{xx}n_x + \sigma_{yx}n_y)_{eli}\,dS + \int_{\text{edge A}} N'_{ik}(\sigma_{xx}n_x + \sigma_{yx}n_y)_{eli}\,dS$$

$$+ \int_{\text{edge A}} N'_{(i+1)l}(\sigma_{xx}n_x + \sigma_{yx}n_y)_{el(i+1)}\,dS + \int_{\text{edge B}} N'_{(i+1)l}(\sigma_{xx}n_x$$

$$+ \sigma_{yx}n_y)_{el(i+1)}\,dS + \int_{\text{edge B}} N'_{(i+2)m}(\sigma_{xx}n_x + \sigma_{yx}n_y)_{el(i+2)}\,dS$$

$$+ \int_{\text{edge C}} N'_{(i+2)m}(\sigma_{xx}n_x + \sigma_{yx}n_y)_{el(i+2)}\,dS + \int_{\text{edge C}} N'_{(i+3)n}(\sigma_{xx}n_x$$

$$+ \sigma_{yx}n_y)_{el(i+3)}\,dS + \int_{\text{edge D}} N'_{(i+3)n}(\sigma_{xx}n_x + \sigma_{yx}n_y)_{el(i+3)}\,dS$$

$$= \int_{\text{edge D}} N'_{ik}(\sigma_{xx}n_x + \sigma_{yx}n_y)_{eli}dS - \int_{\text{edge A}} N'_{(i+1)l}(\sigma_{xx}n_x + \sigma_{yx}n_y)_{el(i+1)}dS$$

$$+ \int_{\text{edge A}} N'_{(i+1)l}(\sigma_{xx}n_x + \sigma_{yx}n_y)_{el(i+1)}dS - \int_{\text{edge B}} N'_{(i+2)m}(\sigma_{xx}n_x$$

$$+ \sigma_{yx}n_y)_{el(i+2)}dS + \int_{\text{edge B}} N'_{(i+2)m}(\sigma_{xx}n_x + \sigma_{yx}n_y)_{el(i+2)}dS$$

$$- \int_{\text{edge C}} N'_{(i+3)n}(\sigma_{xx}n_x + \sigma_{yx}n_y)_{el(i+3)}dS + \int_{\text{edge C}} N'_{(i+3)n}(\sigma_{xx}n_x$$

$$+ \sigma_{yx}n_y)_{el(i+3)}dS - \int_{\text{edge D}} N'_{ik}(\sigma_{xx}n_x - \sigma_{yx}n_y)_{eli}dS = 0 \qquad 3.27.1$$

and for the y direction

$$\int_{S_i} N'_{ik}(\sigma_{xy}n_x + \sigma_{yy}n_y)_{eli}dS + \int_{S_{i+1}} N'_{(i+1)l}(\sigma_{xy}n_x + \sigma_{yy}n_y)_{el(i+1)}dS$$

$$+ \int_{S_{i+2}} N'_{(i+2)m}(\sigma_{xy}n_x + \sigma_{yy}n_y)_{el(i+2)}dS + \int_{S_{i+3}} N'_{(i+3)n}(\sigma_{xy}n_x$$

$$+ \sigma_{yy}n_y)_{el(i+3)}dS = 0 \qquad 3.27.2$$

where the k^{th} node of element i, the l^{th} node of element (i+1), the m^{th} node of element (i+2) and the n^{th} node of element (i+3) are all coincident with the corner node at the right hand end of edge D. Also by the same argument

$$\int_{S_i} N'_{ik}\left(\frac{\partial u_i^*}{\partial x}n_x + \frac{\partial v_i^*}{\partial x}n_y\right)_{eli}dS + \int_{S_{i+1}} N'_{(i+1)l}\left(\frac{\partial u_i^*}{\partial x}n_x + \frac{\partial v_i^*}{\partial x}n_y\right)_{el(i+1)}dS$$

$$+ \int_{S_{i+2}} N'_{(i+2)m}\left(\frac{\partial u_i^*}{\partial x}n_x + \frac{\partial v_i^*}{\partial x}n_y\right)_{el(i+2)}dS + \int_{S_{i+3}} N'_{(i+3)n}\left(\frac{\partial u_i^*}{\partial x}n_x\right.$$

$$\left. + \frac{\partial v_i^*}{\partial x}n_y\right)_{el(i+3)}dS = 0 \qquad 3.28.1$$

and $$\int_{S_i} N'_{ik}\left(\frac{\partial u_i^*}{\partial y}n_x + \frac{\partial v_i^*}{\partial y}n_y\right)_{eli}dS + \int_{S_{i+1}} N'_{(i+1)l}\left(\frac{\partial u_i^*}{\partial y}n_x + \frac{\partial v_i^*}{\partial y}n_y\right)_{el(i+1)}dS$$

$$+ \int_{S_{i+2}} N'_{(i+2)m}\left(\frac{\partial u_i^*}{\partial y}n_x + \frac{\partial v_i^*}{\partial y}n_y\right)_{el(i+2)}dS + \int_{S_{i+3}} N'_{(i+3)n}\left(\frac{\partial u_i^*}{\partial y}n_x + \frac{\partial v_i^*}{\partial y}n_y\right)_{el(i+3)}dS = 0 \qquad 3.28.2$$

Thus by adding the momentum equations in the x and y directions corresponding to node k of element i, node l of element (i+1), node m of element (i+2) and node n of element (i+3) the combined right hand side of the resultant equation reduces to zero. This process can be applied to the momentum and Continuity equations corresponding to all corner nodes not on the boundary of the flow domain. Although the above case considered four elements neighbouring the corner node, it can easily be verified that any number of elements greater than or equal to three, can be treated by the same process.

The surface integrals in the equations corresponding to nodes on the boundary of the flow domain cannot be so easily eliminated. Consider a typical element i with one side, called edge A, on the boundary of the flow domain as shown in diagram c of Figure 3.1. The momentum equations corresponding to any node on this edge have right hand sides given by

$$\int_{S_i} N'_{ik}(\sigma_{xx}n_x + \sigma_{yx}n_y)_{eli}dS + \int_{S_i} N'_{ik}\left(\frac{\partial u_i^*}{\partial x}n_x + \frac{\partial v_i^*}{\partial x}n_y\right)_{eli}dS \qquad 3.29.1.1$$

$$\text{and} \quad \int_{S_i} N'_{ik}(\sigma_{xy}n_x + \sigma_{yy}n_y)_{eli}dS + \int_{S_i} N'_{ik}\left(\frac{\partial u_i^*}{\partial y}n_x + \frac{\partial v_i^*}{\partial y}n_y\right)_{eli}dS \qquad 3.29.1.2$$

where the k^{th} node of element i lies on edge A. If node k is a "non-corner" node then N'_{ik} is zero everywhere except along edge A, and the above integrals reduce to

$$\int_{\text{edge A}} N'_{ik}(\sigma_{xx}n_x + \sigma_{yx}n_y)_{eli}dS + \int_{\text{edge A}} N'_{ik}\left(\frac{\partial u_i^*}{\partial x}n_x + \frac{\partial v_i^*}{\partial x}n_y\right)_{eli}dS \qquad 3.29.2.1$$

$$\text{and} \int_{\text{edge A}} N'_{ik}(\sigma_{xy}n_x + \sigma_{yy}n_y)_{eli}dS + \int_{\text{edge A}} N'_{ik}\left(\frac{\partial u_i^*}{\partial y}n_x + \frac{\partial v_i^*}{\partial y}n_y\right)_{eli}dS \qquad 3.29.2.2$$

Nothing further needs to be done with these since they can now easily be either evaluated if the velocity gradients and pressure (stress tensor components) are specified, or eliminated if the velocity is specified since the corresponding equations then become redundant.

Finally if the k^{th} node of element i is a corner node on the boundary of the flow domain and coincides with the l^{th} node of element (i+1) as shown in diagram d in Figure 3.1, then the shape functions N'_{ik} and $N'_{(i+1)l}$ will be zero everywhere except on the boundary edges A and B and on the common edge C. If at all points along edge C (a) the shape functions for element i and (i+1) have the same value, and (b) the value of the velocity gradients and pressure for element i is the same as their value for element i+1, then for the x direction

$$\int_{S_i} N'_{ik}(\sigma_{xx}n_x + \sigma_{yx}n_y)_{eli}\,dS + \int_{S_i} N'_{ik}\left(\frac{\partial u_i^*}{\partial x}n_x + \frac{\partial v_i^*}{\partial x}n_y\right)_{eli}dS + \int_{S_{i+1}} N'_{(i+1)l}(\sigma_{xx}n_x + \sigma_{yx}n_y)_{el(i+1)}\,dS + \int_{S_{i+1}} N'_{(i+1)l}\left(\frac{\partial u_i^*}{\partial x}n_x + \frac{\partial v_i^*}{\partial x}n_y\right)_{el(i+1)}dS$$

$$= \int_{\text{edge A}} N'_{ik}(\sigma_{xx}n_x + \sigma_{yx}n_y)_{eli}\,dS + \int_{\text{edge C}} N'_{ik}(\sigma_{xx}n_x + \sigma_{yx}n_y)_{eli}\,dS + \int_{\text{edge A}} N'_{ik}\left(\frac{\partial u_i^*}{\partial x}n_x + \frac{\partial v_i^*}{\partial x}n_y\right)_{eli}dS + \int_{\text{edge C}} N'_{ik}\left(\frac{\partial u_i^*}{\partial x}n_x + \frac{\partial v_i^*}{\partial x}n_y\right)_{eli}dS + \int_{\text{edge C}} N'_{(i+1)l}(\sigma_{xx}n_x + \sigma_{yx}n_y)_{el(i+1)}\,dS + \int_{\text{edge B}} N'_{(i+1)l}(\sigma_{xx}n_x + \sigma_{yx}n_y)_{el(i+1)}\,dS + \int_{\text{edge C}} N'_{(i+1)l}\left(\frac{\partial u_i^*}{\partial x}n_x + \frac{\partial v_i^*}{\partial x}n_y\right)_{el(i+1)}dS + \int_{\text{edge B}} N'_{(i+1)l}\left(\frac{\partial u_i^*}{\partial x}n_x + \frac{\partial v_i^*}{\partial x}n_y\right)_{el(i+1)}dS$$

$$= \int_{\text{edge A}} N'_{ik}(\sigma_{xx}n_x + \sigma_{yx}n_y)_{eli}\,dS + \int_{\text{edge C}} N'_{ik}(\sigma_{xx}n_x + \sigma_{yx}n_y)_{eli}\,dS + \int_{\text{edge A}} N'_{ik}\left(\frac{\partial u_i^*}{\partial x}n_x + \frac{\partial v_i^*}{\partial x}n_y\right)_{eli}dS + \int_{\text{edge C}} N'_{ik}\left(\frac{\partial u_i^*}{\partial x}n_x + \frac{\partial v_i^*}{\partial x}n_y\right)_{eli}dS$$

$$
\begin{aligned}
&- \int_{\text{edge C}} N'_{ik}(\sigma_{xx}n_x + \sigma_{yx}n_y)_{eli}\,dS + \int_{\text{edge B}} N'_{(i+1)1}(\sigma_{xx}n_x + \sigma_{yx}n_y)_{el(i+1)}\,dS \\
&- \int_{\text{edge C}} N'_{ik}\left(\frac{\partial u_i^*}{\partial x}n_x + \frac{\partial v_i^*}{\partial x}n_y\right)_{eli}\,dS + \int_{\text{edge B}} N'_{(i+1)1}\left(\frac{\partial u_i^*}{\partial x}n_x + \frac{\partial v_i^*}{\partial x}n_y\right)_{el(i+1)}\,dS \\
&= \int_{\text{edge A}} N'_{ik}(\sigma_{xx}n_x + \sigma_{yx}n_y)_{eli}\,dS + \int_{\text{edge B}} N'_{(i+1)1}(\sigma_{xx}n_x + \sigma_{yx}n_y)_{el(i+1)}\,dS \\
&+ \int_{\text{edge A}} N'_{ik}\left(\frac{\partial u_i^*}{\partial x}n_x + \frac{\partial v_i^*}{\partial x}n_y\right)_{eli}\,dS + \int_{\text{edge B}} N'_{(i+1)1}\left(\frac{\partial u_i^*}{\partial x}n_x + \frac{\partial v_i^*}{\partial x}n_y\right)_{el(i+1)}\,dS
\end{aligned}
\qquad 3.30.1
$$

and for the y direction

$$
\begin{aligned}
&\int_{S_i} N'_{ik}(\sigma_{xy}n_x + \sigma_{yy}n_y)_{eli}\,dS + \int_{S_i} N'_{ik}\left(\frac{\partial u_i^*}{\partial y}n_x + \frac{\partial v_i^*}{\partial y}n_y\right)_{eli}\,dS + \int_{S_{i+1}} N'_{(i+1)1}(\sigma_{xy}n_x \\
&\quad + \sigma_{yy}n_y)_{el(i+1)}\,dS + \int_{S_{i+1}} N'_{(i+1)1}\left(\frac{\partial u_i^*}{\partial y}n_x + \frac{\partial v_i^*}{\partial y}n_y\right)_{el(i+1)}\,dS \\
&= \int_{\text{edge A}} N'_{ik}(\sigma_{xy}n_x + \sigma_{yy}n_y)_{eli}\,dS + \int_{\text{edge B}} N'_{(i+1)1}(\sigma_{xy}n_x + \sigma_{yy}n_y)_{el(i+1)}\,dS \\
&+ \int_{\text{edge A}} N'_{ik}\left(\frac{\partial u_i^*}{\partial y}n_x + \frac{\partial v_i^*}{\partial y}n_y\right)_{eli}\,dS + \int_{\text{edge B}} N'_{(i+1)1}\left(\frac{\partial u_i^*}{\partial y}n_x + \frac{\partial v_i^*}{\partial y}n_y\right)_{el(i+1)}\,dS
\end{aligned}
\qquad 3.30.2
$$

The resulting boundary integrals can again be either evaluated or eliminated and no further manipulation is required. Thus the right hand sides of the equations produced by adding the momentum equations in the x and y directions corresponding to node k of element i to those corresponding to node 1 of element (i+1), can be reduced to boundary integrals that are easily handled. This result can be extended to apply

to the momentum equations corresponding to any boundary corner node that belongs to two or more elements.

From the above discussion it can be seen that the evaluation of the surface integrals on the right hand side of the momentum equations corresponding to any node can be avoided by adding all the respective element equations corresponding to that node. This fact forms the basis for the assembly process. Although only the two-dimensional case has been presented here, it can easily be shown that similar results are obtainable in three dimensions. It should also be noted that although the element continuity equations have no surface integrals on their right hand sides, the above assembly process is equally applicable to them. Finally, all equations corresponding to nodes that lie within an element's volume and not on its surface also have no surface integrals on their right hand sides. These equations need no special assembly process and can simply be included in the global equation system. The actual assembly process can therefore be described as follows. The node for which the global equations are to be asssembled is selected, the element equations for all elements to which that node belongs are examined, and the three momentum and one continuity equations corresponding to that node within each of these equation sub-systems are extracted. By respectively adding these equations, the three global momentum and one global continuity equations corresponding to the selected node are then obtained. Before the element equations are combined it is necessary to ensure that they are all expressed in terms of the same coordinate system. If not, suitable transformations must be applied so that the global equations are all expressed in terms of one global coordinate system.

The first two steps towards obtaining a finite element solution are now established. Firstly the $3K' + K''$ equations for each element at element level are set up and secondly the global equation system is assembled so that, if N_v and N_p are the numbers of velocity and

pressure nodes respectively, within the flow domain, a system of $3N_v + N_p$ simultaneous non-linear equations now remains to be solved. Before proceeding to the solution of these equations however, it is necessary to say something about the continuity of velocity, pressure and velocity gradients across element interfaces. Two major assumptions with regard to the continuity of these quantities were made during the above discussion explaining the assembly process. Firstly it was assumed that any node on an edge common to two elements had associated velocity shape functions in the two elements, that have the same value at all points on the comon edge. For this assumption to be true it is necessary that the velocity shape functions be defined uniquely along each edge of all elements. Therefore only unique functions f_{ij} that satisfy the conditions

$$f_{ij} = 1 \text{ at node } j$$
$$= 0 \text{ at all other nodes in element } i,$$

can be used as velocity shape functions. Such functions ensure continuity of the velocity variables across element interfaces.

Secondly, it was assumed that the stress along any edge common to two elements is the same in both elements; that is, that the velocity gradients and pressure are continuous across element interfaces. By choosing suitable pressure shape functions the pressure continuity can be ensured. However, it is not so easy to guarantee continuity of velocity gradients between elements. To achieve this, additional slope parameters must be introduced and velocity shape functions that ensure continuity of velocity gradients as well as velocity must be found. The difficulty encountered, firstly in establishing a finite element with the above characteristics, and secondly in solving the resulting equation system which will increase considerably in size, makes this condition very difficult to satisfy. As a result, in this study only elements capable of ensuring velocity and pressure continuity will be used. Although this is contrary to what is assumed when the assembly

process is used, to carry the idea of velocity gradient continuity any further would be a major investigation in itself. Therefore no further consideration is given to it in this thesis except to say that this contradiction could be a source of error and instability and therefore should be investigated in future work.

3.4 Solution of Global Simultaneous Equation System

The first two steps towards obtaining a finite element solution to a general viscous flow problem are now completed. That is, the Navier-Stokes equations have been formulated in terms of the finite element procedure, and the global simultaneous non-linear equation system has been constructed. The final two steps will now be discussed in this section. The first is the incorporation of the boundary conditions, and the second, the solution of the final equation system resulting in the required values of velocity components and pressure at all nodes in the flow domain.

The boundary conditions are very easily incorporated in the equation system which, once assembled, contains equations of two types. The first, corresponding to variables at nodes in the interior of the flow domain, all have zero right hand sides, while the second, corresponding to variables at nodes on the outer boundary of the flow domain, all have surface integrals on their right hand sides. Only equations of the second type are normally affected by the application of the boundary conditions. If a velocity component or the pressure is specified at a boundary node the global equation corresponding to that variable is not required and therefore eliminated from the equation system. The effect of the specification is imposed on the remainder of the system by subtracting from the right hand side of each of the other equations, the product of the value of the variable and the coefficient of the linear term corresponding to that variable in each equation. The

non-linear terms are modified by substituting the specified variable into each equation and collecting like terms. If the value of the variable is zero, all terms that contain that variable in each equation are simply eliminated. It should be noted that variables at nodes other than the ones on the outer boundary of the flow domain may be specified in the boundary conditions of a problem. The inclusion of these specifications is identical to that for variables at nodes on the outer boundary of the flow except that in these cases, equations of the first type are involved.

The other type of boundary condition, namely the specification of the stress components and the velocity gradients in a given direction is even more easily incorporated. The values of the stress components and the velocity gradients are simply substituted in the surface integrals on the right hand sides of the remaining type two equations and the integrals evaluated. Once this is done, the right hand sides of all equations should be known, and the number of non-linear global equations in the system should equal the number of unknown nodal velocity components and pressures. The equations are now ready to be solved.

The method that has been recommended by the majority of previous researchers for solving the resulting non-linear simultaneous equation system and the one that was therefore chosen for this study, is the Multi-dimensional Newton-Raphson Iterative Solution Scheme. It can be described basically as a technique for finding the solution to a system of non-linear equations by solving a number of successive related linear systems. That is, the problem is changed from solving one non-linear to several linear systems of equations.

To explain the procedure, consider a system of n non-linear equations expressed in terms of n unknowns $\underset{\sim}{x} = (x_1, x_2, \ldots, x_n)$ and given by

$$f_i(\underset{\sim}{x}) = 0 \quad \text{for } i=1, \ldots n \qquad 3.31$$

A second system of equations can now be constructed by differentiating each of the equations in the first system with respect to each of the n unknowns, and using these derivatives as the coefficients of n terms in the corresponding equations in the second system. Since the initial equation system is non-linear, the above derivatives are not necessarily constant and therefore the second equation system is also non-linear. However by adopting an iterative approach in which an approximate solution, either an initial guess or the solution from the previous iteration, is used to evaluate the derivative coefficients, the second system of equations can be linearized and solved by the usual methods to give an improved approximate solution. This procedure can be conveniently expressed in the equation for the m^{th} iteration of the Newton-Raphson method

$$\sum_{j=1}^{n} J_{ij}(\underset{\sim}{x}^m)\ \delta x_j^{m+1} = -f_i(\underset{\sim}{x}^m) \text{ for } i=1, \ldots n \qquad 3.32$$

and for m=0, ... M

where $J_{ij}(\underset{\sim}{x}^m) = \dfrac{\partial f_i(\underset{\sim}{x})}{\partial x_j}$ evaluated for $\underset{\sim}{x}=\underset{\sim}{x}^m$ 3.33.1

$f_i(\underset{\sim}{x}^m)$ is the value of the equations when $\underset{\sim}{x}=\underset{\sim}{x}^m$ 3.33.2

and $\delta x_j^{m+1} = x_j^{m+1} - x_j^m$ 3.33.3

where $\underset{\sim}{x}^m = (x_1^m, x_2^m, \ldots x_n^m)$ is an estimate of the solution, either an initial guess when m=0 or the solution from the previous iteration, and $\underset{\sim}{x}^{m+1} = (x_1^{m+1}, x_2^{m+1}, \ldots x_n^{m+1})$ is the new estimate of the solution.

It will be noted that at each iteration $\delta \underset{\sim}{x}^{m+1}$, the change in the unknowns is evaluated rather than the unknowns themselves. To start the procedure an initial estimate $\underset{\sim}{x}^0$ of the solution is made with $\underset{\sim}{x}^0$ usually being selected as the null vector. At each subsequent step a new set of equation coefficients $J_{ij}(\underset{\sim}{x}^m)$ are evaluated based upon the solution of the previous step and a change to the previous estimate

of the solution is calculated. When this change becomes sufficiently small the required solution is obtained and the process stopped. The matrix containing the derivative coefficients $J_{ij}(\underset{\sim}{x}^m)$ is commonly known as the Jacobian Matrix and to avoid confusion in the following pages, the system of equations that has $J_{ij}(\underset{\sim}{x}^m)$ as its coefficients at the m^{th} iterative step of the Newton-Raphson method, will be subsequently referred to as the corresponding Jacobian system of equations.

This technique is directly applicable to the solving of the equations derived in Section 3.2 and assembled in Section 3.3. However, rather than assemble the element equations before constructing the global Jacobian equation system it has been found more economical and easier to program if Jacobian equation systems are constructed for each element at element level and these then assembled in the usual manner. Since the assembly process simply involves the addition of element equations, it can easily be shown that the resultant global Jacobian system is the same in both cases, since the derivatives of a sum of equations is identical to the sum of the derivatives of the individual equations. This alternative approach however, presents a slight difficulty when the velocity components or pressure are specified in the boundary conditions since the equations that are actually solved in each iteration are expressed in terms of the changes to the unknown nodal parameters rather than in terms of the nodal parameters themselves. However by letting the first estimate of the solution be zero for all variables and by applying, during the first iteration, boundary conditions that state that the changes in the specified variables equal the value of the variables themselves, then the results of the first iteration can be made to give the required values for the specified velocity components and pressures. In all subsequent iterations, since only changes to all variables are calculated, by ensuring that all changes to the specified velocity components and pressures are zero, the specified variables will retain their correct values when the procedure ends.

The Newton-Raphson method can therefore be used successfully to obtain a solution to the general non-linear simultaneous equation system resulting from the finite element formulation of the Navier-Stokes equations.

To conclude this chapter all that remains to be done is firstly to set up the jk^{th} component of the matrix of coefficients R_i of the equations for element i, and secondly to derive and set up the jk^{th} component of the matrix of coefficients S_i of the Jacobian equations for element i. The full matrix R_i can be obtained by extracting the coefficients of the 3K' + K" variable terms from the 3K' + K" simultaneous equations produced when the approximations given by equations 3.14.1-4 are substituted into equations 3.22.1-4. Since the number of pressure nodes per element K" is less than the number of velocity nodes K', it is not possible to set up the general jk^{th} component of R_i, because the number of equations corresponding to the j^{th} node of element i is either three, if it is a velocity node only, or four if it is a pressure node as well. To overcome this, additional continuity equations consisting of all zeros and corresponding to velocity nodes that are not also pressure nodes, are introduced. To remain consistent, additional zero pressure terms must also be introduced into all equations. The simplest way of doing this is to set up a continuity equation and a pressure term corresponding to all K' velocity nodes and then set $N''_{ij}=0$ or $N''_{ik}=0$ everywhere whenever j or k corresponds to a velocity node that is not a pressure node as well. This results in a system of 4K' equations of which K'-K" are all zero. The general jk^{th} submatrix of R_i for element i is therefore:

$$
[R_i]_{jk} = \left[
\begin{array}{ll}
\dfrac{1}{Re}\displaystyle\int_{V_i}\Big\{(1+C_1-\frac{2}{3}C_3)\frac{\partial N'_{ij}}{\partial x}\frac{\partial N'_{ik}}{\partial x} & \dfrac{1}{Re}\displaystyle\int_{V_i}\Big\{C_1\frac{\partial N'_{ij}}{\partial y}\frac{\partial N'_{ik}}{\partial x} \\
+\dfrac{\partial N'_{ij}}{\partial y}\dfrac{\partial N'_{ik}}{\partial y}+\dfrac{\partial N'_{ij}}{\partial z}\dfrac{\partial N'_{ik}}{\partial z}\Big\}dV & -\dfrac{2}{3}C_3\dfrac{\partial N'_{ij}}{\partial x}\dfrac{\partial N'_{ik}}{\partial y}\Big\}dV \\
+\displaystyle\int_{V_i}\Big\{N'_{ij}\,N'_{ik}\sum_{l=1}^{K'}\Big(\frac{\partial N'_{il}}{\partial x}u_{il}\Big) & +\displaystyle\int_{V_i}\Big\{N'_{ij}\,N'_{ik}\sum_{l=1}^{K'}\Big(\frac{\partial N'_{il}}{\partial y}u_{il}\Big) \\
+C_2\,N'_{ij}\dfrac{\partial N'_{ik}}{\partial x}\sum_{l=1}^{K'}(N'_{ik}u_{il})\Big\}dV & +C_2\,N'_{ij}\dfrac{\partial N'_{ik}}{\partial y}\sum_{l=1}^{K'}(N'_{il}u_{il})\Big\}dV \\
\hline
\dfrac{1}{Re}\displaystyle\int_{V_i}\Big\{C_1\frac{\partial N'_{ij}}{\partial x}\frac{\partial N'_{ik}}{\partial y} & \dfrac{1}{Re}\displaystyle\int_{V_i}\Big\{\frac{\partial N'_{ij}}{\partial x}\frac{\partial N'_{ik}}{\partial x}+(1+C_1-\frac{2}{3}C_3) \\
-\dfrac{2}{3}C_3\dfrac{\partial N'_{ij}}{\partial y}\dfrac{\partial N'_{ik}}{\partial x}\Big\}dV & \dfrac{\partial N'_{ij}}{\partial y}\dfrac{\partial N'_{ik}}{\partial y}+\dfrac{\partial N'_{ij}}{\partial z}\dfrac{\partial N'_{ik}}{\partial z}\Big\}dV \\
+\displaystyle\int_{V_i}\Big\{N'_{ij}\,N'_{ik}\sum_{l=1}^{K'}\Big(\frac{\partial N'_{il}}{\partial x}v_{il}\Big) & +\displaystyle\int_{V_i}\Big\{N'_{ij}\,N'_{ik}\sum_{l=1}^{K'}\Big(\frac{\partial N'_{il}}{\partial y}v_{il}\Big) \\
+C_2\,N'_{ij}\dfrac{\partial N'_{ik}}{\partial x}\sum_{l=1}^{}(N'_{il}v_{il})\Big\}dV & +C_2\,N'_{ij}\dfrac{\partial N'_{ik}}{\partial y}\sum_{l=1}^{K'}(N'_{il}v_{il})\Big\}dV \\
\hline
\dfrac{1}{Re}\displaystyle\int_{V_i}\Big\{C_1\frac{\partial N'_{ij}}{\partial x}\frac{\partial N'_{ik}}{\partial z} & \dfrac{1}{Re}\displaystyle\int_{V_i}\Big\{C_1\frac{\partial N'_{ij}}{\partial y}\frac{\partial N'_{ik}}{\partial z} \\
-\dfrac{2}{3}C_3\dfrac{\partial N'_{ij}}{\partial z}\dfrac{\partial N'_{ik}}{\partial x}\Big\}dV & -\dfrac{2}{3}\dfrac{\partial N'_{ij}}{\partial z}\dfrac{\partial N'_{ik}}{\partial y}\Big\}dV \\
+\displaystyle\int_{V_i}\Big\{N'_{ij}\,N'_{ik}\sum_{l=1}^{K'}\Big(\frac{\partial N'_{il}}{\partial x}w_{il}\Big) & +\displaystyle\int_{V_i}\Big\{N'_{ij}\,N'_{ik}\sum_{l=1}^{K'}\Big(\frac{\partial N'_{il}}{\partial y}w_{il}\Big) \\
+C_2\,N'_{ij}\dfrac{\partial N'_{ik}}{\partial x}\sum_{l=1}^{K'}(N'_{il}w_{il})\Big\}dV & +C_2\,N'_{ij}\dfrac{\partial N'_{ik}}{\partial y}\sum_{l=1}^{K'}(N'_{il}w_{il})\Big\}dV \\
\hline
-\displaystyle\int_{V_i}\Big\{N''_{ij}\frac{\partial N'_{ik}}{\partial x}\Big\}dV & -\displaystyle\int_{V_i}\Big\{N''_{ij}\frac{\partial N'_{ik}}{\partial y}\Big\}dV
\end{array}
\right]
$$

Matrix continues overleaf ...

$$\frac{1}{Re}\int_{V_i}\{C_1\frac{\partial N'_{ij}}{\partial z}\frac{\partial N'_{ik}}{\partial x} - \frac{2}{3}C_3\frac{\partial N'_{ij}}{\partial x}\frac{\partial N'_{ik}}{\partial z}\}dV + \int_{V_i}\{N'_{ij}N'_{ik}\sum_{l=1}^{K'}(\frac{\partial N'_{il}}{\partial z}u_{il}) + C_2 N'_{ij}\frac{\partial N'_{ik}}{\partial z}\sum_{l=1}^{K'}(N'_{il}u_{il})\}dV \qquad -\int_{V_i}\{\frac{\partial N'_{ij}}{\partial x}N''_{ik}\}dV$$

$$\frac{1}{Re}\int_{V_i}\{C_1\frac{\partial N'_{ij}}{\partial z}\frac{\partial N'_{ik}}{\partial y} - \frac{2}{3}C_3\frac{\partial N'_{ij}}{\partial y}\frac{\partial N'_{ik}}{\partial z}\}dV + \int_{V_i}\{N'_{ij}N'_{ik}\sum_{l=1}^{K'}(\frac{\partial N'_{il}}{\partial z}v_{il}) + C_2 N'_{ij}\frac{\partial N'_{ik}}{\partial z}\sum_{l=1}^{K'}(N'_{il}v_{il})\}dV \qquad -\int_{V_i}\{\frac{\partial N'_{ij}}{\partial y}N''_{ik}\}dV$$

$$\frac{1}{Re}\int_{V_i}\{\frac{\partial N'_{ij}}{\partial x}\frac{\partial N'_{ik}}{\partial x} + \frac{\partial N'_{ij}}{\partial y}\frac{\partial N'_{ik}}{\partial y} + (1+C_1-\frac{2}{3}C_3)\frac{\partial N'_{ij}}{\partial z}\frac{\partial N'_{ik}}{\partial z}\}dV + \int_{V_i}\{N'_{ij}N'_{ik}\sum_{l=1}^{K'}(\frac{\partial N'_{il}}{\partial z}w_{il}) + C_2 N'_{ij}\frac{\partial N'_{ik}}{\partial z}\sum_{l=1}^{K'}(N'_{il}w_{il})\}dV \qquad -\int_{V_i}\{\frac{\partial N'_{ij}}{\partial z}N''_{ik}\}dV$$

$$-\int_{V_i}\{N''_{ij}\frac{\partial N'_{ik}}{\partial z}\}dV \qquad 0$$

To derive the Jacobian equations for element i, the element equations must be differentiated with respect to all variables appearing in them. The four j^{th} element equations can be rewritten as:

$$\text{Eq 1} = \sum_{k=1}^{K'} \Big[\frac{1}{Re} \int_{V_i} \Big\{ \Big(1+C_1 - \frac{2}{3}C_3\Big) \frac{\partial N'_{ij}}{\partial x}\frac{\partial N'_{ik}}{\partial x} + \frac{\partial N'_{ij}}{\partial y}\frac{\partial N'_{ik}}{\partial y} + \frac{\partial N'_{ij}}{\partial z}\frac{\partial N'_{ik}}{\partial z} \Big\} dV.u_{ik}$$

$$+ \frac{1}{Re} \int_{V_i} \Big\{ C_1 \frac{\partial N'_{ij}}{\partial y}\frac{\partial N'_{ik}}{\partial x} - \frac{2}{3}C_3 \frac{\partial N'_{ij}}{\partial x}\frac{\partial N'_{ik}}{\partial y} \Big\} dV.v_{ik} + \frac{1}{Re} \int_{V_i} \Big\{ C_1 \frac{\partial N'_{ij}}{\partial z}\frac{\partial N'_{ik}}{\partial x}$$

$$- \frac{2}{3}C_3 \frac{\partial N'_{ij}}{\partial x}\frac{\partial N'_{ik}}{\partial z} \Big\} dV.w_{ik} - \int_{V_i} \Big\{ \frac{\partial N'_{ij}}{\partial x} N''_{ik} \Big\} dV.p_{ik} \Big] + \sum_{k=1}^{K'} \Big[\sum_{l=1}^{K'} \Big\{ \int_{V_i} \Big(N'_{ij}N'_{ik} \frac{\partial N'_{il}}{\partial x}$$

$$+ C_2 N'_{ij} \frac{\partial N'_{ik}}{\partial x} N'_{il} \Big) dV.u_{ik} + \int_{V_i} \Big(N'_{ij} N'_{ik} \frac{\partial N'_{il}}{\partial y} + C_2 N'_{ij} \frac{\partial N'_{ik}}{\partial y} N'_{il} \Big) dV.v_{ik}$$

$$+ \int_{V_i} \Big(N'_{ij}N'_{ik} \frac{\partial N'_{il}}{\partial z} + C_2 N'_{ij} \frac{\partial N'_{ik}}{\partial z} N'_{il} \Big) dV.w_{ik} \Big\} u_{il} \Big] - \text{surface integrals} = 0$$

$$\text{Eq 2} = \sum_{k=1}^{K'} \Big[\frac{1}{Re} \int_{V_i} \Big\{ C_1 \frac{\partial N'_{ij}}{\partial x}\frac{\partial N'_{ik}}{\partial y} - \frac{2}{3}C_3 \frac{\partial N'_{ij}}{\partial y}\frac{\partial N'_{ik}}{\partial x} \Big\} dV.u_{ik} + \frac{1}{Re} \int_{V_i} \Big\{ \frac{\partial N'_{ij}}{\partial x}\frac{\partial N'_{ik}}{\partial x}$$

$$+ \Big(1+C_1 - \frac{2}{3}C_3\Big) \frac{\partial N'_{ij}}{\partial y}\frac{\partial N'_{ik}}{\partial y} + \frac{\partial N'_{ij}}{\partial z}\frac{\partial N'_{ik}}{\partial z} \Big\} dV.v_{ik} + \frac{1}{Re} \int_{V_i} \Big\{ C_1 \frac{\partial N'_{ij}}{\partial z}\frac{\partial N'_{ik}}{\partial y}$$

$$- \frac{2}{3}C_3 \frac{\partial N'_{ij}}{\partial y}\frac{\partial N'_{ik}}{\partial z} \Big\} dV.w_{ik} - \int_{V_i} \Big\{ \frac{\partial N'_{ij}}{\partial y} N''_{ik} \Big\} dV.p_{ik} \Big] + \sum_{k=1}^{K'} \Big[\sum_{l=1}^{K'} \Big\{ \int_{V_i} \Big(N'_{ij}N'_{ik} \frac{\partial N'_{il}}{\partial x}$$

$$+ C_2 N'_{ij} \frac{\partial N'_{ik}}{\partial x} N'_{il} \Big) dV.u_{ik} + \int_{V_i} \Big(N'_{ij}N'_{ik} \frac{\partial N'_{il}}{\partial y} + C_2 N'_{ij} \frac{\partial N'_{ik}}{\partial y} N'_{il} \Big) dV.v_{ik}$$

$$+ \int_{V_i} \Big(N'_{ij}N'_{ik} \frac{\partial N'_{il}}{\partial z} + C_2 N'_{ij} \frac{\partial N'_{ik}}{\partial z} N'_{il} \Big) dV.w_{ik} \Big\} v_{il} \Big] - \text{surface integrals} = 0$$

$$\text{Eq 3} = \sum_{k=1}^{K'} \Big[\frac{1}{Re} \int_{V_i} \Big\{ C_1 \frac{\partial N'_{ij}}{\partial x} \frac{\partial N'_{ik}}{\partial z} - \frac{2}{3} C_3 \frac{\partial N'_{ij}}{\partial z} \frac{\partial N'_{ik}}{\partial x} \Big\} dV.u_{ik} + \frac{1}{Re} \int_{V_i} \Big\{ C_1 \frac{\partial N'_{ij}}{\partial y} \frac{\partial N'_{ik}}{\partial z}$$

$$- \frac{2}{3} C_3 \frac{\partial N'_{ij}}{\partial z} \frac{\partial N'_{ik}}{\partial y} \Big\} dV.v_{ik} + \frac{1}{Re} \int_{V_i} \Big\{ \frac{\partial N'_{ij}}{\partial x} \frac{\partial N'_{ik}}{\partial x} + \frac{\partial N'_{ij}}{\partial y} \frac{\partial N'_{ik}}{\partial y} + (1 + C_1 - \frac{2}{3} C_3) .$$

$$\frac{\partial N'_{ij}}{\partial z} \frac{\partial N'_{ik}}{\partial z} \Big\} dV.w_{ik} - \int_{V_i} \Big\{ \frac{\partial N'_{ij}}{\partial z} N''_{ik} \Big\} dV.p_{ik} \Big] + \sum_{k=1}^{K'} \Big[\sum_{l=1}^{K'} \Big\{ \int_{V_i} \Big(N'_{ij} N'_{ik} \frac{\partial N'_{il}}{\partial x}$$

$$+ C_2 N'_{ij} \frac{\partial N'_{ik}}{\partial x} N'_{il} \Big) dV.u_{ik} + \int_{V_i} \Big(N'_{ij} N'_{ik} \frac{\partial N'_{il}}{\partial y} + C_2 N'_{ij} \frac{\partial N'_{ik}}{\partial y} N'_{il} \Big) dV.v_{ik}$$

$$+ \int_{V_i} \Big(N'_{ij} N'_{ik} \frac{\partial N'_{il}}{\partial z} + C_2 N'_{ij} \frac{\partial N'_{ik}}{\partial z} N'_{il} \Big) dV.w_{ik} \Big\} w_{il} \Big] - \text{surface integrals} = 0$$

$$\text{Eq 4} = \sum_{k=1}^{K'} \Big[- \int_{V_i} \Big\{ N''_{ij} \frac{\partial N'_{ik}}{\partial x} \Big\} dV.u_{ik} - \int_{V_i} \Big\{ N''_{ij} \frac{\partial N'_{ik}}{\partial y} \Big\} dV.v_{ik}$$

$$- \int_{V_i} \Big\{ N''_{ij} \frac{\partial N'_{ik}}{\partial z} \Big\} dV.w_{ik} \Big] = 0$$

The following differentiations must now be carried out in order to set up $[S_i]$.

$\frac{\partial \text{Eq 1}}{\partial u_{im}}$	$\frac{\partial \text{Eq 1}}{\partial v_{im}}$	$\frac{\partial \text{Eq 1}}{\partial w_{im}}$	$\frac{\partial \text{Eq 1}}{\partial p_{im}}$
$\frac{\partial \text{Eq 2}}{\partial u_{im}}$	$\frac{\partial \text{Eq 2}}{\partial v_{im}}$	$\frac{\partial \text{Eq 2}}{\partial w_{im}}$	$\frac{\partial \text{Eq 2}}{\partial p_{im}}$
$\frac{\partial \text{Eq 3}}{\partial u_{im}}$	$\frac{\partial \text{Eq 3}}{\partial v_{im}}$	$\frac{\partial \text{Eq 3}}{\partial w_{im}}$	$\frac{\partial \text{Eq 3}}{\partial p_{im}}$
$\frac{\partial \text{Eq 4}}{\partial u_{im}}$	$\frac{\partial \text{Eq 4}}{\partial v_{im}}$	$\frac{\partial \text{Eq 4}}{\partial w_{im}}$	$\frac{\partial \text{Eq 4}}{\partial p_{im}}$

$$\frac{\partial Eq\ 1}{\partial u_{im}} = \frac{1}{Re} \int_{V_i} \{(1+C_1 - \frac{2}{3} C_3) \frac{\partial N'_{ij}}{\partial x} \frac{\partial N'_{im}}{\partial x} + \frac{\partial N'_{ij}}{\partial y} \frac{\partial N'_{im}}{\partial y} + \frac{\partial N'_{ij}}{\partial z} \frac{\partial N'_{im}}{\partial z}\} dV$$

$$+ \sum_{l=1}^{K'} [\int_{V_i} \{(1+C_2) N'_{ij} N'_{im} \frac{\partial N'_{il}}{\partial x} + (1+C_2) N'_{ij} \frac{\partial N'_{im}}{\partial x} N'_{il}\} dV.u_{il}$$

$$+ \int_{V_i} \{N'_{ij} N'_{il} \frac{\partial N'_{im}}{\partial y} + C_2 N'_{ij} \frac{\partial N'_{il}}{\partial y} N'_{im}\} dV.v_{il} + \int_{V_i} \{N'_{ij} N'_{il} \frac{\partial N'_{im}}{\partial z}$$

$$+ C_2 N'_{ij} \frac{\partial N'_{il}}{\partial z} N'_{im}\} dV.w_{il}]$$

$$\frac{\partial Eq\ 2}{\partial u_{im}} = \frac{1}{Re} \int_{V_i} \{C_1 \frac{\partial N'_{ij}}{\partial x} \frac{\partial N'_{im}}{\partial y} - \frac{2}{3} C_3 \frac{\partial N'_{ij}}{\partial y} \frac{\partial N'_{im}}{\partial x}\} dV + \sum_{l=1}^{K'} [\int_{V_i} \{N'_{ij} N'_{im} \frac{\partial N'_{il}}{\partial x}$$

$$+ C_2 N'_{ij} \frac{\partial N'_{im}}{\partial x} N'_{il}\} dV.v_{il}]$$

$$\frac{\partial Eq\ 3}{\partial u_{im}} = \frac{1}{Re} \int_{V_i} \{C_1 \frac{\partial N'_{ij}}{\partial x} \frac{\partial N'_{im}}{\partial z} - \frac{2}{3} C_3 \frac{\partial N'_{ij}}{\partial z} \frac{\partial N'_{im}}{\partial x}\} dV + \sum_{l=1}^{K'} [\int_{V_i} \{N'_{ij} N'_{im} \frac{\partial N'_{il}}{\partial x}$$

$$+ C_2 N'_{ij} \frac{\partial N'_{im}}{\partial x} N_{il}\} dV.w_{il}]$$

$$\frac{\partial Eq\ 4}{\partial u_{im}} = - \int_{V_i} \{N'_{ij} \frac{\partial N'_{im}}{\partial x}\} dV$$

Similarly

$$\frac{\partial Eq\ 1}{\partial v_{im}} = \frac{1}{Re} \int_{V_i} \{C_1 \frac{\partial N'_{ij}}{\partial y} \frac{\partial N'_{im}}{\partial x} - \frac{2}{3} C_3 \frac{\partial N'_{ij}}{\partial x} \frac{\partial N'_{im}}{\partial y}\} dV + \sum_{l=1}^{K'} [\int_{V_i} \{N'_{ij} N'_{im} \frac{\partial N'_{il}}{\partial y}$$

$$+ C_2 N'_{ij} \frac{\partial N'_{im}}{\partial y} N'_{il}\} dV.u_{il}]$$

$$\frac{\partial Eq\ 2}{\partial v_{im}} = \frac{1}{Re} \int_{V_i} \{\frac{\partial N'_{ij}}{\partial x} \frac{\partial N'_{im}}{\partial x} + (1+C_1 - \frac{2}{3} C_3) \frac{\partial N'_{ij}}{\partial y} \frac{\partial N'_{im}}{\partial y} + \frac{\partial N'_{ij}}{\partial z} \frac{\partial N'_{im}}{\partial z}\} dV$$

$$+ \sum_{l=1}^{K'} [\int_{V_i} \{N'_{ij} N'_{il} \frac{\partial N'_{im}}{\partial x} + C_2 N'_{ij} \frac{\partial N'_{il}}{\partial x} N'_{im}\} dV.u_{il} + \int_{V_i} \{(1+C_2) N'_{ij} N'_{im} \frac{\partial N'_{il}}{\partial y}$$

$$+ (1+C_2) N'_{ij} \frac{\partial N'_{im}}{\partial y} N'_{il}\} dV.v_{il} + \int_{V_i} \{N'_{ij} N'_{il} \frac{\partial N'_{im}}{\partial z} + C_2 N'_{ij} \frac{\partial N'_{il}}{\partial z} N'_{im}\} dV.w_{il}]$$

$$\frac{\partial Eq\ 3}{\partial v_{im}} = \frac{1}{Re} \int_{V_i} \{C_1 \frac{\partial N'_{ij}}{\partial y} \frac{\partial N'_{im}}{\partial z} - \frac{2}{3} C_3 \frac{\partial N'_{ij}}{\partial z} \frac{\partial N'_{im}}{\partial y}\} dV + \sum_{l=1}^{K'} [\int_{V_i} \{N'_{ij} N'_{im} \frac{\partial N'_{il}}{\partial y}$$

$$+ C_2 N'_{ij} \frac{\partial N'_{im}}{\partial y} N'_{il}\} dV.w_{il}]$$

$$\frac{\partial Eq\ 4}{\partial v_{im}} = - \int_{V_i} \{N''_{ij} \frac{\partial N'_{im}}{\partial y}\} dV$$

and

$$\frac{\partial Eq\ 1}{\partial w_{im}} = \frac{1}{Re} \int_{V_i} \{C_1 \frac{\partial N'_{ij}}{\partial z} \frac{\partial N'_{im}}{\partial x} - \frac{2}{3} C_3 \frac{\partial N'_{ij}}{\partial x} \frac{\partial N'_{im}}{\partial z}\} dV + \sum_{l=1}^{K'} [\int_{V_i} \{N'_{ij} N'_{im} \frac{\partial N'_{il}}{\partial z}$$

$$+ C_2 N'_{ij} \frac{\partial N'_{im}}{\partial z} N'_{il}\} dV.u_{il}]$$

$$\frac{\partial Eq\ 2}{\partial w_{im}} = \frac{1}{Re} \int_{V_i} \{C_1 \frac{\partial N'_{ij}}{\partial z} \frac{\partial N'_{im}}{\partial y} - \frac{2}{3} C_3 \frac{\partial N'_{ij}}{\partial y} \frac{\partial N'_{im}}{\partial z}\} dV + \sum_{l=1}^{K'} [\int_{V_i} \{N'_{ij} N'_{im} \frac{\partial N'_{il}}{\partial z}$$

$$+ C_2 N'_{ij} \frac{\partial N'_{im}}{\partial z} N'_{il}\} dV.v_{il}]$$

$$\frac{\partial Eq\ 3}{\partial w_{im}} = \frac{1}{Re} \int_{V_i} \{\frac{\partial N'_{ij}}{\partial x} \frac{\partial N'_{im}}{\partial x} + \frac{\partial N'_{ij}}{\partial y} \frac{\partial N'_{im}}{\partial y} + (1+C_1 - \frac{2}{3} C_3) \frac{\partial N'_{ij}}{\partial z} \frac{\partial N'_{im}}{\partial z}\} dV$$

$$+ \sum_{l=1}^{K'} [\int_{V_i} \{N'_{ij} N'_{il} \frac{\partial N'_{im}}{\partial x} + C_2 N'_{ij} \frac{\partial N'_{il}}{\partial x} N'_{im}\} dV.u_{il} + \int_{V_i} \{N'_{ij} N'_{il} \frac{\partial N'_{im}}{\partial y}$$

$$+ C_2\ N'_{ij} \frac{\partial N'_{il}}{\partial y} N'_{im}\} \, dV . v_{il} + \int_{V_i} \{(1+C_2)\ N'_{ij} N'_{im} \frac{\partial N'_{il}}{\partial z}$$

$$+ (1+C_2)\ N'_{ij} \frac{\partial N'_{im}}{\partial z} N'_{il}\} dV . w_{il}]$$

$$\frac{\partial Eq\ 4}{\partial w_{im}} = - \int_{V_i} \{N''_{ij} \frac{\partial N'_{im}}{\partial z}\} \, dV$$

and

$$\frac{\partial Eq\ 1}{\partial p_{im}} = - \int_{V_i} \{\frac{\partial N'_{ij}}{\partial x} N''_{im}\} \, dV$$

$$\frac{\partial Eq\ 2}{\partial p_{im}} = - \int_{V_i} \{\frac{\partial N'_{ij}}{\partial y} N''_{im}\} \, dV$$

$$\frac{\partial Eq\ 3}{\partial p_{im}} = - \int_{V_i} \{\frac{\partial N'_{ij}}{\partial z} N''_{im}\} \, dV$$

$$\frac{\partial Eq\ 4}{\partial p_{im}} = 0$$

The jk^{th} submatrix of $[S_i]$ for elements i is therefore:

$$[S_i]_{jk} =$$

$$\frac{1}{Re}\int_{V_i}\{(1+C_1-\frac{2}{3}C_3)\frac{\partial N'_{ij}}{\partial x}\frac{\partial N'_{ik}}{\partial x}+\frac{\partial N'_{ij}}{\partial y}\frac{\partial N'_{ik}}{\partial y}+\frac{\partial N'_{ij}}{\partial z}\frac{\partial N'_{ik}}{\partial z}\}dV$$

$$+\int_{V_i}\{(1+C_2)N'_{ij}\sum_{l=1}^{K'}(N'_{ik}\frac{\partial N'_{il}}{\partial x}+\frac{\partial N'_{ik}}{\partial x}N'_{il})u_{il}\}dV$$

$$+\int_{V_i}\{N'_{ij}\sum_{l=1}^{K'}(C_2N'_{ik}\frac{\partial N'_{il}}{\partial y}+\frac{\partial N'_{ik}}{\partial y}N'_{il})v_{il}\}dV$$

$$+\int_{V_i}\{N'_{ij}\sum_{l=1}^{K'}(C_2N'_{ik}\frac{\partial N'_{il}}{\partial z}+\frac{\partial N'_{ik}}{\partial z}N'_{il})w_{il}\}dV$$

$$\frac{1}{Re}\int_{V_i}\{C_1\frac{\partial N'_{ij}}{\partial y}\frac{\partial N'_{ik}}{\partial x}-\frac{2}{3}C_3\frac{\partial N'_{ij}}{\partial x}\frac{\partial N'_{ik}}{\partial y}\}dV$$

$$+\int_{V_i}\{N'_{ij}\sum_{l=1}^{K'}(N'_{ik}\frac{\partial N'_{il}}{\partial y}+C_2\frac{\partial N'_{ik}}{\partial y}N'_{il})u_{il}\}dV$$

$$\frac{1}{Re}\int_{V_i}\{C_1\frac{\partial N'_{ij}}{\partial x}\frac{\partial N'_{ik}}{\partial y}-\frac{2}{3}C_3\frac{\partial N'_{ij}}{\partial y}\frac{\partial N'_{ik}}{\partial x}\}dV$$

$$+\int_{V_i}\{N'_{ij}\sum_{l=1}^{K'}(N'_{ik}\frac{\partial N'_{il}}{\partial x}+C_2\frac{\partial N'_{ik}}{\partial x}N'_{il})v_{il}\}dV$$

$$\frac{1}{Re}\int_{V_i}\{C_1\frac{\partial N'_{ij}}{\partial x}\frac{\partial N'_{ik}}{\partial z}-\frac{2}{3}C_3\frac{\partial N'_{ij}}{\partial z}\frac{\partial N'_{ik}}{\partial x}\}dV$$

$$+\int_{V_i}\{N'_{ij}\sum_{l=1}^{K'}(N'_{ik}\frac{\partial N'_{il}}{\partial x}+C_2\frac{\partial N'_{ik}}{\partial x}N'_{il})w_{il}\}dV$$

$$-\int_{V_i}\{N''_{ij}\frac{\partial N'_{ik}}{\partial x}\}dV$$

$$\frac{1}{Re}\int_{V_i}\{\frac{\partial N'_{ij}}{\partial x}\frac{\partial N'_{ik}}{\partial x}+(1+C_1-\frac{2}{3}C_3)\frac{\partial N'_{ij}}{\partial y}\frac{\partial N'_{ik}}{\partial y}+\frac{\partial N'_{ij}}{\partial z}\frac{\partial N'_{ik}}{\partial z}\}dV$$

$$+\int_{V_i}\{N'_{ij}\sum_{l=1}^{K'}(C_2N'_{ik}\frac{\partial N'_{il}}{\partial x}+\frac{\partial N'_{ik}}{\partial x}N'_{il})u_{il}\}dV$$

$$+\int_{V_i}\{(1+C_2)N'_{ij}\sum_{l=1}^{K'}(N'_{ik}\frac{\partial N'_{il}}{\partial y}+\frac{\partial N'_{ik}}{\partial y}N'_{il})v_{il}\}$$

$$+\int_{V_i}\{N'_{ij}\sum_{l=1}^{K'}(C_2N'_{ik}\frac{\partial N'_{il}}{\partial z}+\frac{\partial N'_{ik}}{\partial z}N'_{il})w_{il}\}dV$$

$$\frac{1}{Re}\int_{V_i}\{C_1\frac{\partial N'_{ij}}{\partial y}\frac{\partial N'_{ik}}{\partial z}-\frac{2}{3}C_3\frac{\partial N'_{ij}}{\partial z}\frac{\partial N'_{ik}}{\partial y}\}dV$$

$$+\int_{V_i}\{N'_{ij}\sum_{l=1}^{K'}(N'_{ik}\frac{\partial N'_{il}}{\partial y}+C_2\frac{\partial N'_{ik}}{\partial y}N'_{il})w_{il}\}dV$$

$$-\int_{V_i}\{N''_{ij}\frac{\partial N'_{ik}}{\partial y}\}dV$$

Matrix continues overleaf ...

$\frac{1}{Re}\int_{V_i}\{C_1\frac{\partial N'_{ij}}{\partial z}\frac{\partial N'_{ik}}{\partial x}-\frac{2}{3}C_3\frac{\partial N'_{ij}}{\partial x}\frac{\partial N'_{ik}}{\partial z}\}dV$ $+\int_{V_i}\{N'_{ij}\sum_{l=1}^{K'}(N'_{ik}\frac{\partial N'_{il}}{\partial z}+C_2\frac{\partial N'_{ik}}{\partial z}N'_{il})u_{il}\}dV$	$-\int_{V_i}\{\frac{\partial N'_{ij}}{\partial x}N''_{ik}\}\ dV$
$\frac{1}{Re}\int_{V_i}\{C_1\frac{\partial N'_{ij}}{\partial z}\frac{\partial N'_{ik}}{\partial y}-\frac{2}{3}C_3\frac{\partial N'_{ij}}{\partial y}\frac{\partial N'_{ik}}{\partial z}\}dV$ $+\int_{V_i}\{N'_{ij}\sum_{l=1}^{K'}(N'_{ik}\frac{\partial N'_{il}}{\partial z}+C_2\frac{\partial N'_{ik}}{\partial z}N'_{il})v_{il}\}dV$	$-\int_{V_i}\{\frac{\partial N'_{ij}}{\partial y}N''_{ik}\}\ dV$
$\frac{1}{Re}\int_{V_i}\{\frac{\partial N'_{ij}}{\partial x}\frac{\partial N'_{ik}}{\partial x}+\frac{\partial N'_{ij}}{\partial y}\frac{\partial N'_{ik}}{\partial y}$ $+(1+C_1-\frac{2}{3}C_3)\frac{\partial N'_{ij}}{\partial z}\frac{\partial N'_{ik}}{\partial z}\}dV$ $+\int_{V_i}\{N'_{ij}\sum_{l=1}^{K'}(C_2N'_{ik}\frac{\partial N'_{il}}{\partial x}+\frac{\partial N'_{ik}}{\partial x}N'_{il})u_{il}\}dV$ $+\int_{V_i}\{N'_{ij}\sum_{l=1}^{K'}(C_2N'_{ik}\frac{\partial N'_{il}}{\partial y}+\frac{\partial N'_{ik}}{\partial y}N'_{il})v_{il}\}dV$ $+\int_{V_i}\{(1+C_2)N'_{ij}\sum_{l=1}^{K'}(N'_{ik}\frac{\partial N'_{il}}{\partial z}+\frac{\partial N'_{ik}}{\partial z}N'_{il})w_{il}\}\ dV$	$-\int_{V_i}\{\frac{\partial N'_{ij}}{\partial z}N''_{ik}\}\ dV$
$-\int_{V_i}\{N''_{ij}\frac{\partial N'_{ik}}{\partial z}\}\ dV$	0

On closer examination it will be noticed that the submatrix $[S_i]_{jk}$ is in fact equal to the sum of the submatrix $[R_i]_{jk}$ and the diagonal matrix given by

$$\int A_{jk} \begin{bmatrix} 1 & 0 & 0 & 0 \\ 0 & 1 & 0 & 0 \\ 0 & 0 & 1 & 0 \\ 0 & 0 & 0 & 1 \end{bmatrix} dV$$

where
$$A_{jk} = N'_{ij} \frac{\partial N'_{ik}}{\partial x} \sum_{l=1}^{K'} (N'_{il} u_{il}) + C_2 N'_{ij} N'_{ik} \sum_{l=1}^{K'} \left(\frac{\partial N'_{il}}{\partial x} u_{il}\right)$$
$$+ N'_{ij} \frac{\partial N'_{ik}}{\partial y} \sum_{l=1}^{K'} (N'_{il} v_{il}) + C_2 N'_{ij} N'_{ik} \sum_{l=1}^{K'} \left(\frac{\partial N'_{il}}{\partial y} v_{il}\right)$$
$$+ N'_{ij} \frac{\partial N'_{ik}}{\partial z} \sum_{l=1}^{K'} (N'_{il} w_{il}) + C_2 N'_{ij} N'_{ik} \sum_{l=1}^{K'} \left(\frac{\partial N'_{il}}{\partial z} w_{il}\right)$$

Therefore for formulations A and B (C_2=0)

$$A_{ij} = N'_{ij} \sum_{l=1}^{K'} \left(\frac{\partial N'_{ik}}{\partial x} N'_{il} u_{il} + \frac{\partial N'_{ik}}{\partial y} N'_{il} v_{il} + \frac{\partial N'_{ik}}{\partial z} N'_{il} w_{il}\right)$$

and for formulations C and D (C_2=1)

$$A_{ij} = N'_{ij} \sum_{l=1}^{K'} \left(\frac{\partial N'_{ik}}{\partial x} N'_{il} u_{il} + \frac{\partial N'_{ik}}{\partial y} N'_{il} v_{il} + \frac{\partial N'_{ik}}{\partial z} N'_{il} w_{il}\right)$$
$$+ N'_{ij} N'_{ik} \sum_{l=1}^{K'} \left(\frac{\partial N'_{il}}{\partial x} u_{il} + \frac{\partial N'_{il}}{\partial y} v_{il} + \frac{\partial N'_{il}}{\partial z} w_{il}\right)$$

CHAPTER 4

FINITE ELEMENT AND COMPUTER PROGRAM DETAILS

4.1 Isoparametric Finite Elements

4.2 Numerical Integration Details

4.3 Some Important Computer Programming Aspects

4. FINITE ELEMENT AND COMPUTER PROGRAM DETAILS

The discussion concerning the first phase of this study is now completed. That is, the fluid dynamics of a general viscous flow have been presented and the governing Navier-Stokes and Continuity equations have been derived. The finite element formulation of these equations has been discussed and the techniques chosen to construct and solve the non-linear simultaneous equation system have been suitably adapted and described. The second phase of this study involved the selection of suitable two- and three-dimensional finite elements and an appropriate numerical integration scheme that could be used to satisfactorily model the particular flow problems that were to be investigated. Details of the finite elements are given in the first section of this chapter, while a description of the integration technique is given in the second. Finally, a number of finite element computer programs were developed and some of the difficulties encountered in so doing are discussed in the last section.

4.1 Isoparametric Finite Elements

The first major decision that must be made whenever the finite element method is chosen to model a particular problem, concerns the selection of element type and the associated order of parameter approximation that will be employed. It has been shown by Hood and Taylor (16) that in modelling a viscous flow, the results obtained when the order of interpolation for both the velocity and pressure is the same, are considerably inferior, especially the pressure, to those obtained when the velocity interpolation is one order higher than that for the pressure. The explanation they presented was based on a consideration of error consistency of the two coupled equations, Momentum and Continuity, for two unknowns, velocity and pressure. A mixed interpolation method of the type described by Hood and Taylor was used exclusively in this study

and, in anticipation of this, the finite element equations given by 3.22.1-4 were arranged so that the number of pressure nodes could, if necessary, be different from the number of velocity nodes in each element.

The actual order of the interpolation used was the quadratic velocity and linear pressure combination. The cubic velocity and quadratic pressure approach, or any of the higher interpolation methods have the obvious advantage of requiring fewer elements to represent the same flow, but results of previous investigations indicated that they do not lead to solutions that are significantly improved. The linear velocity and constant pressure approach was the only other possibility. However an element having this interpolation facility, by its very nature, can have only one pressure node located internally, usually at the centroid. Therefore, because it has no pressure nodes on its edges, it cannot ensure continuity of the pressure variable, a condition that is assumed satisfied whenever the assembly process is used to construct the global simultaneous equation system.

In two dimensions the number of nodes required for a complete interpolation of the n^{th} order can be found from Pascal's Triangle, that is

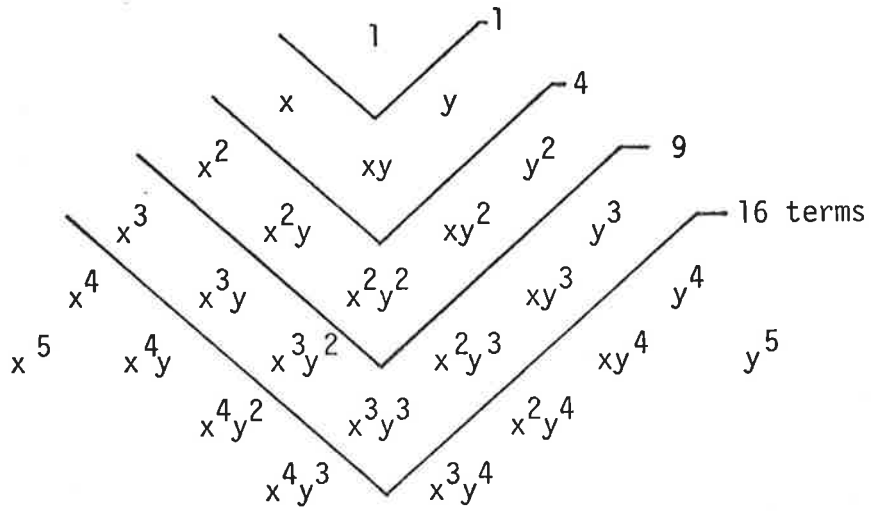

From the above it can be seen that a complete linear pressure and quadratic velocity interpolation requires four unknown pressure and nine unknown velocity nodal parameters and therefore four pressure and nine velocity nodes per element respectively. The nodal arrangements for a triangular and a quadrilateral two-dimensional element with complete quadratic velocity and linear pressure, mixed interpolation facilities are shown in Figure 4.1. The velocity nodes are indicated by a circle and the pressure nodes by a cross. It can therefore be seen that the number of nodes required in the triangular element is ten, while for the quadrilateral it is nine. By using an incomplete velocity interpolation however, the total number of nodes in either element can be reduced. The single internal node of the quadrilateral element can be omitted by removing the x^2y^2 term from the complete quadratic interpolation, thereby reducing the number of nodes to eight. If the same thing is done to the triangular element, all three internal velocity nodes must be removed. This is done by omitting from the complete quadratic interpolation the x^2y, x^2y^2 and xy^2 terms. This however, only reduces the number of nodes to seven, and it becomes evident that the quadrilateral element with either eight or nine nodes should be the best one to use with the quadratic velocity and linear pressure interpolations. It was therefore decided to use both quadrilateral elements and to carry out a comparison to determine the relative merits of each. A comparison similar to this, with the results favouring the eight noded element, was previously performed by Fletcher (11) who used the Galerkin approach to solve an incompressible inviscid flow. On the other hand, Bercovier and Engelman (3) who also solved an incompressible inviscid flow, concluded that the nine noded element was somewhat better than the eight noded. The technique they used was not the Galerkin method but a variational finite element approach with a penalization of the Continuity equation and the consequent elimination from the system of the pressure

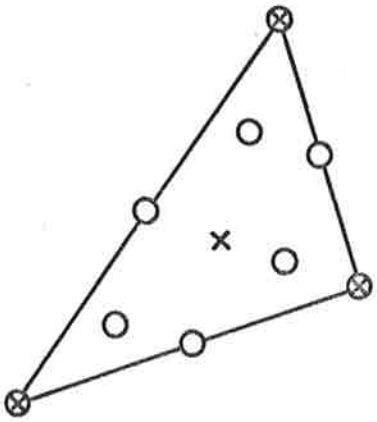

(a) ten noded triangle

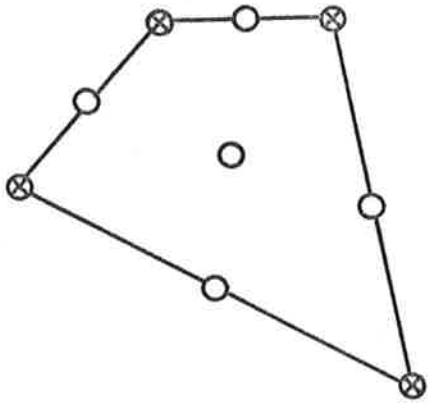

(b) nine noded quadrilateral

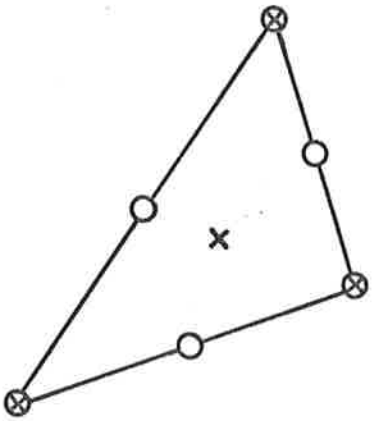

(c) seven noded triangle

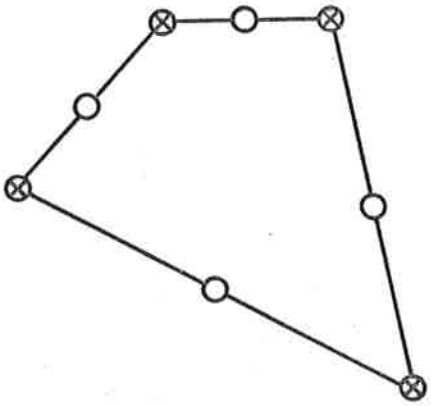

(d) eight noded quadrilateral

Figure 4.1 Typical Triangular and Quadrilateral Two-dimensional Finite Elements, (a) and (b) with complete linear pressure and complete quadratic velocity interpolations, (c) and (d) with complete linear pressure but incomplete quadratic velocity interpolations.

variable. The viscous flow results they presented were obtained using only the nine noded element. In this study however, the results of two viscous flow problems, obtained using firstly the eight and then the nine noded elements, are compared and presented in Chapter 5.

The number of pressure and velocity nodes on each side of both of these elements is two and three respectively. This allows a unique linear pressure and quadratic velocity variation to be described on all edges of each element. These two conditions ensure that the continuity of both pressure and velocity across all element interfaces is maintained. The continuity of velocity gradients however, cannot be guaranteed by either of the above two elements.

The two elements selected above are more commonly known as the eight noded Serendipity and the nine noded Langrangian isoparametric quadrilateral elements. The advantage of these over the standard triangular and rectangular two-dimensional elements is in their ability to represent the relatively complex geometries most likely to be encountered in real flow problems. The term "isoparametric" is used to describe elements that have their geometry expressed in terms of the same set of shape functions used to describe the variations in the fields they are being used to represent. Since it may be necessary in some cases to handle curved flow boundaries, the linear pressure shape functions, which can uniquely describe only a linear variation, are inadequate. The quadratic velocity shape functions must therefore be used to represent the geometry of the elements.

Figure 4.2 shows a typical eight and nine noded element with curved edges. It also shows two coordinate systems, namely the global cartesian x and y system and a local curvilinear ξ and η system. The second system is introduced to facilitate the setting up of the shape functions and their derivatives and is such that ξ and η are either +1 or -1 on the edges of each element. More precisely, given that each element is

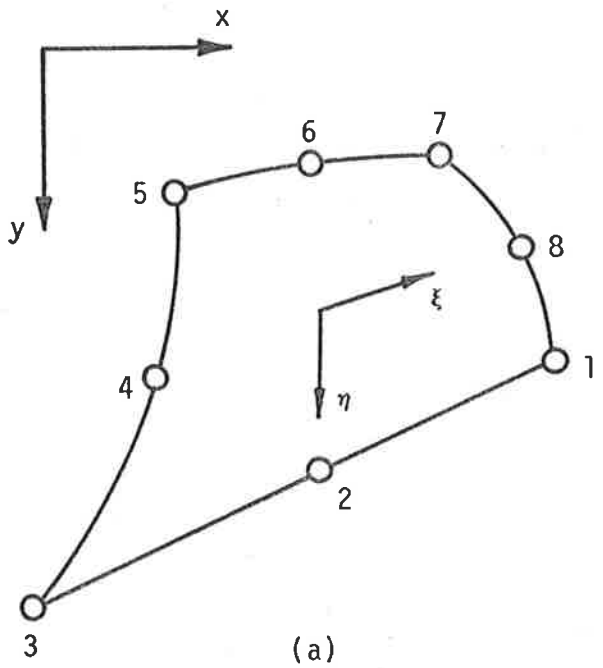

(a)

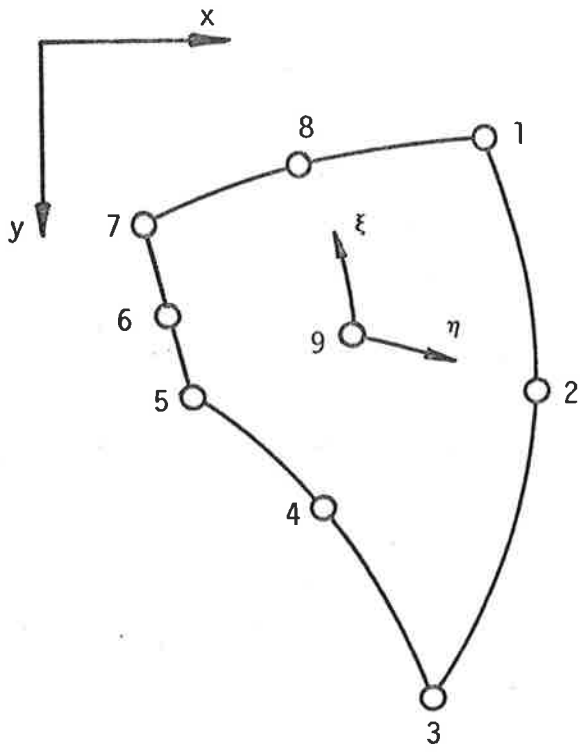

(b)

Figure 4.2 Typical (a) Eight Noded Serendipity and (b) Nine Noded Lagrangian Isoparametric Elements.

defined by listing in a clockwise fashion, firstly the node numbers on its four edges, starting with a corner node, and then any internal nodes, then $\eta=1$ on the first edge, $\xi=-1$ on the second, $\eta=-1$ on the third and $\xi=1$ on the last. For example, if the nine noded element in Figure 4.2 is defined as "123456789", then $\eta=1$ on edge 123, $\xi=-1$ on edge 345, $\eta=-1$ on edge 567 and $\xi=1$ on edge 781. Node 9 is an internal node.

Figure 4.3 shows the same elements as shown in Figure 4.2 but this time with the ξ and η as the cartesian coodinate system. In this system the linear and quadratic shape functions are easily constructed. For any eight noded Serendipity element i, the quadratic velocity shape functions are:

$$N'_{ij} = \tfrac{1}{4}(1+\xi_o)(1+\eta_o)(\xi_o+\eta_o-1) \quad \text{for } j=1,3,5 \text{ and } 7$$

$$N'_{ij} = \tfrac{1}{2}(1-\xi^2)(1+\eta_o) \quad \text{for } j=2 \text{ and } 6$$

and

$$N'_{ij} = \tfrac{1}{2}(1+\xi_o)(1-\eta^2) \quad \text{for } j=4 \text{ and } 8 \qquad 4.1$$

where $\xi_o = \xi\xi_{ij}$

and $\eta_o = \eta\eta_{ij}$ 4.2

and (ξ_{ij}, η_{ij}) are the coordinates of node j in the ξ and η system, and given in Figure 4.3.

The linear pressure shape functions are:

$$N''_{ij} = \tfrac{1}{4}(1+\xi_o)(1+\eta_o) \quad \text{for } j=1,3,5 \text{ and } 7$$

and

$$N''_{ij} = 0 \quad \text{for } j=2,4,6 \text{ and } 8 \qquad 4.3$$

where ξ_o, η_o and (ξ_{ij}, η_{ij}) are as defined above. Similarly, for any nine noded Lagrangian element i, the quadratic velocity shape functions are:

$$N'_{ij} = \tfrac{1}{4}(1+\xi_o)\xi_o(1+\eta_o)\eta_o \quad \text{for } j=1,3,5 \text{ and } 7$$

$$N'_{ij} = \tfrac{1}{2}(1-\xi^2)(1+\eta_o)\eta_o \quad \text{for } j=2 \text{ and } 6$$

$$N'_{ij} = \tfrac{1}{2}(1+\xi_o)\xi_o(1-\eta^2) \quad \text{for } j=4 \text{ and } 8$$

and

$$N'_{ij} = (1-\xi^2)(1-\eta^2) \quad \text{for } j=9 \qquad 4.4$$

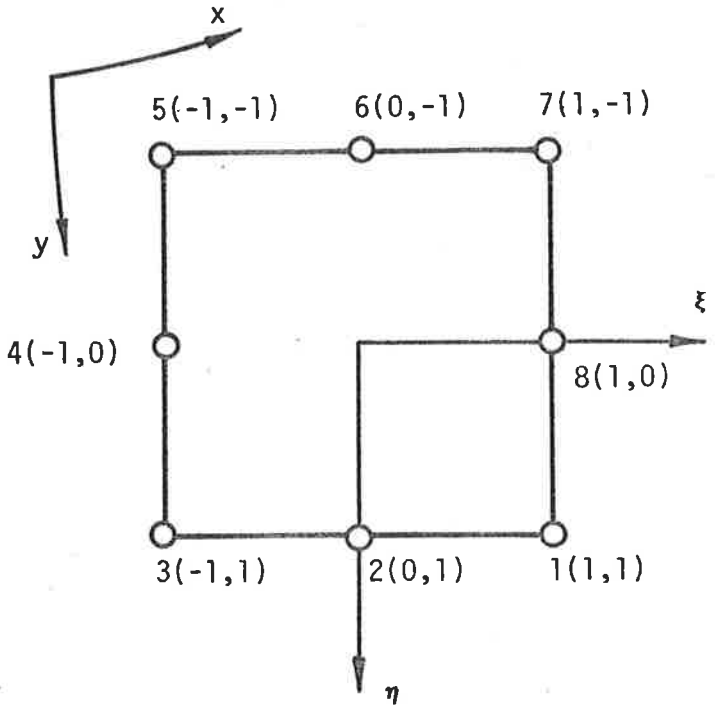

(a)

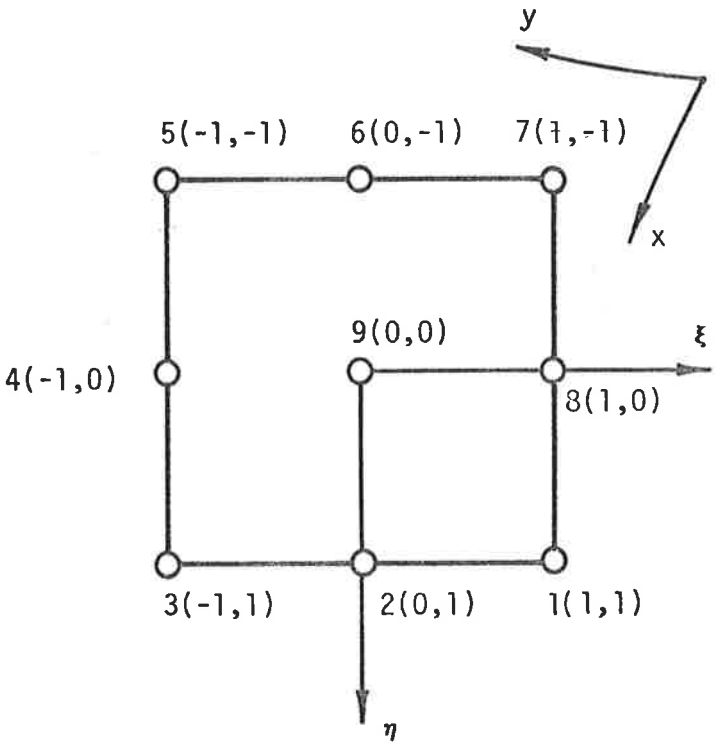

(b)

Figure 4.3 Parent (a) Eight Noded Serendipity and (b) Nine Noded Lagrangian Elements with ξ and η as Cartesian Coordinates.

The linear pressure shape functions are:

$$N''_{ij} = \tfrac{1}{4}(1+\xi_o)(1+\eta_o) \qquad \text{for } j=1,3,5 \text{ and } 7$$

and $$N''_{ij} = 0 \qquad \text{for } j=2,4,6,8 \text{ and } 9 \qquad 4.5$$

where ξ_o, η_o and (ξ_{ij}, η_{ij}) are as defined above.

It must be borne in mind at all times that the shape functions given above are expressed in terms of the local curvilinear coordinates ξ and η. Therefore only derivatives of these shape functions with respect to the coordinates ξ and η may be taken. However, in Chapter 3 it was found that the matrices $[R_i]$ and $[S_i]$ had components that contained terms with first derivatives of the shape functions with respect to the global cartesian coordinates x and y (for two dimensions). Therefore a transformation of the above derivatives between the two ccordinate systems is required and can be set up by making use of the chain rule of partial differentiation. That is

$$\frac{\partial}{\partial \xi} = \frac{\partial}{\partial x}\frac{\partial x}{\partial \xi} + \frac{\partial}{\partial y}\frac{\partial y}{\partial \xi}$$

and $$\frac{\partial}{\partial \eta} = \frac{\partial}{\partial x}\frac{\partial x}{\partial \eta} + \frac{\partial}{\partial y}\frac{\partial y}{\partial \eta} \qquad 4.6.1$$

which in matrix form becomes

$$\begin{Bmatrix} \dfrac{\partial}{\partial \xi} \\ \dfrac{\partial}{\partial \eta} \end{Bmatrix} = \begin{bmatrix} \dfrac{\partial x}{\partial \xi} & \dfrac{\partial y}{\partial \xi} \\ \dfrac{\partial x}{\partial \eta} & \dfrac{\partial y}{\partial \eta} \end{bmatrix} \begin{Bmatrix} \dfrac{\partial}{\partial x} \\ \dfrac{\partial}{\partial y} \end{Bmatrix} = [J] \begin{Bmatrix} \dfrac{\partial}{\partial x} \\ \dfrac{\partial}{\partial y} \end{Bmatrix} \qquad 4.6.2$$

where [J] is the transformation Jacobian and should not be confused with the Jacobian equation system referred to previously in Section 3.4.

By inverting the Jacobian

$$\begin{Bmatrix} \dfrac{\partial}{\partial x} \\ \dfrac{\partial}{\partial y} \end{Bmatrix} = [J]^{-1} \begin{Bmatrix} \dfrac{\partial}{\partial \xi} \\ \dfrac{\partial}{\partial \eta} \end{Bmatrix} \qquad 4.7$$

and by evaluating the derivatives with respect to the local coordinates ξ and η any derivative with respect to the global coordinates x and y can be found.

To obtain the Jacobian matrix a relationship between the two co-ordinate systems must be set up. This can be done by using the isoparametric property of the elements chosen. That is, the geometry, the x and y coordinates of any point inside element i, can be defined using the same shape functions that were used for the velocity interpolation. Therefore

$$\left.\begin{aligned} x_i &= \sum_{j=1}^{K'} N'_{ij} . x_{ij} \\ \text{and} \qquad y_i &= \sum_{j=1}^{K'} N'_{ij} . y_{ij} \end{aligned}\right\} \qquad 4.8$$

where K' is eight for the Serendipity element and nine for the Lagrangian element and (x_{ij}, y_{ij}) are the coordinates of node j in the global x and y system. These two functions describe the mapping of any point (ξ, η) in the curvilinear system to the point (x,y) in the cartesian coordinate system. Therefore

$$[J_i] = \begin{bmatrix} \dfrac{\partial \left\{ \sum_{j=1}^{K'} N'_{ij} . x_{ij} \right\}}{\partial \xi} & \dfrac{\partial \left\{ \sum_{j=1}^{K'} N'_{ij}\, y_{ij} \right\}}{\partial \xi} \\ \dfrac{\partial \left\{ \sum_{j=1}^{K'} N'_{ij}\, x_{ij} \right\}}{\partial \eta} & \dfrac{\partial \left\{ \sum_{j=1}^{K'} N'_{ij}\, y_{ij} \right\}}{\partial \eta} \end{bmatrix} \qquad 4.9.1$$

which expands to

$$= \begin{bmatrix} \dfrac{\partial N'_{i1}}{\partial \xi} & \dfrac{\partial N'_{i2}}{\partial \xi} & \cdots & \dfrac{\partial N'_{iK'}}{\partial \xi} \\ \dfrac{\partial N'_{i1}}{\partial \eta} & \dfrac{\partial N'_{i2}}{\partial \eta} & \cdots & \dfrac{\partial N'_{iK'}}{\partial \eta} \end{bmatrix} \begin{bmatrix} x_{i1} & y_{i1} \\ x_{i2} & y_{i2} \\ \cdot & \cdot \\ \cdot & \cdot \\ \cdot & \cdot \\ x_{iK'} & y_{iK'} \end{bmatrix} \qquad 4.9.2$$

Thus all quantities within the integrals in the matrices $[R_i]$ and $[S_i]$ can be transformed and expressed in terms of the ξ and η coordinates. Then by changing the limits of integration in all integrals, each can be evaluated in the ξ and η system. The element of area dA_i is transformed by the following relationship

$$dA_i = \det J_i \; d\xi d\eta \qquad 4.10$$

This can be verified by any text on the finite element method (36). A typical integral in terms of x and y, say

$$\int_{A_i} \left\{ \frac{\partial N'_{ij}}{\partial x} \frac{\partial N'_{ik}}{\partial x} + \frac{\partial N'_{ij}}{\partial y} \frac{\partial N'_{ik}}{\partial y} \right\} dA$$

becomes

$$\int_{-1}^{1} \int_{-1}^{1} \left\{ \frac{\partial N'_{ij}}{\partial x} \frac{\partial N'_{ik}}{\partial x} + \frac{\partial N'_{ij}}{\partial y} \frac{\partial N'_{ik}}{\partial y} \right\} \det J_i \; d\xi d\eta$$

expressed only in terms of ξ and η. All that remains to be done now is to evaluate these integrals and set up the element equations. However, before the element equations are complete their right hand side surface integrals must be evaluated. It should be remembered that only surface integrals for equations that correspond to nodes on the outer boundary of the flow domain need to be evaluated.

To demonstrate the transformation needed to put these surface integrals into a form that is easily evaluated, consider a typical boundary element with a normal and tangential shear stress applied to the edge that coincides with the portion of the outer boundary of the flow domain on which stresses are applied. Figure 4.4 shows such an element. Let the edge on which the stresses are applied be called edge A. Since the velocity is allowed, at most, a quadratic variation in any element, then the stresses can only vary linearly along any element edge. Therefore the normal stress p and the shear stress s need only be specified at the two corner nodes of edge A and the linear pressure shape functions

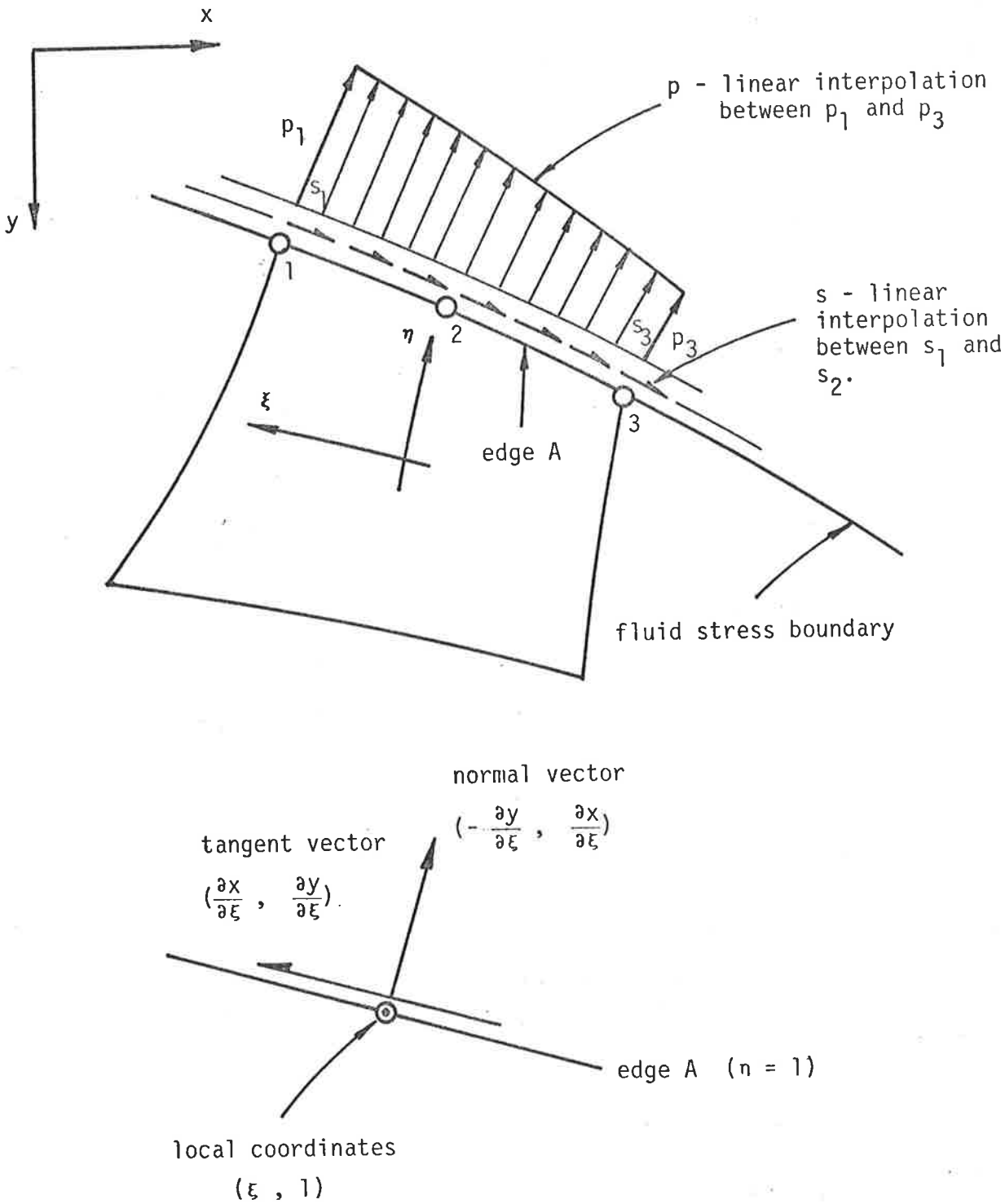

Figure 4.4 Typical Boundary Element with Applied Normal and Tangential Shear Stress Components, p and s.

can then be used to interpolate between these two points. It will be noted that the normal and tangential shear stress components have been used instead of the x and y components. This is because in most real flow problems, on the stress boundary it is usually the normal and shear stresses rather than the x and y components that are known.

It can easily be shown that the vector with components

$$\left(\frac{\partial y}{\partial \eta}, -\frac{\partial x}{\partial \eta}\right) \qquad 4.11.1$$

is normal to the line ξ = constant at any point within an isoparametric element, while the vector with components

$$\left(-\frac{\partial y}{\partial \xi}, \frac{\partial x}{\partial \xi}\right) \qquad 4.11.2$$

is normal to the line η = constant. These vectors are directed outward from the element on the edges $\xi = 1$ and $\eta = 1$ and into the element on the edges $\xi = -1$ and $\eta = -1$. Similarly, it can be shown that at any point within an isoparametric element, the vector with components

$$\left(\frac{\partial x}{\partial \eta}, \frac{\partial y}{\partial \eta}\right) \qquad 4.12.1$$

is tangential to the line ξ = constant while the vector with components

$$\left(\frac{\partial x}{\partial \xi}, \frac{\partial y}{\partial \xi}\right) \qquad 4.12.2$$

is tangential to the line η = constant. The directions of these tangential vectors is always in the positive ξ direction for those tangent to η = constant and in the positive η direction for those tangent to ξ = constant. Remembering that the Jacobian and its inverse matrix are

$$[J] = \begin{bmatrix} \frac{\partial x}{\partial \xi} & \frac{\partial y}{\partial \xi} \\ \frac{\partial x}{\partial \eta} & \frac{\partial y}{\partial \eta} \end{bmatrix} \text{ and } [J]^{-1} = \frac{1}{\det J} \begin{bmatrix} \frac{\partial y}{\partial \eta} & -\frac{\partial y}{\partial \xi} \\ -\frac{\partial x}{\partial \eta} & \frac{\partial x}{\partial \xi} \end{bmatrix}$$

then it can be seen that the above normal vectors can be obtained from the columns of $[J]^{-1}$ multiplied by det J while the tangential vectors

can be obtained from the rows of [J], all of which are expressed in terms of ξ and η.

Thus at any point along edge A, $\eta=1$ and the stress in the x direction is

$$-p\frac{\partial y}{\partial \xi} - s\frac{\partial x}{\partial \xi} \qquad 4.13.1$$

while in the y direction it is

$$p\frac{\partial x}{\partial \xi} - s\frac{\partial y}{\partial \xi} \qquad 4.13.2$$

It should be pointed out that the positive normal stress is always directed outwards from the element and the positive shear stress is always directed in a clockwise sense around the element as shown in Figure 4.4. Therefore a typical integral expressed in terms of x and y, say

$$\int_{\text{edge A}} N_{ij}^{\prime}\{\sigma_{xx}n_x + \sigma_{yx}n_y\}\,dS$$

becomes

$$\int_{-1}^{1} N_{ij}^{\prime}\{-p\frac{\partial y}{\partial \xi} - s\frac{\partial x}{\partial \xi}\}\,d\xi$$

expressed entirely in terms of ξ and η.

Everything that has been discussed so far in this section can easily be extended to three dimensions and for this reason a full discussion of the three-dimensional elements will not be given. The details however must be presented to complete this section.

The three-dimensional hexahedral element used in this study is the twenty noded Serendipity isoparametric element which is capable of allowing a complete linear pressure interpolation but only an incomplete quadratic interpolation for velocity, the terms omitted being x^2y^2, x^2z^2, y^2z^2, x^2y^2z, x^2yz^2, xy^2z^2 and $x^2y^2z^2$. The twenty-seven noded Lagrangian isoparametric hexahedral element which has complete quadratic and linear interpolations for velocity and pressure respectively, was

not used in this study. This is because, unlike in two dimensions where the Lagrangian element only has one node more than the Serendipity and therefore could be used in an analysis without the need of too much extra computer space, in three dimensions it has seven nodes more. The computer space required by the twenty-seven noded Lagrangian element would have been as high as $2\frac{1}{2}$ times that needed by the Serendipity and for this reason was not used. More will be said about this in Chapter 6. Despite this the details of this element have been included here for the sake of completeness.

As can be seen from Figure 4.5 the number of pressure nodes on each face of both three-dimensional elements is four. This allows an exact linear pressure variation to be described uniquely on all faces. For the Langrangian element the number of velocity nodes per face is nine. This allows an exact quadratic velocity variation to be described uniquely also. The Serendipity element however only has eight velocity nodes per face. As a consequence only an incomplete but still unique velocity variation can be described on each face. Therefore for both elements, continuity of both velocity and pressure is ensured.

The shape functions in the curvilinear ξ, η and ζ coordinate system, which is shown and defined in Figure 4.6, are as follows. For the twenty noded Serendipity element i, the quadratic velocity shape functions are:

$$N'_{ij} = \frac{1}{8}(1+\xi_o)(1+\eta_o)(1+\zeta_o)(\xi_o+\eta_o+\zeta_o-2) \quad \text{for } j=1,3,5,7,13,15,17 \text{ and } 19$$

$$N'_{ij} = \tfrac{1}{4}(1-\xi^2)(1+\eta_o)(1+\zeta_o) \quad \text{for } j=4,8,16 \text{ and } 20$$

$$N'_{ij} = \tfrac{1}{4}(1+\xi_o)(1-\eta^2)(1+\zeta_o) \quad \text{for } j=2,6,14 \text{ and } 18$$

and

$$N'_{ij} = \tfrac{1}{4}(1+\xi_o)(1+\eta_o)(1-\zeta^2) \quad \text{for } j=9,10,11 \text{ and } 12 \qquad 4.14$$

where

$$\xi_o = \xi.\xi_{ij}$$

$$\eta_o = \eta.\eta_{ij}$$

and

$$\zeta_o = \zeta.\zeta_{ij} \qquad 4.15$$

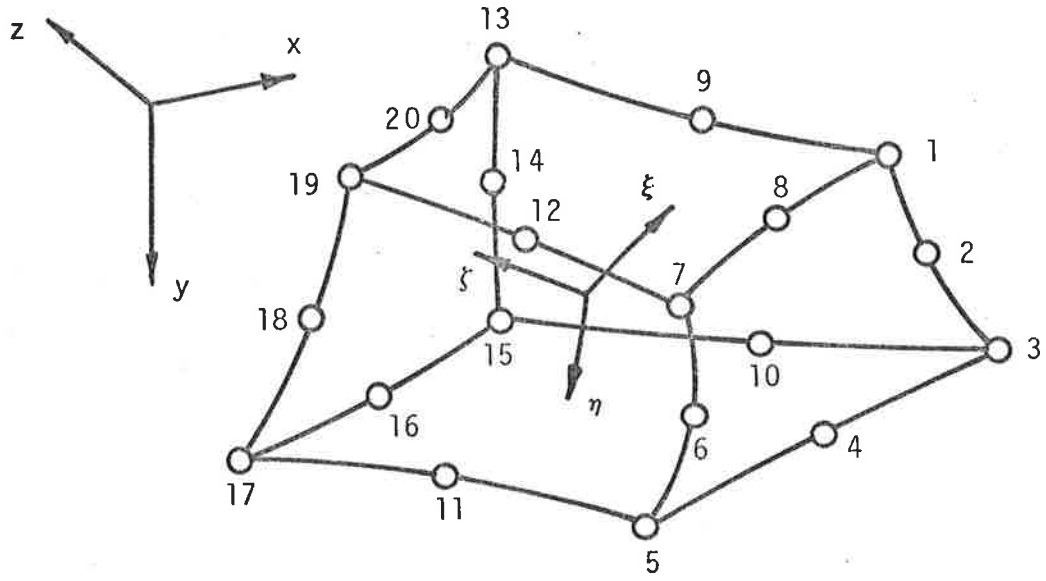

(a)

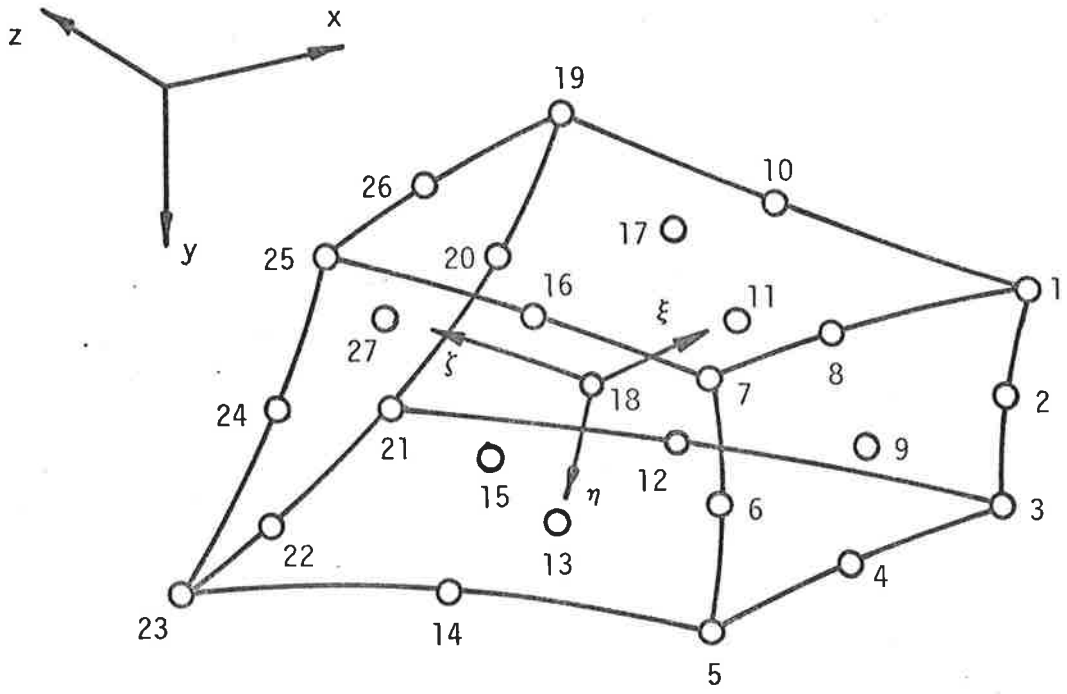

(b)

Figure 4.5 Typical (a) Twenty Noded Serendipity and (b) Twenty-seven Noded Lagrangian Isoparametric Elements.

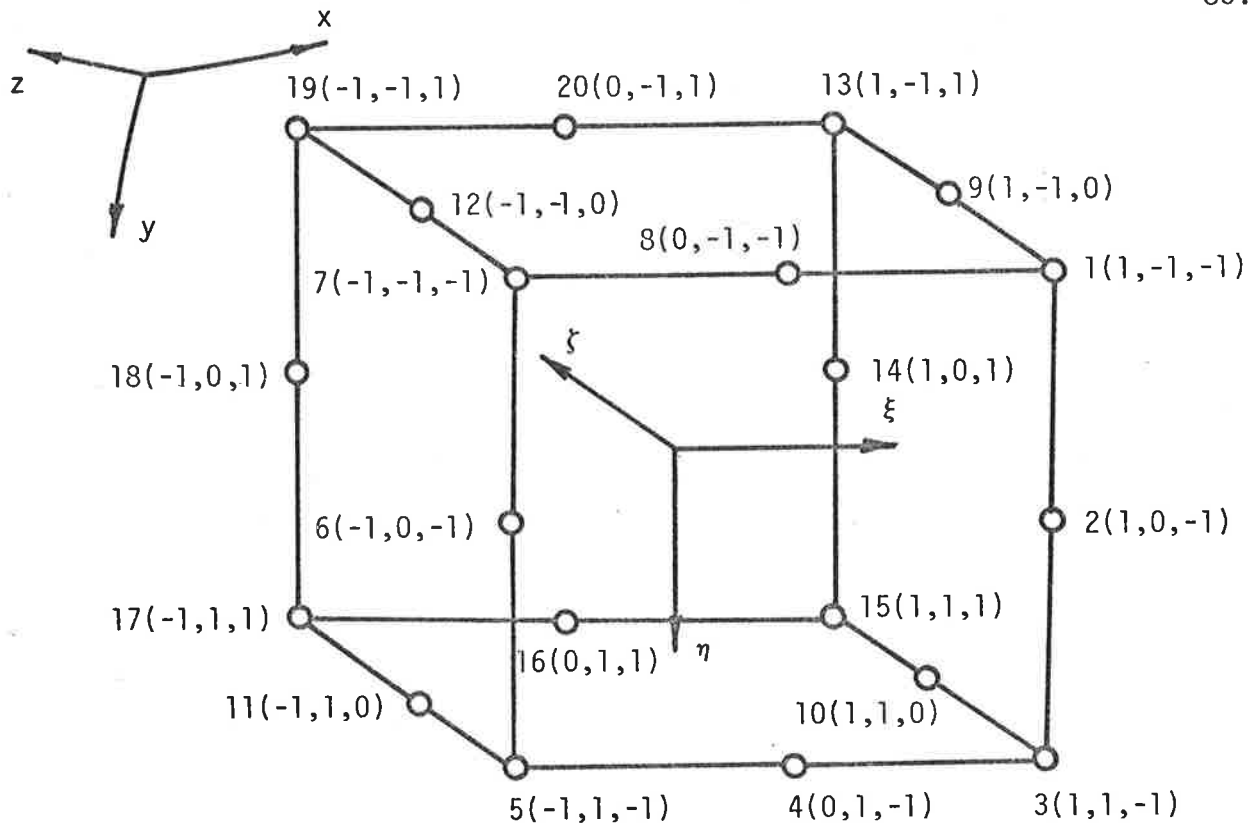

(a)

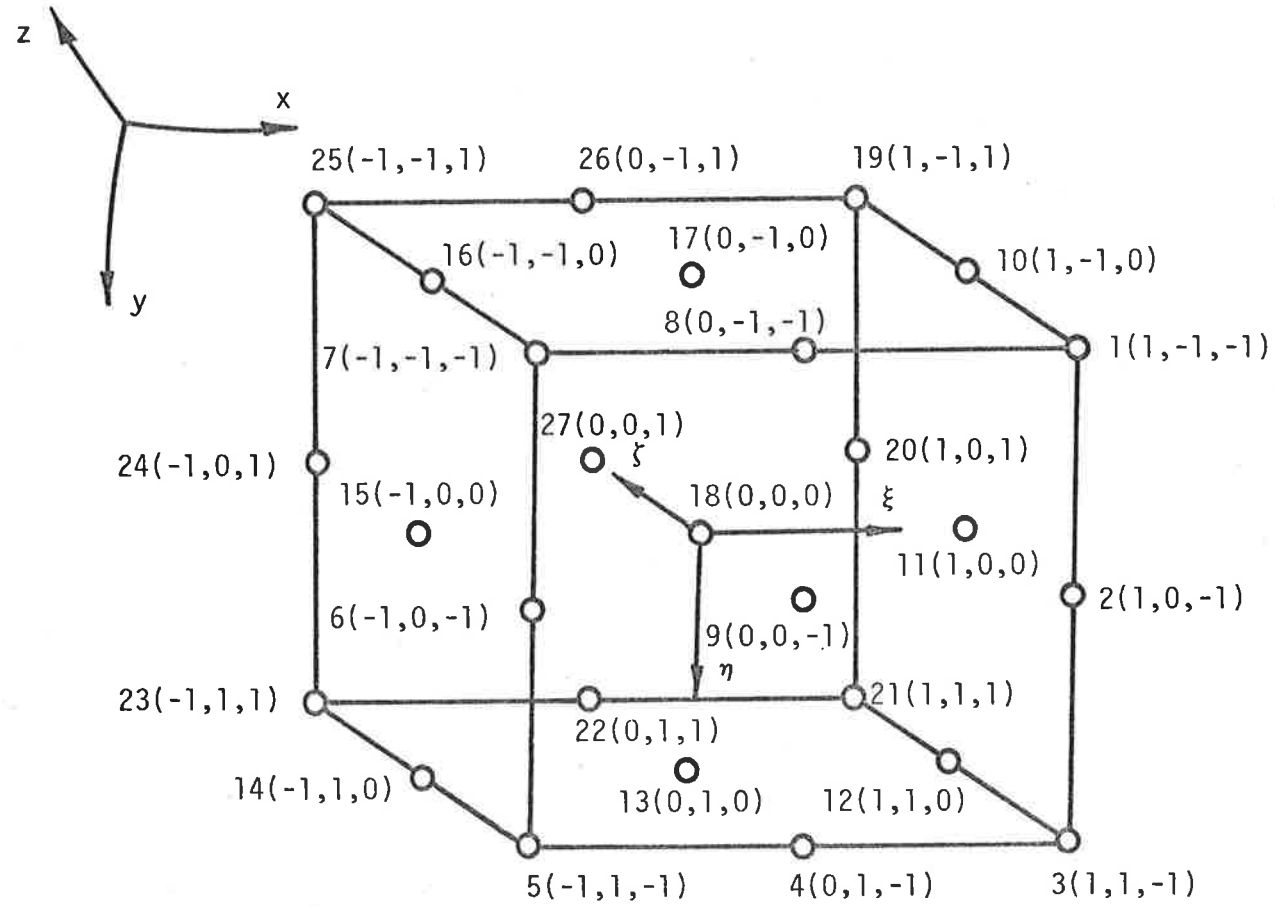

(b)

Figure 4.6 Parent (a) Twenty Noded Serendipity and (b) Twenty-Seven Noded Lagrangian Elements with ξ, η and ζ as Cartesian Coordinates.

and (ξ_{ij}, η_{ij}, ζ_{ij}) are the coordinates of node j in the ξ, η and ζ system, and given in Figure 4.6.

The linear pressure shape functions are:

$$N''_{ij} = \frac{1}{8}(1+\xi_o)(1+\eta_o)(1+\zeta_o) \quad \text{for j=1,3,5,7,13,15,17 and 19}$$

and $$N''_{ij} = 0 \quad \text{for j=2,4,6,8,9,10,11,12,14, 16,18 and 20} \qquad 4.16$$

where ξ_o, η_o, ζ_o, and (ξ_{ij}, η_{ij}, ζ_{ij}) are as defined above.

Similarly, for any twenty-seven noded Lagrangian element i, the quadratic velocity shape functions are:

$$N'_{ij} = \frac{1}{8}(1+\xi_o)\xi_o(1+\eta_o)\eta_o(1+\zeta_o)\zeta_o \quad \text{for j=1,3,5,7,19,21,23 and 25}$$

$$N'_{ij} = \tfrac{1}{4}(1-\xi^2)(1+\eta_o)\eta_o(1+\zeta_o)\zeta_o \quad \text{for j=4,8,22 and 26}$$

$$N'_{ij} = \tfrac{1}{4}(1+\xi_o)\xi_o(1-\eta^2)(1+\zeta_o)\zeta_o \quad \text{for j=2,6,20 and 24}$$

$$N'_{ij} = \tfrac{1}{4}(1+\xi_o)\xi_o(1+\eta_o)\eta_o(1-\zeta^2) \quad \text{for j=10,12,14 and 16}$$

$$N'_{ij} = \tfrac{1}{2}(1+\xi_o)\xi_o(1-\eta^2)(1-\zeta^2) \quad \text{for j=11 and 15}$$

$$N'_{ij} = \tfrac{1}{2}(1-\xi^2)(1+\eta_o)\eta_o(1-\zeta^2) \quad \text{for j=13 and 17}$$

$$N'_{ij} = \tfrac{1}{2}(1-\xi^2)(1-\eta^2)(1+\zeta_o)\zeta_o \quad \text{for j=9 and 27}$$

and $$N'_{ij} = (1-\xi^2)(1-\eta^2)(1-\zeta^2) \quad \text{for j=18} \qquad 4.17$$

The linear pressure shape functions are:

$$N''_{ij} = \frac{1}{8}(1+\xi_o)(1+\eta_o)(1+\zeta_o) \quad \text{for } j=1,3,5,7,19,21,23 \text{ and } 25$$

and $$N''_{ij} = 0 \quad \text{for } j=2,4,6,8,10 \ldots 17,18,20,22, 24 \text{ and } 26 \qquad 4.18$$

where ξ_o, η_o, ζ_o and $(\xi_{ij}, \eta_{ij}, \zeta_{ij})$ are as defined above.

The three-dimensional Jacobian matrix is

$$[J] = \begin{bmatrix} \frac{\partial x}{\partial \xi} & \frac{\partial y}{\partial \xi} & \frac{\partial z}{\partial \xi} \\ \frac{\partial x}{\partial \eta} & \frac{\partial y}{\partial \eta} & \frac{\partial z}{\partial \eta} \\ \frac{\partial x}{\partial \zeta} & \frac{\partial y}{\partial \zeta} & \frac{\partial z}{\partial \zeta} \end{bmatrix} \qquad 4.19$$

and by using the quadratic velocity shape functions to describe the geometry, that is

$$\left.\begin{aligned} x_i &= \sum_{j=1}^{K'} N'_{ij}\, x_{ij} \\ y_i &= \sum_{j=1}^{K'} N'_{ij}\, y_{ij} \end{aligned}\right\} \qquad 4.20$$

and $$z_i \quad \sum_{j=1}^{K'} N'_{ij}\, z_{ij}$$

the Jacobian can be expanded to:

$$[J] = \begin{bmatrix} \frac{\partial N'_{i1}}{\partial \xi} & \frac{\partial N'_{i1}}{\partial \xi} & & \frac{\partial N'_{iK'}}{\partial \xi} \\ \frac{\partial N'_{i1}}{\partial \eta} & \frac{\partial N'_{i1}}{\partial \eta} & \cdots & \frac{\partial N'_{iK'}}{\partial \eta} \\ \frac{\partial N'_{i1}}{\partial \zeta} & \frac{\partial N'_{i1}}{\partial \zeta} & & \frac{\partial N'_{iK'}}{\partial \zeta} \end{bmatrix} \begin{bmatrix} x_{i1}\ y_{i1}\ z_{i1} \\ x_{i2}\ y_{i2}\ z_{i2} \\ \vdots \\ x_{iK'}\ y_{iK'}\ z_{iK'} \end{bmatrix} \qquad 4.21$$

where K' is 20 for the Serendipity element and 27 for the Lagrangian, and (x_{ij}, y_{ij}, z_{ij}) are the coordinates of node j in the global x, y and z system. Therefore

$$\begin{Bmatrix} \frac{\partial}{\partial x} \\ \frac{\partial}{\partial y} \\ \frac{\partial}{\partial z} \end{Bmatrix} = [J]^{-1} \begin{Bmatrix} \frac{\partial}{\partial \xi} \\ \frac{\partial}{\partial \eta} \\ \frac{\partial}{\partial \zeta} \end{Bmatrix} \qquad 4.22$$

As for two dimensions an element of volume dV_i in the x, y and z system can be expressed in the ξ, η and ζ system by using

$$dV_i = \det J_i \, d\xi d\eta d\zeta \qquad 4.23$$

Thus all integrals in the matrices $[R_i]$ and $[S_i]$ can be rewritten in the form

$$\int_{-1}^{1}\int_{-1}^{1}\int_{-1}^{1} f(\xi,\eta,\zeta)\, d\xi d\eta d\zeta$$

by changing the limits of the integration.

The last thing that must be included in this section is the transformation of the surface integrals in each equation corresponding to a node on the portion of the outer boundary of the flow on which stresses can be specified. As for two dimensions, stresses may have at most a linear variation. Therefore on any element face the normal stress and the two shear stress components need only be specified at the four corner nodes and the linear pressure shape functions can then be used to interpolate between these points.

Consider Figure 4.7 which shows a normal stress p and two shear stresses s_1 and s_2 applied to face A of a typical boundary hexahedral element. The positive directions of applied normal and shear stresses are shown in Figure 4.8. It can be shown that at any point within an isoparametric element the vector with components

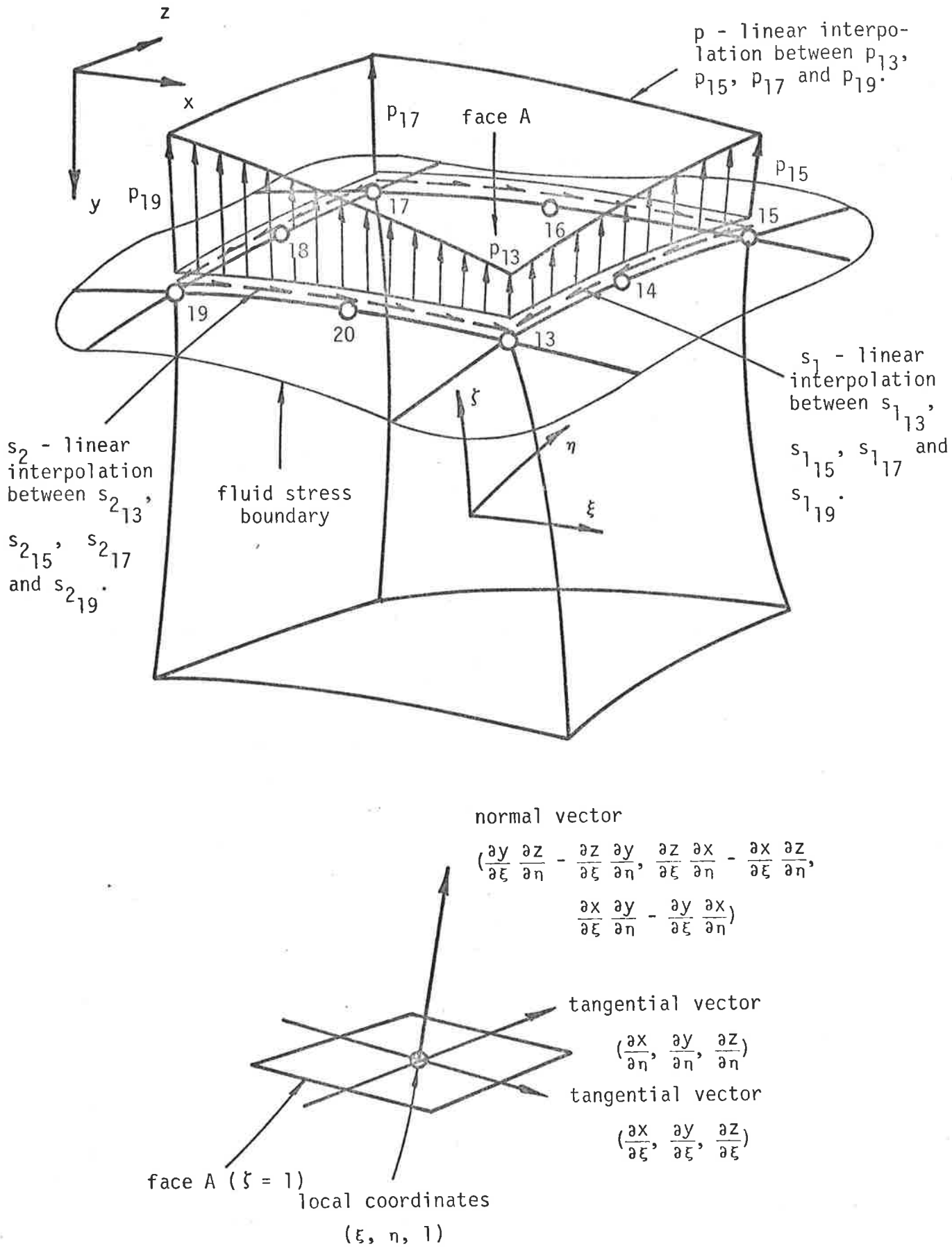

Figure 4.7 Typical Boundary Element with Applied Normal and Tangential Shear Stress Components, p, s_i and s_2.

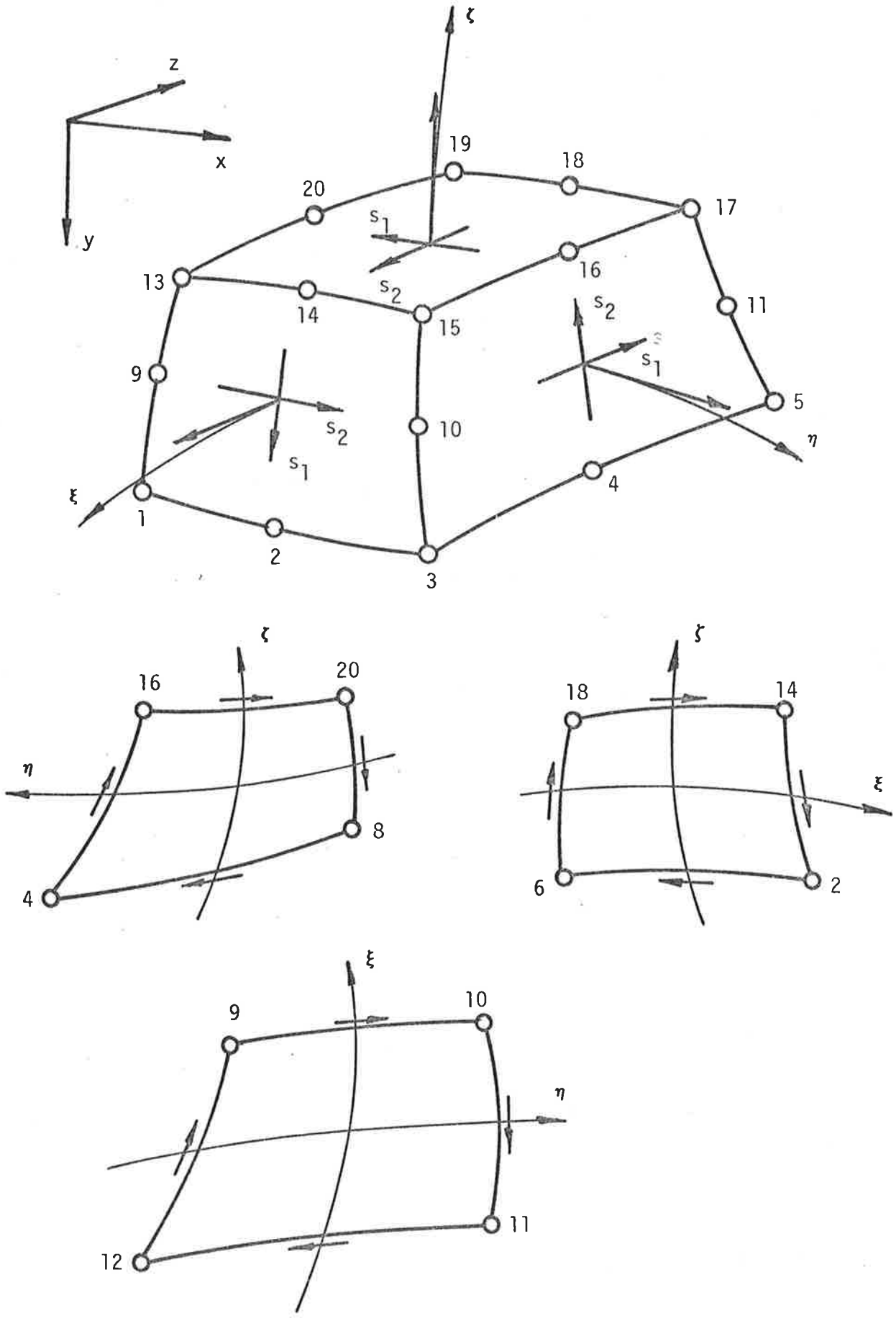

Figure 4.8 Positive Directions of Normal and Shear Stresses in Three Dimensions.

$$\left(\frac{\partial y}{\partial \eta}\frac{\partial z}{\partial \zeta} - \frac{\partial z}{\partial \eta}\frac{\partial y}{\partial \zeta}, \frac{\partial z}{\partial \eta}\frac{\partial x}{\partial \zeta} - \frac{\partial x}{\partial \eta}\frac{\partial z}{\partial \zeta}, \frac{\partial x}{\partial \eta}\frac{\partial y}{\partial \zeta} - \frac{\partial y}{\partial \eta}\frac{\partial x}{\partial \zeta}\right) \qquad 4.24.1$$

is normal to the plane ξ = constant while the vector

$$\left(\frac{\partial y}{\partial \zeta}\frac{\partial z}{\partial \xi} - \frac{\partial z}{\partial \zeta}\frac{\partial y}{\partial \xi}, \frac{\partial z}{\partial \zeta}\frac{\partial x}{\partial \xi} - \frac{\partial x}{\partial \zeta}\frac{\partial z}{\partial \xi}, \frac{\partial x}{\partial \zeta}\frac{\partial y}{\partial \xi} - \frac{\partial y}{\partial \zeta}\frac{\partial x}{\partial \xi}\right) \qquad 4.24.2$$

is normal to the plane η = constant and the vector

$$\left(\frac{\partial y}{\partial \xi}\frac{\partial z}{\partial \eta} - \frac{\partial z}{\partial \xi}\frac{\partial y}{\partial \eta}, \frac{\partial z}{\partial \xi}\frac{\partial x}{\partial \eta} - \frac{\partial x}{\partial \xi}\frac{\partial z}{\partial \eta}, \frac{\partial x}{\partial \xi}\frac{\partial y}{\partial \eta} - \frac{\partial y}{\partial \xi}\frac{\partial x}{\partial \eta}\right) \qquad 4.24.3$$

is normal to the plane ζ = constant. These vectors are directed outward from the element on the faces $\xi = 1$, $\eta = 1$ and $\zeta = 1$ and into the element on the faces $\xi = -1$, $\eta = -1$ and $\zeta = -1$. Similarly it can be shown that the vector with components

$$\left(\frac{\partial x}{\partial \xi}, \frac{\partial y}{\partial \xi}, \frac{\partial z}{\partial \xi}\right) \qquad 4.25.1$$

is tangential to the line η = constant, ζ = constant while the vector

$$\left(\frac{\partial x}{\partial \eta}, \frac{\partial y}{\partial \eta}, \frac{\partial z}{\partial \eta}\right) \qquad 4.25.2$$

is tangential to the line ξ = constant, ζ = constant and the vector

$$\left(\frac{\partial x}{\partial \zeta}, \frac{\partial y}{\partial \zeta}, \frac{\partial z}{\partial \zeta}\right) \qquad 4.25.3$$

is tangential to the line ξ = constant, η = constant. The directions of these tangential vectors are always in the positive ξ direction for the first, positive η direction for the second and the positive ζ direction for the third. It can again be found that the above normal vectors can be obtained from the columns of the inverse Jacobian matrix multiplied by det J, while the tangent vectors can be obtained from the rows of the Jacobian matrix itself.

Thus at any point on face A, $\zeta = 1$ and the stress in the x direction is

$$p\left(\frac{\partial y}{\partial \xi}\frac{\partial z}{\partial \eta} - \frac{\partial z}{\partial \xi}\frac{\partial y}{\partial \eta}\right) - s_1\left(\frac{\widehat{\partial x}}{\partial \xi}\right) + s_2\left(\frac{\widehat{\partial x}}{\partial \eta}\right) \qquad 4.26.1$$

in the y direction it is

$$p\left(\frac{\partial z}{\partial \xi}\frac{\partial x}{\partial \eta} - \frac{\partial x}{\partial \xi}\frac{\partial z}{\partial \eta}\right) - s_1\left(\frac{\widehat{\partial y}}{\partial \xi}\right) + s_2\left(\frac{\widehat{\partial y}}{\partial \eta}\right) \qquad 4.26.2$$

and in the z direction it is

$$p\left(\frac{\partial x}{\partial \xi}\frac{\partial y}{\partial \eta} - \frac{\partial y}{\partial \xi}\frac{\partial z}{\partial \eta}\right) - s_1\left(\frac{\widehat{\partial z}}{\partial \xi}\right) + s_2\left(\frac{\widehat{\partial z}}{\partial \eta}\right) \qquad 4.26.3$$

Thus any surface integral expressed in terms of x, y and z, say

$$\int_{S_i} N_{ij}^{!}\{\sigma_{xx}n_x + \sigma_{yx}n_y + \sigma_{zx}n_z\}\ dS$$

becomes

$$\int_{-1}^{1}\int_{-1}^{1}\{p\left(\frac{\partial y}{\partial \xi}\frac{\partial z}{\partial \eta} - \frac{\partial z}{\partial \xi}\frac{\partial y}{\partial \eta}\right) - s_1\left(\frac{\widehat{\partial x}}{\partial \xi}\right) - s_2\left(\frac{\widehat{\partial x}}{\partial \eta}\right)\}\ d\xi\ d\eta$$

expressed entirely in terms of ξ, η and ζ.

It should be noted that although the rows and columns of the Jacobian matrix and its inverse produce vectors that are respectively, tangent and normal to the surface of an element, the magnitude of these vectors, for the purpose of calculating the x, y and z components of stress are not always correct. In two dimensions this is not so. However in three dimensions, the tangential vectors, as obtained from the rows of the Jacobian matrix lead to incorrect equivalent nodal forces. On the other hand, the normal vectors, as obtained from the columns of the inverse Jacobian multiplied by det J have the correct direction as well as the correct magnitude. Therefore, in order to obtain the correct equivalent nodal force components when shear stresses are involved, at each point on the element's stress boundary (surface) one must first normalize the

tangential vectors and then scale them according to the magnitude of the normal vector at that point. In this way the tangential vectors will have the correct directions and magnitudes suitable for evaluating the equivalent nodal forces without further scaling. The caps on the shear stress terms in equations 4.26.1-3 indicate that they have been adjusted in this manner and that they differ in magnitude from the corresponding components in vectors 4.25.1-3.

4.2 Numerical Integration Details

Having selected an element type and defined associated quadratic and linear shape functions, the integrals in the coefficients and on the right hand sides of the element equations were transformed by making use of the isoparametric property of the element chosen and a change in integration limits, to integrals over a simpler geometric shape but with integrands that are complex rational functions of the local co-ordinates. The exact evaluation of these transformed integrals is difficult even when regular rectangular or brick elements, for which the Jacobian matrix is constant, are used. In these cases, and more so when elements with curved edges or faces are used, the evaluation of these integrals can only be done by computer if a numerical integration technique is employed.

In general, numerical integration of a function of one variable ξ involves the evaluation of the integrand $f(\xi)$ at n Gauss points $\xi=a_j$, $j=1, \ldots n$, multiplying these values by the corresponding prescribed numbers or weights w_j and summing the n results. That is

$$\int_{-1}^{1} f(\xi)\, d\xi \simeq \sum_{j=1}^{n} w_j\, f(a_j) \qquad 4.27$$

The particular form of numerical integration used in this study is the Gauss quadrature or numerical integration. This is the most accurate of the quadrature formulae in ordinary use (36). In this method the values of ξ at the n points at which the integrand is to be evaluated and n weights are chosen so that a polynomial of order less than or equal to 2n-1 can be integrated exactly. Therefore if $f(\xi)$ is any polynomial it can always be evaluated exactly by taking a sufficiently large number of Gauss points, n. However if $f(\xi)$ is not a polynomial, it must first be approximated by one, the order of which depends on the closeness of fit required (only within the limits of integration), and then the

number of Gauss points can be decided. In this case, numerical integration does not produce the exact value of the integral.

The double and triple integrals of functions of more than one variable can be evaluated in the same manner. Thus

$$\int_{-1}^{1}\int_{-1}^{1}\int_{-1}^{1} f(\xi,\eta,\zeta)\, d\xi d\eta d\zeta$$

$$= \int_{-1}^{1}\int_{-1}^{1} \sum_{i=1}^{n} w_i\, f(\xi_i,\eta,\zeta)\, d\eta d\zeta \text{ by treating } \eta \text{ and } \zeta \text{ as constants}$$

$$= \int_{-1}^{1} \sum_{j=1}^{n} w_j \sum_{i=1}^{n} w_i\, f(\xi_i,\eta_j,\zeta)\, d\zeta \text{ by treating } \zeta \text{ as constant}$$

$$= \sum_{k=1}^{n} w_k \sum_{j=1}^{n} w_j \sum_{i=1}^{n} w_i\, f(\xi_i,\eta_j,\zeta_k) \qquad 4.28.1$$

$$= \sum_{k=1}^{n} \sum_{j=1}^{n} \sum_{i=1}^{n} w_i w_j w_k\, f(\xi_i,\eta_j,\zeta_k) \qquad 4.28.2$$

$$= \sum_{l=1}^{n^3} w_l\, f(\xi_l,\eta_l,\zeta_l) \qquad 4.28.3$$

The integrals that were produced after the transformation from the x, y and z system to the ξ, η and ζ have the required limits for the numerical integration, but the integrand is in general not a simple polynomial function. This is because the Jacobian matrix used in the transformation has components that can be functions of ξ, η and ζ. Therefore its inverse, which is used to transform the derivatives, contains the factor $\frac{1}{\det J}$ where detJ is also a function of ξ, η and ζ. Therefore all the derivatives also contain this factor and by examining the integrals in the matrices $[R_i]$ and $[S_i]$, it will be seen that when transformed, the resulting integrands have quotients of two polynomials in the linear portion and a simple polynomial in the non-linear.

In this study it was decided to use n=3 Gauss points per coordinate direction in order to evaluate these integrals numerically. This results in nine and twenty-seven Gauss points in two- and three-dimensional elements respectively. It allows a polynomial of order 5 in terms of ξ, η and ζ to be evaluated exactly. Three Gauss points per direction were also used to evaluate numerically the surface integrals. Figure 4.9 shows the position of the 3x3 Gauss points in the two-dimensional quadrilateral element while Table 4.1 lists the weights associated with each point. The three-dimensional arrangement of Gauss points in a typical hexahedral element is difficult to present and has not been included. However Table 4.1 can also be used to define the location and the weights of each Gauss point in a three-dimensional element.

Recently it has been advocated by some researchers (11) that reduced integration, that is, using less Gauss points than would normally be employed, leads to improved solutions. This aspect, although important since a considerable amount of computation time is saved if fewer Gauss points are used, was not investigated in this study.

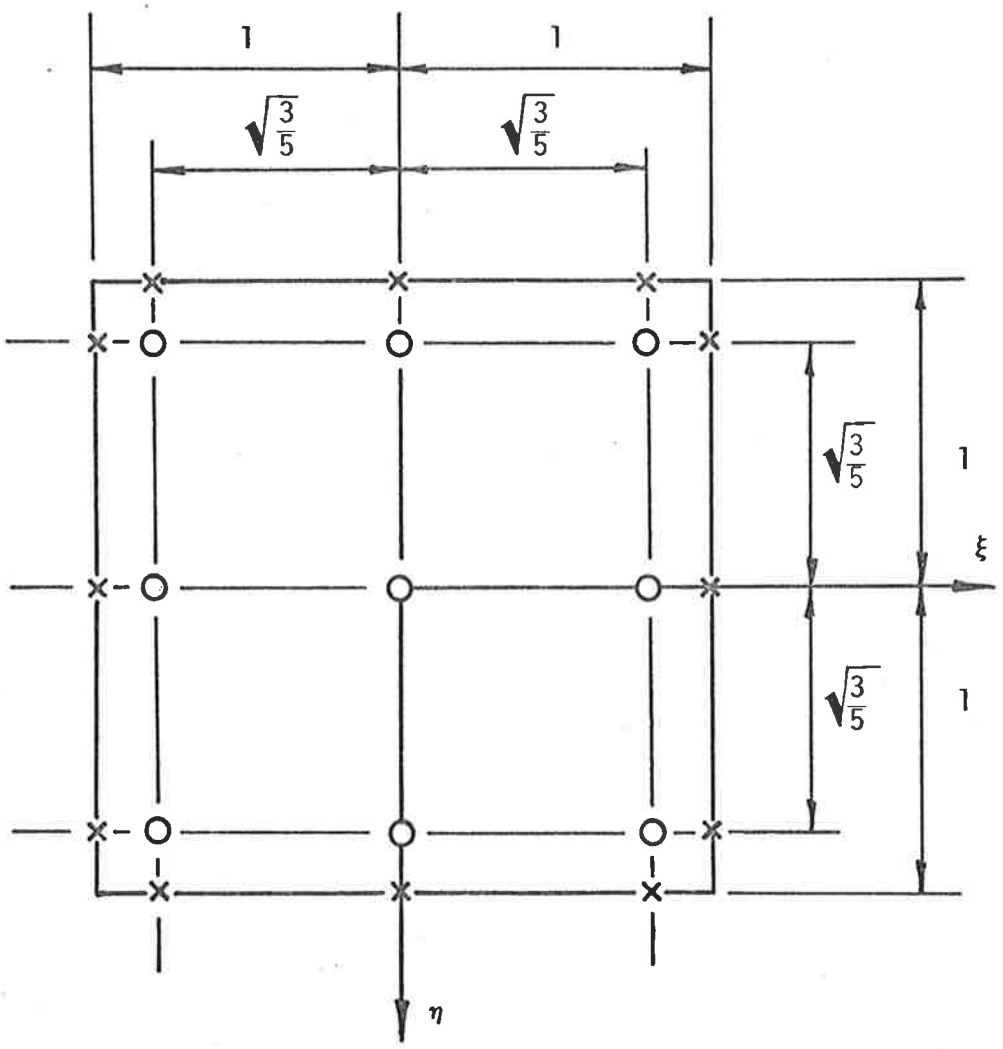

Figure 4.9 Positions of Gauss Points in a Two-Dimensional Element for n=3 for the Evaluation of Area Integrals (O) and Line Integrals (×).

i	ξ_i	η_i	ζ_i	w_i
1	a	a	a	$\frac{5}{9}$
2	0	0	0	$\frac{8}{9}$
3	-a	-a	-a	$\frac{5}{9}$

where $a = \sqrt{\frac{3}{5}} = 0.77459\ 66692\ 41483$

$$\int_{-1}^{1} f(\xi)\, d\xi = \sum_{i=1}^{3} w_i\, f(\xi_i)$$

$$\int_{-1}^{1}\int_{-1}^{1} f(\xi,\eta)\, d\xi d\eta = \sum_{i=1}^{3}\sum_{j=1}^{3} w_i w_j\, f(\xi_i,\eta_j)$$

$$\int_{-1}^{1}\int_{-1}^{1}\int_{-1}^{1} f(\xi,\eta,\zeta)\, d\xi d\eta d\zeta = \sum_{i=1}^{3}\sum_{j=1}^{3}\sum_{k=1}^{3} w_i w_j w_k\, f(\xi_i,\eta_j,\zeta_k)$$

Table 4.1 Positions of Gauss Points and Associated Weights for n=3

4.3 Some Important Computer Programming Aspects

Having established the theoretical background for the selected modelling and solution procedures, the final step in this study was to obtain a solution to a general two- and three-dimensional viscous flow problem. A large amount of time was spent in this section of the research because the development and debugging of the computer programs that were set up to find these solutions was a slow process. In all, four programs were written and developed, debugged and tested. The two two-dimensional programs differed only in the type of element incorporated. Program CR2DVF8 used the eight noded Serendipity isoparametric element, while program CR2DVF9 the nine noded Lagrangian element. The two three-dimensional packages both used the twenty noded Serendipity element but the second, program CR3DVF2 incorporated an additional out of core storage facility in the solution routine that enabled it to handle problems with a larger number of nodes and elements. It was written because it was found that program CR3DVF1 could solve a problem with a finite element mesh no bigger than three elements by three elements in cross-section. Even this required the full core capacity available in the Cyber 173, and as a result program CR2DVF1 was little used. It is important to mention at this stage that all programs were written to be as economical in terms of core requirements as possible, although at times a loss of computing efficiency resulted. Typically, a two-dimensional problem with 150 elements and 500 nodes would require approximately $75{,}000_8$ words of central memory and solution times in the region of 150 central processor seconds per iteration. On the other hand, a three-dimensional problem with 40 elements and 300 nodes and solved using program CR3DVF2 would require $130{,}000_8$ central memory words and 800 central processor seconds per iteration. The above figures are only approximate and are largely dependent on the configuration of the finite element mesh used.

The first two-dimensional program written, CR3DVF8, was based on and followed closely the lines of one written earlier by Yeo for two-dimensional stress analysis and described in detail in the book by Cheung and Yeo (9). It incorporates the eight noded isoparametric element and the well known and efficient solution technique, the Front Solver. Program CR2DVF8 however differed from the one written by Yeo (called ISOP) in three major areas. Firstly, a mixed interpolation was included in program CR2DVF8 resulting in a variable number of unknowns per node, either two or three rather than just two as in ISOP. Secondly, the global stiffness matrix resulting from a viscous flow problem, unlike that for an elasticity problem, is always unsymmetrical. This means that the full matrix rather than just the half above and including the leading diagonal, must be stored and used at all times. Thirdly, because a viscous flow problem has equations that are non-linear, an iterative solution procedure had to be incorporated in program CR2DVF8.

The structure of CR2DVF8 and the three subsequent programs consists of a master main program supported by a number of specialized subroutines to which control is transferred as the need arises. The subprograms perform the basic tasks of accepting and checking the input data, evaluating the Frontal solution parameters, setting up the element equations and their right hand sides, assembling and solving the global equation system and finally, checking the solution at each iteration for convergence. A flow chart showing the basic layout of the four programs is given in Appendix B. In setting up program CR2DVF8, several problems were encountered. A discussion of two of the more troublesome now follows.

The first problem found and probably the most tedious to solve was the incorporation of the mixed interpolation for velocity and pressure. This affected all areas of the program since the number of unknowns per node, now dependent on the node type, is referred to in

almost every subroutine. It was originally intended to treat all nodes alike. This could be done by setting up a zero equation corresponding to the pressure variable at all midside nodes where the only unknowns are the two velocity components. Minor problems occurring when the solution procedure encountered a zero equation could be overcome and a solution with a meaningless zero pressure at all midside nodes could be obtained.

However, after a short calculation, it was found that over half the nodes in a typical two-dimensional mesh are midside nodes. This meant that if a mesh with 600 nodes was used, over 300 zero equations corresponding to pressure and not contributing to the solution, would be processed like normal non-zero equations each iteration. The additional core and execution time required to incorporate mixed interpolation in this fashion were unacceptable. This difficulty was finally overcome by including in the program at every relevant point a facility for adjusting the number of variables for a midside node from three to two. This added a considerable number of lines to each subroutine and was particularly tedious to implement.

The other major problem encountered occurred during the testing of CR2DVF8, when it was found that very small and very large numbers were being combined in the solution procedure, with the consequent loss of accuracy due to rounding off. The large and small numbers appeared as a consequence of the technique adopted for incorporating specified variables, and because the global Continuity equations corresponding to nodes with a pressure unknown have no pressure dependence and therefore have a zero on the leading diagonal of the global stiffness matrix. Whenever a variable is specified in the boundary conditions, a large number, for example 10^{10}, is added to the coefficient corresponding to that variable in the equation corresponding to that variable. As can be seen from the example in Figure 4.10, after sufficient reduction

leading diagonal

...	$a+10^{10}$	b	c	... equation (a) corresponding to a specified velocity
...	d	0	e	... a pressure equation (b)
...	f	g	h	... equation (c) corresponding to an unknown velocity

by round-off, equation system reduces to

...	10^{10}	b	c	... (a)
...	d	0	e	... (b)
...	f	g	h	... (c)

after reduction using equation (a) system is

...	10^{10}	b	c	... (a)
...	0	$-dbx10^{-10}$	$e-cdx10^{-10}$	... (b')
...	0	$g-bfx10^{10}$	$h-fcx10^{-10}$	... (c')

by round-off, equation system reduces to

...	10^{10}	b	c	... (a)
...	0	$-dbx10^{-10}$	e	... (b')
...	0	g	h	... (c')

after reduction using equation (b') system is

...	10^{10}	b	c	... (a)
...	0	$-dbx10^{-10}$	e	... (b')
...	0	0	$h+\frac{eg}{db}x10^{10}$	... (c")

by round-off, equation system reduces to

...	10^{10}	b	c	... (a)
...	0	$-dbx10^{-10}$	e	... (b')
...	0	0	$\frac{eg}{db}x10^{10}$	... (c")

all coefficients in equation (c) have been over-ridden by 10^{10} terms and lost due to round-off.

Figure 4.10 Example of Loss of Information Resulting from Computer Round-Off.

cycles of the Gaussian elimination process, which forms the basis of the Front Solver, numbers of the order of 10^{-10} appear on the leading diagonal in the Continuity equations. When the turn comes for these equations to be used in the reduction elimination process, pivots (leading diagonal coefficients) of order 10^{-10} are used and, as is shown in Figure 4.10, round-off errors are introduced as a result. It is important to stress that this situation would not have occurred if the Continuity equation was a "true" equation containing a pressure dependent term as well as the velocity component terms.

To overcome this problem the Front Solver had to be modified as follows. Firstly in any reduction step, instead of using the first fully assembled equation found in a search from the top of the global stiffness matrix as the equation to be eliminated, a search is made of all the fully assembled equations currently in the global stiffness matrix, and the one with the largest leading diagonal coefficient is used. This resulted in the Continuity equations, all containing pivots of the order of 10^{-10}, remaining in the global stiffness matrix until no other equation could be used. The same problem then occurred when these equations were used. A second modification was then made so that, rather than assembling the equations of each element one at a time and at each stage eliminating all fully assembled equations, the equations for as many elements as possible are assembled in the given working area, and when this is done, only sufficient fully assembled equations are eliminated as will enable the equations of the next element to be assembled. Thus at all stages as many fully assembled equations as possible are present in the global stiffness matrix.

This however still did not prevent the last equations from having very small leading diagonal coefficients. The problem was finally solved by, in addition to the above two modifications, further changing the solution procedure so that at each reduction stage, when the working

area has as many fully assembled equations in it as possible, rather than simply chosing the fully assembled equation with the largest pivot, a pair of fully assembled equations are added and this combined equation used. The equations added must produce the pivot with the largest magnitude and only fully assembled equations for unspecified variables can be considered. This eliminated the round-off errors and program CR2DVF8 then started producing the required solutions.

Program CR2DVF9 is identical to program CR2DVF8 with the exception of the element type used. The nine noded Lagrangian isoparametric element incorporated in CR2DVF9 has one internal node more than the Serendipity element. There is no pressure variable associated with this additional node and the two velocity equations corresponding to it have no surface integrals on their right hand sides. Thus once the element equation system has been constructed, the two velocity equations corresponding to the internal node can be eliminated from it, thereby reducing the number of element equations to 24, the same number as for the eight noded element. Program CR2DVF9 is therefore identical to program CR2DVF8 except in the subroutines that set up the element equations where a pre-assembly reduction is performed, and in the back-substitution subroutine where the two equations per element are used to calculate the two velocity components at each mid-element node.

The three-dimensional program CR3DVF1 is directly analogous to CR2DVF8. It uses the twenty noded Serendipity element and incorporates the same modifications to the solution routine as in programs CR2DVF8 and CR2DVF9. It therefore needs no further discussion other than to say that it is considerably longer and more complex than the corresponding two-dimensional program. A listing of this three-dimensional program is not included because of space limitations. However a listing of CR3DVF2 which incorporates an out of core storage facility in the Front Solver and is the more viable of the two, is given in Appendix B.

The out of core solution technique is essentially a process in which two disc files are used to store the global equations during the assembly and reduction procedures. At any reduction step only a small portion of the global equations are in core at any one time. When required, groups of equations are read from one disc file into core, manipulated, and when they are no longer needed, are written from core to the second file. This process of reading from one file and writing to the other is very time consuming, but since the storage capacity of a disc file is very large, the only limit in size of problem that can be handled by this technique is the in-core working space. In the limit, one equation is read and written at each read-write step. However, the front width for a problem requiring this extreme facility must be in excess of 2000, a very large problem even in three dimensions.

This now completes the discussion on the computer programs. However, before proceeding to the presentation of results, it was considered necessary to include in this thesis the numerical values of the stiffness matrix for at least one particular element. Therefore in Appendix C, the stiffness matrices for a two-dimensional, eight and nine noded, one unit square element have been set out in full. The 24x24 and 27x27 element stiffness matrices have been evaluated using formulation B and programs CR2DVF8 and CR2DVF9. With these, future researchers will be able to check whether the computer programs used in this study operated correctly, and will have some definite numerical values with which to check the operation of their programs.

CHAPTER 5

RESULTS OF ANALYSES AND COMPARISONS IN TWO DIMENSIONS

5.1 Computational Test Program Details

5.2 Entrance Flow Problem Details

5.3 Cavity Flow Problem Details

5.4 Results of Formulation Comparison

5.5 Results of Element Comparison

5.6 Presentation of Entrance and Cavity Flow Problem Results, and Comparison with Other Published Solutions

5. RESULTS OF ANALYSES AND COMPARISONS IN TWO DIMENSIONS

In developing a possible new numerical scheme for solving the Navier-Stokes equations or in improving an existing approach, previous researchers have used a variety of viscous flow problems on which to test and demonstrate the advantages of their proposals. Besides the simpler Poiseuille and Couette flows, two other viscous flow problems that have been traditionally used, are the flow in the entrance region between two semi-infinite parallel plates and the recirculating flow in a square cavity, both of which have no known exact closed-form solution. In this chapter, all aspects concerning the finite element analysis of each of these two flows, including detailed discussions on boundary conditions and mesh configurations, are set out, and the results from these analyses used, firstly in a comparison to determine the optimal formulation of the Navier-Stokes equations, and secondly in a comparison to determine the more efficient of the two two-dimensional finite elements considered. Because the number of lengthy computer runs required for each problem and the amount of results involved is so large, it was decided to use only the above two flow problems in both the formulation and the element comparisons. These two flows are of sufficiently different character to justify one drawing the conclusion that any trend displayed in the results of both these flows may be considered typical of any two-dimensional viscous flow problem.

5.1 Computational Test Program Details

In order to carry out a conclusive comparison of the finite element formulations of the four versions of the Navier-Stokes equations, both the entrance flow problem and the cavity flow problem were used. However, before a full scale test program for each of these flows was undertaken, some preliminary tests on the Poiseuille flow were carried out to ensure that the computer programs written were in fact operating correctly.

It was during these initial tests that a fundamental difference in the performance of the eight and nine noded isoparametric elements became evident. Details of the tests and the solutions obtained are given in Appendix D, but the more important aspects are repeated in the following paragraph.

Essentially, it was found that when the eight noded element was used, the exact solution to the Poiseuille flow was obtained only if the elements in the mesh were rectangular in shape. When trapezoidal or general quadrilateral elements were included, the velocity, and especially the pressure fields obtained, were considerably in error. However when the nine noded element was employed, the exact solution was obtained regardless of which element shapes were used. This behaviour was found to occur with all four finite element formulations of the Navier-Stokes equations and it was therefore concluded that it was not due to a formulation effect. Its explanation was finally found to lie in the choice of quadratic interpolation function used to describe the velocity variation within each element. As was mentioned in Chapter 4, the eight noded Serendipity element has velocity shape functions that result in an incomplete quadratic velocity interpolation. On the other hand, the nine noded Lagrangian element is capable of giving a complete quadratic interpolation for velocity. Although this basic difference did not seem very significant initially, it was found, as is shown in Appendix D, that if a quadratic velocity variation is imposed on a trapezoidal element by speficying its exact value at all the nodes, the function describing the velocity variation at any point within the element and obtained by using the corresponding shape functions, is exact if the Lagrangian element is used, but substantially in error when the Serendipity element is employed. As a result, since the Galerkin finite element procedure is essentially a minimization of a total error or residual in an integrated average sense, when the

eight noded element is used, errors resulting from its inability to represent exactly velocity variations of the type described above are distributed across each element and throughout the variables. Thus even though the pressure may have been interpolated exactly in its own sense, in an overall element and subsequently global approximation, considerable loss of accuracy can occur when trapezoidal or general quadrilateral eight noded Serendipity isoparametric elements are used.

With the above findings in mind, a series of computer runs for the comparison of formulations A to D were planned and carried out on both the entrance flow and the cavity flow problems. In order to avoid problems associated with inadequacies in interpolation, two finite element meshes, one for the entrance flow, ENFLM1 and the other for the cavity flow, CAVFLM1 were constructed entirely of rectangular elements. This was done to enable either the eight or the nine noded element to be used without loss of accuracy. Since it was anticipated that the nine noded Lagrangian element would require considerably more computer storage and execution time, and since the number of computer runs required was quite substantial, it was decided to use only the eight noded Serendipity element in this first series of tests. However, to ensure that the above decision was in fact correct, spot checks were made by rerunning several of the tests using the nine noded element. Table 5.1 shows the runs that were carried out for each of the two problems. The single asterisk indicates that the eight noded Serendipity element was used while the double asterisk indicates that both the eight noded Serendipity and the nine noded Lagrangian elements were used. The results obtained from these runs are used in Section 5.4 to determine the most efficient and most accurate of the formulations A to D.

(a)

Re	Formulation			
	A	B	C	D
1	*	**	*	*
200	*	**	*	*
500	*	**	*	*
1000	**	**	**	**
2000	*	**	*	*

(b)

Re	Formulation			
	A	B	C	D
1	*	**	*	*
100	*	**	*	*
400	**	**	**	**
1000	*	**	*	*
2000	*	**	*	*

Table 5.1 Computer Runs Carried out (a) on mesh ENFLM1 for the entrance flow problem, and (b) on mesh CAVFLM1 for the cavity flow problem, in Computational Test Series 1.

With the first series of runs completed and the comparison performed, a second series of computational tests for the comparison of the eight and nine noded elements was planned and undertaken. In order to verify that the eight noded element was in fact as accurate as the nine noded when all elements in a mesh are rectangular, the first part of this second series involved using meshes ENFLM1 and CAVFLM1 again. For the second part it was necessary to construct two additional meshes, ENFLM2 for the entrance flow and CAVFLM2 for the cavity flow, both incorporating trapezoidal as well as rectangular elements. The results of this second series of tests are presented in Section 5.5 in which the more effecient element is determined. It should be noted that in all tests carried out in the second series, only the optimal formulation determined in the first comparison was used. Table 5.2 shows the computational tests performed in this series.

(a)

Re	8NE		9NE	
	ENFLM1	ENFLM2	ENFLM1	ENFLM2
1	*	*	*	*
200	*	*	*	*
500	*	*	*	*
1000	*	*	*	*
2000	*	*	*	*

(b)

Re	8NE		9NE	
	CAVFLM1	CAVFLM2	CAVFLM1	CAVFLM2
1	*	*	*	*
100	*	*	*	*
400	*	*	*	*
1000	*	*	*	*
2000	*	*	*	*

Table 5.2 Computer Runs Carried out (a) on the entrance flow problem, and (b) on the cavity flow problem, in Computational Test Series 2.

5.2 Entrance Flow Problem Details

As is suggested by its name, this classical fluid mechanics problem involves the prediction at various cross-sections downstream of the entrance edge, of the velocity and pressure profiles of a fluid entering a channel formed by two semi-infinite parallel plates, spaced a distance d apart. It is a well known fact that beyond a critical distance from the entrance edge, full flow development is realized and the parabolic velocity and constant pressure profiles, characteristic of the Poiseuille flow, obtained. The fact that this distance, which is Reynolds number dependent and often referred to as the development length, can be a significant fraction of the channel length, makes its determination a matter of considerable practical importance. Figure 5.1 shows all the essential details required to define the two-dimensional entrance flow problem. However, before proceeding into a detailed discussion of the finite element analysis of this problem, it is worthwhile looking briefly at some of the more important advances made by previous workers in an attempt to solve the entrance flow problem.

Since obtaining an exact analytical solution to this problem is not possible, various approximate solutions, mostly involving some form of boundary layer approximation, have been presented since as early as 1934. Schlichting (28) considered the entrance flow problem and used series expansions near to and far from the entrance, in a velocity profile matching procedure. Van Dyke (33) later improved Schlichting's solution near the entrance edge by using an upstream expansion whose first approximation is the leading edge solution of the flow past a semi-infinite flat plate. Many other analytical approximations, too numerous to mention here but well documented by Van Dyke (33), have been used in an effort to accurately model this problem, but the greatest advance took place when the finite difference method was used. The most frequently cited work in this area was performed by Bodoia and

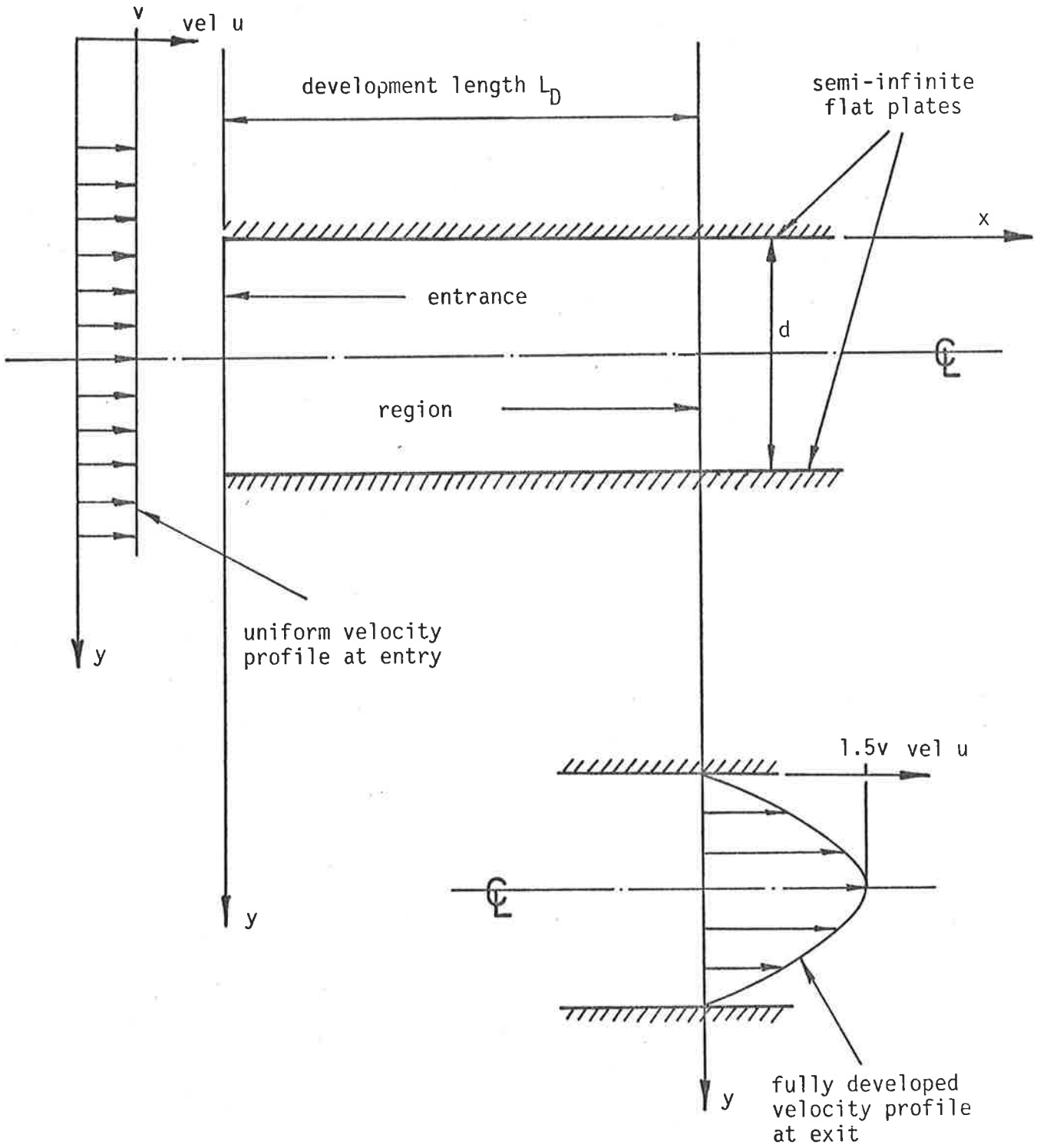

Figure 5.1 Entrance Flow Problem Details.

Osterle (4) who applied the finite difference method to the solving of the boundary layer equations for the entrance problem. However, it was not until several years later that the finite difference technique was finally used to successfully solve the full Navier-Stokes equations. Brandt and Gillis (5) and Morihara and Cheng (21), whose results are used for comparison in this thesis, have obtained stable numerical solutions to the entrance problem for Reynolds numbers based on the channel width as high as 2000. Only recently has the finite element method been applied to the solution of this problem (18, 29).

The entrance flow problem as it is defined in Figure 5.1, must firstly be rendered dimensionless before the non-dimensional form of the Navier-Stokes equations can be used to find its solution. The characteristic velocity and length chosen to do this are the inlet velocity v and the channel width d, respectively. The Reynolds number that appears in the governing equations is therefore defined as $Re = \frac{\rho v d}{\mu}$, and the details defining the corresponding dimensionless problem in which symmetry has been used to reduce the flow domain to the upper half channel, are shown in Figure 5.2.

In applying the finite element method to the solution of the entrance flow problem, it was immediately realized that the finite element mesh, that is, the arrangement of elements chosen to represent the flow, should incorporate relatively small elements close to the channel wall at the entrance edge. This enables the large velocity gradients occurring there as a result of the inlet velocity changing from unity to approximately zero over a very short distance, to be represented accurately. It was anticipated that relatively small elements would also be needed adjacent to the wall for a considerable distance downstream of the entrance edge. This is due to the fact that in viscous flows the effects of viscosity are usually confined to regions adjacent to solid boundaries and commonly known as boundary layers,

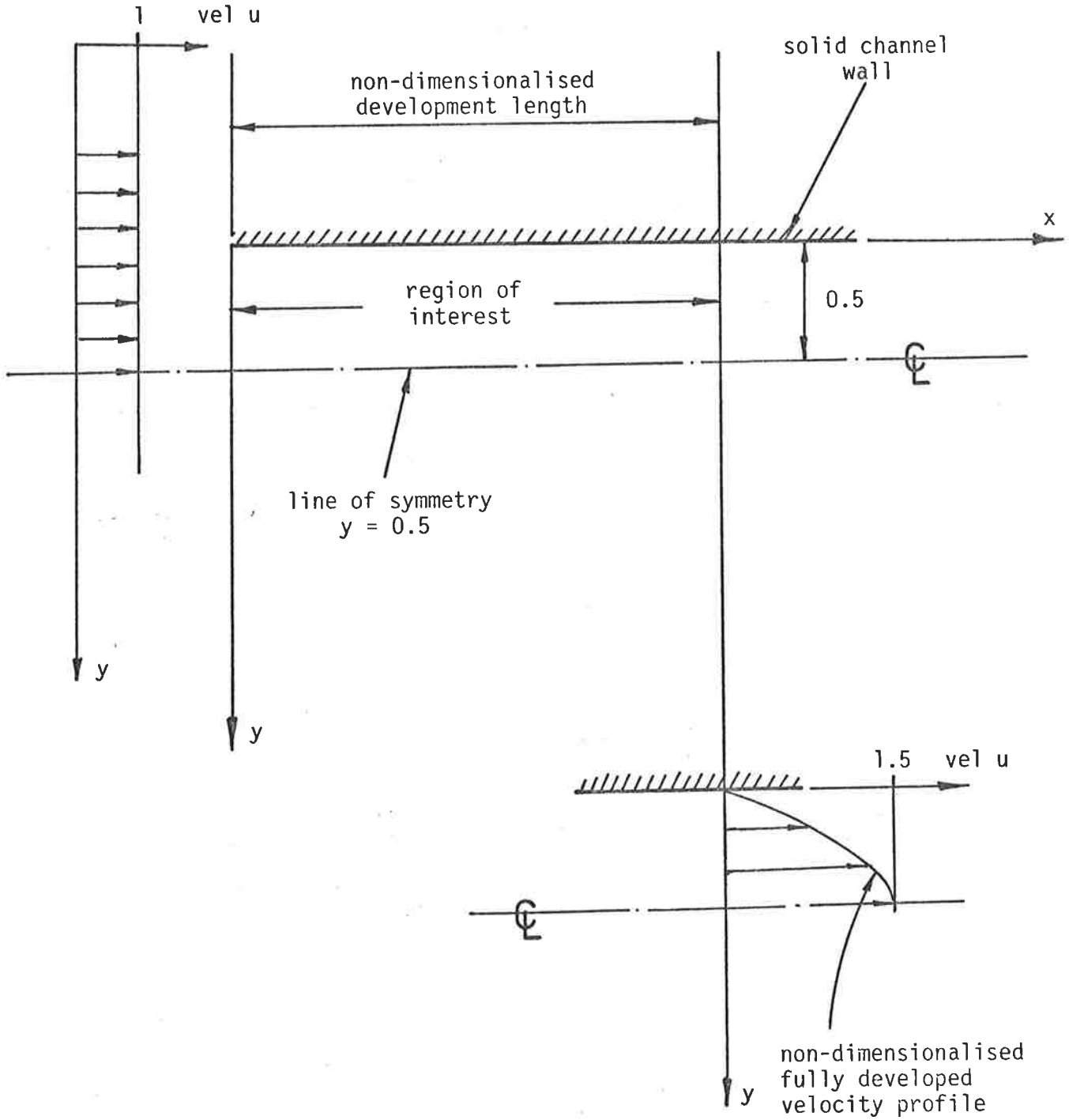

Figure 5.2 Non-dimensionalised Entrance Flow Problem Details.

the thickness of which generally decreases as Reynolds number increases and inside which most of the significant velocity gradients can be found. In the entrance flow problem, a boundary layer of zero thickness at the start of the channel wall and increasing gradually to half the channel width at approximately one development length downstream, can be found along both walls of the channel. In order to adequately represent the large velocity gradients that occur in these regions, at least one, and preferably two, layers of elements should be placed along the wall and within a boundary layer's thickness from it. It is obvious that as the Reynolds number of the flow is increased and the thickness of the boundary layer at any given cross-section decreases, the size of these wall elements can become very small, especially close to the entrance edge.

From the above it can be seen that in order to construct an efficient finite element mesh capable of adequately representing the fluid motion at any point along the wall, an estimate of the thickness of the boundary layer that exists there, must be obtained. As a first approximation, the solution to the flow around a semi-infinite flat plate immersed in a fluid moving parallel to its axis, can be used. A short investigation into some of the analytical studies previously carried out on this problem, such as those performed by Davis (10), revealed that the behaviour of the fluid around the plate can be adequately described by the well known Blasius solution, an excellent description of which has been presented by Rosenhead (26) in his book on laminar boundary layers. However, this solution is only of limited use since it is not valid within a small region at the leading edge of the plate. It is in this region that the size of element is most critical. Improvements to the Blasius solution in the vicinity of the leading edge have recently been proposed; however the exact behaviour of the fluid in this region is still not fully understood and its math-

ematical modelling still not complete. As a consequence it was decided to carry this investigation no further and to fix the size of the smallest element in the wall-leading edge corner of the mesh at 0.1% of the channel width, this figure being selected so that, with a suitable grading of elements from this corner out, a mesh with a reasonable number of elements resulted.

In order to be able to use the properties of a fully developed Poiseuille flow as boundary conditions at the downstream end, the finite element mesh must extend to a section at least one development length downstream of the entrance edge. Since the development length L_D is Reynolds number dependent and given approximately for Reynolds numbers greater than 100 by

$$L_D = k\ Re \qquad 5.1$$

where k, previously determined by other researchers and compared by Brandt and Gillis (5), ranges from 0.040 to 0.048, it is obvious that a different mesh length would be required for each Reynolds number to be considered. To avoid having to modify their meshes for each change in Reynolds number, previous researchers scaled the x coordinate in such a way that allowed full flow development always to be attained within the length of one mesh. In this study however, scaling is not used. Rather it was decided to construct one mesh suitable for solving a flow with Reynolds number equal to 2000, and then to use this mesh to solve all other flows with Reynolds numbers less than this value.

The resulting mesh, incorporating only rectangular elements, is shown in detail in Figure 5.3 and will subsequently be referred to as mesh ENFLM1. It is 200x0.5 in overall size and contains 541 nodes defining 162 elements which range in size from 0.001x0.001 to 0.3x100. The finite element solutions of the entrance flow problem obtained with this mesh are used in both the comparison of formulations A to D and in the comparison of the performance of the eight and nine noded

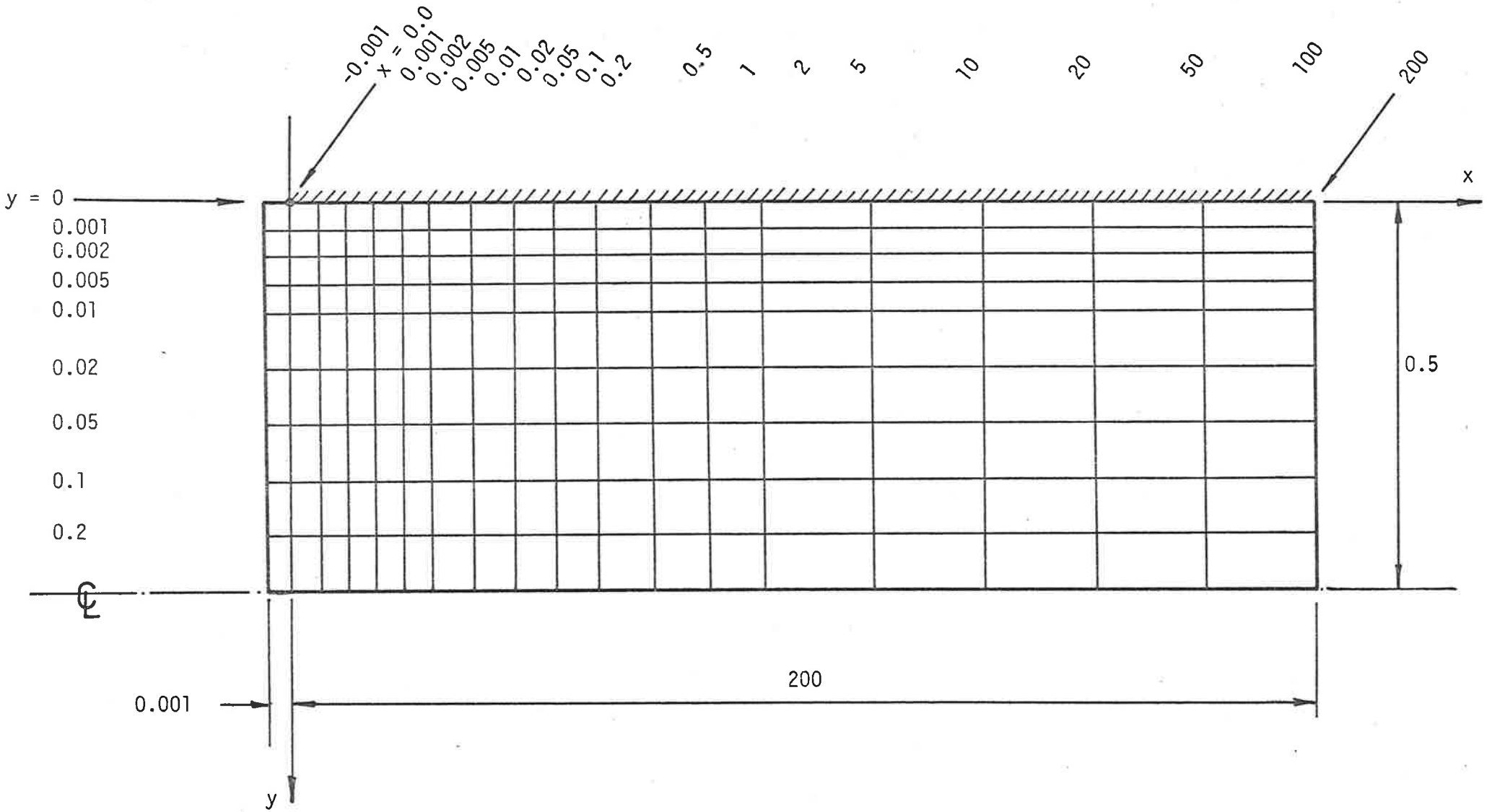

Figure 5.3 Mesh ENFLM1 (not to scale).

isoparametric elements. Because of the fact that only rectangular elements are used in mesh ENFLM1, the grading results in elements with aspect ratios of 100,000 to 1 downstream and close to the wall and 1 to 300 at the entrance edge and near the centreline. The finite element equations for these elements will therefore contain coefficients whose magnitude is as much as five orders larger than the magnitude of others in the same equations. As a result it was feared that, due to round-off errors, instabilities would arise in the solution process leading to solutions that are substantially in error, especially for flows with Reynolds numbers approaching 2000. However on closer investigation it was realized that in the regions occupied by these elements, the velocity components and the pressure have only very small variations and therefore would not be adversely affected by using elements with such high aspect ratios. It was decided to use only rectangular elements in mesh ENFLM1, not only because this would enable the eight noded Serendipity element to be used without loss of accuracy (see Section 5.1), but also because this results in solutions that are evaluated at points on straight lines along and across the channel. This greatly facilitates the plotting of velocity and pressure profiles since the solutions obtained from the finite element analyses can be used directly without having to resort to interpolation.

In order to complete the second comparison, namely the comparison to determine the more efficient of the two elements investigated, a second mesh ENFLM2, the details of which are given in Figure 5.4, was constructed for the entrance flow problem. This second mesh has the same overall dimensions as the first, but is composed of trapezoidal as well as rectangular elements. It contains 410 nodes and 119 elements, and because the trapezoidal elements can be used to achieve a suitable element grading much more effectively, the aspect ratio of the downstream wall elements is reduced to 500 to 1, while that of the elements at

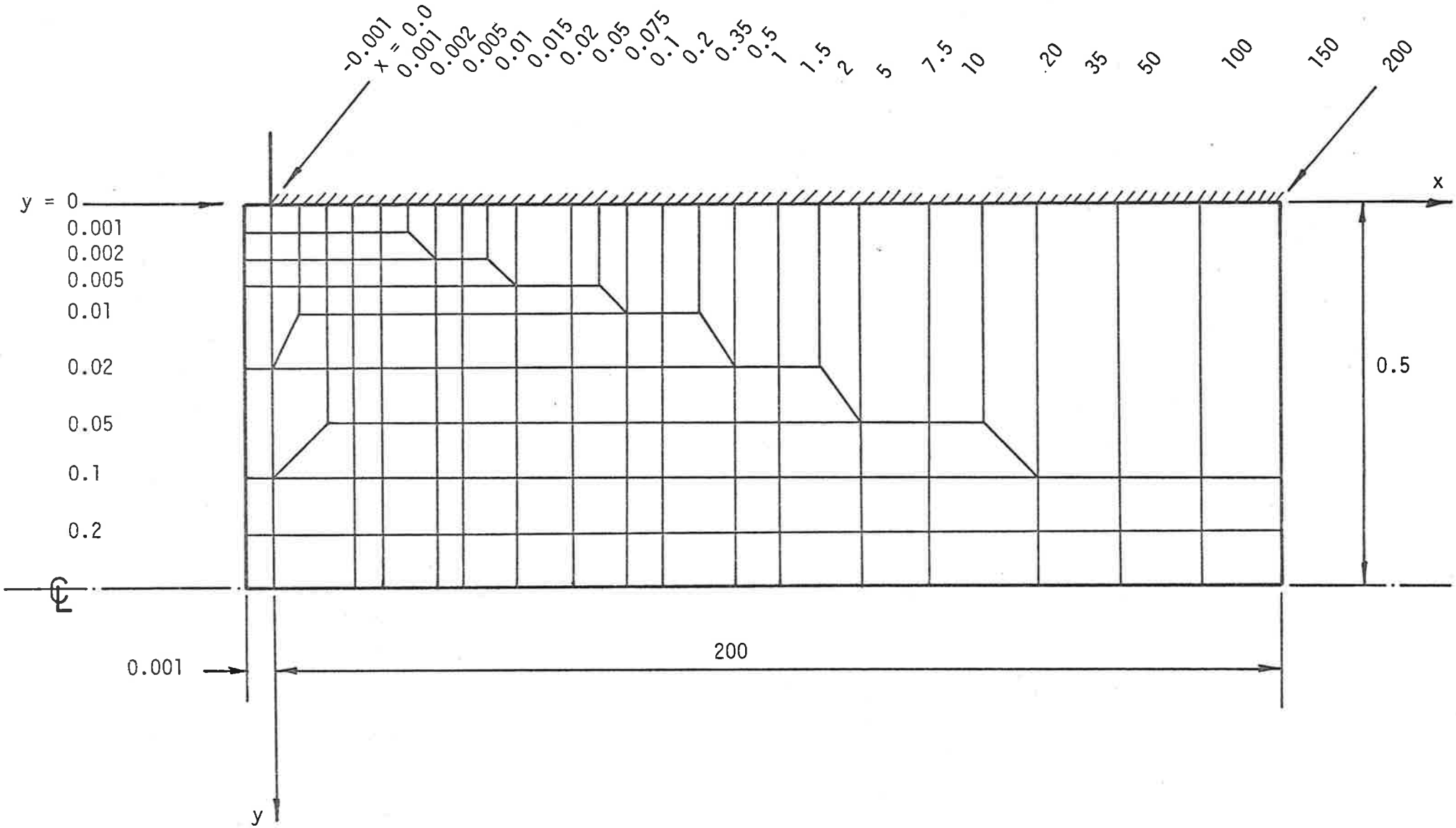

Figure 5.4 Mesh ENFLM2 (not to scale).

the entrance edge near the centreline is reduced to 1 to 60. It should be pointed out that when the nine noded Lagrangian element is used, the number of nodes in both meshes ENFLM1 and ENFLM2 is increased by the number of elements, since each element then contains one extra internal node. Table 5.3 summarizes all the essential details of the meshes used to solve the entrance flow problem.

The only thing that now remains to be discussed in this section is the boundary conditions that were used in the finite element analyses of this problem. As was stated earlier, for a solution to be obtainable, either the velocity component or the corresponding stress tensor component must be specified in each direction at every node on the boundary of the flow domain. The following boundary conditions, a summary of which is shown in Figure 5.5, are sufficient and necessary to enable the correct solution to be obtained at all Reynolds numbers considered. Edges A to D referred to in the following discussion, are defined in Figure 5.5.

Along edge A the fluid velocity must be zero in both directions since this is a solid boundary. Therefore at all nodes on edge A,

$$\left.\begin{aligned} u=0 \quad & \text{(x direction)} \\ \text{and} \quad v=0 \quad & \text{(y direction)} \end{aligned}\right\} \qquad 5.2$$

Since edge B is coincident with the centreline and therefore the line of symmetry of the flow, the shear stress component σ_{yx} parallel, and the velocity component normal to this edge must both be zero. Therefore at all nodes on edge B,

$$\sigma_{xx}n_x + \sigma_{yx}n_y = \sigma_{yx}$$

since the vector normal to edge B has components $n_x=0$ and $n_y=1$. Therefore,

$$\left.\begin{aligned} \sigma_{xx}n_x + \sigma_{yx}n_y = 0 \quad & \text{(x direction)} \\ \text{and} \quad v = 0 \quad & \text{(y direction)} \end{aligned}\right\} \qquad 5.3$$

	ENFLM1		ENFLM2	
	8NE	9NE	8NE	9NE
NE	162	162	119	119
NN_p	190	190	146	146
NN_v	541	703	410	529
NN	541	703	410	529
NP	190	190	146	146
NV	1,082	1,406	820	1,058
NE_q	1,272	1,596	966	1,204
FW	60	60	60	60
FL	$66,000_8$	$74,600_8$	$63,000_8$	$70,200_8$

Table 5.3 Details of Meshes and Elements Used to Solve the Entrance Flow Problem.

(NE = number of elements, NN_p = number of pressure nodes, NN_v = number of velocity nodes, NN = total number of nodes, NP = number of pressure equations, NV = number of velocity equations, NE_q = total number of equations, FW = smallest maximum front width of mesh, and FL = field length or number of computer storage words required to solve the problem.)

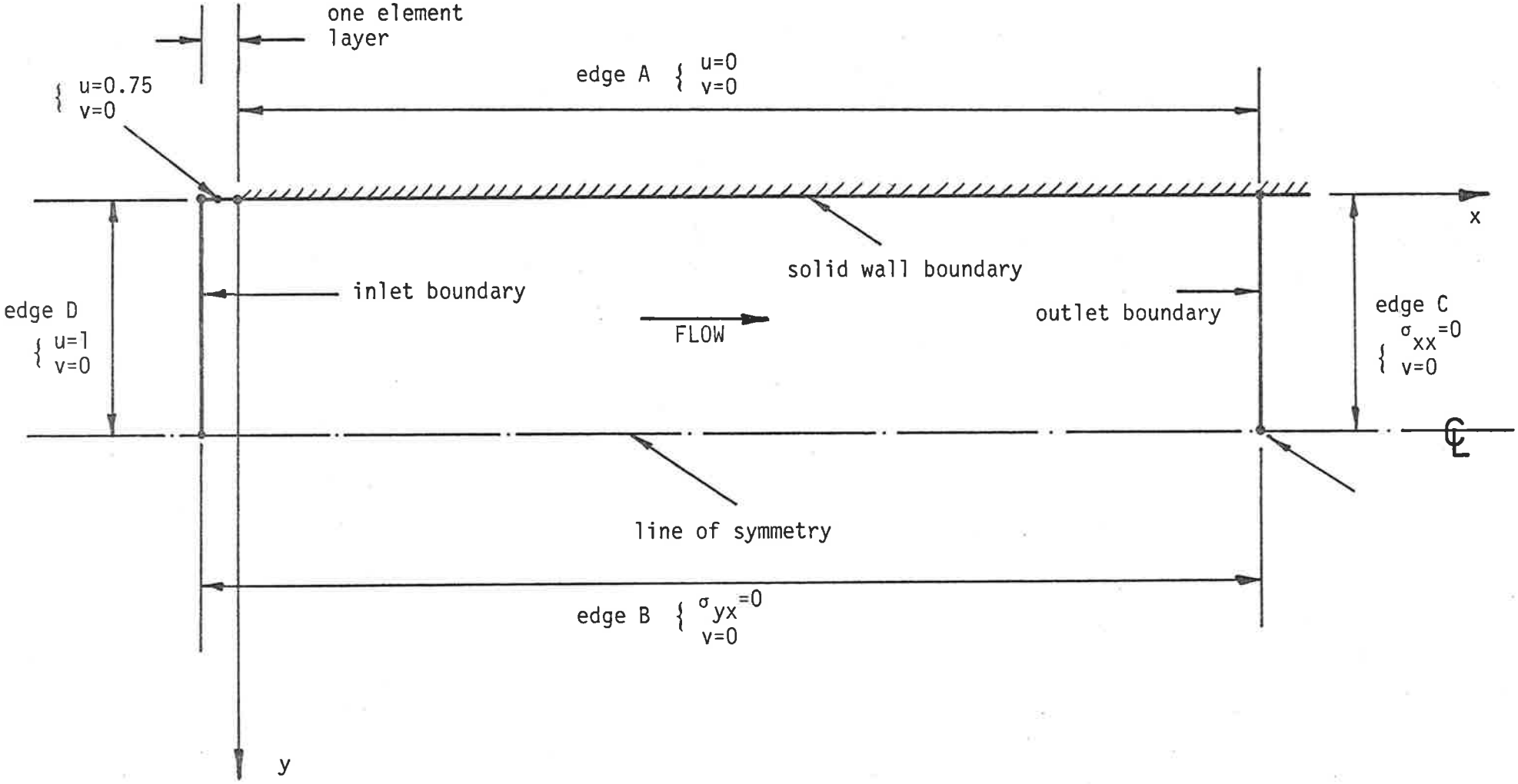

Figure 5.5 Entrance Flow Boundary Conditions.

By ensuring that the finite element mesh is of sufficient length to allow the flow to be fully developed at outlet, the properties of a Poiseuille flow can be used as boundary conditions along edge C. In the direction parallel to the flow either a velocity or a stress type boundary condition can be applied, since both are known for a fully developed Poiseuille flow. In using the former however, the velocity at each node must be calculated, whereas if the stress boundary condition is used, since the normal stress is constant across the channel for a fully developed flow, only one value needs to be evaluated. The latter was therefore chosen for this problem. Also for a fully developed flow, the fluid moves parallel to the channel walls and at a rate that is constant along the channel. Therefore at all nodes on edge C,

$$\sigma_{xx} n_x + \sigma_{yx} n_y$$

$$= \sigma_{xx} \quad \text{since the vector normal to edge C has components } n_x = 1 \text{ and } n_y = 0.$$

$$= \frac{1}{Re}\left(2\frac{\partial u}{\partial x} - \frac{2}{3}C_3\left(\frac{\partial u}{\partial x} + \frac{\partial v}{\partial y}\right)\right) - p \quad \text{by equation 3.21}$$

$$= -p$$

$$= \text{constant, arbitrarily set to zero.}$$

$$\left.\begin{aligned} &\text{Therefore,} \quad \sigma_{xx} n_x + \sigma_{yx} n_y = 0 \qquad \text{(x direction)} \\ &\text{and} \qquad\qquad v = 0 \qquad\qquad\qquad\quad \text{(y direction)} \end{aligned}\right\} \qquad 5.4$$

The value of the pressure at outlet is arbitrarily set to zero to simplify the boundary conditions. By setting it at any other value p_o say, the pressure field for the whole flow is simply either raised or lowered by the same amount p_o. Because of this property of the equations the pressure needs only to be specified at one node, for example, at the corner of edges B and C, to fix a datum relative to which the pressure at any other node is evaluated.

The selection of the boundary conditions that would most accurately model the flow at the inlet edge D presented the most difficulties. Since not all the velocity gradients and the pressure can be predicted a priori in this region, the stress boundary condition cannot be used. Therefore all the velocity components must be specified on edge D. By assuming that the fluid moves parallel to the channel wall at the inlet edge, the transverse velocity component at all nodes on edge D, can be set to zero. The first attempt at solving the entrance flow problem used a finite element mesh whose inlet boundary coincided with the start of the channel. The fluid was given a velocity of one parallel to the channel walls at all nodes on this edge except for the one at the wall where the velocity was specified to be zero. The resulting specified inlet velocity profile is as shown in Figure 5.6(a), the hump resulting from the quadratic interpolation used on the sides of any element with three nodes per side. The solution that was obtained resulted in velocity profiles at sections downstream of the inlet edge, that also have humps close to the wall. A typical profile is shown in Figure 5.6(b). When solutions for the same problem published by other researchers (4, 28, 33) using boundary layer approximations were examined, it was found that no humps existed in their profiles of the velocity component parallel to the channel. It was therefore thought that the above inlet boundary velocity specification had imposed a false velocity profile at inlet and that its effects had been carried downstream to the other velocity profiles.

To overcome this, it was decided to apply the uniform inlet velocity profile one layer of elements before the start of the channel. The velocity immediately in front of the wall therefore, went from one through 0.75 to zero at the start of the wall, over a width of one element, as can be seen in Figure 5.7. The solution obtained using this inlet boundary condition contradicted the above idea since the

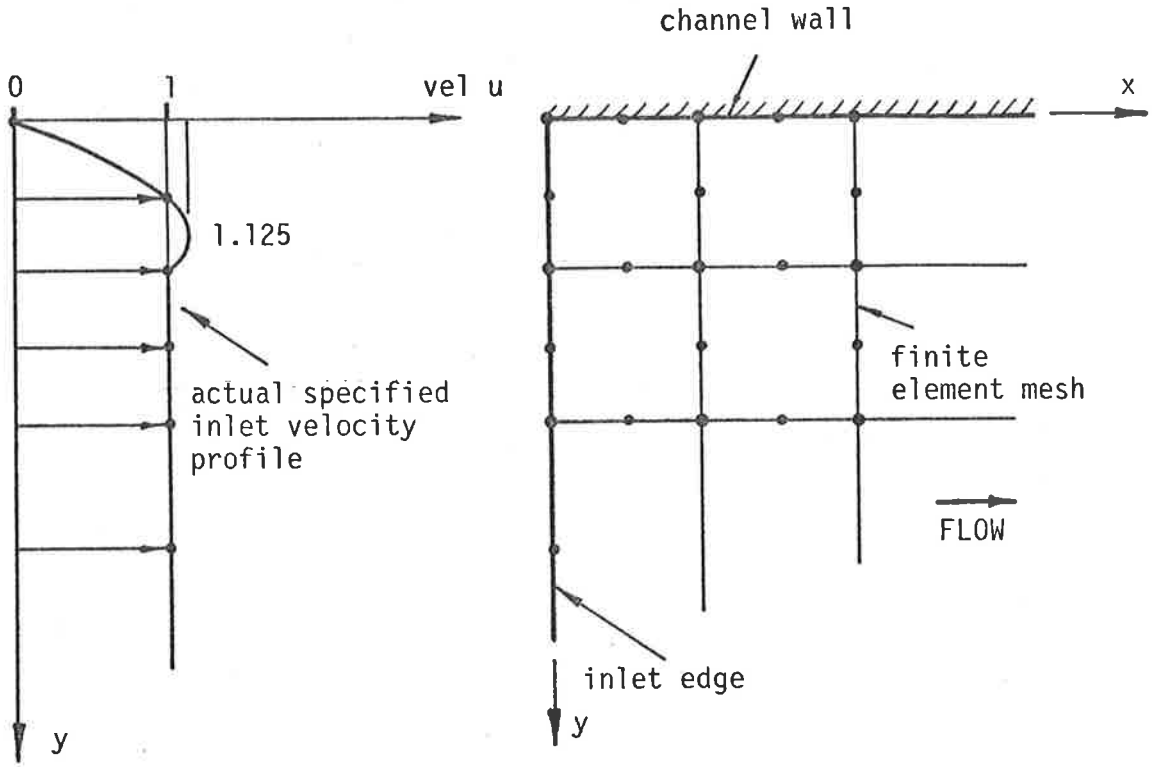

Figure 5.6(a) Specified Entrance Velocity Profile

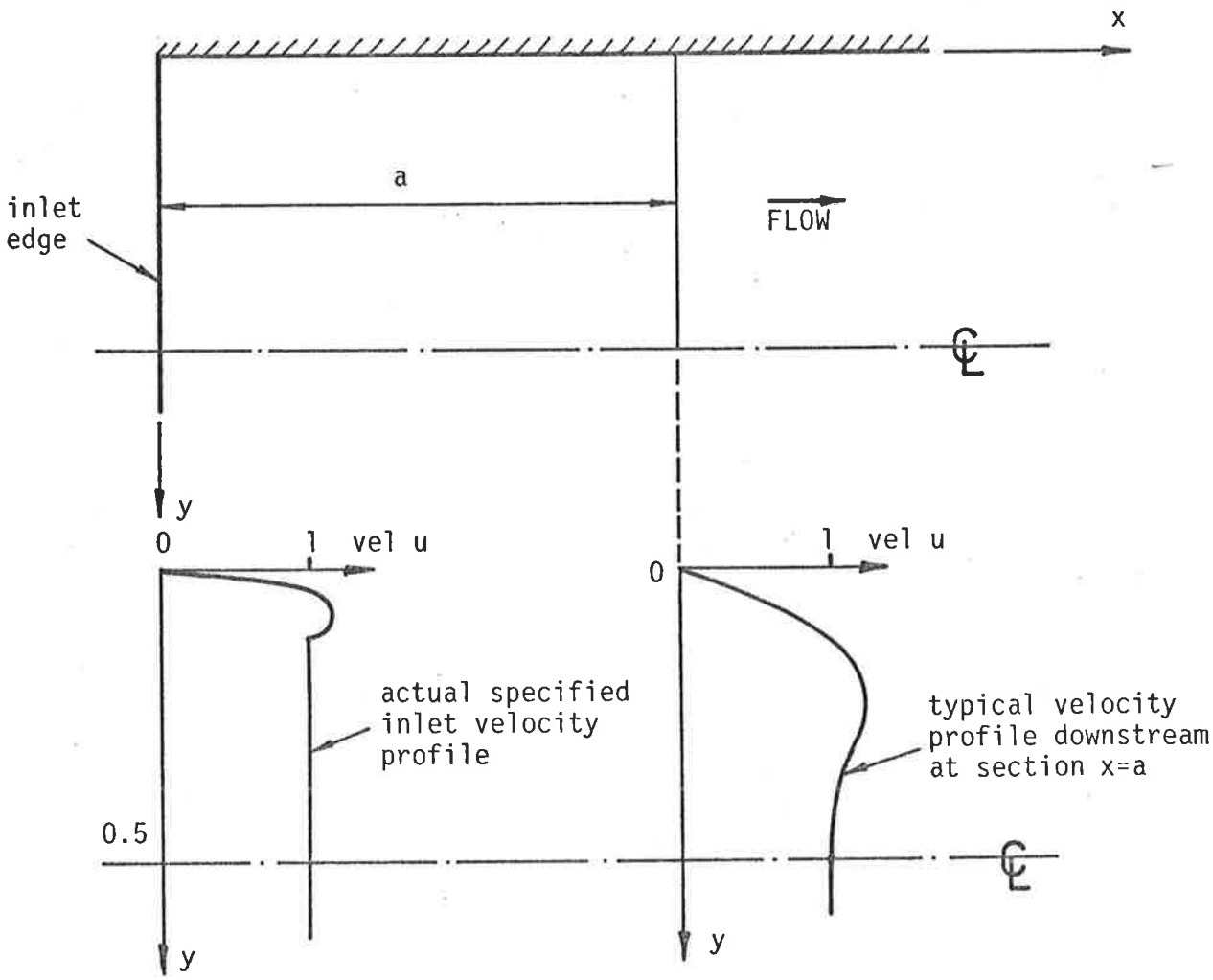

Figure 5.6(b) Typical Downstream Velocity Profile.

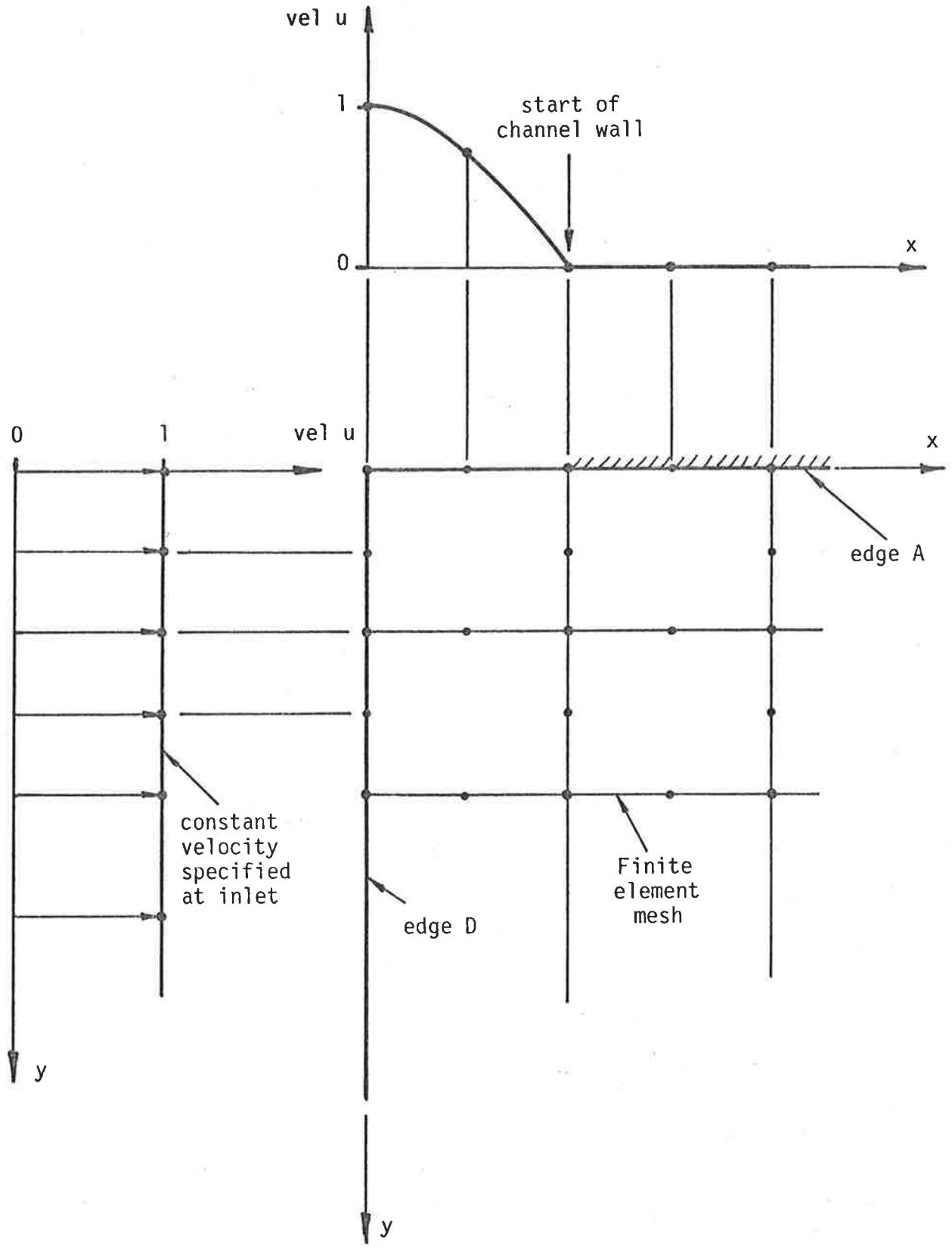

Figure 5.7 Entrance Edge Wall Corner Velocity Specification.

resulting velocity profiles still contained a hump close to the wall. After further investigations it was found that this curious feature of the velocity profiles had in fact been reported by other researchers in this field. Abarbanel and co-workers (1) and all the researchers who had solved this problem using the full Navier-Stokes equations instead of the simpler boundary layer approximations, had recorded similar velocity profiles regardless of whether the finite difference or the finite element method had been used. It was therefore realized that the local maxima occurring in the velocity profiles were a real characteristic of the entrance flow problem and that when the boundary layer equations were used this feature was not represented and therefore not observed. In order to avoid adversely affecting the true velocity profiles by imposing an inlet boundary condition that has a hump in it as well, it was decided to use the second inlet boundary condition for subsequent runs of this problem. The thickness of the additional layer of elements was fixed at 0.1% of the channel width on both meshes ENFLM1 and ENFLM2, so that for all Reynolds numbers considered, the elements at the inlet edge and adjacent to the start of the wall have a width to depth ratio of 1. If scaling of the x coordinate had been used as was suggested earlier in this section, the width of the additional inlet layer of elements would become variable. To avoid introducing additional unknown effects due to changes in the applied velocity gradient immediately in front of the start of the wall, this technique was not adopted. Therefore, for all nodes on edge D,

$$\left.\begin{array}{l} u = 1 \quad \text{(x direction)} \\ \text{except at the node immediately ahead of the wall where } = 0.75, \\ \text{and} \qquad v = 0 \quad \text{(y direction)} \end{array}\right\} \qquad 5.5$$

It should be pointed out that the flow problem that is actually being solved when the above boundary conditions are employed, is the flow in the entrance region in one bay between two semi-infinite flat

plates in an infinite series of such plates, as shown in Figure 5.8. This is because it is assumed in the selected inlet boundary conditions that the transverse velocity component v is zero at all the nodes in front of the start of the wall. To avoid having to make this assumption one must have some knowledge of the stresses that exist in this region. However since it is impossible to know these a priori, some estimate of the velocity field must be made, and as a result the above assumption was adopted.

The only other matter that should be discussed in this section concerns only formulation A. Since this is the only formulation in which $C_1=0$, it is the only formulation that has a second surface integral that must be evaluated on the outer boundary of the flow domain. Along all edges of the entrance region on which the velocity components are specified, the second surface integral is not required since the corresponding equations do not apply. However on edges B and C in the x direction, a stress boundary condition is specified and therefore, for formulation A, surface integrals of the form

$$\int_{S_i} (C_1-1)\,\frac{1}{Re}\left\{\frac{\partial u}{\partial x}\,n_x + \frac{\partial v}{\partial x}\,n_y\right\} dS$$

must be evaluated there. However, on edge B the normal vector component $n_x = 0$ and $v = 0$, while on edge C, $n_y = 0$ and $\frac{\partial u}{\partial x} = 0$. Therefore this integral is zero on both edges B and C and as a result does not have to be evaluated anywhere. For the entrance flow problem then, with boundary conditions as given above, the second surface integral associated with formulation A only, is not required to be evaluated at any point on the outer boundary of the flow domain.

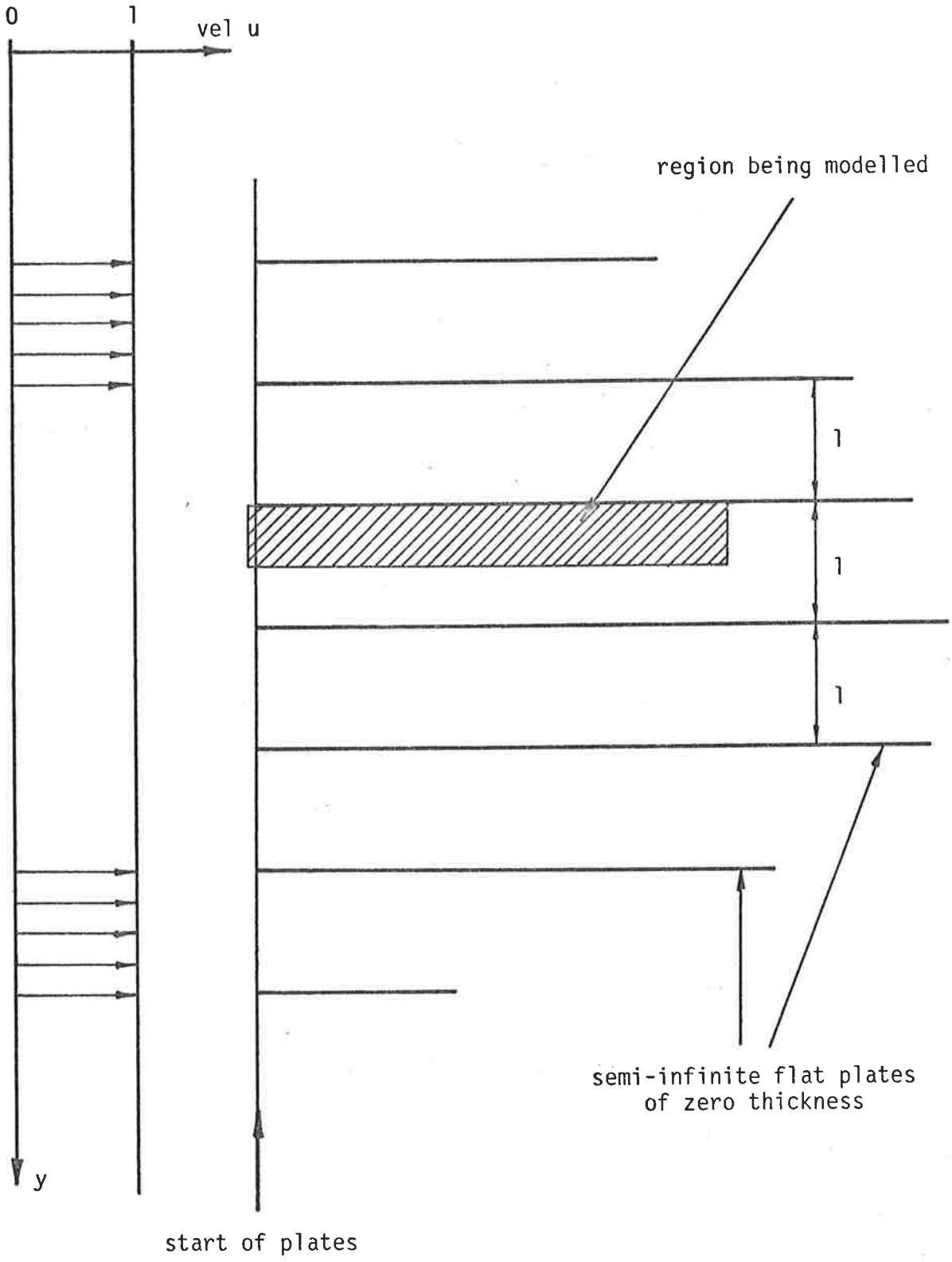

Figure 5.8 Cascade of Plates

5.3 Cavity Flow Problem Details

In order to verify the trends that become apparent in the analyses and solutions of the entrance flow problem, a second classical fluid mechanics problem, namely the recirculating flow in a square cavity, is used. The cavity flow problem involves the prediction of the velocity and pressure fields that occur within a fluid contained in an infinite square cross-section cavity of dimensions DxD and forced to move by the constant lateral motion of one of the four walls. Figure 5.9 shows the real three-dimensional flow that is being studied as well as the simpler two-dimensional arrangement that will actually be used to model it. As was the case with the entrance flow, no exact analytical solution exists for this flow problem, and therefore all solutions published to date involve some form of approximation. However, because there are no inlet or outlet boundaries, this flow problem is somewhat simpler to model than the entrance flow and consequently has sometimes been preferred by previous researchers.

In the last twenty years most of the work that has been done on the cavity flow problem has involved using either the finite difference or the finite element method. A major contribution to the better understanding not only of the cavity flow but also of separated eddies in general, was made by Burggraf (6), who used the finite difference technique to solve the full Navier-Stokes equations. Approximately a decade later, Tuann and Olson (32) published a report in which the cavity flow problem was used to study the advantages and disadvantages of various finite element solution methods. A comparison of their results with those of Burggraf, revealed that both the finite difference and the finite element methods were capable of accurately modelling this flow. More recently, Bercovier and Engelman (3), investigating the difference in performance abilities of the eight and nine noded finite elements of the penalization type, also used the cavity flow problem to demon-

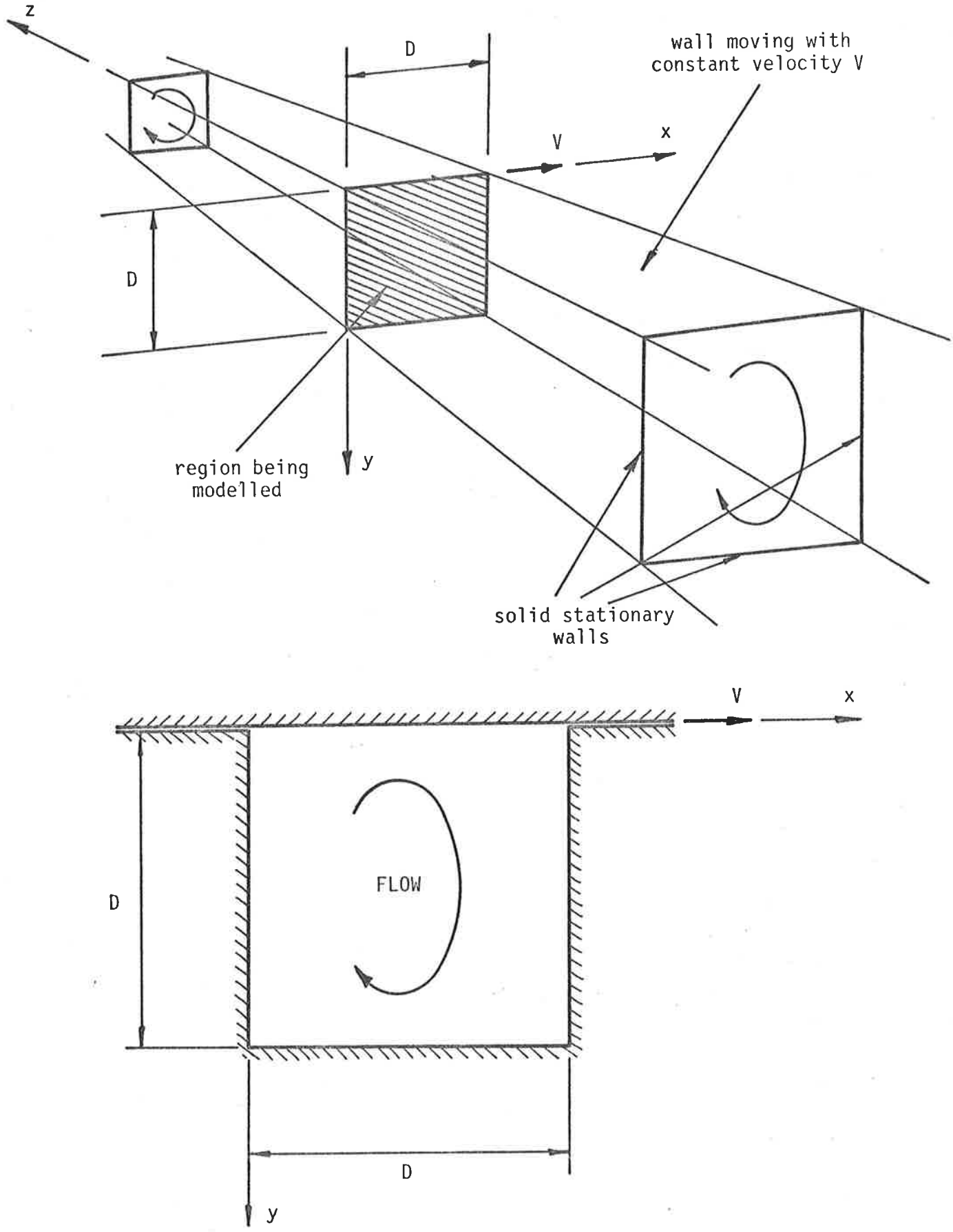

Figure 5.9 Cavity Flow Problem Details.

strate the usefulness of their proposals. It can therefore be seen that, just like the entrance flow, the cavity flow problem has in the past been a popular test case. For this reason and because it is so very different in nature from the entrance flow, it was chosen as the second flow problem with which to confirm the results of the two formulation and element comparisons.

The actual two-dimensional flow problem that is shown in Figure 5.9 is non-dimensionalized by using the velocity of the moving wall V, and the dimension of the cavity D as the characteristic velocity and length respectively. The Reynolds number is therefore defined as $Re = \frac{\rho VD}{\mu}$ and details of the dimensionless problem are given in Figure 5.10.

With the experience gained from the analysis of the entrance flow problem, the construction of the two finite element meshes required for this problem was greatly simplified. It was again realized that boundary layers would exist on all the solid boundaries, but no means by which to estimate their thickness was found. By examining previously published solutions it was also realized that problems associated with singularities in velocity would occur at nodes in the two corners next to the moving wall. This is because at both corners the fluid velocity must be zero since it is next to a stationary wall while at the same time it should be one since it is next to a moving wall. To overcome this problem and in order to adequately represent the large velocity gradients that occur in the boundary layers, significantly smaller elements are used adjacent to all four walls. On the bottom boundary however, the elements are not as small as on the moving wall since it was anticipated that the velocity gradients there, although still significant, would not be as large. This was later confirmed. The size of the smallest elements located in the two top corners was 0.1% of the cavity width, and with a moderate element grading from both these

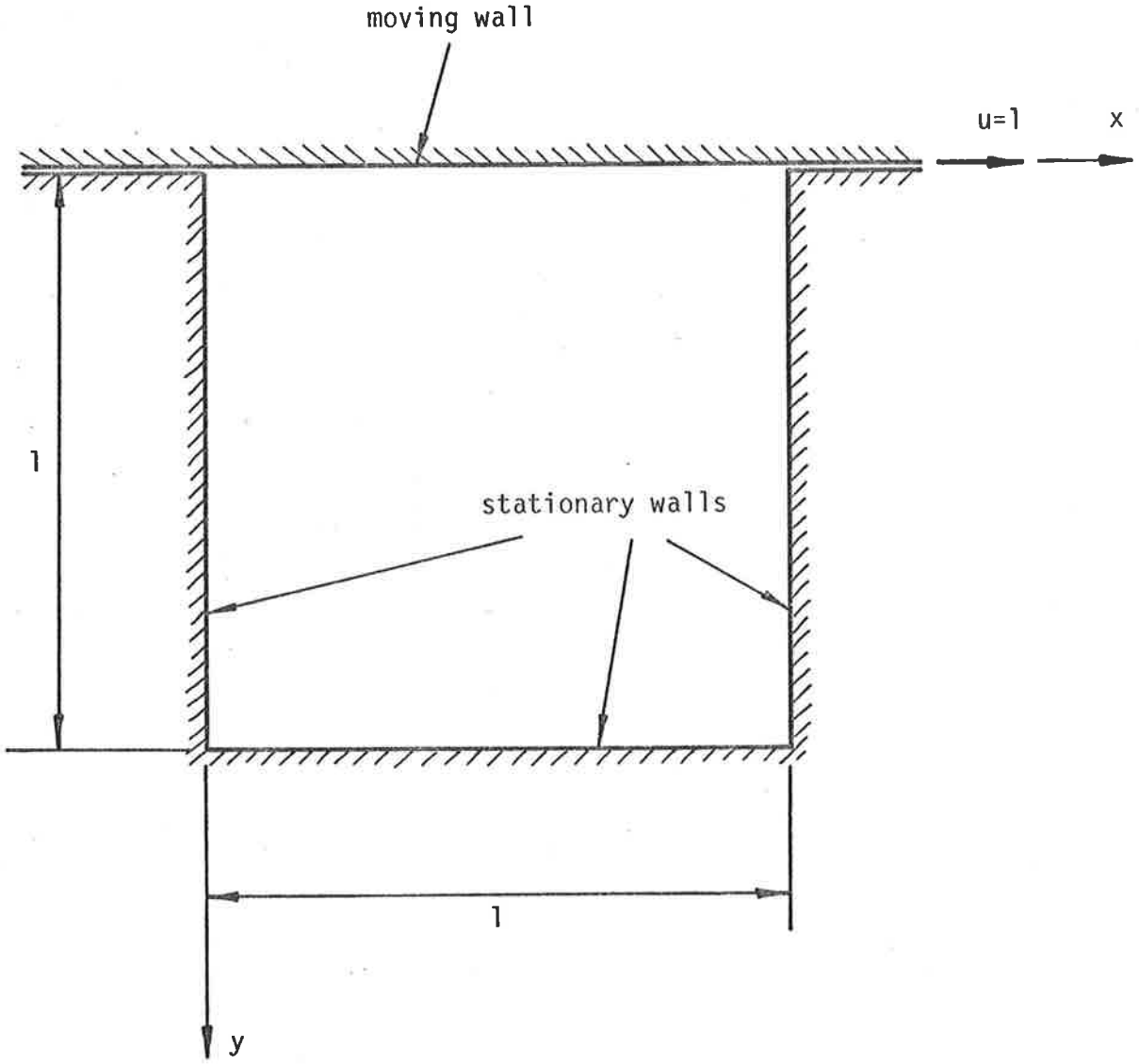

Figure 5.10 Non-dimensionalized Cavity Flow Problem Details.

corners, mesh CAVFLM1, composed entirely of rectangular elements, was constructed.

Mesh CAVFLM1 contains 1133 nodes and 352 elements ranging in size from 0.001x0.001 in the top corners to 0.1x0.1 in the centre of the mesh. As with the entrance flow, the solutions of the cavity flow problem obtained with CAVFLM1 are used in both the formulation as well as the element comparisons. A second mesh labelled CAVFLM2, similar to CAVFLM1 but containing trapezoidal as well as rectangular elements, was also constructed. It contains 709 nodes and 210 elements and was set up to complete the second comparison. Figures 5.11 and 5.12 give the complete details of the element layout for CAVFLM1 and CAVFLM2 while Table 5.4 summarizes all the essential details of both the meshes used to solve the cavity flow problem. Since the cavity flow problem contains no inlet or outlet boundary, the two meshes constructed are suitable for solving cavity flows with any Reynolds number. However it was anticipated that instabilities would arise as Reynolds number is increased and it was therefore decided to limit it to 2000. In both meshes a relatively fine arrangement of elements was retained in the centre of the mesh to enable the vortex centre to be accurately located.

The boundary conditions that are required in order to obtain the solution to the cavity flow problem are given in Figure 5.13. At all nodes on edges B, C and D, which are defined in Figure 5.13, the fluid velocity must be zero in both directions since these edges coincide with stationary solid boundaries. Edge A on the other hand coincides with the moving wall and therefore at all nodes on edge A, the fluid velocity must be one in the x direction and zero in the y. The only other aspect of the boundary conditions used that should be mentioned at this stage is that the actual velocity specification at the nodes on edge A and close to the corners, is as shown in Figure 5.14(a). This avoids the decelerations and accelerations in the flow close to

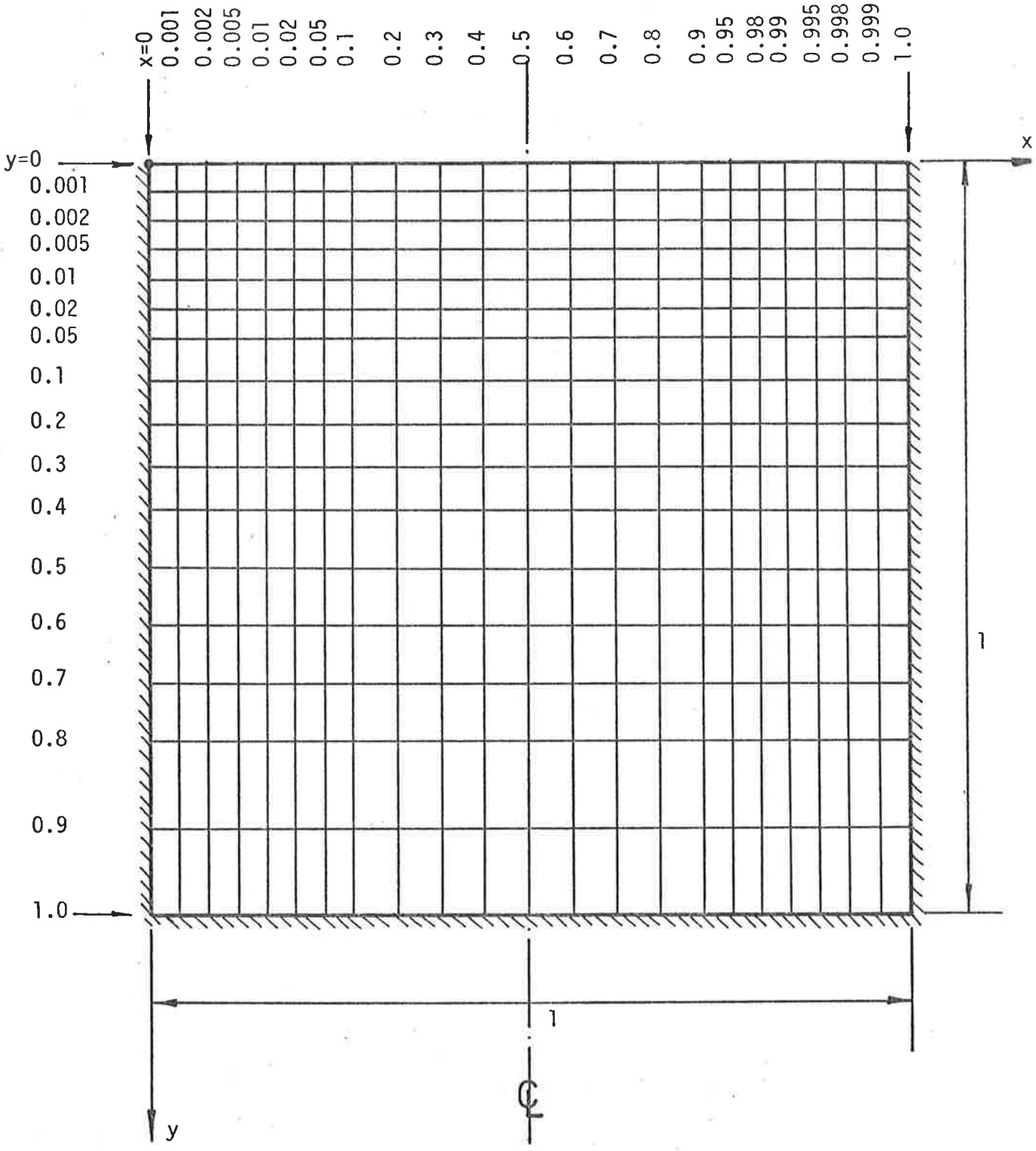

Figure 5.11 Mesh CAVFLM1 (not to scale).

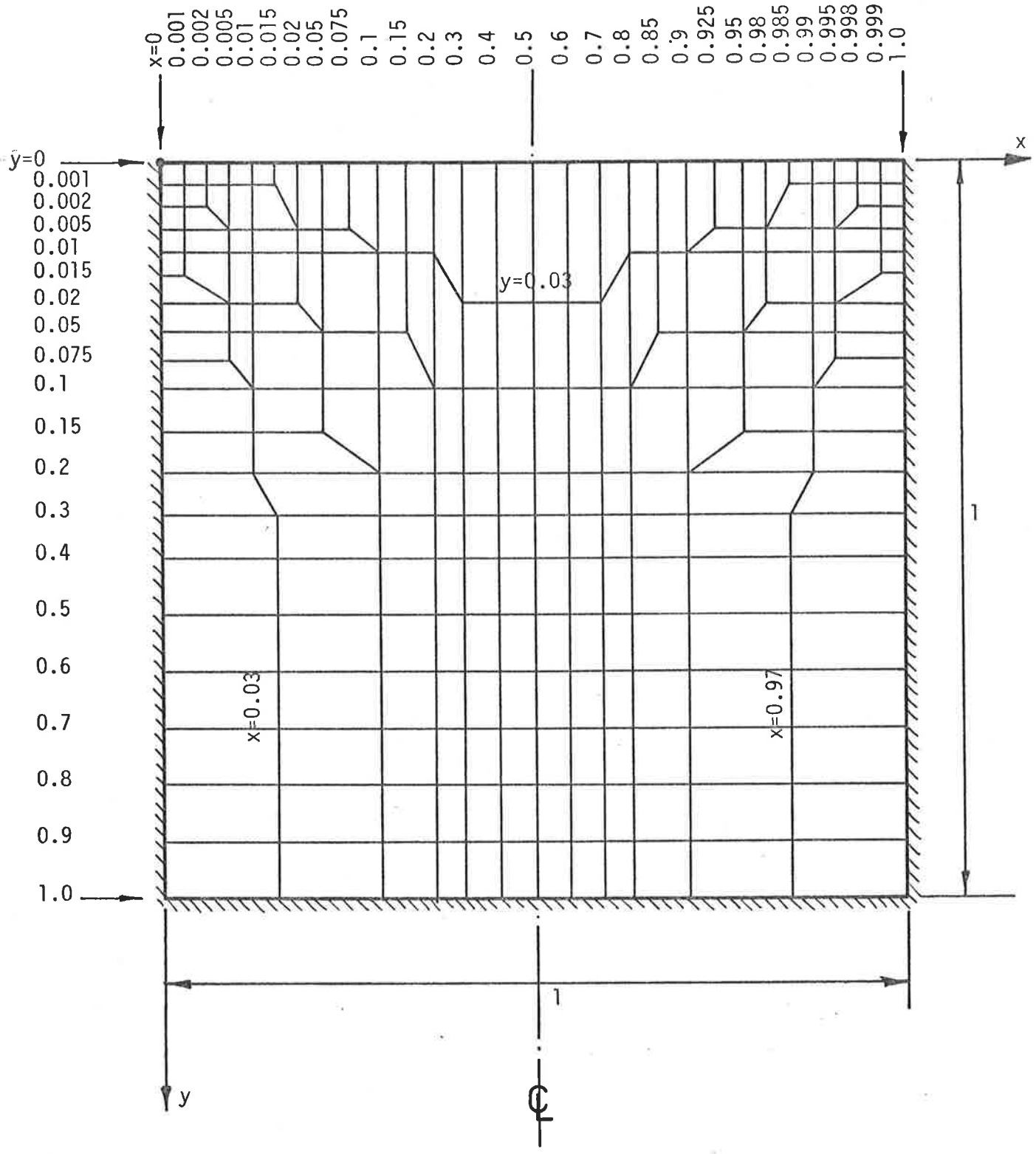

Figure 5.12 Mesh CAVFLM2 (not to scale).

	CAVFLM1		CAVFLM2	
	8NE	9NE	8NE	9NE
NE	352	352	210	210
NN_p	391	391	250	250
NN_v	1,133	1,485	709	919
NN	1,133	1,485	709	919
NP	391	391	250	250
NV	2,266	2,970	1,418	1,838
NE_q	2,657	3,361	1,668	2,088
FW	95	95	95	95
FL	$120,500_8$	$136,100_8$	$107,100_8$	$117,500_8$

Table 5.4 Details of meshes and elements used to solve the cavity flow problem.

(NE = number of elements, NN_p = number of pressure nodes, NN_v = number of velocity nodes, NN = total number of nodes, NP = number of pressure equations, NV = number of velocity equations, NE_q = total number of equations, FW = smallest maximum front width of mesh, and FL = field length or number of computer storage words required to solve the problem.)

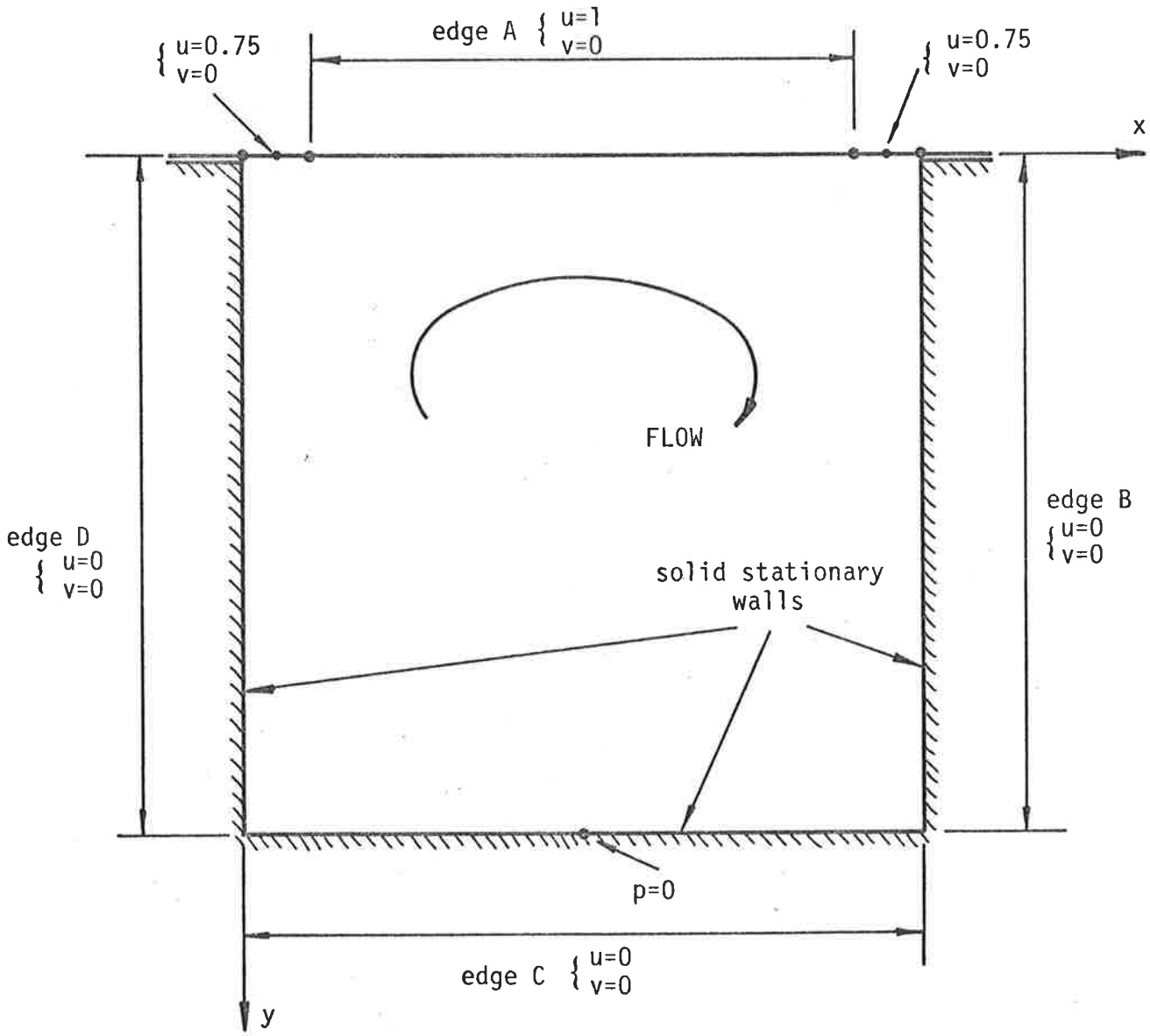

Figure 5.13 Cavity Flow Boundary Conditions.

the downstream and upstream corners that would arise if the velocity normally specified and shown in Figure 5.14(b) were used. Finally, since all boundary conditions are of the velocity type, none of the surface integrals need to be evaluated. All that is required is that the pressure be specified at one node to define the datum. To be consistent with that done by previous workers, the pressure is specified as zero at the node located in the middle of edge C.

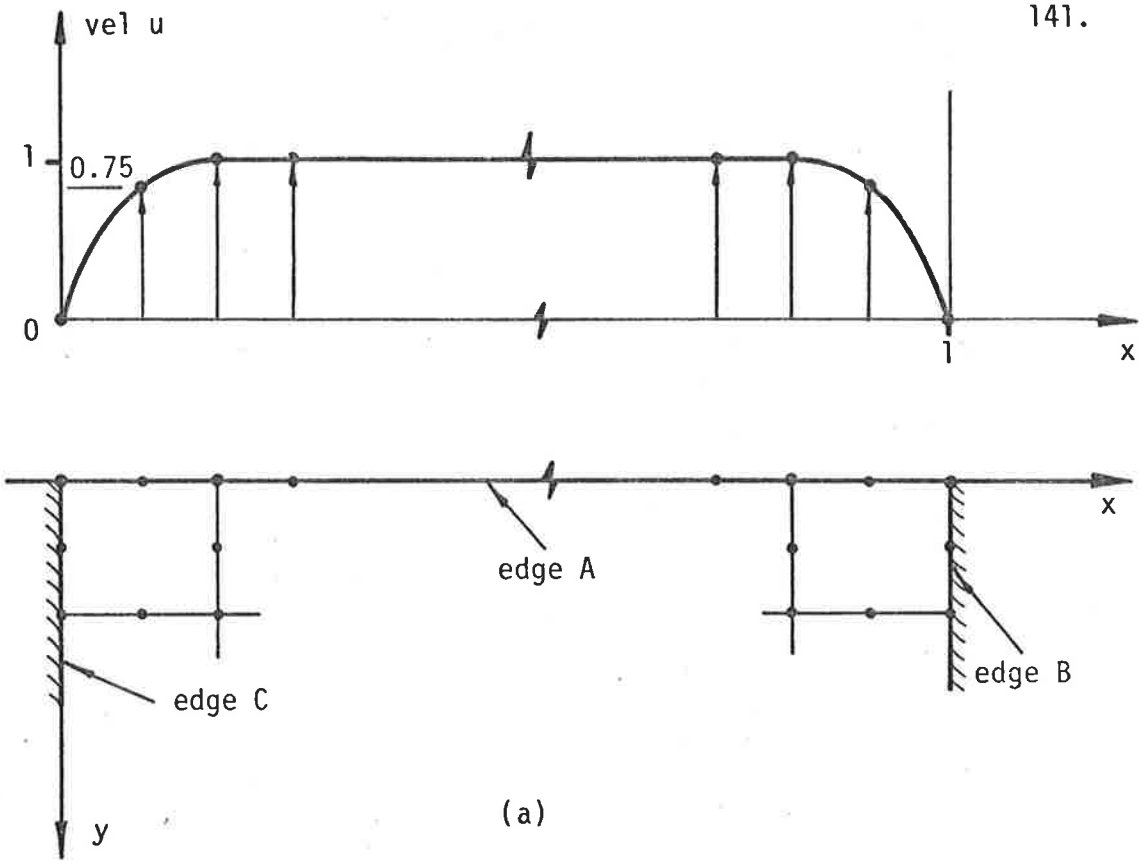

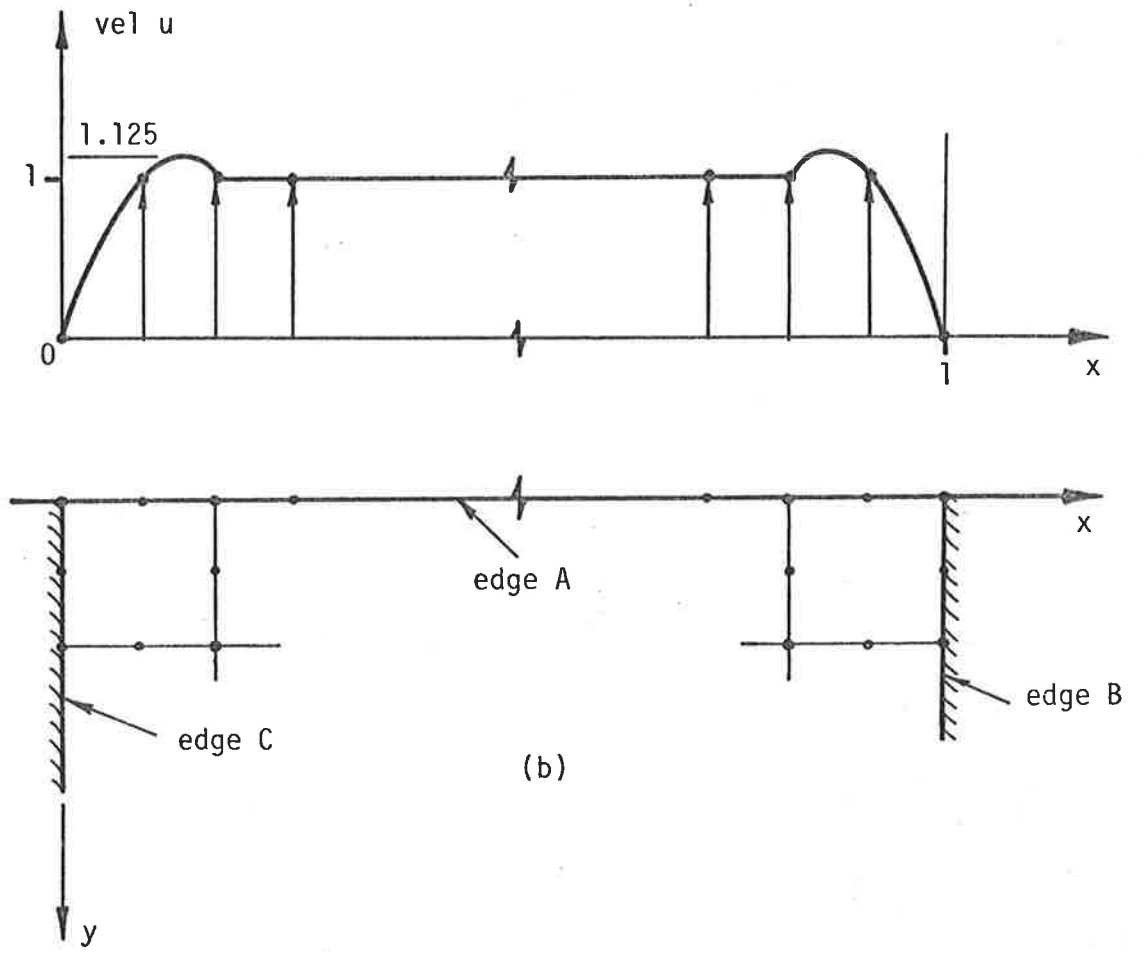

Figure 5.14 (a) Specified Moving Wall Velocity Profile, and
(b) Typical Moving Wall Velocity Profile Specified by Previous Workers.

5.4 Results of Formulation Comparison

As was shown in Section 3.1, several different versions of the Navier-Stokes equations can be obtained by either using or not using the incompressible Continuity equation to eliminate certain of the viscous and acceleration terms that are a normal part of the Navier-Stokes equations. The four versions that have been selected for this comparison are set out again below and briefly described so that the differences in each may be kept in mind as the comparison is made.

Formulation A, which has previously been used by Taylor and Hood (30), Yamada et al. (35), Kawahara et al. (19) and several others, involves the complete elimination of all terms containing the quantity $\frac{\partial v_j}{\partial x_j}$ as a factor. As a direct consequence, the finite element equations for this formulation contain two surface integrals rather than the usual one. However, as was seen earlier in this chapter, the additional surface integral can usually be eliminated by a careful consideration of the quantities involved on the outer boundary of the flow domain. Where elimination is not possible, and this may occur only on that portion of the outer boundary of a flow on which the fluid's stress state is specified, the second surface integral can always be evaluated since all the velocity gradients are known and there the direction of the normal can always be calculated. Nevertheless this second surface integral, whether it can be eliminated or not, introduces an additional inconvenience that does not occur with any of the other formulations. The equations for formulation A are the simplest of all the formulations and contain only one viscous and one acceleration term. They are,

$$\left.\begin{aligned} &\frac{1}{Re}\frac{\partial^2 v_i}{\partial x^2_j} - \frac{\partial p}{\partial x_i} = v_j \frac{\partial v_i}{\partial x_j} \\ \text{and} \quad &\frac{\partial v_j}{\partial x_j} = 0 \end{aligned}\right\}$$

Formulation B has been used by Hutton (17), Zienkiewicz (36, 37), Tuann and Olson (25, 32), and several others also. It involves the retention of an additional viscous term and because of this, its finite element equations do not contain the second surface integral. This is also true for formulations C and D, both of which retain the same extra viscous term. The equations for formulation B are,

$$\left.\begin{aligned} &\frac{1}{Re}\left(\frac{\partial^2 v_i}{\partial x^2_j}+\frac{\partial^2 v_j}{\partial x_i \partial x_j}\right)-\frac{\partial p}{\partial x_i}=v_j\frac{\partial v_i}{\partial x_j} \\ \text{and}\quad &\frac{\partial v_j}{\partial x_j}=0 \end{aligned}\right\}$$

Formulation C, recently proposed by Hutton et al. (18), has equations which include a second acceleration term as well as the second viscous term, and to the author's knowledge, has not previously been used. Because the additional term for this formulation is non-linear, it was anticipated that when formulation C is used, it would require a greater number of iterations of the Newton-Raphson method to attain the given convergence limits, especially at higher Reynolds numbers when the non-linear acceleration terms predominate. The equations for formulation C are,

$$\left.\begin{aligned} &\frac{1}{Re}\left(\frac{\partial^2 v_i}{\partial x^2_j}+\frac{\partial^2 v_j}{\partial x_i \partial x_j}\right)-\frac{\partial p}{\partial x_i}=v_j\frac{\partial v_i}{\partial x_j}+v_i\frac{\partial v_j}{\partial x_j} \\ \text{and}\quad &\frac{\partial v_j}{\partial x_j}=0 \end{aligned}\right\}$$

The last formulation, namely formulation D, has equations that include both the extra viscous and acceleration terms of formulation C, as well as a third viscous term. This formulation, as far as the author can ascertain, has never been proposed before and has been included in this comparison because by retaining the extra viscous term, it is the only formulation in which the variable labelled "p" represents

exactly the pressure in a viscous flow, regardless of whether the Continuity equation has been satisfied exactly or not. This was done by including in the fluid stress-strain rate relationship, a viscous term containing the quantity $\frac{\partial v_j}{\partial x_j}$ that enables either the exact or the approximated pressure to be identically equal to the negative mean of the three exact or approximated normal stresses at any point in a viscous flow. The equations for formulation D are,

$$\left.\begin{aligned} &\frac{1}{Re}\left(\frac{\partial^2 v_i}{\partial x^2_j} + \frac{\partial^2 v_j}{\partial x_i \partial x_j} - \frac{2}{3}\frac{\partial^2 v_j}{\partial x_i \partial x_j}\right) - \frac{\partial p}{\partial x_i} = v_j \frac{\partial v_i}{\partial x_j} + v_i \frac{\partial v_j}{\partial x_j} \\ &\text{and} \quad \frac{\partial v_j}{\partial x_j} = 0 \end{aligned}\right\}$$

In order to determine most effectively which is the optimal formulation, both the computational efficiency as well as the computational accuracy of each is examined. A measure of the computational efficiency of a formulation can be obtained by examining the amount of computer storage and execution time required for a solution to be found when that formulation is used. However, since the only difference between the formulations is an additional term or two in the finite element equations, with the remainder of the solution procedure being the same, the computer storage needed to obtain a solution is almost the same for all formulations. Therefore only the computation time can be used to gauge the relative efficiency of each formulation. From the first few computer runs, it was found that the execution times observed were almost directly proportional to the number of iterations needed to arrive at a solution that satisfied the set convergence limits. Therefore by looking at the number of iterations required to obtain a fully converged solution for each flow with a range of Reynolds numbers and using each of the four formulations, the one which is computationally most efficient can easily be selected. With this in mind, the runs

in test series 1 specified in Table 5.1(a) for the entrance flow and 5.1(b) for the cavity flow were executed and the number of iterations and execution times required by each are listed in Table 5.5. For all formulations and in all flows considered, full convergence was assumed to have been attained when the root mean square of the adjustments calculated at the end of each iteration, became less than 0.1% of the root mean square of the newly adjusted nodal values of velocity and pressure.

From Table 5.5 some interesting points about the performance of the various formulations can be observed. However to fully appreciate these, something must be said about the process by which the solutions are obtained. Since the Navier-Stokes equations, and therefore the corresponding finite element equations are non-linear, the Newton-Raphson iterative solution procedure was used to solve the resulting equation system. In order to start this procedure, an initial guess is required. The initial guess may be identically zero everywhere or it may be any approximation of the velocity and pressure fields being evaluated. However if the initial guess is not sufficiently close to the solution being sought, either the wrong solution is obtained or a large number of iterations is required to obtain the correct solution or no solution at all can be found. The degree of non-linearity of the equation system governs how close the initial guess must be to the correct solution before the Newton-Raphson method can be used effectively to find the correct solution.

In this study it was decided to use an initial guess that is identically equal to zero everywhere for both the entrance and the cavity flow problems. This was done in order to avoid having to estimate the velocity and pressure fields for each flow and so that none of the formulations would be inadvertently advantaged by the fields chosen to start the solution procedure. Because of this it was anticipated that if the same initial guess is used, as Reynolds number increases

(a)

Re	Formulation			
	A	B	C	D
1	2 (222)	2 (222)	2 (223)	2 (223)
200	4 (456)	4 (456)	4 (456)	4 (460)
500	5 (574)	5 (575)	5 (576)	5 (578)
1000	6 (689)	6 (692)	6 (690)	6 (695)
2000	7 (808)	7 (805)	6+3 *	6+3 *

(b)

Re	Formulation			
	A	B	C	D
1	2 (738)	2 (740)	2 (740)	2 (744)
100	3 (1113)	3 (1115)	3 (1115)	3 (1117)
400	6 (2232)	6 (2236)	6 (2237)	6 (2240)
1000	6+3+4 *	6+3+4 *	6+3+4 *	6+3+4 *
2000	13+5 *	13+5 *	13+4+4 **	13+4+ **

Table 5.5 Number of iterations and in brackets execution times for (a) the entrance flow and (b) the cavity flow at various Reynolds numbers for test series 1.

and the dominance of the non-linear terms also increases, the correct solution would become considerably more difficult to obtain and eventually impossible to find. This fact is clearly confirmed by the results given in Table 5.5 and particularly by those for the cavity flow problem.

For both flow problems and for all formulations, it can be observed that as the Reynolds number is increased, the number of iterations needed to obtain a fully converged solution also increases. However, for some tests carried out, a fully converged solution was not obtained. The tests in which this occurred are marked in Table 5.5 with either one or two asterisks. In these cases it was observed that convergence was taking place in the first two or three iterations but thereafter the root mean squared value of the adjustments steadily increased rather than continue decreasing. It was also found that this occurred only for flows with the higher Reynolds numbers and more frequently for formulations C and D. After some consideration it was realized that the reason for this is the increase in non-linearity of the equations describing these cases. Firstly, the increase in Reynolds number causes the ratio of non-linear acceleration terms to linear viscous terms to increase and secondly, when formulations C and D are used, the equations contain additional non-linear acceleration terms. As a consequence, the zero initial guess in these cases, is no longer close enough to the correct solution for the Newton-Raphson method to guarantee convergence on to the correct solution. The inclusion of the additional non-linear acceleration terms in the equations for formulations C and D therefore clearly disadvantage the computational efficiency of these two formulations.

In order to confirm for all cases in which convergence to the correct solution from a zero initial guess did not occur, that the correct solution can still be obtained if the initial guess is close enough to it, all tests marked with either one or two asterisks in

Table 5.5 were rerun using the solution to the same flow but with a lower Reynolds number as the initial guess. For the entrance flow problem, it can be seen from Table 5.5 that when formulations C and D are used, convergence on to the correct solution from a zero initial guess failed to occur only when Reynolds number was equal to 2000. By rerunning these two tests using the solution evaluated with the same formulation but at Reynolds number equal to 1000 as the initial guess, convergence to the correct solution was obtained in three iterations in both cases. The numbers 6+3 that are given in Table 5.5(a) therefore indicate that six iterations were required to solve the flow with Reynolds number equal to 1000 and that a further three iterations were needed to find the solution at Reynolds number equal to 2000.

For the cavity flow problem the situation is considerably worse. Convergence from a zero initial guess was obtained for all formulations only for flows with Reynolds numbers up to 400. In order to obtain the solution to the flow with Reynolds number equal to 1000, the solution to the same flow but with Reynolds number equal to 400 was used. This initial guess however was still not close enough and it was necessary to firstly solve a flow with Reynolds number equal to 600 starting with the Reynolds number equals 400 solution, and then to use this as the starting point to find the solution when Reynolds number equals 1000. For all formulations an additional three iterations were needed to obtain the solution at Reynolds number equals 600 and an additional four iterations to obtain the solution at Reynolds number equals 1000. The numbers in Table 5.5(b) therefore are 6+3+4 for all four formulations.

A difference in the performance of the various formulations was again observed when the solution to the cavity flow problem with Reynolds number equal to 2000 was attempted. With formulations A and B, the Reynolds number equals 1000 solution was used as the initial guess and full convergence was attained after an additional five iterations.

However, when the same initial guess was used with formulations C and D, convergence did not take place, indicating that the Reynolds number equals 1000 solution is not sufficiently close to the correct one for these two formulations. The tests in which this happened are marked with two asterisks in Table 5.5(b). In order to obtain the solution for these cases an additional run per formulation with Reynolds number equals 1500 and starting with the Reynolds number equals 1000 solution was carried out. The results of these runs were then used as the initial guesses for the tests with Reynolds number equal to 2000. However, although formulation C resulted in a converged solution, the Reynolds number equals 1500 solution was still not close enough to the required one for formulation D. At this point it was decided not to carry out any further runs for the cavity flow using formulation D since the general behaviour of the various formulations was already evident. Thus, except for the above case, solutions to all flows using each formulation were evaluated and the total number of iterations required by each recorded in Table 5.5.

From the above discussion and the results in Table 5.5, several points can be noted. Firstly, at low and moderate Reynolds numbers all formulations appear to be equally efficient in terms of computational effort needed to obtain a solution. They all require the same number of iterations and use almost identical amounts of computer time, the small increase for formulations B, C and D being due to the additional terms having to be evaluated in each iteration. Secondly, as Reynolds number increases the efficiency decreases. That is, more iterations are needed to find a solution and as a result the computer time required increases. This trend is displayed by all formulations. Thirdly, and most importantly, since this is the first indication that some of the formulations may not be able to perform as well as the others, at higher Reynolds numbers, formulations C and D appear to be less versatile than

formulations A and B, requiring more overall computation time to obtain the same solution. This is because they require the initial guess to be much closer to the solution being sought and consequently need to have additional runs executed in order to achieve this. Thus, although the above discussion does not prove conclusively which formulation is best, it does show that formulations C and D are considerably disadvantaged by the inclusion of the additional Continuity terms.

The second criterion that is used to decide which is the optimal formulation is the quality of the solution evaluated, since in addition to being the most efficient, the optimal formulation must also be the one that results in the highest computational accuracy. In order to determine which formulation is best able to do this, the solutions obtained in each of the test runs described earlier in this section are examined and compared. This is done by plotting along certain sections, the variations of the velocity and pressure fields calculated for each Reynolds number and flow problem and using each of the four formulations.

For the entrance flow problem the following graphs are plotted: the variations of the x component of velocity along the lines y=0.1 and y=0.5 (the centreline) and the variation of the pressure along the line y=0.5. The variations of the x component of velocity and the pressure along the line x=0.5 for the cavity flow problem are also plotted. These five sets of graphs are shown in Figures 5.15 to 5.19, (a) to (e). In each graph the solutions obtained for a given Reynolds number and using each of the four formulations, are plotted on the same set of axes. By doing this the formulation that results in the highest computational accuracy can easily be found. It will be noted that in all graphs, the logarithm of the x or y coordinate is used rather than the x or y coordinate itself. This mode of presentation was chosen because it represents the most convenient way of showing clearly the

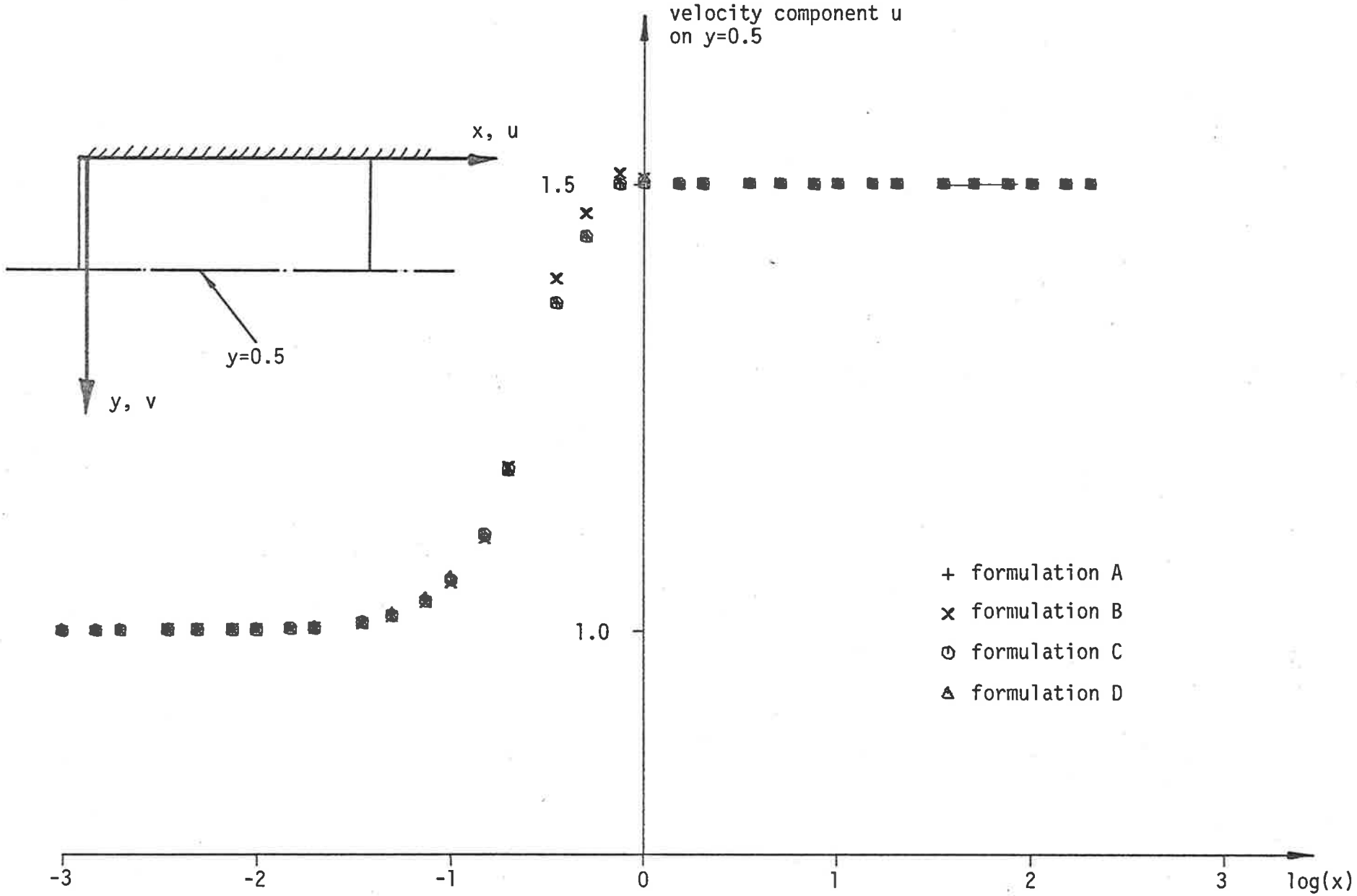

Figure 5.15(a) Formulation Comparison, Entrance Flow, Variation of u on y=0.5 for Re = 1.

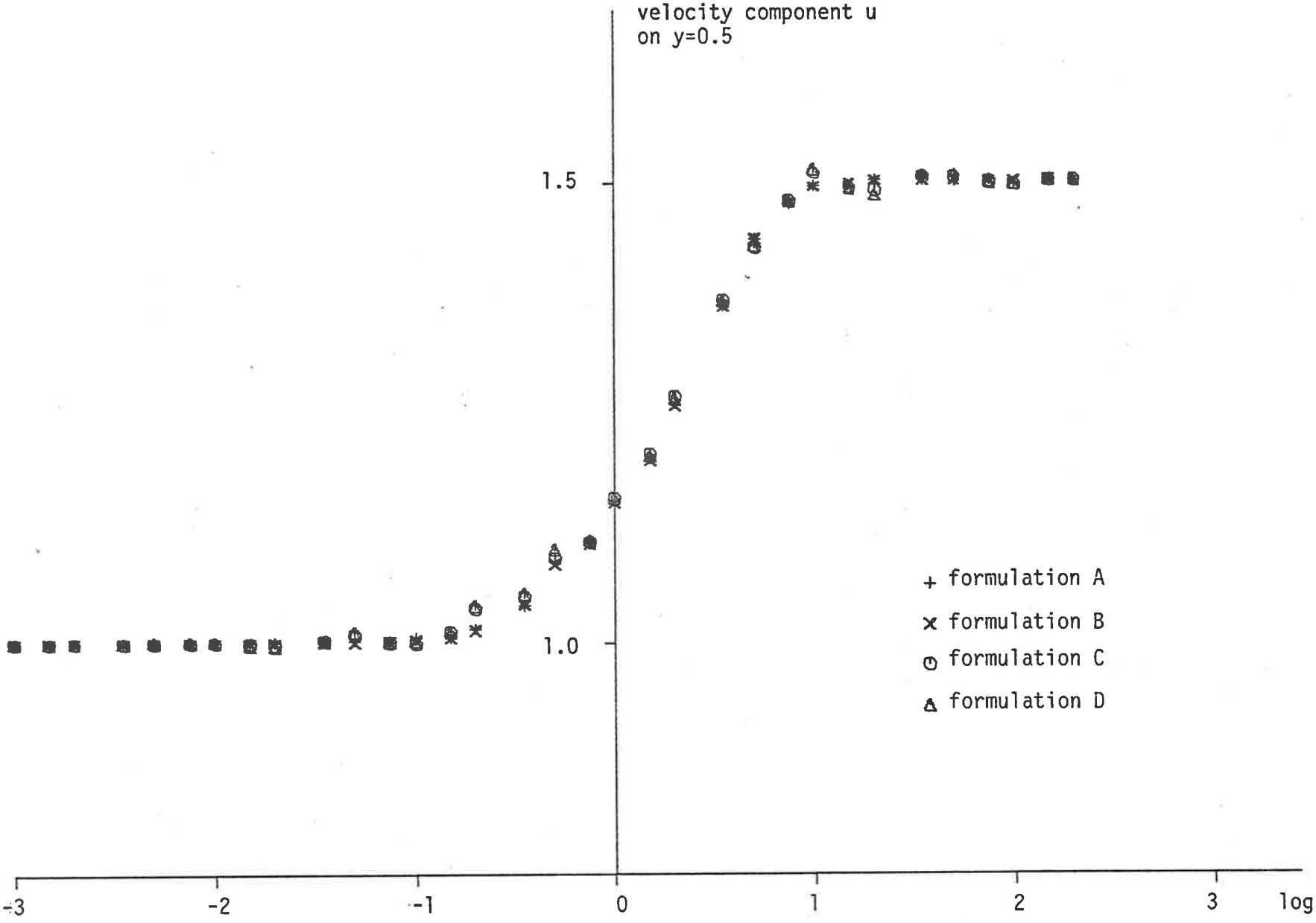

Figure 5.15(b) Variation of u for Re = 200.

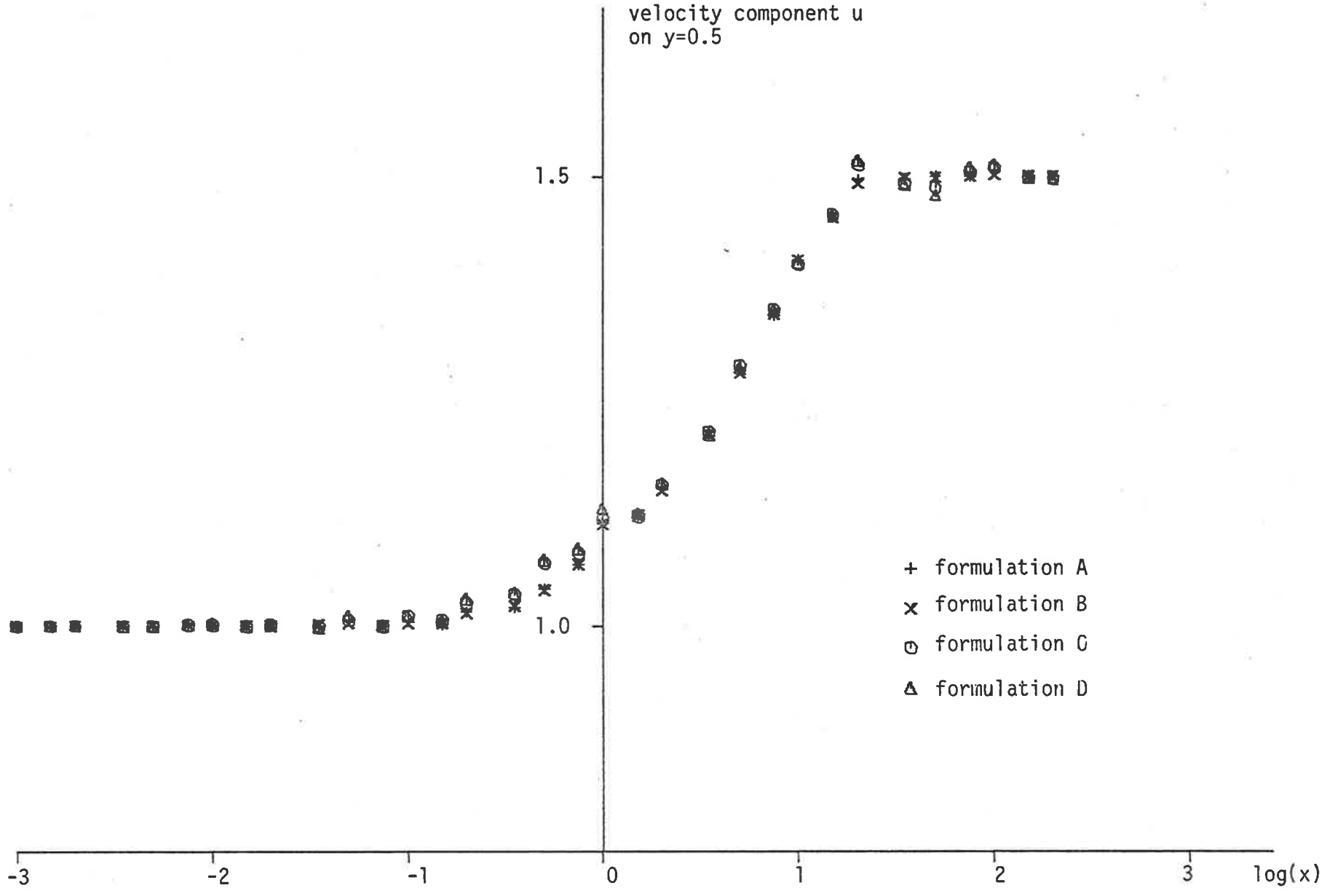

Figure 5.15(c) Variation of u for Re = 500.

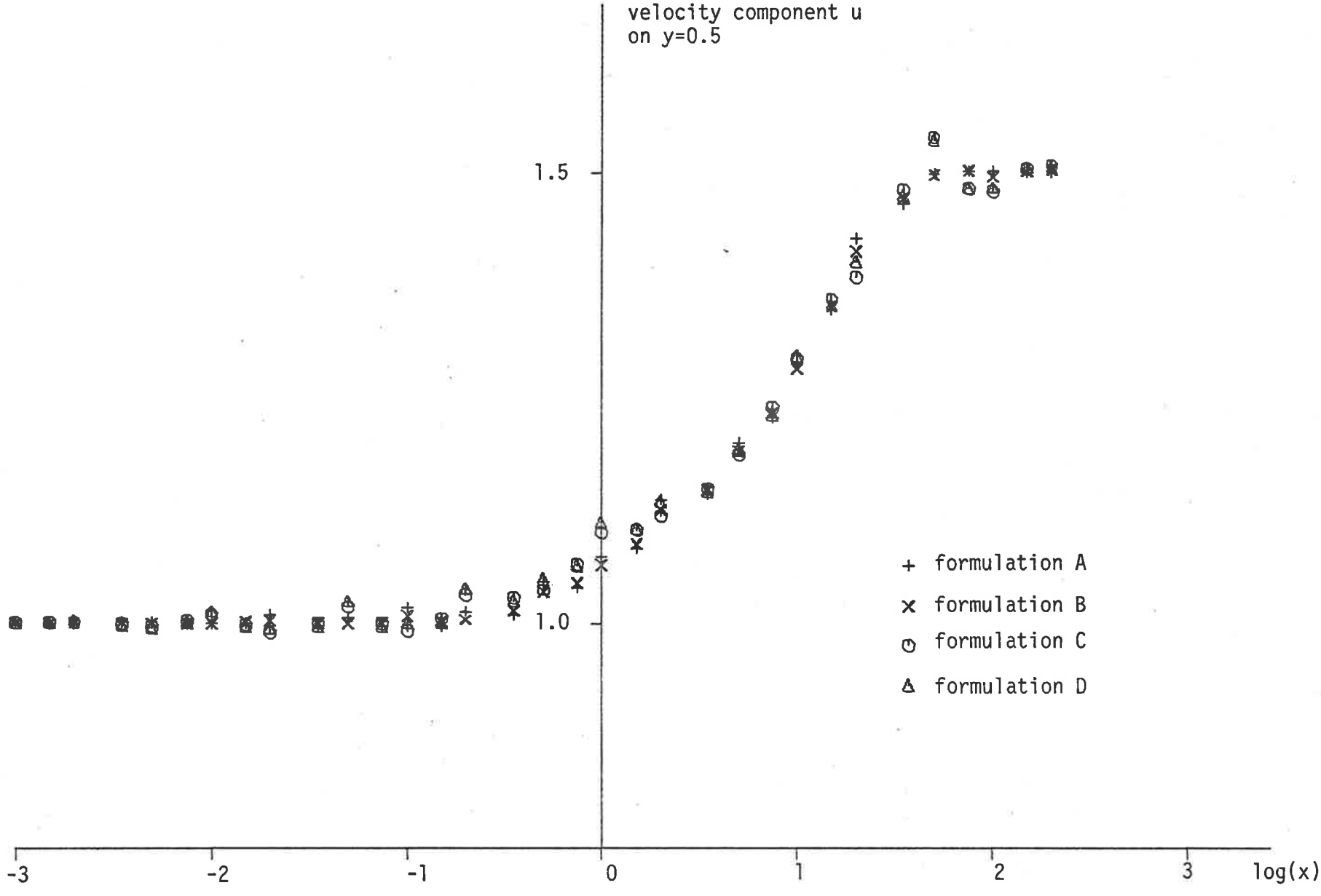

Figure 5.15(d) Variation of u for Re = 1000.

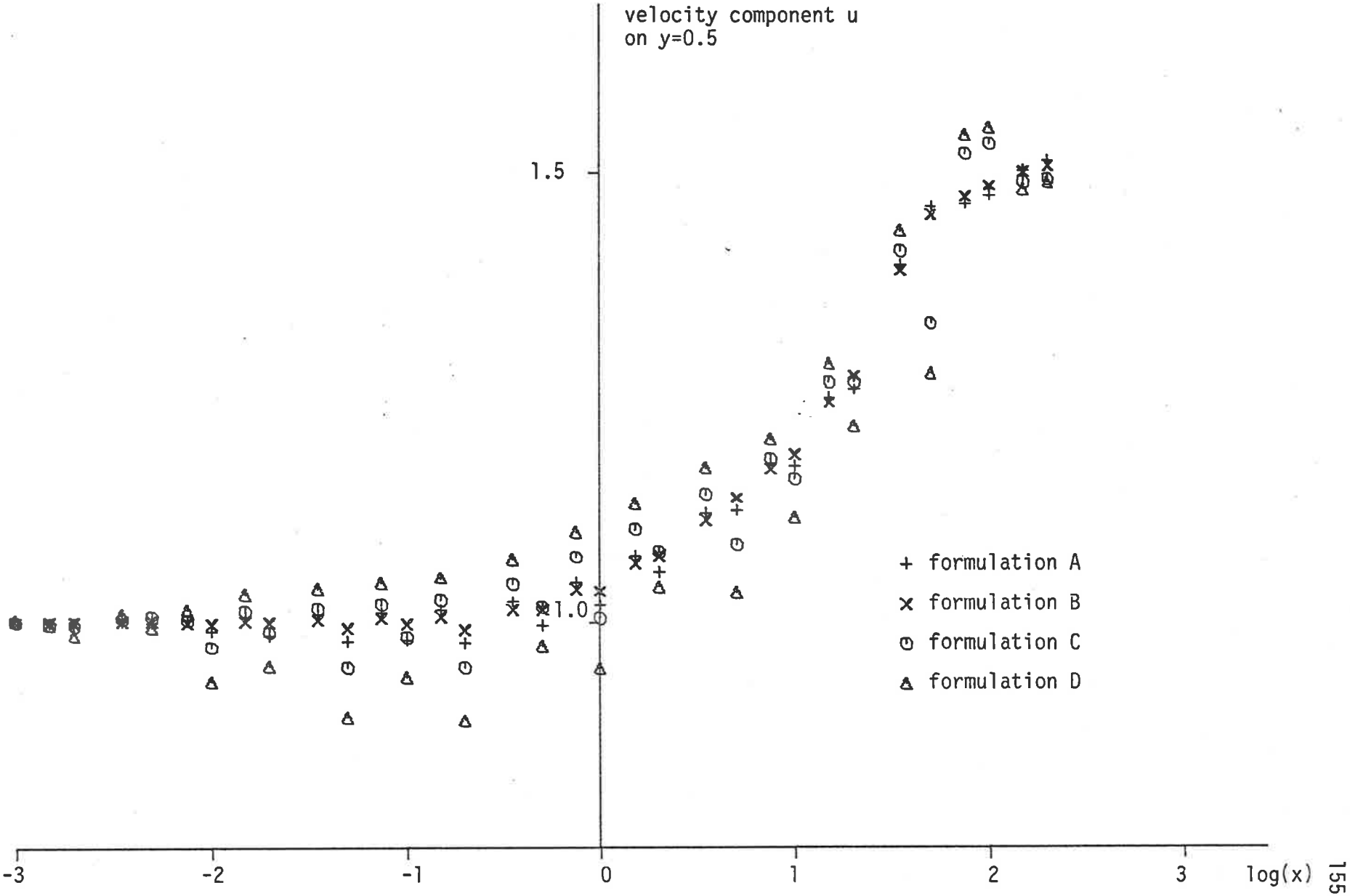

Figure 5.15(e) Variation of u for Re = 2000.

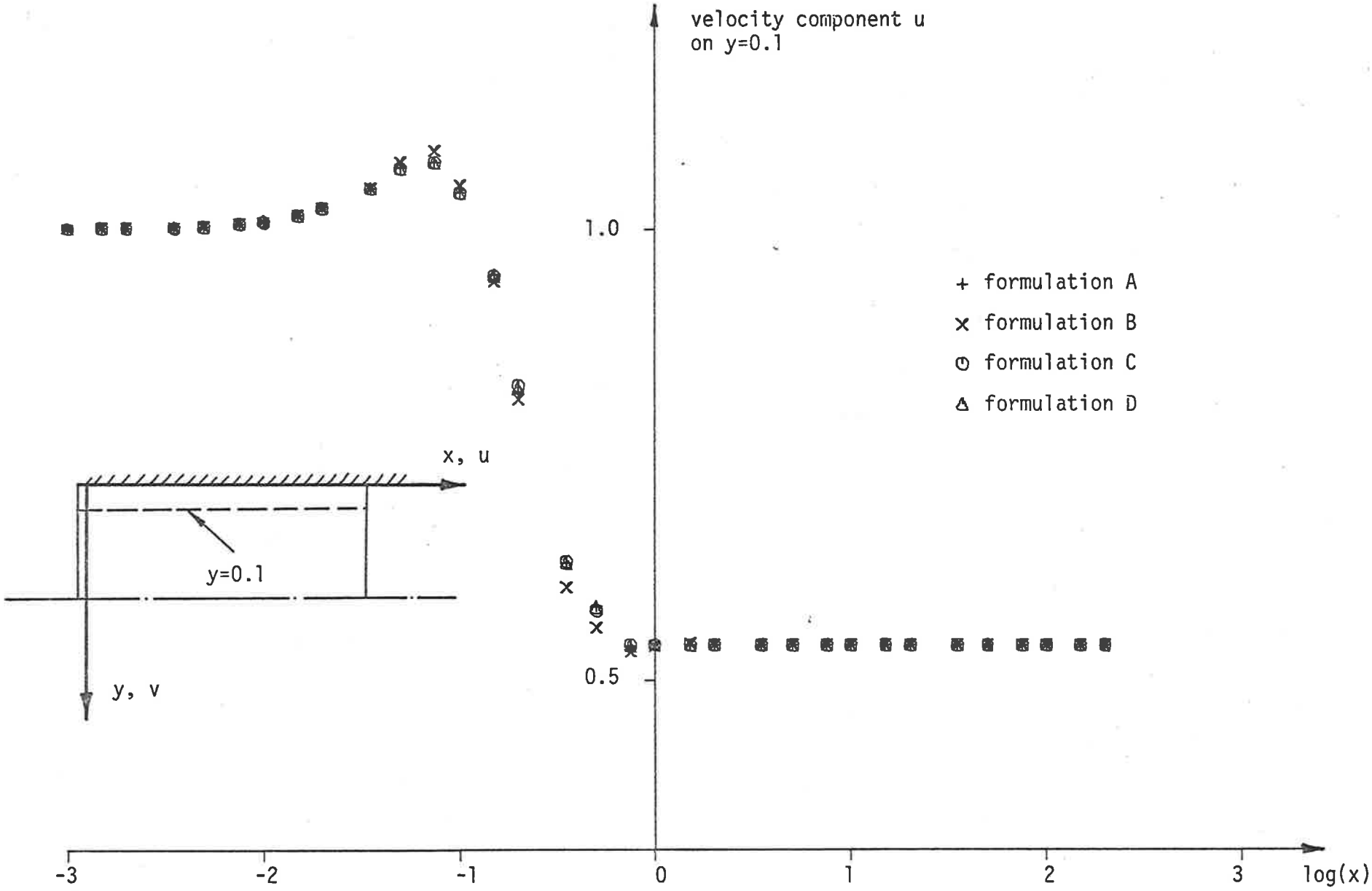

Figure 5.16(a) Formulation Comparison, Entrance Flow, Variation of i on y=0.1 for Re = 1.

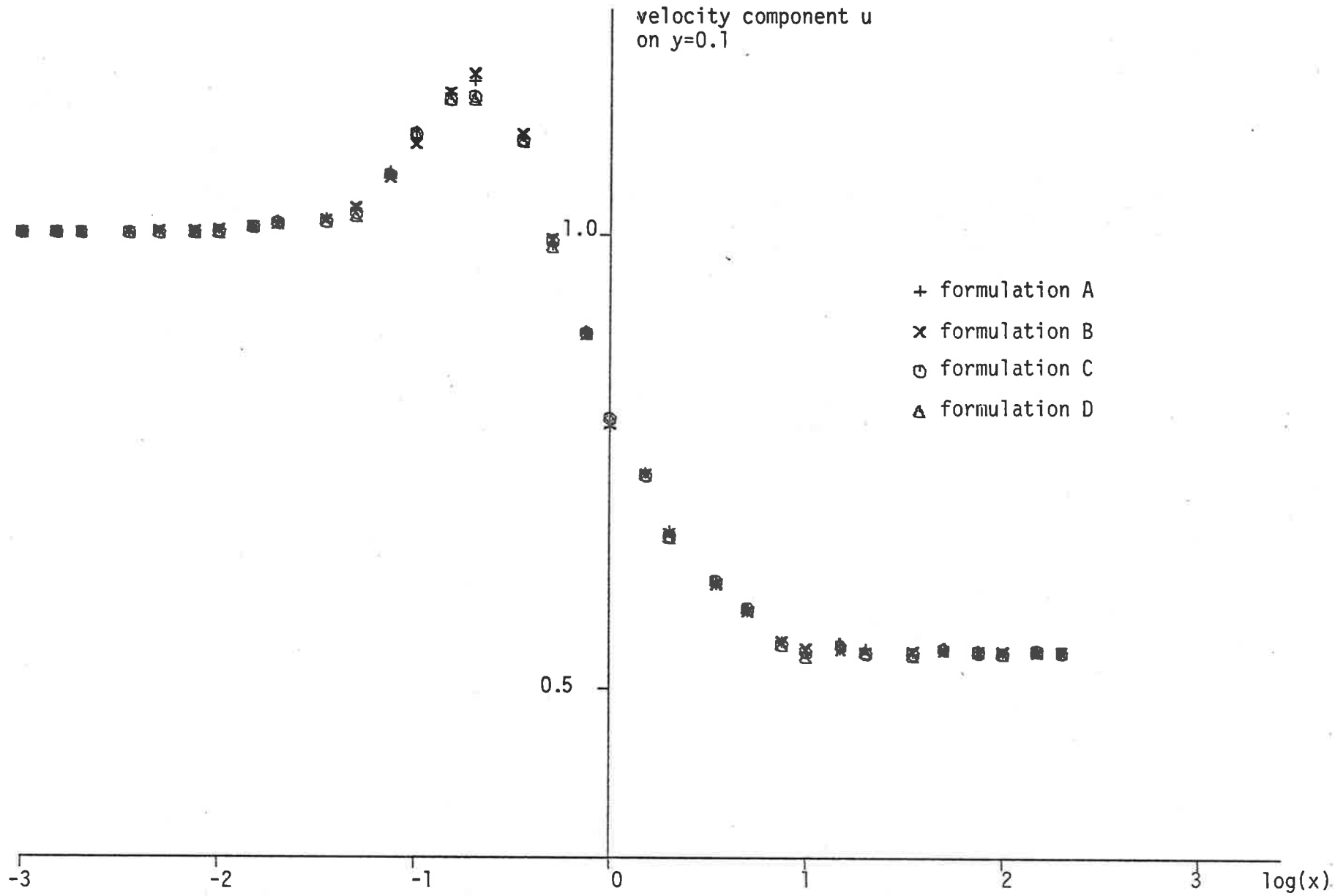

Figure 5.16(b) Variation of u for Re = 200.

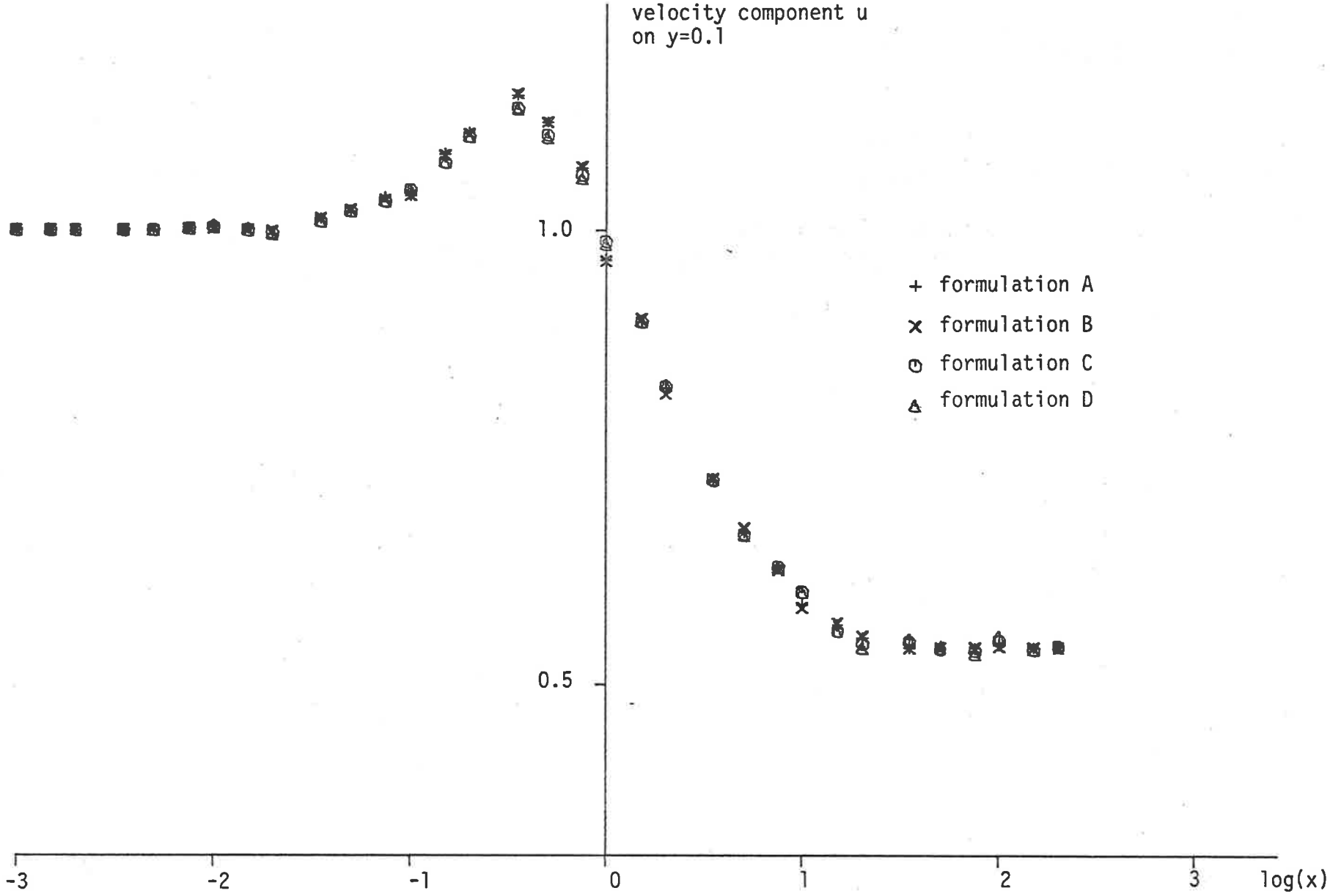

Figure 5.16(c) Variation of u for Re = 500.

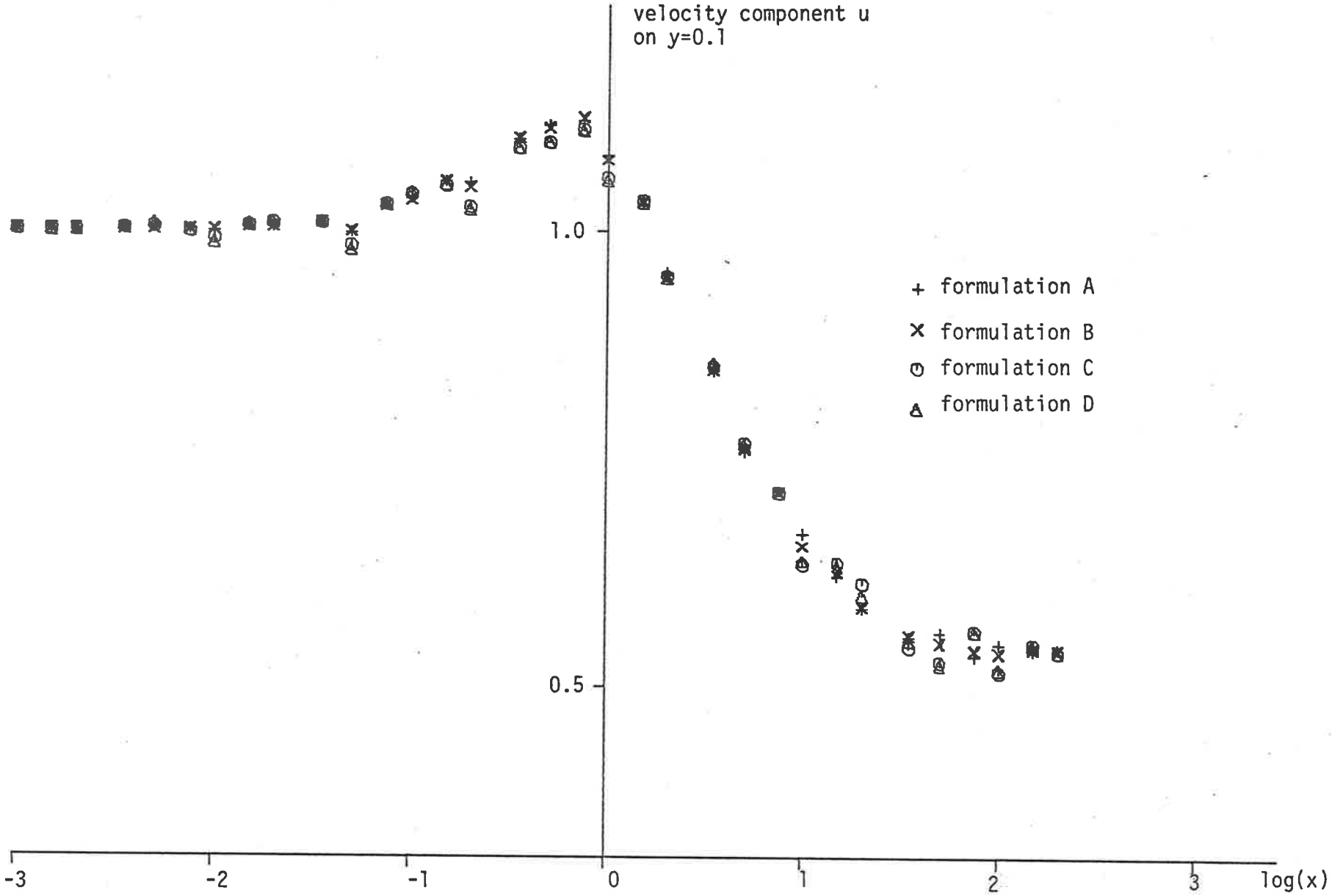

Figure 5.16(d) Variation of u for Re = 1000.

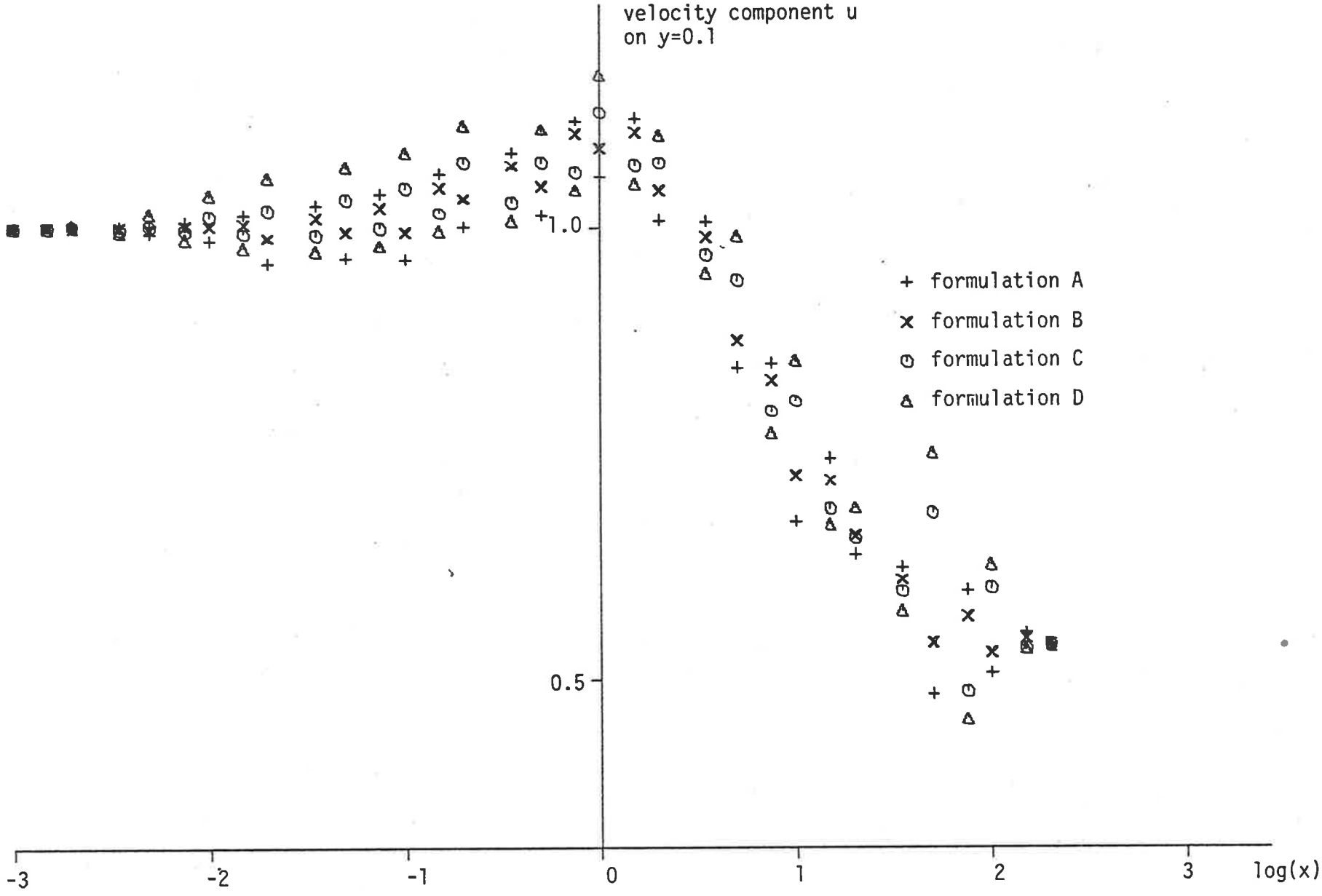

Figure 5.16(e) Variation of u for Re = 2000.

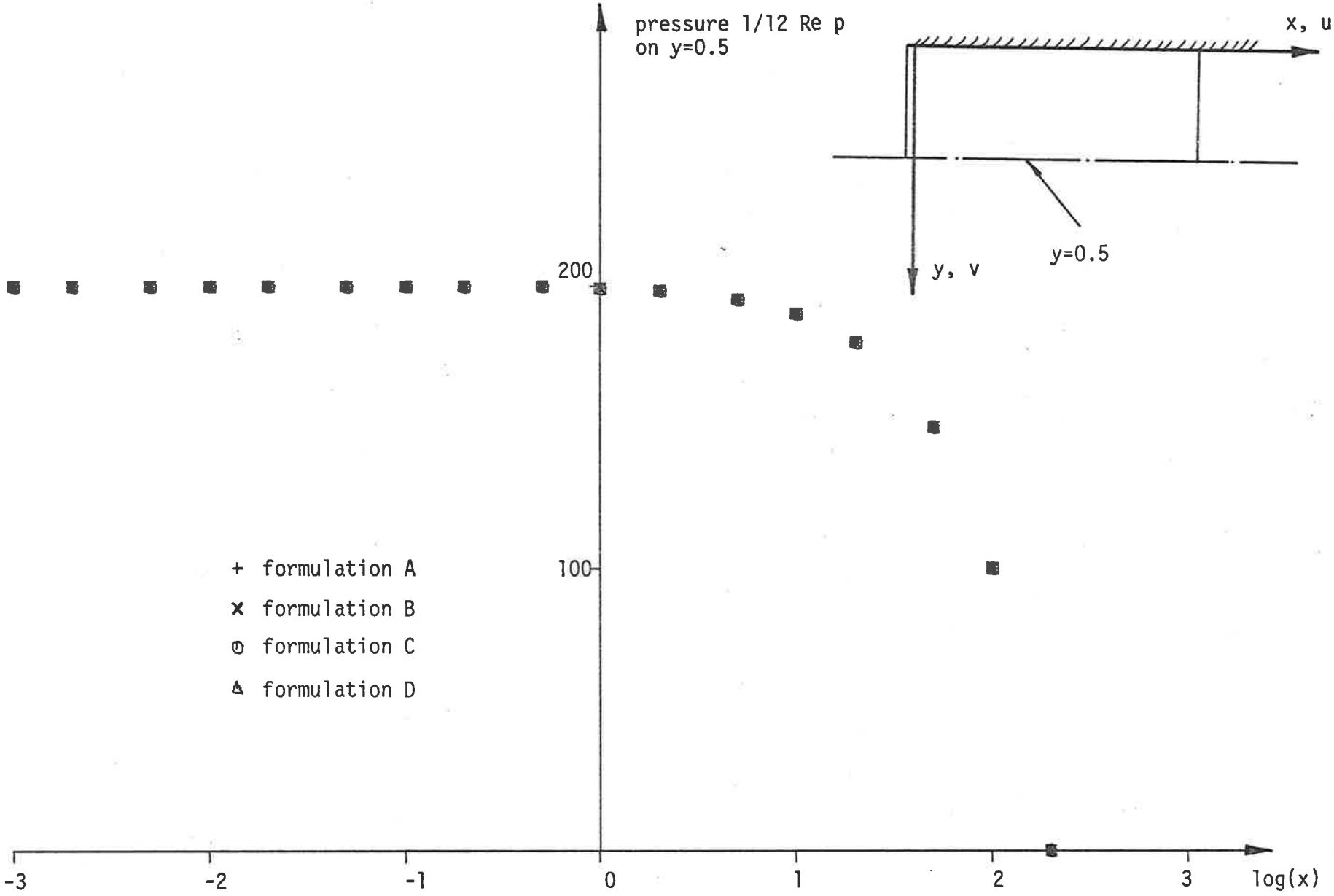

Figure 5.17(a) Formulation Comparison, Entrance Flow, Variation of p on y=0.5 for Re = 1.

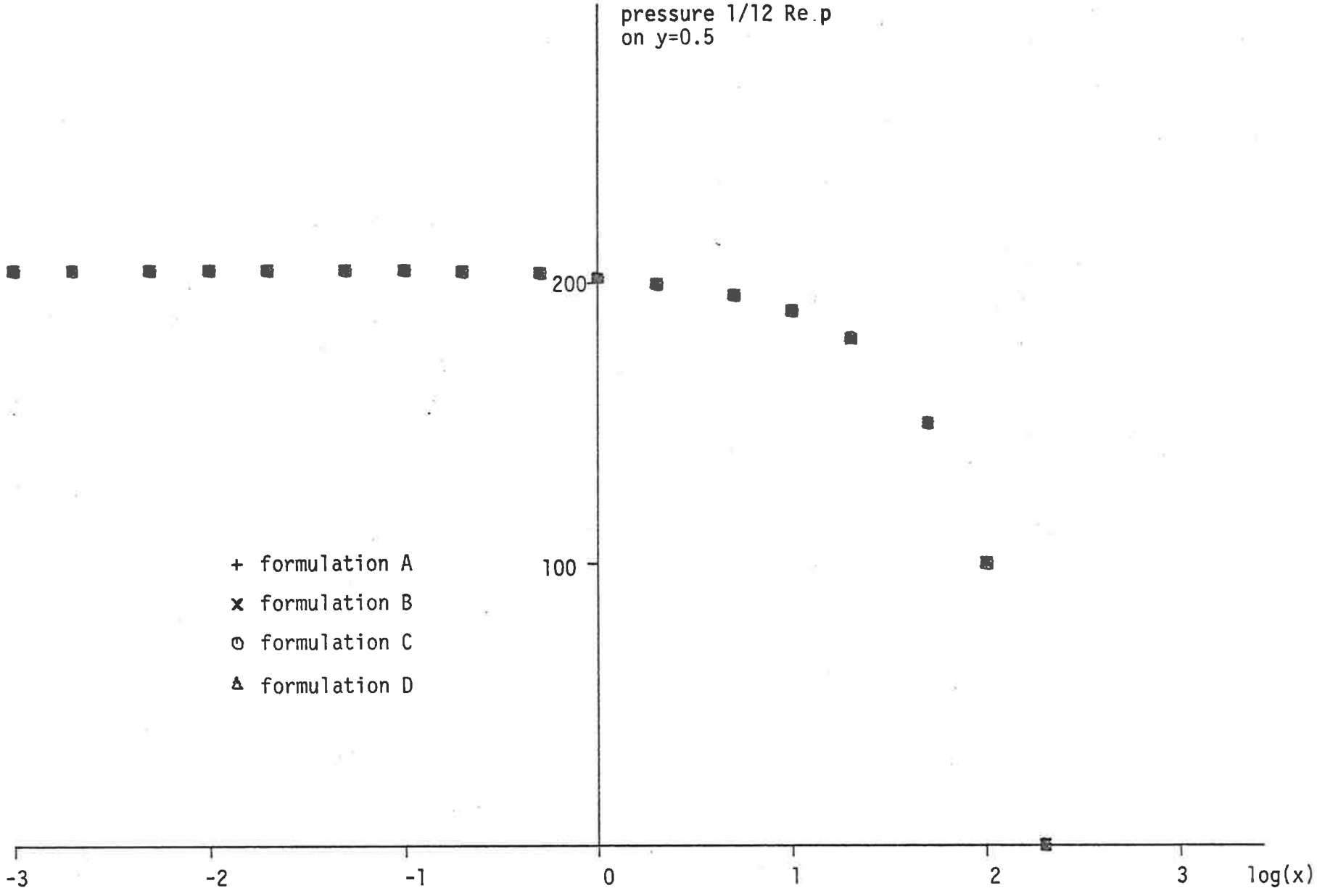

Figure 5.17(b) Variation of p for Re = 200.

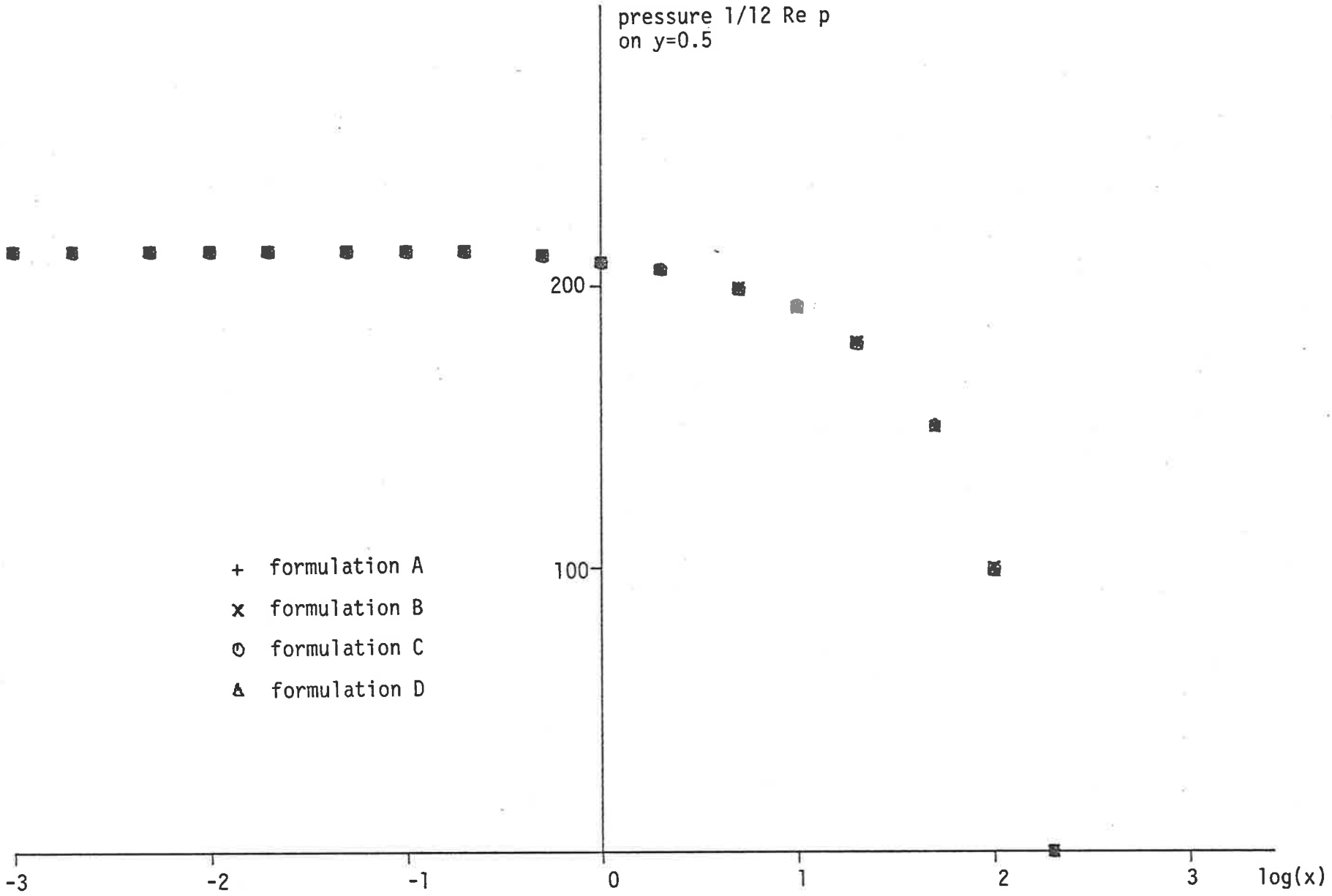

Figure 5.17(c) Variation of p for Re = 500.

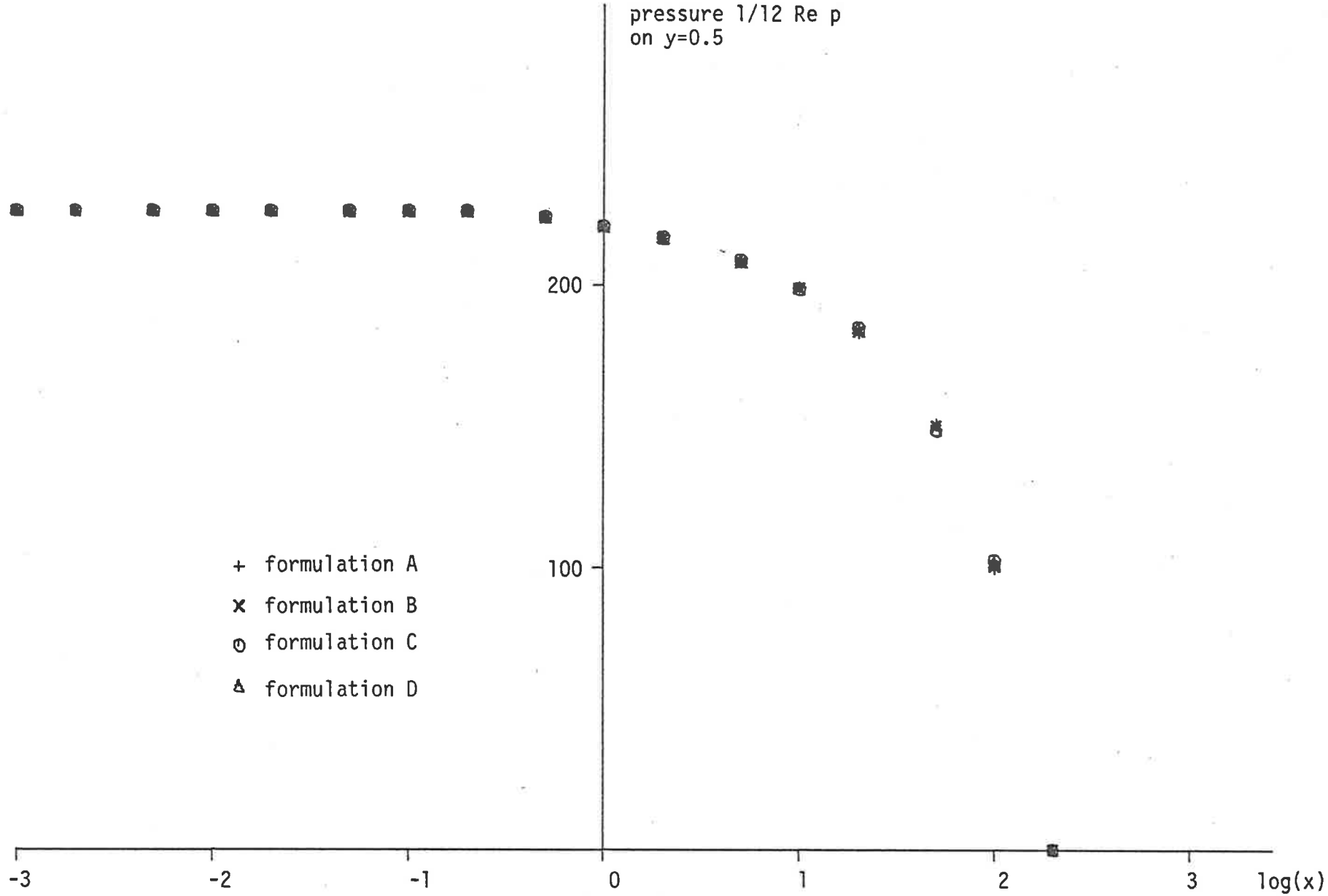

Figure 5.17(d) Variation of p for Re = 1000.

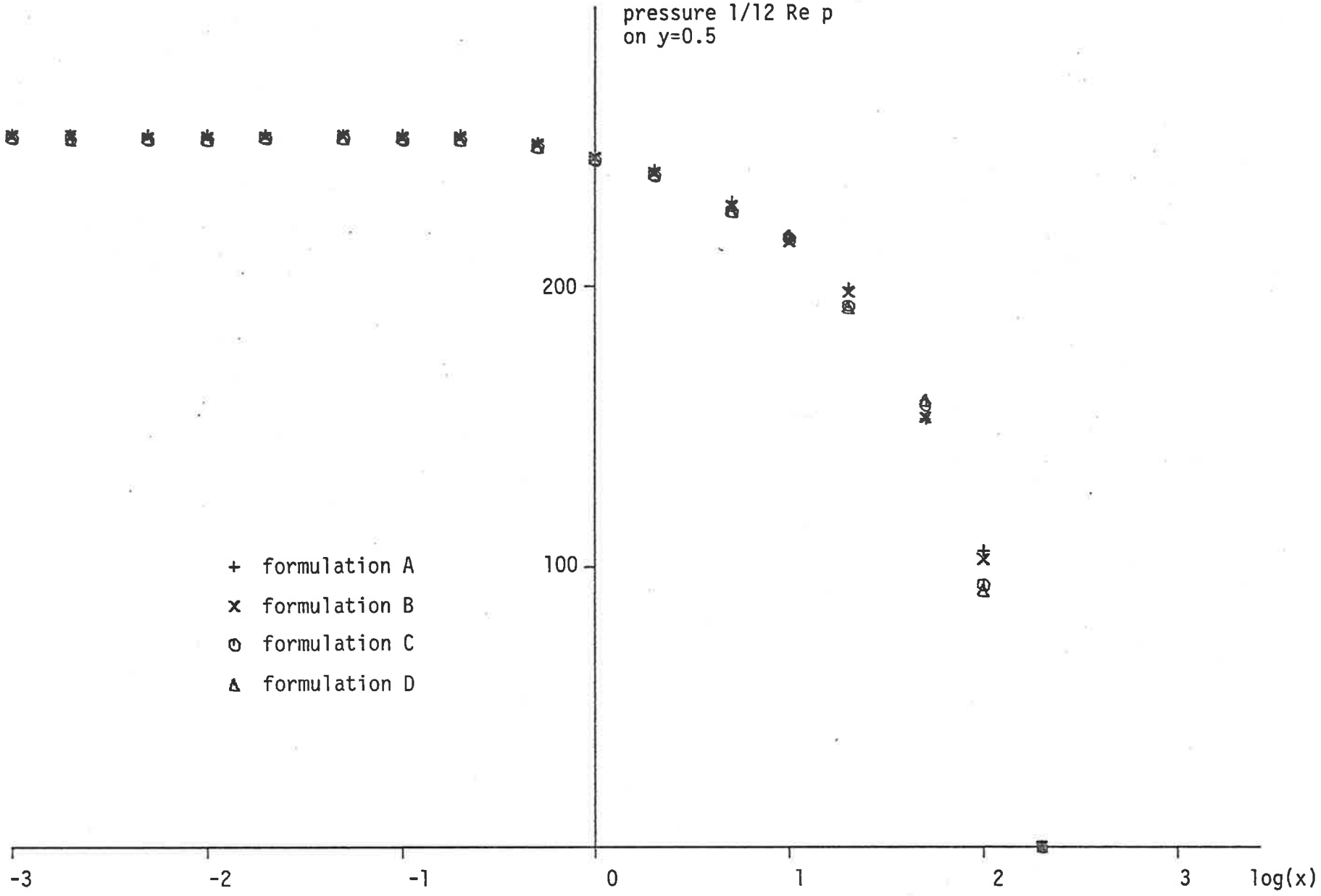

Figure 5.17(e) Variation of p for Re = 2000.

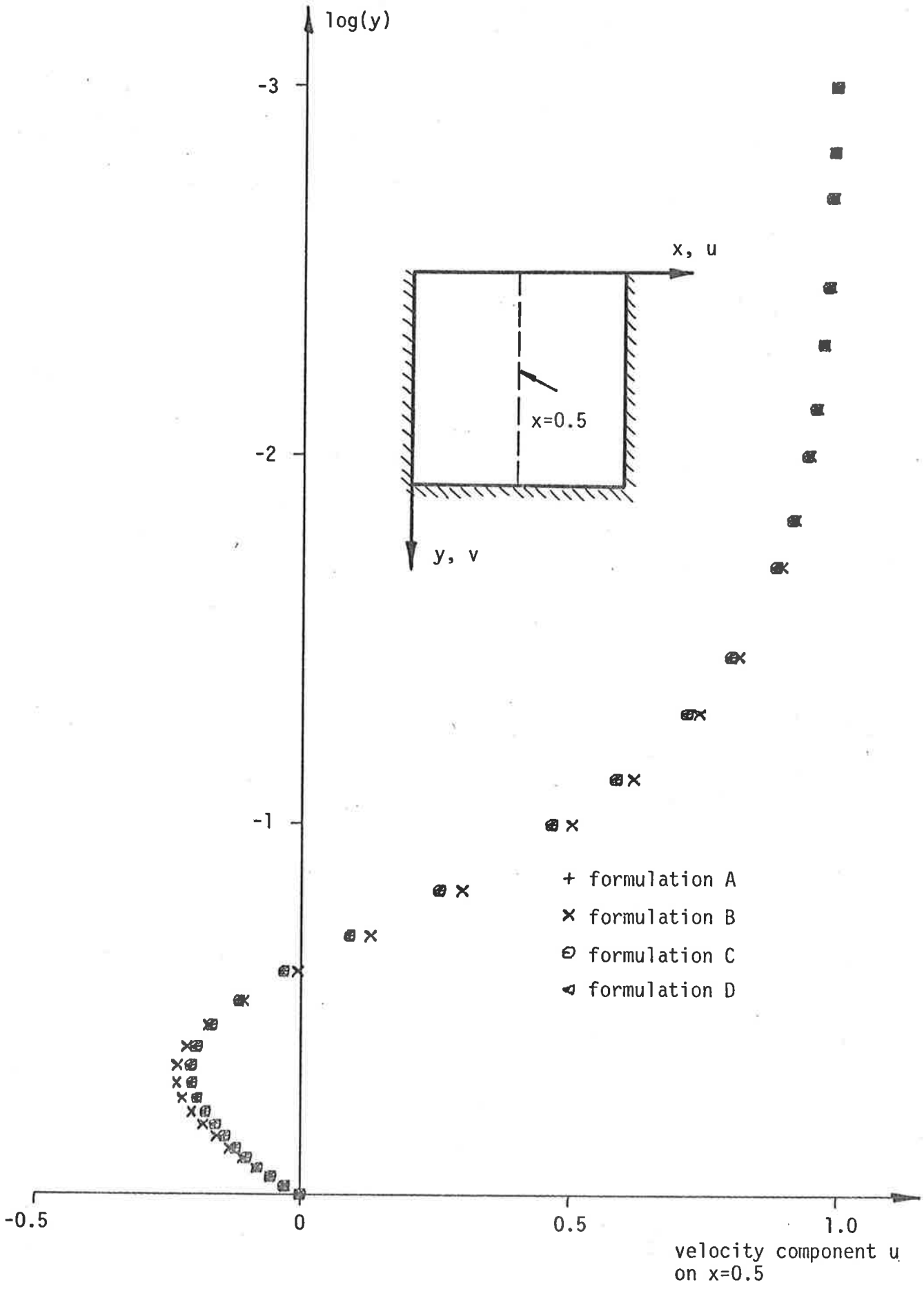

Figure 5.18(a) Formulation Comparison, Cavity Flow, Variation of u on x=0.5 for Re = 1.

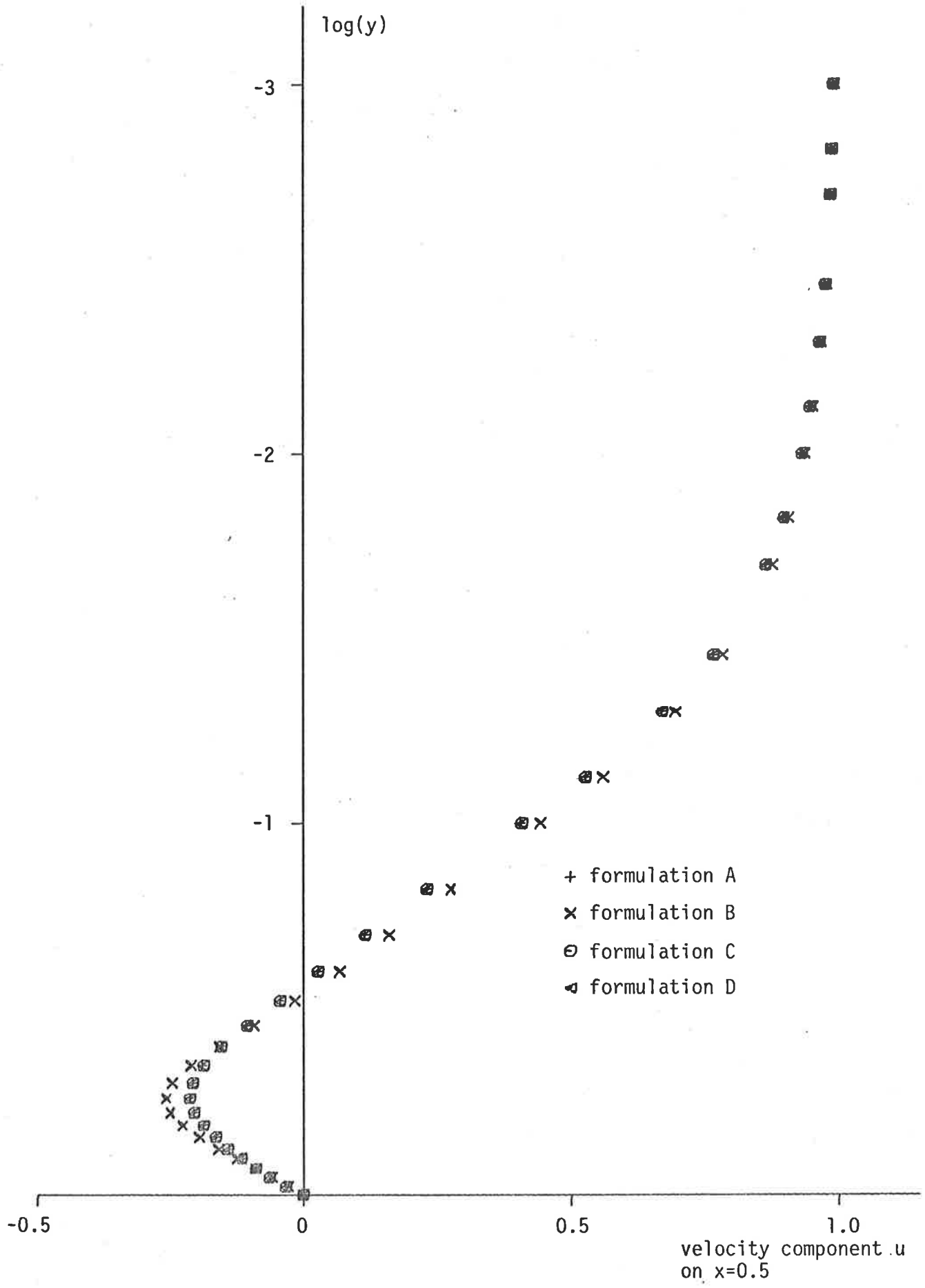

Figure 5.18(b) Variation of u for Re = 100.

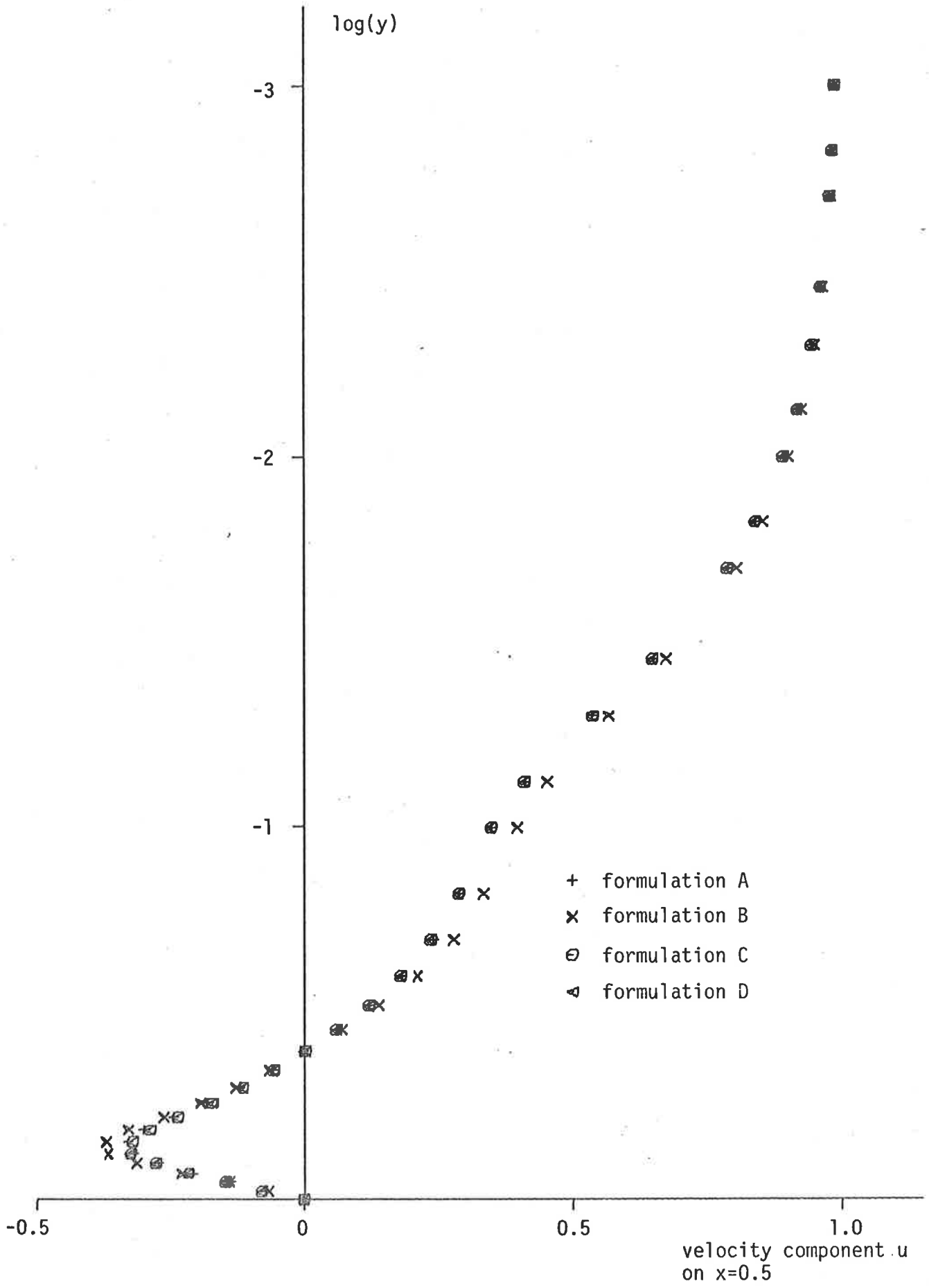

Figure 5.18(c) Variation of u for Re = 400.

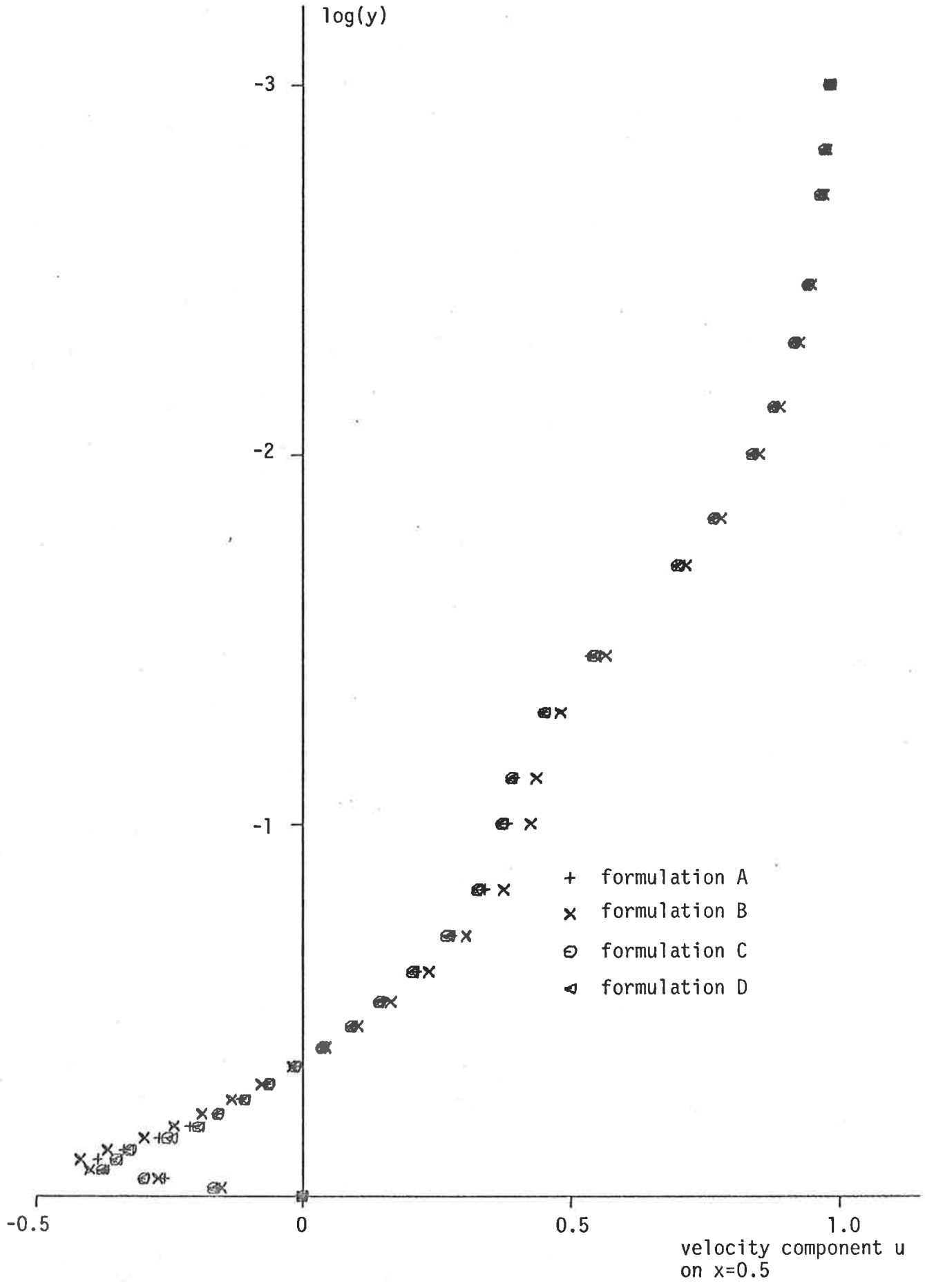

Figure 5.18(d) Variation of u for Re = 1000.

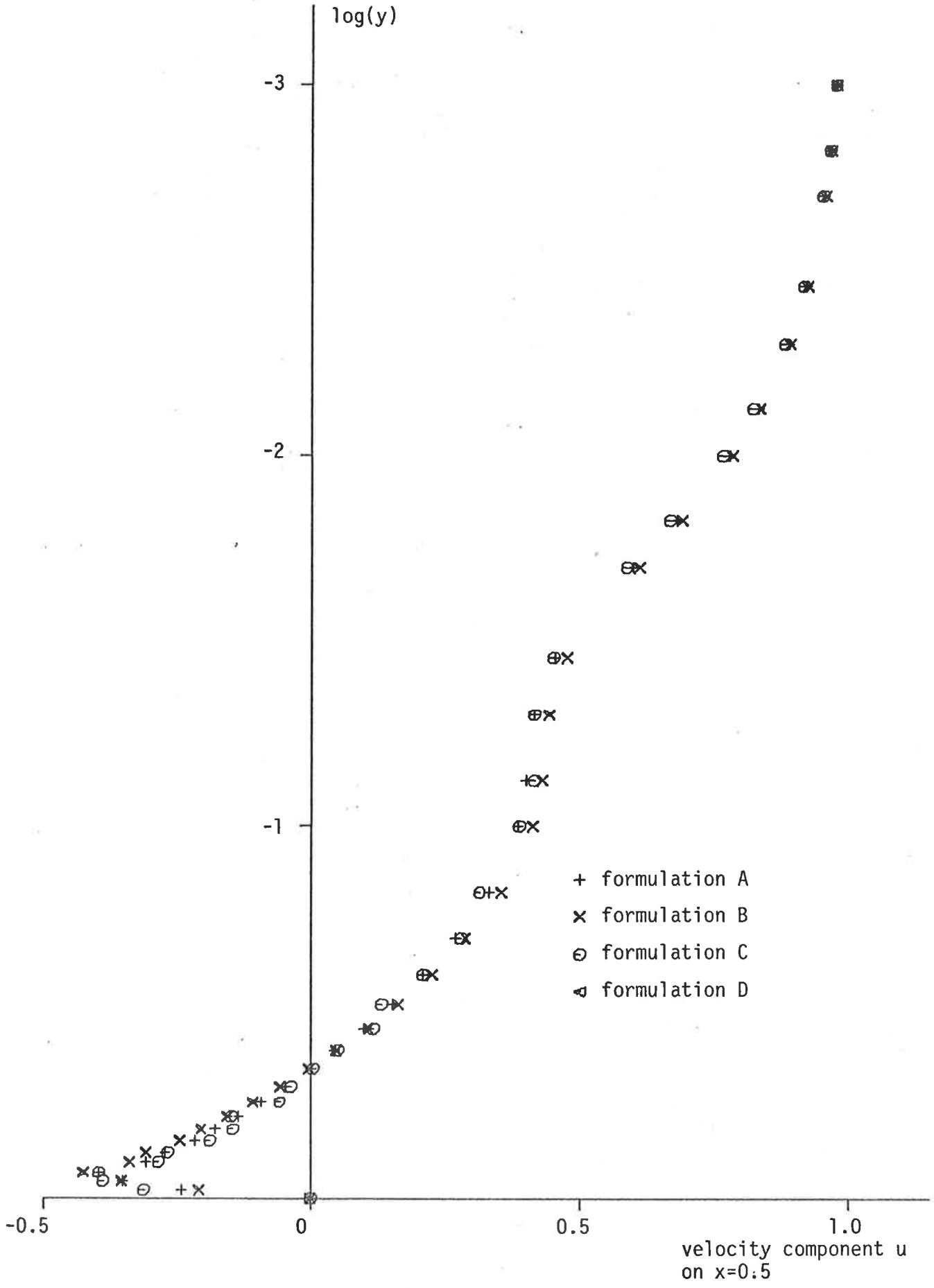

Figure 5.18(e) Variation of u for Re = 2000.

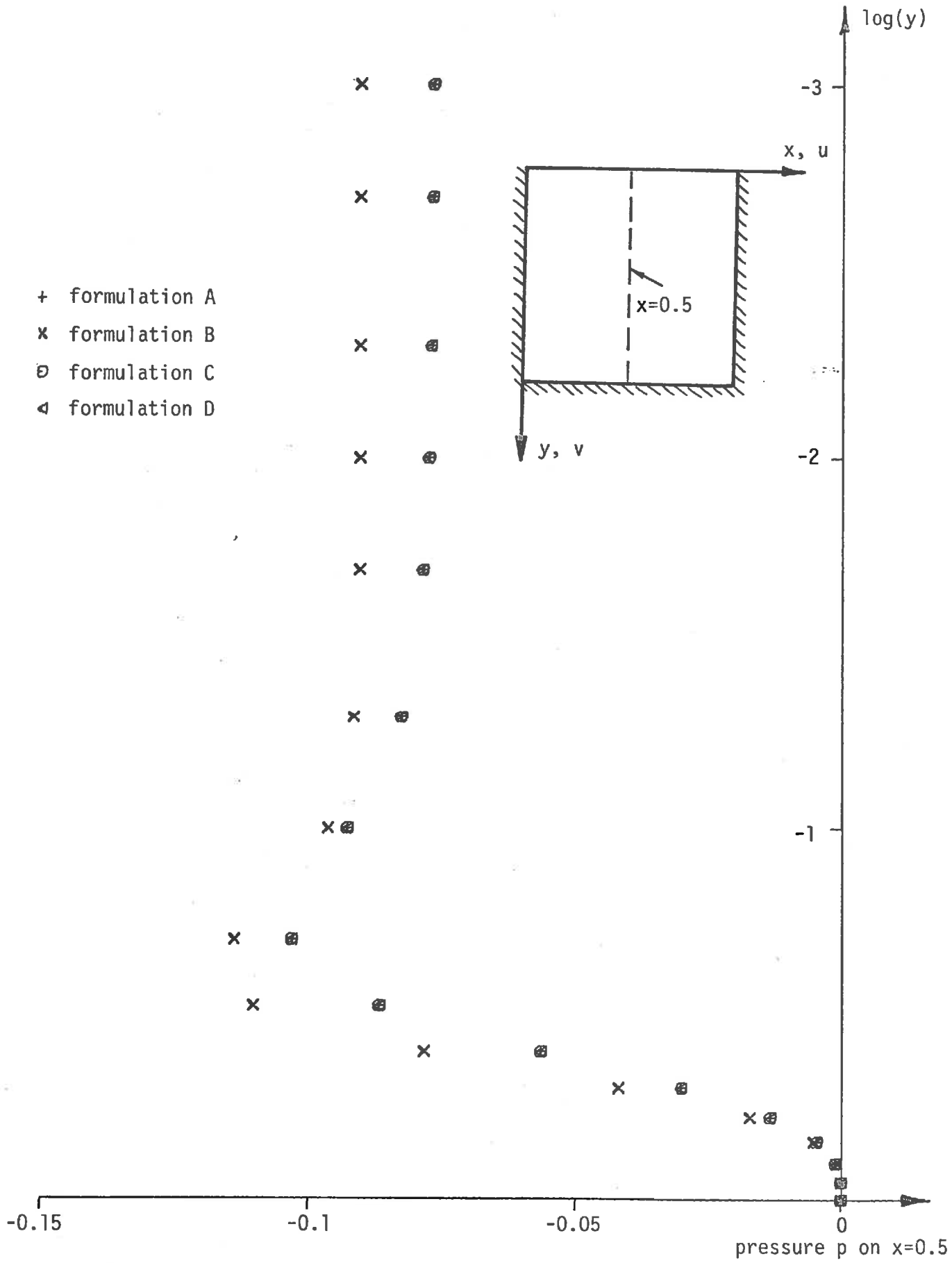

Figure 5.19(a) Formulation Comparison, Cavity Flow, Variation of p on x=0.5 for Re = 1.

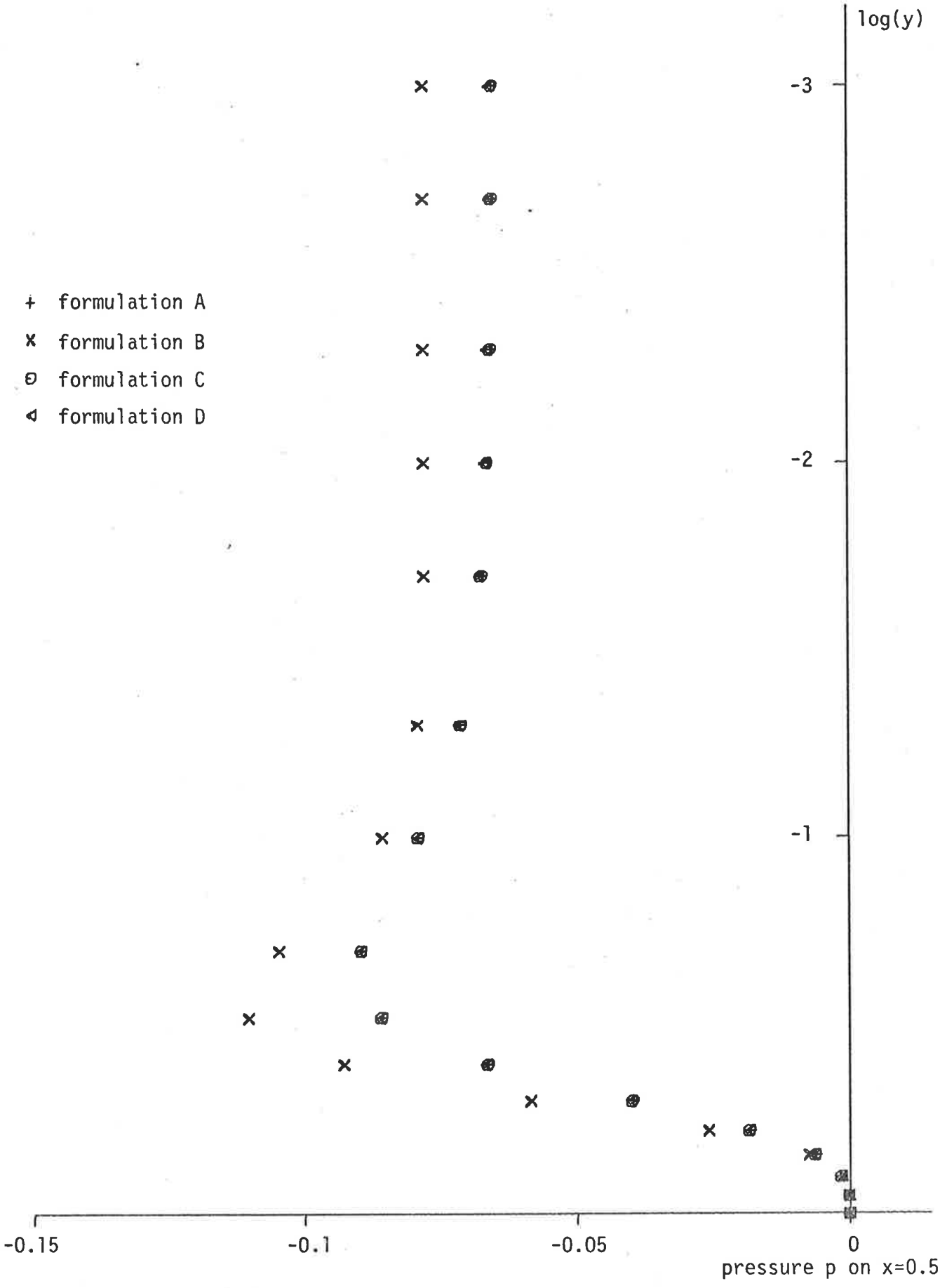

Figure 5.19(b) Variation of p for Re = 100.

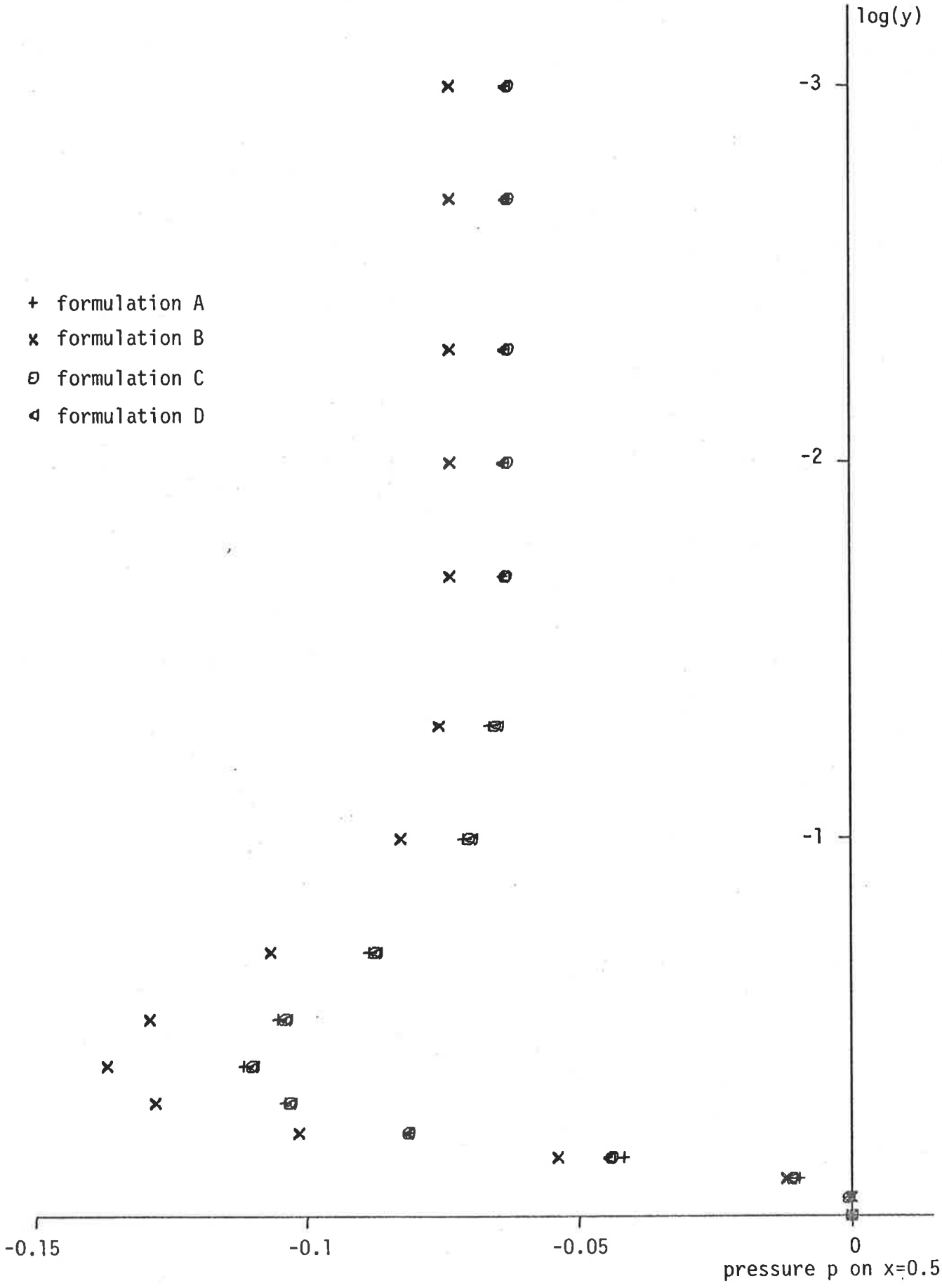

Figure 5.19(c) Variation of p for Re = 400.

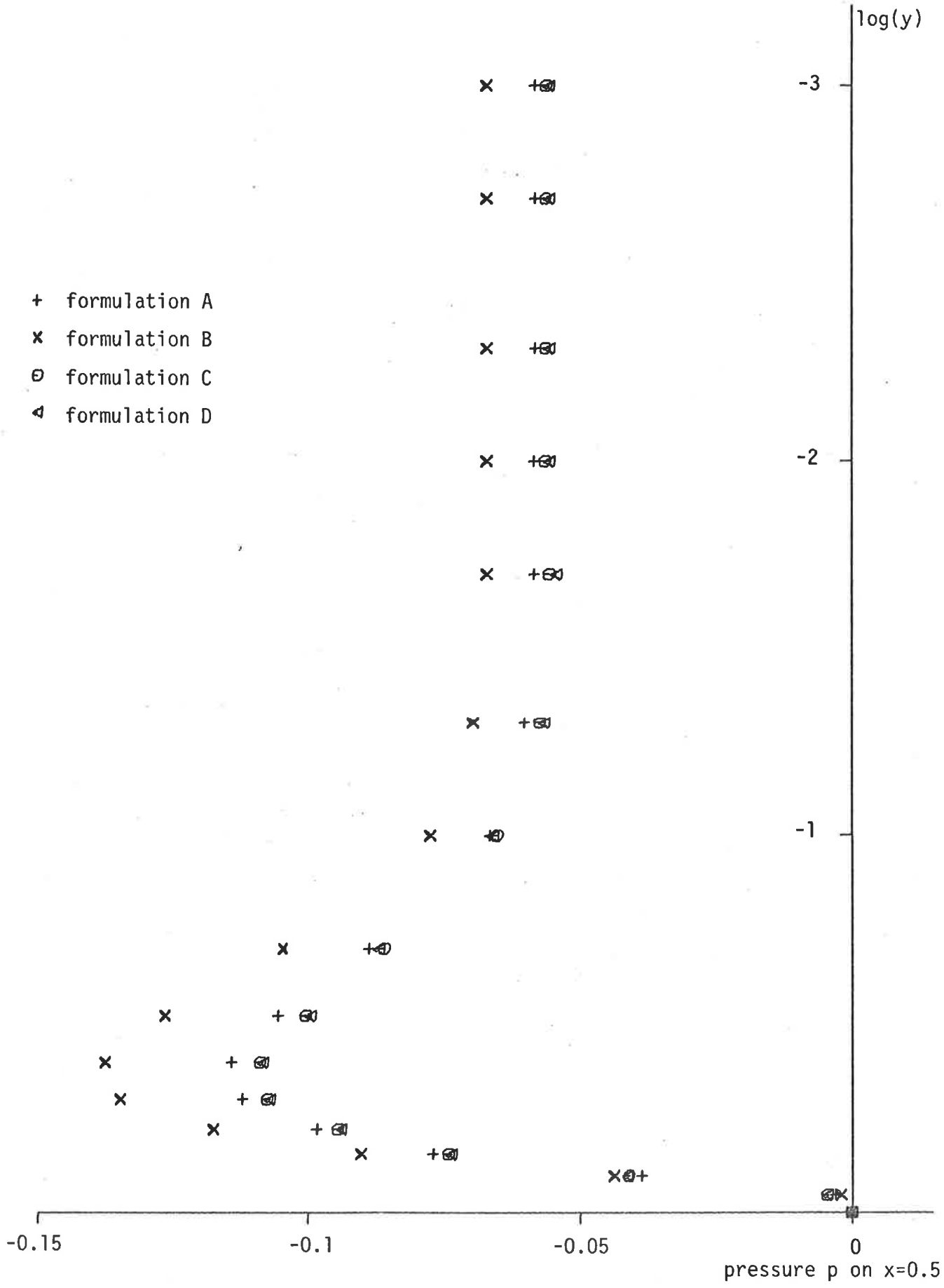

Figure 5.19(d) Variation of p for Re = 1000.

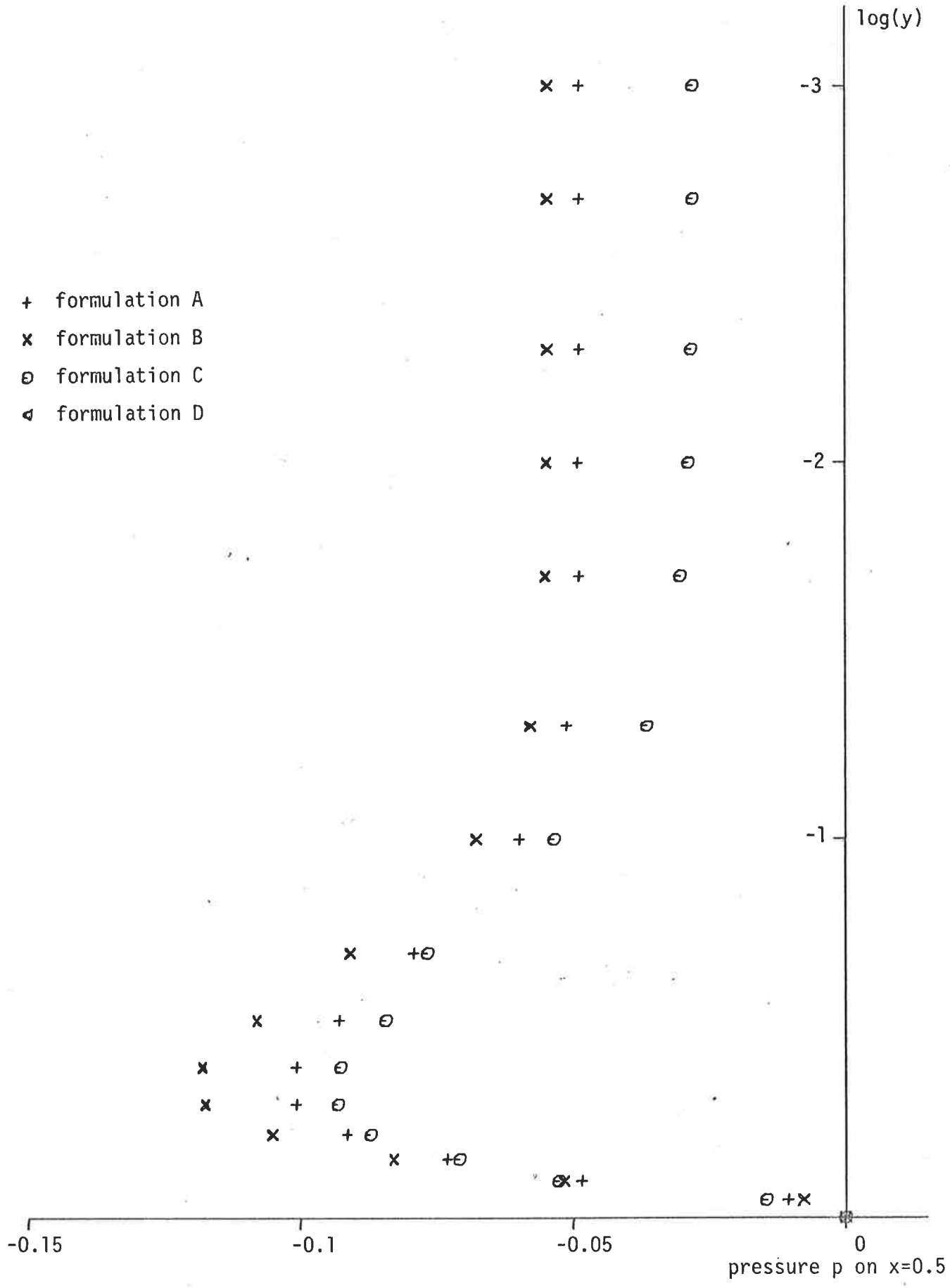

Figure 5.19(e) Variation of p for Re = 2000.

variations in the regions chosen, especially where very small elements are used. If the conventional method of presentation had been used, a loss of information would have occurred since the points on the graphs corresponding to nodes in these regions would be so close together as to make them useless for comparing the various formulation accuracies. It will also be noted that the pressure for the entrance flow problem is plotted as $\frac{1}{12}$ Re.p rather than simply p. This was done so that the same pressure axis could be used for all Reynolds numbers, otherwise a 0 to 200 scale would have been needed for the Reynolds number equals 1 flow while for the Reynolds number equals 2000 flow, a considerably smaller 0 to 0.2 full scale range would have been required.

From the velocity and pressure plots described above, several points can be noted. Firstly, for the entrance flow problem, all formulations result in identical solutions for both the velocity and pressure fields when Reynolds number is below about 500. The plots are smooth with liitle or no spatial oscillations and agree well with solutions previously published. A more precise comparison with existing known numerical solutions is made in Section 5.6. Secondly, at higher Reynolds numbers and particularly at Re=2000, large amplitude spatial oscillations appear in the velocity and pressure fields for all formulations. The severity of these oscillations increases with Reynolds number so that at 2000 the maximum amplitudes of oscillations in the velocity fields produced by formulations A to D are approximately 5%, 2%, 8% and 12% respectively of the fully developed centreline velocity of 1.5. Oscillations in the pressure fields however are not as severe, the maximum amplitude obtained with formulation D being about 2% of the inlet centreline pressure. Thirdly, at all Reynolds numbers considered, formulation B consistently gives the best solution for both the velocity and pressure fields. The spatial oscillations that do occur are always the least severe and lie well within the acceptable limits, even at Re=2000, which

is the maximum value considered in this study. Formulations A, C and D however do not perform as well and at Re=2000, produce oscillations that are unacceptable. From the analyses of the entrance flow problem therefore it can be seen that formulation B results in significantly higher computational accuracy over a considerably larger range of Reynolds numbers. In fact, by examining the rate of increase of oscillation amplitude as Reynolds number increases, one can see that formulation B would probably give acceptable results at Re=3000 and possibly even at 4000 providing the length of the finite element mesh is suitably adjusted.

With the cavity flow problem the situation is slightly different. Firstly, at all Reynolds numbers considered up to the maximum 2000, all formulations result in velocity and pressure variations that are smooth with spatial oscillation amplitudes never exceeding more than 5% of the velocity and pressure values at the centreline of the moving wall. Secondly, when oscillations do occur, mainly at Re=2000, formulation C produces the largest amplitudes both in the velocity and pressure fields. It should be noted at this point that no convergent solution was obtained with formulation D at Reynolds number equals 2000. Lastly, from Figures 5.18 and 5.19, it can be seen that formulation B produces solutions that are consistently and significantly different from those produced by formulations A, C and D. It can also be seen that at least for Reynolds numbers below 400, the solution obtained using formulations A, C and D are identical. Above 400 a variety of solutions are obtained, all with the same basic shape but differing by up to 5% in the velocity variation around the central eddy and by up to 18% in the pressure variation near the moving wall. In order to determine the most accurate formulation, a comparison is made with known existing numerical solutions. However, the two most frequently cited published numerical solutions that are used for this comparison differ so much between themselves

that a conclusive choice of the formulation that is best able to solve the cavity flow problem cannot be made. Nevertheless for the sake of completeness, this comparison is still shown in Section 5.6.

In summary therefore, we see that using both criteria, namely the computational efficiency and computational accuracy to compare the four formulations, B has proven to be the optimal one, requiring the least total computational effort to obtain the most acceptable solution over the widest range of Reynolds numbers. Therefore formulation B is now used in the element comparison and finally in the subsequent three-dimensional analyses.

5.5 Results of Element Comparison

During the early part of this study it was found that various finite elements have, in the past, been used to model viscous flow problems. It was also found that a whole variety of comparisons had been made to show that one particular element was better than another. Most of these comparisons were conclusive and the results accepted by a majority of the workers in this area. Recently, claims that the two-dimensional eight noded Serendipity element is superior to the nine noded Lagrangian element and vice versa have also appeared. However the proof of one element's superiority over the other has never been conclusively established since a comparison of their performance in modelling viscous flow problems has never been made. In order to clarify this contradiction then, at least for the two viscous flows considered in this study, the present comparison was undertaken and carried out.

The second reason for carrying out this comparison was to observe the differences in performance of the eight and nine noded elements when their shapes in a finite element mesh are either only rectangular or trapezoidal as well as rectangular. It was anticipated that when only rectangular elements are used, both element types would be equally

capable of modelling a viscous flow. When trapezoidal as well as rectangular elements are used however, it was expected, following the results shown in Appendix D, that the nine noded element would produce more accurate solutions. For this reason, in the previous formulation comparison, in which the eight noded Serendipity element was used exclusively, only rectangular elements were incorporated in the meshes, thus avoiding, hopefully, additional problems associated with differences in element performance. The present comparison should therefore confirm this assumption and validate the results obtained in the previous section.

In order to keep in mind, as the comparison is made, the differences and similarities between the Serendipity and Lagrangian elements, the essential details of each will now be briefly described again. Firstly and most importantly, the Lagrangian element is capable of representing a complete linear pressure as well as a complete quadratic velocity variation in each coordinate direction. The Serendipity element, on the other hand, is capable of representing in each coordinate direction, a complete linear pressure but only an incomplete quadratic velocity variation, the highest order term being the one omitted. Secondly, in two dimensions, the Lagrangian element has nine nodes, eight of which are the same as the eight of the Serendipity element, while the ninth is located at the intersection point of the two lines joining the midpoints of the opposite edges of the element. It should be pointed out that this point does not coincide with the centroid of the element when a trapezoidal shape is used. Thirdly, both the elements are isoparametric and both are capable of ensuring continuity of velocity and pressure across element interfaces. However, neither can ensure that the first derivative of either the velocity or pressure will also be continuous across element boundaries.

In order to determine conclusively which of the two elements, if either, is the most economical and which leads to the best solution, the same criteria that were used in the formulation comparison can again be applied in this case. Therefore, the computational efficiency can be simply determined by examining the amount of computer time and storage needed to obtain the same solution when each element type is used, and an estimate of the computational accuracy can be obtained by looking at the variations of the velocity and pressure fields along certain cross-sections. To this end, the runs for test series 2, set out in Table 5.2(a) for the entrance flow problem and (b) for the cavity flow problem, were carried out and the results, detailed below, obtained.

Table 5.6 shows the number of iterations and, in brackets, the execution times for each run, while Table 5.7 gives the average execution time per iteration and the computer storage required by each mesh in the four parts of the test series. It should be noted that unlike the formulation comparison in which all formulations required the same amount of computer storage, in this comparison the nine noded element needs additional storage both to hold the slightly longer computer program and to run the problems. Consequently, both the execution times as well as the computer storage requirements should be kept in mind when the more efficient element is selected. It should also be pointed out that the same convergence criterion that was used for the formulation comparison test runs is also used in this test series and that formulation B, the most efficient and accurate of the four considered in the previous section, is used in all runs.

From Tables 5.6 and 5.7 the following points can be noted. Firstly, the same number of iterations is required to obtain a fully converged solution regardless of which element type is used. This is true for all tests with the exception of a few in which it appears that when the nine noded element is used, an additional iteration is needed to

(a)

Re	8NE		9NE	
	ENFLM1	ENFLM2	ENFLM1	ENFLM2
1	2 (222)	2 (161)	2 (300)	2 (218)
200	4 (456)	4 (332)	4 (606)	4 (441)
500	5 (575)	5 (417)	5 (758)	5 (554)
1000	6 (692)	6 (505)	6 (912)	6 (668)
2000	7 (805)	8 (679)	7 (1066)	7 (781)

(b)

Re	8NE		9NE	
	CAVFLM1	CAVFLM2	CAVFLM1	CAVFLM2
1	2 (740)	2 (429)	2 (909)	2 (531)
100	3 (1115)	3 (653)	4 (1805)	4 (1069)
400	6 (2236)	6 (1320)	7 (3171)	7 (1881)
1000	6+3+4 *	6+3+3 *	7+3+4 *	7+3+4 *
2000	13+5 *	12+6+3 *	14+5 *	14+5 *

Table 5.6 Number of iterations and in brackets execution times for (a) the entrance flow and (b) the cavity flow at various Reynolds numbers for test series 2.

Mesh	Execution Time		Computer Storage	
	8NE	9NE	8NE	9NE
ENFLM1	114.1	151.5	66000	74600
ENFLM2	83.2	110.6	63000	70200
CAVFLM1	371.4	452.9	120500	136100
CAVFLM2	217.4	267.2	107100	117500

Table 5.7 Average executive time per iteration in central processor seconds and computer storage in octal words required by each mesh in test series 2.

arrive at the required solution. However this trend is not sufficiently pronounced to prove that the nine noded element is less efficient than the eight. In fact, as can be seen from Table 5.6(a) (at Re=2000) in one of the tests the eight noded element required one iteration more than the nine noded element. Secondly, it can be seen that for the entrance flow problem, the results indicate that the zero initial guess is sufficiently close to the required solution to enable it to be evaluated for the whole Reynolds number range considered. However, with the cavity flow problem for Reynolds numbers above 400, as was the case in the formulation comparison, additional runs had to be executed in order to obtain an initial guess that was sufficiently close. The number of additional iterations required by these preliminary runs is shown in Table 5.6(b), the asterisks indicating the tests for which additional runs were required. Table 5.6(b) also shows that this problem was common to both the eight and nine noded elements, indicating once again that neither of the two elements is significantly more computationally efficient.

The third point, that can be noted from Table 5.7, is the increase in computation time per iteration and computer storage required when the nine noded element is used. It had been anticipated that these would increase because of the greater number of nodes to be treated and therefore the greater number of equations to be solved. This increase in the number of equations is a direct consequence of the decision to use the same meshes and number of elements for the nine noded element tests as were used for the eight noded element tests. If, on the other hand, it had been decided to keep the number of nodes constant in the various sets of tests, then firstly, new meshes would have had to be set up for the nine noded element, secondly the number of elements would have been considerably less in these alternative meshes and thirdly, the element size distribution in them would have been

significantly different, introducing additional complications in the following computational accuracy comparison. Therefore it was decided to use the same meshes with the same number of elements and to let the number of nodes increase accordingly. However, in order to compare more fairly the computational efficiency of each element, and in order to overcome the problem of the variable number of nodes, Table 5.8 is set up. In this table are listed the execution times per iteration per node and from these values it can be seen that both the eight and nine noded elements result in almost identical values for each of the meshes used. From this and the points noted above, the only conclusion that can be drawn is that the Serendipity and Lagrangian elements both appear to be equally efficient in terms of computer requirements when used to model two-dimensional viscous flows. Nevertheless, if a choice must be made, the Serendipity element must be selected, simply because of the slightly shorter and less complex program required and therefore the smaller amount of computer storage needed to hold and execute it. This saving in storage however is still only marginal.

The computational accuracy of the eight noded Serendipity and the nine noded Lagrangian elements can be compared by examining the velocity component and pressure variations along the same cross-sections that were used in the formulation comparison. These are the variations of the x component of velocity along y=0.1 and the centreline y=0.5 and the variation of pressure along y=0.5 for the entrance flow problem, and the variations of the x component of velocity and the pressure both along the centreline x=0.5 for the cavity flow problem. The plots of these variations are given in Figures 5.20 to 5.24 (a) to (e) respectively. In each graph a logarithmic x or y axis has again been used for the same reasons described earlier. Also, in each graph the four solutions obtained with the two meshes and the two element types are plotted for each Reynolds number, on the same set of axes. In this

Mesh	8NE	9NE
ENFLM1	0.21	0.22
ENFLM2	0.20	0.21
CAVFLM1	0.33	0.30
CAVFLM2	0.31	0.29

Table 5.8 Average execution time per iteration per node in central processor seconds.

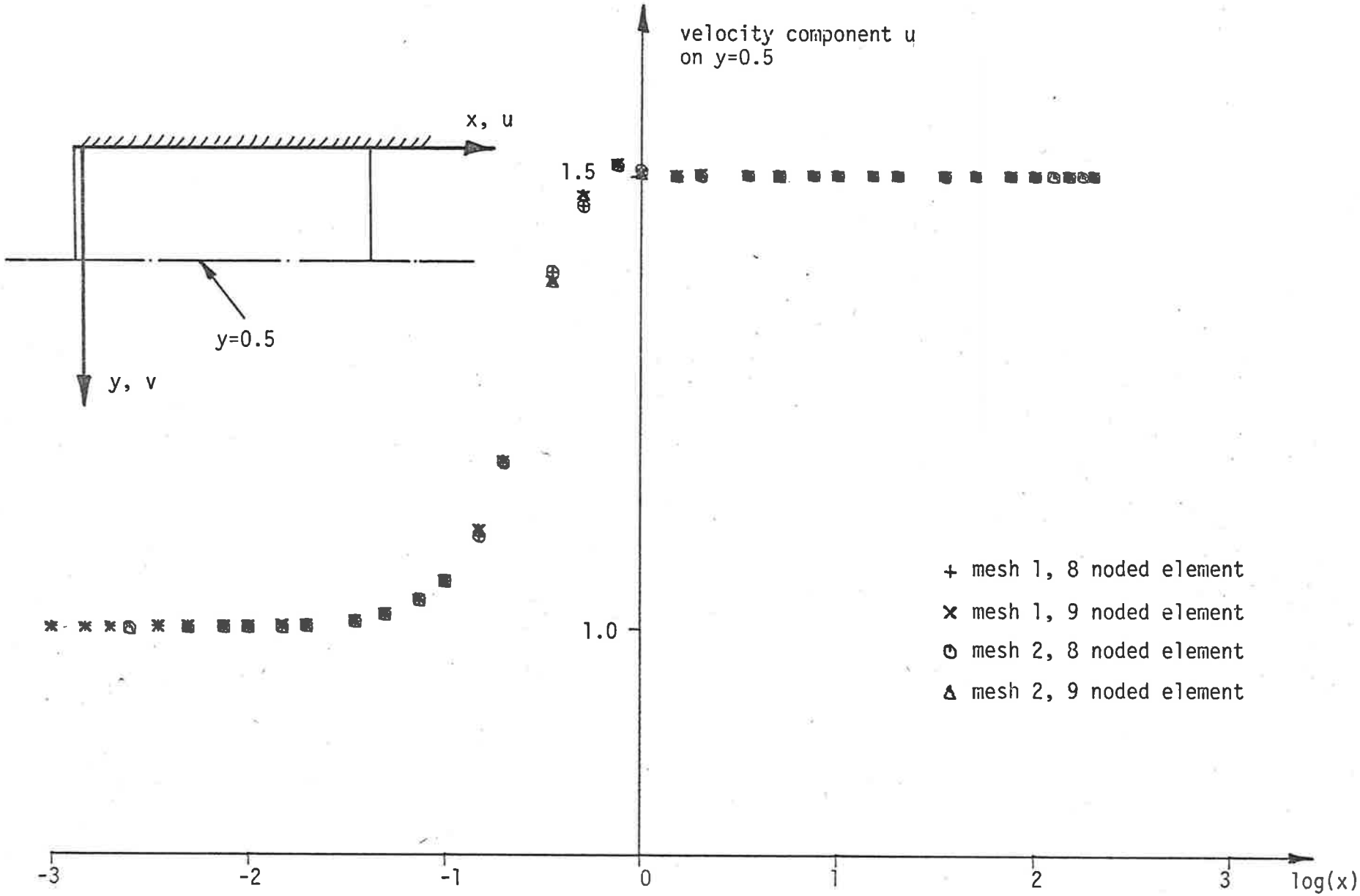

Figure 5.20(a) Element Comparison, Entrance Flow, Variation of u on y=0.5 for Re = 1.

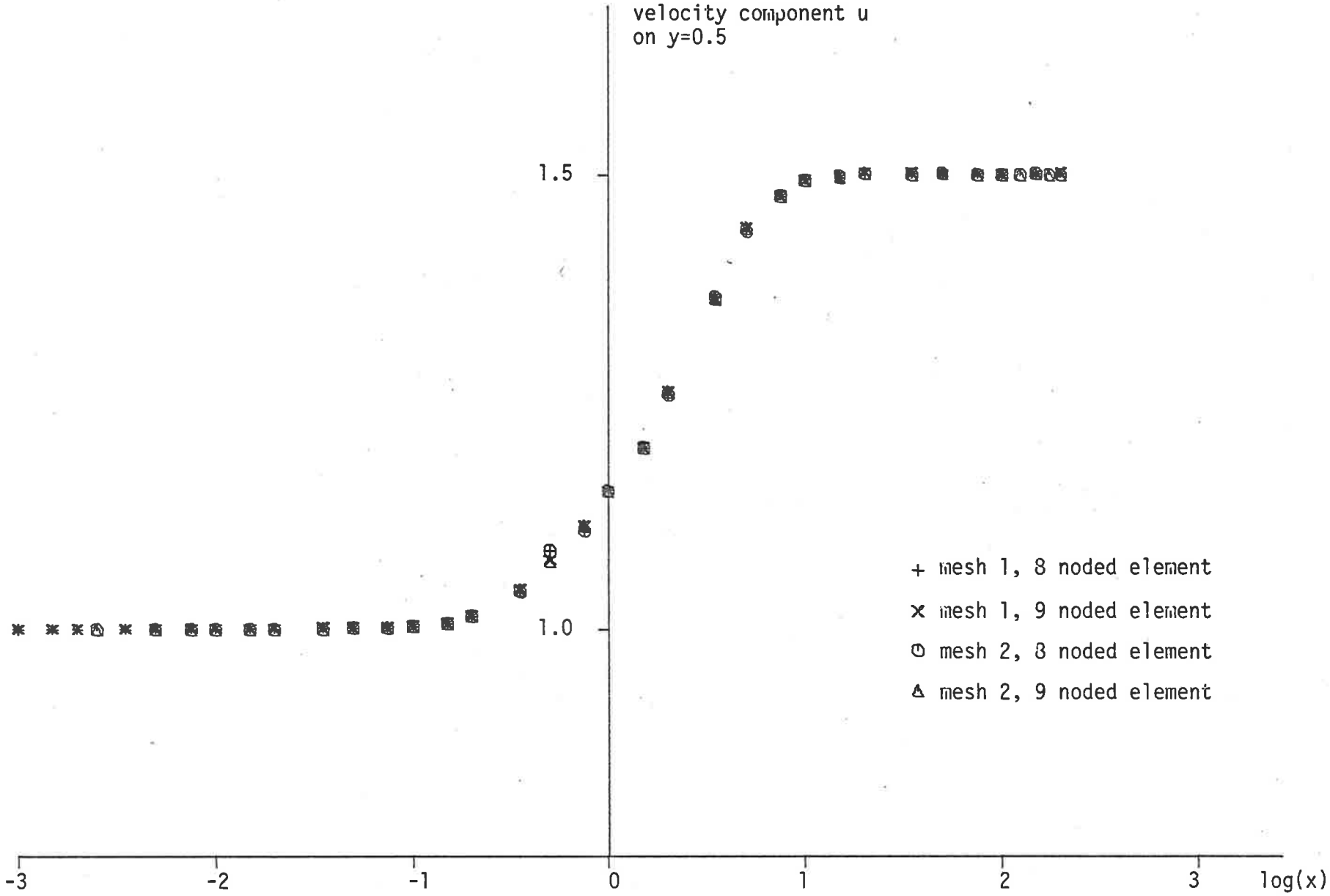

Figure 5.20(b) Variation of u for Re = 200.

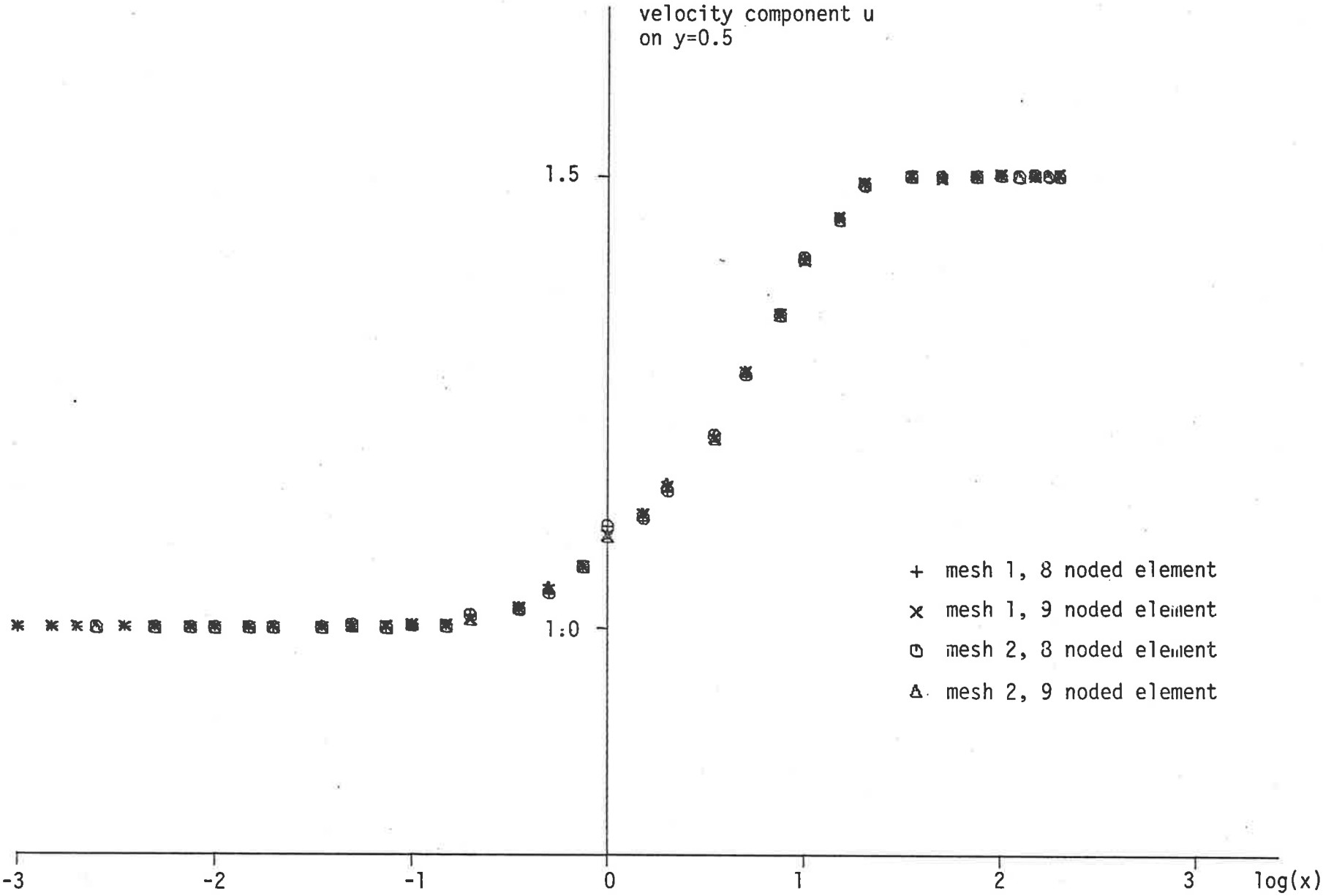

Figure 5.20(c) Variation of u for Re = 500.

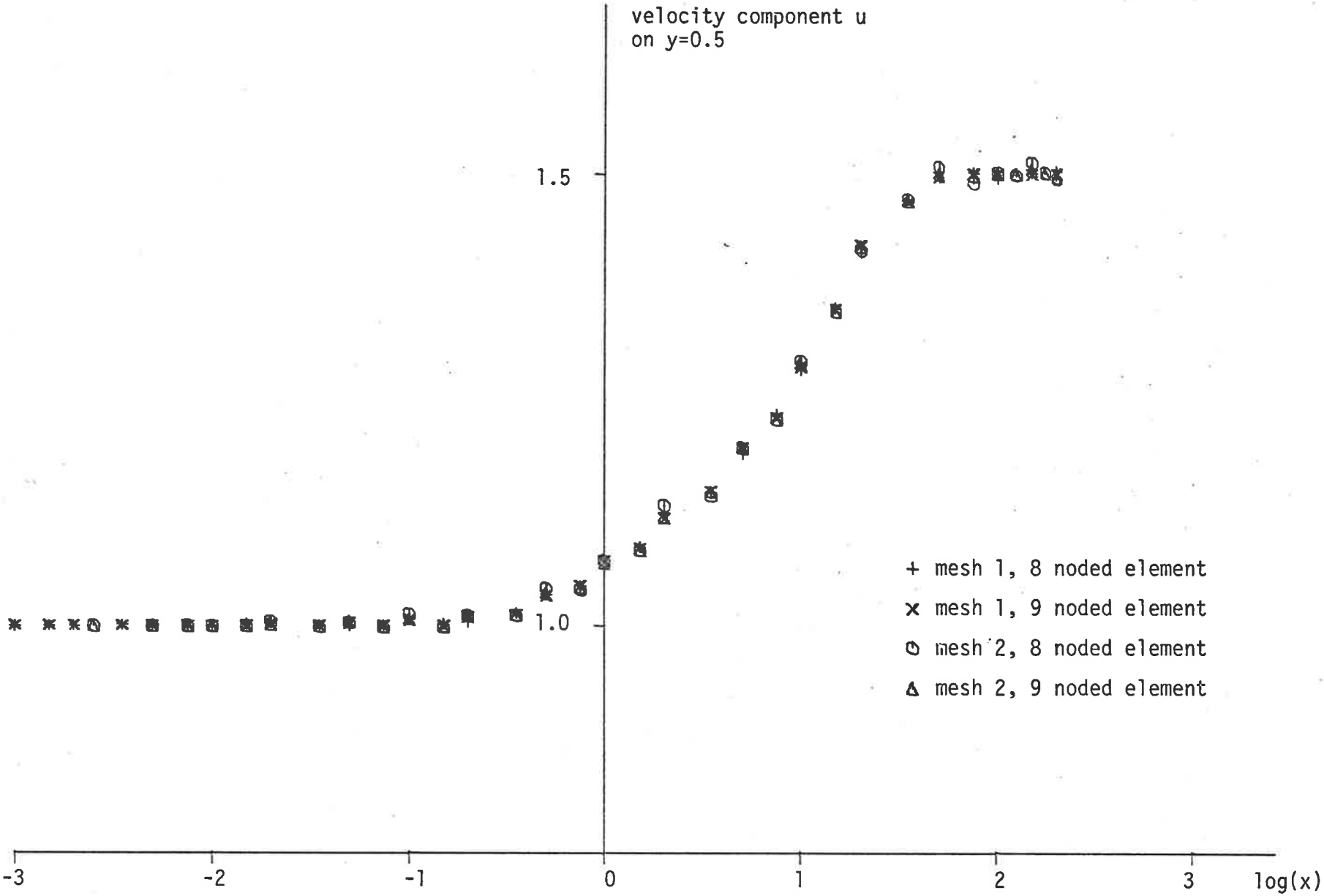

Figure 5.20(d) Variation of u for Re = 1000.

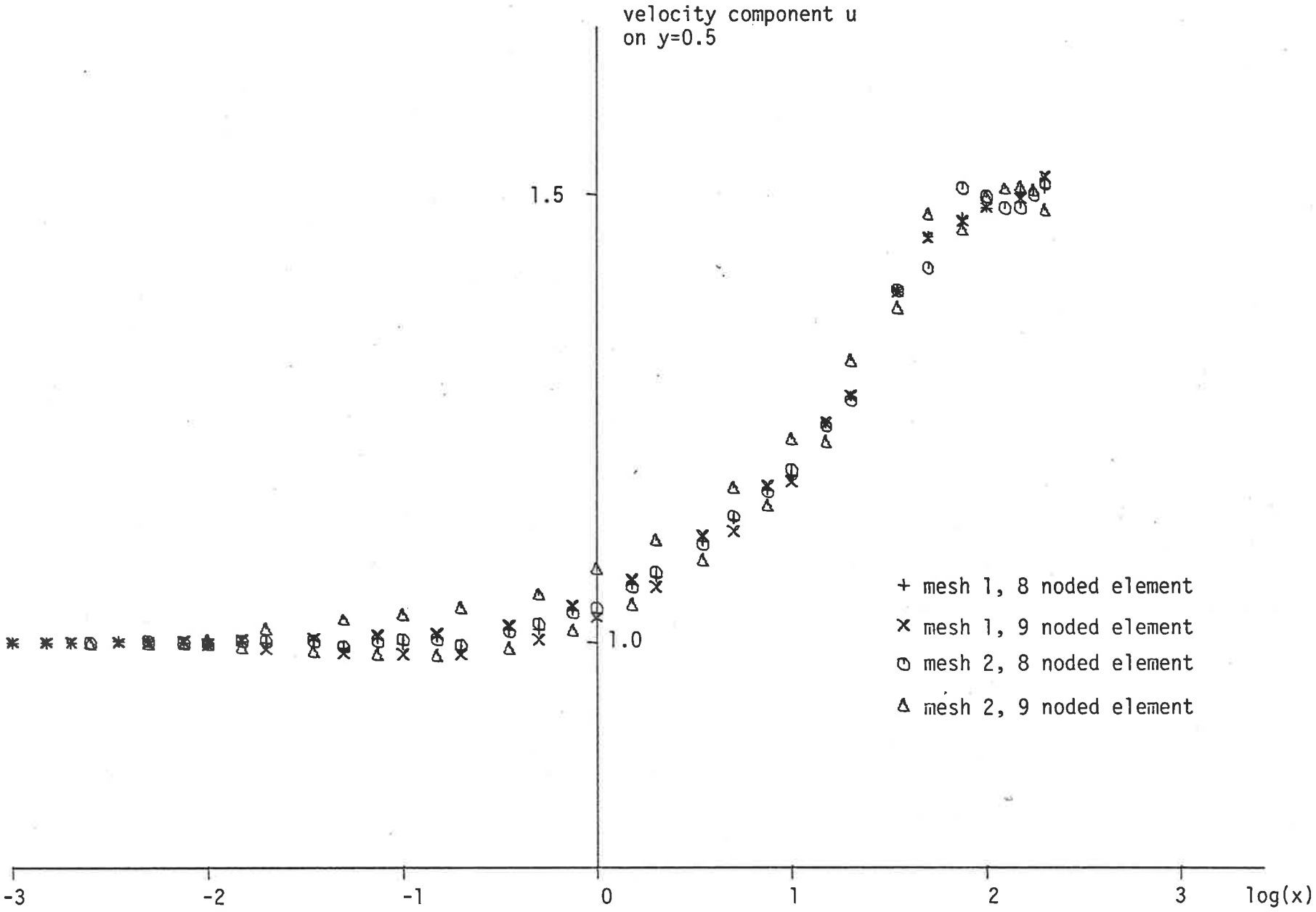

Figure 5.20(e) Variation of u for Re = 2000.

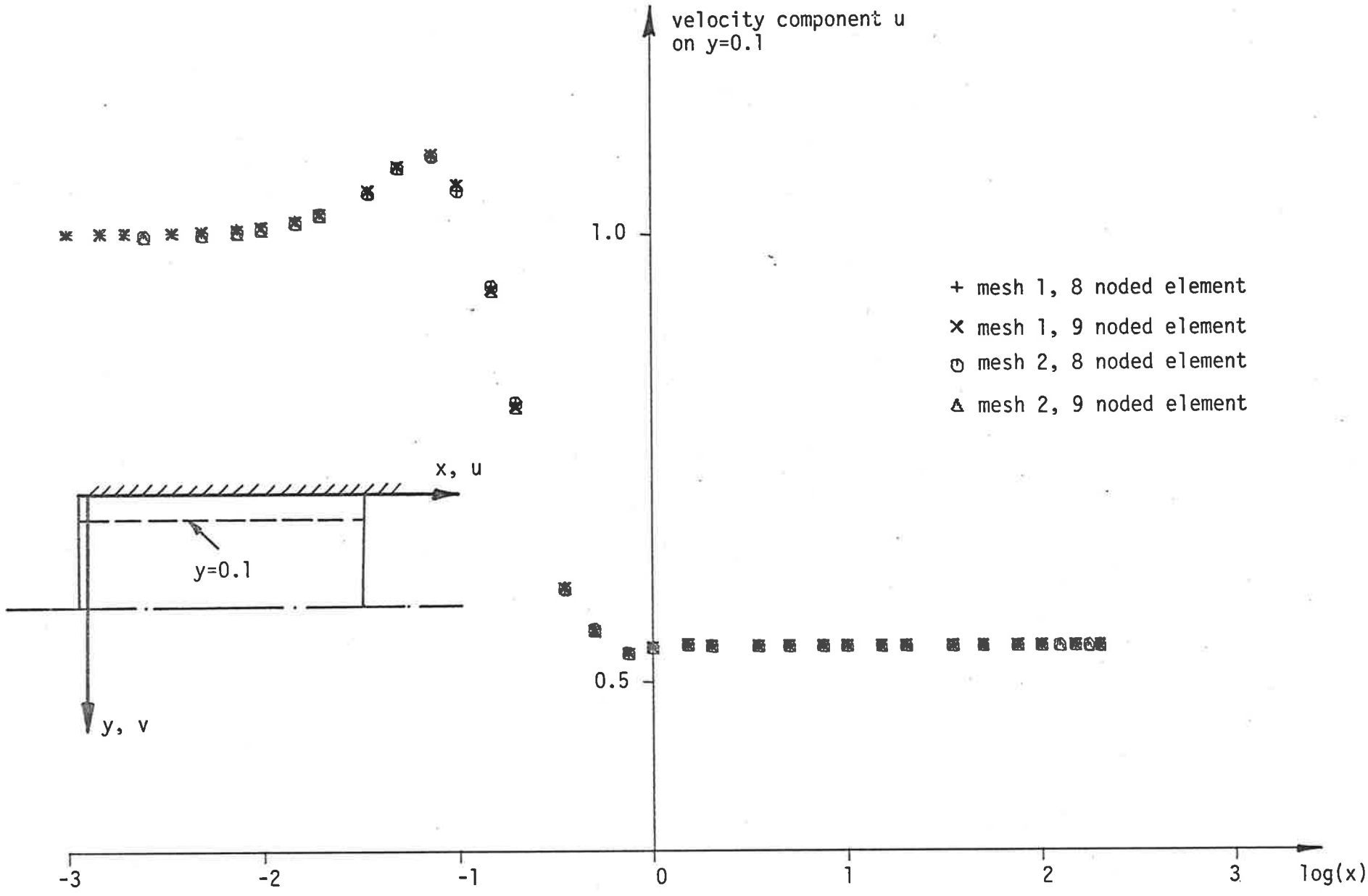

Figure 5.21(a) Element Comparison, Entrance Flow, Variation of u on y=0.1 for Re = 1.

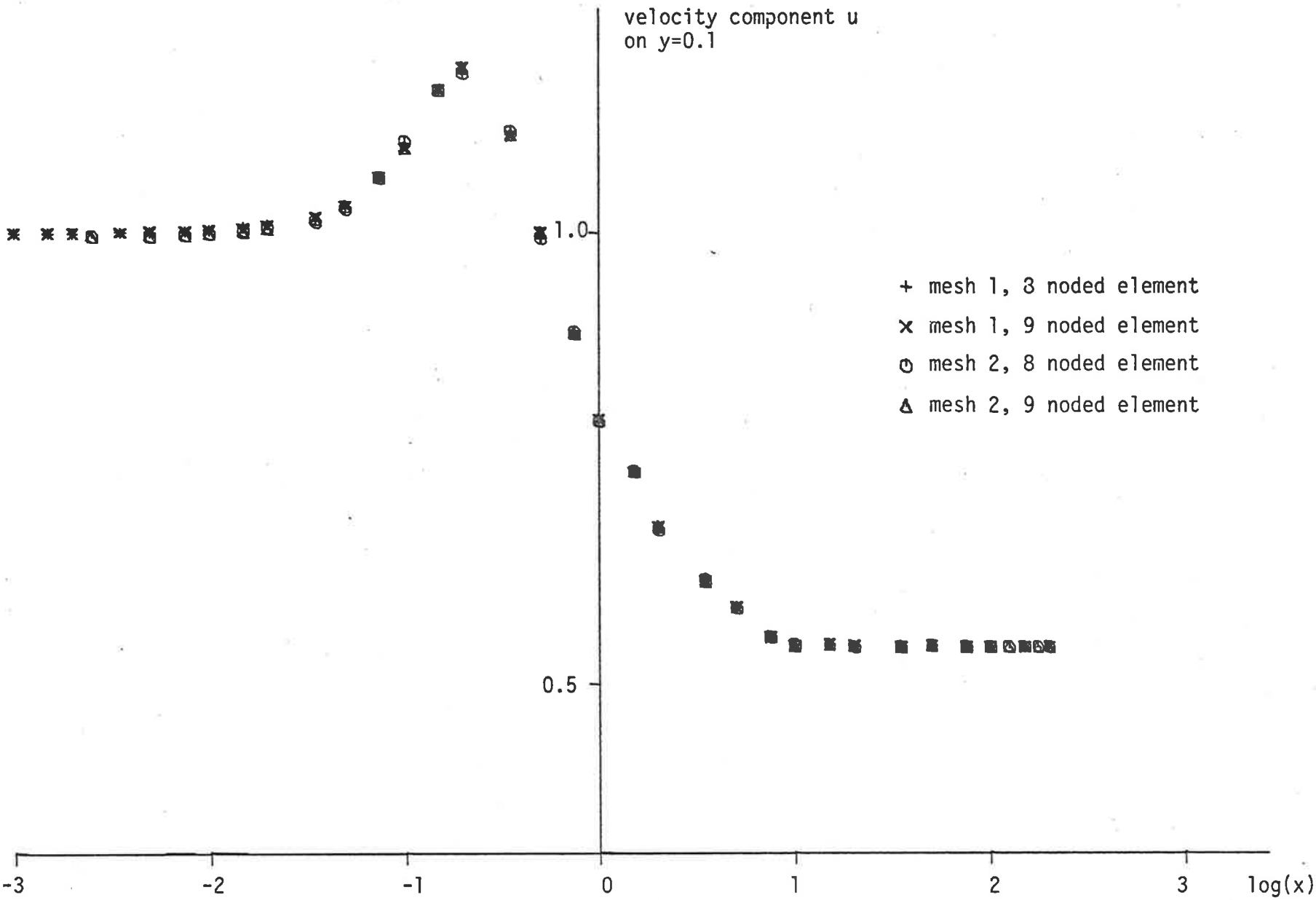

Figure 5.21(b) Variation of u for Re = 200.

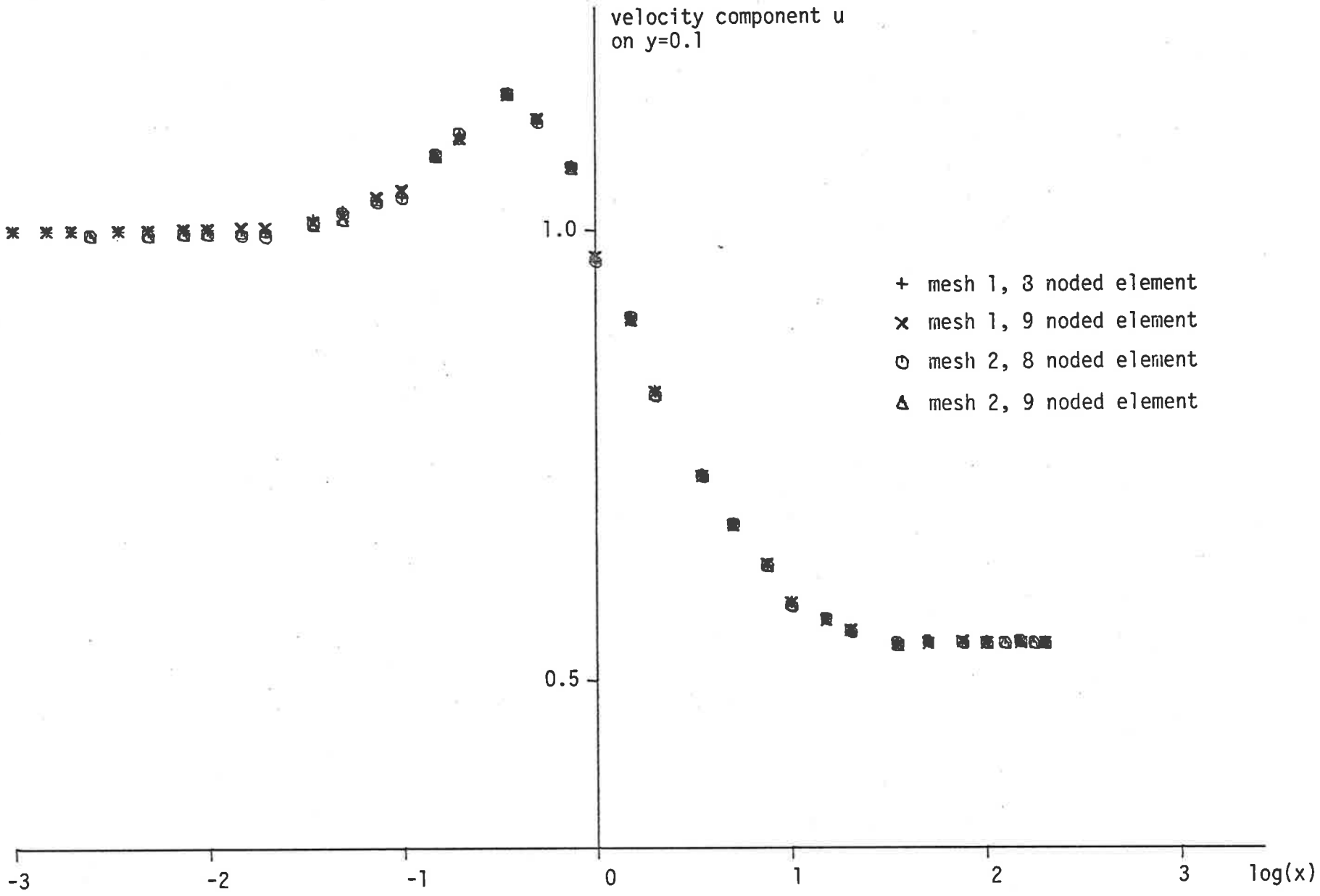

Figure 5.21(c) Variation of u for Re = 500.

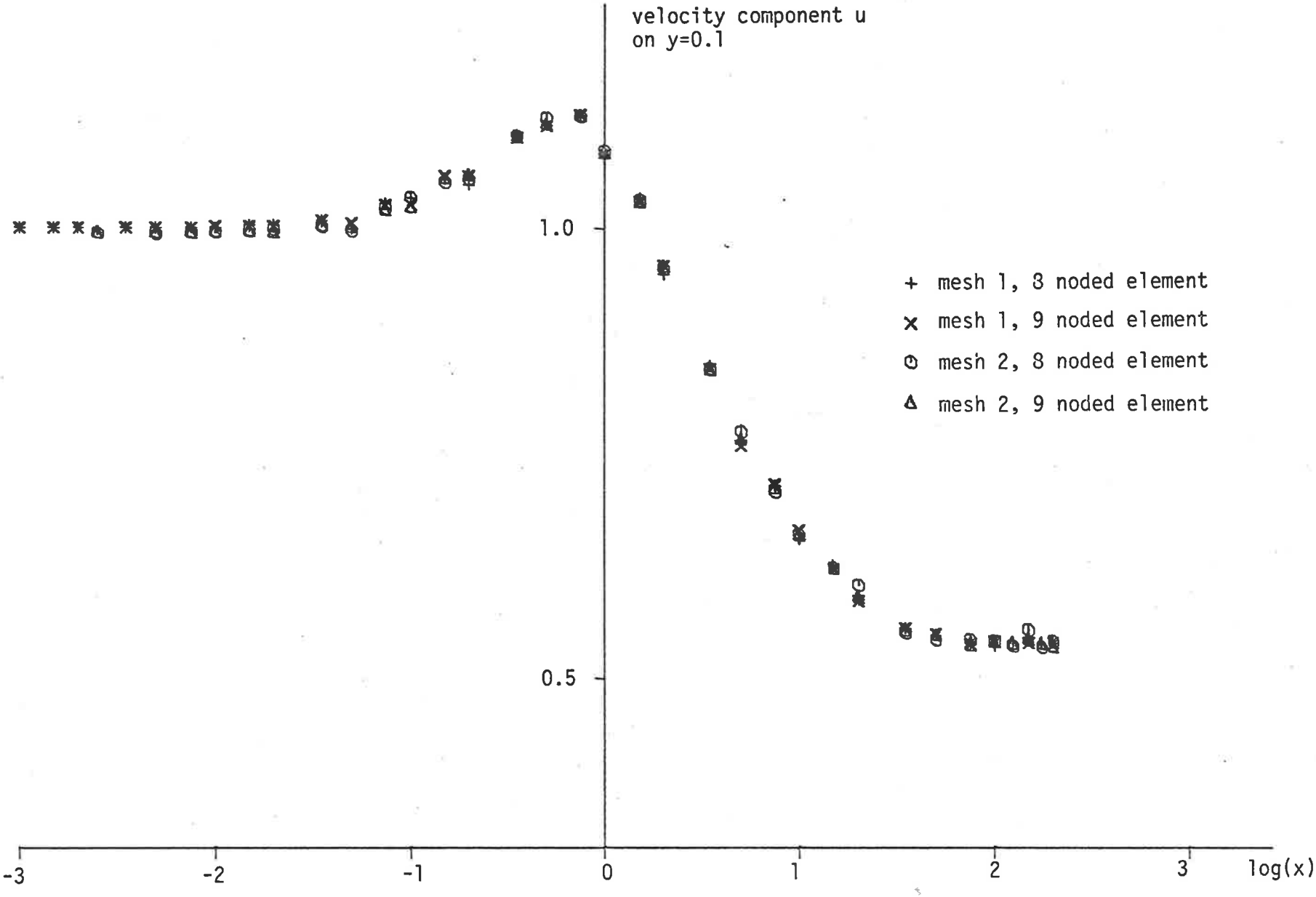

Figure 5.21(d) Variation of u for Re = 1000.

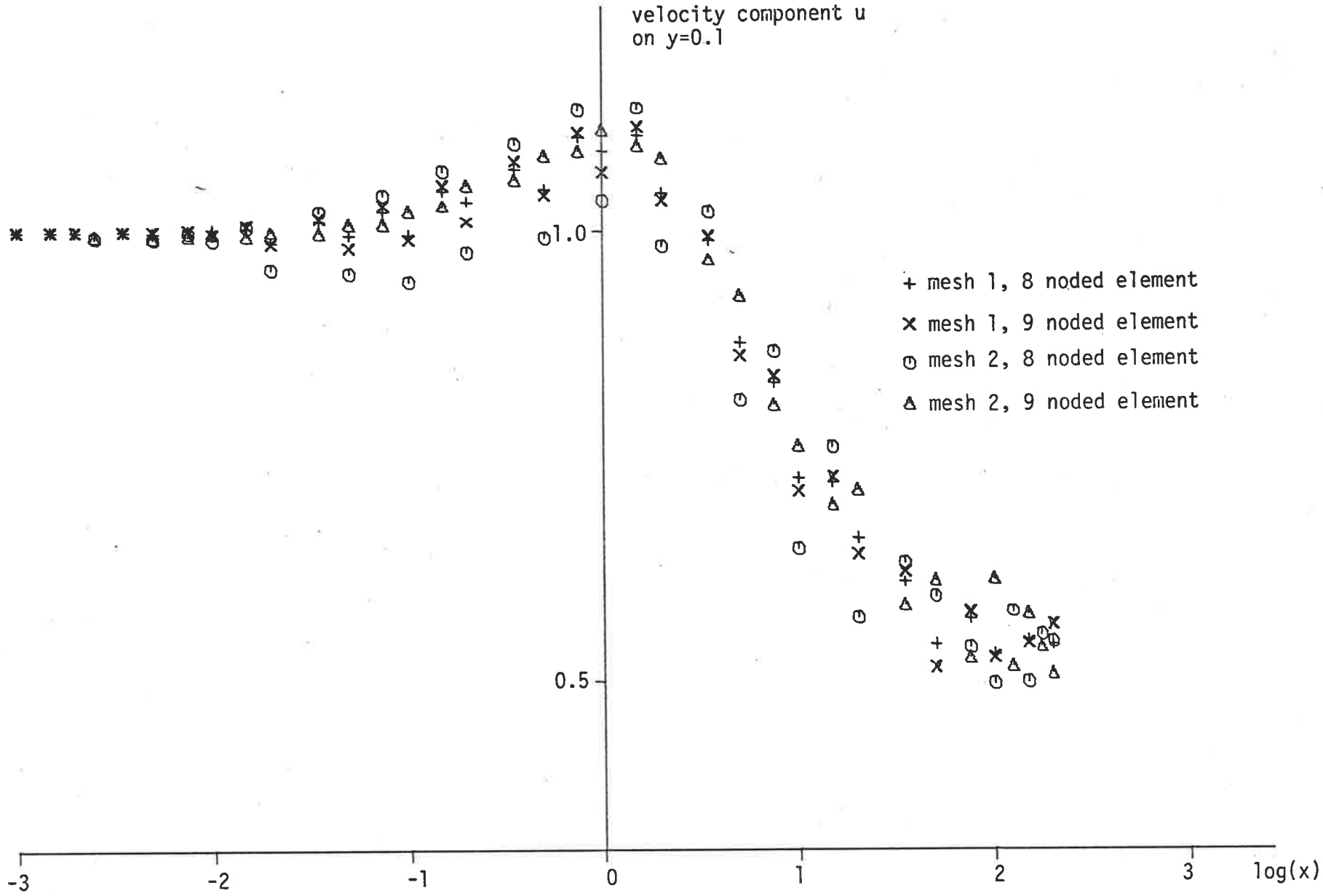

Figure 5.21(e) Variation of u for Re = 2000.

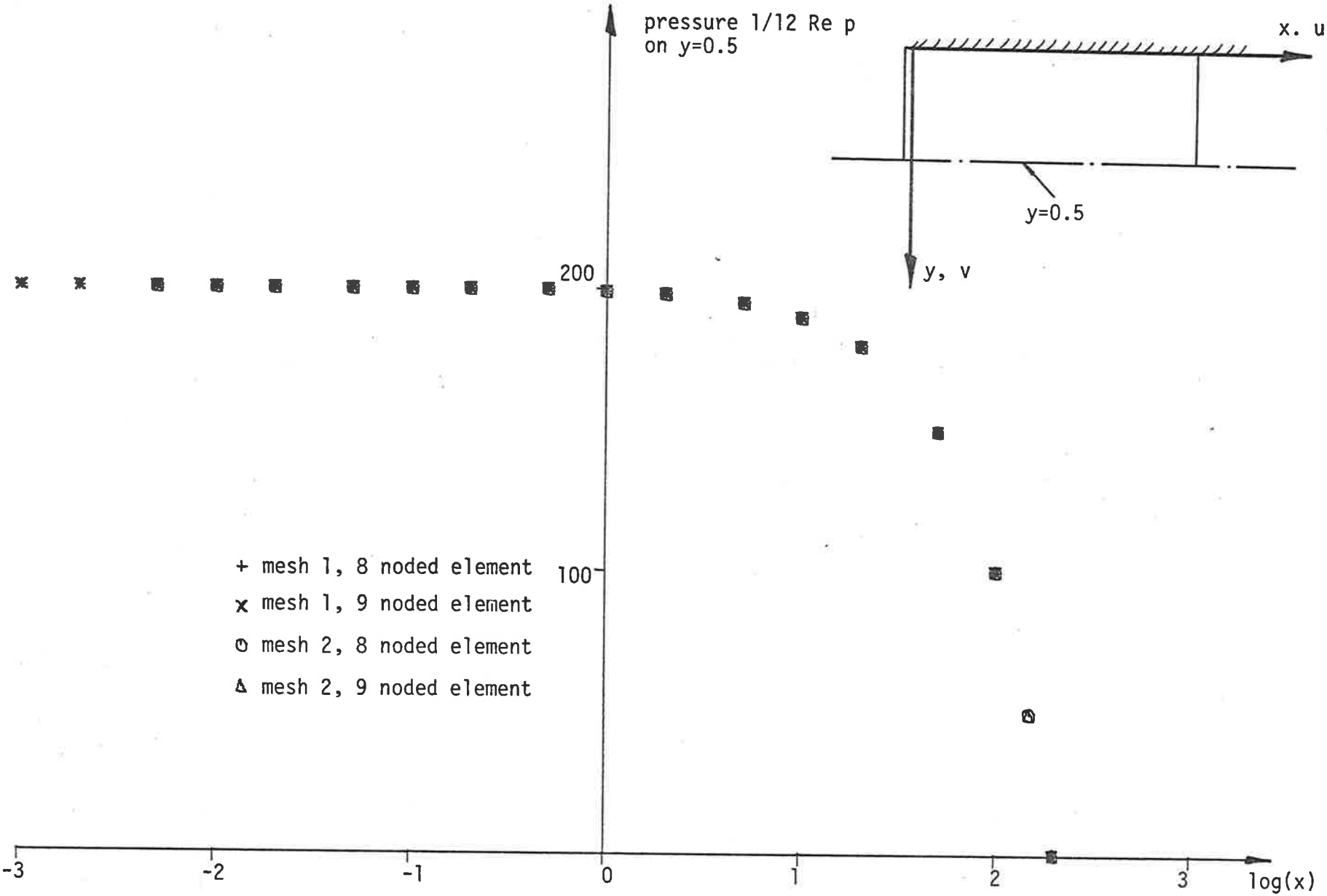

Figure 5.22(a) Element Comparison, Entrance Flow, Variation of p on y=0.5 for Re = 1.

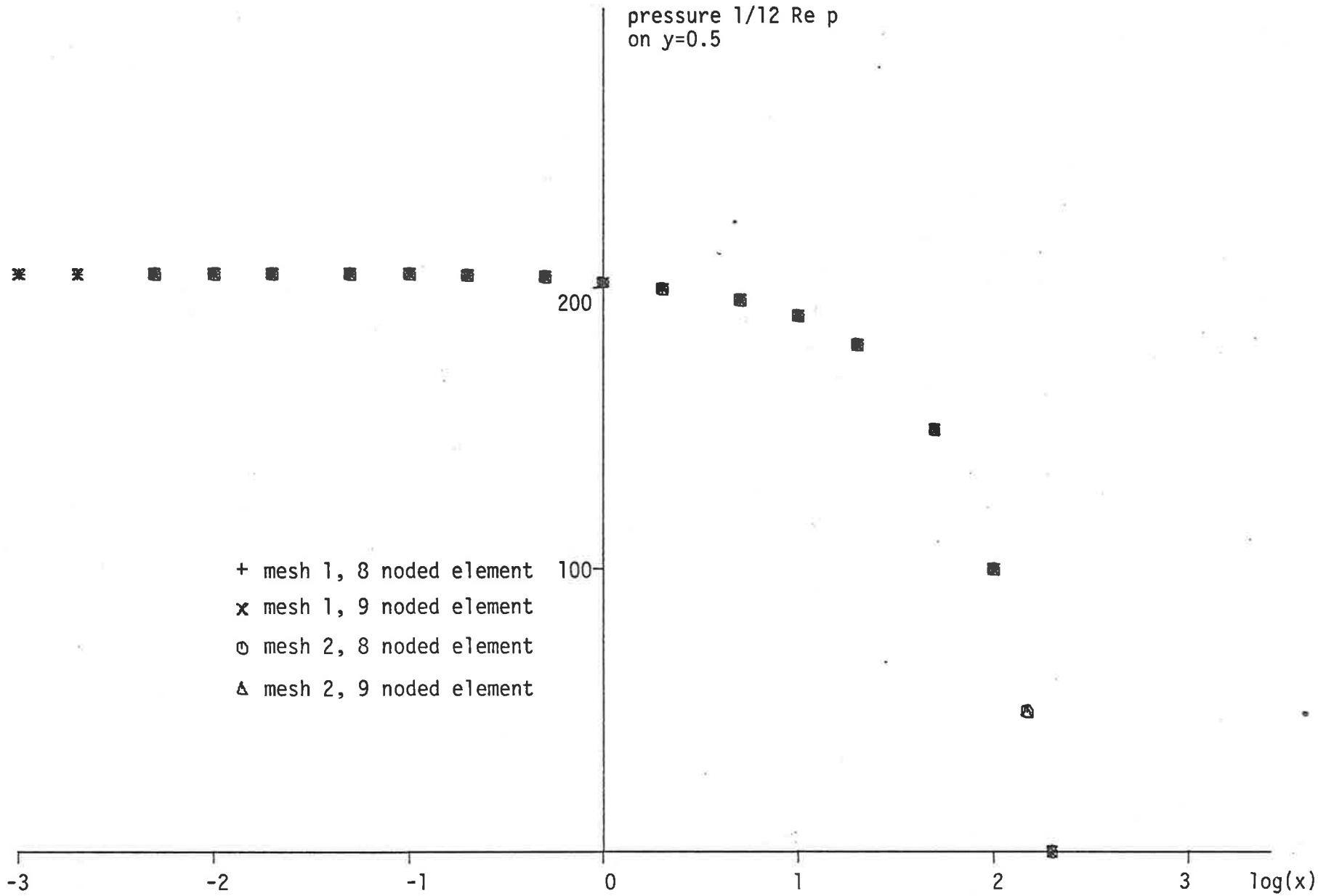

Figure 5.22(b) Variation of p for Re = 200.

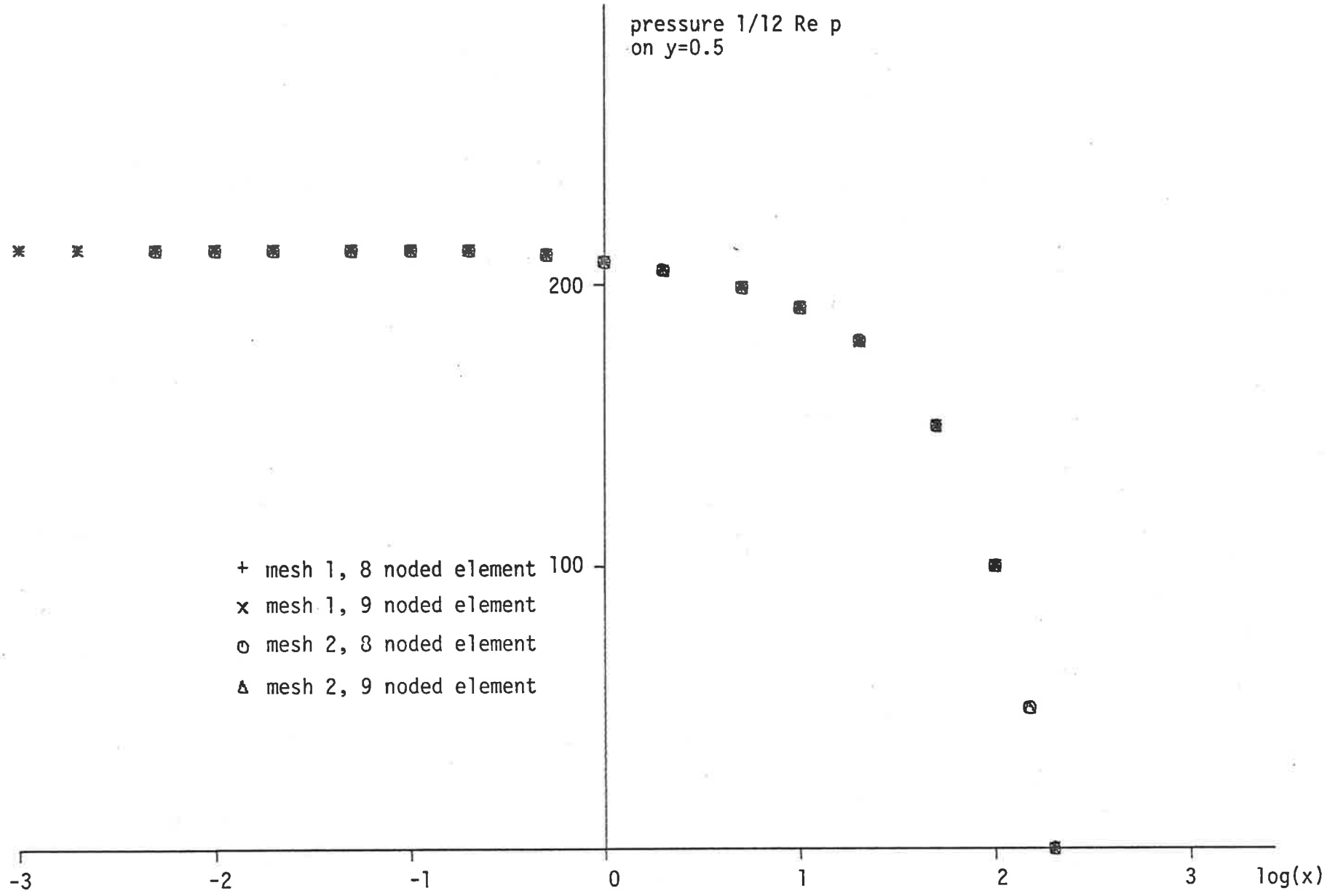

Figure 5.22(c) Variation of p for Re = 500.

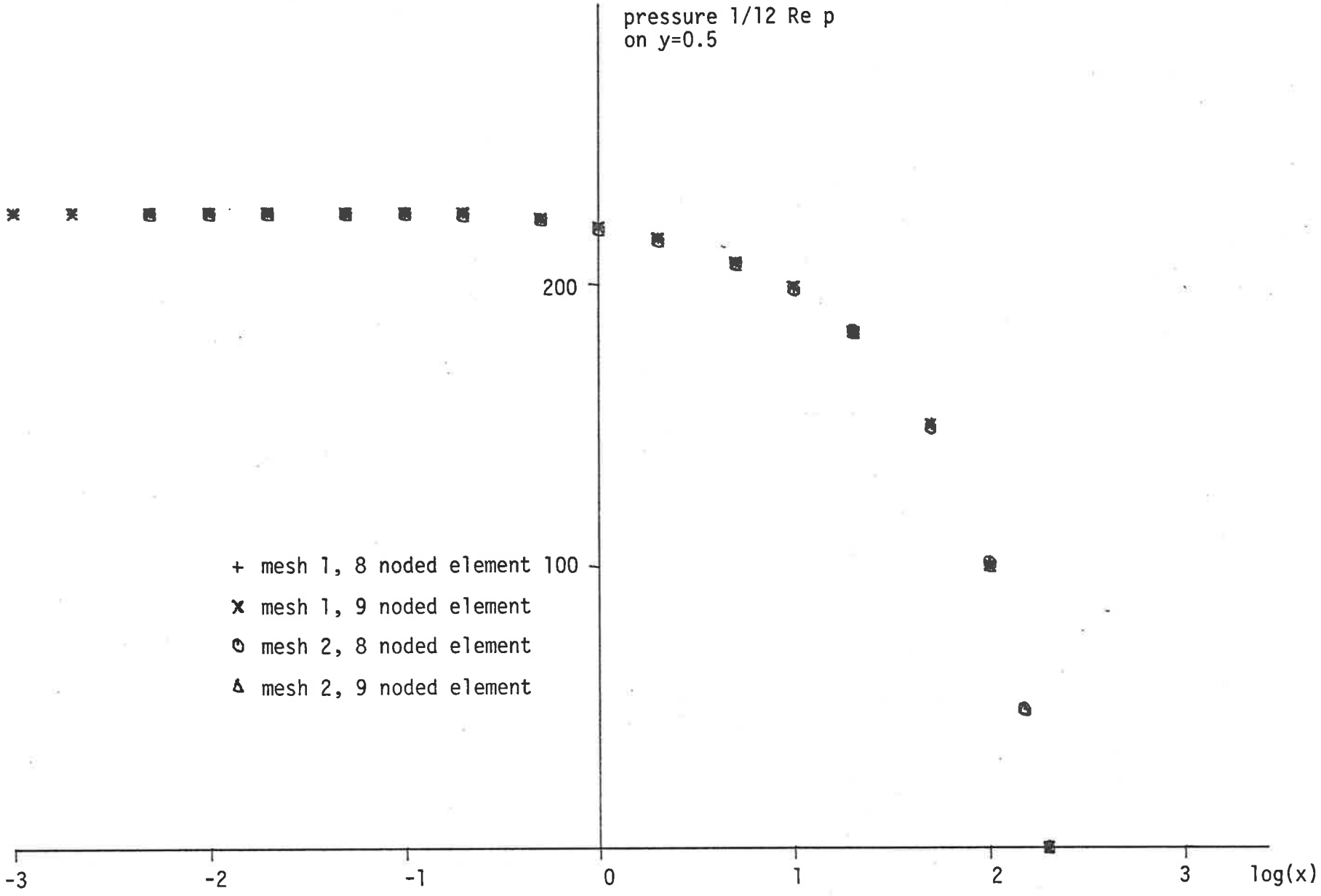

Figure 5.22(d) Variation of p for Re = 1000.

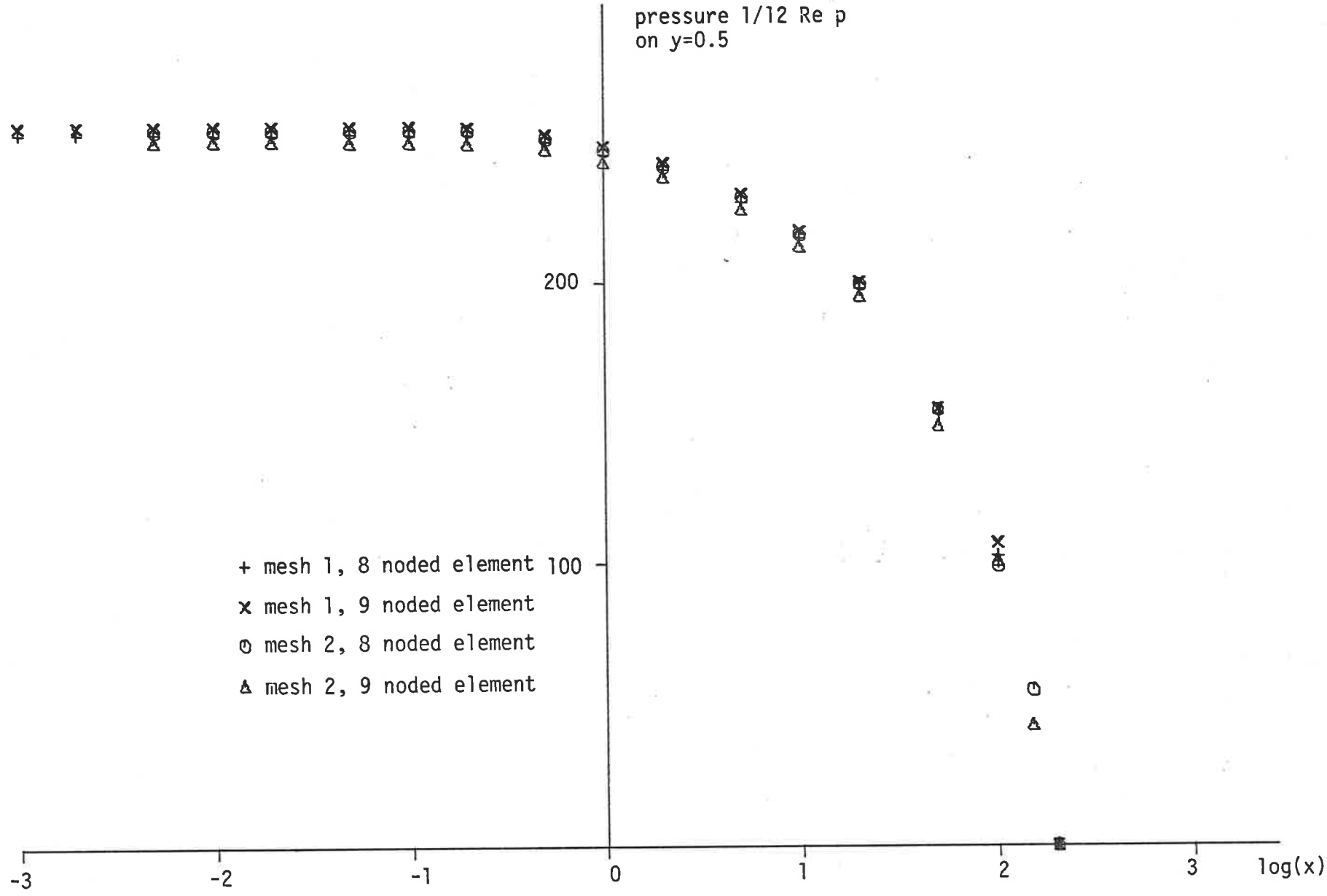

Figure 5.22(e) Variation of p for Re = 2000.

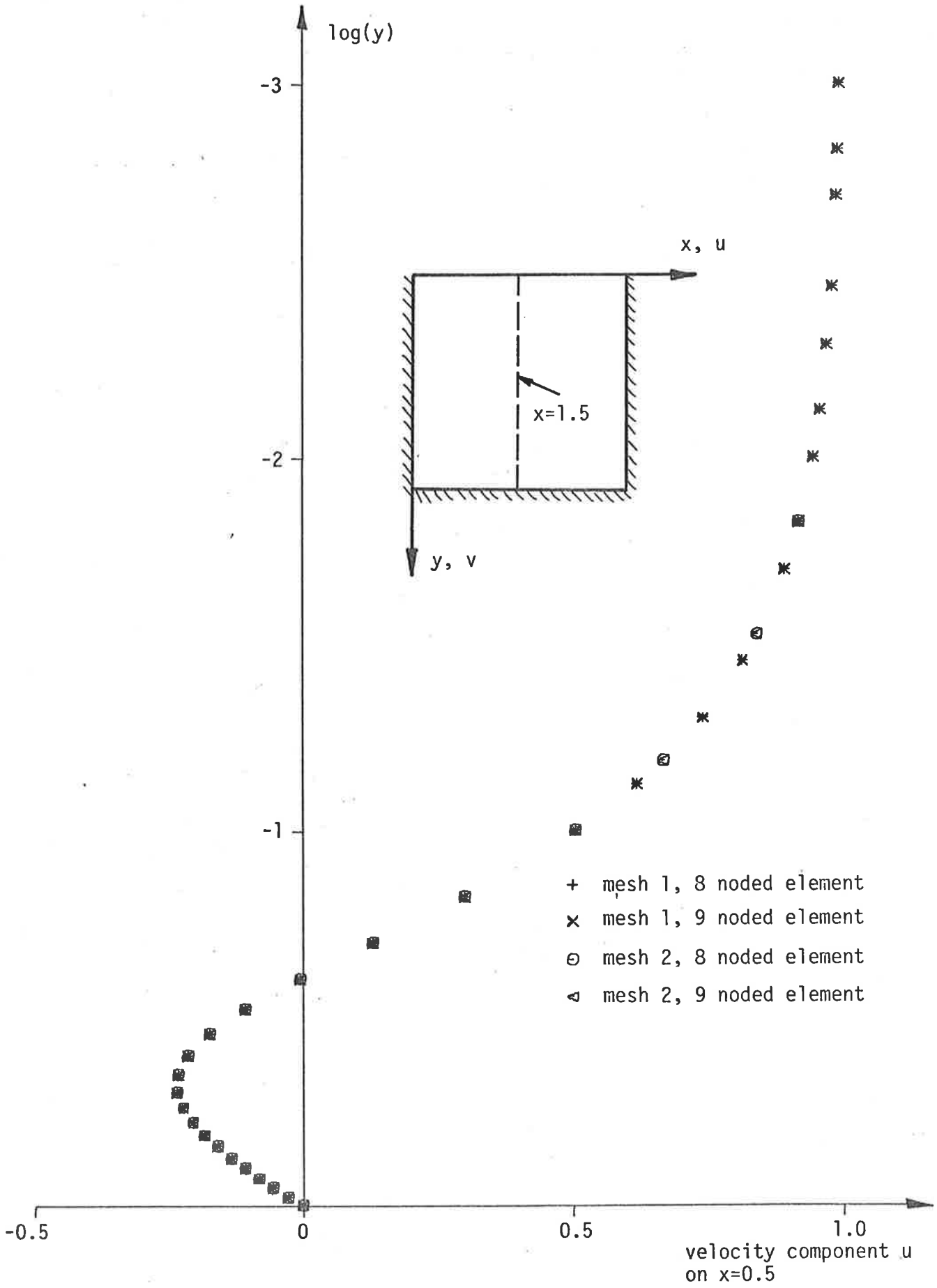

Figure 5.23(a) Element Comparison, Cavity Flow, Variation of u on x=0.5 for Re = 1.

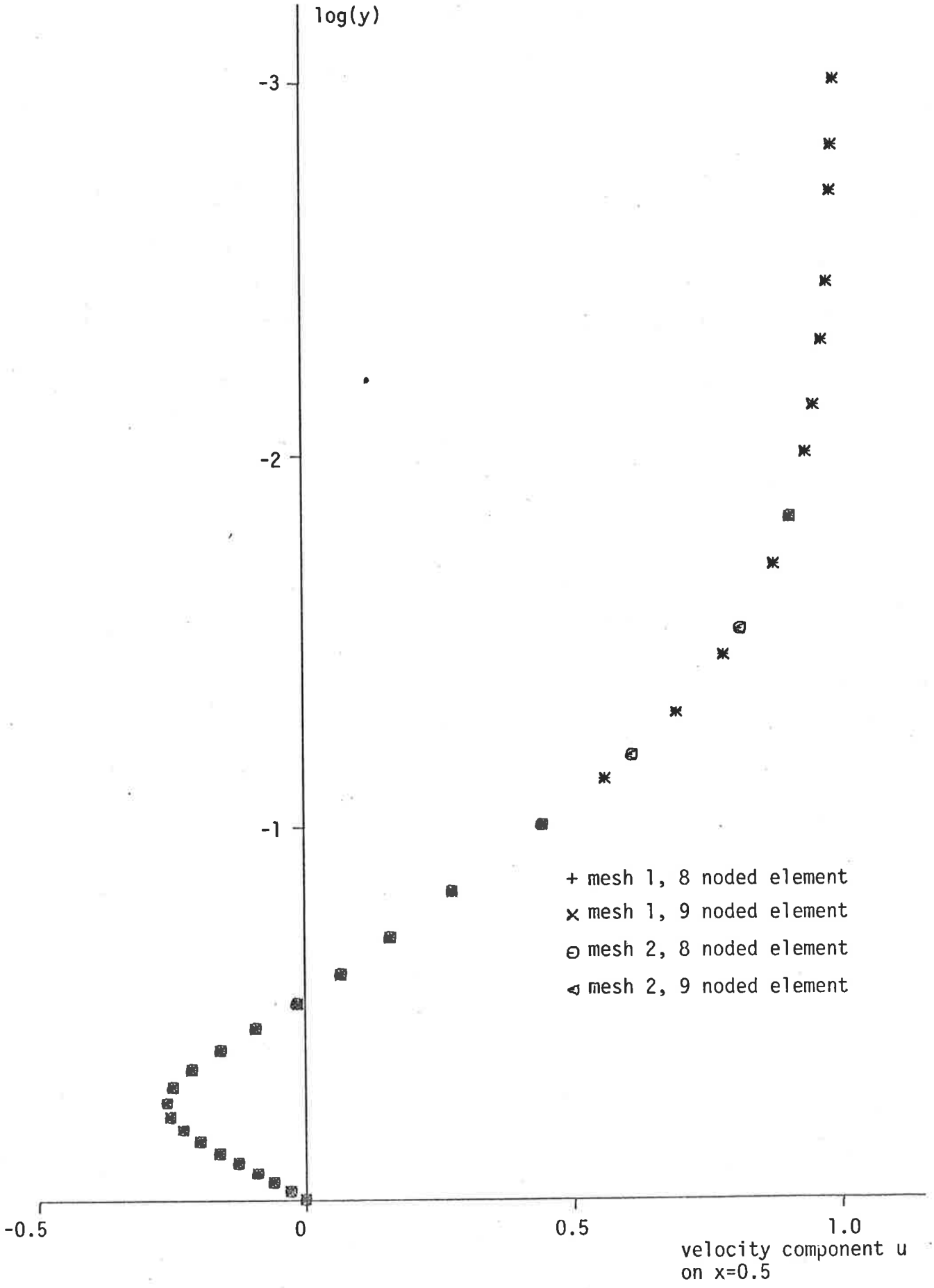

Figure 5.23(b) Variation of u for Re = 100.

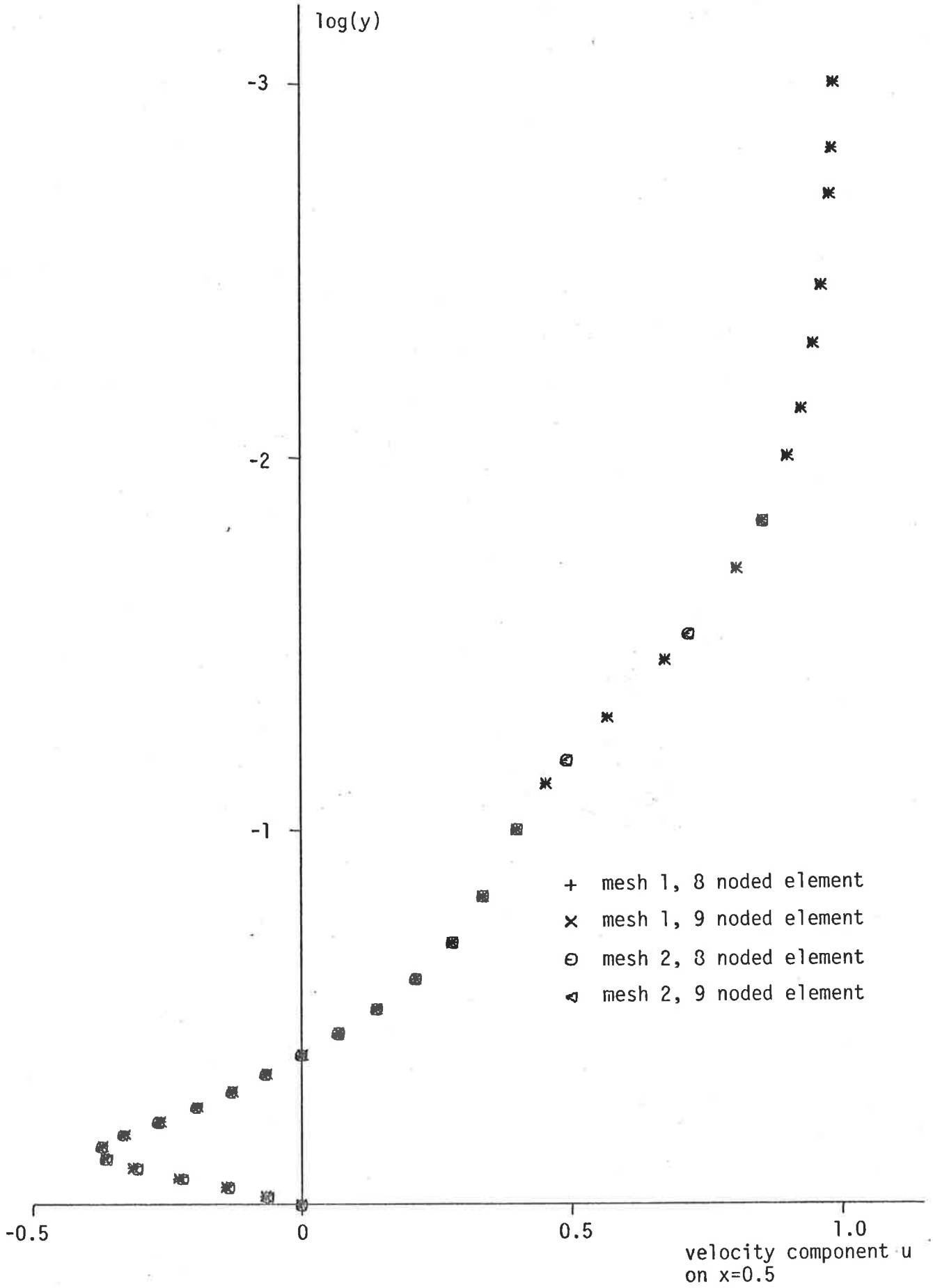

Figure 5.23(c) Variation of u for Re = 400.

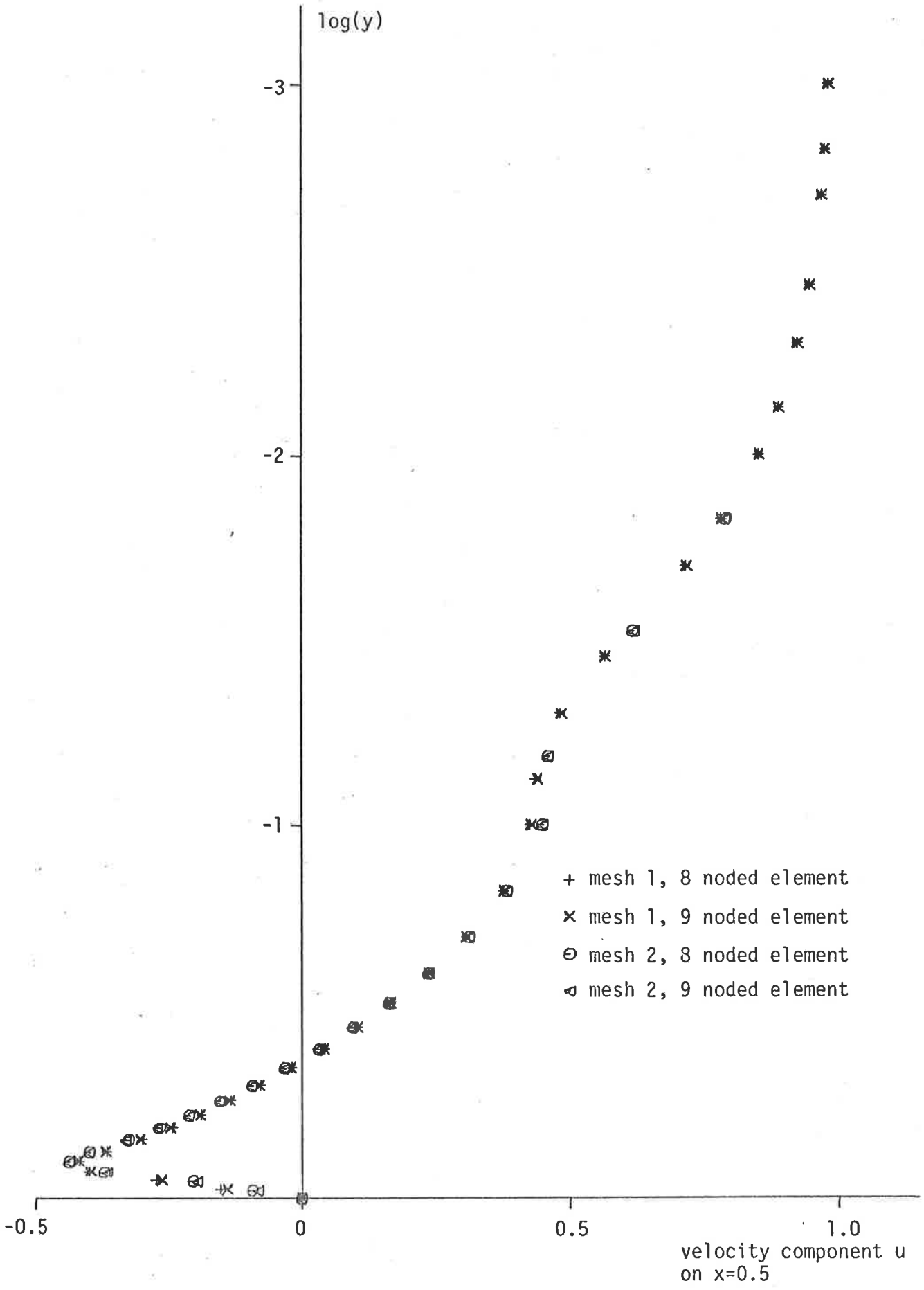

Figure 5.23(d) Variation of u for Re = 1000.

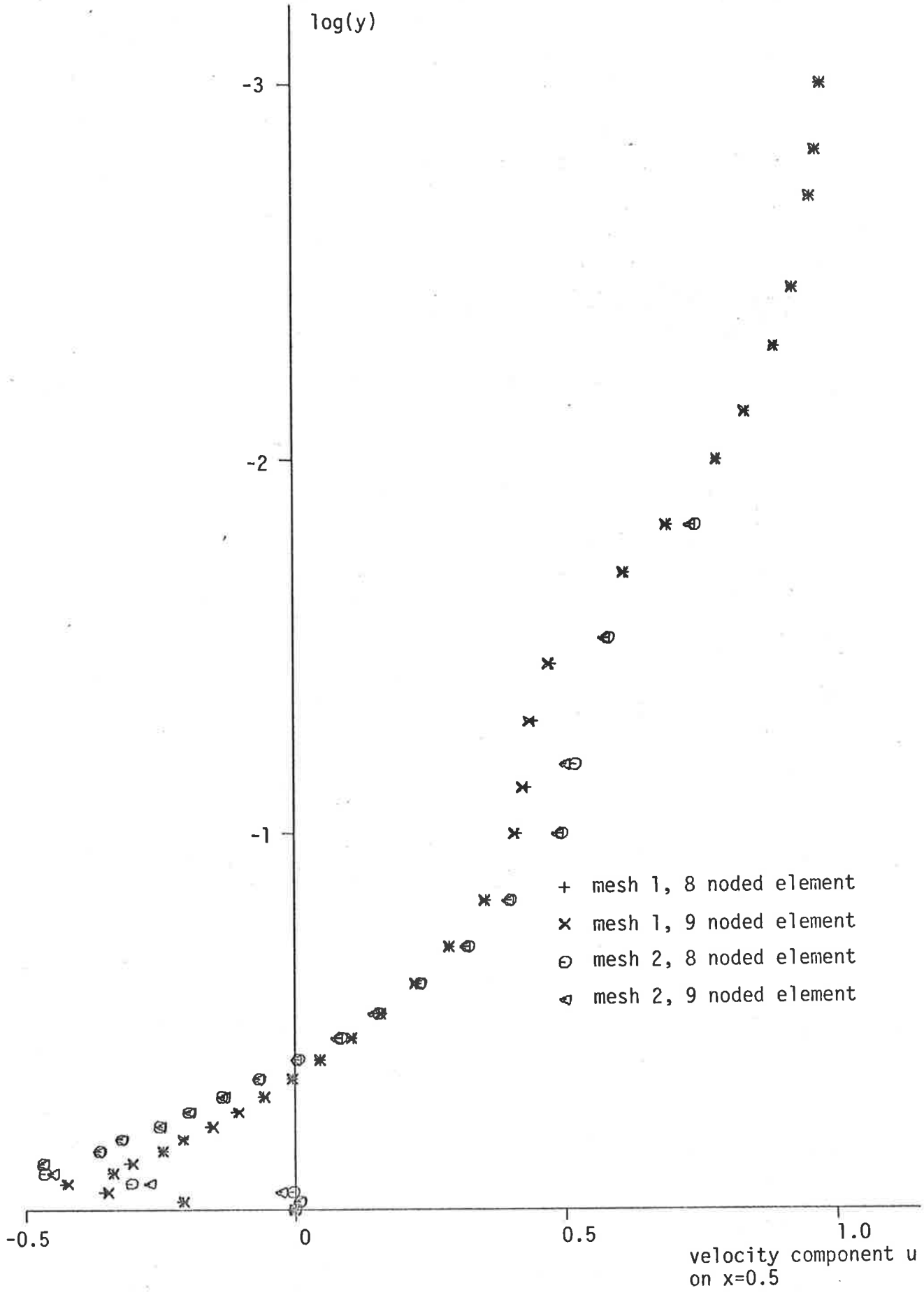

Figure 5.23(e) Variation of u for Re = 2000.

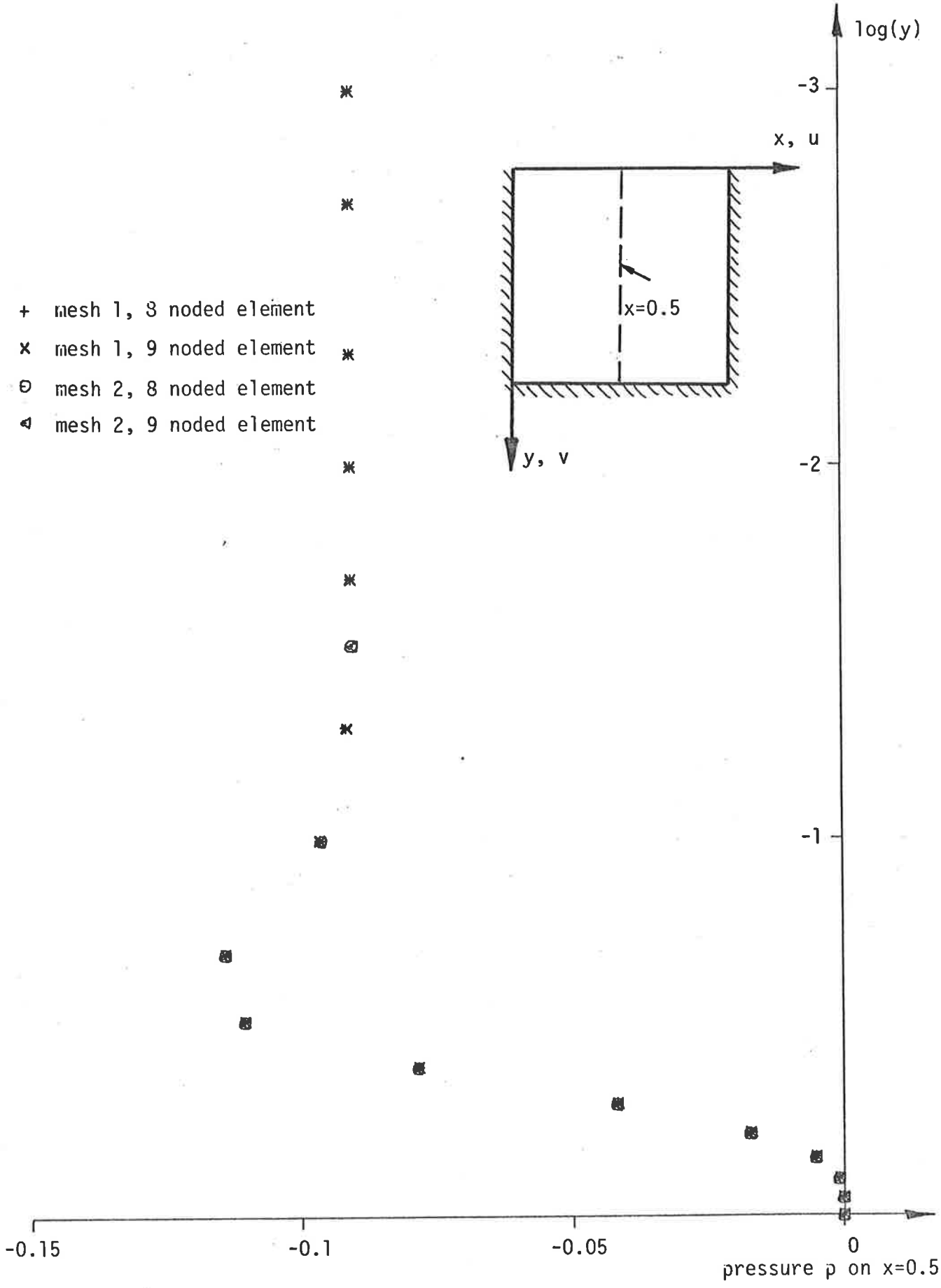

Figure 5.24(a) Element Comparison, Cavity Flow, Variation of p on x=0.5 for Re = 1.

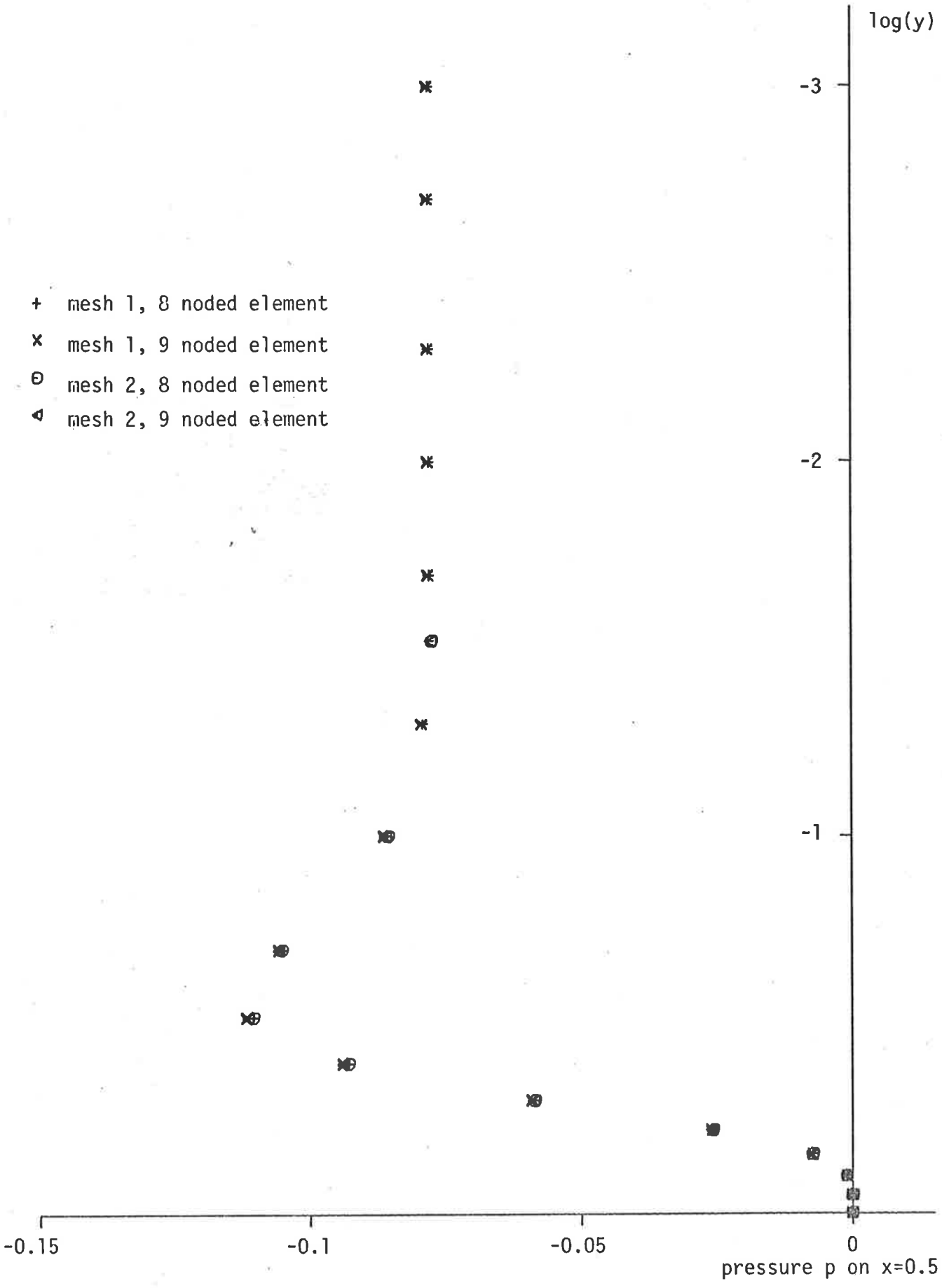

Figure 5.24(b) Variation of p for Re = 100.

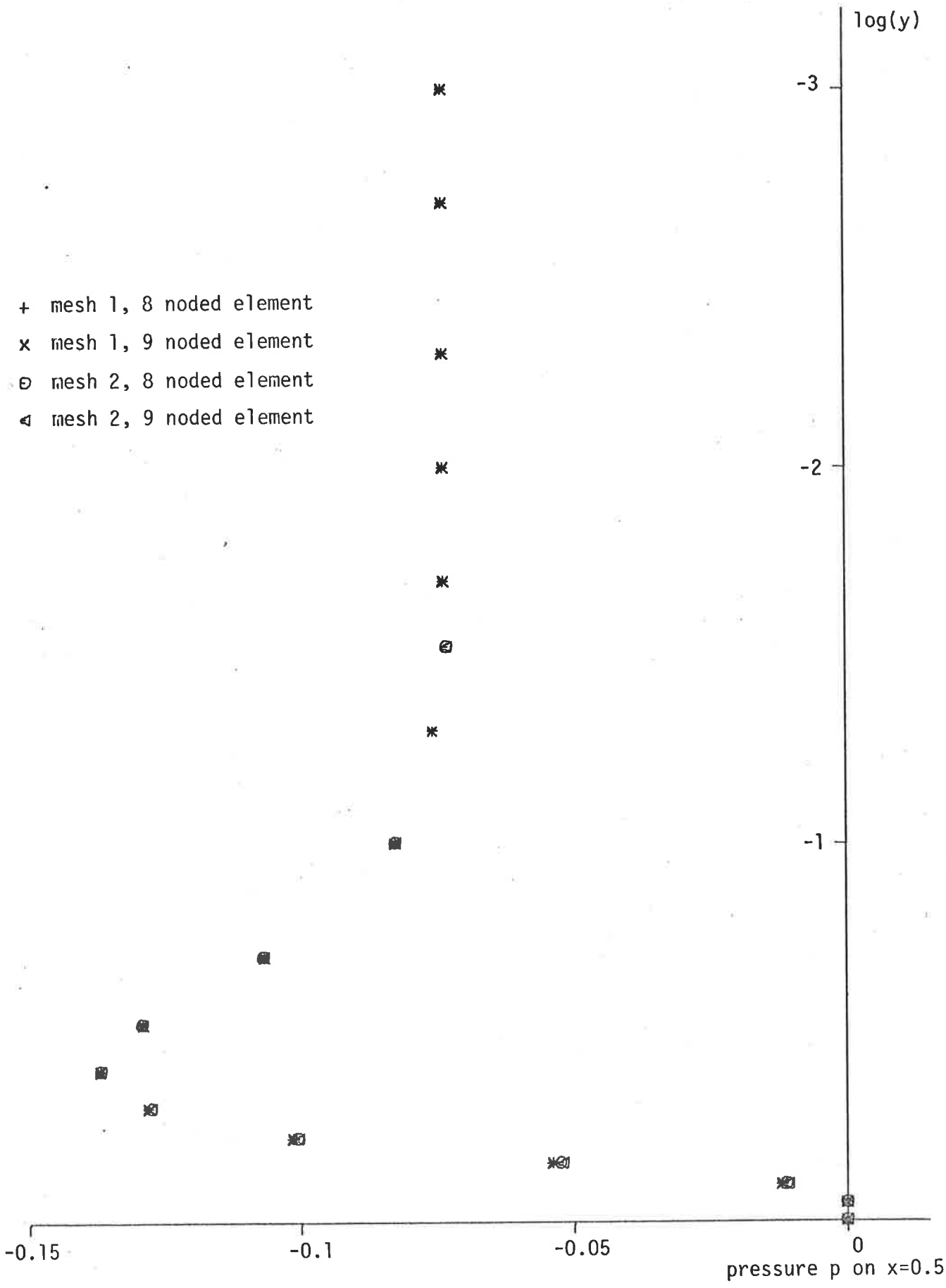

Figure 5.24(c) Variation of p for Re = 400.

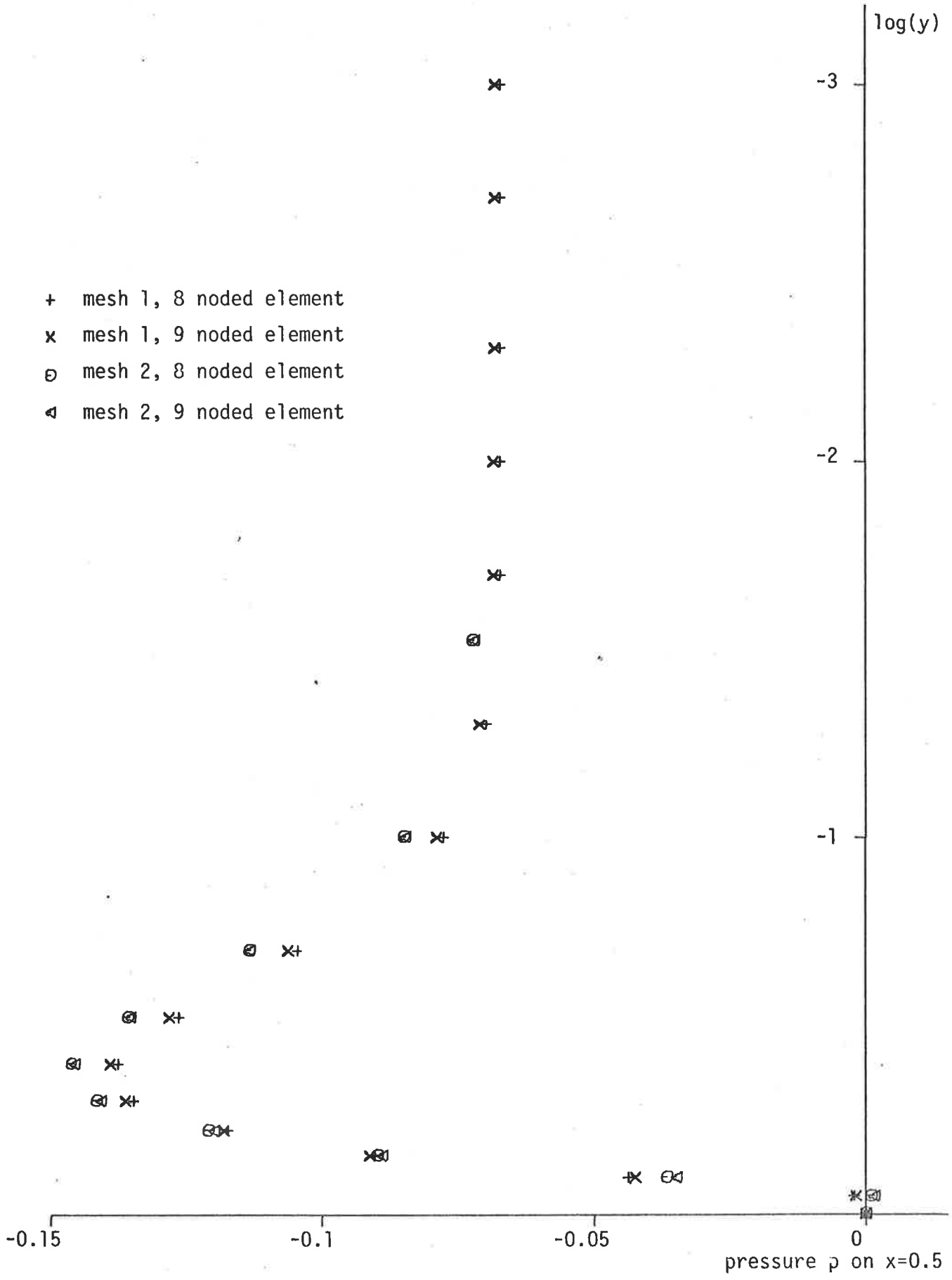

Figure 5.24(d) Variation of p for Re = 1000.

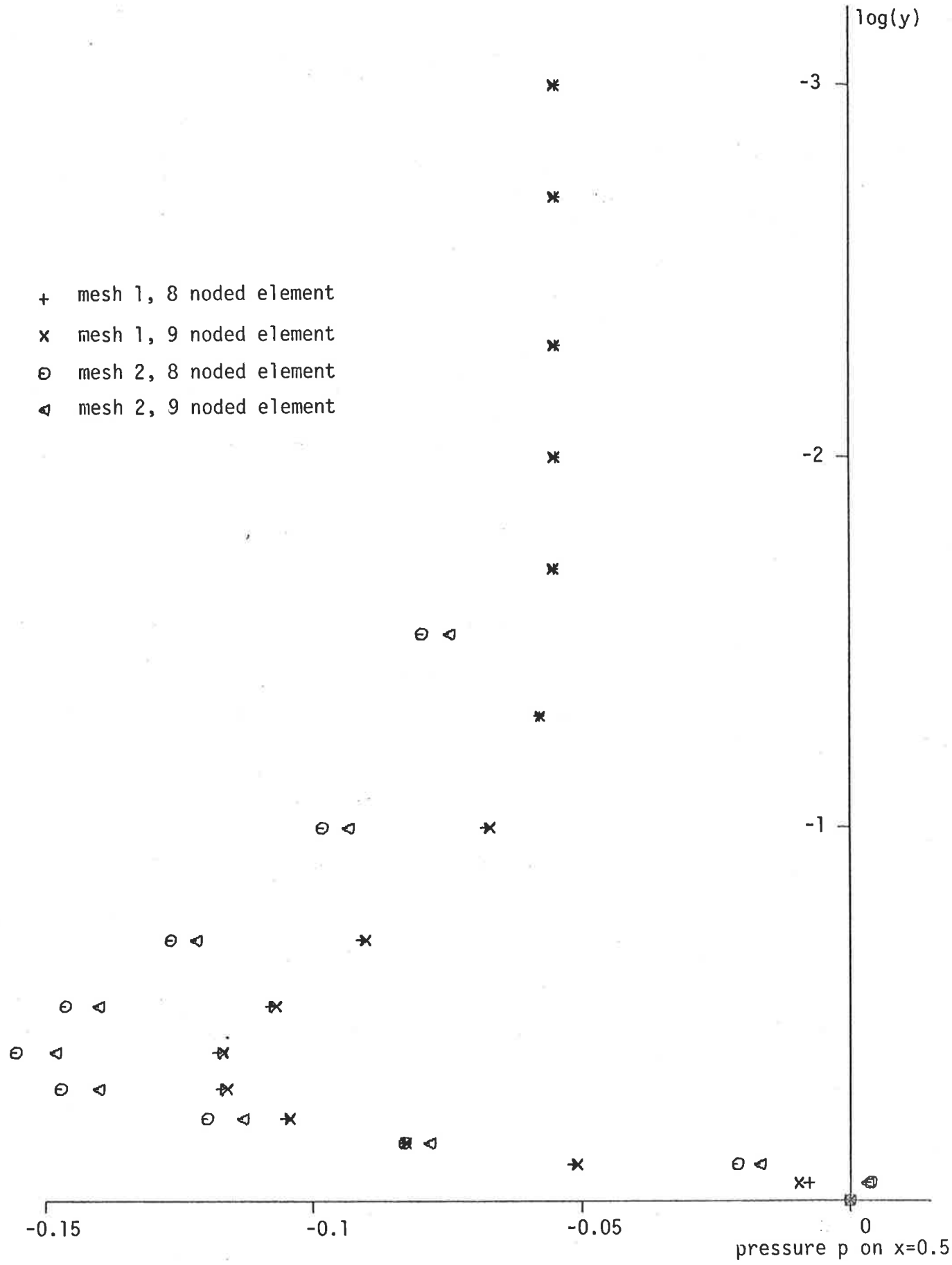

Figure 5.24(e) Variation of ρ for Re = 2000.

way not only can the performances of the two elements be compared, but the effects on these performances of changes in the mesh configurations can also be observed. With this in mind, from Figures 5.20-5.24 the first and most significant fact that can be noted is that for any particular mesh, whether it contains only rectangular elements or not, the eight noded Serendipity and the nine noded Lagrangian elements both result in almost identical solutions. This is true for both the entrance flow and the cavity flow problems and for the pressure as well as the velocity fields. It had been claimed by some previous researchers that the nine noded element would give improved pressure field solutions. However, there was no evidence of this in any of the flow cases considered in this comparison. In fact, with the entrance flow problem at Reynolds number equals 2000, both elements produce the same pressure field but the Lagrangian element results in a considerably inferior velocity solution. the oscillations that occur at Re=2000 in the velocity fields are consistently worse for the Lagrangian element than they are for the Serendipity.

In addition to the above, the following points may also be noted. Firstly for the entrance flow problem. At low Reynolds numbers, up to 1000 at least, exactly the same solution is obtained regardless of which mesh or element type is used. This can be seen from Figures 5.20 to 5.22 (a) to (d). For these Reynolds numbers also, no oscillations are evident in either the velocity or the pressure variations. At Reynolds number equals 2000 however, a slight difference in the performance of the two element types and the two meshes ENFLM1 and ENFLM2 becomes apparent. In the velocity field we see that along the centreline y=0.5, the eight noded element consistently results in a variation that has the smallest amplitude oscillations. This is equally true for both meshes. Along the line y=0.1 however, it can be seen that with mesh ENFLM1, the eight noded element again produces the best solution but

with mesh ENFLM2, the better results are produced, at least in the upstream region, when the nine noded element is used. In the downstream portion of the entrance flow however, the nine noded element solution becomes steadily worse, equalling that obtained with the eight noded element at the exit. Regarding the pressure fields, little can be said about them since at all Reynolds numbers including 2000, the same pressure variation is obtained with both meshes and with either element type.

With the cavity flow problem the situation is similar but some of the results obtained were not as expected. That is, the differences in solutions obtained with the various meshes and element types were not the same as those observed for the entrance flow problem. At Reynolds numbers below 400, both element types and both meshes CAVFLM1 and CAVFLM2 produce identical solutions. Even at Re=1000 the largest difference in solutions is never more than 2% of the maximum for the velocity variation and 4% for the pressure. However at Reynolds number equals 2000, as can be seen from Figures 5.23 and 5.24 (e), the solutions obtained using mesh CAVFLM1 differ by as much as 10% in the velocity and 17% in the pressure from those obtained with mesh CAVFLM2, regardless of which element type is used. This behaviour in the cavity flow problem was also observed to a lesser extent in the formulation comparison. A possible explanation for it is that the larger number of small elements close to the moving edge in mesh CAVFLM1 has the effect of slightly increasing the fluid stiffness in this region at higher Reynolds numbers, thereby resulting in the lower circulatory velocity for the eddy that can be seen for mesh CAVFLM1 in Figures 5.23 (d) and (e). The same explanation can be used to account for the differences observed in the formulation comparison solutions. There, by introducing additional terms in the various formulations, the total fluid stiffness is slightly changed with the effect of either slightly increasing or

slightly decreasing the eddy velocity. This change in eddy velocity can then be used to explain the large differences that occur in the pressure profiles. Since the eddy circulatory velocity is slightly different for the various flows, the vortex centre is in a slightly different position. As a result the line x=0.5 along which the pressure profiles are plotted, is a varying distance from the vortex centre. Therefore the value of the overall pressure field along x=0.5 changes by an amount which is very small when viewed with respect to the whole pressure field, but considerably larger when viewed only in relation to the pressure along x=0.5, since the pressures along x=0.5 are relatively very small. Thus although Figure 5.24(e) shows as much as 17% difference in the pressure variations obtained with the two meshes, when the whole pressure field is taken into account this difference becomes negligible.

The results of this comparison are therefore quite clear. Neither the eight noded Serendipity nor the nine noded Lagrangian element produces significantly better results. The eight noded element gives velocity solutions at higher Reynolds numbers that can be considered marginally better but the improvement is only slight. Therefore, as a result of this comparison, and taking into account both the computational efficiency discussed earlier, as well as the quality of solution produced, it can only be concluded that the eight noded Serendipity and the nine noded Lagrangian elements are equally capable of modelling a steady viscous flow. It can also be concluded that the use of non-rectangular elements in the meshes representing such flows has negligible effect on their ability to accurately represent the fluid motion and that trapezoidal and general quadrilateral elements can be confidently used to vary mesh refinements in regions of particular interest without loss of accuracy. This confirms the assumption made in Section 5.4 about the exclusive use of the eight noded Serendipity element in the formulation comparison and completely validates the results found there.

5.6 Presentation of Entrance and Cavity Flow Problem Results and Comparison with Other Published Solutions

This section has been included to complete the two-dimensional analyses. It serves two purposes: firstly, to compare with existing known solutions the two-dimensional results of the entrance flow and cavity flow problems obtained using the optimal formulation and element type, thereby verifying that the solutions thus evaluated are in fact the same as those currently accepted as correct, and secondly, to present a more complete set of solutions than is currently available for both the entrance and cavity flow problems over a wider range of Reynolds numbers. Although solutions to both these flows have already been obtained and published by other researchers with Reynolds numbers as high as 2000, the results are rarely presented with sufficient information to make them very useful. In this section therefore, care has been taken in the presentation of the solutions to ensure that the maximum usefulness can be derived from them by future workers involved with these two flows. Also, of the published solutions to the entrance and cavity flow problems of which the author is aware, only a small percentage have been obtained using the same approach adopted in this study; that is, the Galerkin finite element solution procedure. Most other workers have used either the finite difference technique or one of the other finite element approaches. Of the few using the Galerkin method, to the author's knowledge none has presented solutions to either the entrance or the cavity flow problem with Reynolds numbers higher than 400. In this section, complete solutions to both the entrance and the cavity flow problems are set out for Reynolds numbers up to and including 2000. All solutions presented have been obtained using formulation B of the two-dimensional Navier-Stokes equations, the eight noded Serendipity isoparametric element and the meshes ENFLM1 and CAVFLM1 incorporating only rectangular elements. These meshes were chosen in

preference to ENFLM2 and CAVFLM2 because the solutions that are obtained are evaluated at nodes on a regular rectangular grid. This enables the variation of velocity and pressure along specific cross-sections to be plotted directly without having to resort to interpolation within elements, as would have been the case had the solutions obtained with the latter two meshes been used.

In order to make the presentation of results as concise and as useful as possible, the following important aspects of the two flows are examined. Firstly for the entrance flow problem,

(a) the variation of the x component of velocity along y=0.5 and y=0.1,

(b) the development length to Reynolds number ratio,

(c) the velocity profiles across the channel and the location and magnitude of the local maxima,

(d) the variation of pressure along y=0.5 and y=0.1,

and (e) the excess pressure drop along y=0.5, y=0.2 and y=0.1,

are considered at Reynolds number equals 1, 200, 500, 1000 and 2000. For the cavity flow problem,

(a) the variation of the x component of velocity along x=0.5,

(b) the velocity vector field,

(c) the pressure contours,

and (d) the position of the vortex centre will be considered at Reynolds number equals 1, 100, 400, 1000 and 2000. Where they are available, solutions calculated by other researchers are plotted or tabulated alongside the results obtained during the present study for both flows. These are those produced by Morihara and Cheng (21) and Brandt and Gillis (5) using the finite difference technique and by Hutton et al. (18) using the finite element method for the entrance flow problem, and those by Burggraf (6) using the finite difference technique and by Tuann and Olson (32) and Bercovier and Engelman (3) using the finite element method for the cavity flow problem.

Consider firstly the entrance flow. The most commonly considered aspect of this problem is the variation of the x component of velocity along the centreline y=0.5. The velocity profile along this longitudinal section is particularly important because it can be used to determine the development length of the flow. Since the velocity along the longitudinal section y=0.5 is the last to attain its fully developed downstream value of 1.5, it can be used to estimate the point at which the transverse velocity profile becomes exactly parabolic and the flow in the channel becomes fully developed. Traditionally, it has been assumed that the flow becomes fully developed when the centreline velocity reaches 99% of its asymptotic value of 1.5. The position at which this occurs is labelled $x_{99\%}$ and is more commonly referred to as the development length of the flow. By plotting the variation of velocity along y=0.5 as is done in Figures 5.25(a)-(e), $x_{99\%}$ can be determined for eachReynolds number. It will be noticed that the horizontal axis in these figures is labelled x/Re. This is usually done to eliminate the dependency of the profiles on Reynolds number. By doing this it is found that as Reynolds number becomes very large, the variation of velocity along y=0.5 approaches a limit and this limit is very close to that predicted by Schlichting using boundary layer theory for large Reynolds numbers. This can easily be verified by plotting the longitudinal velocity profiles along y=0.5 for the various Reynolds numbers on the same set of axes as that used to plot the profile predicted by Schlichting. This however, has not been done here because a very good comparison of this type has already been done both by Morihara and Cheng (21) and by Brandt and Gillis (5).

Also in Figures 5.25(b), (c) and (e), a comparison is made at Reynolds number equals 200, 500 and 2000 with the corresponding solutions obtained by other researchers. In the first two cases agreement is excellent for all values of x/Re. At Re=2000 however, there is a slight

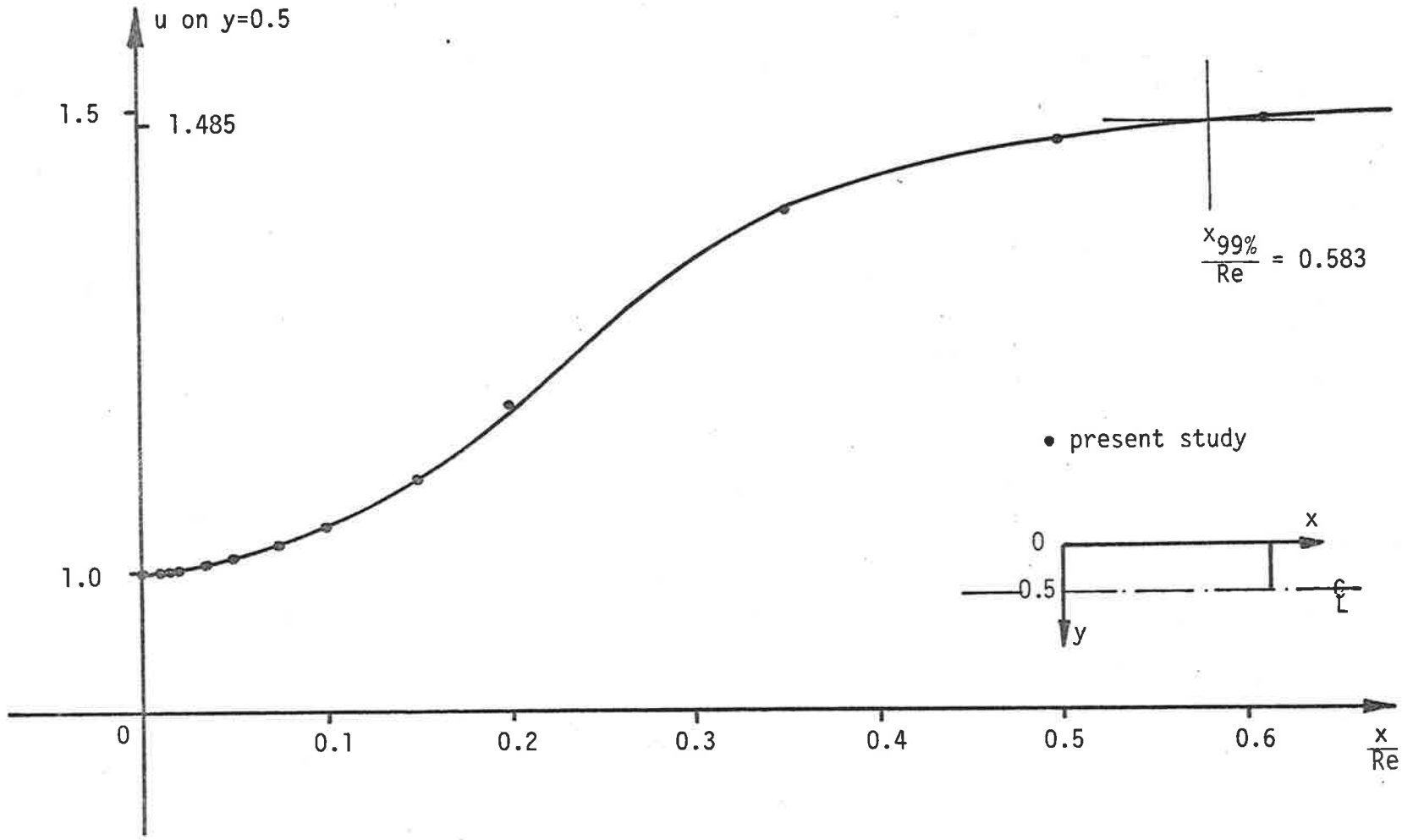

Figure 5.25(a) Variation of u Along y=0.5 for the Entrance Flow Problem at Re = 1.

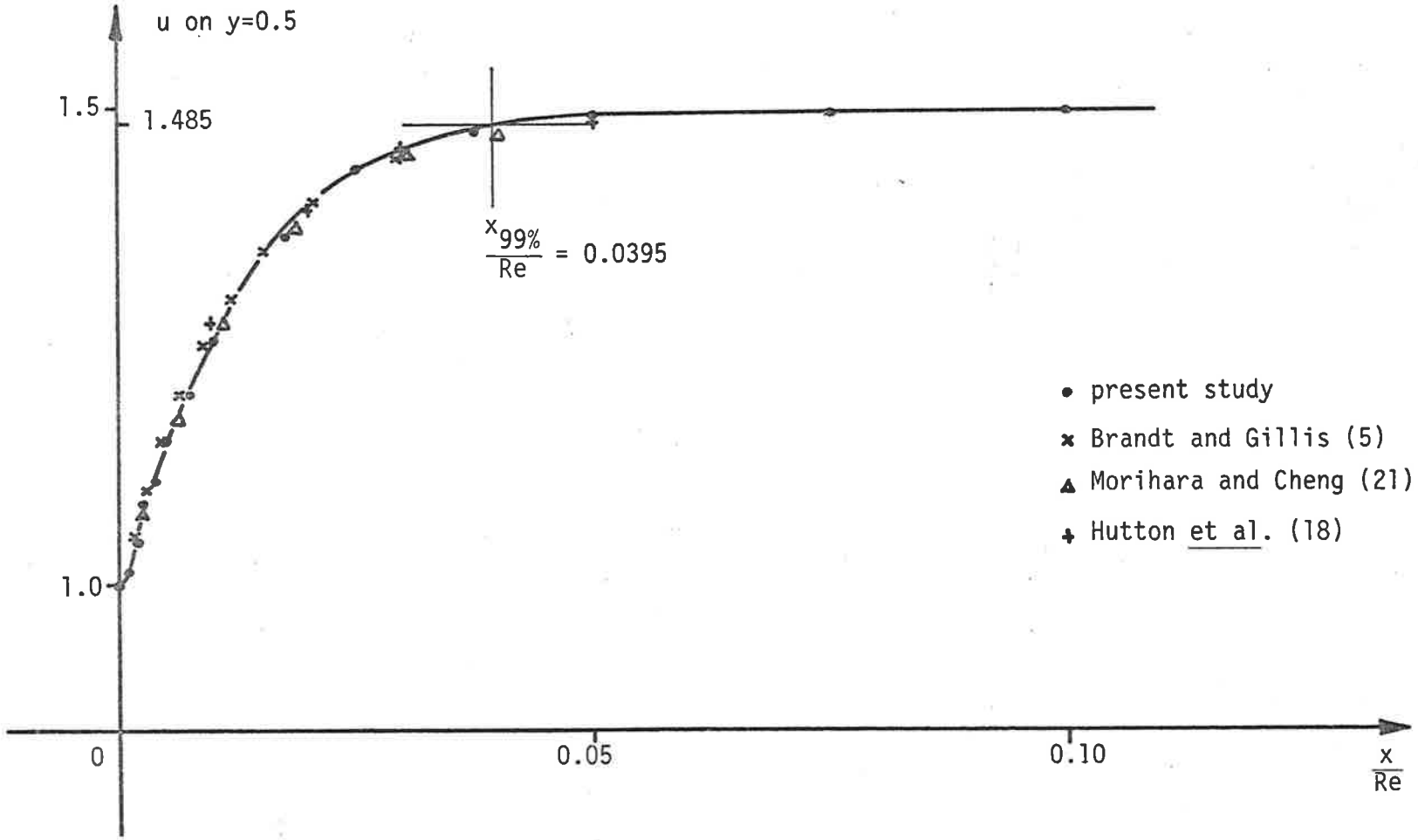

Figure 5.25(b) Variation of u Along y=0.5 for the Entrance Flow Problem at Re = 200.

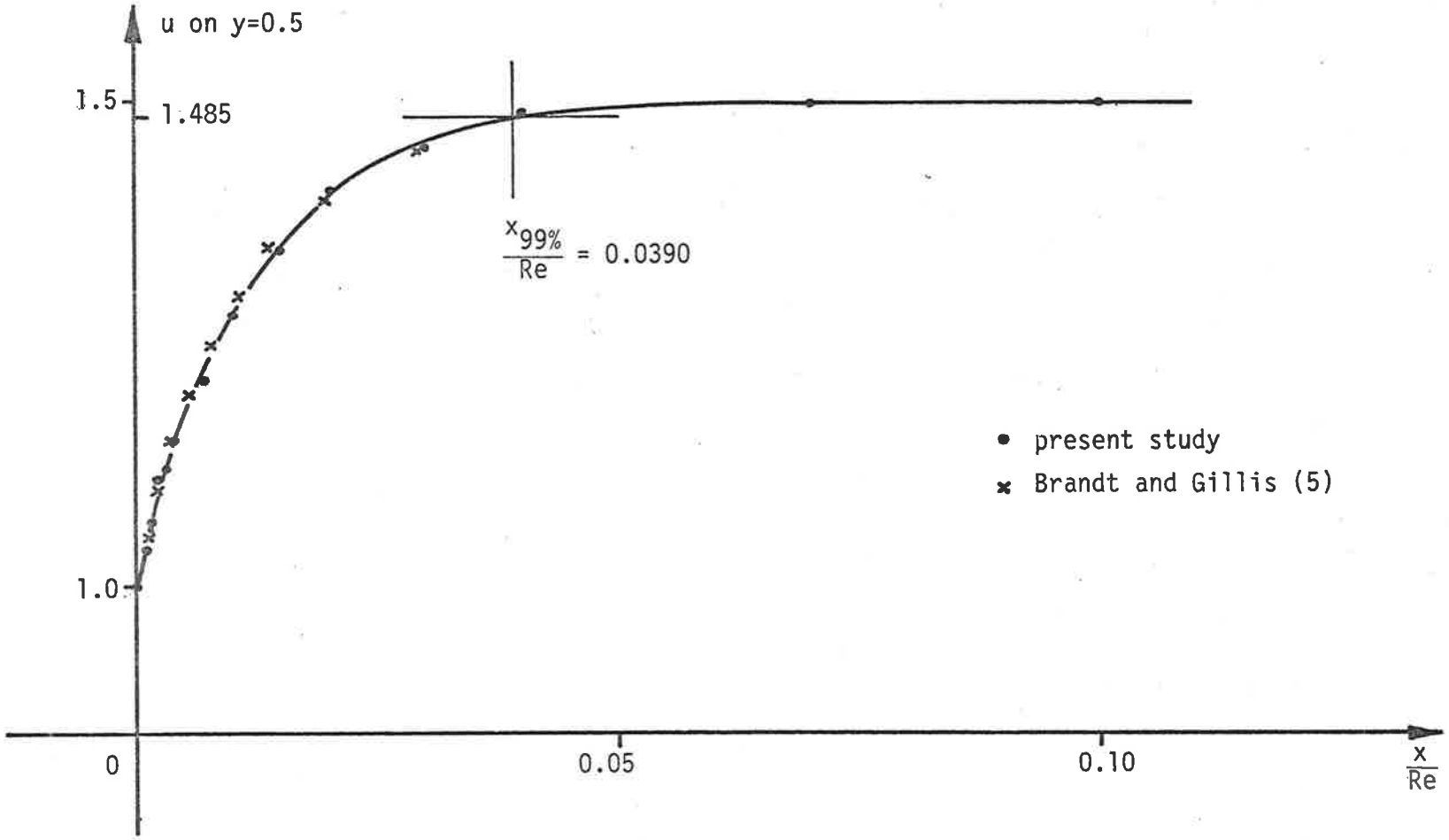

Figure 5.25(c) Variation of u Along y=0.5 for the Entrance Flow Problem at Re = 500.

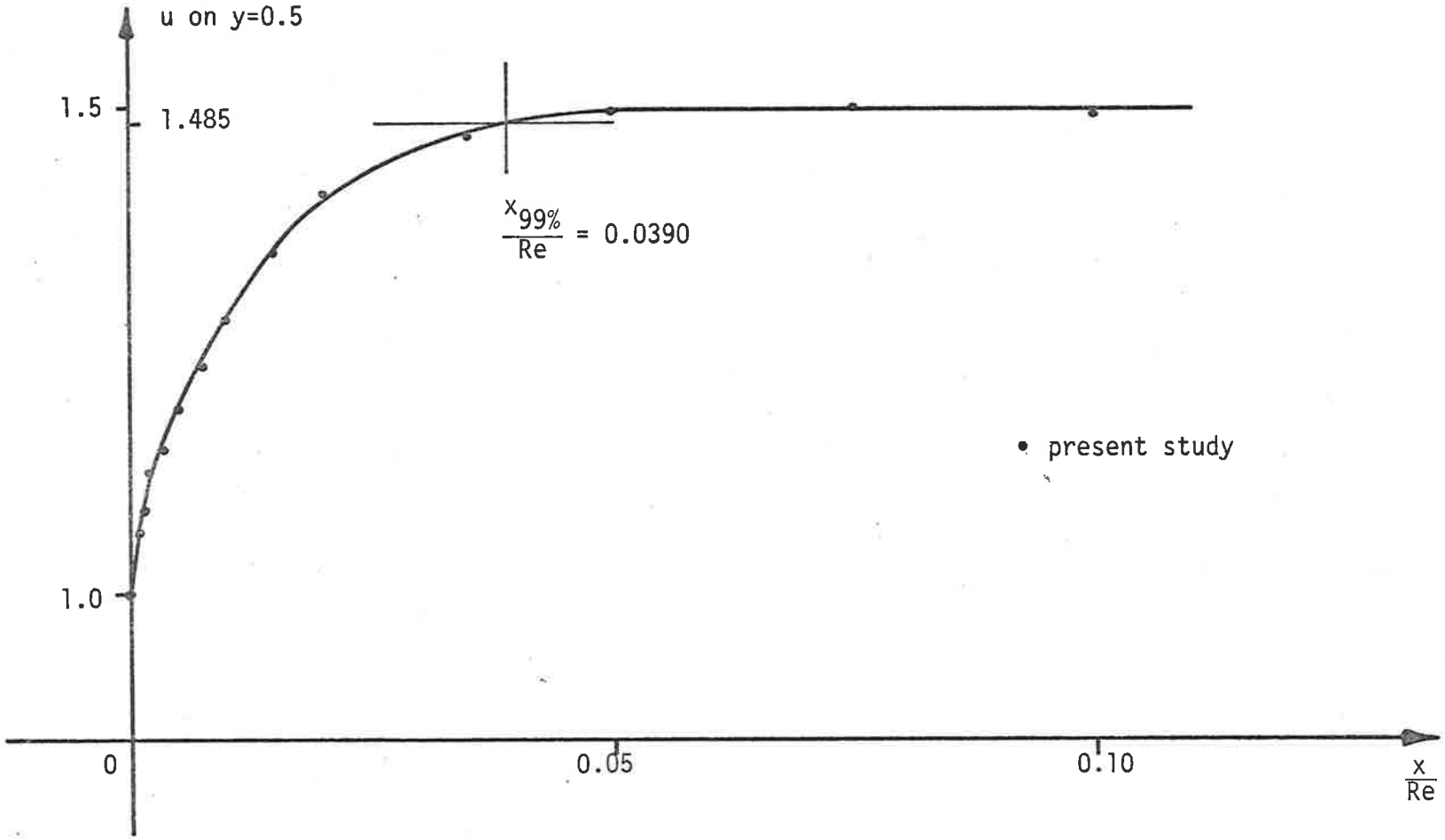

Figure 5.25(d) Variation of u Along y=0.5 for the Entrance Flow Problem at Re = 1000.

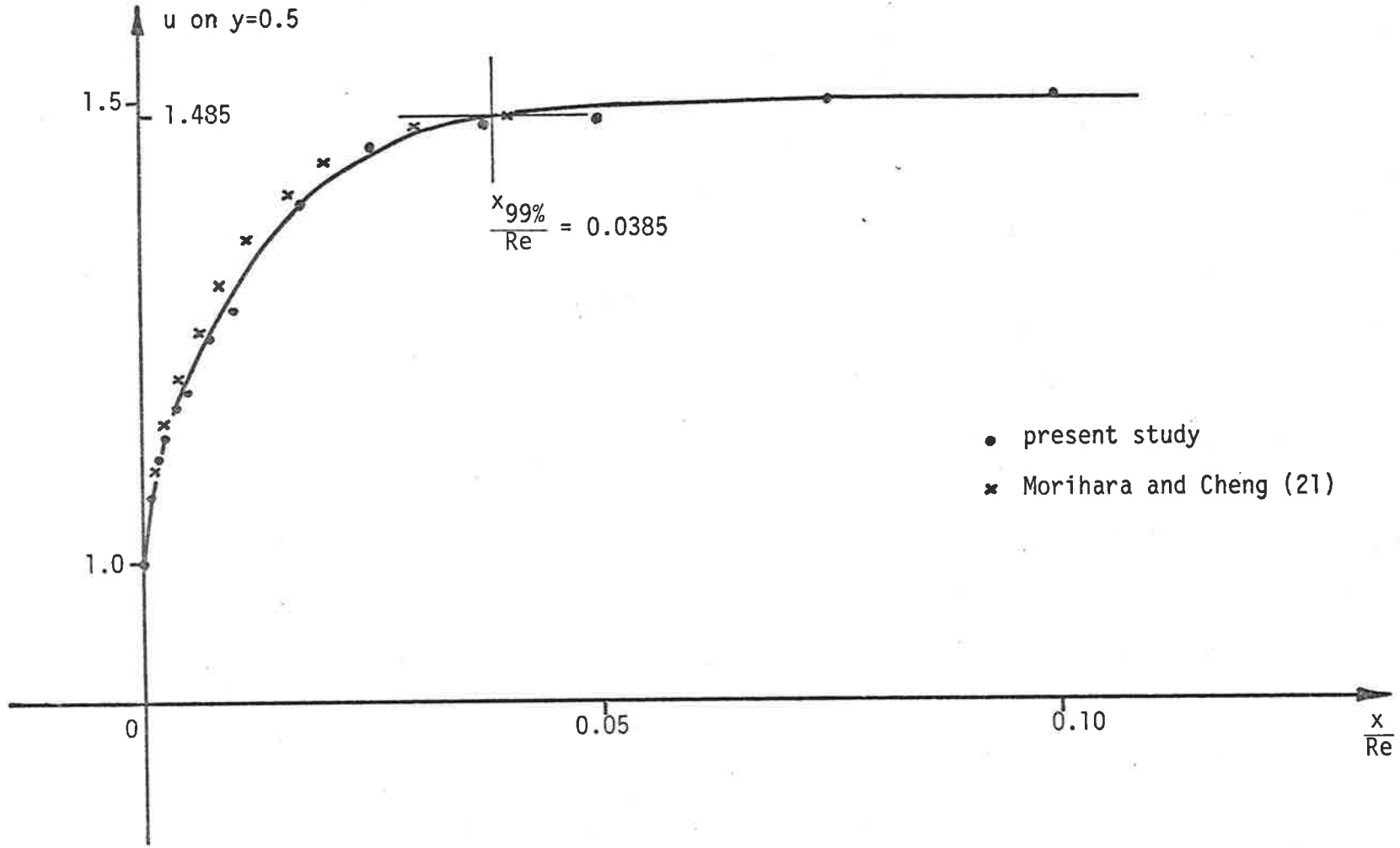

Figure 5.25(e) Variation of u Along y=0.5 for the Entrance Flow Problem at Re = 2000.

discrepancy between the results of the present work and those computed by Morihara and Cheng (21), but the difference is less than 4%. From this comparison it can be concluded that the finite difference and finite element methods both produce essentially the same velocity field when used to solve the entrance flow problem over a wide range of Reynolds numbers. It should be pointed out at this stage that the work done by both Morihara and Cheng (21) and Brandt and Gillis (5) was based on a channel width of 2. Therefore, in order to compare their solutions with those obtained in this study the horizontal axis of their profiles was scaled down by a factor of 2, thereby halving the true width of the channel being modelled. The only finite element solution of the entrance flow problem that was found was that computed by Hutton et al. (18). However only Reynolds number equals 20 and 200 were considered, and a comparison at higher Reynolds numbers with a solution obtained using the finite element method could not be made.

By examining Figures 5.25(a) to (e) the point at which the velocity profiles reach 99% of the fully developed value can be found. From these values it can be seen that the development length $x_{99\%}$, varies from 0.583 at Reynolds number equals 1 to 77.0 at Reynolds number equals 2000. This compares with 0.641 and 85.5 computed by Morihara and Cheng (21). Table 5.9(a) gives the development length obtained during the present study as well as those calculated by Morihara and Cheng (21) and Brandt and Gillis (5) over the range of Reynolds numbers from 1 to 2000. Table 5.9(b) shows the development length computed by various other researchers at the large Reynolds number limit. The results of these comparisons show that the development length for large, medium and low Reynolds numbers computed in this study are consistently between 5 and 15% lower than those calculated by previous researchers. It should be remembered when considering these results, that the present study is the only one in the comparison in which the finite element method

(a)

Re	Present Study		Morihara et al. (21)		Brandt et al. (5)	
	$x_{99\%}$	$x_{99\%}/Re$	$x_{99\%}$	$x_{99\%}/Re$	$x_{97\%}$	$x_{97\%}/Re$
1	0.583	0.583	0.651	0.651	-	-
200	7.9	0.0395	9.04	0.0452	9.12	0.0456
500	19.5	0.0390	-	-	22.4	0.0448
1000	39.0	0.0390	-	-	-	-
2000	77.0	0.0385	85.8	0.0429	-	-

(b)

Researcher	$x_{99\%}/Re$
Present work (28)	0.0380
Schlichting (28)	0.0400
Morihara et al. (21)	0.0423
Bodoia et al. (4)	0.0440
Brandt et al. (5)	0.0442

Table 5.9 Development lengths at Re=1 to 2000 and at the large Reynolds number limit.

is used. All the others used the finite difference method and either the boundary layer approximation or some other linearization of the Navier-Stokes equations. This difference in solution technique could therefore explain why the development length to Reynolds number ratio calculated in this study differs from those calculated by the previous researchers mentioned in Tables 5.9(a) and (b). Also, because the slope of the profiles is very small in the vicinity of $x_{99\%}$, large errors can easily be incurred when determining $x_{99\%}$ especially if the profiles contain some small oscillations. A difference of 10% then becomes less significant when viewed in this light.

The variation of the x component of velocity has also been plotted along the longitudinal section y=0.1, in Figures 5.26(a)-(e). From these figures it can be seen that at $x_{99\%}$, the velocity in the x direction is very close to its fully developed value of 0.54. This confirms the assumption that the whole transverse profile of velocity becomes "acceptably" parabolic when the centreline velocity reaches 1.485 or 99% of its fully developed value. The other point that should be commented upon is the fact that for Reynolds numbers equal to 500, 1000 and 2000, the profiles shown in Figures 5.26(c), (d) and (e) are very similar. In fact, they are identical except in the region where x/Re is less than about 0.02. The same thing was observed in the profiles along y=0.5. This is again in agreement with the results of Schlichting (28) who concluded that as Reynolds number becomes large, for large values of x/Re the velocity field approaches a limiting surface. For small values of x/Re, that is close to the leading edge of flows with large Reynolds numbers, boundary layer theory is not valid and the limiting surface predicted by Schlichting (28) does not apply. This is confirmed by the results in Figures 5.25 and 5.26 which show that for values of x/Re above 0.02, the profiles approach a limit as Reynolds number increases, but for x/Re close to zero, significant changes in the profiles still occur even at Reynolds number as high as 2000.

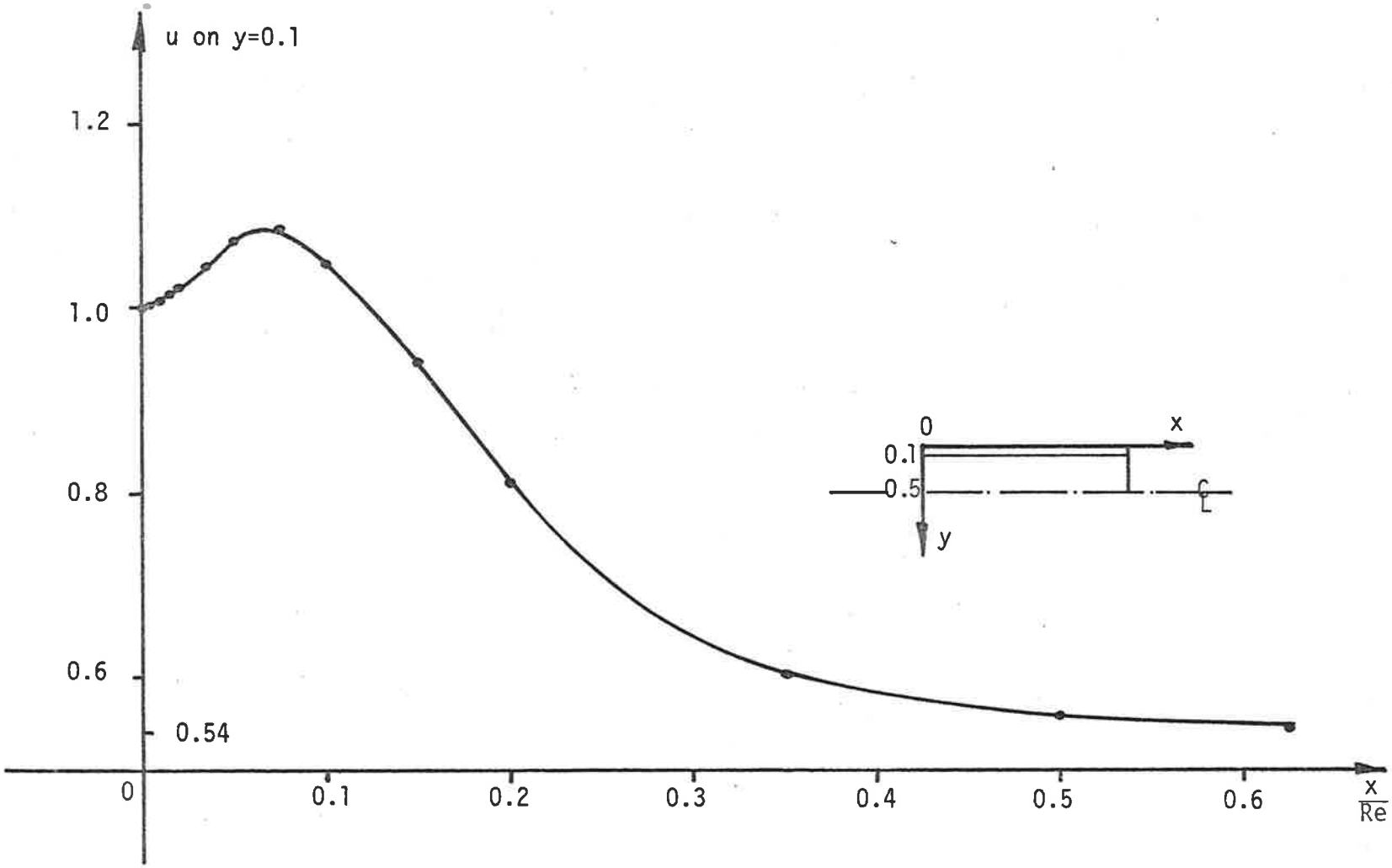

Figure 5.26(a) Variation of u Along y=0.1 for the Entrance Flow Problem at Re = 1.

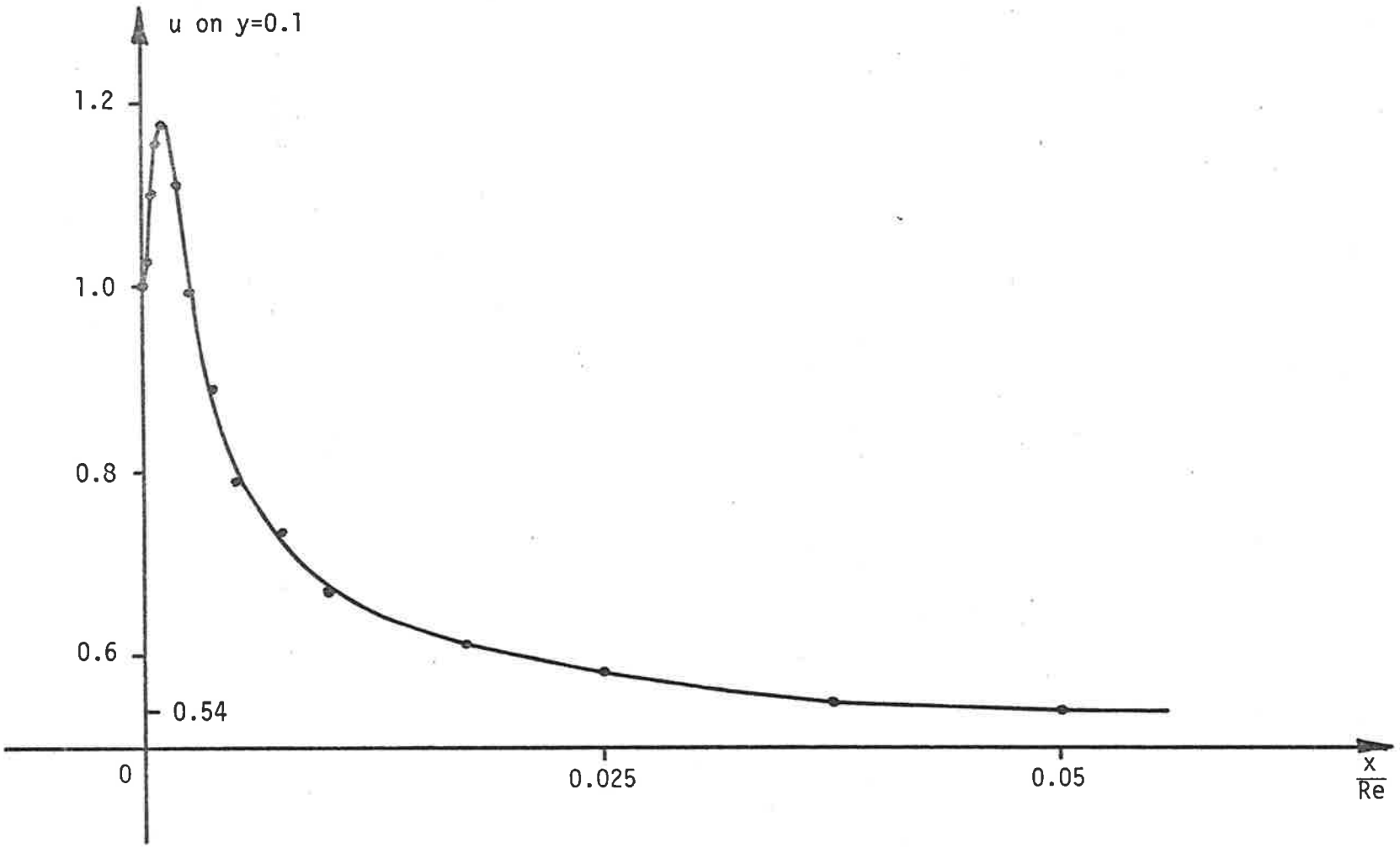

Figure 5.26(b) Variation of u Along y=0.1 for the Entrance Flow Problem at Re = 200.

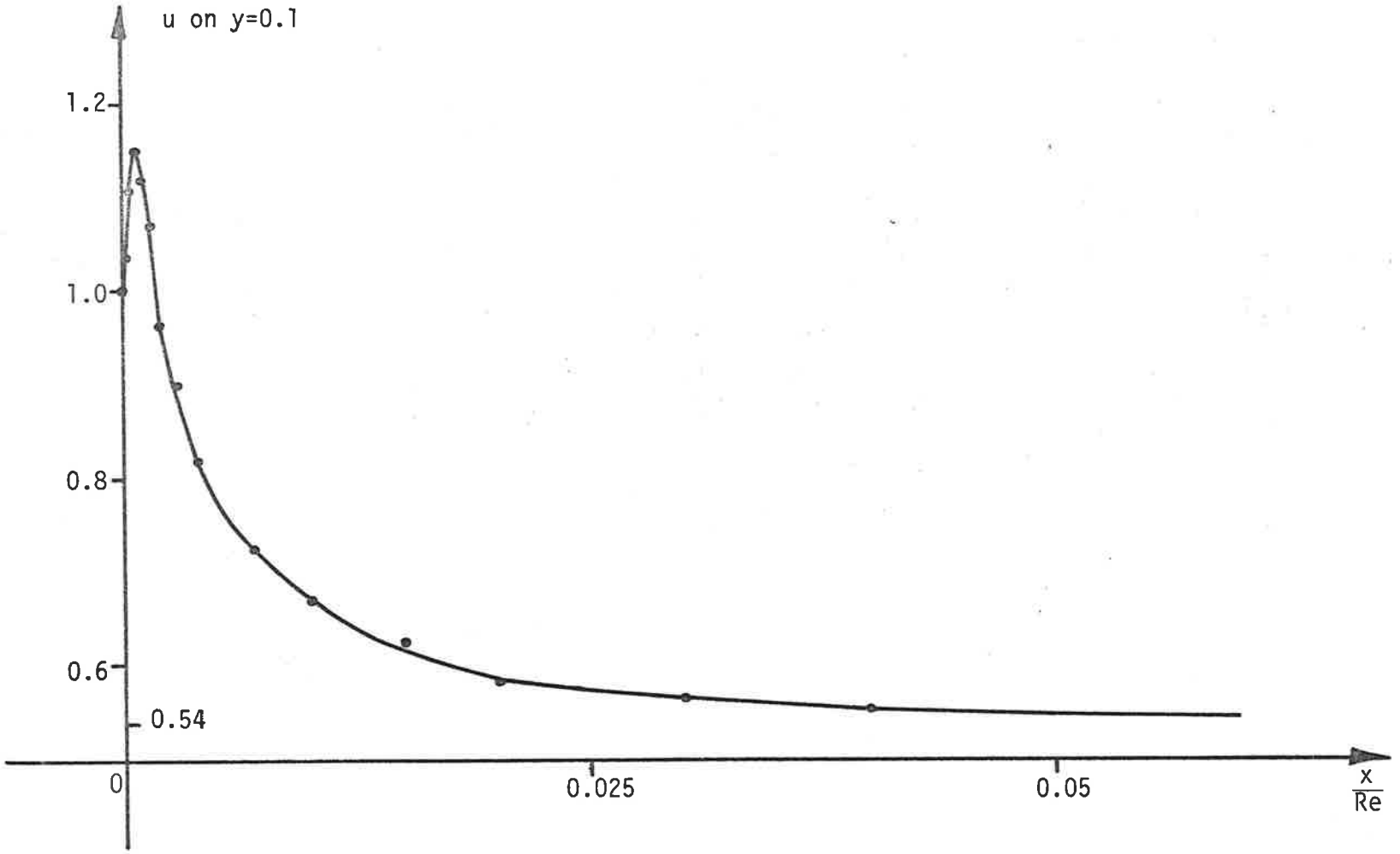

Figure 5.26(c) Variation of u Along y=0.1 for the Entrance Flow Problem at Re = 500.

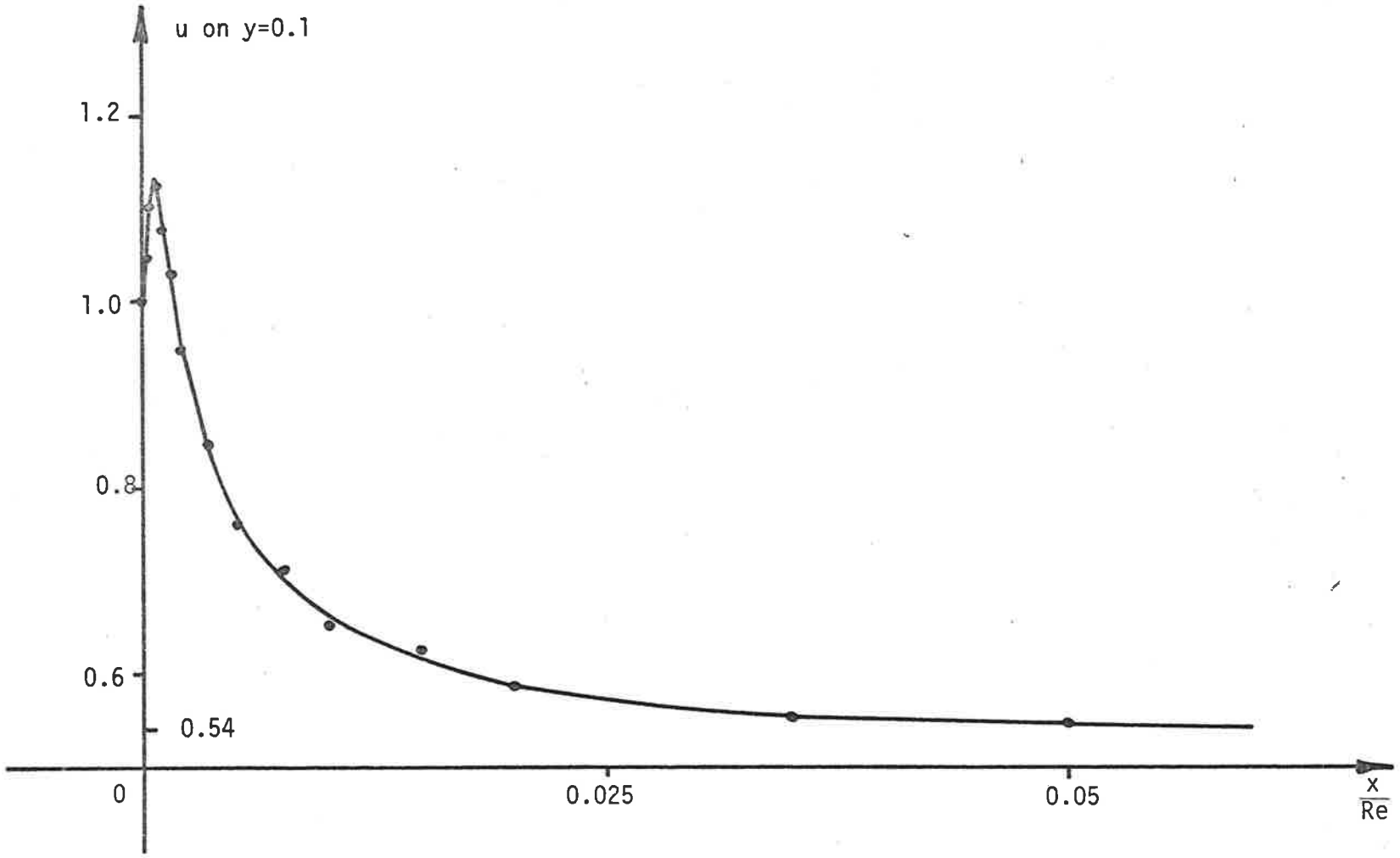

Figure 5.26(d) Variation of u Along y=0.1 for the Entrance Flow Problem at Re = 1000.

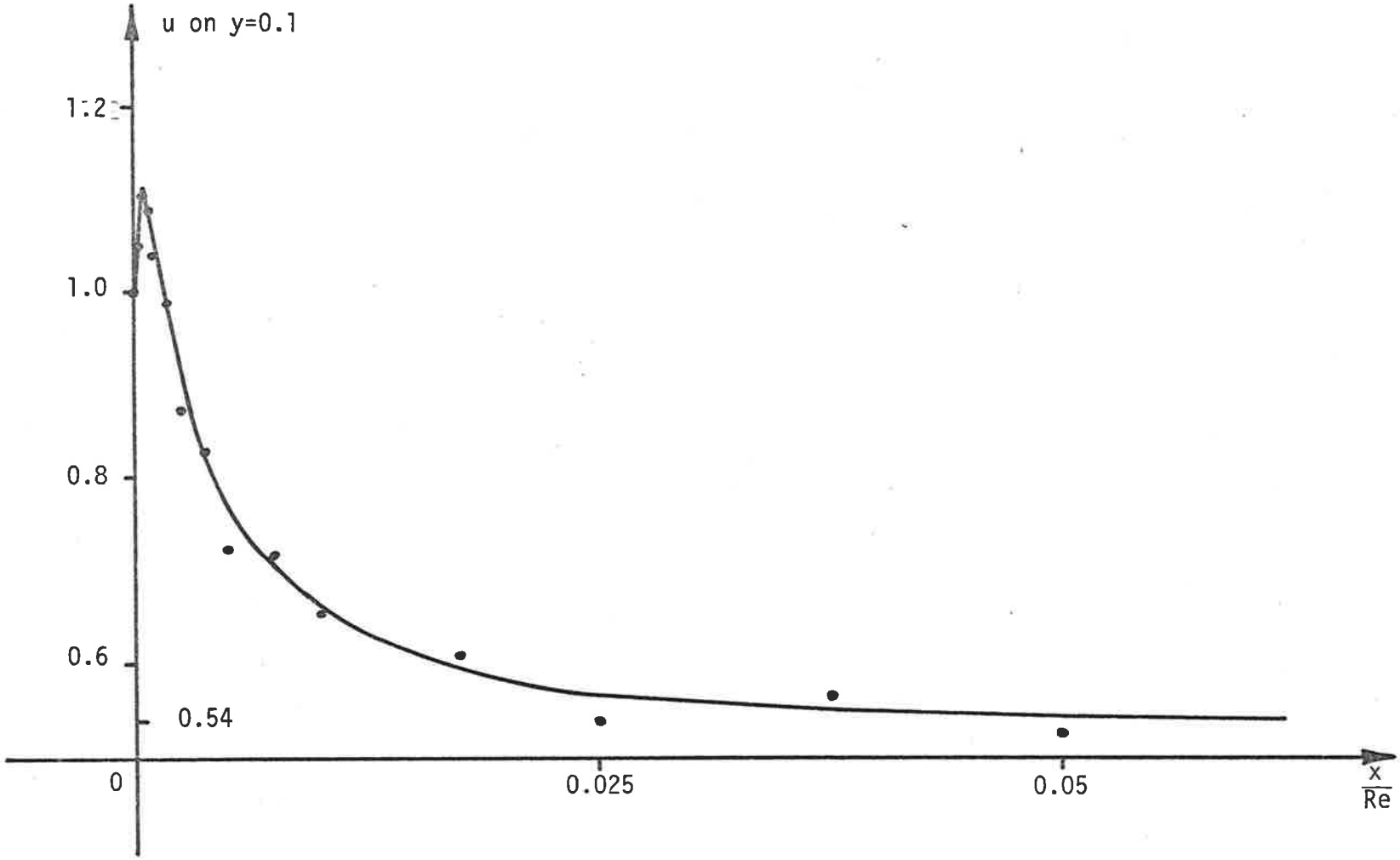

Figure 5.26(e) Variation of u Along y=0.1 for the Entrance Flow Problem at Re = 2000.

A discussion of the entrance flow problem would not be complete without including some mention of the variation of the x component of velocity along various sections across the channel. These transverse velocity profiles are shown in Figures 5.27(a)-(e) for Reynolds numbers 1, 200, 500, 1000 and 2000, and for x=0.001, 0.002, 0.005, 0.01, 0.02, 0.05, 0.1, 0.2, 0.5, 1.0, 2.0, 5.0, 10.0, 20.0, 50.0, 100.0 and 200.0. It will be noted that for small values of x, each profile contains a local minimum on the centreline y=0.5 and a local maximum located close to each of the two channel walls. The presence of these local maxima has been reported by every previous researcher involved with the entrance flow problem except those who used some form of boundary layer approximation. As a result, some confusion arose as to the true nature of the entrance flow solution. Abarbanel et al. (1), using the finite difference method to solve the complete Navier-Stokes equations, have presented evidence indicating the strong possibility that the humps are in fact an intrinsic part of the exact solution. This therefore indicates that boundary layer theory is not capable of allowing a true representation to be made of the flow close to the entrance edge and in the vicinity of the channel walls. The results of this study reinforce this and dispel any suggestion that the humps are due to inherent inadequacies in the solution technique, be it the finite difference or the finite element method.

The commonly accepted physical explanation for the presence of these humps close to the walls in the upstream portion of the entrance region is as follows. With the fluid coming to a sudden standstill at the start of the channel walls, fluid somewhere else must be accelerated in order to conserve mass flow across the entrance section. The particles of fluid most likely to experience this acceleration first are those closest to the fluid that has already been stopped. Therefore, because the flow acceleration does not instantaneously reach the centre-

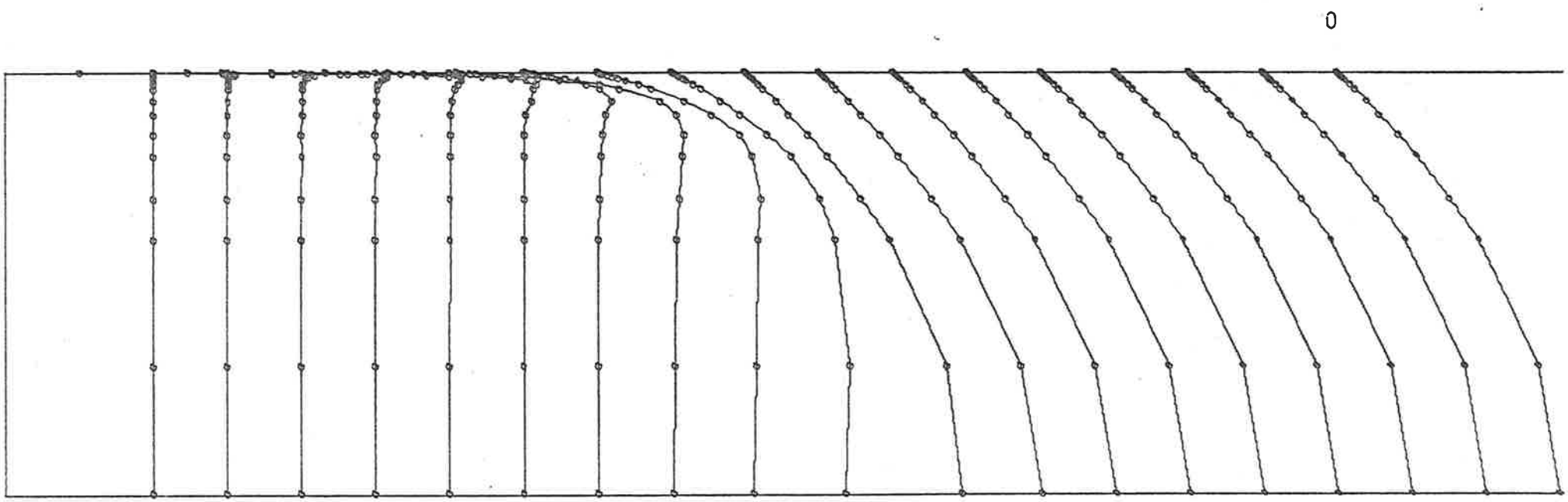

Figure 5.27(a) Transverse Velocity Profiles at x=0.001, 0.002, 0.005, 0.01, 0.02, 0.05, 0.1, 0.2, 0.5, 1.0, 2.0, 5.0, 10.0, 20.0, 50.0, 100.0 and 200.0 at Re = 1.

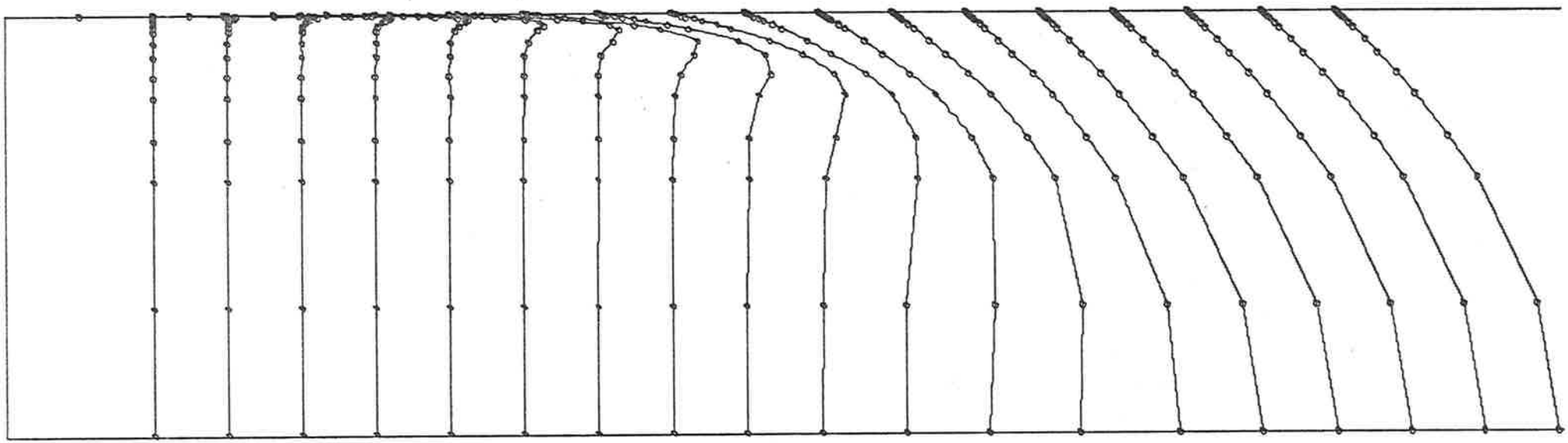

Figure 5.27 (b) Transverse Velocity Profiles at Re = 200.

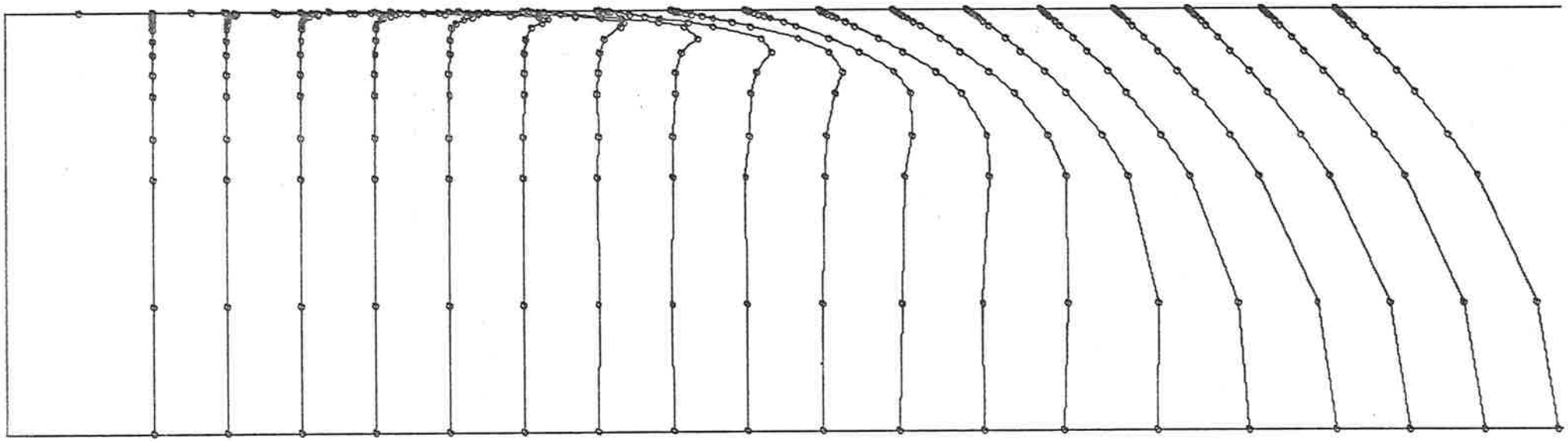

Figure 5.27 (c) Transverse Velocity Profiles at Re = 500.

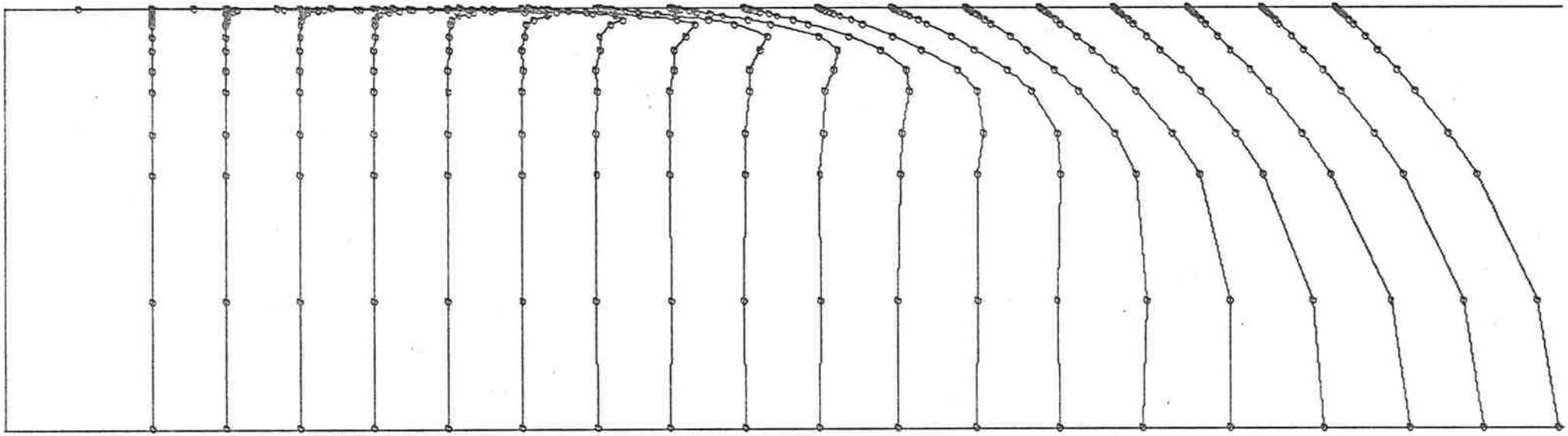

Figure 5.27 (d) Transverse Velocity Profiles at Re = 1000.

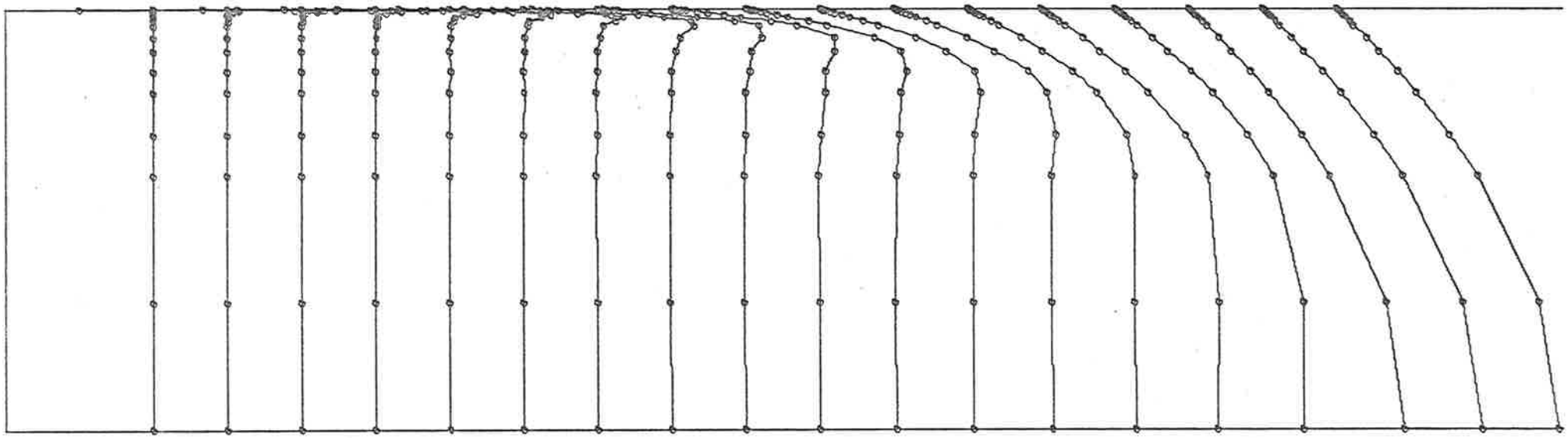

Figure 5.27 (e) Transverse Velocity Profiles at Re = 2000.

line, a local increase in the velocity takes place close to the walls, and the humps observed in the velocity profiles close to the entrance edge result. Also, because the fluid is slowed down so rapidly at the start of the channel walls, large local shear stresses and pressure gradients are experienced by the fluid there. The shear stresses, directed upstream and towards the centreline, have the effect of slowing down more fluid away from the walls and of pushing it towards the centreline. The pressure gradients have a similar effect, accelerating the displaced fluid downstream and also towards the centreline. The final result is that the local maxima occur further and further away from the walls as the fluid moves downstream, so that at the end of the entrance region the two maxima, one either side of the centreline, have merged to produce the single maximum of the fully developed parabolic profile. Table 5.10(a) shows the location of the local maximum at various transverse sections in the top half of the channel for the five Reynolds numbers 1, 200, 500, 1000 and 2000. Table 5.10(b) gives the magnitudes of these maxima. The positions and magnitudes of the local maxima have been calculated by quadratic interpolation along the element boundaries coincident with the cross-sections concerned. Table 5.10(c) shows a comparison of the positions and magnitudes of the local maxima obtained in this study for Reynolds number equals 500 with the results of Brandt and Gillis (5).

From Table 5.10(b) it can be seen that for each Reynolds number the magnitude of the local maxima increases to a peak value, falls slightly and then continues to rise to its maximum of 1.5 at the downstream exit. Morihara and Cheng (21) observed that the peak value was highest at Reynolds number equals 200. In this study however it was found to reach a maximum value of 1.22 at Reynolds number equals 1000. The comparison of results at Reynolds number equals 500 shown in Table 5.10(c) indicates quite satisfactory agreement with the finite difference

a	Reynolds number				
	1	200	500	1000	2000
0.001	0.004	0.004	0.003	0.003	0.002
0.002	0.005	0.004	0.004	0.004	0.003
0.005	0.009	0.008	0.007	0.006	0.005
0.01	0.017	0.015	0.012	0.009	0.008
0.02	0.037	0.026	0.017	0.015	0.012
0.05	0.082	0.041	0.034	0.026	0.021
0.1	0.164	0.071	0.053	0.040	0.031
0.2	0.396	0.114	0.078	0.060	0.042
0.5	0.480	0.187	0.130	0.103	0.075
1	0.5	0.310	0.224	0.150	0.112
2	0.5	0.409	0.323	0.247	0.157
5	0.5	0.475	0.420	0.384	0.329
10	0.5	0.499	0.471	0.427	0.399
20	0.5	0.5	0.494	0.469	0.425
50	0.5	0.5	0.499	0.497	0.494
100	0.5	0.5	0.5	0.5	0.497
200	0.5	0.5	0.5	0.5	0.5

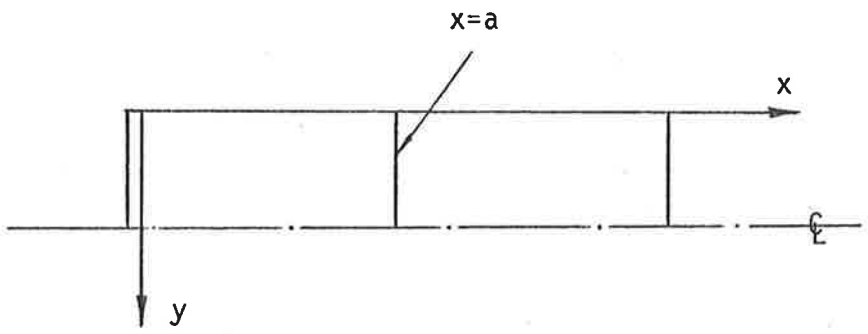

Table 5.10(a) Distance from wall of local maxima at various cross-sections x=a and for various Reynolds numbers.

a	Reynolds number				
	1	200	500	1000	2000
0.001	1.092	1.106	1.119	1.128	1.154
0.002	1.076	1.123	1.149	1.168	1.169
0.005	1.090	1.132	1.154	1.186	1.177
0.01	1.088	1.142	1.172	1.192	1.183
0.02	1.099	1.169	1.188	1.204	1.184
0.05	1.093	1.199	1.179	1.221	1.145
0.1	1.109	1.182	1.177	1.167	1.110
0.2	1.214	1.187	1.163	1.158	1.128
0.5	1.468	1.166	1.129	1.114	1.086
1	1.506	1.191	1.149	1.114	1.094
2	1.5	1.294	1.182	1.148	1.101
5	1.5	1.441	1.309	1.217	1.128
10	1.5	1.494	1.411	1.307	1.207
20	1.5	1.5	1.491	1.417	1.299
50	1.5	1.5	1.498	1.496	1.452
100	1.5	1.5	1.501	1.499	1.484
200	1.5	1.5	1.5	1.502	1.505

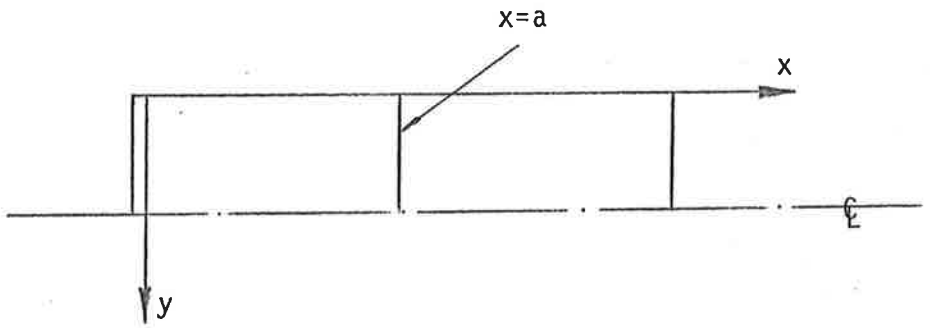

Table 5.10(b) Magnitude of local maxima at various cross-sections x=a and for various Reynolds numbers.

a	Brandt et al. (5)			Present study		
	u_c	u_{max}	$y_{u_{max}}$	u_c	u_{max}	$y_{u_{max}}$
0.05	1.001	1.169	0.030	1.001	-	-
0.1	1.003	1.163	0.048	1.002	1.177	0.053
0.15	1.007	1.156	0.061	1.002	-	-
0.2	1.011	1.151	0.072	1.013	1.163	0.078
0.25	1.017	1.148	0.082	-	-	-
0.5	1.048	1.142	0.123	1.039	1.129	0.130
1.0	1.100	1.151	0.180	1.092	1.149	0.224
1.5	1.135	1.168	0.225	1.121	-	-
2.0	1.162	1.189	0.260	1.151	1.182	0.323
3.0	1.211	1.223	0.315	-	-	-
4.0	1.252	1.256	0.370	-	-	-
5.0	1.288	1.288	0.435	1.280	1.309	0.420

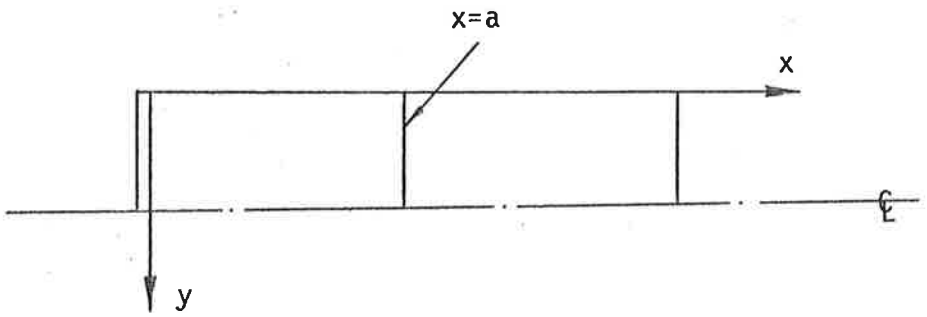

Table 5.10(c) A comparison of the results obtained during the present study with those produced by Brandt and Gillis (5) and Reynolds number equals 500; u_c = the centreline velocity, u_{max} = the maximum velocity in the x direction along section x=a and $y_{u_{max}}$ = the distance from the the wall at which u_{max} occurs.

results of Brandt and Gillis (5). The magnitudes of the local maxima at the various sections considered show a maximum difference of 2%. However the locations of the maxima calculated in this study differ considerably from those evaluated by (5). Their distance from the wall on any section x=a is consistently greater in this study than it is in solutions produced by (5). This implies that the local maxima reach the centreline in a shorter distance from the entrance than that predicted by Brandt and Gillis (5), and that consequently the development length is shorter. This verifies the results presented earlier in this section, namely that the development length to Reynolds number ratio evaluated in this study is about 10% lower than that found by Brandt and Gillis (5).

The variation of pressure along the longitudinal sections y=0.5 and y=0.1 for the five Reynolds numbers considered is plotted in Figures 5.28(a) and (b). From these graphs it can be seen that the pressure varies linearly along most of the channel with the gradients close to the entrance edge decreasing slightly for low Reynolds numbers and increasing quite significantly for high Reynolds numbers. The slope of the linear portion is $-\frac{1}{12}$Re for all Reynolds numbers and corresponds to the pressure gradient existing in a fully developed flow. The increase in pressure close to the entrance edge and more apparently close to the walls for higher Reynolds numbers is produced by the rapid slowing down of the fluid in this region and is consistent with the development of overshoots in the velocity profiles discussed earlier. It will also be noticed that for all Reynolds numbers considered except Re=1 the pressure gradients are always negative. The flow with Reynolds number equals 1 has a small region close to the entrance and on the centreline in which adverse positive pressure gradients develop. This characteristic of low Reynolds number flows was also reported by Morihara and Cheng (21) who observed its presence in a flow with Reynolds number equals 20. This prompted a closer examination of the pressure fields

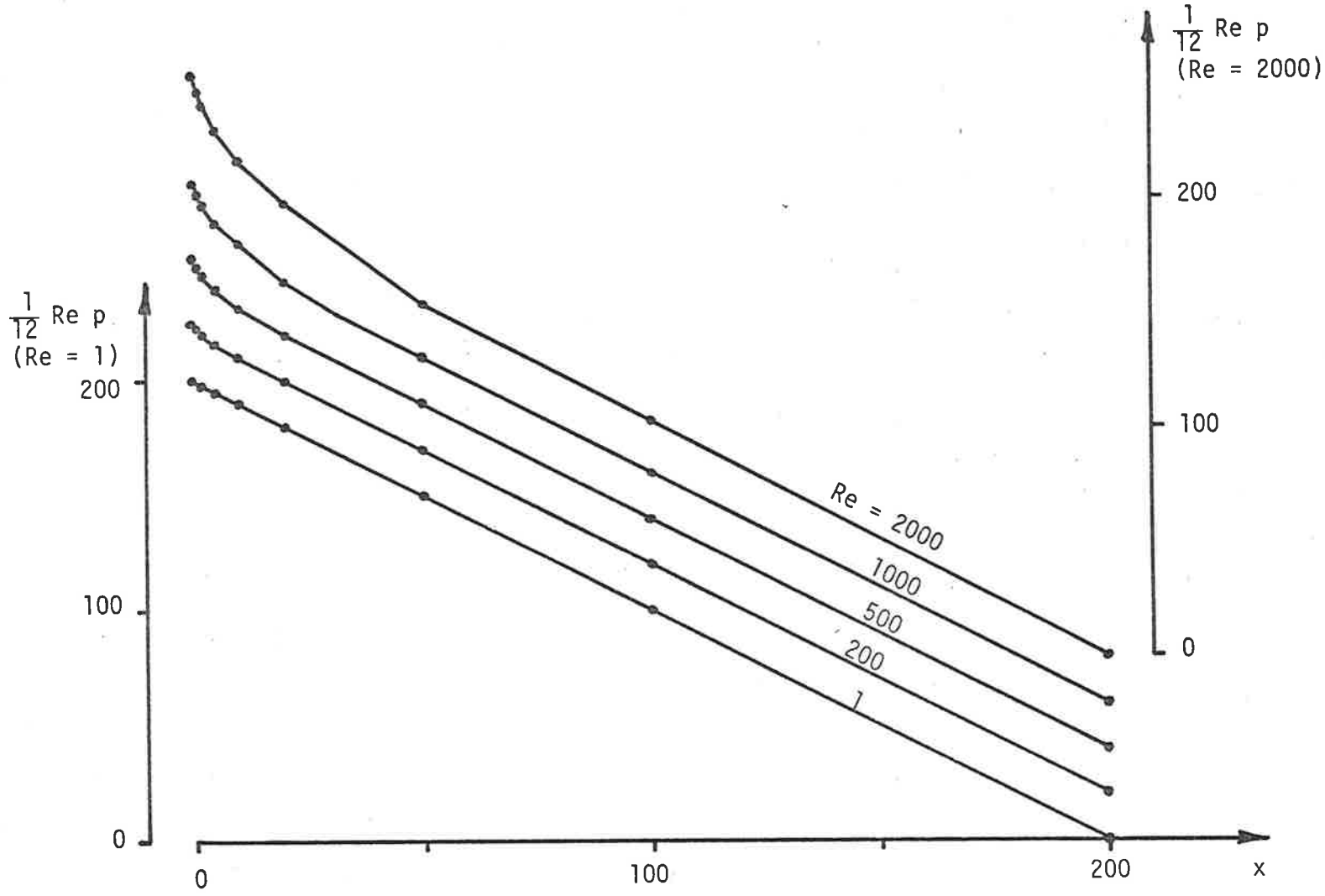

Figure 5.28(a) Variation of p Along y=0.5 for the Entrance Flow Problem.

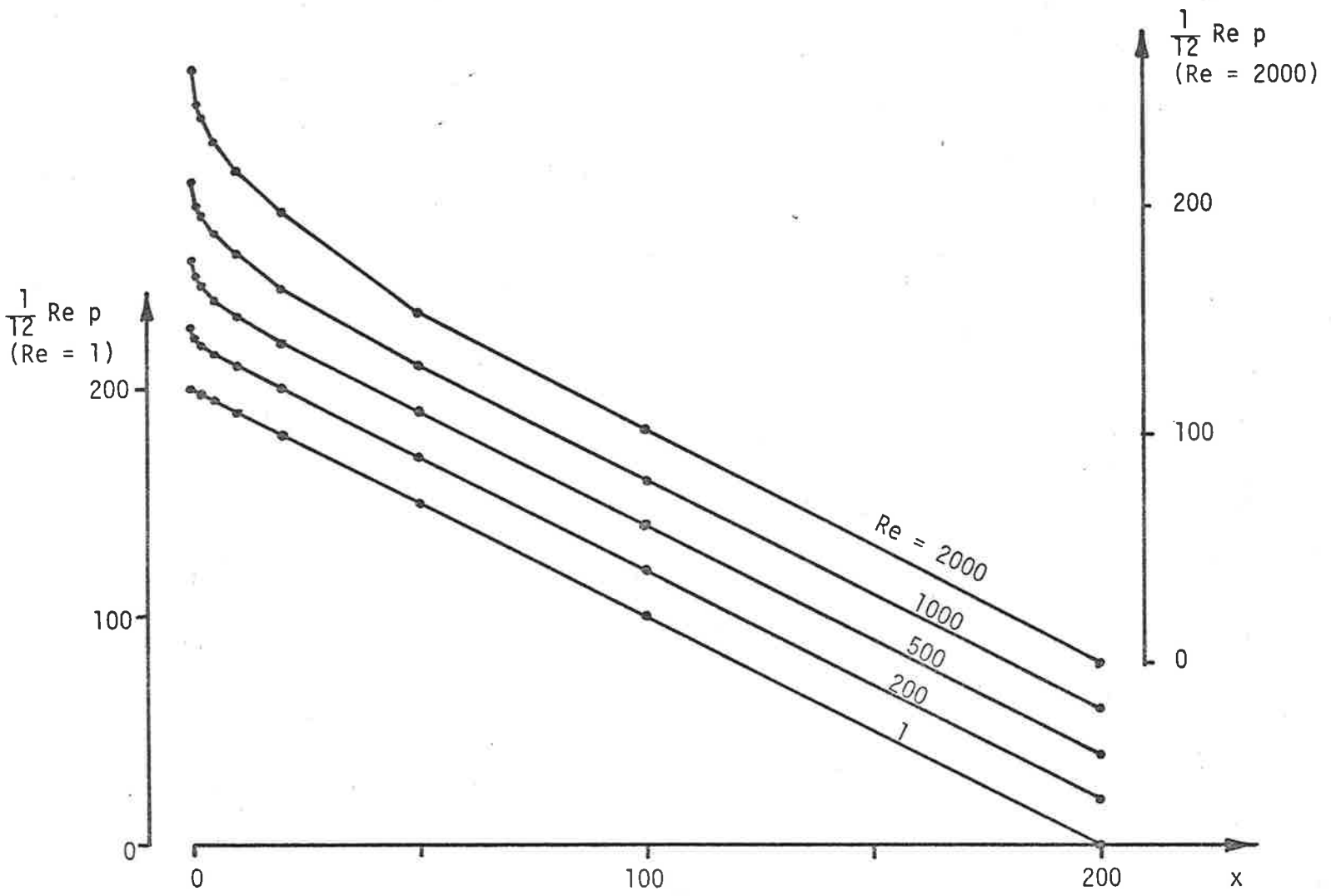

Figure 5.28(b) Variation of p Along y=0.1 for the Entrance Flow Problem.

for flows with higher Reynolds numbers and as expected, regions of adverse pressure gradients were found in all flows. However the extent of these zones is greatly reduced at high Reynolds numbers and only barely evident at Re=2000. Also the magnitude of the maximum positive gradients is only a small fraction of the magnitude of the maximum negative gradients. The reason for the existence of these adverse pressure gradients has not been satisfactorily explained, although Marihara and Cheng (21) suggest that they are probably due to the fact that the inlet velocity profile is forced to be uniform. They also suggest that it is questionable whether in a real flow under steady state conditions a uniform velocity profile as specified in the boundary conditions can be maintained. A satisfactory answer to this question will only be obtained when more information concerning the true nature of the inlet velocity profile becomes available. Until then the assumption that the entrance velocity is uniform is the best that can be made with the information available.

In order to compare the pressure results of this study with those of Brandt and Gillis (5), a quantity referred to by them as "the excess pressure drop" has been evaluated at various sections across the channel and is tabulated in Table 5.11(a) for various Reynolds numbers. From Table 5.11(b), in which a comparison is made at Reynolds number equals 200 and 500, it can be seen that agreement is quite good, the largest difference being 5%. The excess pressure drop is defined by (5) as

$$q(y) = \lim_{x\to\infty} \left\{ p(0,y) - \frac{1}{12} \mathrm{Re}\, x - p(x,y) \right\}$$

and can be considered as the difference between the actual pressure at the end of the entrance region and the pressure that would have been there had the pressure varied linearly from its entrance value with a slope of $\frac{1}{12}$ Re. q(y) is essentially the pressure distribution needed at the entrance edge to maintain the input flow as specified. The term

(a)

y	Reynolds number				
	1	200	500	1000	2000
0.5	-4.78	0.272	0.296	0.309	0.320
0.2	-0.19	0.332	0.332	0.334	0.337
0.1	10.14	0.435	0.393	0.375	0.364
0.05	27.35	0.585	0.477	0.431	0.402
0.02	80.58	0.913	0.664	0.554	0.484
0.01	189.5	1.451	0.927	0.720	0.592
0.005	385.0	2.412	1.331	0.959	0.742
0.002	-	5.297	2.485	1.558	1.081
0.001	-	8.896	3.944	2.310	1.481
0	-	10.32	4.450	2.520	1.576

(b)

y	Present study		Brandt et al. (5)	
	Re=200	500	Re=200	500
0.5	0.272	0.296	0.288	0.308
0.2	0.332	0.332	0.342	0.337
0.1	0.435	0.393	0.434	0.389
0.05	0.585	0.477	0.589	0.474

Table 5.11 Excess pressure drop for various Reynolds numbers.

"excess" refers to the fact that the pressure drops at a faster rate than $\frac{1}{12}$Re close to the entrance.

This completes the presentation of the entrance flow problem solutions.

For the cavity flow problem the variations of the x component of velocity along the centreline x=0.5 for Reynolds numbers 1, 100, 400, 1000 and 2000 are plotted in Figures 5.29(a) to (e) respectively. Where possible, similar profiles produced by Burggraf (6) and Bercovier and Engelman (3) are also plotted in these figures. From this comparison of profiles it can be seen that a significant difference exists between the results of this study and those of other researchers. At low Reynolds numbers the difference is least noticeable and agreement between solutions is quite acceptable. However as Reynolds number increases, the difference between the various profiles also increases, so much so that at Re=1000, the profile produced by Bercovier and Engelman (3) differs from the one obtained in this study by as much as 12% of the maximum moving wall velocity. It is important to note that the profiles produced by (3) and (6) also differ significantly between themselves. The reason for these differences between the various solutions is difficult to determine. Most likely it arises as a consequence of the different solution techniques and mesh point spacings chosen by the researchers, since these are the only quantities which have varied in the three studies compared. This is supported by the results of the previous formulation and element comparisons in which it was observed that changes in equation formulation and mesh configuration both produced significant changes in the numerical values of the velocity along x=0.5. Because the information concerning the cavity flow problem that is currently available is limited and not conclusive, it is not possible to determine which solution is in fact closest to the exact. Therefore no further comment will be made in this section about the accuracy of the various solutions compared.

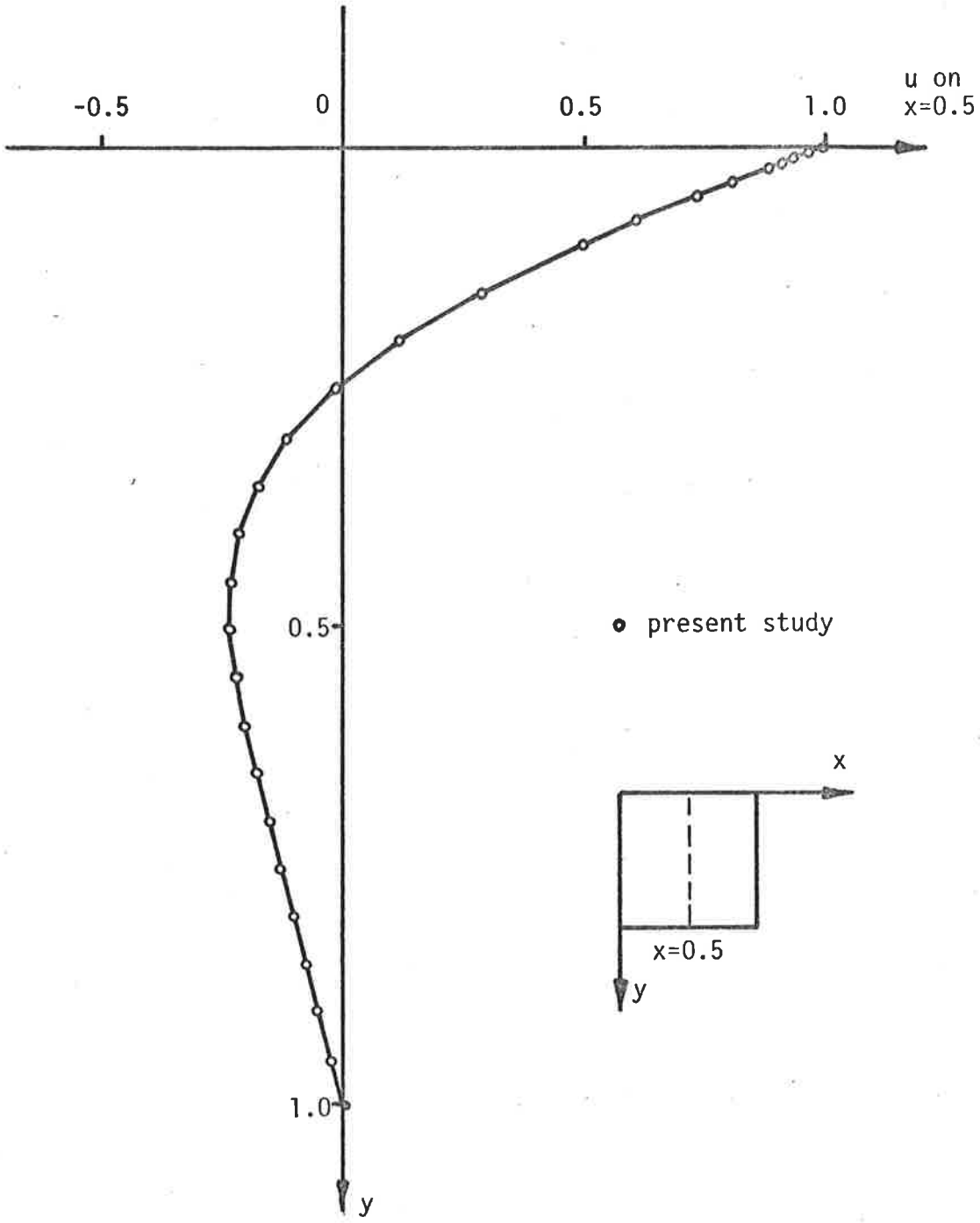

Figure 5.29(a) Variation of u Along x=0.5 for the Cavity Flow Problem at Re = 1.

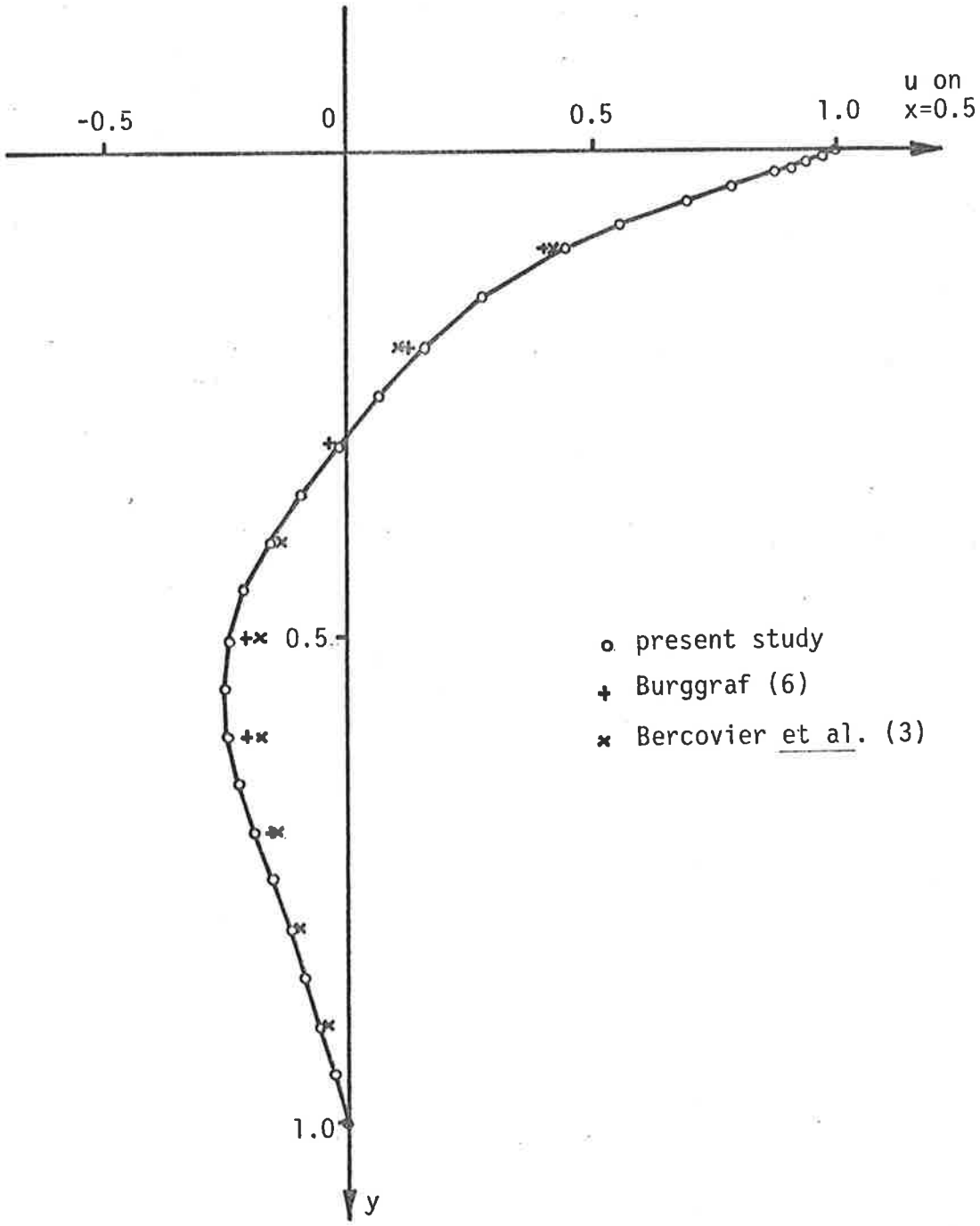

Figure 5.29(b) Variation of u Along x=0.5 for the Cavity Flow Problem at Re = 100.

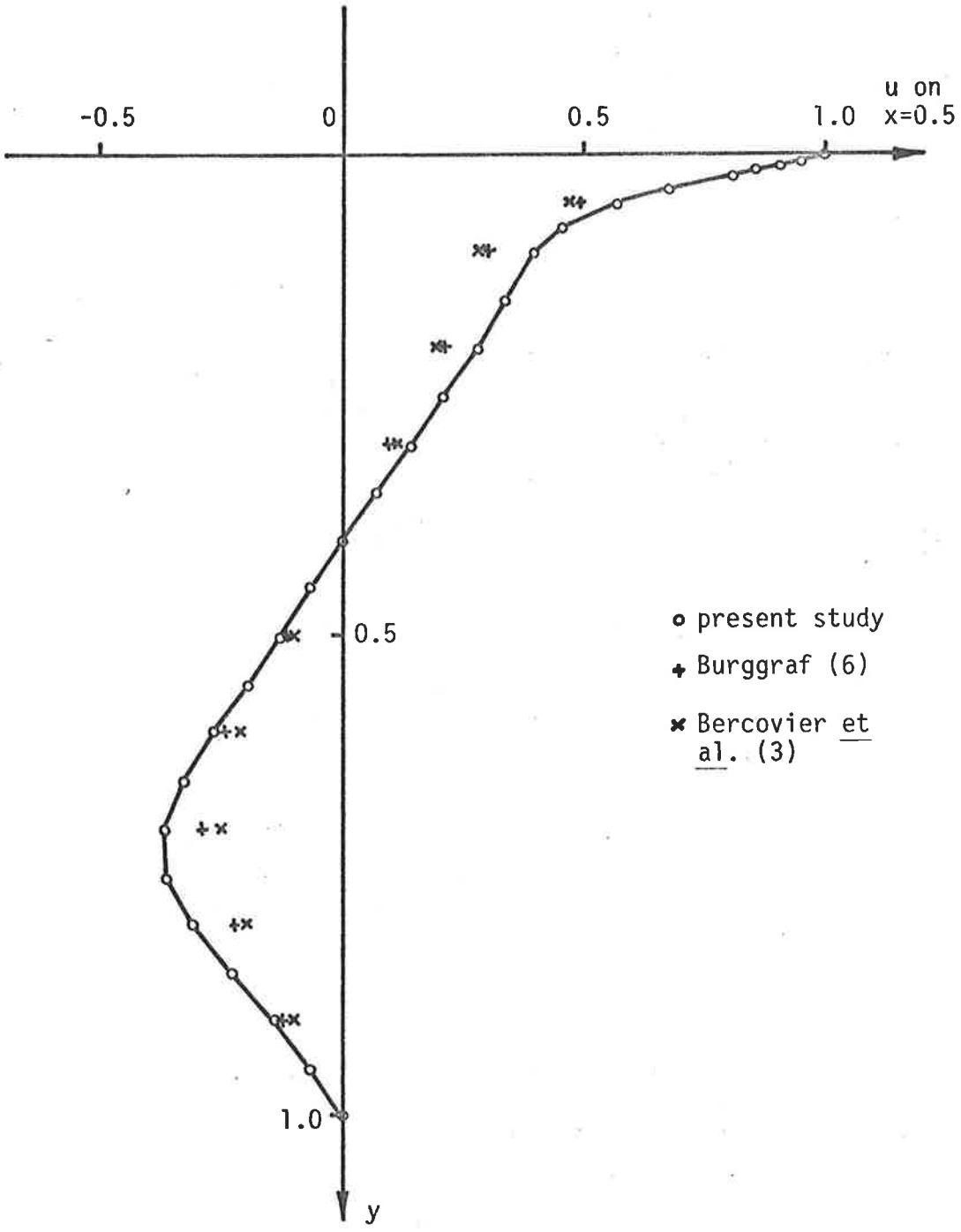

Figure 5.29(c) Variation of u Along x=0.5 for the Cavity Flow Problem at Re = 400.

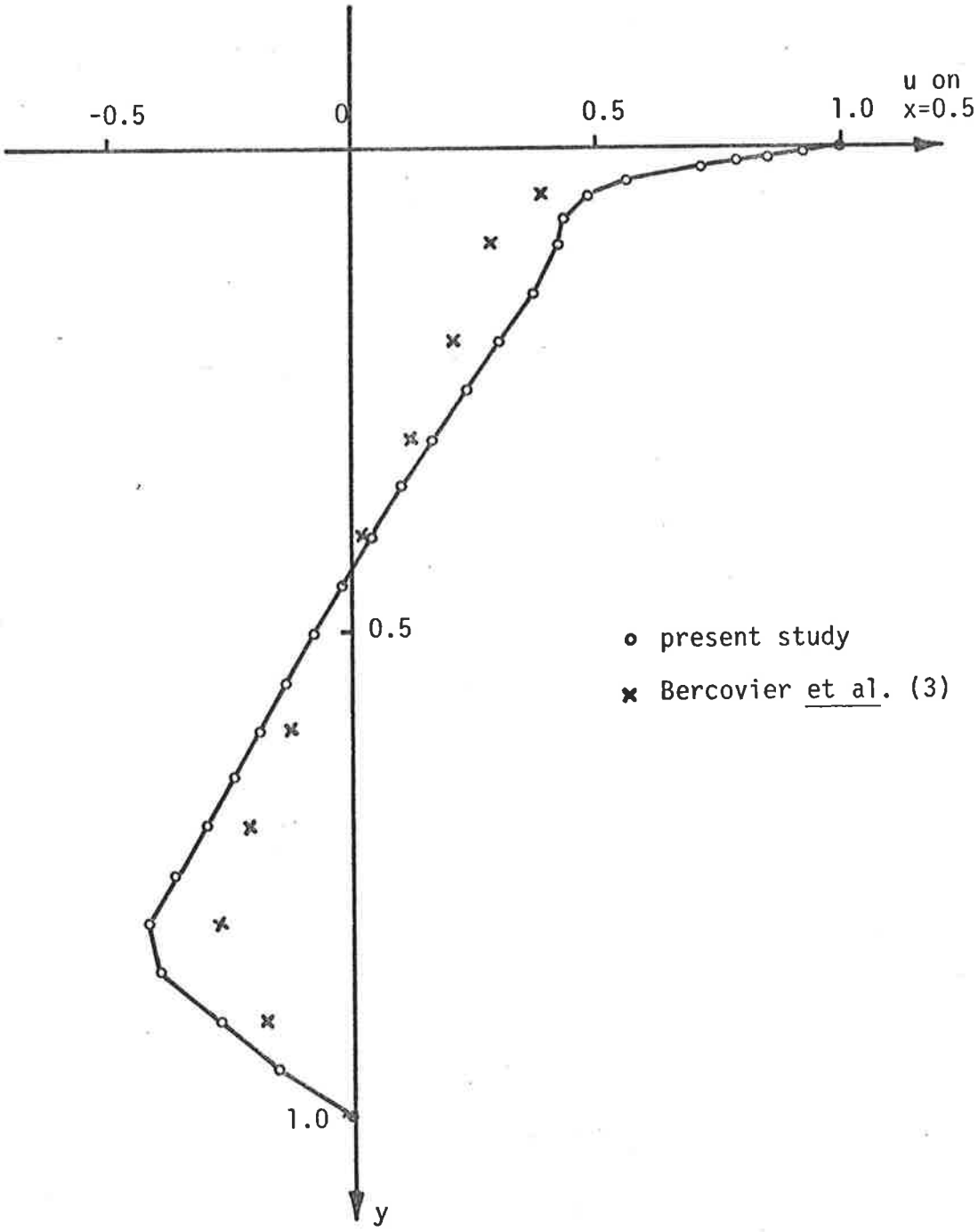

Figure 5.29(d) Variation of u Along x=0.5 for the Cavity Flow Problem at Re = 1000.

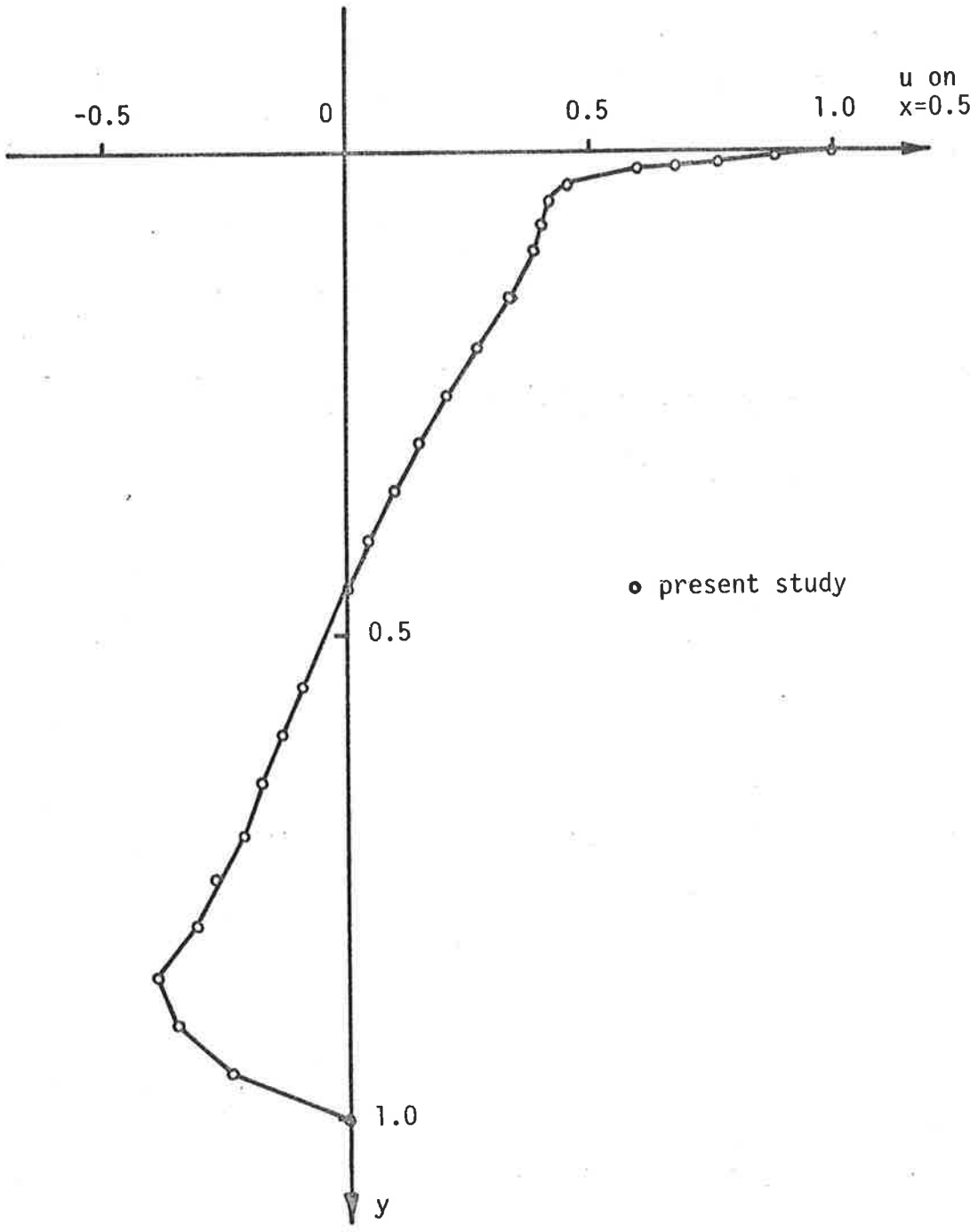

Figure 5.29(e) Variation of u Along x=0.5 for the Cavity Flow Problem at Re = 2000.

From the results of the various studies it can be seen that although the actual values of the x component of velocity along x=0.5 differ quite substantially, the shapes of the profiles are very similar. At low Reynolds numbers the profiles show that fluid particles at various distances from the vortex centre travel with different angular velocities. This means that viscous shear stresses must exist at all points in the flow and that the vortex is essentially viscous in nature. No boundary layers are discernible. At higher Reynolds numbers the central portion of the corresponding profile becomes linear indicating that at least in the vicinity of the vortex centre all fluid particles move with the same angular velocity. As a result there are no viscous shear stresses in this region and the core of the vortex is inviscid in character. The extent of the inviscid core increases with Reynolds number. At Re=2000 it covers approximately 80% of the total cavity area. The remainder is taken up by the boundary layers which exist on all four walls and in which are confined all the viscous effects. The nature of this flow is therefore consistent with that of all viscous flows. The viscous effects are always confined to relatively narrow regions called boundary layers and the thickness of these boundary layers always decreases as Reynolds number increases.

In order to see more clearly the shape of the vortex and how it changes with increasing Reynolds numbers, the velocity vector field for each of the five Reynolds number flows considered has been plotted in Figures 5.30(a) to (e). Figure 5.30(a) shows the vortex for the flow with Reynolds number equal to 1. The vortex centre is located on the centreline and relatively close to the moving wall. The bulk of the vortex is located in the top 70% of the cavity and the fluid in the lower and bottom corner regions undergoes relatively little or no motion. As Reynolds number increases, a shift of the vortex centre becomes clearly evident, first in the downstream direction and then

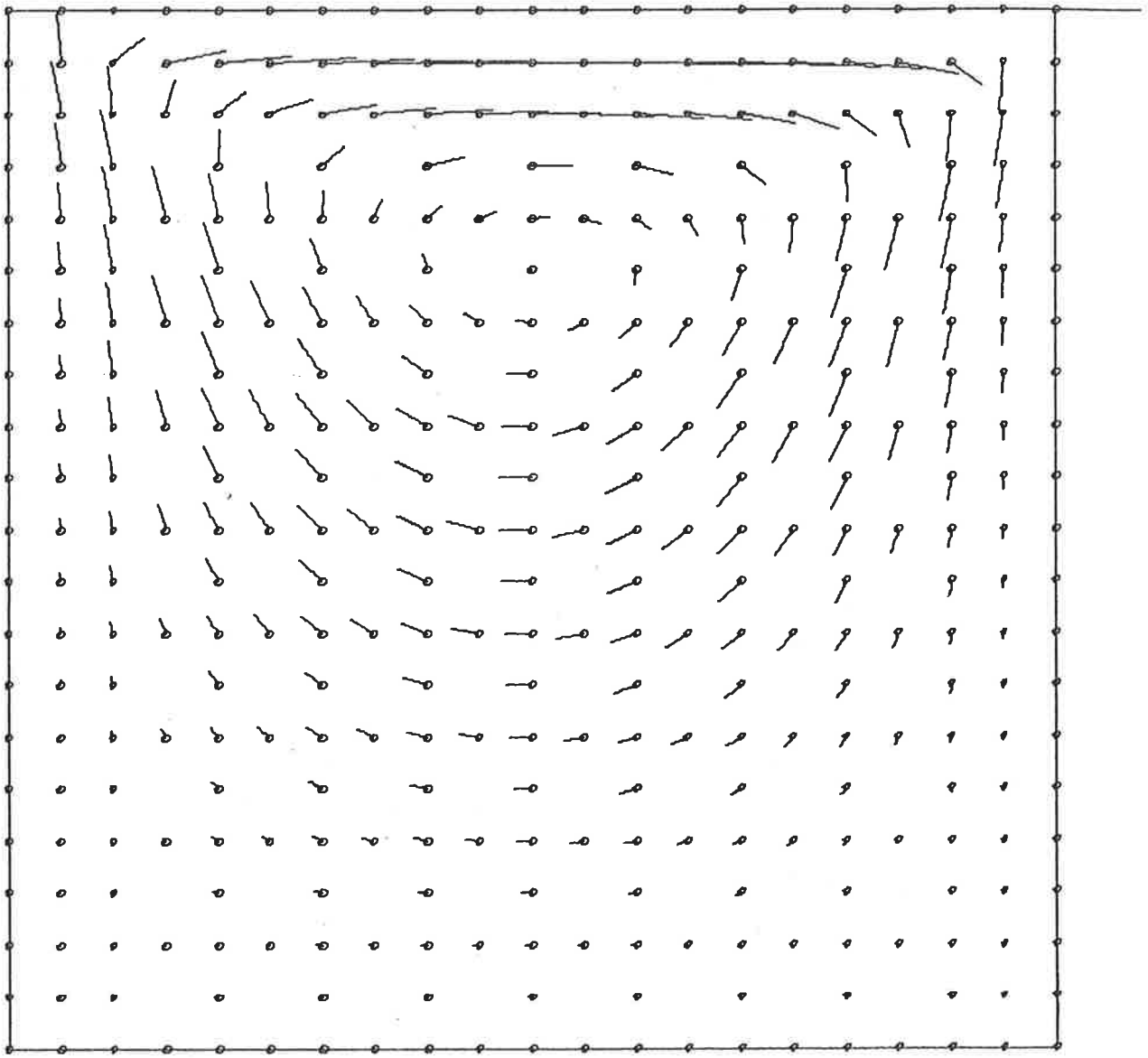

Figure 5.30(a) Velocity Vector Field for Re = 1.

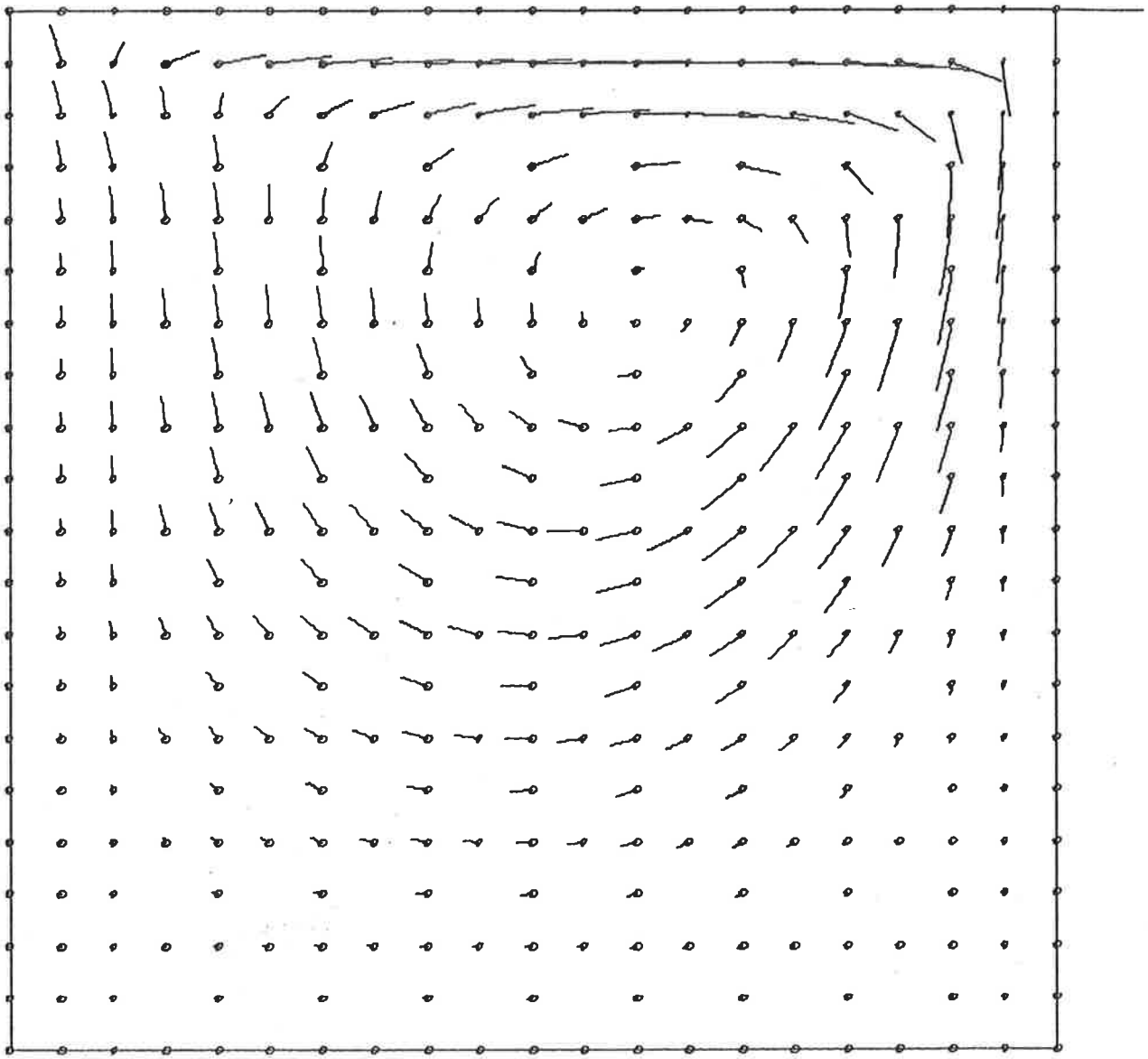

Figure 5.30(b) Velocity Vector Field for Re = 100.

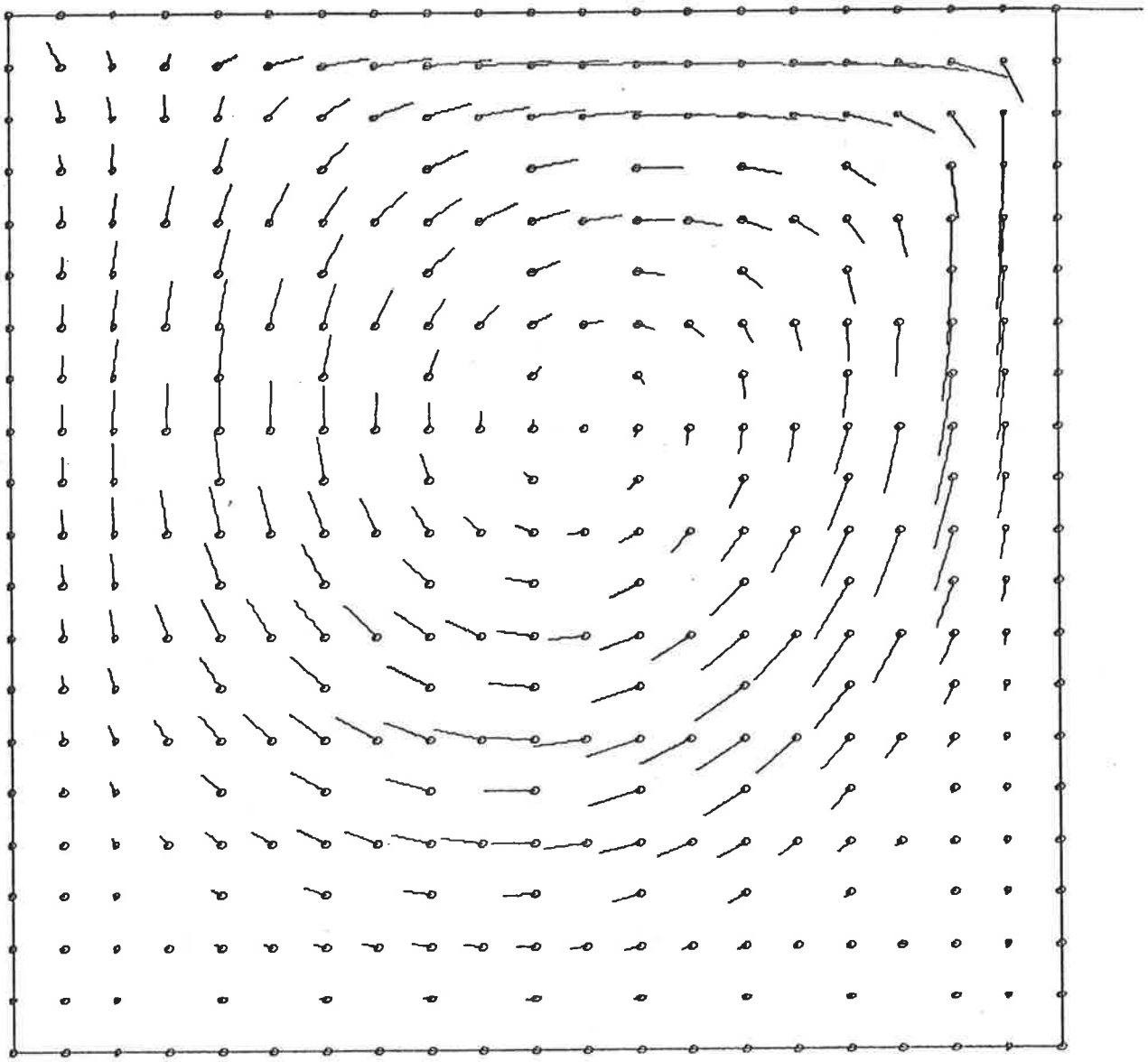

Figure 5.30(c) Velocity Vector Field for Re = 400.

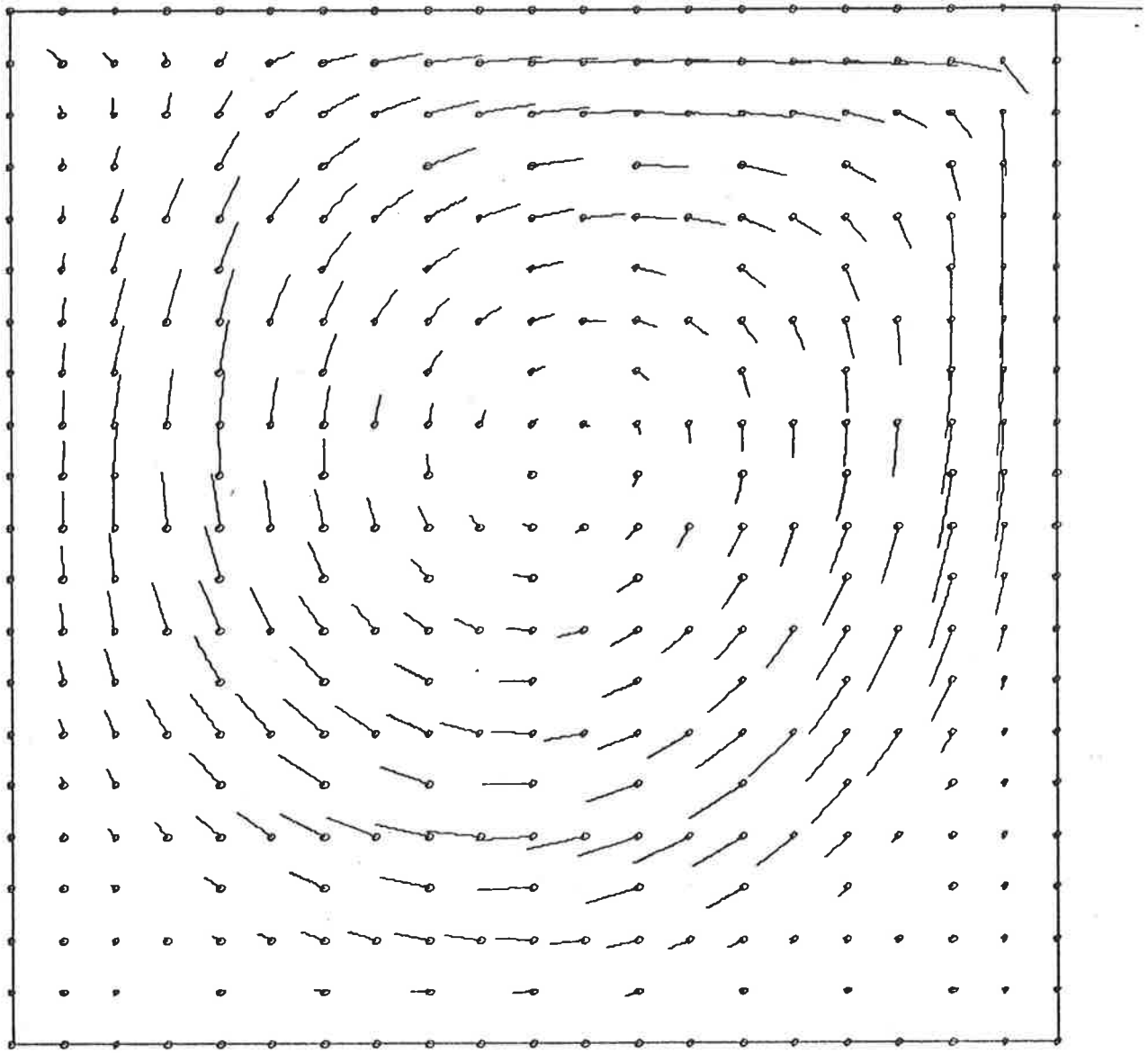

Figure 5.30(d) Velocity Vector Field for Re = 1000.

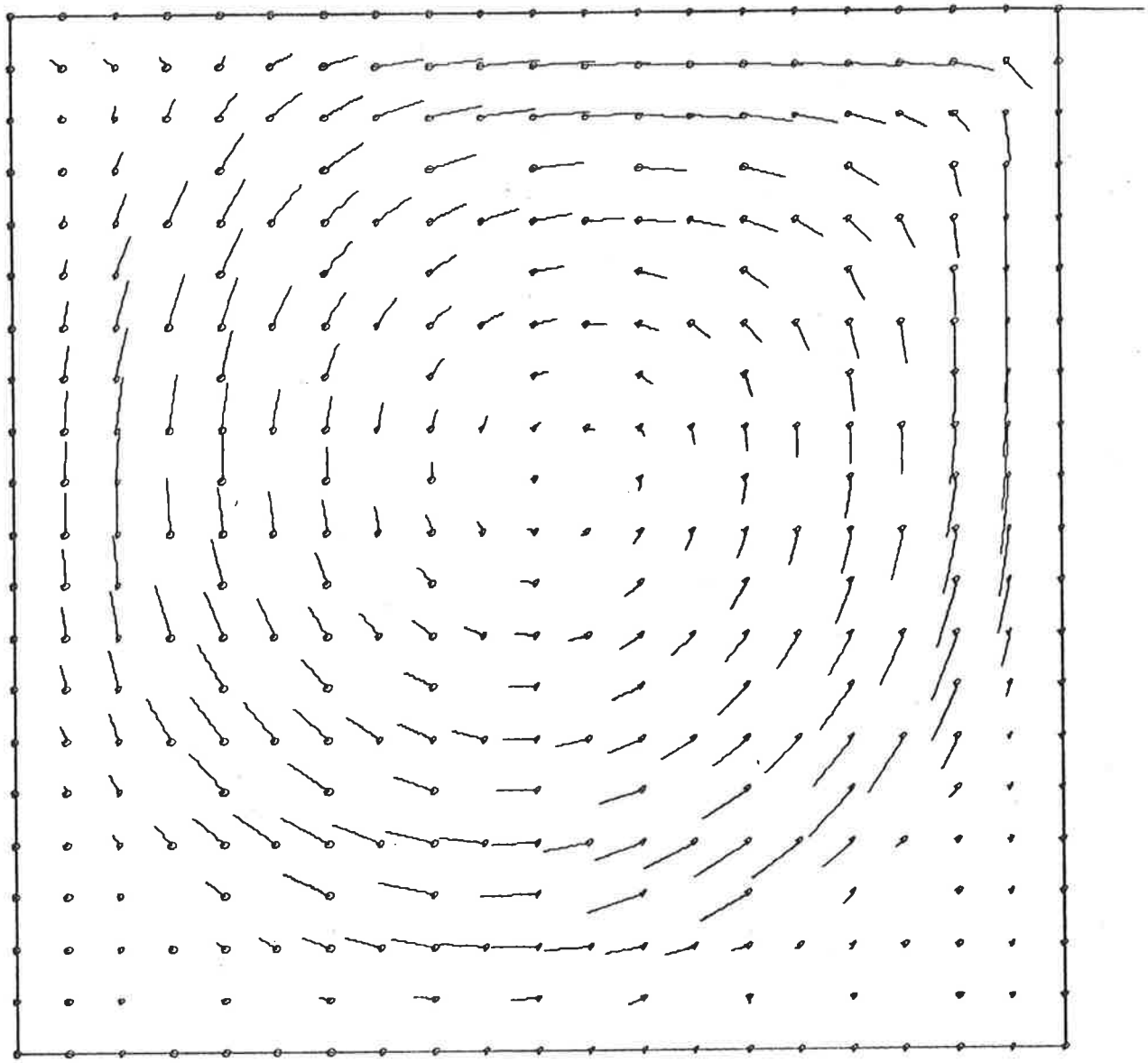

Figure 5.30(e) Velocity Vector Field for Re = 2000.

towards the centre of the cavity. Table 5.12 compares the locations of the vortex centre computed in this study for the five Reynolds numbers with similar results by Bercovier and Engelman (3), Burggraf (6) and Tuann and Olson (32). The agreement between solutions is quite acceptable with the maximum difference being 4%. This indicates that the vortex centre location is much less sensitive to the choice of solution procedure than were the centreline velocity profiles discussed earlier. The change in shape of the vortex with increasing Reynolds numbers is also clearly visible in Figures 5.30(a) to (e). At low Reynolds numbers the vortex is oval in shape, occupying only the upper regions of the cavity, but by Re=1000 it has become almost circular and extends throughout the cavity.

An interesting feature of the cavity flow is the growth of secondary vortices in the two bottom corners and the downstream top corner of the cavity. At low Reynolds numbers no secondary eddies were observed in the velocity fields calculated in this study. Burggraf (6) however stated that they should be present at all Reynolds numbers. Upon closer examination of the Re=1 flow this was found to be true but the extent of these secondary eddies was negligible compared to the size of the main vortex. At Reynolds number equals 400 the two bottom corner vortices are clearly defined and extend to approximately 5% of the cavity size on the upstream wall and 30% on the downstream wall. The third secondary vortex on the top downstream wall corner only appears at Reynolds number equals 2000, at which value the bottom two eddies have grown to 15% and 40% respectively. The presence of these secondary vortices is the main factor preventing the centre of the main vortex from reaching the centre of the cavity.

The final set of results that will be presented for the cavity flow problem is the contour plots of the pressure fields. These are shown in Figures 5.31(a) to (e) for Reynolds numbers 1, 100, 400, 1000

Re	Present Study	Bercovier et al. (3)	Burggraf (6)	Tuann et al. (32)
1	(0.502, 0.248)	-	-	-
100	(0.609, 0.283)	(0.62, 0.27)	(0.61, 0.26)	(0.63, 0.28)
400	(0.547, 0.396)	(0.57, 0.39)	(0.56, 0.37)	(0.55, 0.40)
1000	(0.529, 0.432)	(0.54, 0.44)	-	-
2000	(0.523, 0.444)	-	-	-

Table 5.12 Coordinates of the centre point ($\underset{\sim}{v}$=0) of the main vortex at various Reynolds numbers.

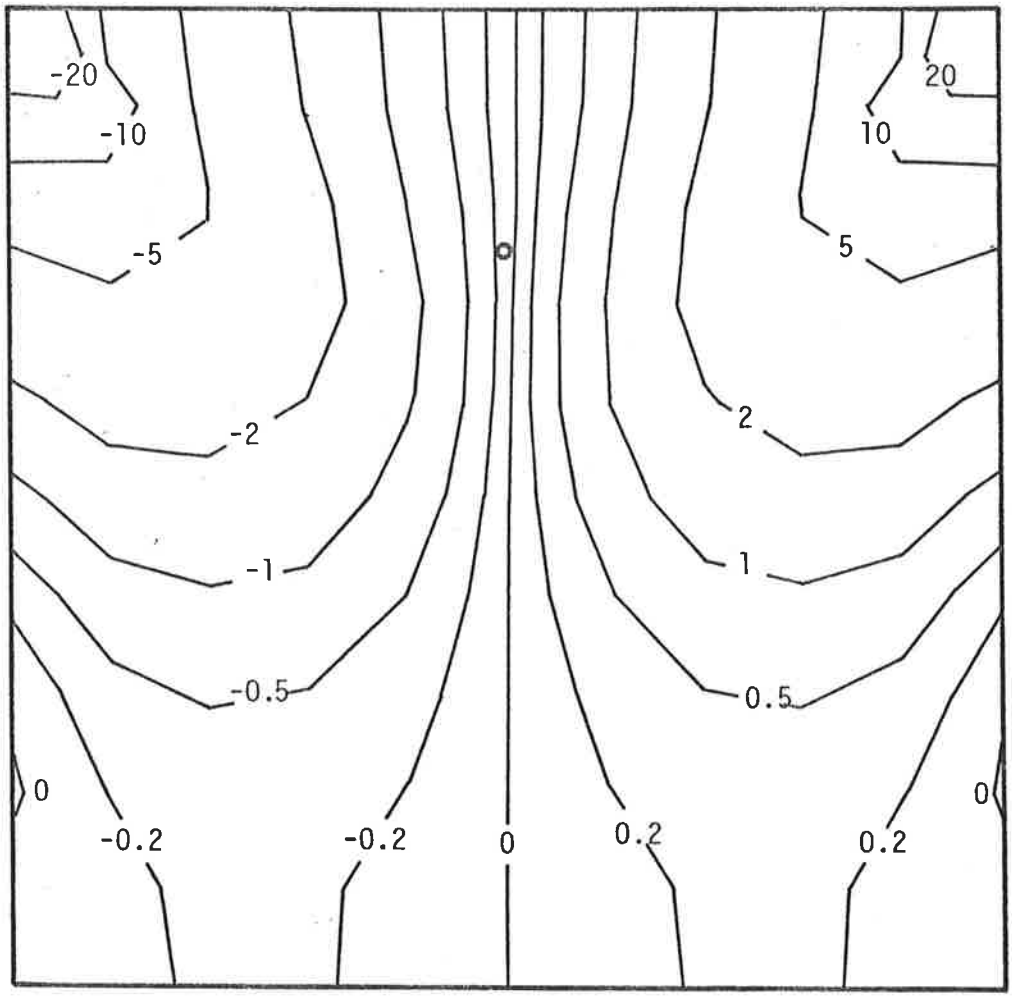

Figure 5.31(a) Pressure Contour Plot for Re = 1.

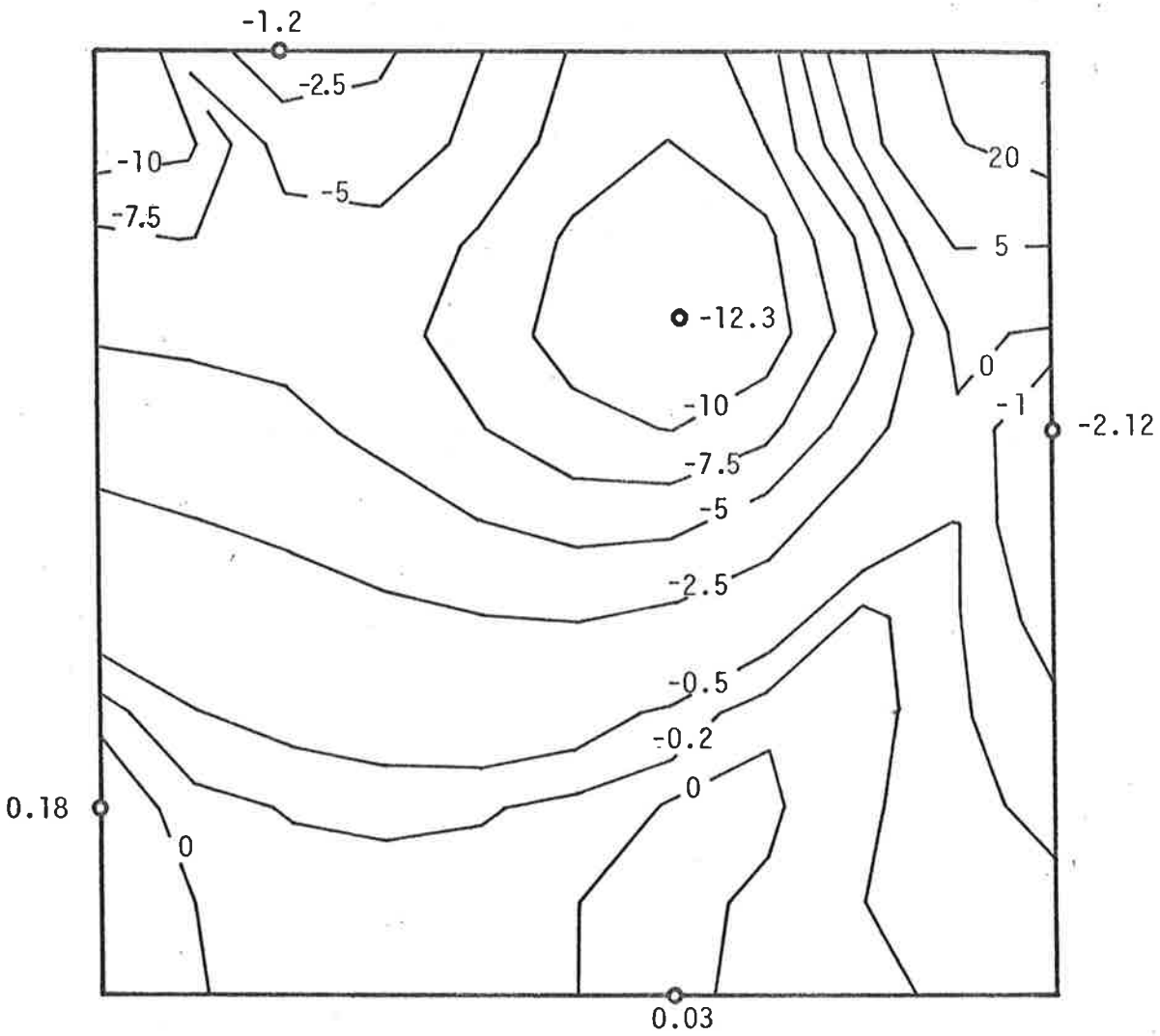

Figure 5.31(b) Pressure Contour Plot for Re = 100.

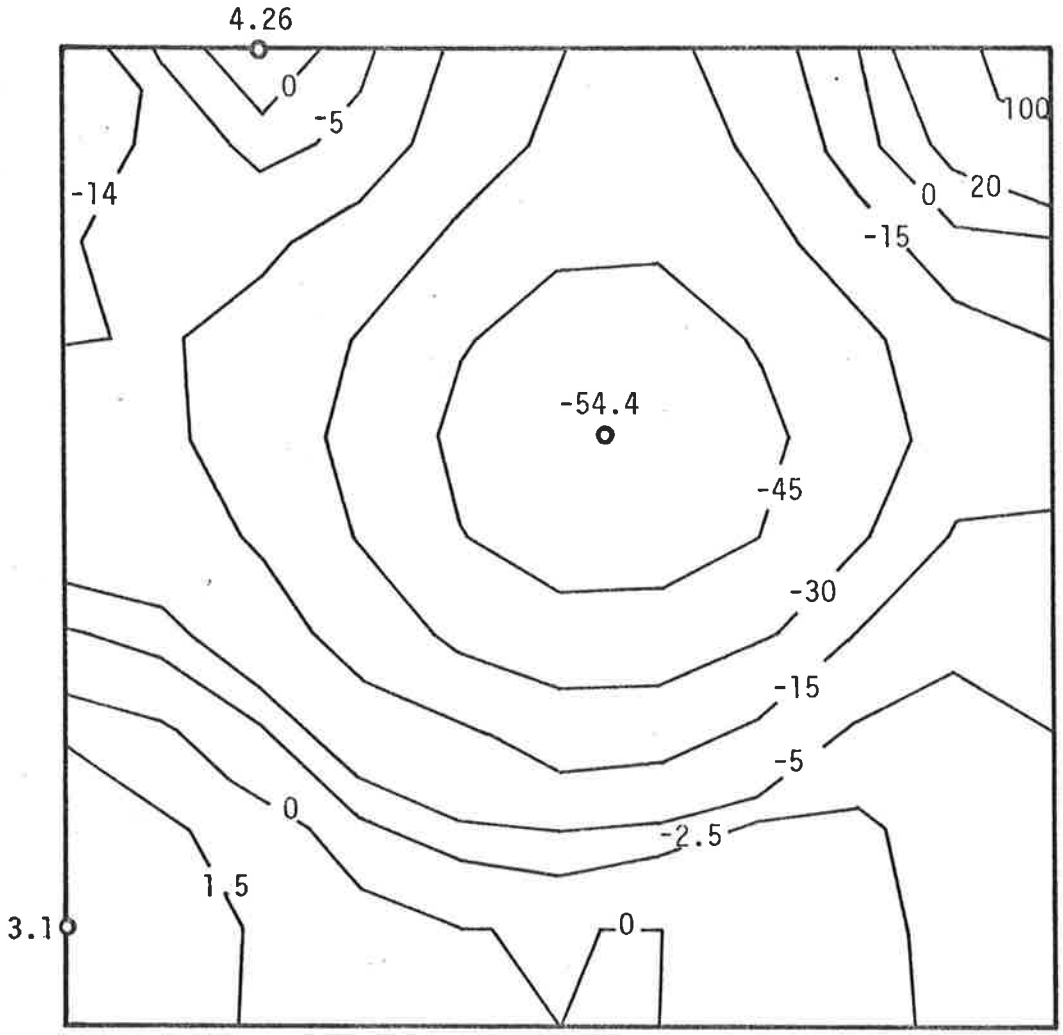

Figure 5.31(c) Pressure Contour Plot for Re = 400.

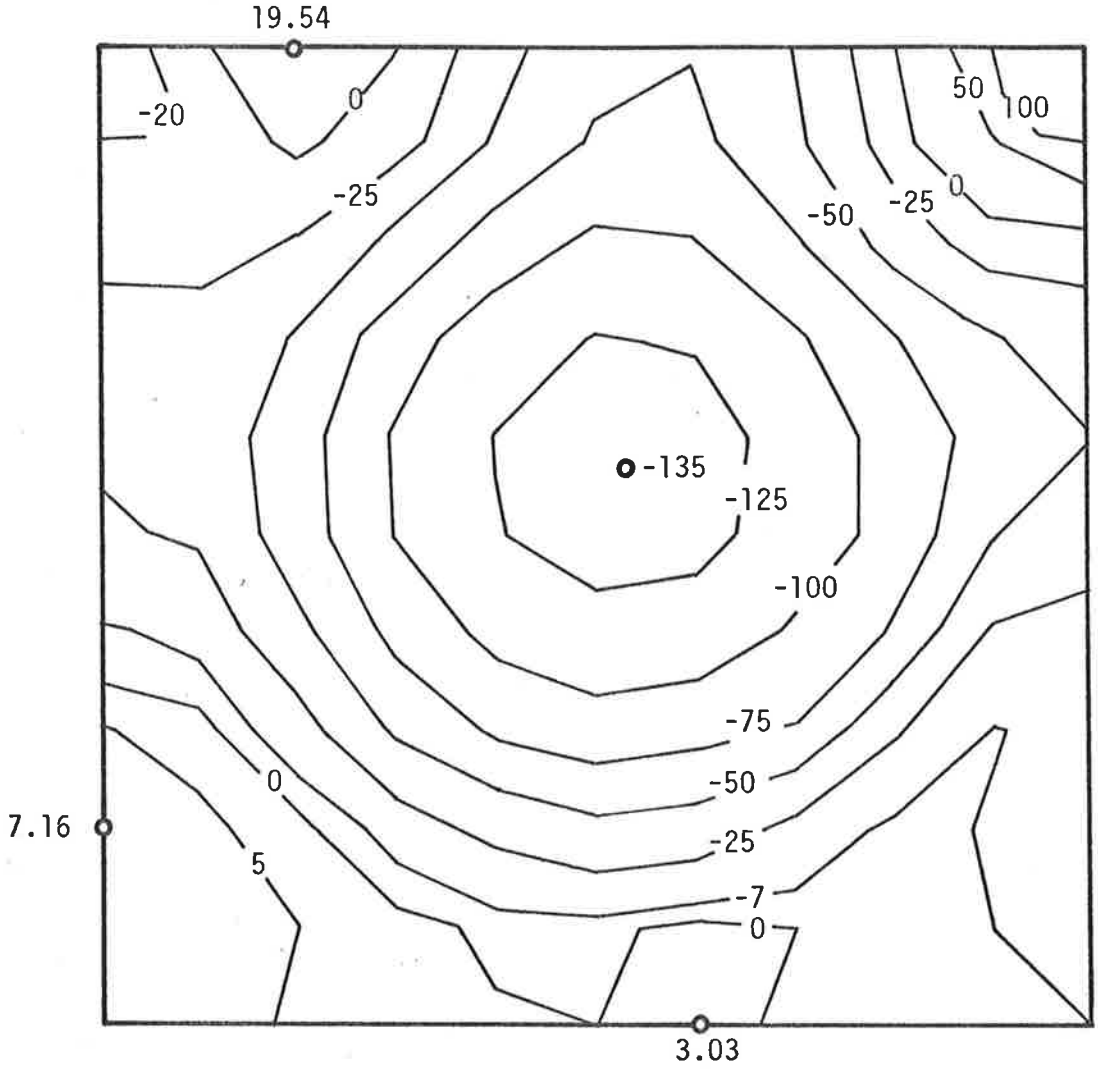

Figure 5.31(d) Pressure Contour Plot for Re = 1000.

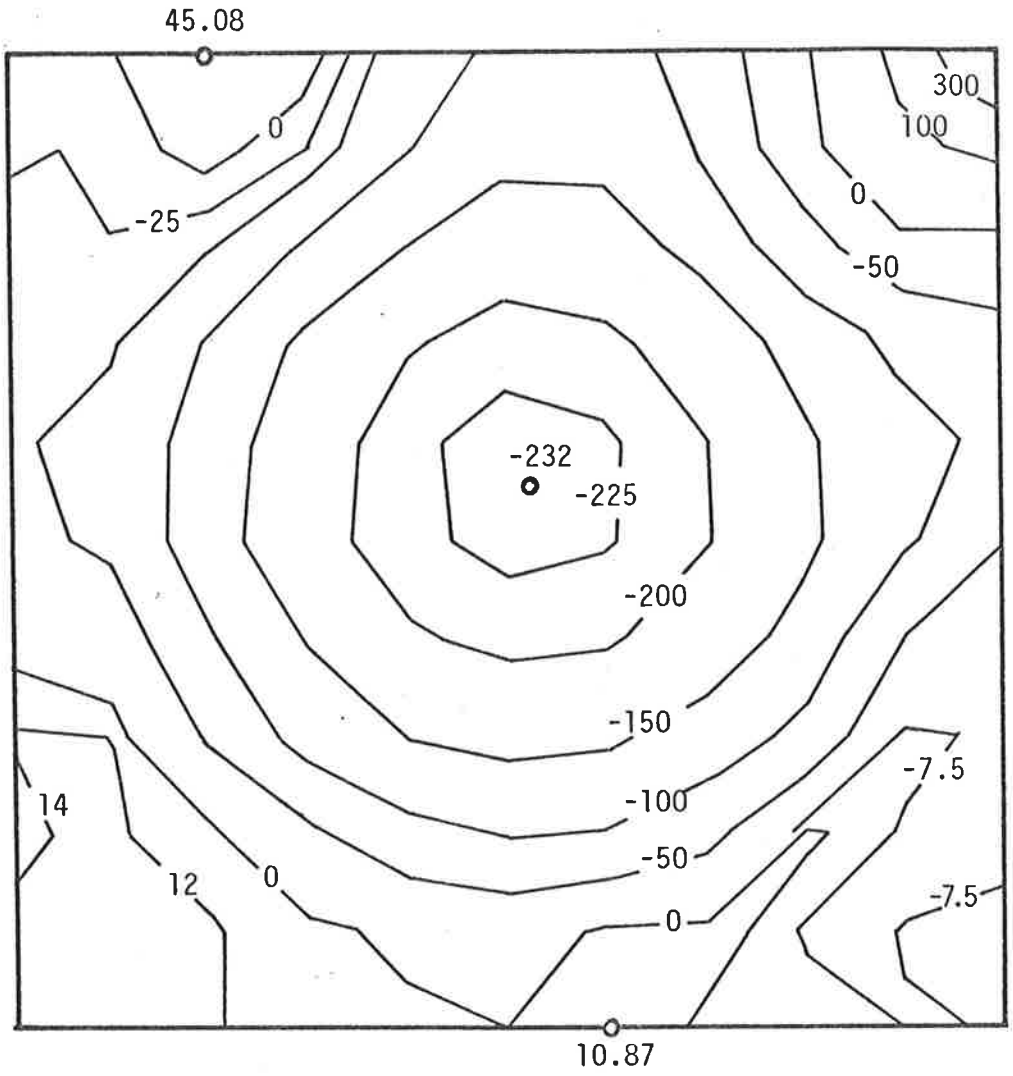

Figure 5.31(e) Pressure Contour Plot for Re = 2000.

and 2000 respectively. The pressure contour plots obtained by other researchers match those of this study quite satisfactorily. However, the magnitude of the pressure at the vortex centre varies widely between researchers. The reason for this is partly due to the fact that different zero pressure reference points were used. Where the same pressure datum was adopted, however, the various studies have all still produced vortex centre pressures that are very different. The pressure results that have been presented here therefore have not been compared with any of the other published solutions.

This completes the presentation of the two-dimensional results and the two-dimensional analyses.

CHAPTER 6

ANALYSES IN THREE DIMENSIONS

6.1 Extension of Two-dimensional Comparisons Results to Three Dimensions

6.2 Details of Three-dimensional Flow Problems

6.3 Results of Three-dimensional Analyses

6. ANALAYSES IN THREE DIMENSIONS

Having completed the first two stages of this study, namely the determination of the optimal finite element formulation of the Navier-Stokes equations and the determination of the more suitable of the two quadrilateral isoparametric elements considered in two dimensions, the final part of the research was undertaken. This involved the extension to three dimensions, of the findings of the above two-dimensional analyses, and then an investigation to determine the suitability of this proposed arrangement for solving a general three-dimensional viscous flow problem. This chapter is used to present and discuss all aspects of this final stage of the research program. The finite element equations and the isoparametric element that were used in the three-dimensional analyses are described in Section 6.1. Sections 6.2 and 6.3 give full details of firstly, the flow problems considered including all mesh configurations and boundary conditions used, and secondly, the results of the analyses of these problems, including a discussion of the difficulties encountered in solving them.

6.1 Extension of Two-dimensional Comparisons Results to Three Dimensions

In Section 5.4 it was shown that, in two dimensions, formulation B of the Navier-Stokes equations is the most efficient and accurate of the four formulations considered. By assuming that the four formulations have similar characteristics in three dimensions, it was decided to use formulation B of the three-dimensional Navier-Stokes equations exclusively in this final section of the research. Therefore the finite element equations, at element level, that are used in the three-dimensional analyses are:

$$\int_{V_i} \frac{1}{Re} \{ \left(\frac{\partial N'_{ij}}{\partial x} \frac{\partial u_i^*}{\partial x} + \frac{\partial N'_{ij}}{\partial y} \frac{\partial u_i^*}{\partial y} + \frac{\partial N'_{ij}}{\partial z} \frac{\partial u_i^*}{\partial z} \right) + \left(\frac{\partial N'_{ij}}{\partial x} \frac{\partial u_i^*}{\partial x} + \frac{\partial N'_{ij}}{\partial y} \frac{\partial v_i^*}{\partial x} + \frac{\partial N'_{ij}}{\partial z} \frac{\partial w_i^*}{\partial x} \right) \}$$

$$- \frac{\partial N'_{ij}}{\partial x} p_i^* + N'_{ij} \left(u_i^* \frac{\partial u_i^*}{\partial x} + v_i^* \frac{\partial u_i^*}{\partial y} + w_i^* \frac{\partial u_i^*}{\partial z} \right) dV$$

$$= \int_{S_i} N'_{ij} \{ \sigma^*_{xx} n_x + \sigma^*_{yx} n_y + \sigma^*_{zx} n_z \} \, dS \qquad 6.1.1$$

$$\int_{V_i} \frac{1}{Re} \{ \left(\frac{\partial N'_{ij}}{\partial x} \frac{\partial v_i^*}{\partial x} + \frac{\partial N'_{ij}}{\partial y} \frac{\partial v_i^*}{\partial y} + \frac{\partial N'_{ij}}{\partial z} \frac{\partial v_i^*}{\partial z} \right) + \left(\frac{\partial N'_{ij}}{\partial x} \frac{\partial u_i^*}{\partial y} + \frac{\partial N'_{ij}}{\partial y} \frac{\partial v_i^*}{\partial y} + \frac{\partial N'_{ij}}{\partial z} \frac{\partial w_i^*}{\partial y} \right) \}$$

$$- \frac{\partial N'_{ij}}{\partial y} p_i^* + N'_{ij} \left(u_i^* \frac{\partial v_i^*}{\partial x} + v_i^* \frac{\partial v_i^*}{\partial y} + w_i^* \frac{\partial v_i^*}{\partial z} \right) dV$$

$$= \int_{S_i} N'_{ij} \{ \sigma^*_{xy} n_x + \sigma^*_{yy} n_y + \sigma^*_{zy} n_z \} \, dS \qquad 6.1.2$$

$$\int_{V_i} \frac{1}{Re} \{ \left(\frac{\partial N'_{ij}}{\partial x} \frac{\partial w_i^*}{\partial x} + \frac{\partial N'_{ij}}{\partial y} \frac{\partial w_i^*}{\partial y} + \frac{\partial N'_{ij}}{\partial z} \frac{\partial w_i^*}{\partial z} \right) + \left(\frac{\partial N'_{ij}}{\partial x} \frac{\partial u_i^*}{\partial z} + \frac{\partial N'_{ij}}{\partial y} \frac{\partial v_i^*}{\partial z} + \frac{\partial N'_{ij}}{\partial z} \frac{\partial w_i^*}{\partial z} \right) \}$$

$$- \frac{\partial N'_{ij}}{\partial z} p_i^* + N'_{ij} \left(u_i^* \frac{\partial w_i^*}{\partial x} + v_i^* \frac{\partial w_i^*}{\partial y} + w_i^* \frac{\partial w_i^*}{\partial z} \right) dV$$

$$+ \int_{S_i} N'_{ij} \{ \sigma^*_{xz} n_x + \sigma^*_{yz} n_y + \sigma^*_{zz} n_z \} \, dS \qquad 6.1.3$$

for $j=1, \ldots K'$

and

$$- \int_{V_i} N''_{ij} \left\{ \frac{\partial u_i^*}{\partial x} + \frac{\partial v_i^*}{\partial y} + \frac{\partial w_i^*}{\partial z} \right\} dV = 0 \qquad 6.1.4$$

for $j=1, \ldots K''$

where

$$u_i^* = \sum_{k=1}^{K'} u_{ik} N'_{ik}$$

$$v_i^* = \sum_{k=1}^{K'} v_{ik} N'_{ik}$$

$$w_i^* = \sum_{k=1}^{K'} w_{ik} N'_{ik}$$

and

$$p_i^* = \sum_{k=1}^{K''} p_{ik} N''_{ik} \quad \text{for } i=1, \ldots Ne$$

where N'_{ik} and N''_{ik} are the velocity and pressure shape functions at node k, u_{ik}, v_{ik}, w_{ik} and p_{ik} are the unknown nodal values for the x, y and z components of velocity and the pressure at node k in element i and K' and K" are the number of velocity and pressure nodes respectively in the three-dimensional finite element chosen to represent the three-dimensional fluid motion.

In Section 5.5 it was shown that the Serendipity and Lagrangian elements are both equally suitable for the analysis of two-dimensional viscous flows. For three-dimensional flows however, it was decided to use the twenty noded Serendipity element rather than the twenty-seven noded Lagrangian. This is because it was realized that in three dimensions, the Lagrangian element would need a much larger field length to hold and execute its program than was found in the two-dimensional analyses. The reason is quite simple. In two dimensions the Lagrangian element has only one additional internal node. At element level the two velocity equations corresponding to this node, there being no pressure equation at an internal node, are eliminated using the Gaussian elimination procedure. The reduced stiffness matrix for a Lagrangian element then becomes the same size as that for an identical Serendipity element, that is 20x20. Consequently, the overall front width of a problem is the same regardless of which element is used.

In three dimensions however, the Lagrangian element has six additional mid-face nodes and one additional internal node. Corresponding to each of these nodes are three velocity equations only, since there is no pressure equation corresponding to internal or mid-face nodes. Therefore, at element level the three velocity equations corresponding to the internal node can be reduced out, but the three equations corresponding to each of the six mid-face nodes must remain in the element equation system. As a consequence, the reduced element stiffness matrix for a Lagrangian element remains much larger than that for an identical Serendipity element. In fact, its size is 86x86 compared with 68x68, an increase of 60%. Also, as a result of not being able to eliminate the equations corresponding to the mid-face nodes, the front width of a problem would also be significantly higher when the Lagrangian element is used. This is illustrated by the example in Figure 6.1 in which is shown a three-dimensional mesh with a three element by three element cross-section. If the twenty noded Serendipity element is used the front width would equal 196 in contrast with 244 if the twenty-seven noded Lagrangian is used. Therefore, since it was anticipated that computer storage would limit the size of finite element mesh that can be employed even with the more efficient program CR3DVF2, the twenty noded Serendipity element was used exclusively in all the three-dimensional analyses.

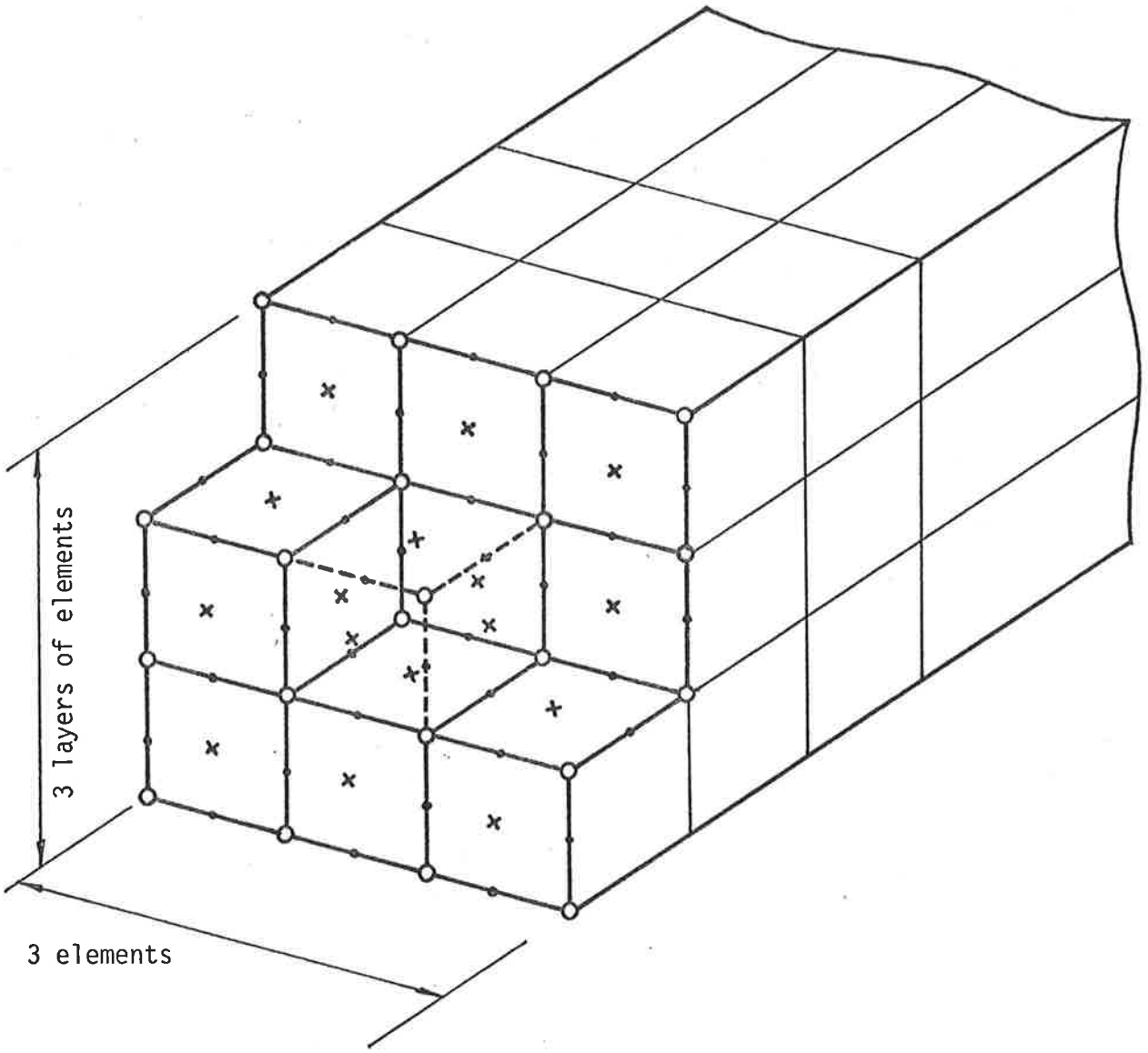

- **o** nodes corresponding to which are three velocity and one pressure equations (same for both Serendipity and Lagrangian elements). Twenty two nodes, eighty eight equations.
- **•** nodes corresponding to which are three velocity equations only (same for both elements).
  Thirty six nodes, one hundred and eight equations.
- **×** nodes corresponding to which are three velocity equations only (Lagrangian element only).
  Sixteen nodes, forty eight equations.

Figure 6.1 Typical Three-dimensional Finite Element Mesh.

6.2 Details of Three-dimensional Flow Problems

In this final section of the research, an attempt was made to solve three different three-dimensional viscous flow problems, each one relatively more complex than the previous. The first of these involved the evaluation of the velocity and pressure fields in a fluid moving between two infinite parallel plates under the action of a pressure gradient; that is, the Poiseuille flow in three dimensions. This problem was used primarily to check and test the operation of the three-dimensional computer package CR3DVF2. The actual dimensionless problem that was solved was set up by non-dimensionalizing the original problem using the distance between the plates, d, and the mean cross-sectional velocity, $\bar{v}$. The resulting Reynolds number is

$$Re = \frac{\rho \bar{v} d}{\mu}$$

Several planes of symmetry were also used to reduce the region to be analysed to the smallest possible. The dimensionless flow that was actually solved extended one unit in the direction of the pressure gradient and half a unit in the other two perpendicular directions.

The second flow problem to be treated was the fully developed flow in a duct of arbitrary cross-section and moving under the action of a pressure gradient. However, because the geometry of the flow region had to be defined beforehand in order to construct a finite element mesh for it, the shape of the duct had to be fixed. The cross-section that was finally selected was square with the width and depth of the duct both equal to a. Symmetry about the vertical and horizontal mid-planes was used to reduce the flow region to be analysed to a quarter of the duct cross-section. The problem was then non-dimensionalized by using the width of the duct, a, and the mean cross-sectional velocity $\bar{v}$, as the characteristic length and velocity respectively. The resulting Reynolds number is

$$Re = \frac{\rho \bar{v} a}{\mu}$$

As with the first flow problem, the actual dimensionless flow that was solved extended one unit in the direction of the pressure gradient and half a unit in the other two perpendicular directions.

For both the first and the second flow problem considered, exact analytical solutions were known and were readily available. The accuracy of the numerical solutions obtained in this study for these two problems could therefore be very easily determined and assessed. The third flow problem that was analysed however was considerably more complicated than the previous two and did not have a known exact analytical solution. It involved the calculation of the velocity and pressure fields in a developing flow in the entrance region of a square duct, with width and depth equal to a. The velocity distribution at the entrance face was specified to be constant and equal to $\bar{v}$, while the normal stress at the exit face was specified to be equal to the outlet pressure which was conveniently assumed to be uniformly zero. The velocities at the entrance and exit faces were further constrained so that the fluid entered and left the duct parallel to its axis. The same planes of symmetry that were used in the previous problem were again used in this case and the region of flow that was to be analysed was reduced to the same quarter duct. Non-dimensionalizing was also carried out in the same fashion and the Reynolds number for this flow was defined as

$$Re = \frac{\rho \bar{v} a}{\mu}$$

The actual dimensionless problem that was solved again extended one unit in the direction of the duct and half a unit in the other two perpendicular directions, with the dimensionless inlet velocity equalling one.

Because an estimate of the required development length for a duct of this type was not available, it was decided to use a mesh of unit length and to start with Reynolds number equal to 1. At this low value of Re it was anticipated that a length of one would be adequate to enable the square duct flow to become fully developed by the time it reached the exit face. Since the fully developed velocity profile for a square duct was also not known, it was assumed that the flow became fully developed when the axial velocity along the axis of the duct reached 99% of its asymptotic value. Having obtained a solution at this Reynolds number, it would then be possible to estimate the maximum value of Re that could be treated with the same unit length mesh.

From the above discussion it can be seen that the region of flow that is analysed in each of the three problems is of the same size. This was arranged so that several different meshes could be used to analyse each of the flows without having to redefine the mesh geometry or the element and nodal configurations. Figure 6.2 shows the five meshes and the number of elements and nodes that were used to solve the above flow problems. Meshes M1, M2, M3 and M4 were used to solve the Poiseuille flow, meshes M3 and M4 were used to analyse the fully developed square duct flow and mesh M5 was used to solve the developing flow in the entrance region of a square duct. The only one of these meshes that needs any further comment is M5. In setting up this mesh for the developing duct flow, the same aspects of the flow that were taken into account when meshes ENFLM1 and ENFLM2 were constructed for the two-dimensional entrance flow, were again considered here. Accordingly, a thin layer of elements was located at the entrance face and next to the two walls in the quarter duct. This arrangement of elements enabled the uniform inlet velocity profile to be specified sufficiently close to the start of the duct and allowed the boundary layers which exist on the duct walls, to be represented as accurately as possible. Only

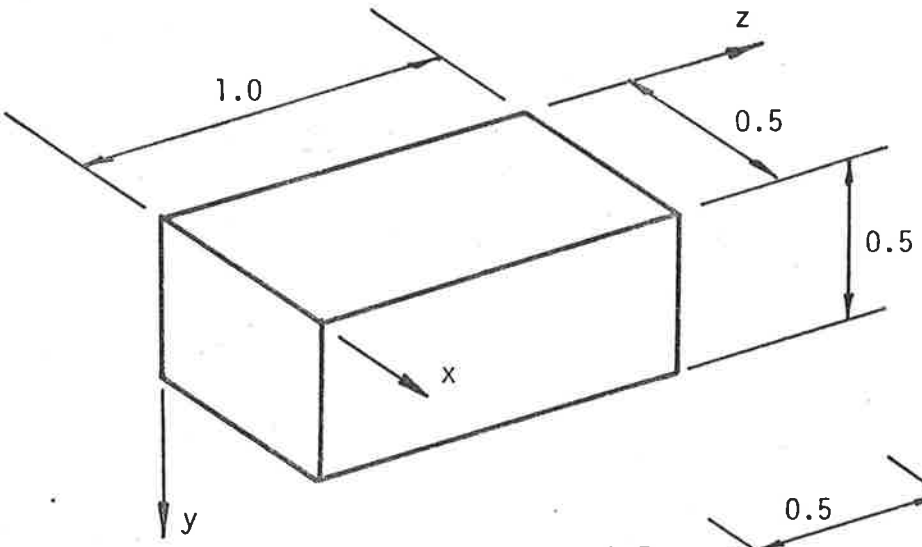

Mesh M1
1 element
20 nodes

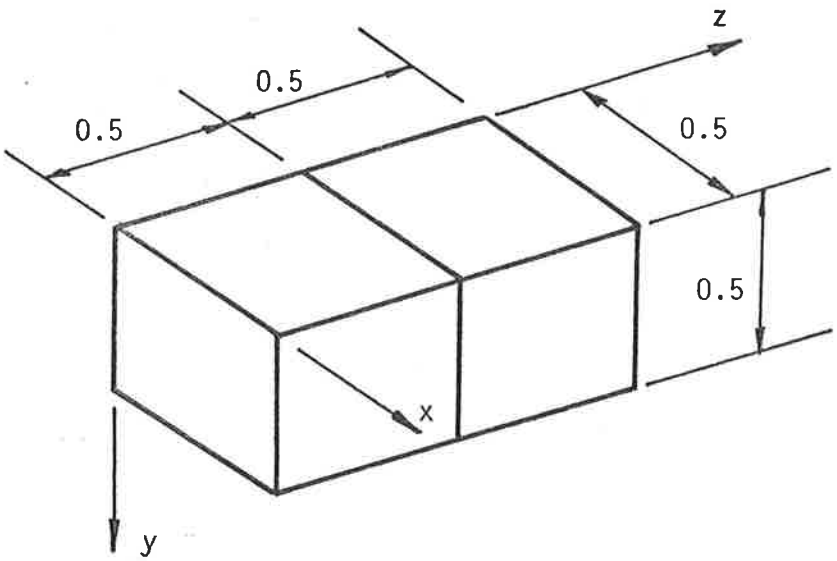

Mesh M2
2 elements
32 nodes

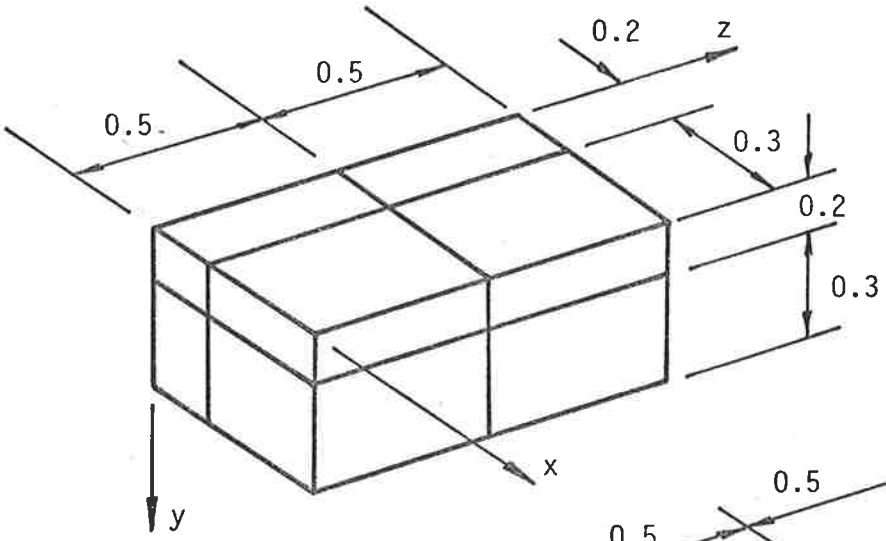

Mesh M3
8 elements
81 nodes

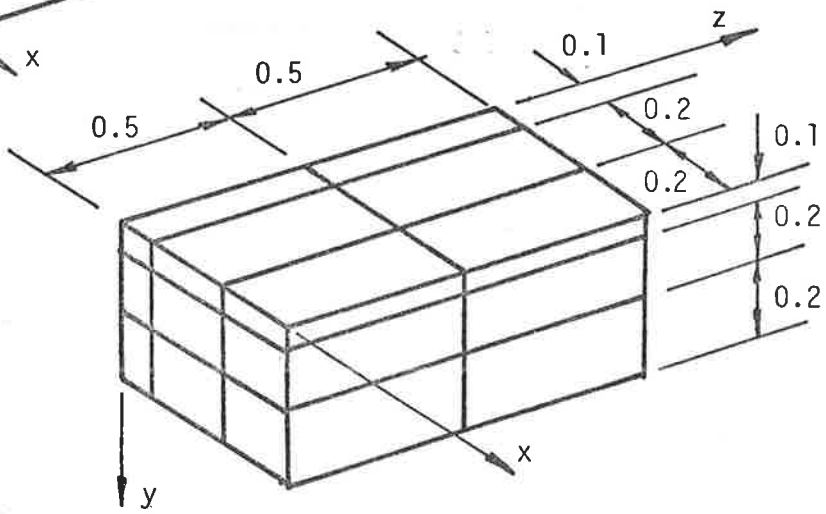

Mesh M4
18 elements
152 nodes

Continued

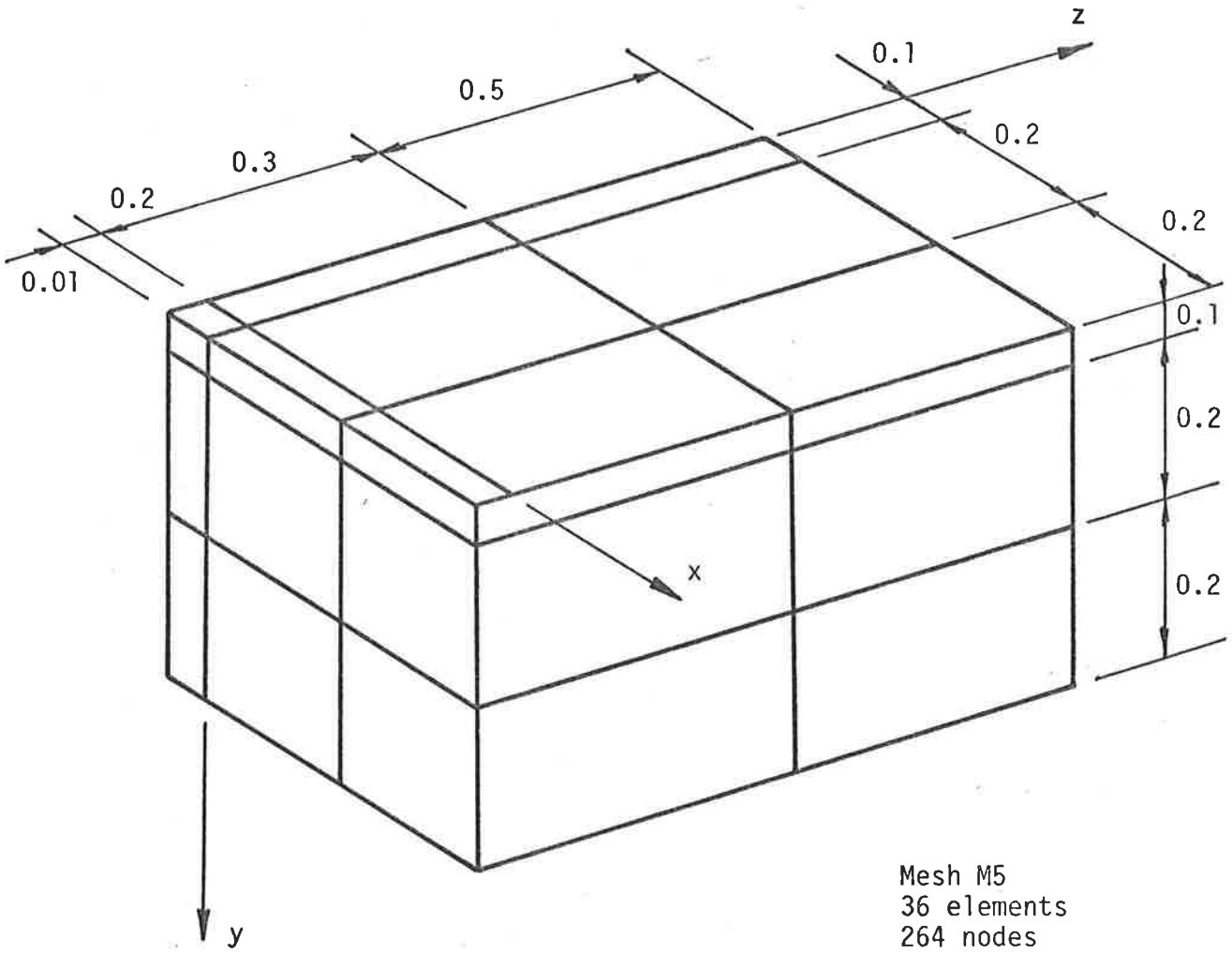

Figure 6.2 Details of Meshes M1, M2, M3, M4 and M5.

a 3x3x4 element mesh was used for the analysis of the developing duct flow because any additional elements would have made the problem too large for it to be solved relatively quickly with the computing facilities available for this study.

It will be noted that all five meshes are composed entirely of regular rectangular-sided "brick" elements. Apart from the fact that this arrangement is the simplest to set up and the easiest to visualize, the main reason that only this type of element was used is because the Serendipity element interpolation was chosen for the three-dimensional analyses. In two dimensions it was found that non-rectangular elements led to small but existent errors when the Serendipity element was used, but gave the exact solution when rectangular elements were used. Assuming the behaviour is analogous in three dimensions, then because the Serendipity rather than the Lagrangian element interpolation was to be used, all meshes were composed entirely of regular rectangular-sided elements so as to minimize any error associated with the incomplete quadratic velocity interpolation inherent in the Serendipity element.

The boundary conditions that were applied in each of the three problems regardless of which mesh was used, are shown in detail in Figure 6.3. It will be noticed that in all three cases the pressure is specified at one node, it being anticipated that this is all that is required to enable the pressure field to be evaluated. With these boundary conditions and the five finite element meshes, several runs were carried out and the results of these runs are described and discussed in the next section.

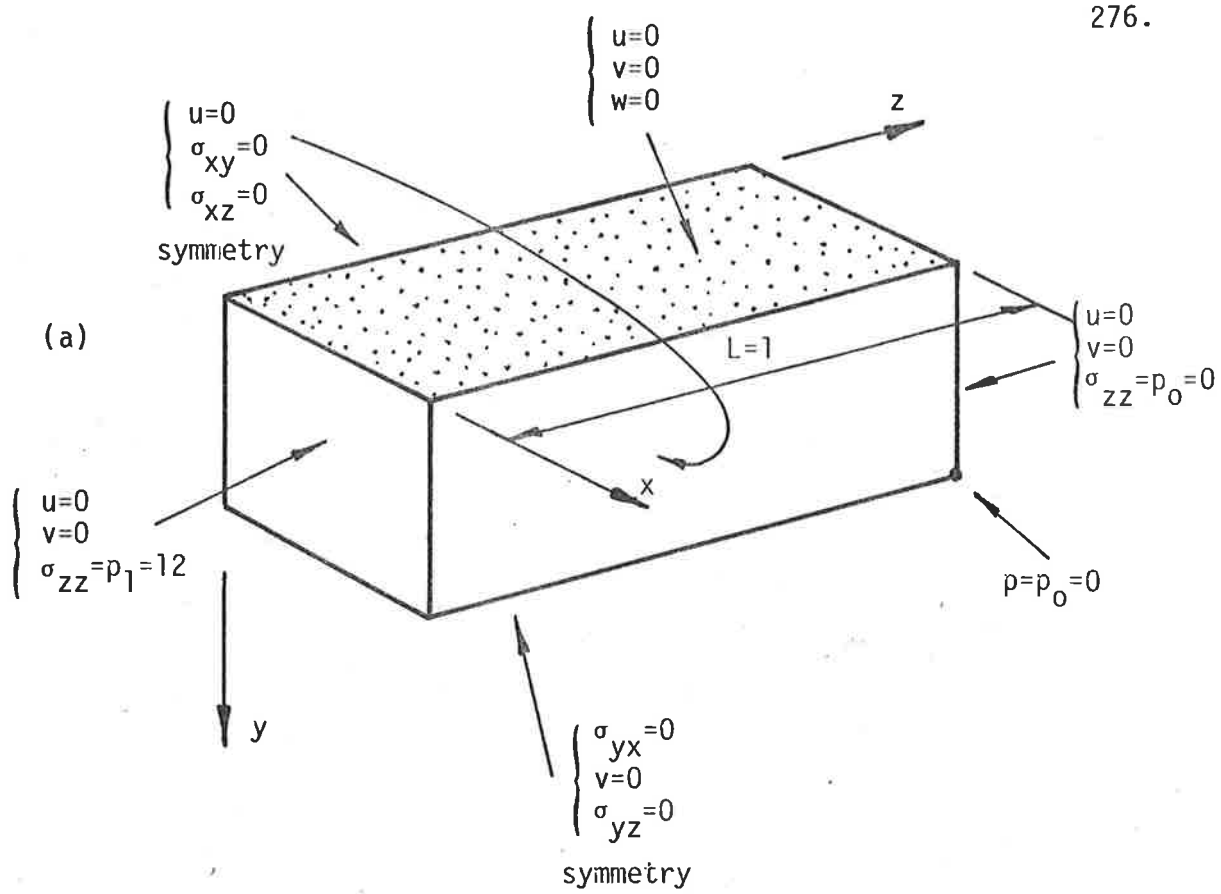
(a)
u=0
v=0
w=0
z
u=0
σxy=0
σxz=0
symmetry
L=1
u=0
v=0
σzz=p0=0
x
u=0
v=0
σzz=p1=12
p=p0=0
y
σyx=0
v=0
σyz=0
symmetry

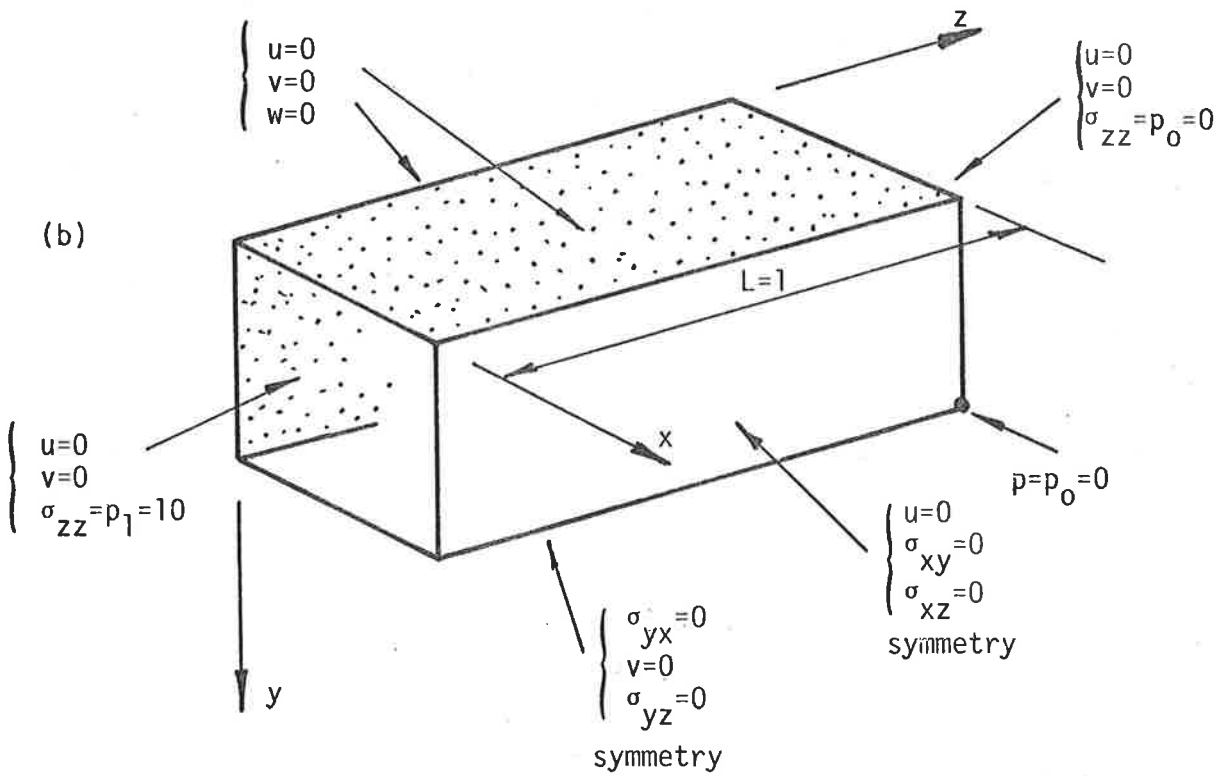
(b)
u=0
v=0
w=0
z
u=0
v=0
σzz=p0=0
L=1
x
u=0
v=0
σzz=p1=10
p=p0=0
y
u=0
σxy=0
σxz=0
symmetry
σyx=0
v=0
σyz=0
symmetry

continued

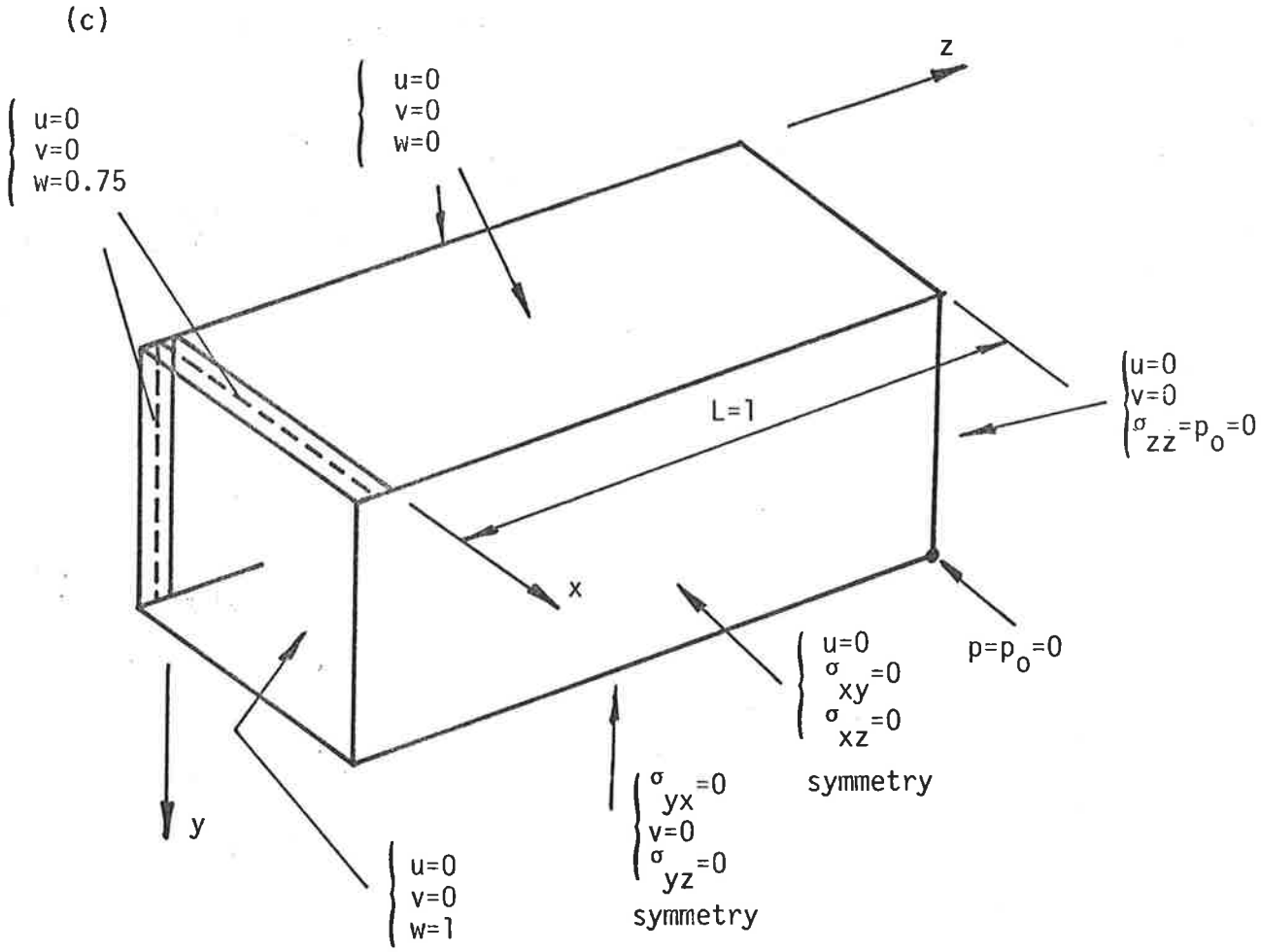

Figure 6.3 Boundary Conditions for (a) Poiseuille Flow, (b) Square Duct Flow and (c) Developing Square Duct Flow.

6.3 Results of Three-Dimensional Analyses

It was anticipated even before the three-dimensional work was commenced that the finite element analysis of a three-dimensional viscous flow problem would require a considerable amount of time and effort, both in setting up the problem and then in solving it. As a result, the flow problem chosen to check that the three-dimensional computer program CR3DVF2 was operating satisfactorily had to be sufficiently simple to enable the necessary tests to be performed as efficiently as possible. The three-dimensional flow problem that was selected for this purpose was the Poiseuille flow in three dimensions and the finite element meshes used to solve it were M1, M2, M3 and M4 as defined in Section 6.2 The exact general solution to this flow is:

$$u(x,y,z) = 0 \qquad 6.2.1$$

$$v(x,y,z) = 0 \qquad 6.2.2$$

$$w(x,y,z) = -\tfrac{1}{2}\,Re\,\frac{dp}{dz}\,y(1-y) \qquad 6.2.3$$

and

$$p(x,y,z) = p_1 + \frac{dp}{dz}\,z \qquad 6.2.4$$

$$\text{where } \frac{dp}{dz} = \frac{p_0 - p_1}{L}$$

The values of p_0 and p_1 were defined in the boundary conditions as being equal to 0 and 12 respectively, while the Reynolds number and the length of channel L were conveniently chosen as 1. The particular solution to this Poiseuille flow is then

$$u(x,y,z) = 0 \qquad 6.3.1$$

$$v(x,y,z) = 0 \qquad 6.3.2$$

$$w(x,y,z) = 6y(1-y) \qquad 6.3.3$$

and

$$p(x,y,z) = 12(1-z) \qquad 6.3.4$$

The following discussion gives a detailed account of the computer program checks carried out using this flow, the results obtained and any conclusions drawn from them.

The analysis of the Poiseuille flow in three dimensions was carried out systematically starting firstly with the single element mesh M1 and finishing with the 18 element mesh M4. The first test, incorporating the boundary conditions given in Figure 6.3(a) successfully evaluated the required velocity field but produced a pressure field that was obviously wrong. As a consequence, the computer program was carefully examined in order to find the reason for the erroneous pressure field. During this examination the equation system for the Poiseuille flow and M1 was printed out and inspected at various stages of its reduction. It was then that the cause of the errors in the pressure field became evident. The computer program proved to be operating correctly, but the equation system it was trying to solve was unexpectedly found to be singular; that is, it contained equations that were composed entirely of other equations in the same system. The boundary conditions were then immediately rechecked to ensure that they were sufficient to uniquely define the flow and to prevent any "free-body" variations appearing in the solutions. Having verified that the boundary conditions were adequate, the equation system was then solved manually. In so doing it was discovered that the redundancy in the equation system was brought about primarily by the fact that the pressure equations, derived from the equation of Continuity, have no pressure dependence. From Figure 6.4(a) which shows a typical layout of the matrix of elementcoefficients of the finite element equations for a general viscous flow, it can be seen that the bottom right hand submatrix D is composed entirely of zeros. If the number of velocity equations corresponding to unknown nodal velocity components is a, and the number of pressure equations is b, then a unique solution to this equation system exists only if $a \geq b$. In the first test run the number of velocity and pressure equations was 12 and 7 respectively. Therefore a unique solution should have been found. However, upon closer examination of the equation system

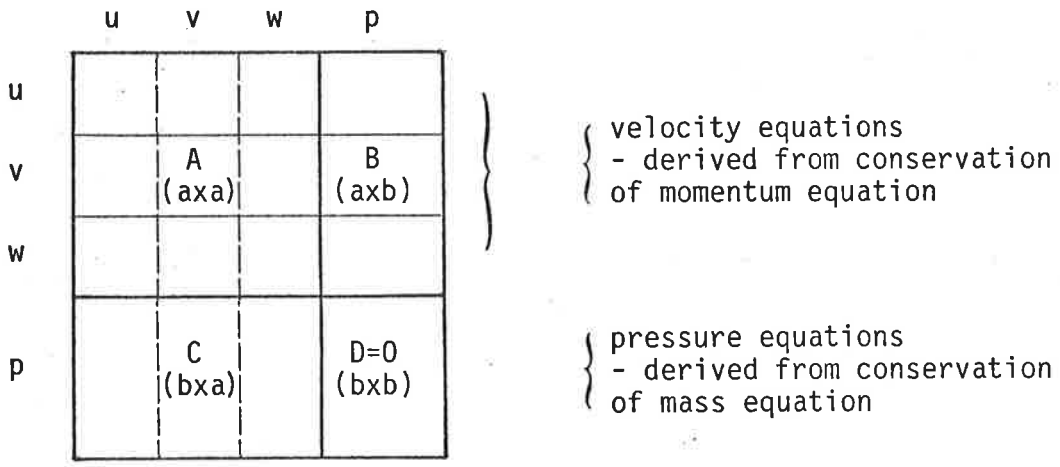

a = number of velocity equations

b = number of pressure equations

(a)

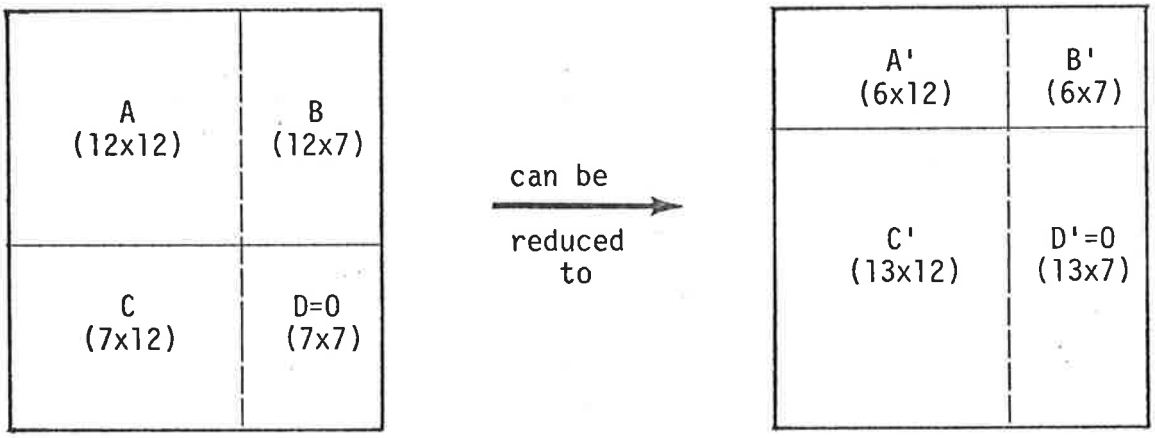

a = 12, b = 7.

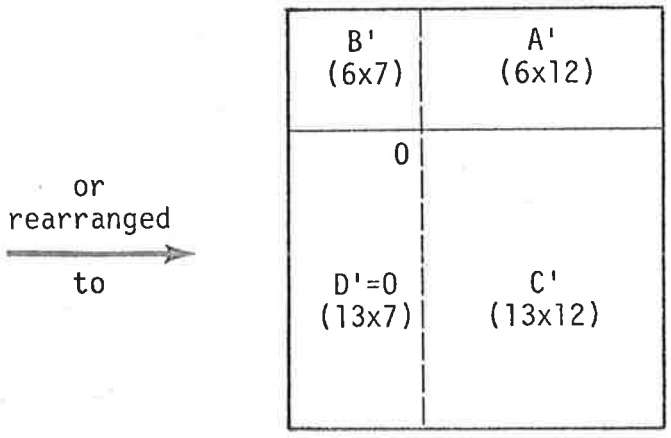

Figure 6.4 (a) Typical Layout of Matrix of Coefficients of Finite Element Equations, and (b) Its Reduced Form.

(b)

it was observed that the pressure coefficients in the velocity equations, that is submatrix B, had a rank of 6 instead of the expected 7. This meant that of the 12 velocity equations, six had linearly dependent pressure coefficients that could be reduced to zero by suitable equation manipulation. Figure 6.4(b) shows the original and the modified equation system layout and clearly demonstrates why the system of equations for the first test run was not uniquely solvable.

Having located the problem, an attempt was made to explain it. However, because of the complexity of the equation system, even for only one element, a precise explanation was not found. The most likely reason, and this was confirmed by subsequent test runs, was the coarseness of the mesh used to analyse the flow. Because only one element was used in mesh M1, the ratio of pressure to velocity equations is high, causing submatrix D, as shown in Figure 6.4(a) to occupy an unusually large portion of the overall matrix of coefficients. As the mesh is refined and more and more elements are incorporated in it however, the ratio of pressure to velocity equations drops. For meshes M1 to M4 the ratio changes from 0.583 to 0.500 to 0.292 to 0.237. The likelihood that the rank of submatrix B (axb) is less than b, the number of pressure equations, is therefore greatly reduced by increasing the number of elements in the mesh. That is, the likelihood of the overall equation system being singular is reduced by increasing the mesh refinement.

Before the second test run was attempted, it was decided to check whether the singular equation system of test run one did in fact have the required velocity and pressure fields as one of its infinite number of solutions. In order to do this it was necessary to remove the singularity from the equation system. This could be done in either of two ways. The first involved introducing into the system an additional equation corresponding to one of the zero specified variables.

However, this could only be done where sufficient information about the surface stress state of the flow in the vicinity of the proposed variable was available to enable the evaluation of its equation's right hand side surface integrals. Fortunately, with the Poiseuille flow the surface stresses at any point are easily calculated and the additional equation can be introduced without too much difficulty. With a more complex flow problem, however, this approach might not have been so easily implemented. By introducing an additional equation the rank of submatrix B is increased by one, the ratio of pressure to velocity equations is reduced and the equation system made solvable. It should also be noted that it is possible that the new equation also has linearly dependent pressure coefficients, in which case the rank of B does not change and the equation system remains singular.

The alternative method of removing the singularity from the equation system involved eliminating one of the redundant equations by specifying in the boundary conditions the value of the variable it corresponds to. If one of the velocity equations was eliminated it would be necessary to specify the value of the corresponding nodal velocity component. If on the other hand, one of the pressure equations was eliminated, the pressure would have to be specified at more than the one point needed to define the pressure datum. It should be noted that if a velocity equation is eliminated, the rank of submatrix B does not change and the equation system remains singular. However, if a pressure equation is eliminated, although the rank of B still does not increase, the value that it should have for the equation system to be solvable is reduced to the required value. Also, by eliminating a pressure equation the ratio of pressure to velocity equations is decreased, whereas if a velocity equation had been eliminated the ratio would have increased, thereby making the system less likely to be solvable.

Therefore to remove the singularity from the equation system of test run one, either an additional velocity equation could be introduced or a pressure equation could be eliminated. To verify this, both approaches were tried and both led to the required exact velocity and pressure fields. The latter however was much simpler to implement since it did not necessitate the evaluation of surfaces stresses in the vicinity of the variables concerned but simply the specification of an additional nodal pressure. The point at which the additional nodal pressure was specified was found to be irrelevant and in all cases the exact solution resulted. This exercise therefore confirmed that the equation system for test run one, although singular, had the exact velocity and pressure fields of the Poiseuille flow as one of its infinite number of solutions.

The second test run for the Poiseuille flow used mesh M2 and behaved similarly to test run one. Using the boundary conditions exactly as given in Figure 6.3(a) the velocity field that was produced was exact but the pressure field was considerably in error. Upon examining the equation system for this test case it was found that, although a solution should have been obtainable since the number of velocity and pressure equations was 22 and 11 respectively, the rank of submatrix B was 10 instead of the required 11; that is one less than that needed for the system to be solvable. Therefore as for the first test run, because the ratio of pressure to velocity equations was high, 0.5, the equation system was again singular.

In order to check that this second equation system had the required velocity and pressure fields as one of its infinite number of solutions, the same techniques that had been used for test run one were again applied. By specifying the pressure at one additional node the solution obtained had the exact velocity and the exact pressure fields. The point at which the additional nodal pressure was specified was again

found to be irrelevant. The exact solution was also obtained when either of several zero specified velocity components were released provided sufficient information about the surface stresses in the vicinity of these variables was supplied to the program. Both these approaches confirmed that the equation system for the second test run also contained the exact velocity and pressure fields of the Poiseuille flow as one of its infinite number of solutions.

Unlike the first two test runs for the Poiseuille flow, the third using mesh M3 and the fourth with M4 and both incorporating the boundary conditions exactly as defined in Figure 6.3(a), both produced the exact Poiseuille flow velocity and pressure fields without requiring the additional pressure specification. For the third test the ratio of pressure to velocity equations was 0.292 while for the fourth test it was 0.237. This result therefore confirmed what had been suggested earlier, namely that provided the number of velocity equations in the overall equation system for a given flow problem is sufficiently larger than the number of pressure equations, then the system should have a unique solution and that solution should be obtainable using a Gaussian reduction and elimination procedure.

Because the Poiseuille flow has no transverse velocity components and because the longitudinal derivative of the axial velocity component is zero, the equations governing this flow are linear; that is, the acceleration or inertia terms are identically equal to zero everywhere. As a result, only the first iteration was required in each of the four test runs for this flow. The computer storage and the execution times required by CR3DVF2 to carry out this one iteration in each of the four tests have been listed in Table 6.1. Also given in this table are the front widths, the execution times per node and the actual physical computer time that the execution of each of these tests required. The unusually high values of physical computer time occur as a result of

Mesh	M1	M2	M3	M4
No. of elements	1	2	8	18
No. of nodes	20	32	81	152
Field length (octal words)	$72{,}000_8$	$72{,}700_8$	$74{,}300_8$	$111{,}400_8$
Execution time (CP seconds)	28.1	55.0	203	459
Front width	68	68	112	176
Execution time per node	1.41	1.72	2.51	3.02
Physical time (minutes)	9.68	20.0	54.3	110

Table 6.1 Details of the four test runs on the three-dimensional Poiseuille flow.

the in and out of core solution technique incorporated in CR3DVF2 and essential if equation systems with even moderate front widths are to be solved. Since the transfer of information from disc to core and from core to disc is essentially carried out by peripheral processors, the construction of the Front solver as it is in CR3DVF2 makes this program very peripheral processor orientated requiring relatively small amounts of central processor time but quite substantial amounts of physical machine time.

By the time the four test runs on the Poiseuille flow were completed, most of the errors in the program had been corrected. The program was then ready for testing on a more complex problem. The second three-dimensional viscous flow problem to be treated in this study was the fully developed flow in a square duct. The exact general solution to the fully developed flow in a rectangular duct with a width to depth ratio of r according to White (34) is:

$$u(x,y,z) = 0 \qquad 6.4.1$$

$$v(x,y,z) = 0 \qquad 6.4.2$$

$$w(x,y,z) = -\frac{4}{\pi^3} Re \frac{dp}{dz} \sum_{i=1,3,5}^{\infty} \left[\frac{(-1)^{\frac{i-1}{2}}}{i^3} \left\{ 1 - \frac{\cosh i\pi(y-\frac{1}{2})}{\cosh \frac{i\pi r}{2}} \right\} \cos i\pi(x - \tfrac{1}{2}) \right] \qquad 6.4.3$$

and

$$p(x,y,z) = p_1 + \frac{dp}{dz} z \qquad 6.4.4$$

$$\text{where } \frac{dp}{dz} = \frac{p_0 - p_1}{L}$$

The values of p_0 and p_1 were defined in the boundary conditions as being equal to 0 and 10 respectively, while the Reynolds number and the length of duct L were conveniently chosen as 1. Since the duct was square, r was also equal to 1. The particular solution to this duct flow is therefore:

$$u(x,y,z) = 0 \qquad 6.5.1$$

$$v(x,y,z) = 0 \qquad 6.5.2$$

$$w(x,y,z) = \frac{40}{\pi^3} \sum_{i=1,3,5}^{\infty} \left[\frac{(-1)^{\frac{i-1}{2}}}{i^3} \left\{ 1 - \frac{\cosh i\pi(y-\frac{1}{2})}{\cosh \frac{i\pi}{2}} \right\} \cos i\pi(x-\tfrac{1}{2}) \right] \qquad 6.5.3$$

and $$p(x,y,z) = 10(1-z) \qquad 6.5.4$$

Figure 6.5 shows the numerical values of w(x,y,z) over a quarter duct cross-section at values of x and y spaced 0.1 apart. The meshes used to analyse the fully developed square duct flow were M3 and M4. Meshes M1 and M2 were not used because in both these cases the boundary conditions as shown in Figure 6.3(b) resulted in an equation system in which b, the number of pressure equations, exceeded the number of velocity equations a. Since a unique solution cannot be found when b>a these two meshes were not considered.

Having set up from the boundary conditions the necessary input data for meshes M3 and M4, the two runs were performed and two numerical solutions for the fully developed square duct flow were obtained. When these solutions were inspected, however, it was observed that a situation similar to that which had occurred with the first two test runs for the Poiseuille flow had again developed. In both cases the velocity field that was obtained gave excellent agreement with the exact solution but the pressure field was obviously wrong. It was therefore anticipated that the equation systems in both cases were singular. Because of the large number of variables involved in these runs it was impossible to examine the two equation systems manually as was done with the Poiseuille flow. Therefore to check if some of the equations in these systems were redundant, it was decided to rerun the two tests and at each reduction step, to print out the elimination equation's leading

$$w(x,y,z) = \frac{40}{\pi^3} \sum_{i=1,3,5}^{\infty} \left[\frac{(-1)^{\frac{i-1}{2}}}{i^3} \left\{ 1 - \frac{\cosh i\pi(y-\frac{1}{2})}{\cosh \frac{i\pi}{2}} \right\} \cos i\pi(x-\tfrac{1}{2}) \right]$$

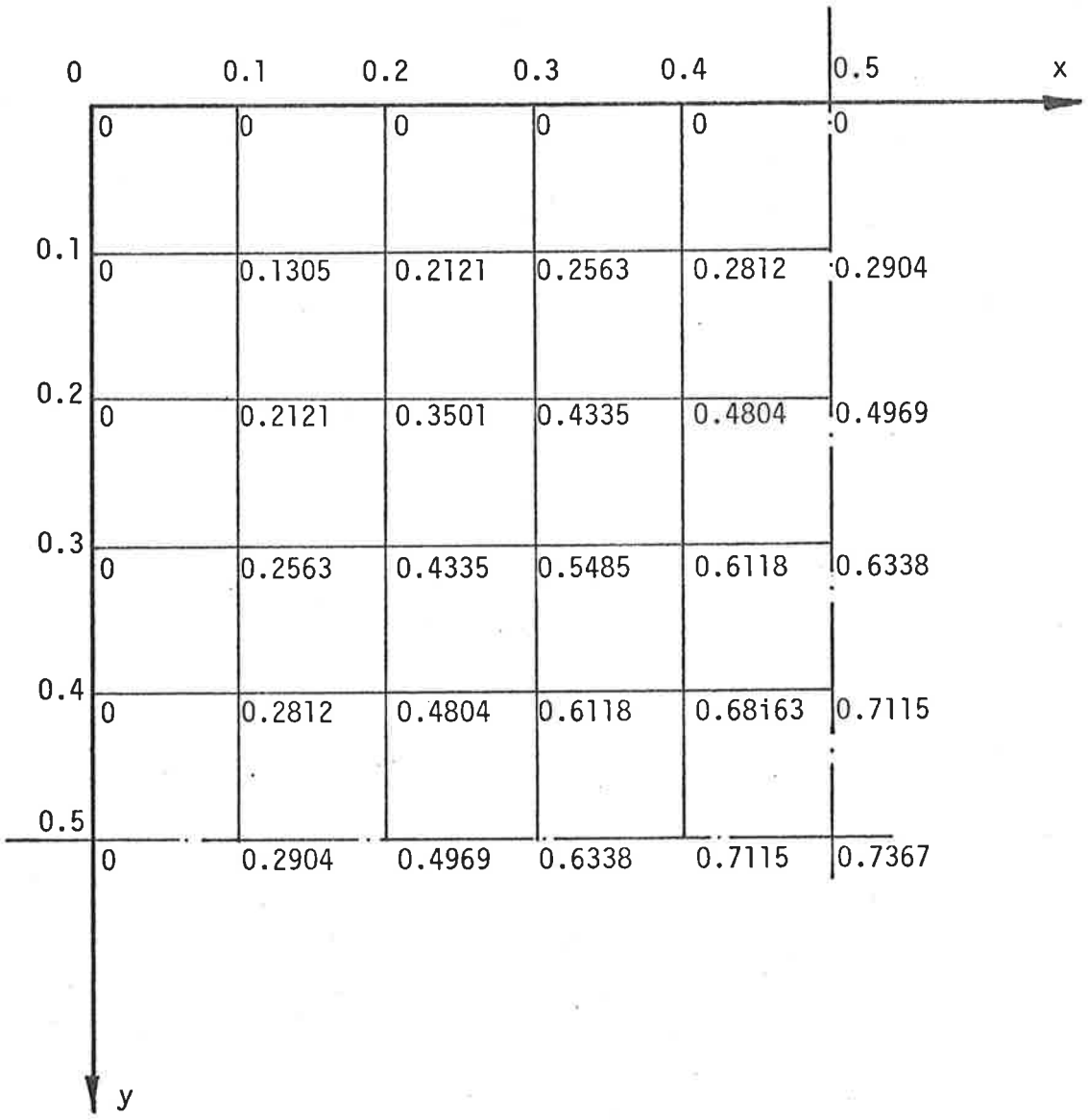

Figure 6.5 Exact Numerical Values of w(x,y,z) Over Quarter Duct Cross-Section.

diagonal coefficient and its right hand side. This was done because if any of the equations in either system were redundant after a finite number of reduction steps, all the coefficients in these equations would be reduced to zero. Actually, they would remain very small numbers because of round-off errors in the computer. Nevertheless, because the computer program CR3DVF2 had been written to select the equation with the largest magnitude leading diagonal coefficient at each reduction step, all redundant equations with the very small leading diagonal coefficients would remain in the system until the end of the reduction procedure. Therefore by printing out the leading diagonal coefficients and the right hand sides, the presence of any redundant equations could easily be detected simply by looking at the last few values printed out. When this was done with the two duct flow runs it was found that in both cases the last coefficient was of the order of 10^{-18} while all the previous coefficients were of the order of 10^{-7} or greater. This proved that one equation in both systems was redundant and explained why the pressure fields produced by the two runs were wrong. However it disproved what had been found previously with the Poiseuille flow.

The first step taken in an attempt to understand the reason for this peculiar behaviour was to check and see if by eliminating the one redundant pressure equation, the correct pressure field could be obtained. To do this the pressure was specified at one additional point in both meshes and the two tests rerun. Both tests then produced the required pressure field as well as the correct velocity field. This confirmed that the equation systems had the required velocity and pressure fields as one of their many solutions.

Several other reruns of these two tests were also carried out, each one with a different pair of points at which the pressure was specified. From these runs it was found that the correct pressure field resulted when the pressure was specified at points on opposite ends

of the duct, but when the two points at which the pressure was specified were on the same end, that is either on the inlet face or on the exit face, the pressure field produced was in error. This further confused rather than clarified the situation, and it now appeared that knowledge of the pressure gradient was necessary before the correct pressure field could be evaluated. This therefore suggested that the two equation systems were singular, not because of the approximations involved in the finite element modelling of such three-dimensional flows, but because sufficient information regarding the pressure gradients as well as the pressure had not been supplied to the program. Conclusive proof for this however was not found. Therefore, despite numerous attempts to explain why the additional pressure information was needed, a satisfactory reason could not be found. As a consequence, it was decided to leave this flow problem and proceed to the last of the three-dimensional viscous flow problems. However before this is done, the velocity fields obtained with meshes M3 and M4 and the additional pressure information are compared with the exact solution for a square duct. Figure 6.6 shows the values of $w(x,y,z)$, both calculated and exact. Since both meshes produced the exact x and y components of velocity, namely $u(x,y,z) = v(x,y,z) = 0$, and the exact pressure field $p(x,y,z) = 10(1-z)$, these have not been tabulated.

One point that should be made before commencing the discussion of the third three-dimensional flow problem, concerns both the Poiseuille flow and the fully developed duct flow. For these flows the x and y components of velocity are zero. Consequently the Continuity equation and the momentum equations for the three directions are

$$-\frac{\partial p}{\partial x} = 0 \qquad 6.6.1$$

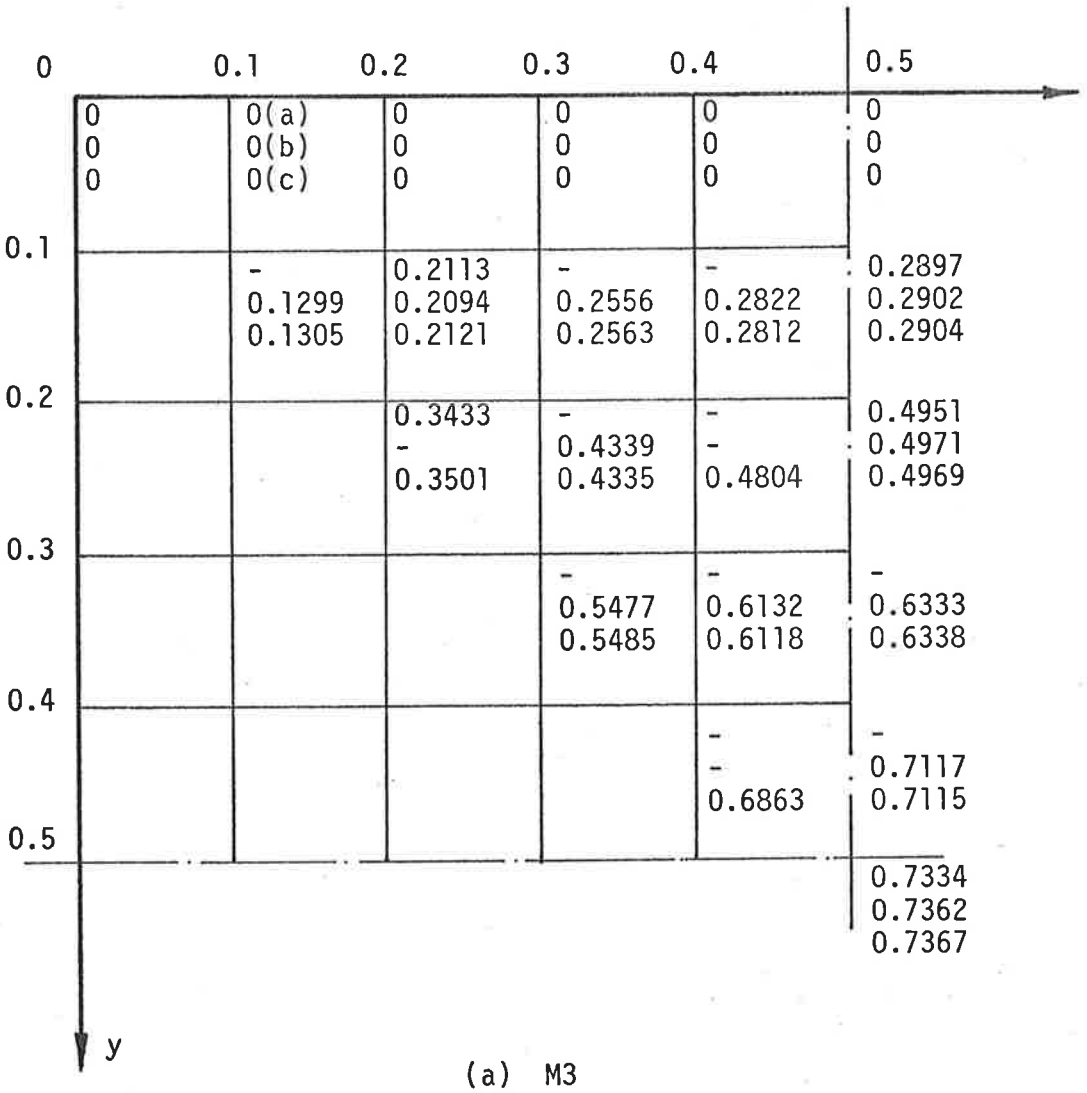

(a) M3
(b) M4
(c) exact

Figure 6.6 Exact and Calculated Values of Axial Component of Velocity for Fully Developed Duct Flow.

$$-\frac{\partial p}{\partial y} = 0 \qquad 6.6.2$$

$$\frac{1}{Re}\left(\frac{\partial^2 w}{\partial x^2} + \frac{\partial^2 w}{\partial y^2}\right) - \frac{\partial p}{\partial z} = 0 \qquad 6.6.3$$

and

$$\frac{\partial w}{\partial z} = 0 \qquad 6.6.4$$

These indicate that the pressure is a function only of z. Further, since w does not vary with z it follows that the velocity and pressure fields can be evaluated independently of each other. For this reason when the equation systems for the Poiseuille flow and the duct flow were singular, the velocity fields that resulted were not wrong as were the pressure fields. That is, the fact that the pressure fields were in error did not necessarily imply that the resulting velocity fields would also be wrong.

Finally, as with the Poiseuille flow the governing equations for the fully developed square duct flow are linear. Therefore only the first iteration was needed in all runs. The execution details for these runs were identical to those for the Poiseuille flow and can be found in Table 6.1.

The last three-dimensional viscous flow problem that was considered in this study is the developing flow in the entrance region of a square duct. This problem does not have a known exact analytical solution and to the best of the author's knowledge has not previously been solved numerically using the finite element method. It has however received considerable attention from researchers, initially using approximate linearization methods to simplify the equations of motion and more recently using the finite difference method to solve one of the many proposed simplfied forms of the non-linear Navier-Stokes equations. Han (15) used the lineary boundary layer approximation to evaluate the

axial velocity and pressure fields downstream of an initial entry region. The square duct flow and the flow between two infinite parallel plates were two limiting cases treated. More recent investigations such as those by Carlson and Hornbeck (7) and by Rubin et al. (27), have centred on the numerical solutions to the finite difference representations of the equations of motion including some of the non-linear terms. Invariably however, in all studies examined to date, some form of approximation has always been used in setting up the governing equations and, as far as the author can ascertain, this study is the first in which an attempt has been made to solve the developing flow in a square duct using the complete Navier-Stokes equations.

Apart from theoretical and numerical modelling, the only other approach available for the investigation of a viscous flow is by experiment. However, because of the difficulties involved in measuring fluid velocities in a real flow, experimental data on most flows is usually very scarce. Nevertheless, Goldstein and Kreid (14) were able to measure precisely the fluid velocity in the entrance region and in the fully developed region of a square duct. As a consequence, in the past their results have often been used as the basis of comparisons to determine the accuracy of various numerical solutions.

The analysis of the developing duct flow was carried out using the boundary conditions exactly as shown in Figure 6.3(c) and with a special mesh M5 constructed with additional elements close to the walls and the inlet face. However, because this study was concerned primarily with checking the suitability of the Galerkin finite element method as it applies to the solution of three-dimensional viscous flow problems as opposed to actually analysing in detail a particular three-dimensional flow, mesh M5 was kept sufficiently simple and relatively coarse to enable several test runs to be carried out without excessive strain on the computing facilities available for this study. As a result mesh

M5 was composed of 36 elements and 264 nodes. It had a minimum front width of 196 and required $126{,}000_8$ words of central memory and 900 central processor seconds per iteration to arrive at a solution. In order to keep the number of iterations to a minimum, the Reynolds number was chosen as one. The flow corresponding to this value was found, from previous work, to require a development length of approximately 0.75. Therefore mesh M5, with an overall length of 1.01, was quite adequate for analysing this flow.

As with the two-dimensional entrance flow, the development length for a square duct was defined as the distance from the start of the duct to the point at which the axial velocity component on the centreline reached 99% of its fully developed value. In order to calculate the theoretical value of this fully developed centreline velocity, it was necessary to use equation 6.5.3 which gives the exact variation of the fully developed axial velocity surface over the duct cross-sectional area for a pressure gradient $\frac{dp}{dz}$ equal to -10. By integrating this axial velocity variation over the area of the duct cross-section, a nett mass flux of 0.3515 was obtained. Since for the developing duct flow problem the nett mass flux prescribed at the inlet face was 1, downstream of the point at which the flow first becomes fully developed, by the law of conservation of mass, the nett mass flux must also be 1. Therefore the pressure gradient in this region must be

$$\frac{1}{0.3515}\ (-10) = \underline{\underline{-28.45}}$$

and the fully developed centreline velocity must, by equation 6.5.3 be

$$\frac{-28.45}{-10}\ 0.7367 = \underline{\underline{2.096}}$$

Therefore the duct flow can be considered fully developed when the centreline velocity reaches 2.075 and the pressure gradient becomes -28.45.

Having completed the preliminary work, the input data for mesh M5 was set up and the program run. However, because of the large amount of computing time required by each iteration, and because it was desirable to avoid wasteful computing of this magnitude, the program was terminated after completion of the first iteration so that the solution could be checked. When this was done it was found that, as with the previous two flows, the velocity field appeared to be correct but the pressure field was obviously wrong. In anticipation of this happening, and so that the equation system for the developing duct flow could be investigated, during the first run the leading diagonal coefficient and the right hand side of the eliminated equation was printed out at each reduction step. When these values were examined it was once again found that one equation was redundant and the equation system indeterminate by one degree. The boundary conditions and the input data were rechecked but by this time, it was realized that the problem was much more fundamental than a simple oversight in the boundary specifications. In fact it was very similar to a problem reported by earlier researchers investigating the use of mixed or common interpolation for the velocity and pressure variables. Hood and Taylor (16) found that in certain circumstances the solutions obtained for two-dimensional viscous flow problems contained accurate velocity fields but the associated pressures were subject to inaccuracies. They then went on to prove, at least qualitatively, that the problem was due to the choice of interpolation for the velocity and pressure variables. More precisely, they showed that the correct pressure field was produced when the pressure interpolation polynomial was one degree less than that for the velocity. The arguments they put forward to support this hold equally well in three dimensions as in two. Therefore, although no mention was made of it earlier in this chapter, it was assumed that in three dimensions a pressure interpolation with one degree less than the velocity interpolation polynomial would be preferable to anything else.

Because of the amount of work involved in checking the effect of a change of interpolation on the pressure solution, this line of investigation was not carried any further. In preference it was decided to try to remove the singularity from the developing duct flow equation system and to proceed, if possible, to obtain a solution. However, because this flow was maintained by a specified inlet flow rather than by a specified pressure gradient as were the previous two flows, this was not as simple as it first appeared. The fluid stress state was not known at any of the nodes where a specified velocity component could be released and the pressure was not known at any of the upstream nodes at which the additional pressure could be specified. Therefore, without additional information regarding either the surface stress field or the pressure field, a solution to this problem could not be obtained.

As a last resort it was decided to estimate the pressure on the centreline at the inlet face by using the pressure gradient calculated above for a fully developed duct flow, and the excess pressure drop reported by Carlson and Hornbeck (7). Several runs were then carried out, each limited to one iteration and with the inlet centreline pressure varying from 28 to 80. From these runs it was observed that the velocity field that resulted was almost totally independent of the value given to the inlet centreline pressure. In fact the velocity field was almost identical to that which resulted from the singular equation system. The difference was less than 1% at all nodes. This confirmed that for low Reynolds number flows in which the non-linear terms are least important, the velocity and pressure fields are once again almost seperable. Some interdependence remains however, due to the existence of transverse velocity components. The variation of the velocity component, $w(x,y,z)$ along the centreline and plotted in Figure 6.7, gives a development length to Reynolds number ratio similar to that of previous researchers. The pressure field that was obtained when the additional pressure was specified at the inlet

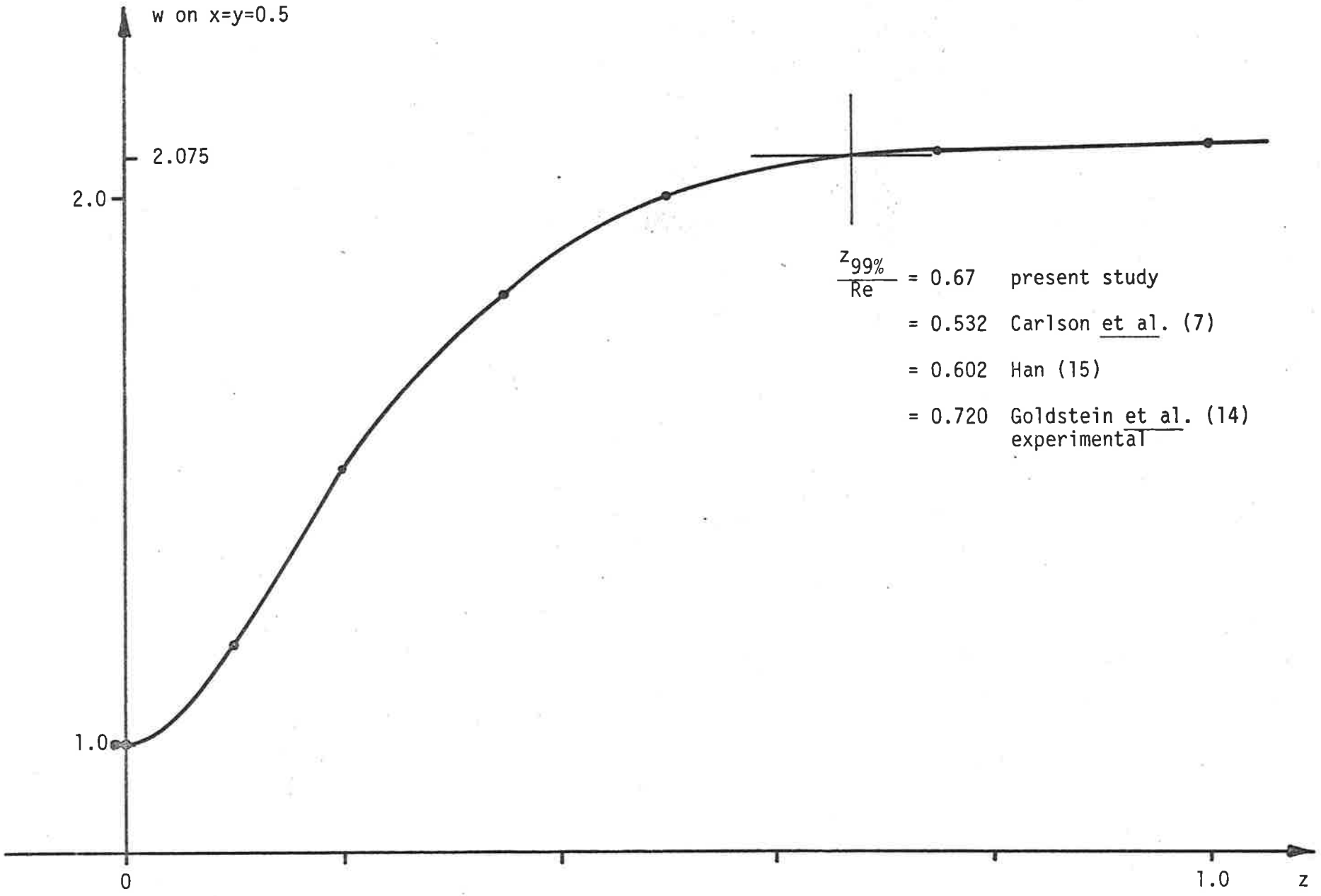

Figure 6.7 Variation of w Along Centreline for Developing Flow in a Square Duct.

centreline also appeared to be almost independent of the inlet pressure value specified. When plotted as in Figure 6.8, the pressure along the centreline showed the expected behaviour with the slope converging to the fully developed pressure gradient at the outlet. However, although the general behaviour of the centreline pressure is as expected, it is evident from Figure 6.8 that the evaluated pressure field has an erroneous oscillatory component. This component is relatively small along the centreline, but closer to the walls becomes so large that it completely overrides the true pressure variations there. This anomoly was found to occur both when the equation system was singular as well as when the singularity was removed by specifying an additional nodal pressure. This was contrary to that which had been found earlier in the investigations of the Poiseuille and the square duct flows, and despite numerous attempts to overcome it, no satisfactory explanation could be arrived at.

During the last stages of the writing up of this thesis however, some work currently being done by Gresho et al. (39) on spurious pressure nodes was brought to the author's attention. In this work it was reported that pressure behaviour similar to that described above had also been found in two dimensions when certain elements were used. The Serendipity and the Lagrangian elements with quadratic velocity and linear pressure mixed interpolation were shown to be free of such spurious oscillatory pressure modes in two dimensions but it was suggested that this would not necessarily be the case in three dimensions.

Their explanation was based on the theory that when the velocity boundary conditions are incorporated in the finite element equation system, additional constraints are imposed on the velocities on the flow boundary resulting in one or more redundant equations. The pressure solutions obtained from such redundant equation systems then contained so-called spurious "checkerboard" modes superimposed

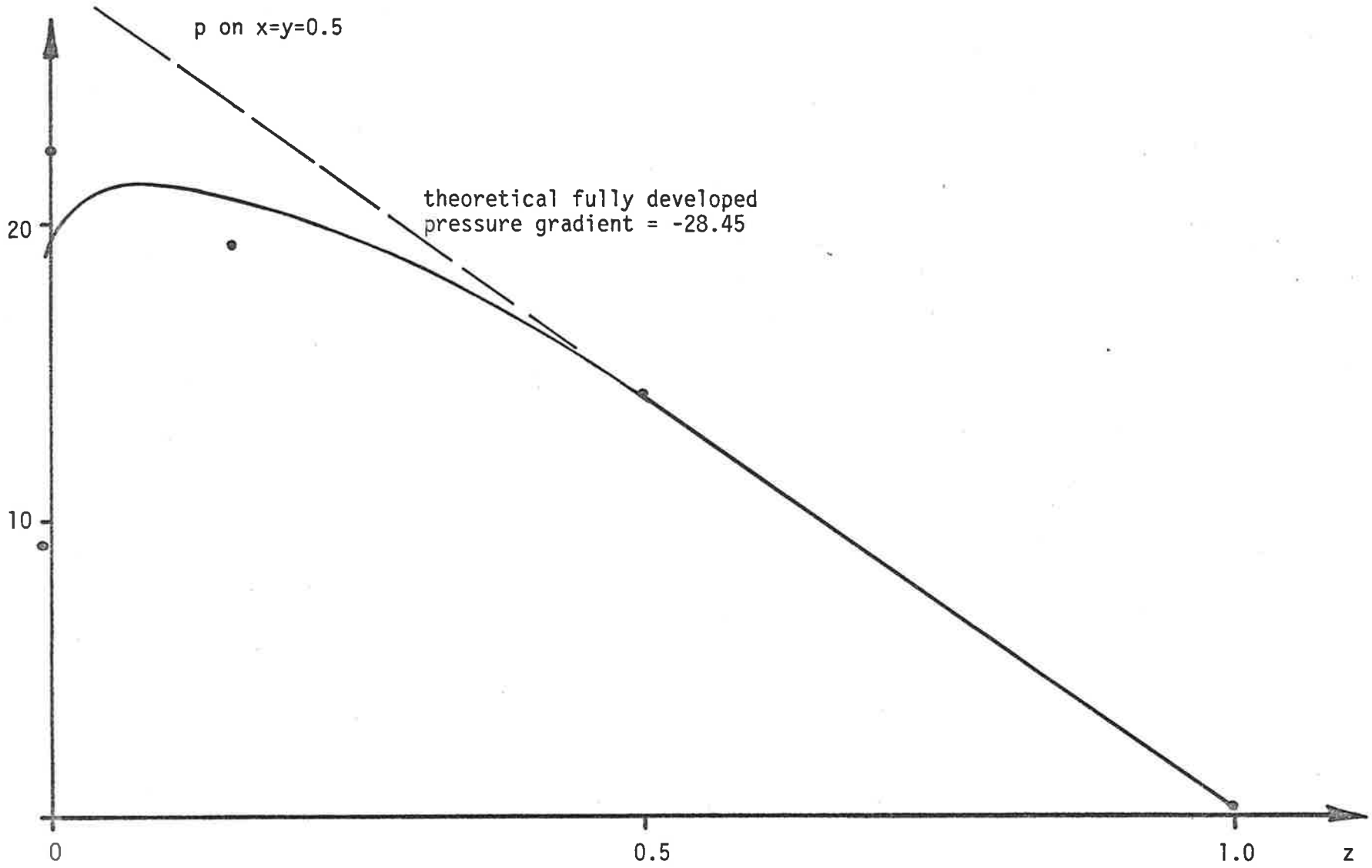

Figure 6.8 Variation of p Along Centreline.

on the true pressure. By filtering off these unwanted modes or by suppressing them by additional pressure specifications, the correct pressure could be evaluated. Unfortunately, because there was insufficient time to test this theory which appears very feasible, it had to be left as a suggestion for future research. Nevertheless, the results of the three-dimensional test runs show that the finite element method can be used successfully to solve a general three-dimensional viscous flow problem.

CHAPTER 7

SUMMARY, CONCLUSIONS AND RECOMMENDATIONS

1. SUMMARY, CONCLUSIONS AND RECOMMENDATIONS

Numerical solutions for the Navier-Stokes equations governing both two- and three-dimensional viscous flows have been obtained. The equations were expressed in terms of the primitive variables velocity and pressure, and the method employed to solve them was the finite element procedure incorporating the Galerkin method as the appropriate weighted residual technique. The Newton-Raphson iterative method and the Frontal Solution technique, built into four computer programs, were used to solve the resulting system of non-linear simultaneous equations.

Within the context of the two-dimensional primitive variables approach, four related versions of the Navier-Stokes equations were formulated, each version including a differing number of terms containing the quantity $(\frac{\partial u}{\partial x} + \frac{\partial v}{\partial y})$. Certain of these terms, historically, have always been eliminated from the momentum equations by use of the Continuity equation. In this study, a comparison of the four formulations was carried out using the solutions for the two-dimensional entrance flow and square cavity flow problems. It was thereby shown that although none of the formulations had pronounced advantages, formulation B, the most commonly used by previous researchers, was slightly more efficient both in terms of computational effort required to obtain a solution, and in the quality of the solution produced.

At low Reynolds numbers all formulations performed equally well, requiring the same number of iterations to obtain a fully converged solution and all producing identical numerical values of velocity and pressure. At high Reynolds numbers however, formulations C and D did not perform as well as the other two. More iterations were required to obtain a converged solution, the quality of the solution was not as high and the initial guess to start the Newton-Raphson

iterative procedure had to be much closer to the required solution for convergence to take place. Although formulation A did not produce as good a quality solution as did formulation B, its efficiency was just as high. However, this formulation had the added difficulty of having an extra surface integral of velocity gradients on the right hand side of its momentum equations. In this study both problems solved were such that the evaluation of these surface integrals could be avoided by making use of the boundary conditions. In a general viscous flow problem however, this may not always be the case and it may be necessary to have prior knowledge of the velocity gradients on the stress boundaries of the flow before formulation A can be used to solve it. As a result of the above findings, formulation B was used in all subsequent two- and three-dimensional work.

In the second part of the two-dimensional study the entrance flow and the cavity flow problems were again used to compare solutions obtained by firstly using eight noded Serendipity and then nine noded Lagrangian elements with quadratic velocity and linear pressure representations. The results of this comparison show that the advantages gained by using the nine noded element, namely a complete quadratic velocity interpolation, did not warrant the additional computer time and space required to obtain solutions that were no better than those obtained using the eight noded Serendipity element with an incomplete velocity interpolation. This, it was found, applied equally to any shape quadrilateral element, rectangular or not. It was therefore concluded in Chapter 5 that the Serendipity element would be the more economical and less difficult to incorporate in a computer package than the Lagrangian element and that by doing so, no loss of accuracy would result. A more comprehensive summary and discussion of the results and conclusions drawn from the two-dimensional

computer studies was presented in Sections 5.5 and 5.6 and will not be repeated here.

By extending the results of the two-dimensional studies to three dimensions, formulation B of the three-dimensional Navier-Stokes equations and the three-dimensional twenty noded Serendipity element were used to model three three-dimensional viscous flow problems. They were the fully developed flow between two parallel plates and in a square duct and the developing flow in a square duct. It was thereby shown that provided a sufficiently large computer facility is available, the Galerkin finite element method using primitive variables can be employed to solve a general three-dimensional steady viscous flow problem. However in order to do so, it was found that additional pressure boundary conditions must be specified. If this was not done the resulting equation system was shown to be singular and a unique solution not obtainable. The exact nature of this restriction was not discovered and must therefore be left for future research. However it was found that solutions could be obtained when a pressure gradient was defined by the pressure boundary conditions rather than simply a pressure datum. In all three cases analysed in Chapter 6, a nodal pressure value at the entry and exit had to be included in the input data before the equation system became non singular and solvable.

As was stated in Chapter 1, the aims of this study were firstly to determine the optimal two-dimensional finite element formulation of the Navier-Stokes equations, secondly to determine the more efficient of two quadrilateral linear pressure and quadratic velocity finite elements, and thirdly to see whether the results of these investigations could be extended to three dimensions and used to obtain a solution to a typical three-dimensional viscous flow. The theoretical

and numerical model developed in Chapters 3 and 4 and the results and conclusions drawn from the studies in Chapters 5 and 6, have fulfilled this objective. This is not to say that the task is complete or that the viscous flow problem is solved. On the contrary, much remains to be gained from future research.

Among the numerous questions that have arisen during the course of this study and that must be answered before the understanding of the primitive variables finite element analysis of steady viscous flows is complete, are:

(a) whether reduced integration can be used to produce the same or better results with less computational effort,

(b) whether the use of elements that do not permit continuity of velocity gradients across element interfaces produces stability, convergence or other problems when it is assumed in the assembly process that the same elements are capable of permitting stress continuity,

(c) why additional pressure boundary conditions are required when the primitive variables Galerkin finite element method is used to solve three-dimensional viscous flows,

(d) whether the use of higher order elements and interpolations is desirable,

and (e) the development of more efficient solution algorithms for three-dimensional problems.

It is clear that the finite element analysis of three-dimensional viscous flows will expand with the increased availability of faster and larger computers. It is therefore hoped that the areas investigated and the results obtained in this study will prove useful in the development of a better technique for the analysis and evaluation of viscous fluid flows.

APPENDICES

A Derivation of Momentum and Mass Conservation Equations and Stress-Strain Rate Relationship

B Three-dimensional Computer Program Details

C Element Stiffness, Numerical Values for 1x1 Element

D Solution of Poiseuille Flow Using Eight and Nine Noded Elements

APPENDIX A

Derivation of Conservation of Momentum Equation

In applying Newton's second law to fluid motion, it is necessary to consider a fixed quantity of fluid matter or system that maintains its identity as it undergoes changes in position and conditions imposed on it by the surrounding flow. To this end let the surfaces S_1 enclose a quantity of moving fluid at some time t and S_2 enclose the same system at a later time, $t + \delta t$. Also let the three regions defined by the surfaces S_1 and S_2 be V_1, V_2 and V_3 as shown in Figure A1.

If we define M_V to be the total linear momentum in a given direction of the fluid in the volume V, then assuming that the flow is steady, the momentum of the above system is $M_{V_1} + M_{V_2}$ at time t and $M_{V_2} + M_{V_3}$ at time $t + \delta t$. The change in momentum during the time δt in the given direction is therefore $M_{V_3} - M_{V_1}$ which equals the net flow of momentum out of the surface S_1. Thus the rate of change of momentum in a given direction of an arbitrary quantity of fluid in a steady flow equals the net rate at which momentum flows out of the surface containing it (any inflow taken as negative outflow).

To facilitate the derivation of the momentum equation consider the steady flow of an incompressible fluid through an element $\delta x \delta y \delta z$ centred on a point P with coordinates (x,y,z) as shown in Figure A2. Let the fluid density (constant for incompressible fluids) be ρ at all points in the flow and at P let the fluid velocity be $v_i(x,y,z)$ in the x_i direction (i.e. u, v and w in the x, y and z directions respectively) and the stress tensor be $\sigma_{ij}(x,y,z)$. Consider initially the x direction. By using Newton's second law of motion one may state that the rate of change of momentum in the x direction of the fluid passing through the element equals the sum of the body and surface forces acting on the element in the x direction. Then by applying the argument presented above, the rate of change of momentum in the x direction

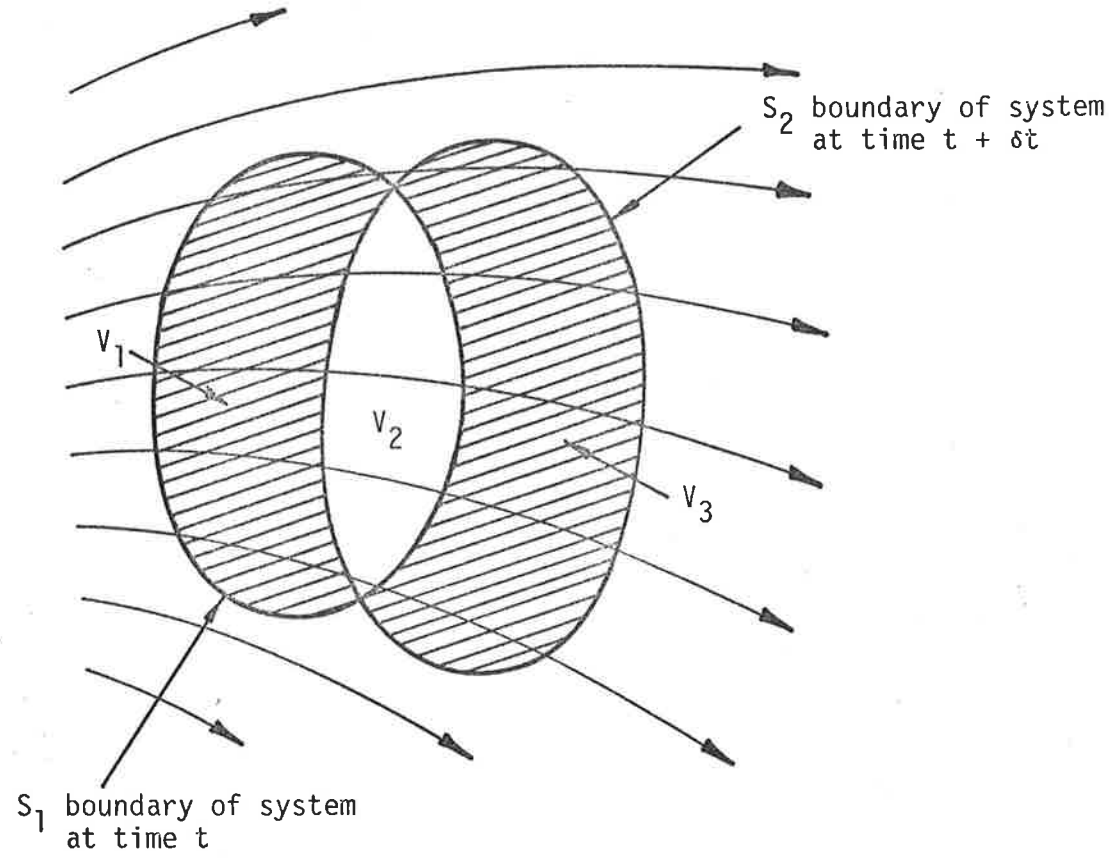

Figure A1 Position of a Mass of Viscous Fluid at Times t and t+δt.

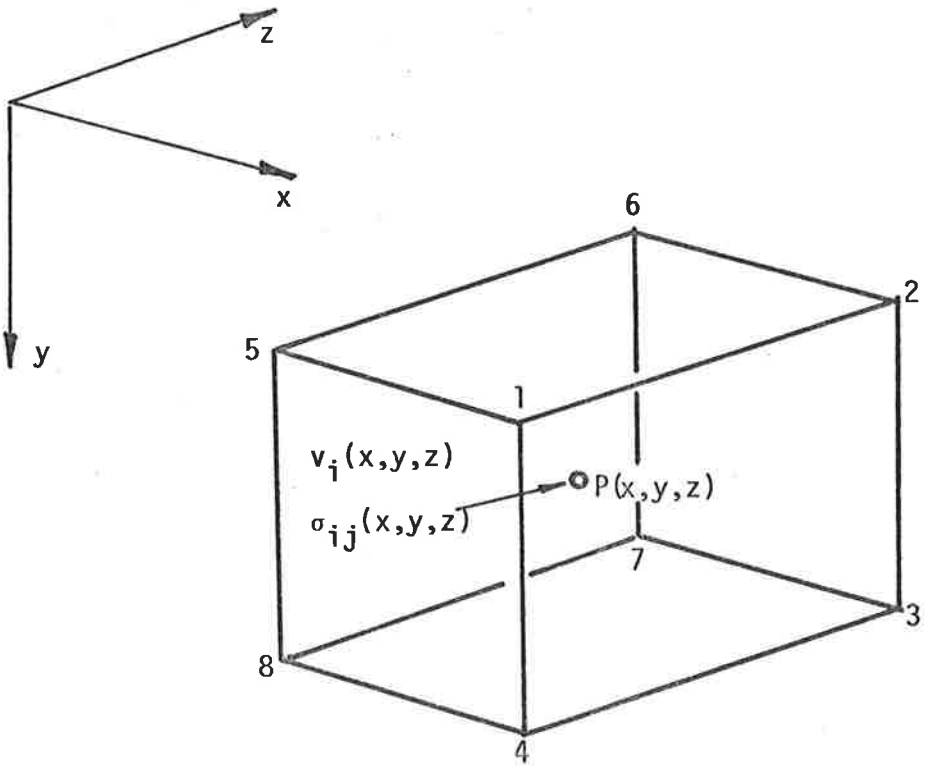

Figure A2 Typical Element of Fluid, δxδyδz.

of the fluid in the volume $\delta x \delta y \delta z$ may be replaced by the rate at which momentum in the x direction is carried out of the element's surfaces. Thus, to set up the incompressible momentum equation for the x direction it is necessary to derive expressions for the rate of flow of momentum in the x direction out of the element, and for the sum of the body and surface forces acting on the element in the x direction. Since the flow is steady these forces are constant with respect to time.

The first of these two expressions can be set up by considering the flow through the element in a time δt. Throughout this time, since the flow is assumed to be steady and incompressible, at each of the six faces (1) 1234, (2) 5678, (3) 4378, (4) 1265, (5) 3267 and (6) 4158, the momentum per unit volume in the x direction is:

$$\rho(u + \frac{\partial u}{\partial x}\frac{\delta x}{2}), \quad \rho(u - \frac{\partial u}{\partial x}\frac{\delta x}{2}),$$

$$\rho(u + \frac{\partial u}{\partial y}\frac{\delta y}{2}), \quad \rho(u - \frac{\partial u}{\partial y}\frac{\delta y}{2}),$$

$$\rho(u + \frac{\partial u}{\partial z}\frac{\delta z}{2}), \quad \rho(u - \frac{\partial u}{\partial z}\frac{\delta z}{2}). \qquad \text{A1.1}$$

Similarly, the outward normal velocity at each of the six faces is:

$$(u + \frac{\partial u}{\partial x}\frac{\delta x}{2}), \quad -(u - \frac{\partial u}{\partial x}\frac{\delta x}{2}),$$

$$(v + \frac{\partial v}{\partial y}\frac{\delta y}{2}), \quad -(v - \frac{\partial v}{\partial y}\frac{\delta y}{2}),$$

$$(w + \frac{\partial w}{\partial z}\frac{\delta z}{2}), \quad -(w - \frac{\partial w}{\partial z}\frac{\delta z}{2}). \qquad \text{A1.2}$$

In the same time δt, the total momentum in the x direction flowing out of the element is therefore:

$$\{\rho(u + \frac{\partial u}{\partial x}\frac{\delta x}{2})(u + \frac{\partial u}{\partial x}\frac{\delta x}{2})\ \delta t$$

$$-\rho(u - \frac{\partial u}{\partial x}\frac{\delta x}{2})(u - \frac{\partial u}{\partial x}\frac{\delta x}{2})\ \delta t\}\ \delta y\delta z$$

$$+\{\rho(u + \frac{\partial u}{\partial y}\frac{\delta y}{2})(v + \frac{\partial v}{\partial y}\frac{\delta y}{2})\ \delta t$$

$$-\rho(u - \frac{\partial u}{\partial y}\frac{\delta y}{2})(v - \frac{\partial v}{\partial y}\frac{\delta y}{2})\ \delta t\}\ \delta x\delta z$$

$$+\{\rho(u + \frac{\partial u}{\partial z}\frac{\delta z}{2})(w + \frac{\partial w}{\partial z}\frac{\delta z}{2})\ \delta t$$

$$-\rho(u - \frac{\partial u}{\partial z}\frac{\delta z}{2})(w - \frac{\partial w}{\partial z}\frac{\delta z}{2})\ \delta t\}\ \delta x\delta y \qquad \text{A1.3}$$

And simplifying becomes:

$$\rho\{(u\frac{\partial u}{\partial x} + u\frac{\partial u}{\partial x}) + (u\frac{\partial v}{\partial y} + v\frac{\partial u}{\partial y})$$

$$+ (u\frac{\partial w}{\partial z} + w\frac{\partial u}{\partial z})\}\delta x\delta y\delta z\ \delta t$$

$$= \rho\{(u\frac{\partial u}{\partial x} + v\frac{\partial u}{\partial y} + w\frac{\partial u}{\partial z})$$

$$+ u(\frac{\partial u}{\partial x} + \frac{\partial v}{\partial y} + \frac{\partial w}{\partial z})\}\delta x\delta y\delta z\ \delta t$$

$$= \rho(v_j\frac{\partial u}{\partial x_j} + u\frac{\partial v_j}{\partial x_j})\delta x\delta y\delta z\ \delta t \qquad \text{A1.4}$$

Thus the rate at which momentum in the x direction is carried out of the element is:

$$\rho(v_j\frac{\partial u}{\partial x_j} + u\frac{\partial v_j}{\partial x_j})\ \delta x\delta y\delta z \qquad \text{A1.5}$$

The second expression, the sum of the body and surface forces acting on the element in the x direction, can be set up as follows. On each of the six element faces the stress tensor component that acts

in the x direction is:

$$(\sigma_{xx} + \frac{\partial \sigma_{xx}}{\partial x}\frac{\delta x}{2}), \quad -(\sigma_{xx} - \frac{\partial \sigma_{xx}}{\partial x}\frac{\delta x}{2}),$$

$$(\sigma_{yx} + \frac{\partial \sigma_{yx}}{\partial y}\frac{\delta y}{2}), \quad -(\sigma_{yx} - \frac{\partial \sigma_{yx}}{\partial y}\frac{\delta y}{2}),$$

$$(\sigma_{zx} + \frac{\partial \sigma_{zx}}{\partial z}\frac{\delta z}{2}) \text{ and } -(\sigma_{zx} - \frac{\partial \sigma_{zx}}{\partial z}\frac{\delta z}{2}), \qquad \text{A1.6}$$

where σ_{ij} is a stress component acting at a point in space in the positive j^{th} direction and on a plane whose normal points in the positive i^{th} direction. The positive direction of the nine stress components is shown in Figure A3.

The total force acting on the element in the x direction is therefore:

$$\{(\sigma_{xx} + \frac{\partial \sigma_{xx}}{\partial x}\frac{\delta x}{2}) - (\sigma_{xx} - \frac{\partial \sigma_{xx}}{\partial x}\frac{\delta x}{2})\}\delta y \delta z$$

$$+ \{(\sigma_{yx} + \frac{\partial \sigma_{yx}}{\partial y}\frac{\delta y}{2}) - (\sigma_{yx} - \frac{\partial \sigma_{yx}}{\partial y}\frac{\delta y}{2})\}\delta x \delta z$$

$$+ \{(\sigma_{zx} + \frac{\partial \sigma_{zx}}{\partial z}\frac{\delta z}{2}) - (\sigma_{zx} - \frac{\partial \sigma_{zx}}{\partial z}\frac{\delta z}{2})\}\delta x \delta y + \rho F_x \delta x \delta y \delta z \qquad \text{A1.7}$$

where the last term is the part contributed by the body force per unit mass $F_i(x,y,z)$ at point P.

By simplifying, the total force becomes:

$$(\frac{\partial \sigma_{xx}}{\partial x} + \frac{\partial \sigma_{yx}}{\partial y} + \frac{\partial \sigma_{zx}}{\partial z})\ \delta x \delta y \delta z + \rho F_x \delta x \delta y \delta z$$

$$= \frac{\partial \sigma_{jx}}{\partial x_j} \delta x \delta y \delta z + \rho F_x \delta x \delta y \delta z \qquad \text{A1.8}$$

Thus the general momentum equation for the x direction is:

$$\rho(v_j \frac{\partial u}{\partial x_j} + u \frac{\partial v_j}{\partial x_j})\ \delta x \delta y \delta z$$

$$= \frac{\partial \sigma_{jx}}{\partial x_j} \delta x \delta y \delta z + \rho F_x \delta x \delta y \delta z$$

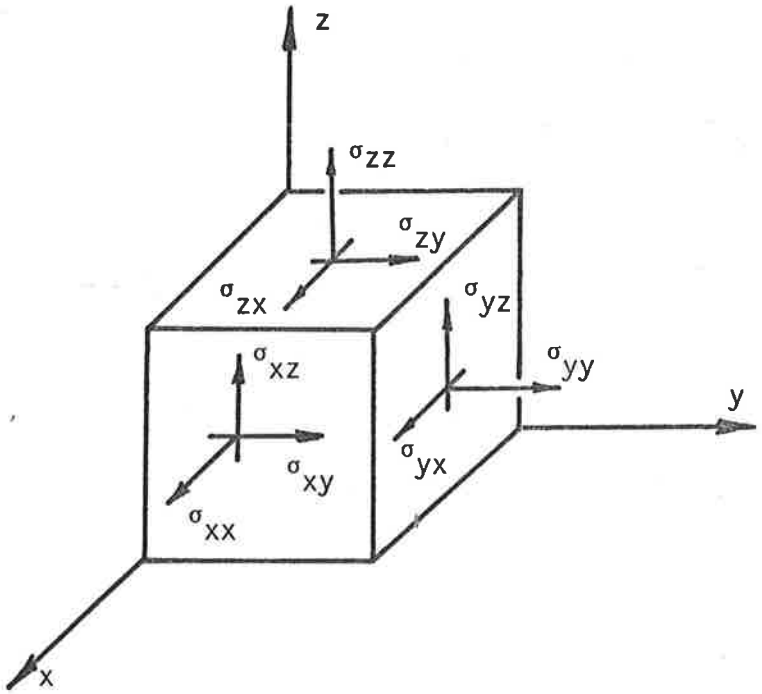

Figure A3 Positive Directions of Nine Three-dimensional Stress Components.

$$\text{i.e.}\quad \rho\left(v_j \frac{\partial u}{\partial x_j} + u \frac{\partial v_j}{\partial x_j}\right) = \frac{\partial \sigma_{jx}}{\partial x_j} + \rho F_x$$

$$\text{i.e.}\quad \frac{\partial \sigma_{jx}}{\partial x_j} = \rho\left(v_j \frac{\partial u}{\partial x_j} + u \frac{\partial v_j}{\partial x_j} - F_x\right) \qquad \text{A1.9.1}$$

As is traditionally done the term $u \cdot \frac{\partial v_j}{\partial x_j}$ is now set to zero by making use of the steady incompressible Continuity equation. In this study however this term will be prefixed by a constant C_3 whose value is either zero or one depending on whether the term is to be discarded or retained. Thus the effects of the inclusion of this term can be investigated by simply changing the value of C_3 from zero to one.

By applying the same arguments to the y and z directions, one can obtain the remaining two momentum equations.

$$\frac{\partial \sigma_{jy}}{\partial x_j} = \rho\left(v_j \frac{\partial v}{\partial x_j} + C_3\, v \frac{\partial v_j}{\partial x_j} - F_y\right) \qquad \text{A1.9.2}$$

$$\frac{\partial \sigma_{jz}}{\partial x_j} = \rho\left(v_j \frac{\partial w}{\partial x_j} + C_3\, w \frac{\partial v_j}{\partial x_j} - F_z\right) \qquad \text{A1.9.3}$$

The three equations for the x, y and z directions can now be combined and expressed in tensor notation form to give the general steady and incompressible Navier-Stokes equation.

$$\frac{\partial \sigma_{ji}}{\partial x_j} = \rho\left(v_j \frac{\partial v_i}{\partial x_j} + C_3\, v_i \frac{\partial v_j}{\partial x_j} - F_i\right) \qquad \text{A1.10}$$

Derivation of Conservation of Mass Equation

The law of conservation of mass states that the rate of change of the total mass of a given quantity of fluid (system) must be zero as the system moves within the remainder of the flow. By employing techniques similar to those used in the derivation of the momentum equation, the Continuity equation can be set up as follows. As defined previously, let the surfaces S_1 and S_2 enclose the same quantity of

fluid at times t and $t + \delta t$, and let the volumes V_1, V_2 and V_3 be the three regions bounded by S_1 and S_2 (see Figure A1). If we define m_V to be the total mass of the fluid in the volume V, then assuming that the flow is steady, the mass of the above system is $m_{V_1} + m_{V_2}$ at time t and $m_{V_2} + m_{V_3}$ at time $t + \delta t$. The change in the total mass during the time δt is therefore $m_{V_3} - m_{V_1}$ which equals the net flow of mass out of the surface S_1. Thus the rate of change of the mass of an arbitrary volume of fluid in a steady flow equals the net rate at which mass flows out of the surface containing it.

An expression for this rate can be derived by considering the steady flow of an incompressible fluid through the element $\delta x \delta y \delta z$ described earlier and shown in Figure A2 in a time δt. During this time, at each of the six faces of the element, the outward normal velocity is:

$$\left(u + \frac{\partial u}{\partial x}\frac{\delta x}{2}\right), \quad -\left(u - \frac{\partial u}{\partial x}\frac{\delta x}{2}\right),$$

$$\left(v + \frac{\partial v}{\partial y}\frac{\delta y}{2}\right), \quad -\left(v - \frac{\partial v}{\partial y}\frac{\delta y}{2}\right),$$

$$\left(w + \frac{\partial w}{\partial z}\frac{\delta z}{2}\right) \text{ and } -\left(w - \frac{\partial w}{\partial z}\frac{\delta z}{2}\right). \qquad \text{A1.11}$$

Since the fluid density is constant, in a time δt the mass flowing out of the element is therefore:

$$\left\{\rho\left(u + \frac{\partial u}{\partial x}\frac{\delta x}{2}\right)\delta t - \rho\left(u - \frac{\partial u}{\partial x}\frac{\delta x}{2}\right)\delta t\right\}\delta y \delta z$$

$$+ \left\{\rho\left(v + \frac{\partial v}{\partial y}\frac{\delta y}{2}\right)\delta t - \rho\left(v - \frac{\partial v}{\partial y}\frac{\delta y}{2}\right)\delta t\right\}\delta x \delta z$$

$$+ \left\{\rho\left(w + \frac{\partial w}{\partial z}\frac{\delta z}{2}\right)\delta t - \rho\left(w - \frac{\partial w}{\partial z}\frac{\delta z}{2}\right)\delta t\right\}\delta x \delta z \qquad \text{A1.12}$$

And simplifying, becomes:

$$\rho\left(\frac{\partial u}{\partial x} + \frac{\partial v}{\partial y} + \frac{\partial w}{\partial z}\right)\delta x \delta y \delta z \; \delta t$$

$$= \rho \frac{\partial v_i}{\partial x_i}\delta x \delta y \delta z \; \delta t \qquad \text{A1.13}$$

Thus the rate at which mass is carried out of the element is:

$$\rho \frac{\partial v_i}{\partial x_i} \delta x \delta y \delta z \qquad \text{A1.14}$$

By the law of conservation of mass this rate must always be zero. The steady and incompressible Continuity equation is therefore:

$$\rho \frac{\partial v_i}{\partial x_i} \delta x \delta y \delta z = 0$$

i.e.
$$\frac{\partial v_i}{\partial x_i} = 0 \qquad \text{A1.15}$$

Derivation of Stress Strain-Rate Relationship for a Newtonian Fluid

The general form of the stress tensor σ_{ij} was first suggested by Stokes who derived it on the basis of three assumptions. He assumed that

(a) the fluid is continuous and that the stress tensor is at most a linear function of the strain rate,

(b) the fluid is isotropic, that is its properties are independent of direction,

and (c) when the strain rate is zero the deformation law must reduce to the hydrostatic pressure condition $\sigma_{ij} = -p\,\delta_{ij}$, where δ_{ij} is the Kronecker delta function.

The process of internal friction occurs in a fluid only when adjacent fluid particles move with different velocities; that is, when there is relative motion between them. Therefore σ_{ij} must be dependent on the spatial derivatives of velocity. If the velocity gradients are small, we may assume that only the first derivatives are involved and by assumption (a) above, that σ_{ij} is a linear function of these first derivatives. There can be no terms in σ_{ij} independent of $\frac{\partial v_i}{\partial x_j}$ since by assumption (c) above, σ_{ij} must reduce to the hydrostatic pressure condition when the fluid velocity is spatially constant. Also the same

condition must prevail when the whole fluid is in uniform rotation since it is clear that in such motion no internal friction occurs in the fluid. It can easily be shown that the sum

$$\frac{\partial v_i}{\partial x_j} + \frac{\partial v_j}{\partial x_i} \qquad \text{A1.16}$$

vanishes when the fluid is in a state of uniform rotation. According to Reference 20, the most general tensor satisfying the above condition is

$$\sigma_{ij} = a\left(\frac{\partial v_i}{\partial x_j} + \frac{\partial v_j}{\partial x_i}\right) + b\frac{\partial v_k}{\partial x_k}\delta_{ij} - p\,\delta_{ij} \qquad \text{A1.17}$$

where a and b are independent of the velocity. In making this statement, use is made of assumption (b) above.

By considering the shear flow between two parallel plates moving relative to each other as shown in Figure A4, it can easily be verified that

$$a = \mu \qquad \text{A1.18}$$

where μ is the property of the fluid which relates the stress applied to the top plate and the velocity gradient produced in the fluid, and defined as

$$\mu = \frac{\sigma_{yx}}{\left(\frac{\partial u}{\partial y}\right)} \qquad \text{A1.19}$$

The other constant b, is independent of μ, is usually given the symbol λ and is customarily called the coefficient of bulk viscosity since it is associated only with volume expansion. Therefore

$$\sigma_{ij} = \mu\left(\frac{\partial v_i}{\partial x_j} + \frac{\partial v_j}{\partial x_i}\right) + \lambda\frac{\partial v_k}{\partial x_k}\delta_{ij} - p\,\delta_{ij} \qquad \text{A1.20}$$

Equation A1.20 as it stands is not in an immediately usable form since λ has not been defined. In order to clarify the quantity λ it is necessary to examine more closely the pressure variable. By

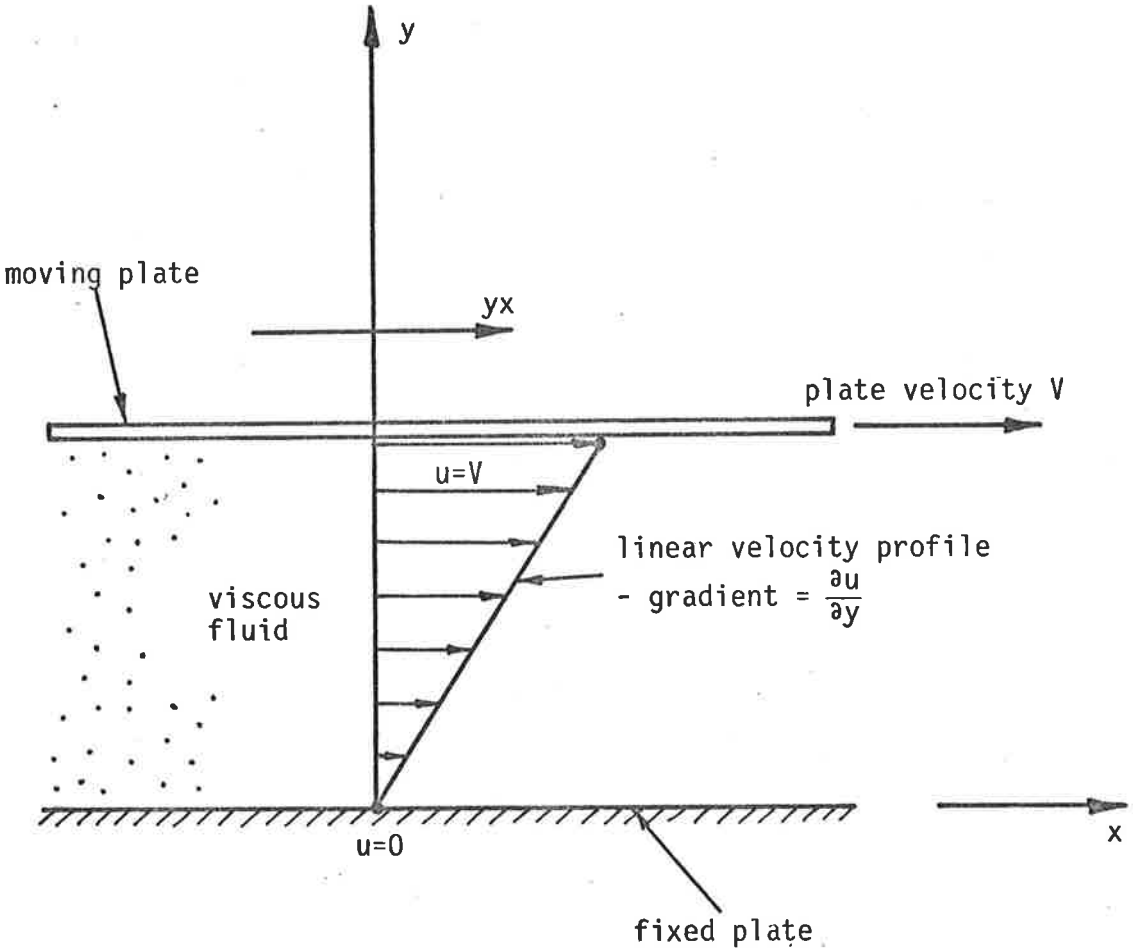

Figure A4 Flow Between Two Parallel Plates Moving Relative to Each Other.

definition the pressure is the average compressive stress on an element of fluid. Using equation A1.20 therefore

$$\text{pressure} = p - (\lambda + \frac{2}{3}\mu)\frac{\partial v_k}{\partial x_k} \qquad \text{A1.21}$$

Thus the pressure in a deforming fluid is equal to the thermodynamic quantity p only if $\lambda = -\frac{2}{3}\mu$ or $\frac{\partial v_k}{\partial x_k} = 0$. In an incompressible fluid the latter is true and equation A1.20 has only two terms and is immediately usable. If however $\frac{\partial v_k}{\partial x_k}$ is not equal to zero, as might be the case in a finite element approximation sense, then the problem can only be resolved by setting $\lambda = -\frac{2}{3}\mu$.

Thus the stress strain rate relationship for this study must be written as

$$\sigma_{ij} = \mu(\frac{\partial v_i}{\partial x_j} + \frac{\partial v_j}{\partial x_i} - \frac{2}{3} C_3 \delta_{ij} \frac{\partial v_k}{\partial x_k}) - p \delta_{ij} \qquad \text{A1.22}$$

$$\text{or} \quad \sigma_{ij} = \mu(v_{i,j} + v_{j,i} - \frac{2}{3} C_3 \delta_{ij} v_{k,k}) - p \delta_{ij} \qquad \text{A1.23}$$

where C_3, which can have the value 1 or 0, has been included so that the term it prefixes can be either included if it is assumed that $\frac{\partial v_k}{\partial x_k}$ is not identically equal to zero everywhere or excluded if it is.

APPENDIX B

Three-dimensional Computer Program Details

Basic flow chart for CR3DVF2

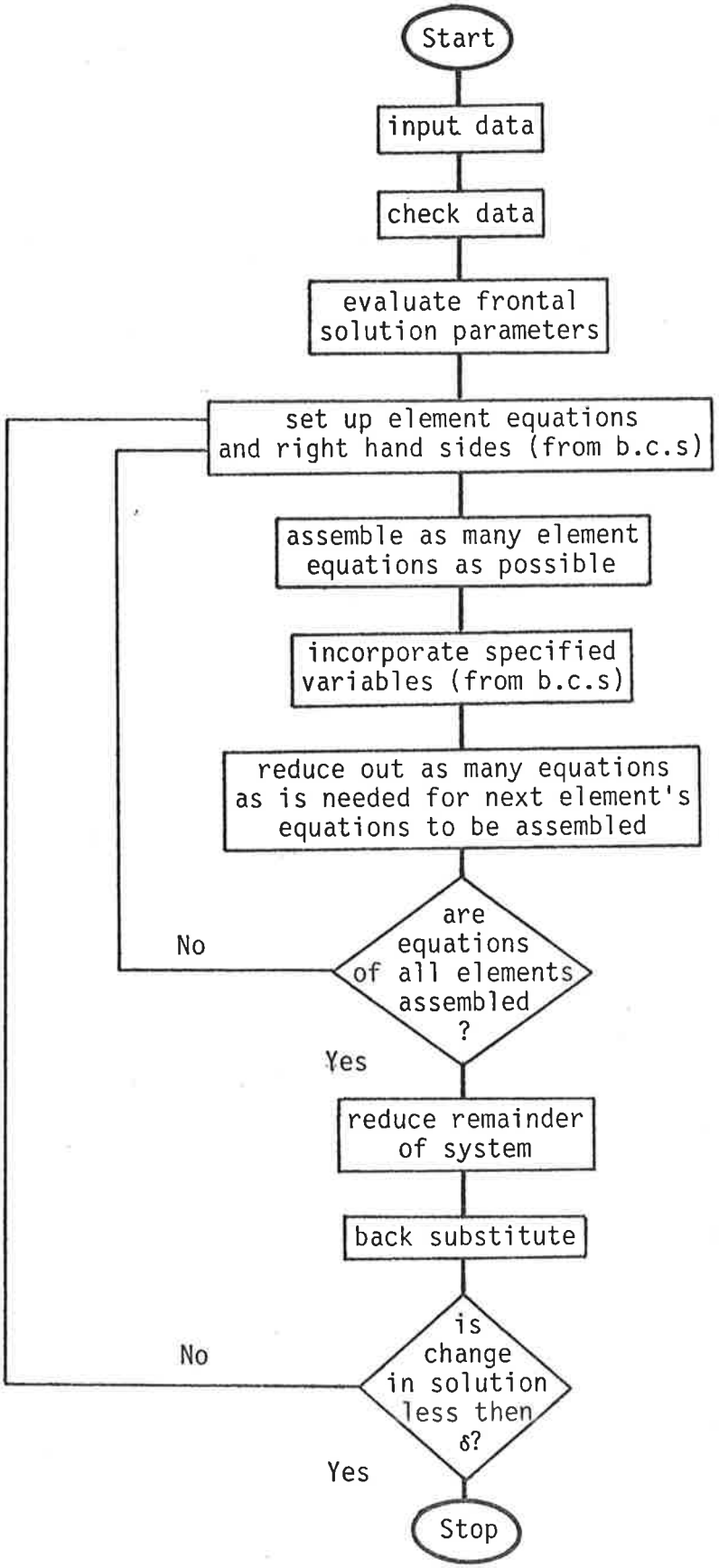

```
      PROGRAM CR3DVF2(INPUT=65,OUTPUT=65,TAPE5=INPUT,TAPE6=OUTPUT,TAPE2,
     1 TAPE4=0,TAPE20=0,TAPE21=0,TAPE3)

C     PROGRAM CR3DVF CALCULATES THE VELOCITY AND PRESSURE DISTRIBUTIONS
C     IN A 3D VISCOUS FLOW ASSUMING QUADRATIC VELOCITY AND LINEAR
C     PRESSURE VARIATIONS AND USING THE 20-NODED ISOPARAMETRIC ELEMENT
C     AND THE GALERKIN METHOD OF WEIGHTED RESIDUALS

C     ALL VARIABLES WILL BE DEFINED IN THE SUBROUTINE IN WHICH THEY
C     FIRST APPEAR

**********     ENTER COMMON BLOCK HERE     **********

C     MAXIT = MAXIMUM NUMBER OF ITERATIONS ALLOWED
C     MAXNW = MAXIMUM SIZE OF PROBLEM THAT CAN BE HANDLED BY PROGRAM
C     MAXSS = MAXIMUM SIZE OF STRUCTURAL STIFFNESS MATRIX AVAILABLE
C     MAXND = MAXIMUM NUMBER OF EQUATIONS IN CORE AT ONE TIME
C     MAXNS = MAXIMUM NUMBER OF STRUCTURAL STIFFNESS MATRIX SUBDIVISIONS
C     MAXLD = MAXIMUM SIZE OF VECTOR LDEST IN PREFNT
      MAXNW=150
      MAXSS=MAXNW
      MAXND=50
      MAXLD=128
      MAXNS=MAXNW/MAXND
      REWIND 3

      L20=20
      L21=21

C     TAPES 20 AND 21 ARE USED TO HOLD THE TOTAL STRUCTURAL STIFFNESS
C     MATRIX WHILE IT IS MANIPULATED

      REWIND L20
      REWIND L21

C     INPUT DATA FOR PROBLEM

      CALL INDAT

C     CHECK INPUT DATA

      CALL CHKPLT

C     CALCULATE MAXIMUM FRONT WIDTH FOR PROBLEM

      CALL PREFNT(ADSPL,MAXLD)

C     INITIALIZE SOLUTION VECTOR

      DO 1 I=1,MAXNOD
      DO 2 J=1,NVABZ
      ADSPL(I,J)=0.0
    2 CONTINUE
    1 CONTINUE

C     ITERATE UNTIL CONVERGENCE IS ACHIEVED

      CALL REMARK(3HONE)
      DO 3 ITER=1,MAXIT

C     CALCULATE ELEMENT STIFFNESS MATRICES AND STORE ON TAPE 4

      CALL STIFN
      ENDFILE 4

#
```

```
C     INITIALIZE STRUCTURAL STIFFNESS MATRIX AND RIGHT HAND SIDE FORCE
C     VECTOR

      DO 5 J=1,MAXNW
      DO 6 I=1,MAXND
      SS(I,J)=0.0
    6 CONTINUE
      SRS(J)=0.0
    5 CONTINUE

C     INITIALIZE TAPES 20 AND 21

      DO 9 I=1,MAXNS
      BUFFER OUT (L20,1) (SS(1,1),SS(MAXND,MAXNW))
      IF(UNIT(L20)) 4,7,8
    4 CONTINUE
      BUFFER OUT (L21,1) (SS(1,1),SS(MAXND,MAXNW))
      IF(UNIT(L21)) 9,7,8
    9 CONTINUE
      ENDFILE 20
      ENDFILE 21

      REWIND L20
      REWIND L21
      BUFFER IN (L20,1) (SS(1,1),SS(MAXND,MAXNW))
      IF(UNIT(L20)) 10,7,8
   10 CONTINUE
      KS=1
      KF=MAXND

C     REDUCE EQUATIONS TO UPPER TRIANGULAR FORM USING MODIFIED
C     FRONTAL SOLUTION TECHNIQUE

      CALL REMARK(3HTWO)
      CALL ASMBLE

C     CALCULATE ADJUSTED NODAL PARAMETERS

      CALL REMARK(5HTHREE)
      CALL BAKSUB

      CALL REMARK(4HFOUR)
    3 CONTINUE

      WRITE(3) MAXNOD,MAXNEL,RE,ADSPL
      ENDFILE 3
      STOP

    7 STOP "1 EOF ENCOUNTERED IN BUFFER IN OR OUT"
    8 STOP "1 PATITY ERROR IN BUFFER IN OR OUT"

      END
      SUBROUTINE INDAT

C     SUBROUTINE INDAT ACCEPTS ALL DATA REQUIRED TO SOLVE A FLOW PROBLEM

**********     ENTER COMMON BLOCK HERE     **********

      DIMENSION HEAD(9)

C     NNODZ = NUMBER OF NODES PER ELEMENT
      NNODZ=20

C     MAXNEL = MAXIMUM NUMBER OF ELEMENTS
C     MAXNOD = MAXIMUM NODE NUMBER
#
```

```
C     MAXDIS = MAXIMUM NUMBER OF SPECIFIED NON-ZERO VARIABLES
C     MAXNDZ = MAXIMUM NUMBER OF SPECIFIED ZERO (EARTHED) VARIABLES
C     MAXPRS = MAXIMUM NUMBER OF NODES AT WHICH A PRESSURE IS SPECIFIED
C     MAXSHR = MAXIMUM NUMBER OF NODES AT WHICH A SHEAR IS SPECIFIED

      WRITE(6,2000)
    1 READ(5,1001) ICODE,NCODE
    2 WRITE(6,1000) ICODE,NCODE

C     IF ICODE = 99, NO MORE DATA ACCEPTED

      IF(ICODE.NE.99) GO TO 3
      WRITE(6,2013)
      RETURN
    3 CONTINUE

      GOTO(100,200,300,400,500,700),ICODE

C     READ IN HEADINGS (NCODE = 01)

  100 GOTO(101,103),NCODE
  101 WRITE(6,2001)
  102 READ(5,1002) ICODE,NCODE,HEAD
      IF(ICODE.NE.0) GO TO 2
      WRITE(6,1003) HEAD
      GO TO 102

C     READ IN PROGRAM PARAMETERS (NCODE = 02)
C     MAXIT = MAXIMUM NUMBER OF ITERATIONS ALLOWED
C     NFORM = FORMULATION NUMBER

  103 WRITE(6,2014)
  104 READ(5,1012) ICODE,NCODE,(NW(I),I=1,2)
      IF(ICODE.NE.0) GO TO 2
      MAXIT=NW(1)
      NFORM=NW(2)
      WRITE(6,1013) MAXIT,NFORM
      GO TO 104

C     READ IN FLOW PROPERTIES (ICODE = 02)
C     RE IS THE REYNOLDS NUMBER OF THE FLOW

  200 WRITE(6,2002)
  201 READ(5,1004) ICODE,NCODE,NMAT,A
      IF(ICODE.NE.0) GO TO 2
      RE=A
      WRITE(6,1005) NMAT,RE
      GO TO 201

C     READ IN COORDINATES (ICODE = 03)

  300 GO TO(301,303),NCODE

C     CARTESIAN COORDINATES (NCODE = 01)

  301 WRITE(6,2003)
  302 READ(5,1004) ICODE,NCODE,NIC,COX,COY,COZ
      IF(ICODE.NE.0) GO TO 2
      WRITE(6,1005) NIC,COX,COY,COZ
      CORD(NIC,1)=COX
      CORD(NIC,2)=COY
      CORD(NIC,3)=COZ
      GO TO 302

C     CYLINDRICAL COORDINATES (NCODE = 02)
#
```

```
C     ANG IS DEFINED BY THE RIGHT HANDED SYSTEM

  303 WRITE(6,2004)
  304 READ(5,1004) ICODE,NCODE,NIC,RAD,ANG,COZ,COCX,COCY,COCZ
      IF(ICODE.NE.0) GO TO 2
      WRITE(6,1005) NIC,RAD,ANG,COZ,COCX,COCY,COCZ
      A1=0.0174532925*ANG
      CORD(NIC,1)=RAD*COS(A1)+COCX
      CORD(NIC,2)=RAD*SIN(A1)+COCY
      CORD(NIC,3)=COZ+COCZ
      GO TO 304

C     READ IN ELEMENT DEFINITIONS (ICODE = 04)

  400 WRITE(6,2005)
      NEL=0
  401 NEL=NEL+1
      READ(5,1006) ICODE,NCODE,(NW(I),I=1,12)
      IF(ICODE.NE.0) GO TO 402
      READ(5,1006) ICODE,NCODE,(NW(I),I=13,NNODZ)
      DO 403 I=1,NNODZ
      LDEF(NEL,I)=NW(I)
  403 CONTINUE
      WRITE(6,1007) NEL,(LDEF(NEL,I),I=1,NNODZ)
      MAXNEL=NEL
      GO TO 401
  402 DO 405 NEL=1,MAXNEL
      DO 404 LNOD=1,NNODZ
      IF(MAXNOD.LT.LDEF(NEL,LNOD)) MAXNOD=LDEF(NEL,LNOD)
  404 CONTINUE
  405 CONTINUE
      GO TO 2

C     READ IN FLOW CONSTRAINT DATA (ICODE = 05)

  500 NCOUNT=0
      GO TO(501,503),NCODE

C     NON-ZERO SPECIFIED VELOCITIES AND PRESSURES (NCODE = 01)

  501 WRITE(6,2006)
  502 NCOUNT=NCOUNT+1
      READ(5,1008) ICODE,NCODE,(NW(I),I=1,5),(CW(I),I=1,4)
      IF(ICODE.NE.0) GO TO 2
      DO 506 I=1,5
      NDISP(NCOUNT,I)=NW(I)
  506 CONTINUE
      DO 507 I=1,4
      DISP(NCOUNT,I)=CW(I)
  507 CONTINUE
      WRITE(6,1009) (NDISP(NCOUNT,I),I=1,5),(DISP(NCOUNT,I),I=1,4)
      MAXDIS=NCOUNT
      GO TO 502

C     ZERO-SPECIFIED VELOCITIES AND PRESSURES (NCODE = 02)

  503 WRITE(6,2007)
  504 READ(5,1010) ICODE,NCODE,NFIXU,NFIXV,NFIXW,NFIXP,(NW(I),I=1,14)
      IF(ICODE.NE.0) GO TO 2
      WRITE(6,1011) NFIXU,NFIXV,NFIXW,NFIXP,(NW(I),I=1,14)
      DO 505 I=1,14
      IF(NW(I).EQ.0) GO TO 504
      NCOUNT=NCOUNT+1
      NDISPZ(NCOUNT,1)=NFIXU
      NDISPZ(NCOUNT,2)=NFIXV
#
```

```
      NDISPZ(NCOUNT,3)=NFIXW
      NDISPZ(NCOUNT,4)=NFIXP
      NDISPZ(NCOUNT,5)=NW(I)
      MAXNDZ=NCOUNT
  505 CONTINUE
      GO TO 504

C     READ IN SPECIFIED SIDE STRESS DATA (ICODE = 07)

  700 NCOUNT=0
      GO TO(701,703),NCODE

C     SIDE PRESSURE (NCODE = 01)
C     PRESSURE IS ASSUMED POSITIVE IF IT ACTS ONTO THE SIDE

  701 WRITE(6,2010)
  702 NCOUNT=NCOUNT+1
      READ(5,1017) ICODE,NCODE,N,A1
      IF(ICODE.NE.0) GO TO 2
      NPRES(NCOUNT)=N
      PRES(NCOUNT)=A1
      WRITE(6,1018) NPRES(NCOUNT),PRES(NCOUNT)
      MAXPRS=NCOUNT
      GO TO 702

C     SIDE SHEAR STRESS (NCODE = 02)

  703 WRITE(6,2011)
  704 NCOUNT=NCOUNT+1
      READ(5,1017) ICODE,NCODE,N,A1,A2
      IF(ICODE.NE.0) GO TO 2
      NSHEAR(NCOUNT)=N
      SHEAR(NCOUNT,1)=A1
      SHEAR(NCOUNT,2)=A2
      WRITE(6,1018) NSHEAR(NCOUNT),(SHEAR(NCOUNT,I),I=1,2)
      MAXSHR=NCOUNT
      GO TO 704

 1000 FORMAT(1X,2I2)
 1001 FORMAT(2I2)
 1002 FORMAT(2I2,1X,9A8)
 1003 FORMAT(6X,9A8)
 1004 FORMAT(2I2,1X,I5,6E10.3)
 1005 FORMAT(6X,I5,6E10.3)
 1006 FORMAT(2I2,6X,12I5)
 1007 FORMAT(6X,21I5)
 1008 FORMAT(2I2,1X,4I1,1X,I5,5X,4E10.3)
 1009 FORMAT(6X,4I1,1X,I5,5X,4E10.3)
 1010 FORMAT(2I2,1X,4I1,1X,14I5)
 1011 FORMAT(6X,4I1,1X,14I5)
 1012 FORMAT(2I2,1X,2I5)
 1013 FORMAT(6X,2I5)
 1017 FORMAT(2I2,1X,I5,3E10.3)
 1018 FORMAT(6X,I5,3E10.3)

 2000 FORMAT(1H1)
 2001 FORMAT(2X,7HHEADING)
 2002 FORMAT(2X,15HREYNOLDS NUMBER)
 2003 FORMAT(2X,27HNODAL CARTESIAN COORDINATES)
 2004 FORMAT(2X,29HNODAL CYLINDRICAL COORDINATES)
 2005 FORMAT(2X,19HELEMENT DEFINITIONS)
 2006 FORMAT(2X,28HNON-ZERO SPECIFIED VARIABLES)
 2007 FORMAT(2X,24HZERO SPECIFIED VARIABLES)
 2010 FORMAT(2X,28HAPPLIED SIDE NORMAL STRESSES)
#
```

```
 2011 FORMAT(2X,27HAPPLIED SIDE SHEAR STRESSES)
 2013 FORMAT(2X,13HDATA COMPLETE)
 2014 FORMAT(2X,34HPROGRAM PARAMETERS MAXIT AND NFORM)

      END
      SUBROUTINE CHKPLT

C     SUBROUTINE CHKPLT CHECKS INPUT DATA FOR OBVIOUS ERRORS

**********     ENTER COMMON BLOCK HERE     **********

C     CHECK FOR ANY UNDEFINED NODAL COORDINATES AND CALCULATE THE
C     COORDINATES OF UNDEFINED MIDSIDE NODES

      WRITE(6,1000)
      DO 1 NEL=1,MAXNEL
      DO 2 NOD=1,NNODZ
      NIC=LDEF(NEL,NOD)
      COX=CORD(NIC,1)
      COY=CORD(NIC,2)
      COZ=CORD(NIC,3)
      DO 3 I=1,12
      N2=INT2(I)
      IF(NOD.EQ.N2) GO TO 4
    3 CONTINUE
      IF(COX.EQ.0.0.AND.COY.EQ.0.0.AND.COZ.EQ.0.0) WRITE(6,1001) NIC
      GO TO 2
    4 CONTINUE
      IF(COX.NE.0.0.OR.COY.NE.0.0.OR.COZ.NE.0.0) GO TO 2
      N1=INT1(I)
      N3=INT3(I)
      NIC1=LDEF(NEL,N1)
      NIC3=LDEF(NEL,N3)
      CORD(NIC,1)=(CORD(NIC1,1)+CORD(NIC3,1))*0.5
      CORD(NIC,2)=(CORD(NIC1,2)+CORD(NIC3,2))*0.5
      CORD(NIC,3)=(CORD(NIC1,3)+CORD(NIC3,3))*0.5
    2 CONTINUE
    1 CONTINUE

C     CHECK ELEMENT DEFINITIONS

      DO 5 NELI=1,MAXNEL
      DO 6 I=1,12
      NODI=INT2(I)
      N1=INT1(I)
      N2=INT3(I)
      NIC1=LDEF(NELI,N1)
      NIC2=LDEF(NELI,NODI)
      NIC3=LDEF(NELI,N2)
      DO 7 NELJ=1,MAXNEL
      DO 8 J=1,12
      NODJ=INT2(J)
      NIC5=LDEF(NELJ,NODJ)
      IF(NIC5.NE.NIC2) GO TO 8
      N3=INT1(J)
      N4=INT3(J)
      NIC4=LDEF(NELJ,N3)
      NIC6=LDEF(NELJ,N4)
      IF(NIC1.EQ.NIC4.AND.NIC3.EQ.NIC6) GO TO 8
      IF(NIC1.EQ.NIC6.AND.NIC3.EQ.NIC4) GO TO 8
      WRITE(6,1002) NELI,NELJ,NIC2
    8 CONTINUE
    7 CONTINUE
    6 CONTINUE
    5 CONTINUE
#
```

```
 1000 FORMAT(1H1,///)
 1001 FORMAT(5X,19HCOORDINATES OF NODE,I5,18H ARE (0.0,0.0,0.0))
 1002 FORMAT(5X,35HELEMENT DEFINITION ERRORS, ELEMENTS,2I5,5H NODE,I5)

      RETURN

      END
      SUBROUTINE PREFNT(LDEST,MAXLD)

C     SUBROUTINE PREFNT CALCULATES THE MAXIMUM FRONT WIDTH NEEDED BY
C     CR3DVF TO SOLVE THE FLOW PROBLEM

**********     ENTER COMMON BLOCK HERE     **********

      DIMENSION LDEST(MAXLD)

C     NVABZ = NUMBER OF VARIABLES PER NODE
C     MVABZ = NUMBER OF VARIABLES PER ELEMENT
C     MAXFW = MAXIMUM FRONT WIDTH ENCOUNTERED IN PROBLEM
C     IF MAXFW EXCEEDS MAXNW ALL MATRIX SIZES MUST BE ADJUSTED
      NVABZ=4
      MVABZ=NVABZ*NNODZ

C     INITIALIZE HEADING VECTOR NW
C     IF NW(I)=0 COLUMN I CAN ACCEPT A NEW NODAL VARIABLE

      MAXNW1=MAXNW+50
      DO 1 I=1,MAXNW1
      NW(I)=0
    1 CONTINUE

C     SET LDEST(NIC) EQUAL TO THE NUMBER OF THE ELEMENT IN WHICH NODE
C     NIC APPEARS FOR THE LAST TIME
C     SET LFRST(NIC) EQUAL TO THE NUMBER OF THE ELEMENT IN WHICH NODE
C     NIC APPEARS FOR THE FIRST TIME

      DO 2 NEL=1,MAXNEL
      DO 3 I=1,NNODZ
      NIC=LDEF(NEL,I)
      LDEST(NIC)=NEL
      IF(LFRST(NIC).EQ.0) LFRST(NIC)=NEL
    3 CONTINUE
    2 CONTINUE

C     CHANGE THE SIGN OF LDEF(NEL,I) FOR ELEMENTS NEL IN WHICH NODE
C     NUMBER I APPEARS FOR THE LAST TIME

      DO 5 NIC=1,MAXNOD
      NEL=LDEST(NIC)
      DO 6 I=1,NNODZ
      IF(LDEF(NEL,I).NE.NIC) GO TO 6
      LDEF(NEL,I)=-NIC
      LDEST(NIC)=0
      GO TO 5
    6 CONTINUE
    5 CONTINUE

C     CALCULATE MAXFW

      DO 7 NEL=1,MAXNEL
      DO 8 I=1,NNODZ
      N1=IABS(LDEF(NEL,I))
      DO 9 J=1,NVABZ
      DO 10 K=1,12
#
```

```
      IF(I.NE.INT2(K)) GO TO 10
      IF(J.EQ.NVABZ) GO TO 9
      GO TO 15
   10 CONTINUE
   15 CONTINUE
      NVAB=(N1-1)*NVABZ+J
      IF(LDEST(NVAB).NE.0) GO TO 8
      DO 11 K=1,MAXNW1
      IF(NW(K).NE.0) GO TO 11
      NW(K)=NVAB
      LDEST(NVAB)=K
      IF(MAXFW.LT.K) MAXFW=K
      GO TO 9
   11 CONTINUE
      WRITE(6,999) MAXNW1
      STOP1
    9 CONTINUE
    8 CONTINUE

      DO 12 I=1,NNODZ
      NIC=LDEF(NEL,I)
      N1=IABS(LDEF(NEL,I))
      IF(NIC.GT.0) GO TO 12
      DO 13 J=1,NVABZ
      DO 14,K=1,12
      IF(I.NE.INT2(K)) GO TO 14
      IF(J.EQ.NVABZ) GO TO 13
      GO TO 16
   14 CONTINUE
   16 CONTINUE
      NVAB=(N1-1)*NVABZ+J
      K=LDEST(NVAB)
      NW(K)=0
   13 CONTINUE
   12 CONTINUE
    7 CONTINUE
      WRITE(6,1001) NVABZ
      WRITE(6,1002) NNODZ
      WRITE(6,1003) MVABZ
      WRITE(6,1004) MAXNEL
      WRITE(6,1005) MAXNOD
      WRITE(6,1006) MAXFW,MAXNW
      WRITE(6,1007) MAXNS
      WRITE(6,1008) MAXNW,MAXND
      WRITE(6,1009) NFORM

C     STOP IF MAXNW IS EXCEEDED

      IF(MAXFW.LE.MAXNW)RETURN
      WRITE(6,1000) MAXFW
      STOP2

  999 FORMAT(45H1INSUFFICIENT ROOM TO CALCULATE FRONT WIDTH
     1       21HINCREASE MAXNW TO 50+,I3)
 1000 FORMAT(55H1MAXIMUM FRONT WIDTH DURING PREFNT EXCEEDS SIZE OF SS
     1       18HINCREASE MAXNW TO ,I5)
 1001 FORMAT(///,5X,30HNUMBER OF VARIABLES PER NODE =,I5,5X,
     130HWITH ONE LESS AT MIDSIDE NODES)
 1002 FORMAT(/,5X,29HNUMBER OF NODES PER ELEMENT =,I5)
 1003 FORMAT(/,5X,33HNUMBER OF VARIABLES PER ELEMENT =,I5,5X,
     150HINCLUDING 12 MIDSIDE VARIABLES THAT ARE NEVER USED,/)
 1004 FORMAT(/,5X,28HMAXIMUM NUMBER OF ELEMENTS =,I5)
 1005 FORMAT(/,5X,25HMAXIMUM NUMBER OF NODES =,I5,/)
 1006 FORMAT(/,5X,21HMAXIMUM FRONT WIDTH =,I5,5X,
     117HSHOULD NOT EXCEED,I5,/)
#
```

```
 1007 FORMAT(/,5X,69HMAXIMUM NUMBER OF SUBDIVISIONS IN TOTAL STRUCTURAL
     1STIFFNESS MATRIX =,I5)
 1008 FORMAT(/,5X,35HMAXIMUM SIZE OF EACH SUBDIVISION IS,I5,2H X,I5,/)
 1009 FORMAT(/,5X,14HFORMULATION = ,I5,/////)

      END
      SUBROUTINE STIFN

C     SUBROUTINE STIFN SETS UP THE ELEMENT STIFFNESS MATRIX FOR EACH
C     ELEMENT AT EACH ITERATION STEP

**********     ENTER COMMON BLOCK HERE     **********

      DIMENSION R(80,80)
      EQUIVALENCE (R(1,1),SS(1,1))

      REWIND 4

C     NRULE = NUMBER OF INTEGRATION POINTS PER DIMENSION
      NRULE=3

      DO 1 NEL =1,MAXNEL

      WRITE(6,1000) NEL
 1000 FORMAT(5X,*ELEMENT*,I3)

C     INITIALIZE LINEAR AND NON-LINEAR STIFFNESS MATRICES AND RIGHT
C     HAND SIDE FORCE VECTOR

      DO 2 I=1,MVABZ
      DO 3 J=1,MVABZ
      S(I,J)=0.0
      R(I,J)=0.0
    3 CONTINUE
      RS(I)=0.0
    2 CONTINUE

C     SET UP ELEMENT VARIABLES

      DO 4 J=1,NNODZ
      NIC=IABS(LDEF(NEL,J))
      X(J)=CORD(NIC,1)
      Y(J)=CORD(NIC,2)
      Z(J)=CORD(NIC,3)
      ELDISP(J,1)=ADSPL(NIC,1)
      ELDISP(J,2)=ADSPL(NIC,2)
      ELDISP(J,3)=ADSPL(NIC,3)
      ELDISP(J,4)=ADSPL(NIC,4)
    4 CONTINUE

C     EVALUATE STIFFNESS MATRIX COMPONENTS

      DO 6 JA=1,NRULE
      XL=VECTLC(JA)
      WX=WTFUN(JA)
      DO 7 JB=1,NRULE
      YL=VECTLC(JB)
      WY=WTFUN(JB)
      DO 8 JC=1,NRULE
      ZL=VECTLC(JC)
      WZ=WTFUN(JC)
      CALL JACOB(0)
      CALL MULT1
    8 CONTINUE
    7 CONTINUE
#
```

```
    6 CONTINUE

      CALL MULT2
      CALL MULT3

C     EVALUATE RIGHT HAND SIDE FORCE VECTOR COMPONENTS

      IF(MAXPRS.NE.0) CALL PRES1
      IF(MAXSHR.NE.0) CALL SHEAR1

C     STORE ON TAPE 4 EACH ELEMENT STIFFNESS AND FORCE ARRAYS

      BUFFER OUT (4,1) (RS(1),RS(80))
      IF(UNIT(4)) 5,10,11
    5 CONTINUE
      BUFFER OUT (4,1) (S(1,1),S(80,80))
      IF(UNIT(4)) 1,10,11
    1 CONTINUE

C     NSTOP IS SET TO ZERO IN SUBROUTINE JACOB IF ERRORS ARISE IN ANY
C     ELEMENT GEOMETRY

    9 IF(NSTOP.EQ.0) RETURN
      STOP3

   10 STOP "2 EOF ENCOUNTERED IN BUFFER IN OR OUT"
   11 STOP "2 PARITY ERROR IN BUFFER IN OR OUT"

      END
      SUBROUTINE JACOB(I1)

C     SUBROUTINE JACOB CALCULATES THE VALUES OF THE SHAPE FUNCTIONS,
C     THEIR FIRST DERIVATIVES AND THE JACOBIAN AT EACH GAUSS POINT

**********     ENTER COMMON BLOCK HERE     **********

C     INITIALIZE THE JACOBIAN ARRAY

      DO 1 I=1,9
      CW(I)=0.0
    1 CONTINUE

C     SHP1 AND SHP2 ARE THE LINEAR AND NON-LINEAR SHAPE FUNCTIONS
C     DX DY AND DZ ARE THE FIRST DERIVATIVES OF SHP1 WITH RESPECT
C     TO THE LOCAL COORDINATES

      A4=XL*XL
      A5=YL*YL
      A6=ZL*ZL
      DO 2 I=1,NNODZ
      A1=XL*XX(I)
      A2=YL*YY(I)
      A3=ZL*ZZ(I)
      GO TO(10,30,10,20,10,30,10,20,40,40,
     1      40,40,10,30,10,20,10,30,10,20),I
   10 DX(I)=0.125*(1+A2)*(1+A3)*(2*A1+A2+A3-1)*XX(I)
      DY(I)=0.125*(1+A1)*(1+A3)*(A1+2*A2+A3-1)*YY(I)
      DZ(I)=0.125*(1+A1)*(1+A2)*(A1+A2+2*A3-1)*ZZ(I)
      SHP1(I)=0.125*(1+A1)*(1+A2)*(1+A3)*(A1+A2+A3-2)
      SHP2(I)=0.125*(1+A1)*(1+A2)*(1+A3)
      GO TO 3
   20 DX(I)=-0.5*XL*(1+A2)*(1+A3)
      DY(I)=0.25*YY(I)*(1-A4)*(1+A3)
      DZ(I)=0.25*ZZ(I)*(1-A4)*(1+A2)
      SHP1(I)=0.25*(1-A4)*(1+A2)*(1+A3)
#
```

```
      SHP2(I)=0.0
      GO TO 3
   30 DX(I)=0.25*XX(I)*(1-A5)*(1+A3)
      DY(I)=-0.5*YL*(1+A1)*(1+A3)
      DZ(I)=0.25*ZZ(I)*(1-A5)*(1+A1)
      SHP1(I)=0.25*(1+A1)*(1-A5)*(1+A3)
      SHP2(I)=0.0
      GO TO 3
   40 DX(I)=0.25*XX(I)*(1-A6)*(1+A2)
      DY(I)=0.25*YY(I)*(1-A6)*(1+A1)
      DZ(I)=-0.5*ZL*(1+A1)*(1+A2)
      SHP1(I)=0.25*(1+A1)*(1+A2)*(1-A6)
      SHP2(I)=0.0
    3 CONTINUE

C     SET UP THE 9 COMPONENTS OF THE JACOBIAN MATRIX J

      CW(1)=CW(1)+DX(I)*X(I)
      CW(2)=CW(2)+DX(I)*Y(I)
      CW(3)=CW(3)+DX(I)*Z(I)
      CW(4)=CW(4)+DY(I)*X(I)
      CW(5)=CW(5)+DY(I)*Y(I)
      CW(6)=CW(6)+DY(I)*Z(I)
      CW(7)=CW(7)+DZ(I)*X(I)
      CW(8)=CW(8)+DZ(I)*Y(I)
      CW(9)=CW(9)+DZ(I)*Z(I)
    2 CONTINUE

C     EVALUATE THE DETERMINANT OF J

      DETJ=CW(1)*(CW(5)*CW(9)-CW(8)*CW(6))+
     1     CW(2)*(CW(7)*CW(6)-CW(4)*CW(9))+
     2     CW(3)*(CW(4)*CW(8)-CW(7)*CW(5))

C     IF THE DETERMINANT OF J IS ZERO OR NEGATIVE SET NSTOP TO 1 AND
C     EXECUTION WILL TERMINATE IN SUBROUTINE STIFN

      IF(DETJ.GT.0.0) GO TO 4
      WRITE(6,1000) NEL,DETJ
      NSTOP=1
    4 CONTINUE

C     INVERT J

      RDETJ=1.0/DETJ
      AW(1)=(CW(5)*CW(9)-CW(6)*CW(8))*RDETJ
      AW(2)=(CW(3)*CW(8)-CW(2)*CW(9))*RDETJ
      AW(3)=(CW(2)*CW(6)-CW(3)*CW(5))*RDETJ
      AW(4)=(CW(6)*CW(7)-CW(4)*CW(9))*RDETJ
      AW(5)=(CW(1)*CW(9)-CW(3)*CW(7))*RDETJ
      AW(6)=(CW(3)*CW(4)-CW(1)*CW(6))*RDETJ
      AW(7)=(CW(4)*CW(8)-CW(5)*CW(7))*RDETJ
      AW(8)=(CW(2)*CW(7)-CW(1)*CW(8))*RDETJ
      AW(9)=(CW(1)*CW(5)-CW(2)*CW(4))*RDETJ

C     IF SUBROUTINE JACOB IS CALLED FROM PRES2 OR SHEAR2 I1=1
C     NO FURTHER CALCULATION NEEDED IN JACOB

      IF(I1.EQ.1) RETURN

C     SET UP DERIVATIVES WITH RESPECT TO GLOBAL COORDINATES

      DO 5 I=1,NNODZ
      DXI=DX(I)
      DYI=DY(I)
#
```

```
      DZI=DZ(I)
      DX(I)=AW(1)*DXI+AW(2)*DYI+AW(3)*DZI
      DY(I)=AW(4)*DXI+AW(5)*DYI+AW(6)*DZI
      DZ(I)=AW(7)*DXI+AW(8)*DYI+AW(9)*DZI
    5 CONTINUE
      RETURN

 1000 FORMAT(//,5X,28HNEGATIVE OR ZERO DETERMINENT,/,5X,8HELEMENT ,I5,
     1       12H DETERMINENT,2X,E10.3)

      END
      SUBROUTINE MULT1

C     SUBROUTINE MULT1 EVALUATES THE INTEGRALS OF ALL THE CROSS PRODUCTS
C     OF DERIVATIVES OF THE SHAPE FUNCTIONS BY NUMERICAL INTEGRATION

**********     ENTER COMMON BLOCK HERE     **********

      DIMENSION R(80,80)
      EQUIVALENCE (R(1,1),SS(1,1))

      WAIT=WX*WY*WZ*DETJ
      DO 1 I=1,NNODZ
      DXI=DX(I)*WAIT
      DYI=DY(I)*WAIT
      DZI=DZ(I)*WAIT
      SHP1I=SHP1(I)*WAIT
      SHP2I=SHP2(I)*WAIT
      II=(I-1)*NVABZ
      DO 2 J=1,NNODZ
      DXJ=DX(J)
      DYJ=DY(J)
      DZJ=DZ(J)
      SHP1J=SHP1(J)
      SHP2J=SHP2(J)
      JJ=(J-1)*NVABZ

C     EVALUATE INTEGRALS FOR THE LINEAR STIFFNESS S

      S(II+1,JJ+1)=S(II+1,JJ+1)+DXI*DXJ
      S(II+1,JJ+2)=S(II+1,JJ+2)+DYI*DXJ
      S(II+1,JJ+3)=S(II+1,JJ+3)+DZI*DXJ
      S(II+1,JJ+4)=S(II+1,JJ+4)+DXI*DYJ
      S(II+2,JJ+1)=S(II+2,JJ+1)+DYI*DYJ
      S(II+2,JJ+2)=S(II+2,JJ+2)+DZI*DYJ
      S(II+2,JJ+3)=S(II+2,JJ+3)+DXI*DZJ
      S(II+2,JJ+4)=S(II+2,JJ+4)+DYI*DZJ
      S(II+3,JJ+1)=S(II+3,JJ+1)+DZI*DZJ
      S(II+3,JJ+2)=S(II+3,JJ+2)+DXI*SHP2J
      S(II+3,JJ+3)=S(II+3,JJ+3)+DYI*SHP2J
      S(II+3,JJ+4)=S(II+3,JJ+4)+DZI*SHP2J
      S(II+4,JJ+1)=S(II+4,JJ+1)+DXJ*SHP2I
      S(II+4,JJ+2)=S(II+4,JJ+2)+DYJ*SHP2I
      S(II+4,JJ+3)=S(II+4,JJ+3)+DZJ*SHP2I

C     EVALUATE THE INTEGRALS FOR THE NON-LINEAR STIFFNESS R

      DO 3 K=1,NNODZ
      DXK=DX(K)
      DYK=DY(K)
      DZK=DZ(K)
      SHP1K=SHP1(K)
      R(II+1,JJ+1)=R(II+1,JJ+1)+SHP1I*SHP1J*DXK*ELDISP(K,1)
      R(II+1,JJ+2)=R(II+1,JJ+2)+SHP1I*SHP1J*DXK*ELDISP(K,2)
      R(II+1,JJ+3)=R(II+1,JJ+3)+SHP1I*SHP1J*DXK*ELDISP(K,3)
#
```

```
      R(II+1,JJ+4)=R(II+1,JJ+4)+SHP1I*SHP1J*DYK*ELDISP(K,1)
      R(II+2,JJ+1)=R(II+2,JJ+1)+SHP1I*SHP1J*DYK*ELDISP(K,2)
      R(II+2,JJ+2)=R(II+2,JJ+2)+SHP1I*SHP1J*DYK*ELDISP(K,3)
      R(II+2,JJ+3)=R(II+2,JJ+3)+SHP1I*SHP1J*DZK*ELDISP(K,1)
      R(II+2,JJ+4)=R(II+2,JJ+4)+SHP1I*SHP1J*DZK*ELDISP(K,2)
      R(II+3,JJ+1)=R(II+3,JJ+1)+SHP1I*SHP1J*DZK*ELDISP(K,3)
      R(II+3,JJ+2)=R(II+3,JJ+2)+SHP1I*SHP1K*DXJ*ELDISP(K,1)
      R(II+3,JJ+3)=R(II+3,JJ+3)+SHP1I*SHP1K*DYJ*ELDISP(K,2)
      R(II+3,JJ+4)=R(II+3,JJ+4)+SHP1I*SHP1K*DZJ*ELDISP(K,3)
    3 CONTINUE
    2 CONTINUE
    1 CONTINUE

      RETURN

      END
      SUBROUTINE MULT2

C     SUBROUTINE MULT2 COMBINES THE INDIVIDUAL INTEGRALS FROM MULT1 TO
C     GIVE THE COMPONENTS OF THE ELEMENT STIFFNESS MATRIX S AND THE
C     MATRIX OF COEFFICIENTS OF THE ORIGINAL EQUATIONS

**********     ENTER COMMON BLOCK HERE     **********

      DIMENSION R(80,80)
      EQUIVALENCE (R(1,1),SS(1,1))

      DO 1 I=1,NNODZ
      II=(I-1)*NVABZ
      DO 2 J=1,NNODZ
      JJ=(J-1)*NVABZ
      S1=S(II+1,JJ+1)
      S2=S(II+1,JJ+2)
      S3=S(II+1,JJ+3)
      S4=S(II+1,JJ+4)
      S5=S(II+2,JJ+1)
      S6=S(II+2,JJ+2)
      S7=S(II+2,JJ+3)
      S8=S(II+2,JJ+4)
      S9=S(II+3,JJ+1)
      S10=S(II+3,JJ+2)
      S11=S(II+3,JJ+3)
      S12=S(II+3,JJ+4)
      S13=S(II+4,JJ+1)
      S14=S(II+4,JJ+2)
      S15=S(II+4,JJ+3)

      R1=R(II+1,JJ+1)
      R2=R(II+1,JJ+2)
      R3=R(II+1,JJ+3)
      R4=R(II+1,JJ+4)
      R5=R(II+2,JJ+1)
      R6=R(II+2,JJ+2)
      R7=R(II+2,JJ+3)
      R8=R(II+2,JJ+4)
      R9=R(II+3,JJ+1)
      RR=R(II+3,JJ+2)+R(II+3,JJ+3)+R(II+3,JJ+4)

      R(II+1,JJ+1)=(2*S1+S5+S9)/RE+(R1)
      R(II+1,JJ+2)=(S2)/RE+(R4)
      R(II+1,JJ+3)=(S3)/RE+(R7)
      R(II+1,JJ+4)=-S10
      R(II+2,JJ+1)=(S4)/RE+(R2)
      R(II+2,JJ+2)=(S1+2*S5+S9)/RE+(R5)
      R(II+2,JJ+3)=(S6)/RE+(R8)
#
```

```
      R(II+2,JJ+4)=-S11
      R(II+3,JJ+1)=(S7)/RE+(R3)
      R(II+3,JJ+2)=(S8)/RE+(R6)
      R(II+3,JJ+3)=(S1+S5+2*S9)/RE+(R9)
      R(II+3,JJ+4)=-S12
      R(II+4,JJ+1)=-S13
      R(II+4,JJ+2)=-S14
      R(II+4,JJ+3)=-S15

      S(II+1,JJ+1)=R(II+1,JJ+1)+RR
      S(II+1,JJ+2)=R(II+1,JJ+2)
      S(II+1,JJ+3)=R(II+1,JJ+3)
      S(II+1,JJ+4)=-S10
      S(II+2,JJ+1)=R(II+2,JJ+1)
      S(II+2,JJ+2)=R(II+2,JJ+2)+RR
      S(II+2,JJ+3)=R(II+2,JJ+3)
      S(II+2,JJ+4)=-S11
      S(II+3,JJ+1)=R(II+3,JJ+1)
      S(II+3,JJ+2)=R(II+3,JJ+2)
      S(II+3,JJ+3)=R(II+3,JJ+3)+RR
      S(II+3,JJ+4)=-S12
      S(II+4,JJ+1)=-S13
      S(II+4,JJ+2)=-S14
      S(II+4,JJ+3)=-S15

    2 CONTINUE
    1 CONTINUE
      RETURN

      END
      SUBROUTINE MULT3

C     SUBROUTINE MULT3 CALCULATES THE VALUES OF THE RIGHT HAND SIDES OF
C     THE ORIGINAL EQUATIONS USING THE NODAL VALUES OF VELOCITY AND
C     PRESSURE FROM THE PREVIOUS ITERATION. IF THE RIGHT HAND SIDES ARE
C     ALL ZERO THE EXACT SOLUTION HAS BEEN FOUND

**********     ENTER COMMON BLOCK HERE     **********

      DIMENSION R(80,80)
      EQUIVALENCE (R(1,1),SS(1,1))

      DO 1 I=1,NNODZ
      II=(I-1)*NVABZ
      NIC=IABS(LDEF(NEL,I))
      DO 2 J=1,NNODZ
      JJ=(J-1)*NVABZ
      DO 3 K=1,NVABZ
      DO 4 L=1,NVABZ
      RS(II+K)=RS(II+K)+R(II+K,JJ+L)*ELDISP(J,L)
    4 CONTINUE
    3 CONTINUE
    2 CONTINUE
    1 CONTINUE
      RETURN

      END
      SUBROUTINE PRES1

C     SUBROUTINE PRES1 FINDS THE FACES THAT HAVE A PRESSURE APPLIED ON
C     THEM

**********     ENTER COMMON BLOCK HERE     **********

      DIMENSION IP(20)
#
```

```
      LOGICAL IP
      N=0
      DO 1 I=1,NNODZ
      P(I)=0.0
      IP(I)=.FALSE.
    1 CONTINUE

      DO 2 J=1,MAXPRS
      NOD=NPRES(J)
      DO 3 I=1,NNODZ
      IF(IABS(LDEF(NEL,I)).NE.NOD) GO TO 3
      P(I)=PRES(J)
      N=N+1
      IP(I)=.TRUE.
      GO TO 2
    3 CONTINUE
    2 CONTINUE

      IF(N.LT.4) RETURN
      IF(IP(13).AND.IP(15).AND.IP(17).AND.IP(19)) CALL PRES2(1)
      IF(IP(15).AND.IP( 3).AND.IP( 5).AND.IP(17)) CALL PRES2(2)
      IF(IP( 1).AND.IP( 3).AND.IP(15).AND.IP(13)) CALL PRES2(3)
      IF(IP( 1).AND.IP( 3).AND.IP( 5).AND.IP( 7)) CALL PRES2(4)
      IF(IP(13).AND.IP( 1).AND.IP( 7).AND.IP(19)) CALL PRES2(5)
      IF(IP( 7).AND.IP( 5).AND.IP(17).AND.IP(19)) CALL PRES2(6)
      RETURN

      END
      SUBROUTINE PRES2(I1)

C     SUBROUTINE PRES2 EVALUATES THE ORIENTATIONS OF THE FACES AT THE
C     NINE GAUSS POINTS ON EACH FACE

**********     ENTER COMMON BLOCK HERE     **********

      GO TO(1,2,3,4,5,6),I1

    1 WZ=-1.0
      ZL=1.0
      GO TO 7
    4 WZ=1.0
      ZL=-1.0
    7 DO 8 JA=1,NRULE
      WX=WTFUN(JA)
      XL=VECTLC(JA)
      DO 9 JB=1,NRULE
      WY=WTFUN(JB)
      YL=VECTLC(JB)
      CALL JACOB(1)
      CALL PRES3(3,6,9)
    9 CONTINUE
    8 CONTINUE
      RETURN

    2 WY=-1.0
      YL=1.0
      GO TO 10
    5 WY=1.0
      YL=-1.0
   10 DO 11 JA=1,NRULE
      WX=WTFUN(JA)
      XL=VECTLC(JA)
      DO 12 JB=1,NRULE
      WZ=WTFUN(JB)
      ZL=VECTLC(JB)
#
```

```
      CALL JACOB(1)
      CALL PRES3(2,5,8)
   12 CONTINUE
   11 CONTINUE
      RETURN

    3 WX=-1.0
      XL=1.0
      GO TO 13
    6 WX=1.0
      XL=-1.0
   13 DO 14 JA=1,NRULE
      WY=WTFUN(JA)
      YL=VECTLC(JA)
      DO 15 JB=1,NRULE
      WZ=WTFUN(JB)
      ZL=VECTLC(JB)
      CALL JACOB(1)
      CALL PRES3(1,4,7)
   15 CONTINUE
   14 CONTINUE
      RETURN

      END
      SUBROUTINE PRES3(I1,I2,I3)

C     SUBROUTINE PRES3 EVALUATES THE X  Y AND Z COMPONENTS OF THE FACE
C     PRESSURE AT THE NINE GAUSS POINTS ON EACH FACE AND THEN USES
C     NUMERICAL INTEGRATION TO CALCULATE THE X  Y AND Z COMPONENTS OF
C     THE EQUIVALENT NODAL FORCES

**********     ENTER COMMON BLOCK HERE     **********

      APRES=0.0
      DO 1 I=1,NNODZ
      APRES=APRES+P(I)*SHP2(I)
    1 CONTINUE

      WAIT=WX*WY*WZ*APRES*DETJ

      M=0
      DO 2 I=1,NNODZ
      SHPI=SHP1(I)*WAIT
      RS(M+1)=RS(M+1)-SHPI*AW(I1)
      RS(M+2)=RS(M+2)-SHPI*AW(I2)
      RS(M+3)=RS(M+3)-SHPI*AW(I3)
      M=M+NVABZ
    2 CONTINUE
      RETURN

      END
      SUBROUTINE SHEAR1

C     SUBROUTINE SHEAR1 FINDS THE FACES THAT HAVE A SHEAR STRESS APPLIED
C     ON THEM

**********     ENTER COMMON BLOCK HERE     **********

      DIMENSION IS(20)
      LOGICAL IS
      N=0
      DO 1 I=1,NNODZ
      SH1(I)=0.0
      SH2(I)=0.0
#
```

```
      IS(I)=.FALSE.
    1 CONTINUE

      DO 2 J=1,MAXSHR
      NOD=NSHEAR(J)
      DO 3 I=1,NNODZ
      IF(IABS(LDEF(NEL,I)).NE.NOD) GO TO 3
      SH1(I)=SHEAR(J,1)
      SH2(I)=SHEAR(J,2)
      N=N+1
      IS(I)=.TRUE.
      GO TO 2
    3 CONTINUE
    2 CONTINUE

      IF(N.LT.4) RETURN
      IF(IS(13).AND.IS(15).AND.IS(17).AND.IS(19)) CALL SHEAR2(1)
      IF(IS(15).AND.IS( 3).AND.IS( 5).AND.IS(17)) CALL SHEAR2(2)
      IF(IS( 1).AND.IS( 3).AND.IS(15).AND.IS(13)) CALL SHEAR2(3)
      IF(IS( 1).AND.IS( 3).AND.IS( 5).AND.IS( 7)) CALL SHEAR2(4)
      IF(IS(13).AND.IS( 1).AND.IS( 7).AND.IS(19)) CALL SHEAR2(5)
      IF(IS( 7).AND.IS( 5).AND.IS(17).AND.IS(19)) CALL SHEAR2(6)
      RETURN

      END
      SUBROUTINE SHEAR2(I1)

C     SUBROUTINE SHEAR2 EVALUATES THE ORIENTATIONS OF THE FACES AT THE
C     NINE GAUSS POINTS ON EACH FACE

**********     ENTER COMMON BLOCK HERE     **********

      GO TO(1,2,3,4,5,6),I1

    1 WZ=-1.0
      ZL=1.0
      GO TO 7
    4 WZ=1.0
      ZL=-1.0
    7 DO 8 JA=1,NRULE
      WX=WTFUN(JA)
      XL=VECTLC(JA)
      DO 9 JB=1,NRULE
      WY=WTFUN(JB)
      YL=VECTLC(JB)
      CALL JACOB(1)
      CALL SHEAR3(3,6,9,4,5,6,1,2,3)
    9 CONTINUE
    8 CONTINUE
      RETURN

    2 WY=-1.0
      YL=1.0
      GO TO 10
    5 WY=1.0
      YL=-1.0
   10 DO 11 JA=1,NRULE
      WX=WTFUN(JA)
      XL=VECTLC(JA)
      DO 12 JB=1,NRULE
      WZ=WTFUN(JB)
      ZL=VECTLC(JB)
      CALL JACOB(1)
      CALL SHEAR3(2,5,8,1,2,3,7,8,9)
#
```

```
   12 CONTINUE
   11 CONTINUE
      RETURN

    3 WX=-1.0
      XL=1.0
      GO TO 13
    6 WX=1.0
      XL=-1.0
   13 DO 14 JA=1,NRULE
      WY=WTFUN(JA)
      YL=VECTLC(JA)
      DO 15 JB=1,NRULE
      WZ=WTFUN(JB)
      ZL=VECTLC(JB)
      CALL JACOB(1)
      CALL SHEAR3(1,4,7,7,8,9,4,5,6)
   15 CONTINUE
   14 CONTINUE
      RETURN

      END
      SUBROUTINE SHEAR3(I1,I2,I3,I4,I5,I6,I7,I8,I9)

C     SUBROUTINE SHEAR3 EVALUATES THE X Y AND Z COMPONENTS OF THE FACE
C     SHEAR STRESS AT THE NINE GAUSS POINTS ON EACH FACE AND THEN USES
C     NUMERICAL INTEGRATION TO CALCULATE THE X  Y AND Z COMPONENTS OF
C     THE EQUIVALENT NODAL FORCES

**********     ENTER COMMON BLOCK HERE     **********

      ASHR1=0.0
      ASHR2=0.0
      DO 1 I=1,NNODZ
      ASHR1=ASHR1+SH1(I)*SHP2(I)
      ASHR2=ASHR2+SH2(I)*SHP2(I)
    1 CONTINUE

      A1=SQRT(AW(I1)*AW(I1)+AW(I2)*AW(I2)+AW(I3)*AW(I3))*DETJ*WX*WY*WZ
      A2=SQRT(CW(I4)*CW(I4)+CW(I5)*CW(I5)+CW(I6)*CW(I6))
      A3=SQRT(CW(I7)*CW(I7)+CW(I8)*CW(I8)+CW(I9)*CW(I9))

      WAIT1=ASHR1*A1/A2
      WAIT2=ASHR2*A1/A3

      M=0
      DO 2 I=1,NNODZ
      RS(M+1)=RS(M+1)-SHP1(I)*WAIT1*CW(I4)+SHP1(I)*WAIT2*CW(I7)
      RS(M+2)=RS(M+2)-SHP1(I)*WAIT1*CW(I5)+SHP2(I)*WAIT2*CW(I8)
      RS(M+3)=RS(M+3)-SHP1(I)*WAIT1*CW(I6)+SHP2(I)*WAIT2*CW(I9)
      M=M+NVABZ
    2 CONTINUE
      RETURN

      END
      SUBROUTINE ASMBLE

C     SUBROUTINE ASMBLE ASSEMBLES THE ELEMENT STIFFNESS MATRIX INTO THE
C     GLOBAL ARRAY

**********     ENTER COMMON BLOCK HERE     **********

      REWIND 2
      REWIND 4

#
```

```
C     INITIALIZE HEADING VECTOR NW

      DO 1 I=1,MAXNW
      NW(I)=0
    1 CONTINUE
      NUMEQ=0

C     INITIALIZE STORAGE CONTROL VARIABLES MZM AND NZN

      MZM=0
      NZN=0

C     INTRODUCE ELEMENTS ONE AT A TIME

      DO 2 NEL=1,MAXNEL
      BUFFER IN (4,1) (RS(1),RS(80))
      IF(UNIT(4)) 30,31,32
   30 CONTINUE
      BUFFER IN (4,1) (S(1,1),S(80,80))

C     FOR EACH NEW ELEMENT CALCULATE THE NUMBER OF NEW VARIABLES THAT
C     WILL BE INTRODUCED WHEN THE ELEMENT IS ASSEMBLED IN SS

      N=0
      DO 3 I=1,NNODZ
      NIC=IABS(LDEF(NEL,I))
      DO 4 J=1,NVABZ
      DO 5 K=1,12
      IF(I.NE.INT2(K)) GO TO 5
      IF(J.EQ.NVABZ) GO TO 4
      GO TO 24
    5 CONTINUE
   24 CONTINUE
      IF(LFRST(NIC).LT.NEL) N=N+1
    4 CONTINUE
    3 CONTINUE

C     CALCULATE THE NUMBER OF VACANT POSITIONS IN THE SS MATRIX

      DO 6 I=1,MAXNW
      IF(NW(I).EQ.0) N=N+1
    6 CONTINUE

      IF(UNIT(4)) 33,31,32
   33 CONTINUE

C     REDUCE OUT THE REQUIRED NUMBER OF EQUATIONS IF THERE IS
C     INSUFFICIENT ROOM IN SS FOR THE NEXT ELEMENT TO BE ASSEMBLED

      M=68-N
      IF(N.LT.68) CALL FRONT(M)

C     SET UP THE VARIABLE DESTINATION VECTOR NELDES AND THE HEADING
C     VECTOR NW

      DO 7 I=1,NNODZ
      NIC=IABS(LDEF(NEL,I))
      DO 8 J=1,NVABZ
      DO 9 K=1,12
      IF(I.NE.INT2(K)) GO TO 9
      IF(J.EQ.NVABZ) GO TO 8
      GO TO 25
    9 CONTINUE
   25 CONTINUE
      N1=(I-1)*NVABZ+J
#
```

```
      NVAB=(NIC-1)*NVABZ+J
      IF(LFRST(NIC).GE.NEL) GO TO 10
      DO 11 K=1,MAXNW
      IF(NW(K).NE.NVAB) GO TO 11
      NELDES(N1)=K
      GO TO 8
   11 CONTINUE
   10 CONTINUE

      DO 12 K=1,MAXNW
      IF(NW(K).NE.0) GO TO 12
      NELDES(N1)=K
      NW(K)=NVAB
      GO TO 8
   12 CONTINUE
    8 CONTINUE
    7 CONTINUE

C     ASSEMBLE THE NEW ELEMENT

      DO 29 KK=1,MAXNS
      DO 13 I=1,NNODZ
      DO 14 II=1,NVABZ
      DO 15 K=1,12
      IF(I.NE.INT2(K)) GO TO 15
      IF(II.EQ.NVABZ) GO TO 14
      GO TO 26
   15 CONTINUE
   26 CONTINUE
      N1=(I-1)*NVABZ+II
      ISTRST=NELDES(N1)
      IELEMT=N1
      IF(KK.EQ.1) SRS(ISTRST)=SRS(ISTRST)+RS(IELEMT)
      ISTRST=ISTRST-KS+1
      IF(ISTRST.LT.1.OR.ISTRST.GT.MAXND) GO TO 14
      DO 16 J=1,NNODZ
      DO 17 JJ=1,NVABZ
      DO 18 K=1,12
      IF(J.NE.INT2(K)) GO TO 18
      IF(JJ.EQ.NVABZ) GO TO 17
      GO TO 27
   18 CONTINUE
   27 CONTINUE
      N1=(J-1)*NVABZ+JJ
      JSTRST=NELDES(N1)
      JELEMT=N1
      SS(ISTRST,JSTRST)=SS(ISTRST,JSTRST)+S(IELEMT,JELEMT)
   17 CONTINUE
   16 CONTINUE
   14 CONTINUE
   13 CONTINUE
      BUFFER OUT (L21,1) (SS(1,1),SS(MAXND,MAXNW))
      IF(UNIT(L21)) 34,31,32
   34 CONTINUE
      IF(KK.EQ.MAXNS) GO TO 29
      BUFFER IN (L20,1) (SS(1,1),SS(MAXND,MAXNW))
      KS=KS+MAXND
      KF=KF+MAXND
      IF(UNIT(L20)) 29,31,32
   29 CONTINUE

      CALL RESET

C     CHANGE THE SIGN OF THE HEADING VECTOR NW FOR ANY VARIABLE THAT
C     CAN NOW BE REDUCED OUT OF THE EQUATION SYSTEM
#
```

```
      DO 19 I=1,NNODZ
      NIC=LDEF(NEL,I)
      N1=IABS(LDEF(NEL,I))
      IF(NIC.GT.0) GO TO 19
      DO 20 J=1,NVABZ
      DO 21 K=1,12
      IF(I.NE.INT2(K)) GO TO 21
      IF(J.EQ.NVABZ) GO TO 20
      GO TO 28
   21 CONTINUE
   28 CONTINUE
      NVAB=(N1-1)*NVABZ+J

      DO 22 K=1,MAXNW
      IF(NW(K).NE.NVAB) GO TO 22
      NW(K)=-NW(K)
      GO TO 20
   22 CONTINUE
   20 CONTINUE
   19 CONTINUE

    2 CONTINUE

C     REDUCE OUT ALL THE REMAINING EQUATIONS ONCE ALL THE ELEMENTS
C     HAVE BEEN ASSEMBLED

      N=0
      DO 23 K=1,MAXNW
      IF(NW(K).NE.0) N=N+1
   23 CONTINUE
      CALL FRONT(N)
      RETURN

   31 STOP "3 EOF ENCOUNTERED IN BUFFER IN OR OUT"
   32 STOP "3 PARITY ERROR IN BUFFER IN OR OUT"

      END
      SUBROUTINE FRONT(MREQ)

C     SUBROUTINE FRONT REDUCES THE EQUATION SYSTEM TO UPPER TRIANGULAR
C     FORM USING THE GAUSS REDUCTION TECHNIQUE

**********      ENTER COMMON BLOCK HERE      **********

C     MAXREQ = MAXIMUM SIZE OF STORAGE VECTOR FOR REDUCED EQUATIONS
C     IF MAXREQ IS EXCEEDED REDUCED EQUATIONS STORED ON TAPE 2
C     LIV IS THE NUMBER OF THE EQUATION THAT IS TO BE USED IN THE
C     REDUCTION PROCESS
C     NUMEQ IS THE TOTAL NUMBER OF SIMULTANEOUS EQUATIONS IN THE PROBLEM

      MAXREQ=1000
      MAXLREQ=200
      NUMEQ=NUMEQ+MREQ

      DO 1 IEQ=1,MREQ
      IND=0

C     INITIALIZE HEADING VECTOR LIMITS

      NSNW=1
      NFNW=MAXNW

C     ADJUST HEADING VECTOR LIMITS

#
```

```
    3 IF(NW(NSNW).NE.0) GO TO 4
      NSNW=NSNW+1
      GO TO 3
    4 IF(NW(NFNW).NE.0) GO TO 5
      NFNW=NFNW-1
      GO TO 4
    5 CONTINUE

C     FIND THE VARIABLE WHOSE EQUATION LIV HAS THE LARGEST PIVOT
C     ONLY VARIABLES THAT CORRESPOND TO NODES THAT CAN BE REDUCED OUT
C     NEED BE CONSIDERED

      AMAX=0.0
      DO 2 K=NSNW,NFNW
      IF(NW(K).GE.0) GO TO 2
      IF(K.GT.KF) CALL CHECK(K)
      N1=K-KS+1
      IF(ABS(SS(N1,K)).LE.AMAX) GO TO 2
      AMAX=ABS(SS(N1,K))
      LIV=K
      DO 19 I=NSNW,NFNW
      STEQ(I)=SS(N1,I)
   19 CONTINUE
    2 CONTINUE
      CALL RESET

      NVAB=IABS(NW(LIV))
      N1=(NVAB-1)/NVABZ
      NUMVAB=NVAB-N1*NVABZ
      NIC=N1+1
      LOC=NVAB

C     FIND AN EQUATION LIN THAT CAN BE ADDED TO EQUATION LIV SO THAT THE
C     LARGEST ABSOLUTE VALUE OF PIVOT IS OBTAINED
C     ONLY EQUATIONS THAT CORRESPOND TO VARIABLES THAT ARE FREE AND FOR
C     NODES THAT CAN BE REDUCED OUT NEED BE CONSIDERED

      BMAX=0.0
      LIN=0
      DO 12 I=NSNW,NFNW
      IF(NW(I).GE.0) GO TO 12
      IF(I.EQ.LIV) GO TO 12
      IF(I.GT.KF) CALL CHECK(I)
      N1=I-KS+1
      SUM=SS(N1,LIV)+STEQ(LIV)
      IF(ABS(SUM).LE.ABS(BMAX)) GO TO 12
      N=IABS(NW(I))
      N1=(N-1)/NVABZ
      N2=N-N1*NVABZ
      N1=N1+1
      DO 15 J=1,MAXDIS
      IF(N1.NE.NDISP(J,5)) GO TO 15
      IF(NDISP(J,N2).EQ.1) GO TO 12
      GO TO 16
   15 CONTINUE
   16 CONTINUE

      DO 17 J=1,MAXNDZ
      IF(N1.NE.NDISPZ(J,5)) GO TO 17
      IF(NDISPZ(J,N2).EQ.1) GO TO 12
      GO TO 18
   17 CONTINUE
   18 CONTINUE
      BMAX=SUM
      LIN=I
#
```

```
   12 CONTINUE
      CALL RESET

      IF(LIN.EQ.0) GO TO 14
      CALL CHECK(LIN)
      N1=LIN-KS+1
      DO 13 I=NSNW,NFNW
      STEQ(I)=STEQ(I)+SS(N1,I)
   13 CONTINUE
      SRS(LIV)=SRS(LIV)+SRS(LIN)
      CALL RESET
   14 CONTINUE

C     CHECK IF THERE IS SUFFICIENT ROOM ON BUFFER FOR THE NEXT EQUATION
C     IF NOT WRITE STORED EQUATIONS TO TAPE 2 AND RESET STORAGE CONTROL
C     VARIABLES TO ZERO

      IF((NZN-NSNW+NFNW+1).LT.MAXREQ.AND.(MZM+4).LT.MAXLREQ) GO TO 6
      WRITE(2)  MZM,NZN,REQ,LREQ
      MZM=0
      NZN=0
    6 CONTINUE

C     ADJUST THE RHS IF THE NODE IS TO HAVE SPECIFIED VARIABLES

      CALL PRECON

      PIVOT=STEQ(LIV)
      WRITE(6,1000) PIVOT,NIC,LOC,SRS(LIV)
 1000 FORMAT(5X,E13.6,2I7,E13.6)
      N1=NZN

C     STORE EQUATION LIV AND ITS RHS ON BUFFER AND SET THE CORRESPONDING
C     POSITIONS IN THE GLOBAL STIFFNESS MATRIX, RHS VECTOR AND THE
C     HEADING VECTOR TO ZERO

      CALL CHECK(LIV)
      DO 7 I=NSNW,NFNW
      NZN=NZN+1
      K1=LIV-KS+1
      REQ(NZN)=STEQ(I)
      SS(K1,I)=0.0
    7 CONTINUE
      NZN=NZN+1
      REQ(NZN)=SRS(LIV)
      SRS(LIV)=0.0
      NW(LIV)=0
      CALL RESET

C     REDUCE REMAINING EQUATIONS

      IF(IND.EQ.1) GO TO 11
      DO 8 I=NSNW,NFNW
      IF(NW(I).EQ.0) GO TO 8
      IF(I.GT.KF) CALL CHECK(I)
      K1=I-KS+1
      FACT=SS(K1,LIV)/PIVOT
      N2=N1-NSNW+1
      DO 9 J=NSNW,NFNW
      SS(K1,J)=SS(K1,J)-FACT*REQ(N2+J)
    9 CONTINUE
      SRS(I)=SRS(I)-FACT*REQ(NZN)
      SS(K1,LIV)=0.0
    8 CONTINUE
      CALL RESET
#
```

```
   11 CONTINUE

C     MAKE COLUMN LIV ZERO

      IF(IND.NE.1) GO TO 21
      DO 10 I=NSNW,NFNW
      IF(I.GT.KF) CALL CHECK(I)
      K1=I-KS+1
      SS(K1,LIV)=0.0
   10 CONTINUE
      CALL RESET
   21 CONTINUE

C     STORE HEADING VECTOR LIMITS LIV AND LOC FOR LATER USE IN THE BACK
C     SUBSTITUTION PROCESS

      LREQ(MZM+1)=NSNW
      LREQ(MZM+2)=NFNW
      LREQ(MZM+3)=LIV
      LREQ(MZM+4)=LOC
      MZM=MZM+4

    1 CONTINUE
      RETURN

      END
      SUBROUTINE RESET

C     SUBROUTINE RESET RESETS TAPES 20 AND 21 AT THEIR STARTS AND PUTS
C     THE FIRST SUBDIVISION OF THE STRUCTURAL STIFFNESS MATRIX BACK
C     INTO SS

**********     ENTER COMMON BLOCK HERE     **********

    1 CONTINUE
      IF(KS.EQ.1) RETURN
      IF(KF.GE.MAXNW) GO TO 2
      BUFFER OUT (L21,1) (SS(1,1),SS(MAXND,MAXNW))
      IF(UNIT(L21)) 3,4,5
    3 CONTINUE
      BUFFER IN (L20,1) (SS(1,1),SS(MAXND,MAXNW))
      IF(UNIT(L20)) 6,4,5
    6 CONTINUE
      KS=KS+MAXND
      KF=KF+MAXND
      GO TO 1

    2 CONTINUE
      BUFFER OUT (L21,1) (SS(1,1),SS(MAXND,MAXNW))
      IF(UNIT(L21)) 7,4,5
    7 CONTINUE
      REWIND L20
      REWIND L21
      L=L21
      L21=L20
      L20=L
      BUFFER IN (L20,1) (SS(1,1),SS(MAXND,MAXNW))
      IF(UNIT(L20)) 8,4,5
    8 CONTINUE
      KS=1
      KF=MAXND
      RETURN

    4 STOP "4 EOF ENCOUNTERED IN BUFFER IN OR OUT"
    5 STOP "4 PARITY ERROR IN BUFFER IN OR OUT"
#
```

```
      END
      SUBROUTINE PRECON

C     SUBROUTINE PRECON ADJUSTS THE STIFFNESS AND THE RHS VECTOR TO
C     INCORPORATE SPECIFIED ZERO AND NON-ZERO NODAL VARIABLES

**********     ENTER COMMON BLOCK HERE     **********

      IF(MAXDIS.EQ.0) GO TO 1

C     ASSEMBLE NON-ZERO SPECIFIED VARIABLES AND MODIFY THE RHS VECTOR

      DO 2 I=1,MAXDIS
      IF(NIC.NE.NDISP(I,5)) GO TO 2
      DO 3 J=1,NVABZ
      IF(NDISP(I,J).EQ.0) GO TO 3
      IF(J.NE.NUMVAB) GO TO 3
      DSP=-DISP(I,J)

C     AFTER THE FIRST ITERATION ALL SPECIFIED ZERO OR NON-ZERO VARIABLES
C     MUST BE SET TO ZERO

      IF(ITER.GT.1) DSP=0.0

      DO 4 K=NSNW,NFNW
      IF(K.GT.KF) CALL CHECK(K)
      N1=K-KS+1
      SRS(K)=SRS(K)-DSP*SS(N1,LIV)
    4 CONTINUE
      STEQ(LIV)=1.0E+10
      CALL RESET
      IND=1
      RETURN

    3 CONTINUE
    2 CONTINUE

    1 CONTINUE
      IF(MAXNDZ.EQ.0) RETURN

C     ASSEMBLE ZERO SPECIFIED VARIABLES

      DO 5 I=1,MAXNDZ
      IF(NIC.NE.NDISPZ(I,5)) GO TO 5
      DO 6 J=1,NVABZ
      IF(NDISPZ(I,J).EQ.0) GO TO 6
      IF(J.NE.NUMVAB) GO TO 6
      STEQ(LIV)=1.0E+10
      IND=1
      RETURN

    6 CONTINUE
    5 CONTINUE
      RETURN

      END
      SUBROUTINE CHECK(N)

C     SUBROUTINE CHECK ENTERS THE SUBDIVISION OF THE STRUCTURAL
C     STIFFNESS MATRIX WHICH CONTAINS EQUATION N INTO SS

**********     ENTER COMMON BLOCK HERE     **********

    1 CONTINUE
#
```

```
      IF(KF.GE.N) RETURN
      BUFFER OUT (L21,1) (SS(1,1),SS(MAXND,MAXNW))
      IF(UNIT(L21)) 2,3,4
    2 CONTINUE
      BUFFER IN (L20,1) (SS(1,1),SS(MAXND,MAXNW))
      IF(UNIT(L20)) 5,3,4
    5 CONTINUE
      KS=KS+MAXND
      KF=KF+MAXND
      GO TO 1

    3 STOP "5 EOF ENCOUNTERED IN BUFFER IN OR OUT"
    4 STOP "5 PARITY ERROR IN BUFFER IN OR OUT"

      END
      SUBROUTINE BAKSUB

C     SUBROUTINE BAKSUB USES THE EQUATIONS REDUCED TO TRIANGULAR FORM
C     AND THE PROCESS OF BACK SUBSTITUTION TO OBTAIN THE NODAL
C     VELOCITIES AND PRESSURES

**********     ENTER COMMON BLOCK HERE     **********

      TOT=0.0
      ERROR=0.0
      DO 1 I=1,NUMEQ
      IF(NZN.NE.0) GO TO 5

C     READ STORED EQUATIONS FROM TAPE 2

      BACKSPACE 2
      READ(2) MZM,NZN,REQ,LREQ
      BACKSPACE 2

    5 CONTINUE

      MZM=MZM-4
      NSNW=LREQ(MZM+1)
      NFNW=LREQ(MZM+2)
      LIV=LREQ(MZM+3)
      LOC=LREQ(MZM+4)

C     SET UP EQUATION PARAMETERS

      GASH=REQ(NZN)
      PIVOT=REQ(NZN-NFNW-1+LIV)
      REQ(NZN-NFNW-1+LIV)=0.0
      N2=NZN-NFNW-2+NSNW
      NZN=N2

C     BACKSUBSTITUTE KNOWN VARIABLES

      DO 6 J=NSNW,NFNW
      N2=N2+1
      GASH=GASH-SRS(J)*REQ(N2)
    6 CONTINUE

      SRS(LIV)=GASH/PIVOT
      N1=(LOC-1)/NVABZ
      NUMVAB=LOC-N1*NVABZ
      NIC=N1+1
      ADS=GASH/PIVOT

C     REASSIGN SPECIFIED NODAL VARIABLES

#
```

```
      CALL POSTCN

C     MODIFY PREVIOUS ITERATIONS SOLUTION BY CALCULATED NEW ADJUSTMENTS

      ADSPL(NIC,NUMVAB)=ADSPL(NIC,NUMVAB)-ADS
      TOT=TOT+ADSPL(NIC,NUMVAB)*ADSPL(NIC,NUMVAB)
      ERROR=ERROR+ADS*ADS

    1 CONTINUE

C     EVALUATE CONVERGENCE PARAMETERS

      WRITE(6,999) ITER
      TOT=SQRT(TOT/NUMEQ)
      ERROR=SQRT(ERROR/NUMEQ)
      IF(ERROR/TOT.LE.1.0E-03) ITER=MAXIT

C     WRITE OUT FINAL SOLUTION

      IF(ITER.NE.MAXIT) GO TO 2
      WRITE(6,1000)
      DO 7 I=1,MAXNOD
      WRITE(6,1001) I,(ADSPL(I,J),J=1,NVABZ)
    7 CONTINUE
    2 CONTINUE
      WRITE(6,1002) ERROR,TOT,(ERROR/TOT)
      RETURN

  999 FORMAT(/////,5X,7HITER = ,I3)
 1000 FORMAT(1H1,///,5X,30HNODAL VELOCITIES AND PRESSURES,/,
     15X,4HNODE,8X,6HX-VEL ,9X,6HY-VEL ,9X,6HZ-VEL ,8X,8HPRESSURE)
 1001 FORMAT(4X,I5,4(5X,F10.5))
 1002 FORMAT(//,5X,36HMEAN SQUARED VALUE OF ADJUSTMENTS = ,E10.3,/,
     1      5X,43HMEAN SQUARED VALUE OF ADJUSTED VARIABLES = ,E10.3,/,
     1      5X,35HRATIO OF ADJUSTMENTS TO ADJUSTED = ,E10.3,/)

      END
      SUBROUTINE POSTCN

C     SUBROUTINE POSTCN REASSIGNS THE CORRECT SPECIFIED VALUE TO NODAL
C     VARIABLES WHOSE VALUES WERE ORIGINALLY KNOWN

**********     ENTER COMMON BLOCK HERE     **********

      IF(MAXDIS.EQ.0) GO TO 1

C     REASSIGN NON-ZERO SPECIFIED VARIABLES

      DO 2 I=1,MAXDIS
      IF(NIC.NE.NDISP(I,5)) GO TO 2
      DO 3 J=1,NVABZ
      IF(NDISP(I,J).EQ.0) GO TO 3
      IF(J.NE.NUMVAB) GO TO 3
      DSP=-DISP(I,J)
      IF(ITER.GT.1) DSP=0.0
      ADS=DSP
      SRS(LIV)=DSP
      RETURN

    3 CONTINUE
    2 CONTINUE
    1 CONTINUE
      IF(MAXNDZ.EQ.0) RETURN

C     REASSIGN ZERO SPECIFIED VARIABLES
#
```

```
      DO 4 I=1,MAXNDZ
      IF(NIC.NE.NDISPZ(I,5)) GO TO 4
      DO 5 J=1,NVABZ
      IF(NDISPZ(I,J).EQ.0) GO TO 5
      IF(J.NE.NUMVAB) GO TO 5
      ADS=0.0
      SRS(LIV)=0.0
      RETURN

    5 CONTINUE
    4 CONTINUE
      RETURN

      END
      BLOCK DATA

**********     ENTER COMMON BLOCK HERE     **********

      DATA INT1/1,3,5,7,1,3,5,7,13,15,17,19/
      DATA INT2/2,4,6,8,9,10,11,12,14,16,18,20/
      DATA INT3/3,5,7,1,13,15,17,19,15,17,19,13/

      DATA XX/1.0,1.0,1.0,0.0,-1.0,-1.0,-1.0,0.0,1.0,1.0,
     1       -1.0,-1.0,1.0,1.0,1.0,0.0,-1.0,-1.0,-1.0,0.0/
      DATA YY/-1.0,0.0,1.0,1.0,1.0,0.0,-1.0,-1.0,-1.0,1.0,
     1       1.0,-1.0,-1.0,0.0,1.0,1.0,1.0,0.0,-1.0,-1.0/
      DATA ZZ/-1.0,-1.0,-1.0,-1.0,-1.0,-1.0,-1.0,-1.0,0.0,0.0,
     1       0.0,0.0,1.0,1.0,1.0,1.0,1.0,1.0,1.0,1.0/

      DATA VECTLC/-0.774596669241148,0.0,0.774596669241148/
      DATA WTFUN/0.555555555555556,0.888888888888889,0.555555555555556/

      END



**********     COMMON BLOCK     **********

      COMMON MAXNEL,MAXNOD,NNODZ,NVABZ,MAXFW,MAXNW,MAXDIS,MAXNDZ,MAXND
      COMMON MAXPRS,MAXSHR,NRULE,MAXSS,MAXREQ,MAXIT,NFORM,ADS,MAXNS
      COMMON ITER,RE,XL,YL,ZL,WX,WY,WZ,DETJ,PIVOT,NSTOP,NUMVAB,NUMEQ
      COMMON MZM,NZN,NSNW,NFNW,NEL,NIC,LIV,MVABZ,IND,L20,L21,KS,KF
      COMMON ADSPL(32,4),CORD(32,3),LFRST(32)
      COMMON DISP(8,4),NDISP(8,5),NDISPZ(32,5)
      COMMON NPRES(8),PRES(8),NSHEAR(8),SHEAR(8,2)
      COMMON NW(200),SRS(150),SS(50,150),STEQ(150)
      COMMON LDEF(2,20)
      COMMON AW(9),CW(9),X(20),Y(20),Z(20),DX(20),DY(20),DZ(20)
      COMMON NELDES(80),SHP1(20),SHP2(20)
      COMMON P(20),SH1(20),SH2(20)
      COMMON ELDISP(20,4),S(80,80),RS(80),REQ(1000),LREQ(200)
      COMMON/CR1/INT1(12),INT2(12),INT3(12),XX(20),YY(20),ZZ(20)
      COMMON/CR2/VECTLC(3),WTFUN(3)
#
```

Typical input data for program CR3DVF2.

```
1 1                                        Heading 5X,9A8
        POISEUILLE FLOW
        MESH 2
        REYNOLDS NUMBER IS 1.0
1 2                                        Program parameters MAXIT and NFORM 5X,2I5
       1    2
2 1                                        Reynolds number 5X,I5,E10.3
        1 0.100E+01
3 1                                            Nodal Cartesian coordinates
        1 0.000E+00 0.000E+00 0.000E+00        5X,I5,3E10.3
        3 0.500E+00 0.000E+00 0.000E+00
        5 0.500E+00 0.500E+00 0.000E+00
        7 0.000E+00 0.500E+00 0.000E+00
       13 0.000E+00 0.000E+00 0.500E+00
       15 0.500E+00 0.000E+00 0.500E+00
       17 0.500E+00 0.500E+00 0.500E+00
       19 0.000E+00 0.500E+00 0.500E+00
       25 0.000E+00 0.000E+00 0.100E+01
       27 0.500E+00 0.000E+00 0.100E+01
       29 0.500E+00 0.500E+00 0.100E+01    Element
       31 0.000E+00 0.500E+00 0.100E+01    Element definitions
4 1                                        10X,12I5/10X,8I5
             1   2   3   4   5   6   7   8   9  10  11  12
            13  14  15  16  17  18  19  20
            13  14  15  16  17  18  19  20  21  22  23  24
            25  26  27  28  29  30  31  32
5 1                                        Non-zero specified variables 5X,4I1,X,4E10.
   0001    29       0.000E+00 0.000E+00 0.000E+00
5 2                                        Zero specified variables 5X,4I1,X,14I5
   1110     1   2   3   9  10  13  14  15  21  22  25  26  27
   1100     4   5   6   7   8  11  12  16  17  18  19  20  23
   1100    28  29  30  31  32
6 1                                        Applied side normal stresses 5X,I5,E10.3
        1 0.120E+02
        3 0.120E+02
        5 0.120E+02
        7 0.120E+02
       25 0.000E+00
       27 0.000E+00
       29 0.000E+00
       31 0.000E+00
99 0                                       Data complete
```

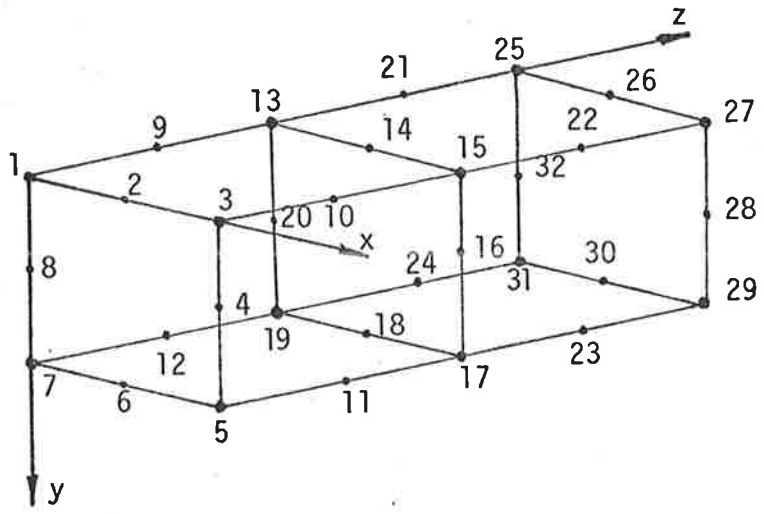

APPENDIX C

Element Stiffness, Numerical Values for 1x1 Element

The numerical values of the element stiffness matrix for a 1x1 square eight noded Serendipity element and for a 1x1 square nine noded Lagrangian element have been calculated using programs CR2DVF8 and CR2DVF9 respectively and formulation B, and are as follows.

$$\frac{1}{180}\begin{bmatrix}
312 & -308 & 146 & -104 & 138 & -172 & 124 & -136 & 85 & -100 & 15 & -20 & 35 & -20 & -15 & 20 & 35 & -5 & -10 & 10 \\
-308 & 736 & -308 & 0 & -172 & 224 & -172 & 0 & 20 & 0 & -20 & -80 & -20 & 0 & 20 & 80 & -40 & 40 & 20 & -20 \\
146 & -308 & 312 & -136 & 124 & -172 & 138 & -104 & -15 & 100 & -85 & -20 & 15 & 20 & -35 & 20 & 5 & -35 & -10 & 10 \\
-104 & 0 & -136 & 512 & -136 & 0 & -104 & -32 & -20 & -80 & 100 & 0 & -100 & 80 & 20 & 0 & -30 & -30 & -30 & -30 \\
138 & -172 & 124 & -136 & 312 & -308 & 146 & -104 & 35 & -20 & -15 & 20 & 85 & -100 & 15 & -20 & 10 & -10 & -35 & 5 \\
-172 & 224 & -172 & 0 & -308 & 736 & -308 & 0 & -20 & 0 & 20 & 80 & 20 & 0 & -20 & -80 & -20 & 20 & 40 & -40 \\
124 & -172 & 138 & -104 & 146 & -308 & 312 & -136 & 15 & 20 & -35 & 20 & -15 & 100 & -85 & -20 & 10 & -10 & -5 & 35 \\
-136 & 0 & -104 & -32 & -104 & 0 & -136 & 512 & -100 & 80 & 20 & 0 & -20 & -80 & 100 & 0 & 30 & 30 & 30 & 30 \\
\hline
85 & 20 & -15 & -20 & 35 & -20 & 15 & -100 & 312 & -136 & 124 & -172 & 138 & -104 & 146 & -308 & 35 & 10 & -10 & -5 \\
-100 & 0 & 100 & -80 & -20 & 0 & 20 & 80 & -136 & 512 & -136 & 0 & -104 & -32 & -104 & 0 & 30 & 30 & 30 & 30 \\
15 & -20 & -85 & 100 & -15 & 20 & -35 & 20 & 124 & -136 & 312 & -308 & 146 & -104 & 138 & -172 & 10 & 35 & -5 & -10 \\
-20 & -80 & -20 & 0 & 20 & 80 & 20 & 0 & -172 & 0 & -308 & 736 & -308 & 0 & -172 & 224 & -20 & -40 & 40 & 20 \\
35 & -20 & 15 & -100 & 85 & 20 & -15 & -20 & 138 & -104 & 146 & -308 & 312 & -136 & 124 & -172 & 10 & 5 & -35 & -10 \\
-20 & 0 & 20 & 80 & -100 & 0 & 100 & -80 & -104 & -32 & -104 & 0 & -136 & 512 & -136 & 0 & -30 & -30 & -30 & -30 \\
-15 & 20 & -35 & 20 & 15 & -20 & -85 & 100 & 146 & -104 & 138 & -172 & 124 & -136 & 312 & -308 & 5 & 10 & -10 & -35 \\
20 & 80 & 20 & 0 & -20 & -80 & -20 & 0 & -308 & 0 & -172 & 224 & -172 & 0 & -308 & 736 & -40 & -20 & 20 & 40 \\
\hline
35 & -40 & 5 & -30 & 10 & -20 & 10 & 30 & 35 & 30 & 10 & -20 & 10 & -30 & 5 & -40 & 0 & 0 & 0 & 0 \\
-5 & 40 & -35 & -30 & -10 & 20 & -10 & 30 & 10 & 30 & 35 & -40 & 5 & -30 & 10 & -20 & 0 & 0 & 0 & 0 \\
-10 & 20 & -10 & -30 & -35 & 40 & -5 & 30 & -10 & 30 & -5 & 40 & -35 & -30 & -10 & 20 & 0 & 0 & 0 & 0 \\
10 & -20 & 10 & -30 & 5 & -40 & 35 & 30 & -5 & 30 & -10 & 20 & -10 & -30 & -35 & 40 & 0 & 0 & 0 & 0
\end{bmatrix}$$

Stiffness matrix for a 1x1 eight noded element and formulation B

$$\frac{1}{180}\begin{bmatrix}
168 & -100 & 2 & 24 & -6 & 36 & -20 & -8 & -96 & 45 & -60 & 15 & 20 & -5 & 20 & -15 & 60 & -80 & 25 & 5 & 0 & 0 \\
-100 & 480 & -100 & -96 & 36 & -32 & 36 & -96 & -128 & 60 & 0 & -60 & -80 & 20 & 0 & -20 & 80 & 0 & -20 & 20 & 0 & 0 \\
2 & -100 & 168 & -8 & -20 & 36 & -6 & 24 & -96 & -15 & 60 & -45 & -60 & 15 & -20 & 5 & -20 & 80 & -5 & -25 & 0 & 0 \\
24 & -96 & -8 & 576 & -8 & -96 & 24 & 32 & -448 & 20 & -80 & 60 & 0 & -60 & 80 & -20 & 0 & 0 & -10 & -50 & -50 & -10 \\
-6 & 36 & -20 & -8 & 168 & -100 & 2 & 24 & -96 & -5 & 20 & -15 & 60 & 45 & -60 & 15 & 20 & -80 & 0 & 0 & -25 & -5 \\
36 & -32 & 36 & -96 & -100 & 480 & -100 & -96 & -128 & 20 & 0 & -20 & 80 & 60 & 0 & -60 & -80 & 0 & 0 & 0 & 20 & -20 \\
-20 & 36 & -6 & 24 & 2 & -100 & 168 & -8 & -96 & 15 & -20 & 5 & -20 & -15 & 60 & -45 & -60 & 80 & 0 & 0 & 5 & 25 \\
-8 & -96 & 24 & 32 & 24 & -96 & -8 & 576 & -448 & -60 & 80 & -20 & 0 & 20 & -80 & 60 & 0 & 0 & 50 & 10 & 10 & 50 \\
-96 & -128 & -96 & -448 & -96 & -128 & -96 & -448 & 1536 & -80 & 0 & 80 & 0 & -80 & 0 & 80 & 0 & 0 & -40 & 40 & 40 & -40 \\
45 & 60 & -15 & 20 & -5 & 20 & 15 & -60 & -80 & 168 & -8 & -20 & 36 & -6 & 24 & 2 & -100 & -96 & 25 & 0 & 0 & 5 \\
-60 & 0 & 60 & -80 & 20 & 0 & -20 & 80 & 0 & -8 & 576 & -8 & -96 & 24 & 32 & 24 & -96 & -448 & 50 & 50 & 10 & 10 \\
15 & -60 & -45 & 60 & -15 & -20 & 5 & -20 & 80 & -20 & -8 & 168 & -100 & 2 & 24 & -6 & 36 & -96 & 0 & 25 & 5 & 0 \\
20 & -80 & -60 & 0 & 60 & 80 & -20 & 0 & 0 & 36 & -96 & -100 & 480 & -100 & -96 & 36 & -32 & -128 & 0 & -20 & 20 & 0 \\
-5 & 20 & 15 & -60 & 45 & 60 & -15 & 20 & -80 & -6 & 24 & 2 & -100 & 168 & -8 & -20 & 36 & -96 & 0 & -5 & -25 & 0 \\
20 & 0 & -20 & 80 & -60 & 0 & 60 & -80 & 0 & 24 & 32 & 24 & -96 & -8 & 576 & -8 & -96 & -448 & -10 & -10 & -50 & -50 \\
-15 & -20 & 5 & -20 & 15 & -60 & -45 & 60 & 80 & 2 & 24 & -6 & 36 & -20 & -8 & 168 & -100 & -96 & -5 & 0 & 0 & -25 \\
60 & 80 & -20 & 0 & 20 & -80 & -60 & 0 & 0 & -100 & -96 & 36 & -32 & 36 & -96 & -100 & 480 & -128 & -20 & 0 & 0 & 20 \\
-80 & 0 & 80 & 0 & -80 & 0 & 80 & 0 & 0 & -96 & -448 & -96 & -128 & -96 & -448 & -96 & -128 & 1536 & -40 & -40 & 40 & 40 \\
25 & -20 & -5 & -10 & 0 & 0 & 0 & 50 & -40 & 25 & 50 & 0 & 0 & 0 & -10 & -5 & -20 & -40 & 0 & 0 & 0 & 0 \\
5 & 20 & -25 & -50 & 0 & 0 & 0 & 10 & 40 & 0 & 50 & 25 & -20 & -5 & -10 & 0 & 0 & -40 & 0 & 0 & 0 & 0 \\
0 & 0 & 0 & -50 & -25 & 20 & 5 & 10 & 40 & 0 & 10 & 5 & 20 & -25 & -50 & 0 & 0 & 40 & 0 & 0 & 0 & 0 \\
0 & 0 & 0 & -10 & -5 & -20 & 25 & 50 & -40 & 5 & 10 & 0 & 0 & 0 & -50 & -25 & 20 & 40 & 0 & 0 & 0 & 0
\end{bmatrix}$$

Stiffness matrix for a 1x1 nine noded element and formulation B

APPENDIX D

Solution of Poiseuille Flow using Eight and Nine Noded Elements

The Poiseuille flow is the steady flow that occurs between two parallel infinite flat plates spaced at a distance of one unit apart, as a result of the application of a constant pressure gradient. The actual three-dimensional flow and its more common two-dimensional representation are shown in Figure D1. Almost all researchers in numerical viscous fluid dynamics at one stage or another, use this flow problem as a test case during the development of their particular solution technique. The exact solution for the Poiseuille flow is:

$$u(x,y) = -\tfrac{1}{2}\, Re \frac{dp}{dx}\, y(1-y) \qquad D1.1$$

$$v(x,y) = 0 \qquad D1.2$$

and

$$p(x,y) = p_1 + \frac{dp}{dx}\, x \quad \text{where} \quad \frac{dp}{dx} = \frac{p_2 - p_1}{L} \qquad D1.3$$

In this study the Poiseuille flow was solved initially using the eight noded Serendipity element and a regular rectangular arrangement of elements in the various meshes. Figure D2 shows the meshes and the actual numerical values of the boundary conditions used. The solutions obtained using each of the meshes 1 to 3 correspond exactly with the values calculated from equations D1, as expected.

In order to investigate as fully as possible all aspects of the solution of the Poiseuille flow using the Galerkin finite element method and the eight noded Serendipity element, various changes to the geometry of the elements in mesh 2 were made and the problem was rerun. Firstly, the regularity of the rectangular elements was altered so that long thin and short wide elements were incorporated, thus destroying the symmetry of the element arrangement. The results obtained again correspond exactly with the exact analytical solution. Secondly, the shape

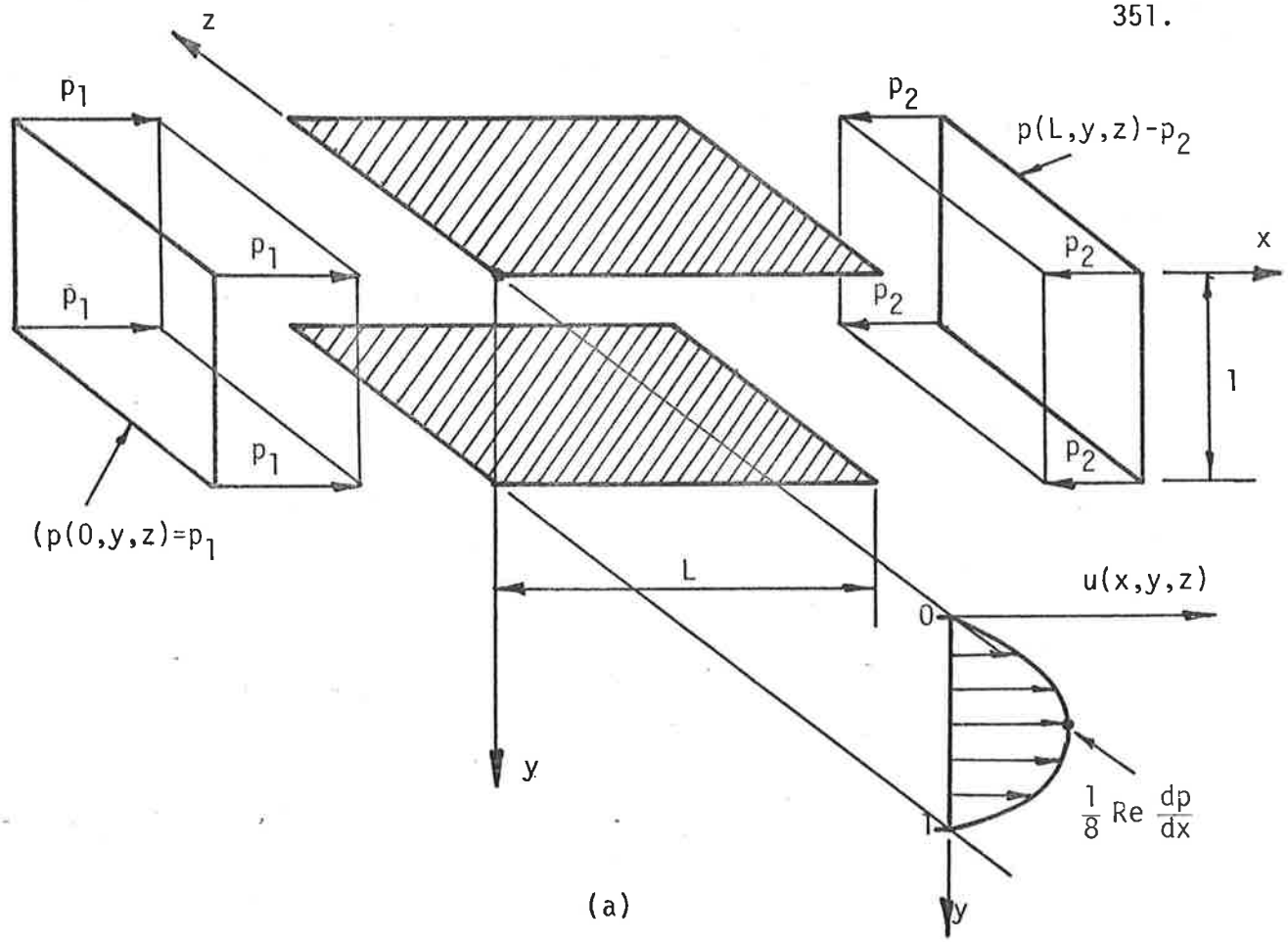

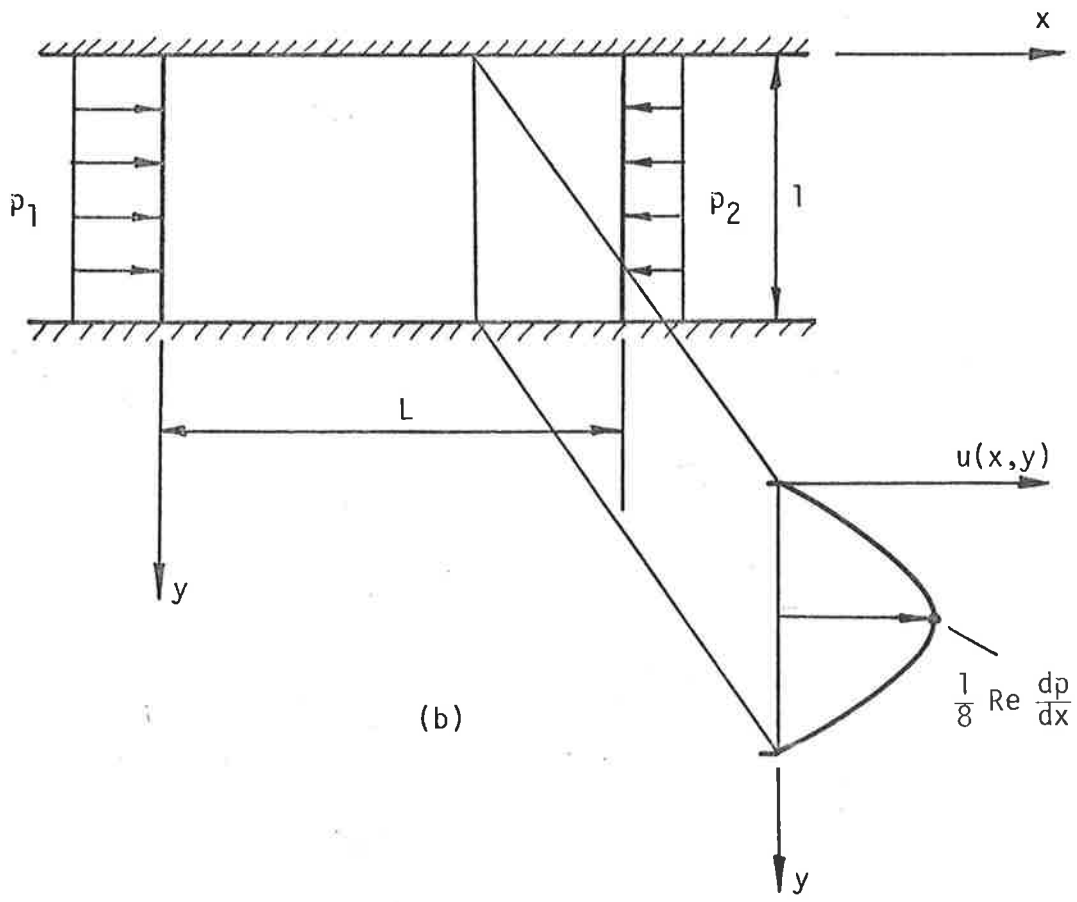

Figure D1 (a) Actual Three-dimensional Poiseuille Flow, and (b) Two-dimensional Representation.

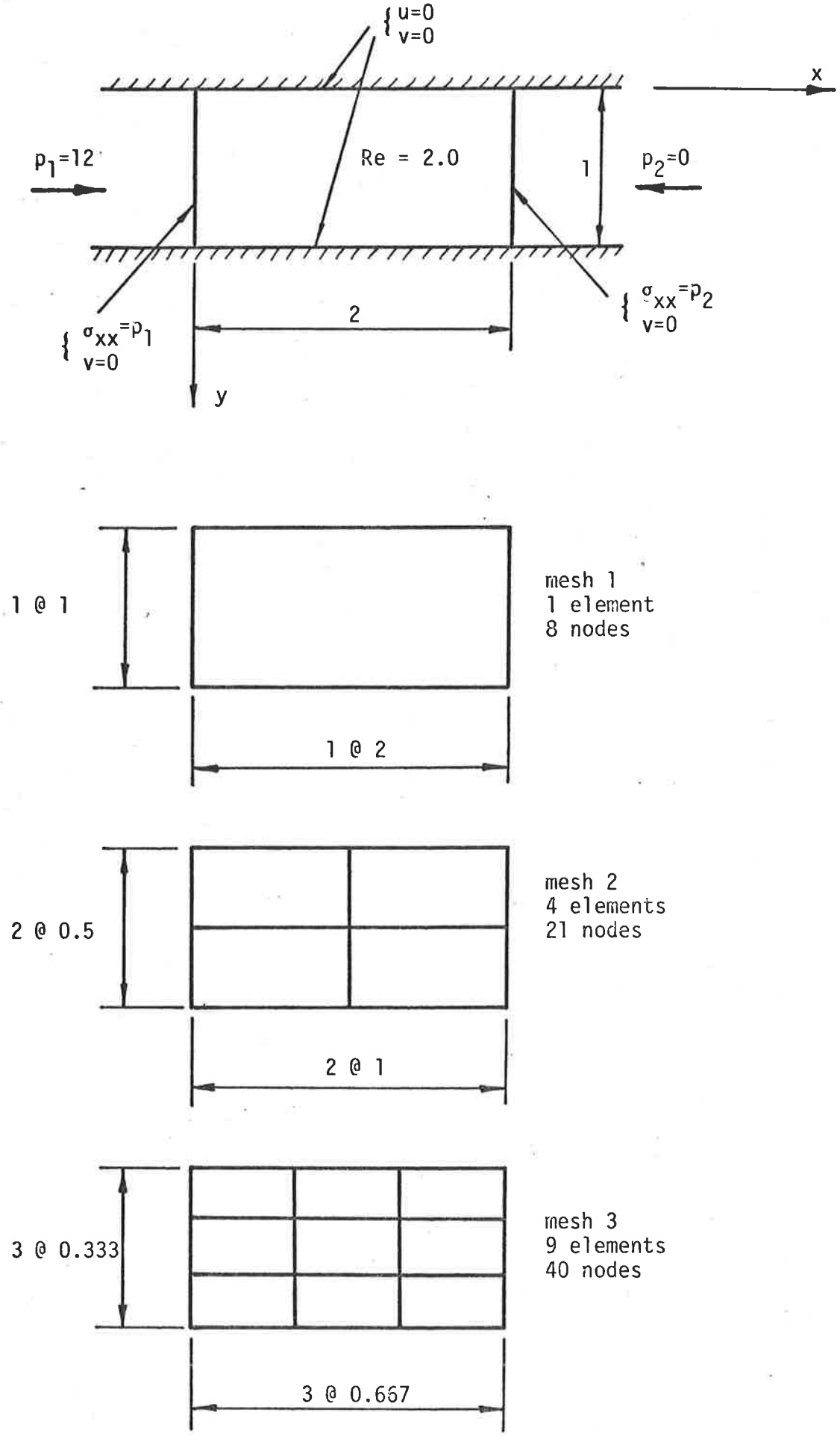

Figure D2 Details of Meshes 1, 2 and 3.

of the elements was changed from rectangular to arbitrary quadrilateral by relocating the central node slightly off centre as shown in Figure D3. In this case the solution obtained differed by varying amounts from the exact solution in both the x and y components of velocity and in the pressure. Although the differences are quite small, they still caused concern since it had been expected that the exact solution would be obtained. This is because it had been anticipated that the eight noded Serendipity element would be quite capable of representing exactly the velocity variation which is at most quadratic and the pressure variation which is at most linear.

When the nine noded Lagrangian element was used to solve the Poiseuille flow, the same results were obtained with all meshes except 2C. In this case, whereas the Serendipity element had given slightly erroneous results, the Lagrangian element gave the exact solution for both the velocity components as well as the pressure. The results obtained using mesh 2C and the eight and nine noded elements are given in Table D1. From this table it can be seen that the eight noded element produces quite good results with errors no larger than 1% but that the Lagrangian element produces the exact solution. This finding prompted a closer investigation into the relative abilities of the eight and nine noded elements to represent a quadratic velocity variation when the element shape is non rectangular. To this end, an arbitrary quadrilateral was set up, the details of which are given in Figure D4(a), and a quadratic velocity variation given by

$$u(x,y) = 2y(4-y) \qquad \text{D2}$$

was imposed on it by specifying its exact value at all the nodes. Then by using the shape functions of firstly the Serendipity element and secondly the Lagrangian element, two expressions for the variation of u at any point within the element were set up. The two expressions are:

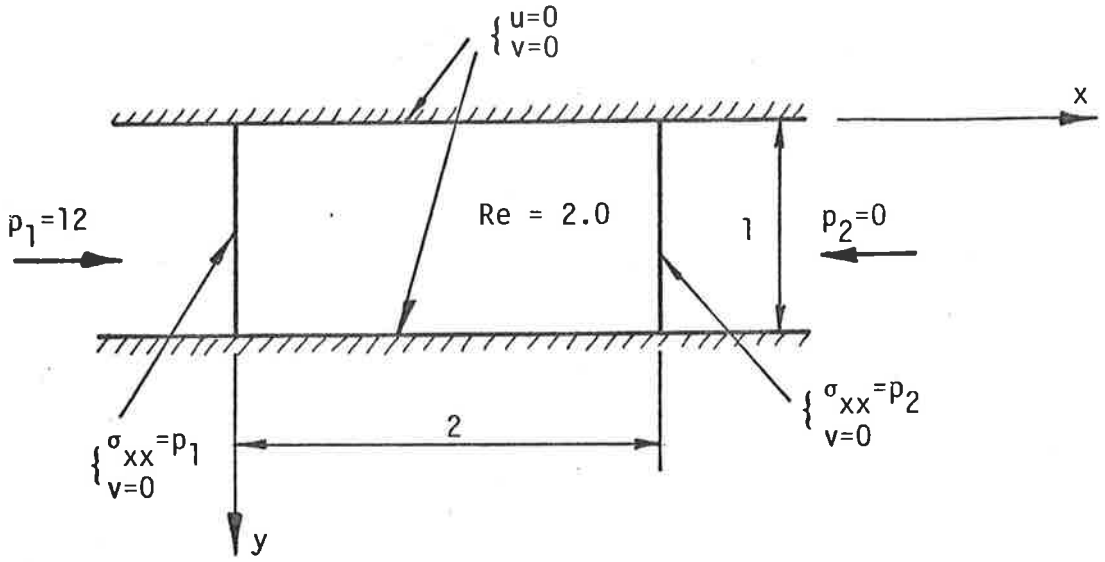

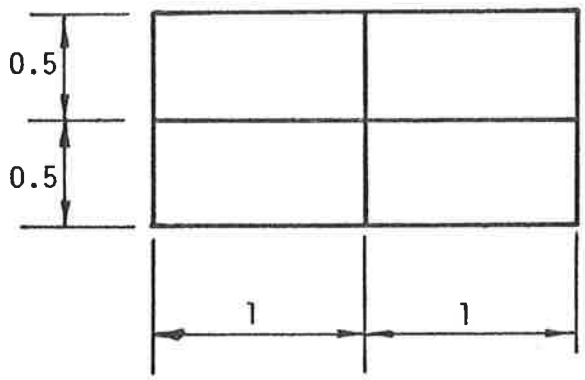

mesh 2A

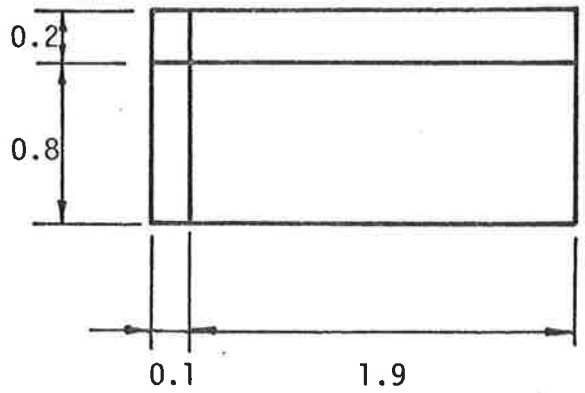

mesh 2B

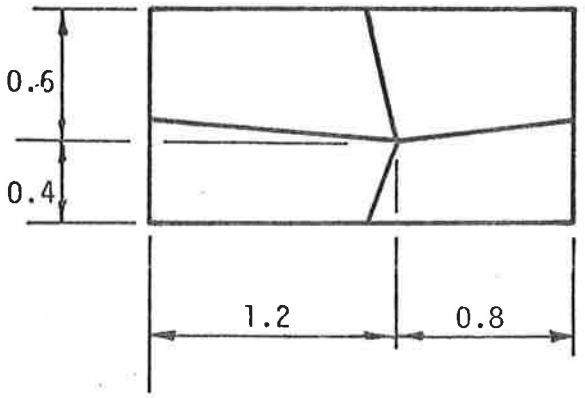

mesh 2C

Figure D3 Details of Meshes 2A, 2B and 2C.

Node	Coords		8NE			9NE		
			Velocity		Press	Velocity		Press
	x	y	x	y		x	y	
1	0	0	0	0	12.000	0	0	12.000
2	0.5	0	0	0		0	0	
3	1	0	0	0	5.949	0	0	6.000
4	1.5	0	0	0		0	0	
5	2	0	0	0	0.188	0	0	0
6	0	0.25	1.124	0		1.125	0	
7	1.1	0.3	1.258	-0.0005		1.260	0	
8	2	0.25	1.126	0		1.125	0	
9	0	0.5	1.501	0	12.015	1.500	0	12.000
10	0.6	0.55	1.484	0.0002		1.485	0	
11	1.2	0.6	1.444	-0.0005	4.814	1.440	0	4.800
12	1.6	0.55	1.483	-0.0003		1.485	0	
13	2	0.5	1.499	0	-0.095	1.500	0	0
14	0	0.75	1.125	0		1.125	0	
15	1.1	0.8	0.957	-0.0001		0.960	0	
16	2	0.75	1.125	0		1.125	0	
17	0	1	0	0	11.958	0	0	12.000
18	0.5	1	0	0		0	0	
19	1	1	0	0	5.963	0	0	6.000
20	1.5	1	0	0		0	0	
21	2	1	0	0	0.197	0	0	0
22	0.55	0.275				1.196	0	
23	1.55	0.275				1.196	0	
24	0.55	0.775				1.046	0	
25	1.55	0.775				1.046	0	

Table D1 Solution to Poiseuille flow obtained using mesh 2C and the eight and nine noded Serendipity and Lagrangian elements.

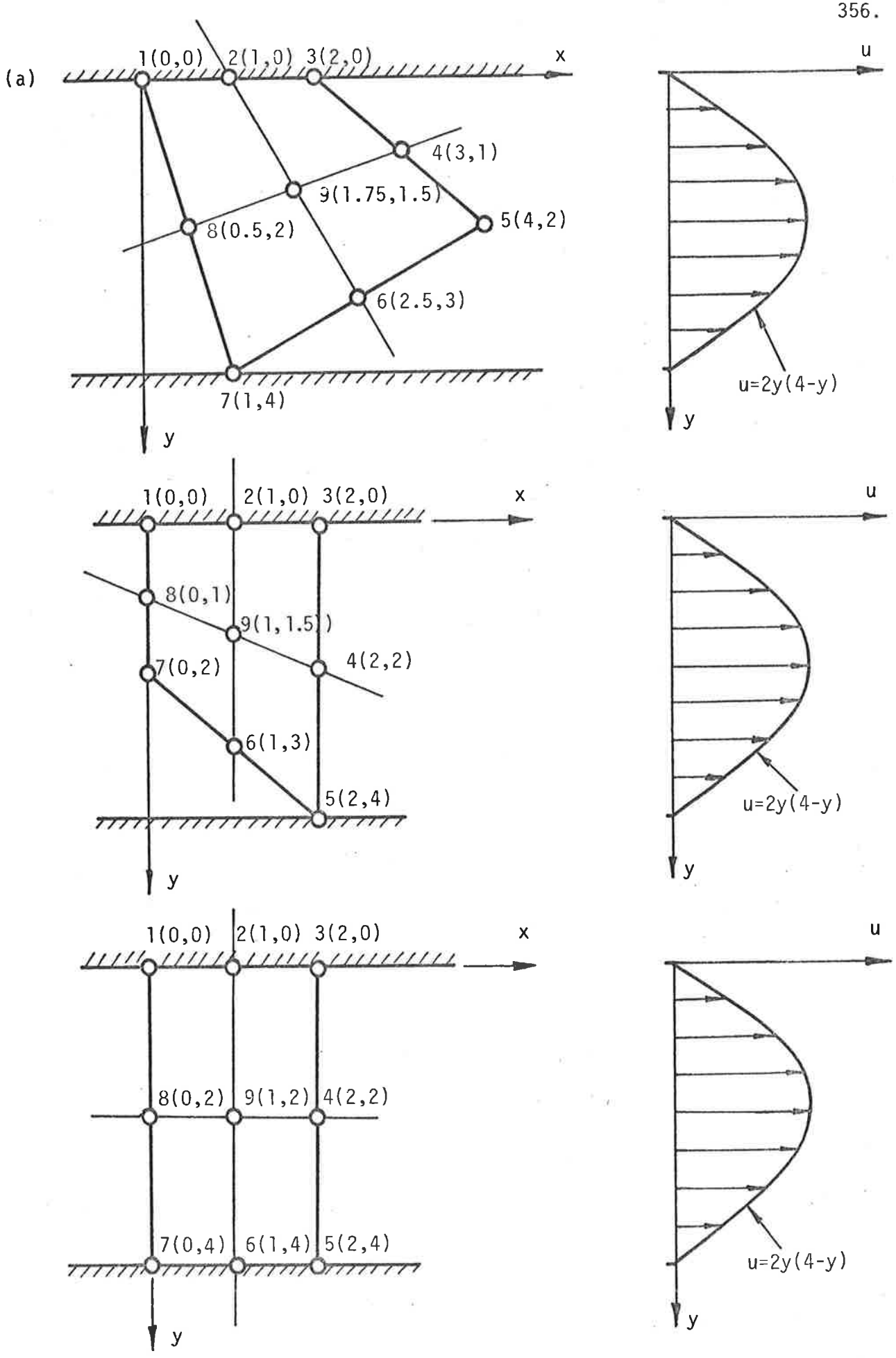

Figure D4 Typical Elements (a) General Quadrilateral, (b) Trapezoidal, and (c) Rectangular.

$$u_8(\xi,\eta) = 8 + \xi + 2\xi\eta - 3\eta - \xi^2 - 5\eta^2 - 3\xi\eta^2 + \xi^2\eta \qquad \text{D3}$$

and $$u_9(\xi,\eta) = 7.5 + \xi + 2\xi\eta - 3\eta - 0.5\xi^2 - 4.5\eta^2 - 3\xi\eta^2 + \xi^2\eta - 0.5\xi^2\eta^2 \qquad \text{D4}$$

where $$\left.\begin{aligned} x &= 1.75 - 1.25\xi - 0.75\eta + 0.25\xi\eta \\ \text{and}\quad y &= 1.5 + 0.5\xi - 1.5\eta - 0.5\xi\eta \end{aligned}\right\} \qquad \text{D5}$$

Since these functions are expressed in terms of the local coordinates ξ and η and the transformation back to x and y is complicated, it is easier to use the transformation from x and y to ξ and η to rewrite $u(x,y) = 2y(4-y)$ in terms of ξ and η. Therefore $u(x,y) = 2y(4-y)$ becomes

$$u(\xi,\eta) = 7.5 + \xi + 2\xi\eta - 3\eta - 0.5\xi^2 - 4.5\eta^2 - 3\xi\eta^2 + \xi^2\eta - 0.5\xi^2\eta^2 \qquad \text{D6}$$

It can now be seen that $u_9(\xi,\eta)$ is identical to $u(\xi,\eta)$ while $u_8(\xi,\eta)$ differs from it by

$$\begin{aligned} & 0.5 - 0.5\xi^2 - 0.5\eta^2 + 0.5\xi^2\eta^2 \\ = \; & 0.5(1-\xi^2)(1-\eta^2) \end{aligned} \qquad \text{D7}$$

Since this difference is equal to zero when $\xi = \pm 1$ or $\eta = \pm 1$ we see that $u_8(\xi,\eta)$ represents $u(\xi,\eta)$ exactly only on the boundary of the element where $\xi = \pm 1$ or $\eta = \pm 1$. Within the element however, the error can be quite significant, in this case as high as 6.7%. Therefore the Serendipity element is not able to represent exactly a quadratic variation in the velocity when the element shape is a general quadrilateral. On the other hand, $u_9(\xi,\eta)$ being identically equal to $u(\xi,\eta)$ indicates that the Lagrangian element can represent a quadratic velocity variation adequately regardless of what shape the element is.

The above process can be repeated for a trapezoidal and finally a rectangular element as shown in Figures D4(b) and (c). The expressions obtained for the trapezoidal element are:

$$u_8(\xi,\eta) = 8 - \xi - 2\xi\eta - 3\eta - \xi^2 - 5\eta^2 + 3\xi\eta^2 + \xi^2\eta \qquad \text{D8}$$

$$u_9(\xi,\eta) = 7.5 - \xi - 2\xi\eta - 3\eta - 0.5\xi^2 - 4.5\eta^2 + 3\xi\eta^2 + \xi^2\eta - 0.5\xi^2\eta^2 \qquad D9$$

and $$u(\xi,\eta) = 7.5 - \xi - 2\xi\eta - 3\eta - 0.5\xi^2 - 4.5\eta^2 + 3\xi\eta^2 + \xi^2\eta - 0.5\xi^2\eta^2 \qquad D10$$

while the expressions obtained for the rectangular element are:

$$u_8(\xi,\eta) = 8 - 8\eta^2 \qquad D11$$

$$u_9(\xi,\eta) = 8 - 8\eta^2 \qquad D12$$

and $$u(\xi,\eta) = 8 - 8\eta^2 \qquad D13$$

From all the above we see that $u_9(\xi,\eta)$ is always equal to $u(\xi,\eta)$. Therefore the Lagrangian element is capable of representing a quadratic velocity variation exactly regardless of which element shape is used. On the other hand, $u_8(\xi,\eta)$ is only equal to $u(\xi,\eta)$ when the element is rectangular. Therefore the Serendipity element is capable of representing a quadratic velocity variation exactly only when the element shape is rectangular. For this reason therefore it was found that when the eight noded element was used to solve the Poiseuille flow with mesh 2C, the solution obtained was slightly wrong, whereas when the nine noded element was used it corresponded exactly with the exact solution.

The last point that should be mentioned here is that, although it is only the velocity representation that is inadequate when non rectangular elements are used, it is found that the resulting pressure field, which is linear and should be adequately handled by both the Serendipity and the Lagrangian elements, also contains errors. The reason for this is that the Galerkin finite element method is a process in which integral rather than discrete quantities are considered. As a consequence, inadequacies in the representation of one variable produces errors not only in that variable but also in all the other variables to which it is connected by the governing equation system.

BIBLIOGRAPHY

1. ABARBANEL, S., BENETT, S., BRANDT, A. and GILLIS, J., "Velocity Profiles of Flow at Low Reynolds Numbers", Journal of Applied Mechanics, Transactions of the ASME, March 1970, pp. 2-4.

2. BAKER, A.J., "Finite Element Solution Algorithm for Viscous Incompressible Fluid Dynamics", International Journal for Numerical Methods in Engineering, Vol. 6, 1973, pp. 89-101.

3. BERCOVIER, M. and ENGELMAN, M., "A Finite Element for the Numerical Solution of Viscous Flows", Journal of Computational Physics, No. 30, 1979, pp. 181-201.

4. BODOIA, J.R. and OSTERLE, J.F., "Finite Difference Analysis of Plane Poiseuille and Couette Flow Developments", Applied Scientific Research, Section A, Vol. 10, 1961, pp. 265-276.

5. BRANDT, A. and GILLIS, J., "Magnetohydrodynamic Flow in the Inlet Region of a Straight Channel", The Physics of Fluids, Vol. 9, No. 4, April, 1966, pp. 690-699.

6. BURGGRAF, O.R., "Analytical and Numerical Studies of the Structure of Steady Separated Flows", Journal of Fluid Mechanics, Vol. 24, Pt 1, 1966, pp. 113-151.

7. CARLSON, G.A. and HORNBECK, R.W., "A Numerical Solution for Laminar Entrance Flow in a Square Duct", Journal of Applied Mechanics, Transactions of the ASME, March, 1973, pp. 25-30.

8. CHENG, R.T., "Numerical Solution of the Navier-Stockes Equations by the Finite Element Method", The Physics of Fluids, Vol. 15, No. 12, 1972, pp. 2098-2105.

9. CHUNG, Y.K. and YEO, M.F., A Practical Introduction to Finite Element Analysis, Pitman International Text, 1979.

10. DAVIS, R.T., "Lamina Incompressible Flow Past a Semi-Infinite Flat Plate", Journal of Fluid Mechanics, Vol. 27, Pt 4, 1967, pp. 691-704.

11. FLETCHER, C.A.J., Improved Integration Techniques for Fluid Flow Finite Element Formulations", Department of Defence, Weapons Research Establishment, Salisbury, South Australia, Technical Report 1810 (W), April, 1977.

12. FORTIN, M., "Approximation des Fonctions à Divergence Nulle par la Méthode des Elements Finis", Proceedings of the Third International Conference on Numerical Methods in Fluid Mechanics, edited by Richtmyer, R.D., 1974, pp. 392-395.

13. GARTLING, D.K., NICKELL, R.E. and TANNER, R.I., "A Finite Element Convergence Study for Accelerating Flow Problems", International Journal for Numerical Methods in Engineering, Vol. 11, 1977, pp. 1155-1174.

14. GOLDSTEIN, R.J. and KREID, D.K., "Measurement of Laminar Flow Development in a Square Duct Using a Laser-Doppler Flowmeter", Journal of Applied Mechanics, Transactions of the ASME, December, 1967, pp. 813-818.

15. HAN, L.S., "Hydrodynamic Entrance Lengths for Incompressible Flow in Rectangular Ducts", Journal of Applied Mechanics, Transactions of the ASME, September, 1960, pp. 403-409.

16. HOOD, P. and TAYLOR, C., "Navier-Stokes Equations Using Mixed Interpolation", Finite Elements in Flow Problems, UAH Press, Huntsville, 1974, pp. 121-132.

17. HUTTON, A.G., "On Flow Near Singular Points of a Wall Boundary", Finite Element Methods in Flow Problems, UAH Press, Huntsville, 1974, pp. 67-83.

18. HUTTON, S.G., EXETER, M.K., FUSSEY, D.E., WEBSTER, J.J. and RIGON, C., "Primitive Variable Finite Element Formulations for Steady Viscous Flows", International Journal for Numerical Methods in Engineering, Vol. 15, 1980, pp. 209-223.

19. KAWAHARA, M., YOSHIMURA, N., NAKAGAWA, K. and OHSAKA, H., "Steady and Unsteady Finite Element Analysis of Incompressible Viscous Fluid", International Journal for Numerical Methods in Engineering, Vol. 10, 1976, pp. 437-456.

20. LANDAU, L.D. and LIFSHITZ, E.M., Fluid Mechanics, Pergamon Press, London, 1959.

21. MORIHARA, H. and CHENG, R.T., "Numerical Solution of the Viscous Flow in the Entrance Region of Parallel Plates", Journal of Computational Physics, Vol. 11, 1973, pp. 550-572.

22. NORRIE, D.H. and DE VRIES, G., A Survey of Finite Element Applications in Fluid Mechanics, Department of Mechanical Engineering, University of Calgary, Alberta, Canada, Report No. 83, December, 1976.
(A shorter version, "Recent Advances in Finite Element Methods Applied to Fluid Dynamics" is included in Proceedings of the 1976 International Conference on Finite Element Methods in Engineering, University of Adelaide, December, 1976.)

23. OLSON, M.D., "Variational-Finite Element Methods for Two-Dimensional and Axisymmetric Navier-Stokes Equations", Finite Elements in Fluids, Vol. 1, John Wiley and Sons, London, 1975, pp. 57-72.

24. OLSON, M.D., "Comparison of Various Finite Element Solution Methods for the Navier-Stokes Equations", Proceedings of the International Conference on Finite Elements in Water Resources, Princeton University, July, 1976, pp. 4.185-203.

25. OLSON, M.D. and TUANN, S.Y., "Primitive Variables Versus Stream Function Finite Element Solutions of the Navier-Stokes Equations", Proceedings of the Second International Conference on Finite Element Methods in Flow Problems, St Margherita, Italy, 1976, pp. 57-68.

26. ROSENHEAD, L., Lamina Boundary Layers, Clarendon Press, 1963.

27. RUBIN, S.G., KHOSLA, P.K. and SAARI, S.,"Laminar Flow in Rectangular Channels", Computers and Fluids, Vol. 5, 1977, pp. 151-173.

28. SCHLICHTING, H., Boundary Layer Theory, 6th edition, McGraw-Hill Book Co., 1968, pp. 146-149.

29. SMITH, R.M., A Study of Lamina Flow Entrance Sections Using the Finite Element Method, CEGB Report No. RD/13/N3513, December, 1975.

30. TAYLOR, C. and HOOD, P., "A Numerical Solution of the Navier-Stokes Equations Using the Finite Element Technique", Computers and Fluids, Vol. 1, 1973, pp. 73-100.

31. TONG, P., "On the Solution of the Navier-Stokes Equations in Two-Dimensional and Axial Symmetric Problems", Finite Element Methods in Flow Problems, UAH Press, Huntsville, 1974, pp. 57-66.

32. TUANN, S.Y. and OLSON, M.D., A Study of Various Finite Element Solution Methods for the Navier-Stokes Equations, Structural Research Series Report No. 14, University of British Columbia, Department of Civil Engineering, Vancouver, May, 1976.

33. VAN DYKE, M., "Entry Flow in a Channel", Journal of Fluid Mechanics, Vol. 44, Pt 4, 1970, pp. 813-823.

34. WHITE, F.M., Viscous Fluid Flow, McGraw-Hill Book Co., 1974, pp. 123-124.

35. YAMADA, Y., ITO, K., YOKOUCHI, Y., TAMANO, T. and OHTSUBO, T., "Finite Element Analysis of Steady Fluid and Metal Flow, Finite Elements in Fluids, Vol. 1, John Wiley and Sons, London, 1975, pp. 73-94.

36. ZIENKIEWICZ, O.C., The Finite Element Method in Engineering Science, McGraw-Hill Book Co., New York, 1971, pp. 44-46.

37. ZIENKIEWICZ, O.C. and PAREKH, C.J., "Transient Field Problems: Two-dimensional and Three-dimensional Analysis by Isoparametric Finite Elements", International Journal for Numerical Methods in Engineering, Vol. 2, 1970, pp. 61-71.

38. ZIENKIEWICZ, O.C. and CHEUNG, Y.K., "Finite Elements in the Solution of Field Problems", The Engineer, September, 1965, pp. 507-510.

39. SANI, R.L., GRESHO, P.M., LEE, R.L., GRIFFITHS, D.F. and ENGELMAN, M., "The Cause and Cure (?) of the Spurious Pressures Generated by Certain FEM Solutions of the Incompressible Navier-Stokes Equations", Parts I and II, Unpublished Report prepared for publication in the International Journal for Numerical Methods in Fluids, January, 1981.